

THE 2015 AMMCS-CAIMS CONGRESS



JUNE 7-12

WATERLOO, ONTARIO, CANADA

BOOK OF ABSTRACTS

Technical Design by
Michael Murray

Mathematics and Computation in Biological Sciences and Medicine
Partial Differential and Integral Equations in Mathematics and Applications
Applications of Dynamical Systems and Differential Equations
Computational Physics and Chemistry
Computational Algebra, Combinatorics and Optimization
Mathematical Models in Social Sciences
Computational Mechanics and Engineering
Financial Mathematics and Computation
Statistical Modelling
Mathematical Methods in Environmental Sciences
Mathematical Education in Biological Sciences and Medicine
Partial Differential and Integral Equations in Mathematics and Applications
Applications of Dynamical Systems and Differential Equations
Mathematics and Computation in Biological Sciences and Medicine
Partial Differential and Integral Equations in Mathematics and Applications
Applications of Dynamical Systems and Differential Equations
Computational Physics and Chemistry
Computational Algebra, Combinatorics and Optimization
Mathematical Models in Social Sciences
Computational Mechanics and Engineering
Financial Mathematics and Computation
Statistical Modelling



The AMMCS–CAIMS 2015 Congress

Book of Abstracts

Waterloo, Ontario, Canada

June 7–12, 2015

Disclaimer

This book contains abstracts of the AMMCS-CAIMS 2015 Congress. Authors are responsible for the contents and accuracy. Opinions expressed may not necessarily reflect the position of the AMMCS-CAIMS 2015 scientific and organizing committees.

Technical Designer: Michael J. Murray

Publisher: CAIMS-AMMCS 2015

ISBN: 978-0-9918856-1-9

General Chairs

Jacques Bélair (University of Montreal)

Roman Makarov (Wilfrid Laurier University, Waterloo)

Roderick Melnik (Wilfrid Laurier University, Waterloo)

Scientific Committee

Alberto Bressan (Penn State University)

David Cai (New York University)

Ronald Coifman (Yale University)

Carlos Garcia-Cervera (University of California, Santa Barbara)

Anatoli Ivanov (Penn State University)

Shaofan Li (University of California, Berkeley)

John Lowengrub (University of California, Irvine)

Andrew Majda (New York University)

Boris Malomed (Tel Aviv University)

Olof Runborg (KTH Royal Institute of Technology)

Chi-Wang Shu (Brown University)

Konstantina Trivisa (University of Maryland)

Dimitri Vvedensky (Imperial College London)

Nicholas Zabaras (University of Warwick)

Maciej Zworski (University of California, Berkeley)

Organizing Committee

Herb Kunze (Congress Program Chair, University of Guelph)

Zilin Wang (Congress Treasurer, Wilfrid Laurier University, Waterloo)

Chester Weatherby (Student Prize Committee Chair, Wilfrid Laurier University, Waterloo)

Hasan Shodiev (Local OC, Wilfrid Laurier University, Waterloo)

Ian Frigaard (Global OC, University of British Columbia, Vancouver)

Raymond Spiteri (Global OC, University of Saskatchewan, Saskatoon)

Technical Support Committee

George Lifchits (Web Coordinator)

Jeanette Haas (Administrative Support)

Michael Murray (Electronic Publishing Coordinator)

Sanjay Prabhakar (Computer Support)

Shyam Badu (Digital Media Support)

SIAM Representative

Roderick Melnik (Wilfrid Laurier University, Waterloo)

AMMCS-CAIMS2015 Students Team

Saqif Abdullah (WLU, Waterloo)	Adrian Lee (UofG, Guelph)
Alysha Ahlin (WLU, Waterloo)	Moriah Magcalas (UW, Waterloo)
Shazma Ameen (WLU, Waterloo)	Anisha Mahant (WLU, Waterloo)
Zaamilah Balasubramaniam (WLU, Waterloo)	Zhijun Mao (WLU, Waterloo)
Moosa Baque (WLU, Waterloo)	Philip McCarthy (UW, Waterloo)
Amenda Chow (UW, Waterloo)	Katia McDougall (WLU, Waterloo)
Lorena Cid Montiel (UW, Waterloo)	Mbika Nfor (WLU, Waterloo)
Asiya Gul (WLU, Waterloo)	Kenneth Onuma (WLU, Waterloo)
Andrew Harris (WLU, Waterloo)	Diogo Poças (McMaster, Hamilton)
Alexander Howse (UW, Waterloo)	Krishan Rajaratnam (UW, Waterloo)
Bowen Hu (WLU, Waterloo)	Januka Shanmugarajah (WLU, Waterloo)
Syeda Hussain (WLU, Waterloo)	Shada Tabet (WLU, Waterloo)
Maryo Ibrahim (WLU, Waterloo)	Yuchen Zhu (WLU, Waterloo)
Igor Ivashev (WLU, Waterloo)	Bingxia Zong (WLU, Waterloo)
Nilam Lakhani (WLU, Waterloo)	

Sponsors



Contents

Lists of Sessions	1
Plenary Lectures	9
Semi-Plenary Lectures	34
Special Sessions	40
Session SS-AAIP Inverse Problem	42
Session SS-CMPMC Computational Methods in Physical and Macromolecular Chemistry	52
Session SS-CNT Computational Number Theory	59
Session SS-CP Computational Physics	80
Session SS-DASO Data Analytics for System Optimization	87
Session SS-DDEMM Delay Differential Equations as Mathematical Models of Real World Phenomena	94
Session SS-DDMDS Data-Driven Methods for Dynamical Systems	108
Session SS-EBMSAHS Equation-Based Modeling: Structural Analysis and Hybrid Systems	119
Session SS-FCP Fractional Calculus and Probability	125
Session SS-GAMCCM Geometric and Analytic Methods in Classical and Celestial Mechanics	131

Session SS-GLS Geocomputational Landscapes and Spaces	145
Session SS-GTA Game Theory: Applications and Evolutionary Games	152
Session SS-MACHS Modeling, Analysis and Control in Hybrid Systems	169
Session SS-MFMC Mathematical Finance - Modeling, Computation and Risk Management	180
Session SS-MMNN Mathematical Models for Nanoscience and Nanotechnology	196
Session SS-MMPND Matrix Manifold Problems subject to Noisy Data	207
Session SS-MSMB Modeling & Simulation in Medicine and Biology	213
Session SS-RALSMCL Recent Advances in Lie Symmetry Methods and Conservation Laws for Differential Equations and Applications	226
Session SS-SSMMBP Simulations in Soft Matter and Molecular Bio-Physics .	240
Session SS-TMN Topics In Mathematical Neuroscience	250
Session SS-WDSEE Wealth Distribution and Statistical Equilibrium in Economics	260
Session SS-WPA Wave Propagation and Applications	267
CAIMS Scientific Themes	280
Session ST-AADS Applied Analysis and Dynamical Systems	282
Session ST-ACM Applied and Computational Mechanics	299
Session ST-IM Industrial Mathematics	321
Session ST-MB Mathematical Biology	337
Session ST-SCNA The 2nd Canadian Symposium on Scientific Computing and Numerical Analysis	380
Session ST-CFDSC The 23rd Conference of the CFD Society of Canada	421

Contributed Sessions	576
Session CS-AMPRE Applied Problems and Methods in Research & Education	578
Session CS-BSM Mathematics and Computation in Biological Sciences and Medicine	584
Session CS-CACO Computational Algebra, Combinatorics and Optimization .	600
Session CS-CPC Computational Physics and Chemistry	607
Session CS-DSDE Applications of Dynamical Systems and Differential Equations	614
Session CS-ENV Mathematical Modeling in Environmental Sciences and Models for Complex Media	628
Session CS-FINANCE Financial Mathematics and Computation	633
Session CS-MECH Computational Mechanics and Engineering	642
Session CS-MODELING Partial Differential and Integral Equations in Mathematical Modeling	651
Session CS-POST AMMCS-CAIMS2015 Poster Session	661
Index of Authors	689

Lists of Sessions

List of Congress Plenary Lectures

Title	Speaker
Graph Analysis and Discrete Dynamic Modeling Elucidates the Outcomes of Within-cell Networks	Réka Albert (Pennsylvania State University)
Dependence Between Components of Multivariate Conditional Markov Chains: Markov Consistency and Markov Copulae	Tomasz Bielecki (Illinois Institute of Technology)
Eight Great Reasons to Do Maths	Chris Budd (University of Bath)
Multiscale Modeling of Soft Materials and Related Biological Responses	Wing Kam Liu (Northwestern University)
Learning in High Dimension: from Images to Quantum Chemistry	Stéphane Mallat (École Normale Supérieure)
On Fourier Cosine Expansions and Wavelets for Derivative Pricing and Risk Management in Computational Finance	Kees Oosterlee (Delft University of Technology and CWI)
Species Coexistence in Stochastic Environments: A Mathematical Perspective	Sebastian Schreiber (University of California, Davis)
Multiscale Modeling in a Stochastic Setting	Eric Vanden-Eijnden (Courant Institute, New York University)
Noise Impact on Finite Dimensional Dynamical Systems	Yingfei Yi (University of Alberta)
An information theoretic approach to computational modelling in engineering and the sciences	Nicholas Zabaras (University of Warwick)

List of CFDSC Plenary Lectures

Title	Speaker
Recent Progresses in the Development of Parameter Free Continuous Finite Element Methods for Compressible Fluids	Rémi Abgrall (University of Zurich)
DNS/LES of Complex Turbulent Flows Beyond Petascale	Paul Fischer (University of Illinois)

List of Semi-Plenary Lectures

Title	Speaker
Conservation Laws of Fluid Flow on Riemannian Manifolds	Stephen Anco (Brock University)
Computing Elliptic Curves of Fixed Conductor	Mike Bennett (University of British Columbia)
Modelling the Collapse of Financial Systems	Tom Hurd (McMaster University)
On Long Time Dynamics in Nonlinear Wave Equations	Eduard-Wilhelm Kirr (University of Illinois at Urbana-Champaign)
Sustainability of Cooperation in Dynamic Games Played over Event Trees	Georges Zaccour (École des Hautes Études commerciales de Montréal)

AMMCS Special Sessions (SS-AAIP — SS-GTA)

SESSION	ORGANIZERS
SS-AAIP	Kim Herder (University of Guelph) Herb Kunze (University of Guelph)
Inverse Problems	Davide La Torre (Khalifa University, UAE, and Univiversity of Milan, Italy)
SS-CMPMC	
Computational Methods in Physical and Macromolecular Chemistry	Styliani Consta (Western University)
SS-CNT	Chester Weatherby (WLU, Waterloo)
Computational Number Theory	Kevin Hare (University of Waterloo) Renate Scheidler (University of Calgary)
SS-CP	Alex Fedoseyev (CFD Research Corporation, USA)
Computational Physics	Marek Wartak (WLU, Waterloo)
SS-DASO	Jianhong Wu (York University)
Data Analytics for System Optimization	Jimmy Huang (York University) Wenying Feng (Trent University)
SS-DDEMM	Elena Braverman (University of Calgary)
Delay Differential Equations as Mathematical Models of Real World Phenomena	Anatoli Ivanov (Penn State University)
SS-DDMDS	Dimitris Giannakis (New York University)
Data-Driven Methods for Dynamical Systems	Tyrus Berry (Penn State University)
SS-EBMSAHS	Ned Nedialkov (McMaster University)
Equation-Based Modeling: Structural Analysis and Hybrid Systems	John Pryce (Cardiff University)
SS-FCP	József Lörinczi (Loughborough University)
Fractional Calculus and Probability	Mark Meerschaert (Michigan State University) Enrico Scalas (University of Sussex)
SS-GAMCCM	Manuele Santoprete (WLU, Waterloo)
Geometric and Analytic Methods in Classical and Celestial Mechanics	Lennard Bakker (Brigham Young University) Ray McLenaghan (University of Waterloo)
SS-GLS	Steven A. Roberts (WLU, Waterloo)
Geocomputational Landscapes and Spaces	Colin Robertson (WLU, Waterloo)
SS-GTA	Monica Cojocaru (University of Guelph)
Game Theory: Applications and Evolutionary Games	Joe Apaloo (St. Francis Xavier) Ross Cressman (WLU, Waterloo)

AMMCS Special Sessions (SS-MACHS – SS-WPA)

SESSION	ORGANIZERS
SS-MACHS Modeling, Analysis and Control in Hybrid Systems	Xinzhi Liu (University of Waterloo) Mohamad Alwan (U of Waterloo) Peter Stechlinski (MIT)
SS-MFMCR Mathematical Finance — Modelling, Computation and Risk Management	Joe Campolieti (WLU, Waterloo) Adam Metzler (WLU, Waterloo)
SS-MMNN Mathematical Models for Nanoscience and Nanotechnology	Zoran Miskovic (University of Waterloo) Hamed Majedi (University of Waterloo)
SS-MMPND Matrix Manifold Problems subject to Noisy Data	Forbes Burkowski (University of Waterloo) Henry Wolkowicz (University of Waterloo)
SS-MSMB Modeling & Simulation in Medicine and Biology	Suzanne Shontz (University of Kansas) Corina Drapaca (Penn State University) Siv Sivaloganathan (University of Waterloo)
SS-RALSMCL Recent Advances in Lie Symmetry Methods and Conservation Laws for Differential Equations and Applications	M. Abudiab (Texas A&M University, USA) C.M. Khalique (North-West University, USA) M.L. Gandarias (Universidad de Cadiz, Spain)
SS-SSMMBP Simulations in Soft Matter and Molecular Bio-Physics	Cristiano Dias, Zhaoqian Su, and Farbod Mahmoudinoba (New Jersey Institute of Technology)
SS-TMN Topics in Mathematical Neuroscience	Lydia Bilinsky (Duke University) Priscilla Greenwood (Duke University)
SS-WDSEE Wealth Distribution and Statistical Equilibrium in Economics	Enrico Scalas (University of Sussex) Bertram Düring (University of Sussex)
SS-WPA Wave Propagation and Applications	Eduard Kirr (University of Illinois) Nicolae Tarfulea (Purdue University Calumet) Catalin Turc (New Jersey Institute of Technology)

CAIMS Scientific Themes

THEME	ORGANIZERS
ST-AADS Applied Analysis and Dynamical Systems	Xingfu Zou (Wester University) Dmitry Pelinovsky (McMaster University) David Iron (Dalhousie University)
ST-ACM Applied and Computational Mechanics	Marek Stastna (University of Waterloo) Bartek Protas (McMaster University) Il Yong Kim (Queens University)
ST-IM Industrial Mathematics	Huaxiong Huang (York University) John Stockie (SFU) Odile Marcotte (UQAM & CRM) Sean Bohun (UOIT)
ST-MB Mathematical Biology	Frithjof Lutscher (Ottawa) Lea Popovic (Concordia) Rebecca Tyson (U of British Columbia) Connell McCluskey (WLU, Waterloo)
ST-SCNA The 2nd Canadian Symposium on Scientific Computing and Numerical Analysis	Scott MacLachlan (MUN) Justin Wan (University of Waterloo) Hans de Sterck (University of Waterloo) Ben Adcock (SFU)
ST-CFDSC The 23rd Conference of the CFD Society of Canada	Lilia Krivodonova (University of Waterloo) Lucian Ivan (University of Waterloo)

List of Contributed Sessions

CODE	TITLE
CS-APMRE	Applied Problems and Methods in Research & Education
CS-BSM	Mathematics and Computation in Biological Sciences and Medicine
CS-CACO	Computational Algebra, Combinatorics and Optimization
CS-CPC	Computational Physics and Chemistry
CS-DSDE	Applications of Dynamical Systems and Differential Equations
CS-ENV	Mathematical Modelling in Environmental Sciences and Models for Complex Media
CS-FINANCE	Financial Mathematics and Computation
CS-MECH	Computational Mechanics and Engineering
CS-MODELING	Partial Differential and Integral Equations in Mathematical Modeling
CS-POST	AMMCS-CAIMS2015 Poster Session

Plenary Lectures

Graph Analysis and Discrete Dynamic Modeling Elucidates the Outcomes of Within-Cell Networks

Réka Albert (Pennsylvania State University)

Abstract: Interaction networks formed by gene products form the basis of cell behavior (growth, survival, apoptosis, movement). Experimental advances in the last decade helped uncover the structure of many molecular-to-cellular level networks, such as protein interaction or metabolic networks. These advances mark the first steps toward a major goal of contemporary biology: to map out, understand and model in quantifiable terms the various networks that control the behavior of the cell. Such an understanding would also allow the development of comprehensive and effective therapeutic strategies.

This talk will focus on my group's recent work on discrete dynamic modeling of signal transduction networks in various organisms. These models can be developed from qualitative information yet show a dynamic repertoire that can be directly related to the real system's outcomes. For example, our model of the signaling network inside T cells predicted therapeutic targets for the blood cancer T-LGL leukemia, several of which were validated experimentally. I will then present an enriched network representation that includes the regulatory logic. Extension of existing graph measures and analyses, performed on this expanded network, allows an efficient way to determine the dynamic repertoire of the network and to predict manipulations that can stabilize or, conversely, block, certain outcomes.

About the Speaker: Prof. Réka Albert received her Ph.D. in Physics from the University of Notre Dame (2001), working with Prof. Albert-Laszlo Barabasi. She did post-doctoral research in mathematical biology at the University of Minnesota with Prof. Hans Othmer. Prof. Albert then joined the Pennsylvania State University, where she currently is a Professor of Physics with adjunct appointments in the Department of Biology and the College of Information Science and Technology. Dr. Albert works on predictive modeling of biological regulatory networks at multiple levels of organization. Her pioneering publications on the structural heterogeneities of complex networks had a large impact on the field, reflected in their identification as “Fast breaking paper” and “High impact paper” by Thomson Reuters. Dr.

Albert is a fellow of the American Physical Society, where she served as a member-at-large in the Division of Biological Physics. She was a recipient of a Sloan Research Fellowship (2004), an NSF Career Award (2007), and the Maria Goeppert–Mayer award (2011). Her service to the profession includes serving on the editorial board of the journals Physical Review E, The New Journal of Physics, IET Systems Biology, Biophysical Journal, SIAM Journal of Applied Dynamical Systems and Bulletin of Mathematical Biology, on the scientific advisory board of the Mathematical Biosciences Institute at Ohio State, and as a peer reviewer for more than 35 journals.



Dependence Between Components of Multivariate Conditional Markov Chains: Markov Consistency and Markov Copulae

Tomasz Bielecki (Illinois Institute of Technology)

Abstract: Modeling of evolution of dependence between processes occurring in financial markets is important. Typically, one can identify marginal statistical properties of individual processes, and then one is confronted with the task of modeling dependence between these individual processes so that the marginal properties are obeyed. We have been advocating, for some time now, to address this modeling problem via the theory of Markov consistency and Markov copulae. In this talk we shall examine the problem of existence and construction of a non-trivial multivariate conditional Markov chain with components that are given conditional Markov chains. In this regard we shall give sufficient and necessary conditions, in terms of relevant conditional expectations, for a component of a multivariate Markov chain to be a Markov chain in the filtration of the entire chain – a property called strong Markov consistency, as well as in its own filtration a property called weak Markov consistency. These characterization results are proved via analysis of the semi-martingale structure of the chain. Several financial applications will be indicated.

About the Speaker: Tomasz R. Bielecki is a Professor of Applied Mathematics and the Director of the Master of Mathematical Finance program at Illinois Institute of Technology. He received his Ph.D. degree from the Warsaw School of Economics. Prof. Bielecki's fields of expertise include Stochastic Analysis, Mathematical Finance, and Credit Risk Modeling. He is an Associate Editor of six well-known journals in areas of Mathematics and Finance, including Mathematical Finance and International Journal of Theoretical and Applied Finance. Prof. Bielecki is a co-author of three books in the area of Credit Risk Modeling and Financial Mathematics including his most recent book "Counterparty Risk and Funding: A Tale of Two Puzzles" co-authored with Stphane Crpey and Damiano Brigo.



Eight Great Reasons to Do Maths

Chris Budd (University of Bath)

Abstract: The UK government has identified 8 great technologies which it believes will lead the advancement of science and technology into the future. Mathematics underpins all of these and developments of mathematics will be the engine for future growth in all of them. In this talk I will describe the 8 technologies and look at some of the maths behind them, from Big Data through to Energy.

About the Speaker: I have broad research interests in interdisciplinary industrial and applied mathematics with a particular interest in complex nonlinear problems arising in real applications. Typically these involve the solution (analytically or numerically) of partial differential equations. A large amount of my work for the last ten years has been in numerical weather prediction and data assimilation in close collaboration with the Met Office (which I visit very frequently). My algorithms are now incorporated into the Met Office operational weather forecasting code where they have made a significant difference to their accuracy and received a Knowledge Transfer Award. I am also working on climate modelling using modern mathematical and computational methods and am actively involved in a number of international climate modelling networks, including CliMathNet which I co-direct and the Maths of Planet Earth programme. I also collaborate with the energy industry, the aerospace industry, the telecommunications industry and the food industry. Anywhere that maths can be applied is of interest to me.



Multiscale Modeling of Soft Materials and Related Biological Responses

Wing Kam Liu (Northwestern University)

Abstract: Liquids, polymers, gels, foams and a number of biological materials are soft materials, which can be easily deformed by thermal stress or thermal fluctuations. Predominate physical behaviors of these soft materials occur at energy scale comparable with room temperature thermal energy. These behaviors cannot be, or are not easily, to be directly predicted from its atomic or molecular constituents. This is because the soft materials are always self-assemble into mesoscopic structures, which are much larger than the microscopic scale, and yet much smaller than the macroscopic scale of these materials. Especially, the mechanical and physical properties of soft materials originate from the interplay of phenomena at different spatial and temporal scales. As such, it is necessary to adopt multiscale methods when dealing with soft materials in order to account for all important mechanisms. The offerings of this lecture are twofold: (1) establishing a multiscale modeling framework to predict viscoelastic behaviors of polymers through fractional derivatives, (2) rapid computational prototyping and testing of drug carriers in tumor microvasculature through immersed molecular finite element method (IMFEM). In (1), we have incorporated the fractional diffusion of free chains into the integration kernel for the viscoelastic response of polymers and polymer nanocomposites using the Mittag-Leffler function. While conventional models for viscoelastic materials employ a discrete relaxation spectrum, the fractional-order model exhibits a continuous relaxation distribution, which is in accordance with experimental observations. In (2), the IMFEM is used to simulate the whole blood including blood plasma, red blood cells and nanoparticles. We elucidate how the size, shape and stiffness of nanoparticles will affect their dispersions in the microvasculature, with the accurate molecular interactions informed by molecular mean-field theory.

About the Speaker: Dr. Wing Kam Liu, Walter P. Murphy Professor of Northwestern University, has made fundamental, innovative contributions to the theory, methodologies, and applications of multiscale simulations towards the understanding and design of nano-materials, polymers science, and multiresolution mechanics. His ISI and Google citations and H factors are (14,200, 60) and (37,750, 88), respectively. In 2014, Liu is selected as a highly cited researcher in Computer Science and a member of the Worlds Most Influential Scientific Minds by Thompson Reuters. Liu developed new exceptional accuracy meshfree methods for simulation of extremely deformation of solids and fluids including additive manufacturing; fractional-order viscoelasticity polymer science; fluid-structure interaction, and applicable to medical imaging. He was the PI of a multi-year multi-million research grant from Goodyear Tire and Rubber Company to develop and integrated design strategy to enable prediction, synthesis and characterization of new polymer nanocomposites to achieve enhanced performance. Liu is current the President of IACM and Chair of USNCTAM; Founding Director of the Summer Institute on Nano Mechanics and Materials; Founding Chair of the ASME NanoEngineering Council; Editors of Computational Mechanics and Int. J. of Applied Mathematics and Mechanics; Honorary Editor of Int. J. of Computational Methods; serve on numerous editorial boards; Consultant to 20+ organizations. Liu has written three books; and he is a Fellow of ASME, ASCE, USACM, AAM, and IACM. Lius selected awards and honors including: 2014 Japan Society for Computational Engineering and Science Grand Prize in recognition of his outstanding contributions in the field of computational mechanics; the Honorary Professorship from Dalian University of Technology in 2013; the 2012 IACM Gauss-Newton Medal; the 2012 ASME Design Automation Conference Best Paper Award; the 2009 ASME Dedicated Service Award, the 2007 ASME Robert Henry Thurston Lecture Award, the 2007 USACM John von Neumann Medal, the 2004 JSME Computational Mechanics Award, the 2002 IACM Computational Mechanics Award, the 2001 USACM Computational Structural Mechanics Award, the 1995 ASME Gustus L. Larson Memorial Award, the 1985 ASME Pi Tau Sigma Gold Medal, the 1979 ASME Melville Medal, the 1989 Thomas J. Jaeger Prize of the ISMIRT, and the 1983 Ralph R. Teetor Educational Award, American Society of Automotive Engineers.



Learning in High Dimension: from Images to Quantum Chemistry

Stéphane Mallat (École Normale Supérieure)

Abstract: Learning from data means approximating functionals in high dimensional spaces. Finding strong sources of regularity is necessary to avoid the curse of dimensionality. Invariance to action of small groups such as rigid displacements is too weak, but stability to action of diffeomorphisms is a much stronger property, satisfied by many physical functionals and most signal and image classification problems. We show that it is sufficient to approximate complex high-dimensional classification and regression functionals.

We introduce scattering operators, which are invariants to low-dimensional Lie groups, and Lipschitz continuous to actions of diffeomorphisms. They are computed with iterated multiscale wavelet transforms. These scattering operators provide a Euclidean embedding of geometric distances and a representation of stationary random processes, which captures intermittency phenomena. Applications will be shown for several image classification problems, and for learning quantum chemistry energy functionals.

About the Speaker: Stéphane Mallat received the Ph.D. degree in electrical engineering from the University of Pennsylvania, in 1988. He was then Professor at the Courant Institute of Mathematical Sciences. In 1995, he became Professor in Applied Mathematics at École Polytechnique, Paris. From 2001 to 2007 he was co-founder and CEO of a semiconductor start-up company. In 2012 he joined the Computer Science Department of École Normale Supérieure, in Paris.

Stéphane Mallat's research interests include signal processing, computer vision, harmonic analysis and learning. He wrote a "Wavelet tour of signal processing: the sparse way". In 1997, he received the Outstanding Achievement Award from the SPIE Society and was a plenary lecturer at the International Congress of Mathematicians in 1998. He also received the 2004 European IST Grand prize, the 2004 INIST-CNRS prize for most cited French researcher in engineering and computer science, and the CNRS innovation medal in 2014. He was elected at the French Academy of Sciences in 2014.



On Fourier Cosine Expansions and Wavelets for Derivative Pricing and Risk Management in Computational Finance

Kees Oosterlee (Delft University of Technology and CWI)

Abstract: In this talk, we discuss applications of Fourier cosine expansions and wavelets in computational finance. Next to the accurate and efficient valuation of various financial options, we recently generalized the methods towards risk management and the numerical solution of backward stochastic differential equations (BSDEs). Typically Fourier techniques in finance rely on the availability of the asset dynamics' characteristic function (ie. the Fourier transform of the asset's density function). We will discuss a numerical Fourier method for which the characteristic function need not be available. The resulting methods can then also be employed for problems with varying coefficients (local volatility, stochastic local volatility) models), such as for the Stochastic Alpha Beta Rho (SABR) method.

About the Speaker: Prof. Kees Oosterlee (<http://www.cwi.nl/people/2098>, <http://ta.twi.tudelft.nl/mf/users/oosterle/>) works in numerical analysis and scientific computing at the CWI, center for mathematics and computer science, in Amsterdam, the Netherlands, as well as in the Delft University of Technology. His field of expertise is Computational Finance, working at the interface of numerical and financial mathematics. In Oosterlee's group the COS method, pricing financial derivatives efficiently with Fourier cosine expansions, has been developed, which is in use at financial institutions world-wide. Prof. Oosterlee is the Editor-in-Chief of the Journal of Computational Finance. He has organized several international workshops and conferences, and taught Summer Schools abroad (in Spain, Japan, South Africa) on Computational Finance. His 90 journal publications range from multigrid solution methods for fluid flow problems to Monte Carlo methods in finance.



Species Coexistence in Stochastic Environments: A Mathematical Perspective

Sebastian Schreiber (University of California, Davis)

Abstract: Stochastic fluctuations in temperature, precipitation and a host of other environmental factors occur at multiple spatial and temporal scales. As the survival and reproduction of organisms, whether they be plants, animals, or viruses, depend on these environmental factors, these stochastic fluctuations often drive fluctuations in population abundances. This simple observation leads to a fundamental question in population biology. Namely, under what conditions do stochastic environmental fluctuations hinder or facilitate the maintenance of biodiversity? This question is particularly pressing in light of global climate models predicting increasing temporal variation in many climatic variables over the next century.

One fruitful approach to tackling this question from population biology is the development and analysis of models accounting for nonlinear feedbacks among species, population structure, and environmental stochasticity. In this talk, I will discuss progress in the development of a mathematical theory for stochastic coexistence where the dynamics of the interacting species are encoded by random difference equations and coexistence corresponds to the limit points of empirical measures being bounded away from an extinction set. I will illustrate the theory with empirical based examples involving checkerspot butterflies, Kansas prairies, and coastal dunes.

About the Speaker: Sebastian J. Schreiber is a Professor of Ecology and Evolution and member of the Center of Population Biology at the University of California, Davis. Prior to coming to Davis, he was an Associate Professor of Mathematics at the College of William and Mary and Western Washington University. Professor Schreibers research on the development and application of methods in stochastic processes and nonlinear dynamics to ecology, evolution, and epidemiology has been supported by grants from the U.S. National Science Foundation, the U.S. National Oceanic and Atmospheric Administration, the Bureau for Land Management, and the U.S. Fisheries and Wildlife Service. He has authored nearly eighty scientific papers in peer-reviewed mathematics and biology journals. Professor Schreiber is currently on the editorial boards of five research journals including Ecology and the Journal of Mathematical Biology.



Multiscale Modeling in a Stochastic Setting

Eric Vanden-Eijnden (Courant Institute, New York University)

Abstract: Applications from molecular dynamics, material science, biology, or atmosphere/ocean sciences present new challenges for applied and numerical mathematics. These applications typically involve systems whose dynamics span a very wide range of spatio-temporal scales, and are subject to random perturbations of thermal or other origin. This second aspect especially complicates the modeling and computation of these systems and requires one to revisit standard tools from numerical analysis from a probabilistic perspective. In this talk I will discuss recent advances that have been made in this context. For example, I will show how tools from Freidlin-Wentzell theory of large deviations and potential theoretic approaches to metastability can be used to develop numerical algorithms to accelerate the computations of reactive events arising in metastable systems. I will also explain how averaging theorems for singularly perturbed Markov processes can help develop schemes bridging micro- to macro-scales of description or compute free energies, etc. As illustrations, I will use a selection of examples from molecular dynamics, material sciences, and fluid dynamics and show how the confrontation with actual problems not only profits from the theory but also enriches it.

About the Speaker: My main focus is the development of mathematical tools and numerical methods for the analysis of dynamical systems which are both stochastic and multiscale. The particular areas of applications I am interested in include molecular dynamics, chemical and biological networks, materials science, atmosphere-ocean science, and fluids dynamics. My main objectives are to understand the pathways and rate of occurrence of rare events in complex systems; to develop and analyze multiscale algorithms for the simulation of random dynamical systems; and, more generally, to quantify the effects of random perturbations on the systems dynamics.



Noise Impact on Finite Dimensional Dynamical Systems

Yingfei Yi (University of Alberta)

Abstract: Dynamical systems are often subjected to noise perturbations either from external sources or from their own intrinsic uncertainties. While it is well believed that noises can have dramatic effects on the stability of a deterministic system at both local and global levels, mechanisms behind noise surviving or robust dynamics have not been well understood especially from distribution perspectives. This talk attempts to outline a mathematical theory for making a fundamental understanding of these mechanisms in white noise perturbed systems of ordinary differential equations, based on the study of stationary measures of the corresponding Fokker-Planck equations. New existence and non-existence results of stationary measures will be presented by relaxing the notion of Lyapunov functions. Limiting behaviors of stationary measures as noises vanish will be discussed in connection to important issues such as stochastic stability and bifurcations.

About the Speaker: Yingfei Yi obtained his B.Sc. degree in classical mechanics from Jilin University in 1984 and his Ph.D. degree in applied mathematics from the University of Southern California in 1990. His professional career started at Georgia Institute of Technology, first as a Postdoctoral Fellow at the Center for Dynamical Systems and Nonlinear Studies from 1990-1992, then at the School of Mathematics as an Assistant Professor from 1992-1997, an Associate Professor from 1997-2000, and a Professor from 2000. He joined the Department of Mathematical and Statistical Sciences, the University of Alberta in 2014 as a Killam Memorial Chair in Dynamical Systems. He received a Rosenbaum Fellowship from the University of Cambridge in 1995, a University Research Fellowship from Jilin University in 1998, an Outstanding Young Scientist Award from NSFC in 2004, a Changjiang Scholarship from MoE, China and Li Ka Shing Foundation in 2008, and a Chinese National Qianren Research Chair Professorship in 2009 from MoE, China. He is a Co-editor in Chief for the Journal of Dynamics and Differential Equations, a handling editor for the Journal of Differential Equations, an editor for the Proceedings of the American Mathematical Society, an editor for the SIAM DSweb Magazine, and he is also an associate editor or a member of editorial board of three other professional journals. His research interests lie in dynamical systems and qualitative theory of differential equations.



An Information Theoretic Approach to Computational Modelling in Engineering and the Sciences

Nicholas Zabaras (University of Warwick)

Abstract: Predictive modelling and design of materials gives rise to unique mathematical and computational challenges including (i) Modelling of hierarchical random heterogeneous material structures; (ii) Propagating uncertainties in a quantifiable manner across spatial and temporal length scales (stochastic coarse graining); (iii) Addressing the curse of stochastic dimensionality; (iv) Addressing the phenomenology typical of most materials science models; (v) Modelling failure and rare events in random media; and many more. We will advocate an information theoretic approach to address some of these challenges. In particular, we will discuss data-driven models of material structure, forward uncertainty propagation in high dimensions using limited data, variational approaches to stochastic coarse graining, and quantifying epistemic uncertainty when using surrogate models. We will finally address the importance of using probabilistic graphical models for predictive modelling of multiscale and multiphysics problems. With synergistic developments in materials physics, computational mathematics/statistics, and machine learning there is potential for developing data-driven materials models that allow us to understand where observable variabilities in properties arise and provide means to control them for accelerated materials design.

About the Speaker: Nicholas Zabaras received his Ph.D. at Cornell University (1987) in the area of Theoretical and Applied Mechanics. Upon graduation he joined the faculty of Engineering at the University of Minnesota. In 1991 he returned to Cornell as a faculty member of the Sibley School of Mechanical and Aerospace Engineering where he was also member of various other academic fields including Applied Mathematics, Materials Science and Engineering and Computational Science and Engineering. He was the founding director of the Materials Process and Design Laboratory that integrated materials modelling and design with innovative mathematical approaches including inverse problems, uncertainty quantification, robust design, and scientific computing. In the summer of 2014 he joined the University of Warwick to establish and lead the Warwick Centre for Predictive Modelling. WCPM is a university wide initiative across many colleges and departments with emphasis on the integration of computational mathematics, computational statistics and scientific computing to address modelling and design of complex systems in the presence of uncertainties. He has received several awards including a Presidential Young Investigator Award in 1991. He is Fellow and member of various societies. In 2014, Prof. Zabaras was appointed as Hans Fisher Senior Fellow at the Institute of Advanced Study at the Technische Universität München. The same year he received the Royal Society's Wolfson Research Merit Award for his work on predictive modelling. He is currently an Associate Editor of the Journal of Computational Physics and the Editor in Chief of the International Journal for Uncertainty Quantification.



Recent progress in the development of parameter free continuous finite element methods for compressible fluids

Rémi Abgrall (University of Zurich)

Abstract: In this talk, I will review the current status of the so-called Residual Distribution schemes applied, in particular, to compressible fluid dynamics problems. Other physical models include the Shallow Water equation and generalization, MHD, etc.

After the early work of R. Ni at Bombardier, and the seminal work of P.L. Roe, in particular his 1981 JCP paper and its extensions to scalar multidimensional schemes, these schemes can be considered as finite element methods of the streamline diffusion type. The emphasis is put on non-oscillatory properties, in order to be able to compute flow discontinuities, so that they are nonlinear by construction. Indeed shock capturing is done in a totally different manner as for streamline diffusion, allowing for a class of parameter free schemes. In a way, the Residual Distribution methods can be seen as a kind of compromise between high order TVD-like finite difference/finite volume schemes and classical finite element methods, in that they borrow ideas from both communities: geometrical flexibility, the residual concept on one side, and non oscillatory, maximum principle on the other one.

In the talk, we will first consider the case of steady scalar hyperbolic problems, showing how one can systematically construct parameter free essentially non-oscillatory schemes. Then we will move towards steady advection diffusion problems, showing how uniform accuracy, whatever the Peclet/Reynolds number is. The last part of the talk we will consider recent work on unsteady problems. Examples of compressible flows (laminar and turbulent) will be also shown, in order to demonstrate the efficiency of the method, both in accuracy, memory footprint and CPU time.

This is joint work with many colleagues and students among whom Dante de Santis, Mario Ricchiuto, Algiane Froehly, Adam Larat, Mohamed Mezine at INRIA, and many discussions with H. Deconinck (VKI, Belgium) as well as Phil Roe (Michigan, USA). This work has been funded by several EU contracts: the FP6 ADIGMA project (contract AST5-CT-2006-030719), the FP7 IDIHOM project (contract AAT-2010-RTD-1-265780) and the ERC Advanced Grant ADDECCO (contract #226316), as well as a grant of the Swiss National Fund.

About the Speaker: Rémi Abgrall is a former student of École Normale Supérieure de Saint Cloud. After his Ph.D., he has been engineer at ONERA, then research scientist at INRIA. Since January 2014, he is professor at the University of Zürich, Institute of Mathematics, after having been Professor in the University of Bordeaux (Institut Polytechnique de Bordeaux) since 1996 and in secondment at INRIA from 2008 till the end of 2013. He has been awarded an Advanced Research Grant from the ERC in December 2008 and has been invited speaker at the International Conference of Mathematicians (ICM 2014) in Seoul. He is associate editor of several international journals, including the Journal of Computational Physics, Mathematics of Computation, Computers and Fluids, the Journal of Scientific Computing. He is also co-chief editor of the International Journal on Numerical Methods in Fluids. His research is about efficient algorithms for the simulation of compressible materials (single fluids, multiphase, interface problems, compressible solids) using high order schemes designed for unstructured meshes. He also has interest in (curved) meshes generation for high order scheme and model reduction for transport dominated problems with and without discontinuities. in the solution.



DNS/LES of Complex Turbulent Flows beyond Petascale

Paul Fischer (University of Illinois)

Abstract: Petascale computing platforms currently feature million-way parallelism and it is anticipated that exascale computers with billion-way concurrency will be deployed in the early 2020s. In this talk, we explore the potential of computing at these scales with a focus on turbulent fluid flow and heat transfer in a variety of applications including nuclear energy, combustion, oceanography, vascular flows, and astrophysics. Following Kreiss and Oliger'72, we argue that high-order methods are essential for scalable simulation of transport phenomena. We demonstrate that these methods can be realized at costs equivalent to those of low-order methods having the same number of gridpoints. We further show that, with care, efficient multilevel solvers having bounded iteration counts will scale to billion-way concurrency. Using data from leading-edge platforms over the past 25 years, we analyze the scalability of state-of-the-art solvers to predict parallel performance on exascale architectures. The analysis sheds light on the expected scope of exascale physics simulations and provides insight to design requirements for future algorithms, codes, and architectures.

About the Speaker: Paul Fischer is a Blue Waters Professor at the University of Illinois, Urbana-Champaign in the departments of Computer Science and Mechanical Science & Engineering. He received his Ph.D. in mechanical engineering from MIT and was a post-doc in applied mathematics at Caltech, where he was the first Center for Research in Parallel Computation fellow. His work is in the area of high-order numerical methods for partial differential equations, scalable linear solvers, and high-performance computing. He is the architect of the open source SEM-based fluid dynamics/heat transfer code Nek5000, which has been recognized with the Gordon Bell Prize in high-performance computing and which has successfully scaled beyond a million processes. Nek5000 is currently used by over 200 researchers for a variety of applications in turbulence and heat transfer.



Semi-Plenary Lectures

Conservation Laws of Fluid Flow on Riemannian Manifolds

Stephen Anco (Brock University)

Abstract: All local conservation laws of kinematic type on moving domains and moving surfaces for inviscid compressible fluid flow on curved Riemannian manifolds are derived. In particular, any such conservation laws will be found that hold only for (1) special dimensions of the manifold or the surface; (2) special conditions on the geometry of the manifold or the surface; (3) special equations of state. Importantly, the general form of these kinematic conservation laws will be allowed to depend on the intrinsic Riemannian metric, volume form, and curvature tensor of the manifold or the surface. All kinematic constants of motion that arise from the resulting kinematic conservation laws also will be determined. These results generalize earlier work on finding all kinematic local conservation laws on moving domains for inviscid compressible fluid flow in n-dimensional Euclidean space.

About the Speaker: Stephen Anco is a full professor in the Department of Mathematics and Statistics at Brock University, Canada. He is a co-author of two books in the Springer Applied Mathematics Series and has published over 60 papers. His research encompasses several areas of mathematical physics, including classical gauge field theory, General Relativity, symmetries and conservation laws of differential equations, integrable systems, and geometric curve flows. At Brock, he has served as Department Chair from 2009 to 2012 and Graduate Program Director from 2005 to 2007.



Computing elliptic curves of fixed conductor

Mike Bennett (University of British Columbia)

Abstract: I will discuss new, old and older still methods for computing elliptic curves with bad reduction outside given sets of primes. Applying these, we are now able to find models for all elliptic curves over the rationals with prime conductor bounded by 10^{10} and, conjecturally, by 10^{12} . I will then mention extensions of these results to the case of more general conductors and to curves over number fields. This is a joint work with Andrew Rechnitzer.

About the Speaker: Michael Bennett is Professor and Head of the Mathematics Department at the University of British Columbia. Prior to coming to UBC, he held positions at The University of Illinois, The Institute for Advanced Study in Princeton, The University of Michigan and the University of Waterloo. He has authored more than 60 papers in Number Theory. In 2004, he was a recipient of the Ribenboim prize of the Canadian Number Theory Association.



Modelling the Collapse of Financial Systems

Tom Hurd (McMaster University)

Abstract: The list of possible channels of systemic risk (SR) includes correlated asset shocks, default contagion, funding liquidity contagion and market illiquidity effects. A number of deliberately simplified modelling frameworks, beginning with the Eisenberg–Noe 2001 model, aim to reveal the pure contagion effects that can lead to cascading chains of defaulted and illiquid financial institutions. It turns out that analytic methods can be brought to bear to determine the characteristics of such cascades on large random financial networks (RFN) that have a property we call local tree-like independence (LTI). In this talk, we review the conceptual basis of these methods in percolation theory on random graphs, and investigate how to extend them to interesting models of complex financial networks.

About the Speaker: Tom Hurd is Professor of Mathematics at McMaster University. He turned to the mathematical study of financial markets in the late 1990s, following his earlier research in mathematical physics. Since then he has written on a wide range of financial topics, with publications in portfolio theory, interest rate modelling, and credit risk. Over the past few years, his work has focussed on the mathematical modelling of systemic risk, that is, the stability of financial networks. His new book entitled “Contagion! The Spread of Systemic Risk in Financial Networks” is soon to be published. He has delivered a number of minicourses on this subject and, most recently, a one-semester PhD course at ETH Zurich. In addition to cofounding the M-Phimac Master program in Financial Mathematics at McMaster, which he continues to direct, he has supervised numerous undergraduate, M.Sc., Ph.D. and Postdoctoral researchers working in financial mathematics.



On Long Time Dynamics in Nonlinear Wave Equations

Eduard-Wilhelm Kirr (University of Illinois at Urbana-Champaign)

Abstract: Since the first description in 1834 of the “wave of translation”, currently called soliton, by John Scott Russell, scientist have studied intensely such particular solutions of nonlinear wave equations i.e., coherent structures that do not change shape as they propagate. They have been put to good use in nonlinear optics and telecommunications, and play an important role in understanding the formation of large waves in oceans and in analyzing large systems of quantum particles. Moreover their importance in describing the large time behavior of nonlinear wave models is summarized by the following: Asymptotic Completeness Conjecture: any initial data of a nonlinear wave equations evolves into a superposition of coherent structures plus a part that radiates to infinity. My presentation will summarize both our current knowledge on existence of coherent structures and recent progress towards solving the asymptotic completeness conjecture.

About the Speaker: Eduard-Wilhem Kirr is currently an associate professor in the Mathematics Department at University of Illinois Urbana-Champaign. He obtained his Ph.D. in Mathematics from University of Michigan in 2002 under the direction of Michael I. Weinstein and Anthony Bloch and was a Dickson Instructor at University of Chicago from 2002 to 2005 under the direction of Peter Constantin. During his graduate studies he was also a summer intern at Bell Laboratories. His main research interests focus on studying wave propagation and wave interaction using both theoretical methods and numerical simulations.



Sustainability of Cooperation in Dynamic Games Played over Event Trees

Georges Zaccour
(École des Hautes Études commerciales de Montréal)

Abstract: A well-known problem in dynamic cooperative games is the sustainability of cooperation over time. The literature addressed this issue following different approaches, namely, the design of time-consistent payments, incentive equilibrium strategies and trigger strategies that deter credibly and effectively deviation from cooperation. In this talk, I will apply these different approaches to dynamic games played over event trees, that is, stochastic games where the uncertainty is not influenced by players' actions but it is nature's decision. After introducing the main elements of this class of games, I will introduce node-consistent cooperative payments based on the Shapley value and imputations in the core as means for sustaining cooperation over nodes (and time). Further, I will show how incentive and trigger strategies can be constructed to strategically support the cooperative agreement designed at the starting date of the game.

About the Speaker: Georges Zaccour holds the Chair in Game Theory and Management and is a full professor of Department of Management Sciences at HEC Montréal. He holds a Ph.D. in management science, an M.Sc. in international business from HEC Montréal and a licence in mathematics and economics from Université Paris-Dauphine. He served as the director of GERAD, an interuniversity research center and the director of marketing department and Ph.D. program at HEC Montréal. His research areas are differential games, optimal control and operations research applied to marketing, energy sector and environmental management, areas in which he has published more than 140 papers and co-edited thirteen volumes. He coauthors the books Differential Games in Marketing and Games and Dynamic Games. His research is regularly funded by the Natural Sciences and Engineering Research Council of Canada. He is the editor-in-chief of Dynamic Games and Applications and associate editor of the International Game Theory Review, Environmental Modeling and Assessment, Computational Management Science, INFOR, and other journals. He is a fellow of The Royal Society of Canada and was the president of the International Society of Dynamic Games (2002-2006).



Special Sessions

SS-AAIP Inverse Problem

A smoothing technique for image processing with sparsity

D. La Torre¹, D. Otero² and E.R. Vrscay²

¹ Khalifa University, Abu Dhabi, UAE and University of Milan, Italy, davide.latorre@kustar.ac.ae

² University of Waterloo, Waterloo, Ontario, Canada, {dotero,ervrscay}@uwaterloo.ca

Many problems in image analysis may be cast as the following optimization problem: Given a $y \in \mathbf{R}^m$ and a compact subset $D \subset \mathbf{R}^n$, determine the solution to the following problem,

$$\min_{x \in D} \frac{1}{2} \|Ax - y\|_2^2 + \gamma \|x\|_1. \quad (1)$$

Here, A is an appropriate $m \times n$ transformation matrix (e.g., wavelet, DCT, Fourier, etc.). The first term in (1) is commonly known as the “data fitting term”. The non-smooth L^1 regularization term is typically applied in an effort to enforce *sparsity*, i.e., to make the number of nonzero components of x as small as possible.

In this paper, we consider a modification of the above optimization problem in which the L^1 -norm regularization function $\|x\|_1$ is approximated by a family of smooth functions $\phi_c \in C_0^\infty(\mathbf{R}^n)$ that satisfy the following properties,

1. $\phi_c(x) \geq 0$, for all $x \in \mathbf{R}^n$,
2. $\text{supp}(\phi_c) \subseteq \{x \in \mathbf{R}^n : \|x\|_2 \leq c\}$,
3. $\int_{\mathbf{R}^n} \phi_c(x) dx = 1$.

Such functions are called *mollifiers* [1]. We consider the following smooth version of the problem in (1),

$$\min_{x \in D} \frac{1}{2} \|Ax - y\|_2^2 + \gamma \|x\|_1^c, \quad (2)$$

where

$$\|x\|_1^c = \int_{\mathbf{R}^n} \|x - z\| \phi_c(z) dz = \int_{\mathbf{R}^n} \|z\|_1 \phi_c(x - z) dz. \quad (3)$$

Because the functions $\|\cdot\|_1^c$ are epi-converging to $\|\cdot\|_1$, the sequence of minimizers x_c^* of (2) converges to a minimizer x^* of (1).

We also introduce a new set of algorithms that solve the following optimization problem via mollifiers,

$$\min_{x \in D} T(Ax, y) + \gamma \|x\|_1. \quad (4)$$

Here, $T(x, y) = 1 - S(x, y)$, where $S(x, y)$ denotes the Structural Similarity (SSIM) measure between x and y , $x, y \in \mathbf{R}^n$ [2]. This technique allows us to employ classical approaches such as gradient descent and generalized Newton’s method to solve the non-smooth problem in (4). Some numerical results will be presented.

References

- [1] Y.M Ermoliev, V.I. Norkin and R.J.B. Wets, *The minimization of semicontinuous functions: Mollifier subgradients*, SIAM J. Control Opt. **33**, pp. 1490167 (1995).
- [2] Z. Wang, A.C. Bovik, H.R. Sheikh and E.P. Simoncelli, *Image quality assessment: From error visibility to structural similarity*, IEEE Transactions on Image Processing **13**, 4, pp. 600-612 (2004).

A V-variable approach to fractal image compression

F. Mendivil¹, Ö. Stenflo²

¹ Acadia University, Wolfville, Canada, franklin.mendivil@acadiau.ca

² Uppsala University, Uppsala, Sweden, stenflo@math.uu.se

Most methods of using fractal-based methods in image compression rely on variations of A. Jacquin's fractal "block coding" algorithm [1]. In his approach, the image is first partitioned twice, once into "large" blocks and again into "small" blocks; the small blocks are typically one-half the size of the large blocks. Given these two block partitions, the algorithm works by scanning through all the small blocks and, for each one, searching the large blocks to find the "best" match. In matching, we allow ourselves to scale, α , and shift, β , (the reduced version of) the intensity values of the pixels in the large block. The compressed code consists of the collection of triples (*which large block, α , β*). The theory underlying fractal block coding is that of IFS fractals (more particularly, "local" IFS fractals).

In this talk, I will discuss a completely new fractal-based algorithm for image compression, one which is inspired by the theory of V-variable fractals [2, 3, 4]. V-variable fractals are intuitively fractals with at most V different "forms" at each level of magnification. In the context of a block partition, this means that for a given size of block, there are at most V different blocks of that size.

Our algorithm also works with a block decomposition of the image and progresses down the size scale. However, we define no contractive mappings from larger scale to smaller scale, but instead we sort and cluster blocks of a given size to find V "representatives." The inspiration from V-variable fractals is in the way the structure of the image is encoded into the V-variable tree representation. At each size "level" there are only V types and so we need only store how each type at level n is composed of the types at level $n + 1$.

This talk is based on our joint paper [5].

References

- [1] A. Jacquin. Image coding based on a fractal theory of iterated contractive image transformations *IEEE Trans. Image Process.*, 1:18–30, 1992.
- [2] M. F. Barnsley, J. E. Hutchinson and Ö. Stenflo. A fractal valued random iteration algorithm and fractal hierarchy *Fractals*, 13:111–146, 2005.
- [3] M. F. Barnsley, J. E. Hutchinson and Ö. Stenflo. V-variable fractals: Fractals with partial self similarity. *Adv. Math.*, 218:2051–2088, 2008.
- [4] M. F. Barnsley, J. E. Hutchinson and Ö. Stenflo. V-variable fractals: dimension results. *Forum Math.*, 24:445–470, 2012.
- [5] F. Mendivil, Ö. Stenflo, V-variable image compression, to appear in *Fractals*.

Circle Inversion Map and Star-shaped Set Inversion Map Fractals

B. Boreland¹, H. Kunze²

¹ University of Guelph, Guelph, Canada, bborelan@mail.uoguelph.ca

² University of Guelph, Guelph, Canada, hkunze@uoguelph.ca

Given a circle C with centre o and radius r , inversion with respect to C transforms the point p to the point p' such that p and p' lie on the same radial half-line from o and $d(o, p)d(o, p') = r^2$, where d is Euclidean distance. Circle inversion was introduced in Apollonius of Perga's book, *Plane Loci*, and has drawn interest in geometry. In *The Fractal Geometry of Nature*, Mandelbrot briefly discusses successive inversion with respect to a family of M circles. In subsequent literature, approximations of fractal sets are drawn using a version of the chaos game [1, 2]. Most recently, the idea was extended to star-shaped set inversion [3]: The key observation is that the circle inversion framework essentially relies on the fact that any radial half-line from the inversion centre o hits the circle at exactly one point. A star-shaped set in the plane is a closed and bounded set containing at least one interior point o that has the preceding property. All of these recent papers focus on graphics, presenting many pretty pictures of fractals; some other recent papers present three-dimensional pictures that extend the idea to spheres.

In this talk, we present some mathematical underpinnings of these ideas that appear to be absent from the literature. We establish that the fractals in the circle inversion case are set attractors of an iterated system of contractive maps on the union of all of the circles, and we discuss the star-shaped set case. Some inverse problems are suggested.

References

- [1] C. Clancy and M. Frame, Fractal Geometry of Restricted Sets of Circle Inversions, *Fractals* 3(4), 1995.
- [2] M. Frame and T. Cogevina, An Infinite Circle Inversion Limit Set Fractal, *Comput. Graph.* 24(5), 2000.
- [3] K. Gdawiec, Star-shaped Set Inverstion Fractals, *Fractals*, 22(4), 2014.

Collage-based Approach to Inverse Problems for Elliptic PDEs on Perforated Domains

H. Kunze¹, D. La Torre²

¹ University of Guelph, Guelph, Canada, hkunze@uoguelph.ca

² University of Milan, Milan, Italy, and Khalifa University, Abu Dhabi, UAE, davide.latorre@unimi.it and davide.latorre@kustar.ac.ae

A perforated domain or porous medium is a material characterized by a partitioning of the total volume into a solid portion often called the “matrix” and a pore space usually referred to as “holes” that can be either materials different from that of the matrix or real physical holes. When formulating differential equations over porous media, the term “porous” implies that the state equation is written in the matrix only, while boundary conditions should be imposed on the whole boundary of the matrix, including the boundary of the holes. Porous media can be found in many areas of applied sciences and engineering, as well as other research disciplines.

Since porosity in materials can take different forms and appear in varying degrees, solving differential equations over porous media is often a complicated task and the holes’ size and their distribution play an important role in its characterization. Furthermore numerical simulations over perforated domains need a very fine discretization mesh which often requires a significant computational time. The mathematical theory of differential equations on perforated domains is usually based on the theory of “homogenization” in which heterogeneous material is replaced by a fictitious homogeneous one [3]. Of course this implies the need of convergence results linking together the model on a perforated domain and on the associated homogeneous one. In the case of porous media, or heterogeneous media in general, characterizing the properties of the material is a tricky process and can be done on different levels, mainly the microscopic and macroscopic scales, where the microscopic scale describes the heterogeneities and the macroscopic scale describes the global behavior of the composite.

In this talk, we focus on the analysis of inverse problems for elliptic partial differential equations (PDEs) on perforated domains. In the typical problem, we are given a target function, which may be the interpolation of observational data value. This target function is supposed to be the solution (or an approximation thereof) to a PDE on a perforated domain for certain values of unknown parameters. We aim to estimate these parameters by solving an inverse problem on a homogenized domain with no holes. We discuss an inverse problem framework based on the generalized collage theorem for elliptic PDEs [1, 2] and establish several results linking the inverse problem on a perforated domain with the inverse problem on the domain with no holes. We illustrate the results with examples.

References

- [1] H. Kunze, D. La Torre and E.R. Vrscay, A generalized collage method based upon the Lax–Milgram functional for solving boundary value inverse problems, *Nonlinear Anal.* 71 (12), 2009, 1337–1343.
- [2] H. Kunze, D. La Torre, and E.R. Vrscay, Solving inverse problems for variational equations using the “generalized collage methods,” with applications to boundary value problems, *Nonlinear Analysis Real World Applications*, 11 (5), 2010, 3734–3743.
- [3] V.A. Marchenko and E.Y. Khruslov, *Homogenization of Partial Differential Equations*, Birkhauser, Boston, 2006.

Inverse problems via the “Generalized Collage Theorem” for vector-valued Lax Milgram-based variational problems

H. Kunze¹, D. La Torre², K. Levere³, M. Ruiz Galán⁴

¹ University of Guelph, Guelph, Canada, hkunze@uoguelph.ca

² Khalifa University, Abu Dhabi, UAE, and University of Milan, Milan, Italy, davide.latorre@kustar.ac.ae, davide.latorre@unimi.it

³ University of Guelph, Guelph, Canada, klevere@uoguelph.ca

⁴ University of Granada, Granada, Spain, mruizg@ugr.es

In the recent years a great deal of attention has been paid to the problem of parameter estimation in distributed systems, that is the determination of unknown parameters in the functional form of the governing model of the phenomenon under study. In the mathematical literature this kind of problem is called *inverse problem*. We call two problems *inverse* of one another if the formulation of each involves all or part of the solution of the other. Often, for historical reasons, one of the two problems has been studied extensively for some time, while the other one is newer and not so well understood. In such cases, the former is called the *direct problem*, while the latter is the *inverse problem*". There is a fundamental difference between the direct and the inverse problem; often the direct problem is *well-posed* while the corresponding inverse problem is *ill-posed*.

Many inverse problems may be recast as the approximation of a target element x in a complete metric space (X, d) by the fixed point \bar{x} of a contraction mapping $T : X \rightarrow X$. Thanks to a simple consequence of Banach's Fixed Point Theorem known as the *Collage Theorem*, most practical methods of solving the inverse problem for fixed point equations seek an operator T for which the *collage distance* $d(x, Tx)$ is as small as possible.

This method of *collage coding* may be applied in other situations where contractive mappings are encountered. These ideas have been extended to inverse problems for Initial Value Problems (IVP). In this setting, the contractive Picard operator plays the role of T and the space X contains continuous and appropriately bounded functions on a closed interval of observation.

In a manner analogous to the Collage Theorem we have also formulated a Generalized Collage Theorem for solving Boundary Value Problems (BVP), replacing the minimization of the true error by the minimization of something akin to the collage distance. In place of Banach's fixed point theorem for contraction maps on a complete metric space, we have appealed to the Lax-Milgram representation theorem.

These results have been extended to a wider class of elliptic equations problems, by considering not only Hilbert but also reflexive Banach spaces.

The paper is concerned with an extension of the *Collage Theorem* to a finite-dimensional vector-valued context, as well as with a discretization scheme based on the use of suitable Schauder bases. We also present three different numerical examples which show how to solve inverse problems for systems of elliptic differential equations.

References

- [1] M.I. Berenguer, H. Kunze, D. La Torre, and M. Ruiz Galan, *Galerkin schemes and inverse boundary value problems in reflexive Banach spaces*, Journal of Computational and Applied Mathematics **275**, pp. 100-112 (2015).
- [2] H. Kunze, D. La Torre, F. Mendivil, M. Ruiz Galan, and R. Zaki, *Fractal-based methods and inverse problems for differential equations: current state-of-the-art*, Mathematical Problems in Engineering **2014**, Article ID 737694 (2014).
- [3] K. Levere, H. Kunze, and D. La Torre, *A collage-based approach to solving inverse problems for second-order nonlinear parabolic PDEs*, Journal of Mathematical Analysis and Applications **406**, 1, pp. 120-133 (2013).

Modelling an Aquaponic Ecosystem using Ordinary Differential Equations

C. Bobak¹, H. Kunze²,

^{1,2} University of Guelph, Guelph, Canada, cpesweb@uoguelph.ca

Aquaponics is a closed-loop agricultural system which uses a symbiotic relationship between aquatic organisms and aquatic macrophytes that has been gathering in popularity globally [5]. However, relatively little academic research, particularly in the mathematics field, has been conducted on the practice. The two major populations of interest are fish and plants, however the system is dependent on ammonia concentrations and nitrate concentrations to function sustainably [2]. Organic nitrogen in fish waste naturally converts to ammonia through biological degradation [1]. Ammonia is highly toxic to fish, and is an inefficient nutrient source for plants [2]. In order for ammonia to be used as fertilizer for the plants, it must go through a natural microbial process called the Nitrogen Cycle and be transformed to Nitrate. Nitrate is a nutrient rich food source for plants and essential to the nutrient uptake process [1].

In this work, we develop a mathematical model for the dynamics of an aquaponic system in the form of a system of ordinary differential equations. We are able to establish that the model has physically reasonable qualitative properties. A review of the aquaponics literature helps us determine estimates for some of the model parameters. Solutions to the model at these baseline parameter values also have appealing properties, reflecting the real-life expectations of the physical system. Sensitivity analysis was performed using the SensSB Matlab toolbox [3, 4].

Collaborations with facilities that have established aquaponic systems are in progress with the goal of obtaining data relevant to this model. We are optimistic that the data obtained can be used to solve a parameter estimation inverse problem for the model.

References

- [1] A. Endut, A.Jusoh and N.Ali, Nitrogen budget and effluent nitrogen components in aquaponics circulation systems, *Desalinations and Water Treatments*, 52:744-752, 2014.
- [2] J.L. Liang and Y.H. Chien, Effects of feeding frequency and photoperiod on water quality and crop production in a tilapia-water spinach raft aquaponics system, *International Biodeterioration & Biodegradation*, 83:693-700, 2013.
- [3] M. Rodriguez-Fernandez and J. R. Banga, SensSB: a software toolbox for the development and sensitivity analysis of systems biology models, *Bioinformatics*, 26(13):1675-1676, 2010.
- [4] M. Rodriguez-Fernandez and J. R. Banga, SensSB.- A software toolbox for sensitivity analysis in systems biology models. International Conference on Systems Biology *ICSB 2009*, August 30 - Sept 4, Stanford University, Palo Alto, CA, 2009. (PDF)
- [5] A. Pattillo, Aquaponic System Design and Management, *Aquaculture Extension*, 2014.

Normalization of Eigenvectors and Certain Properties of Parameter Matrices Associated with the Inverse Problem for Vibrating Systems

M. El-Gebeily¹, Y. Khulief²

¹*King Fahd University of Petroleum and Minerals, Saudi Arabia, mgebeily@kfupm.edu.sa*

²*King Fahd University of Petroleum and Minerals, Saudi Arabia, khulief@kfupm.edu.sa*

There is a great deal of interest and vast literature devoted to the problem of identifying mass, damping and stiffness matrices of a vibrating system from a given complete set of eigenvalues and eigenvectors. System monitoring and fault detection depend essentially on identification of such matrices. The analysis of a discretized free vibrating system

$$M\ddot{q} + D\dot{q} + Kq = 0 \quad (1)$$

amounts to solving the eigenvalue problem for the second order matrix equation

$$\lambda^2 Mx + \lambda Dx + Kx = 0 \quad (2)$$

The inverse problem [1] is one of identifying the real definite matrices $M > 0, K > 0$ and $D \geq 0$ from a specified pair (Λ, X_c) of eigenvalues and corresponding eigenvectors. We assume here that $\Lambda = U + iW$, where $U \leq 0$ and $W > 0$ are diagonal matrices. The well posedness of the inverse problem requires that the matrix X_c be properly normalized in the sense that there is a diagonal matrix γ such that the normalized matrix

$$\tilde{X}_c := X_c \gamma \quad (3)$$

satisfies

$$\tilde{X}_R \tilde{X}_R^T = \tilde{X}_I \tilde{X}_I^T, \text{ where } \tilde{X}_R = \Re(\tilde{X}_c) \text{ and } \tilde{X}_I = \Im(\tilde{X}_c). \quad (4)$$

To the best of our knowledge, no formula has been given for finding a normalization matrix γ – except solving case by case a quadratic system of equations involving the elements of γ . In this work we show how to derive an explicit expression of a class of such normalization matrices.

Furthermore, it is known that for the properly normalized \tilde{X}_c , there exist a nonsingular matrix X_R and an orthogonal matrix Θ , both real, such that

$$\tilde{X}_c = X_R(I - i\Theta) \quad (5)$$

We also show that the spectrum of Θ satisfies

$$\sigma(\Theta) \subset \left\{ z \in \mathbb{C} : |\arg(z)| < \frac{\pi}{2} \right\} \quad (6)$$

- [1] P. Lancaster, and U. Prells, *Inverse problems for damped vibrating systems*, J. Sound Vib., 283 (2005) 891–914.

Parameter estimation for discrete-time models through goal programming with application to economics and management

C. Colapinto¹, D. La Torre², D. Liuzzi³, S. Marsiglio⁴

¹ Ca' Foscari University of Venice, Venice, Italy, cinzia.colapinto@unive.it

² Khalifa University, Abu Dhabi, UAE, and University of Milan, Milan, Italy, davide.latorre@kustar.ac.ae, davide.latorre@unimi.it

³ University of Milan, Milan, Italy, danilo.liuzzi@unimi.it

⁴ University of Wollongong, Wollongong, Australia, simonem@uow.edu.au

The proliferation of non-linear dynamic models in economics and management has set new challenges and perspectives. Examples of applications of non-linear dynamic models are related to macroeconomic dynamics, demographic change, pricing models, diffusion processes and others. Often, these models take the form of an evolution equation driven by discrete-time equation as follows:

$$x(t+1) = g(x(t), t), \quad x(0) = x_0 \quad (1)$$

where $x(t)$ describes the evolution process over time and x_0 is the initial condition. For instance in population dynamics the function $x(t)$ typically describes the population size at the time t , in innovation diffusion $x(t)$ can model the level of technological progress/adoption over time, in media studies $x(t)$ depicts the level of popularity over time, and so on. Many times these models include several parameters that need to be estimated in order to predict the long run behaviour of the solution $x(t)$. In other words, in practical applications, the above system takes the form of

$$x(t+1) = g_\lambda(x(t), t), \quad x(0) = x_0 \quad (2)$$

where λ is a vector of parameters. A parameter estimation procedure for system (2) (sometimes called inverse problem) starts with a given target time-dependent function $\bar{x}(t)$, which is constructed by interpolating available data. The aim of a parameter estimation technique consists of determining the values of unknown parameters $\bar{\lambda}$ such that $\bar{x}(t)$ is a solution to the above system (2) once we replace λ with $\bar{\lambda}$.

In this paper we propose a method for solving parameter identification problems based on the Goal Programming (GP) model. The idea behind this approach is based on the following observation: for solving an inverse problem for the above system (2) one has to minimize the distance between the left and right side of equation (2). This leads quite to distance function model where the deviations between the left and the right side of (2) are to be minimized. This is basically the scope of the GP model.

References

- [1] C. Colapinto, E. Sartori, M. Tolotti, *Awareness, persuasion, and adoption: Enriching the Bass model*, Physica A **395**, pp. 1-10 (2014).
- [2] C. Colapinto, E. Benecchi, *Dynamics and Motivations of Media Marketing: The Role of Globalization and Empowerment*, Abstract and Applied Analysis **2014**, Article ID 393168 (2014).
- [3] D. La Torre, S. Marsiglio, *Endogenous technological progress in a multi-sector growth model*, Economic Modeling **27**, 5, pp. 1017-1028 (2010).

Predicting visual degradation of image subblocks produced by JPEG and JPEG2000 compression

A. Cheeseman, I.A. Kowalik-Urbaniak and E.R. Vrscay

University of Waterloo, Waterloo, Ontario, Canada, {akcheese,iakowali,ervrscay}@uwaterloo.ca

Much of the “raw” data of a digital image (i.e., greyscale values) – in fact, well over 90% – can be removed with no loss in visual quality, due to the high correlations between neighbouring pixels, resulting in *lossless image compression*. Exponentially-increasing amounts of data being generated in countless applications, however, have led to an increased use of higher compression rates which produce degradations in images. Even radiological communities have recognized the need for such *lossy image compression*, but only to the extent that the diagnostic quality of the image is not compromised. In this study, which arose from an initial interest in “diagnostically lossless medical image compression,” [1] we examine whether it is possible to predict which regions of an image – typically pixel subblocks – will exhibit greater degrees of *visual degradation* when compressed.

Traditional image processing methods have mostly employed *root mean squared error* (RMSE) and its relatives. It is well known, however, that these Euclidean-based distances correspond quite poorly to visual quality [2]. This has led us to consider a number of *image quality measures* which provide much improved assessments of visual quality. In this study, we focus on the structural similarity (SSIM) index [3], which is recognized in the research literature as one of the best measures of visual quality.

In JPEG compression, a 2D discrete cosine transform (DCT) is first applied to each 8×8 -pixel block \mathbf{b} of an image. The DCT coefficient array, c_{ij} , $0 \leq i, j \leq 7$, is conveniently viewed as a collection of the counter-diagonals $c(i, j)$, $i + j = K$, where K ranges from 0 (low-frequency end) to 14 (high-frequency end). In JPEG compression, the DCT coefficients are quantized, which typically affects the high-frequency coefficients most significantly, often setting them to zero. From Parseval’s identity, we expect that DCT blocks \mathbf{c} with significant *high-frequency content* – (total norm of the DCT diagonals $8 \leq K \leq 14$) will exhibit higher amounts of degradation as measured by RMSE. This is confirmed by numerical experiments. On the other hand, we predict that DCT coefficient blocks \mathbf{c} with (i) high *high-frequency fraction* – the ratio of high-frequency norm to total energy norm – and (ii) low *total energy* will exhibit the greatest visual degradation as measured by SSIM. This is also confirmed by numerical experiments. Most remarkably, we find that *these blocks also exhibit the smallest RMSE-based degradation*.

The final test is to compare these predictions with subjective assessments. At various JPEG quality factors Q , (lower Q implies greater compression ratio), subjects were asked to identify blocks in images which were noticeably degraded. These blocks generally exhibited high SSIM-based error but, quite remarkably, *also exhibited the lowest RMSE values*, a striking confirmation that RMSE is not a good measure of visual quality.

Preliminary experiments indicate that our DCT-based approach can also be used to predict relative visual degradations produced by the JPEG2000 compression scheme.

References

- [1] I.A. Kowalik-Urbaniak, *The quest for “diagnostically lossless” medical image compression using objective image quality measures*, Ph.D. Thesis, Department of Applied Mathematics, University of Waterloo (2015).
- [2] Z. Wang and A.C. Bovik, *Mean squared error: love it or leave it? - A new look at signal fidelity measures*, IEEE Trans. Signal Processing **26**, 1, 98-117 (2007).
- [3] Z. Wang, A.C. Bovik, H.R. Sheikh and E.P. Simoncelli, *Image quality assessment: From error visibility to structural similarity*, IEEE Transactions on Image Processing **13**, 4, pp. 600-612 (2004).

SS-CMPMC Computational Methods in Physical and Macromolecular Chemistry

Charge-induced instabilities of droplets containing macromolecular complexes

F. Sheriff¹, S. Consta²

¹ Department of Biochemistry, The University of Western Ontario, London, Canada

² Department of Chemistry, The University of Western Ontario, London, Canada, stylianiconstas@gmail.com

Solvated macromolecular complexes are ubiquitous in nature, notably in biological systems containing proteins and nucleic acids. Studies of the interactions within a macromolecular complex and between the complex and the solvent in droplet environments are critical for understanding the stability of macromolecular complexes in electrospray ionization (ESI) and nanofluidic experiments. In this study, two distinct cases of macromolecular complexes in aqueous nanodrops are examined by using molecular dynamics simulations: (*i*) a pair of sodiated poly(ethylene) glycol (PEG) macroions and (*ii*) a double-stranded DNA (dsDNA). PEG represents a case in which the surface energy of the aqueous droplet is larger than the solvent–macromolecule energy. Conversely, in a droplet solvating dsDNA, the solvent–macromolecule interaction energy overcomes the solvent interaction energy. We report that charge-induced instabilities previously identified for single macroions also appear in the case of complexes, but with a higher level of complexity. In the case of a pair of PEG macroions, we found that their conformations on the surface of a droplet “sense” each other. The charged PEGs are each released from a droplet at different times through contiguous extrusion or drying-out mechanisms. In the case of the DNA, the charge-induced instability manifests as a spine droplet morphology. Narrow regions of the spines promote break down of the hydrogen bonds that hold the dsDNA together. The dsDNA separates into two single strands as it is increasingly exposed to vacuum. These findings elucidate charge-induced instabilities of macromolecular complexes in droplets, which are critical intermediates in ESI and nanofluidic experiments.

Conformational selection or induced-fit docking: results of computational studies.

Anatoly Malevanets¹

¹ *Cyclica Inc., Toronto, Canada, anatoly.malevanets@cyclicarx.com*

We apply a new efficient sampling technique[MW11], termed Multiple Replica Repulsion (MRR) method to study docking of small molecules to proteins. In the study we merged advantages of two receptor based methods for computational ligand docking; rigid docking and induced-fit docking. Rigid docking is an effective strategy when the binding pocket preserves its conformation upon the docking. It is very efficient as the coordinates of the protein atoms are considered to be fixed and simulations involve only a limited subset of ligand atoms. The induced fit docking is more computationally demanding as the protein conformations need to be sampled in order to find a suitable transient binding pocket.

Using Multiple Replica Repulsion (MRR) approach we generated low lying conformers of proteins in energy landscape and used them to find protein-ligand complexes. The determined complexed were compared with known structures and were found to be in good agreement. We demonstrated that rigid docking of ligands with an ensemble of low energy conformations of a given protein is an enticing alternative to an induced fit docking approach.

References

- [MW11] Anatoly Malevanets and Shoshana J. Wodak. Multiple replica repulsion technique for efficient conformational sampling of biological systems. *BIOPHYSICAL JOURNAL*, 101(4):951–960, AUG 17 2011.

Effect of Counterions on the Charging Mechanisms of a Poly(ethylene glycol) in Aqueous Nanodrops

M. Sharawy¹, S. Consta²,

¹ University of Western Ontario, Canada, msharawy@uwo.ca

² University of Western Ontario, Canada, styliani.constas@gmail.com

Nanodrops that carry excess charge play a critical role in aerosols and in electrospray ionization (ESI) processes. We report the first molecular dynamics study of the effect of counterions on the charging mechanisms of a macromolecule found in an aqueous droplet that contains excess charge. The droplets under study are composed of a poly(ethylene glycol) (PEG) molecule with sixty four monomers embedded in an aqueous droplet, where the charge carriers are sodium and chloride ions. The sodiated PEG is used here as a general model for investigating the principles of the charging mechanism of a macromolecule. We study the effect of counterions by varying the temperature of the droplets and the concentration of the chloride ions. We find that the size of the droplet from which the macromolecule will be released and its charge state are determined by the competition of the counterions and the macromolecule for the sodium ions (Fig. 1). We also find that the counterions form ion complexes and crystallites into the droplet that for certain sizes of droplets they may deprive a macromolecule from immediate access to the sodium ions and facile sodiation. We also report that regardless of the concentration of the counterions, the temperature plays a critical role in determining the nature of the droplet shape fluctuations that are responsible for the charging of a macromolecule and its extrusion from a droplet. At high temperature the macromolecule is released by the formation of a Taylor cone that transports ions onto the macromolecule. Differently, at lower temperature the Taylor cones are absent or substantially less pronounced. These findings provide insight into the mechanisms that macromolecules acquire their charge in droplets produced in electrospray ionization experiments.

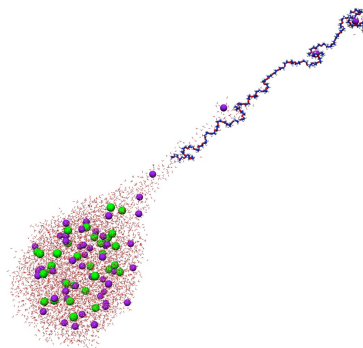


Figure 1: The release of a sodiated 64-mer Poly(ethylene glycol) from positively charged droplet in the presence of counterions. The nanodrop is composed of ~ 5000 water molecules (red dots), 47 Na^+ ions (green spheres), and 32 Cl^- ions (blue spheres).

Effect of Solvent on Solvation and Sodiation Mechanisms of Poly(ethylene glycol) in Droplets

M. Oh¹, S. Consta²

¹ University of Western Ontario, London, Canada, moh22@uwo.ca

² University of Western Ontario, London, Canada, sconstas@uwo.ca

Charged macromolecules, such as peptides and nucleic acids, are ubiquitous in chemical and biological systems as well as in industrial applications. These macromolecules may be solvated in bulk solution or droplets. Even though conformational and thermodynamic properties of the macromolecules in bulk solution have been extensively studied by experiments, macromolecular interactions with ions and solvent molecules have not been well understood at the atomistic level due to the complex nature of the interactions. Besides, the computational studies are relatively limited, which is attributable to highly challenging statistical sampling problems. Hence, the primary aim of our research project is to study the macromolecules-ion-solvent interactions in various bulk and droplet environments with atomistic details. This presentation will focus particularly on the computational studies of poly(ethylene glycol) (PEG) in nanosized charged droplets of aqueous and acetonitrile solvents, where all atoms are explicitly represented (Figure 1).

The effect of solvent on solvation and charging mechanisms of methylated PEG in charged droplets was investigated using constant-temperature molecular dynamics simulations. The droplet was placed in vacuo and no periodic boundary condition was applied, allowing solvent and ion evaporation to occur. Sodium cations were added as simple charge carriers for charged droplets, and the TIP3P model was used for water molecules. Interatomic interactions were modelled using the OPLS-AA force field.

A critical observation is that PEG prefers different locations of solvation, depending on the type of solvent, as shown in Figure 1. PEG diffuses outwards to the surface of the aqueous droplet, while it resides inside the acetonitrile droplet. Also, PEG may be charged temporarily at the water/vacuum interface, but it is charged “permanently” as the parent droplet reduces excess charges via sequential partial extrusions of the macroion. On the other end, PEG does not release sodium ions back into solvent once it is sodiated in an acetonitrile droplet. Consequently, the parent droplet loses charges through a series of Coulomb fissions, and the macroion is released as the solvent dries out. Moreover, the final charge state on PEG dissolved in the aqueous droplets is found to be $\text{PEG}-4\text{Na}^+$, whereas the fewer numbers of the final charge state ($\text{PEG}-2\text{Na}^+$ or $\text{PEG}-3\text{Na}^+$) are observed when it is dissolved in the acetonitrile droplets.

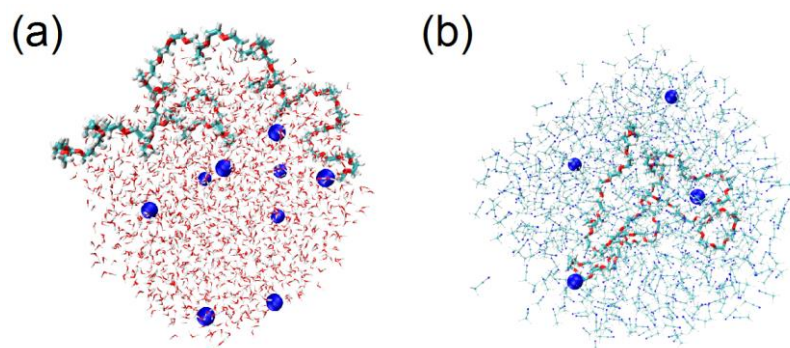


Figure 1: Poly(ethylene glycol) in (a) water and (b) acetonitrile droplets, both charged with sodium ions (blue spheres).

Interactions between carbon nanoparticles and fragmentation of a droplet of organic solvent

M. Paliy¹, S. Consta², J. Yang³

¹ Department of Chemistry and Department of Mechanical and Materials Engineering, The University of Western Ontario, London, Ontario, Canada, mpaliy@uwo.ca

² Department of Chemistry and Department of Physics and Astronomy The University of Western Ontario, London, Ontario, Canada, sconstas@uwo.ca

³ Department of Mechanical and Materials Engineering, The University of Western Ontario, London, Ontario, Canada, jyang@eng.uwo.ca

We report the first detailed Molecular Dynamics study of two carbon nanoparticles (nanotubes or fullerenes) embedded in a droplet of a typical organic solvent chloroform. The nanoparticles are negatively charged and are accompanied by the positive counterions of sodium. On the one hand, this setup is inspired by the carbon nanoparticle salts - “nanotubides” and “fullerides” [1], proposed recently as a promising answer to difficult problem of the dispersion of carbon nanoparticulates in the organic solvents. On the other hand, the electrospray [2] of carbon nanoparticle suspensions has been shown to be a promising technique for their dispersion and the production of nanoparticle coatings [3]. We explore the combination of these two approaches by molecular simulations [4].

The stability of a droplet depends on the subtle balance between the electrostatic repulsion of the ionic species and the cohesive action of the solvent. We find that depending on the overall electrostatic charge balance the two nanoparticles can exist in the droplet either in the “salted-out” bound state or in a “solvent-separated” state. The latter opens up the possibility for the efficient dispersion of the nanoparticles in the charged droplet environment.

Depending on the overall droplet charge, we found two distinct regimes of droplet fragmentation -namely, (i) even regime, when the original droplet breaks up into two nearly equal fragments, versus (ii) uneven regime, where one of the meso-ions carries away only small amount of the solvent. We interpret the difference between these two regimes with the help of a simple model. For the case of the even droplet fragmentation, we observe pronounced hysteresis between the states of the single droplet containing both meso-ions, and two separate droplets carrying one single meso-ion each. The source of such hysteresis is the different rearrangement of the solvent during the processes of the droplets break-up and coalescence.

The understanding of the fragmentation paths and the intermolecular interactions of the nanoparticles in droplets provide insight into the manner that the droplet chemistry can be manipulated so as effective dispersion of nanoparticulates can be achieved [5]. Relation of the observed phenomena to the fragmentation phase transition in clusters is discussed [6].

References

- [1] D. Voiry, C. Drummond, and A. Penicaud. Portrait of carbon nanotube salts as soluble polyelectrolytes. *Soft Matter*, 7(18):7998–8001, 2011.
- [2] J. Iribarne and B. Thomson. On the evaporation of small ions from charged droplets *J. Chem. Phys.*, 64:2287–2294, 1976.
- [3] Bon Ku and Pramod Kulkarni. Morphology of single-wall carbon nanotube aggregates generated by electrospray of aqueous suspensions. *J. Nanopart. Res.*, 11(6):1393–1403, 2009.
- [4] S. Consta. Fragmentation reactions of charged aqueous clusters *J. Mol. Struct.*, 591:131–140, 2002.
- [5] M. Paliy, S. Consta, and J. Yang. Interactions between carbon nanoparticles in a droplet of organic solvent. *J. Phys. Chem. C*, 118(29):16074–16086, 2014.
- [6] D.H.E. Gross, M.E. Madjet, and O. Schapiro. Fragmentation phase transition in atomic clusters I. *Z. Phys. D Atom. Mol. Cl.*, 39(1):075–083, 1997.

Effect of Methanol on the Charging Mechanisms of Poly(ethylene glycol) in Droplets

S. Soltani¹, S. Constas²

¹ Department of Physics and Astronomy, The University of Western Ontario, Canada, {ssoltan3}@uwo.ca

² Department of Chemistry, The University of Western Ontario, Canada, sconstas@uwo.ca

Electrospray ionization (ESI) is a technique that has many application in analytical chemistry[1]. The role of ESI is to transfer chemical species that are often macromolecules from a bulk solution into the gaseous state. In this process droplets are generated by spraying the solution into an electric. Due to high voltage in ESI and Coulomb explosion droplet shrinks and analyte can appear. So we use classical molecular dynamics to study the role of the methanol as solvent on the charge state and on manner that a macromolecule emerges from a droplet. The excess charge is carried by Na⁺ ions that charge PEG. The sodiated PEG64 in MeOH droplets resides in the interior of the droplet and emerges from the droplet by a drying-out process of the solvent and escape of solvated ions in contrast to previous studies in my group (PEG in aqueous droplet)[2, 3]. Key finding of our study is that the solvent plays a critical role in the mechanism of the charging and release of PEG.

A poly(ethylene glycol) molecule with 64 monomers (PEG64) was modelled in droplets of methanol (MeOH) that contained Na⁺ ions charge carriers. The droplets were modelled in vacuo with constant temperature at 280 K. The interatomic interactions were described using the OPLS-AA force field.

Typical snapshots of the charging of PEG64 and the drying-out process in a MeOH droplet with initial size of 800 MeOH molecules and 11 Na⁺ ions are shown in Fig. 1.

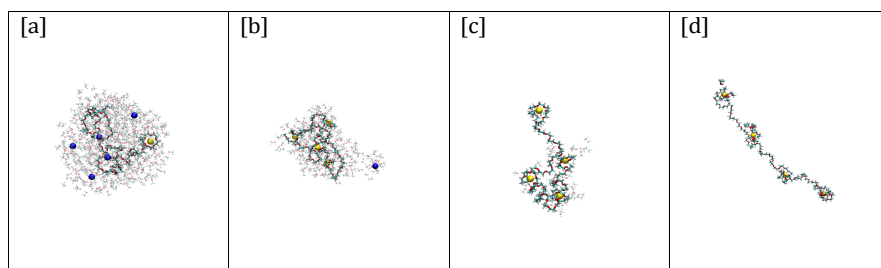


Figure 1: Typical snapshots of the charging and drying-out of PEG64 in a MeOH droplet. The color coding of the atomic sites is: blue spheres represent Na⁺ ions, the red sites represent oxygen, the white sites hydrogen and the turquoise carbon. The captured Na⁺ ions by PEG64 are shown in yellow color. The MeOH molecules are transparent in order to not obscure the visibility of PEG64 charging. For the four configurations, the time t from the initiation of the simulation run, the radius of the droplet (r), the number of MeOH molecules (N_{MeOH}) and the number of Na⁺ ions (N_{Na}) are: (a) $t = 2.7$ ns, $r \approx 2.3$ nm, $N_{\text{MeOH}} = 626$, $N_{\text{Na}} = 6$, (b) $t = 9.4$ ns, $r \approx 1.7$ nm, $N_{\text{MeOH}} = 269$, $N_{\text{Na}} = 5$, (c) $t = 14.4$ ns, $N_{\text{MeOH}} = 39$, $N_{\text{Na}} = 4$, (d) $t = 16.9$ ns, $N_{\text{MeOH}} = 10$, $N_{\text{Na}} = 4$.

References

- [1] S. Washito and K. Karabashi, *Soft landing of complex molecules on surfaces*, in *Annu. Rev. Anal. Chem.* (4), pp. 83-104 (2011).
- [2] T. M. Chang, J. S. Prell, E. R. Warrick, E. R. Williams, *Where's the Charge? Protonation Sites in Gaseous Ions Change with Hydration*, in *ACS Publications* (134), 38, pp. 15805-15813 (2012).
- [3] S. Consta and A. Malevanets, *Disintegration Mechanisms of Charged Nanodroplets: Novel Systems for Applying Methods of Activated Processes*, in *Mol. Simulat.*, (41), 1-3, pp. 73-85 (2014).

SS-CNT Computational Number Theory

Binary sequences with merit factors greater than 6.34

S. Choi

Simon Fraser University, Canada, schoia@sfu.ca

It had been decades for Turyn's binary sequences having the largest known asymptotic merit factor 6. In 2004, by considering truncated rotated Legendre sequences, Borwein, Jedwab and Choi conjectured that there are binary sequences having the asymptotic merit factor greater than 6.34. Until very recently, the conjecture is proved by Jedwab, Katz and Schmidt. In this talk, I will discuss this result.

Common Subexpression Algorithms for Space-Complexity Reduction of Gaussian Normal Basis Multiplication

R. Azarderakhsh¹, D. Jao², H. Lee²

¹ Rochester Institute of Technology, Rochester, New York, USA, rxaeec@rit.edu

² University of Waterloo, Waterloo, Ontario, Canada, {djaao,h96lee}@waterloo.ca

The use of normal bases for representing elements in a binary field is attractive in some applications because it is easy to perform squaring operations in hardware. In such cases, the costs of implementing the multiplication operation become a primary concern. We present new algorithms for reducing the space complexity of Gaussian normal basis (GNB) multipliers over binary fields $GF(2^m)$, where m is odd. Compared to previous results, our approach incurs no additional costs in time complexity, and achieves improvements in space complexity over a wide range of finite fields and digit sizes. For the binary fields specified in the NIST FIPS 186-3 elliptic curve digital signature algorithm (ECDSA) standards document, our algorithms reduce by 16% (respectively, 27%) the number of XOR gates needed for the implementation of a digit-level parallel-input parallel-output multiplier over a 163-bit (respectively, 409-bit) binary field.

Computing elliptic curves of fixed conductor

M. A. Bennett¹, A. Rechnitzer²

¹ University of British Columbia, Vancouver, Canada bennett@math.ubc.ca

² University of British Columbia, Vancouver, Canada andrewr@math.ubc.ca

I will discuss new, old and older still methods for computing elliptic curves with bad reduction outside given sets of primes. Applying these, we are now able to find models for all elliptic curves over the rationals with prime conductor bounded by 10^{10} and, conjecturally, by 10^{12} . I will then mention extensions of these results to the case of more general conductors and to curves over number fields.

Computing Galois groups with Magma

A.-S. Elsenhans¹

¹ Universität Paderborn, Germany, {Stephan.Elsenhans}@math.upb.de

The computation of the Galois group of a polynomial with rational coefficients is done in `magma` by using Stauduhar's method. On a first glance this approach looks quite simple. But in its initial form it could only give heuristic results for polynomials of degree at most 7.

In this talk I will explain variations of the method that enable us to determine the Galois group of a degree 20 polynomial with moderate coefficients in about 1 second. Finally, we will have a try with a degree 63 polynomial.

References

- [1] A.-S. Elsenhans: *Invariants for the computation of intransitive and transitive Galois groups*, J. Symbolic Comput. 47 (2012), no. 3, 315 – 326.
- [2] A.-S. Elsenhans: *On the construction of relative invariants*, Preprint 2014
- [3] A.-S. Elsenhans: *A note on short cosets*, Experimental Mathematics 23 (2014) 411 – 413
- [4] C. Fieker, J. Klüners: *Computation of Galois groups of rational polynomials*, LMS J. Comput. Math. 17 (2014), no. 1, 141 – 158
- [5] K. Geißler: *Berechnung von Galoisgruppen über Zahl- und Funktionenkörpern*, Dissertation, Berlin, 2003.
- [6] R. Stauduhar: *The determination of Galois groups*, Math. Comp. 27 (1973), 981 – 996.

Computing periodic points for Hénon maps over number fields

P. Ingram¹

¹ Colorado State University, Fort Collins, USA, pingram@math.colostate.edu

Hénon maps are automorphisms of the plane of the form

$$f(x,y) = (ay, x + P(y)),$$

for P a polynomial of degree at least two. They are of interest in part due to their relation to the Lorenz system [2], but also because of the role they play in classifying all automorphisms of the plane [1]. If one works over an algebraically closed field, one is perhaps not surprised that f will in general have infinitely many periodic points. Over a number field, however, one can show that there are only finitely many [4].

In this talk we will discuss a few approaches to finding all of the periodic points of a Hénon map over a number field, and some conjectures about how uniform one should expect the number of such points to be as one varies the map.

References

- [1] S. Friedland and J. Milnor, Dynamical properties of plane polynomial automorphisms. *Ergodic Theory Dynam. Systems* **9** (1989), no. 1, pp. 67–99.
- [2] M. Hénon, A two-dimensional mapping with a strange attractor. *Comm. Math. Phys.* **50** (1976), no. 1, pp. 69–77.
- [3] P. Ingram, Canonical heights for Hénon maps. *Proc. London Math. Soc.*, **108** (2014), no. 3, pp. 780–808.
- [4] J. H. Silverman, Geometric and arithmetic properties of the Hénon map. *Math. Z.* **215** (1994), no. 2, pp. 237–250.

Computing rational curves on quasihyperbolic surfaces

Navid Alaei¹, Nils Bruin²,

^{1, 2} Simon Fraser University, Canada, nbruin@sfsu.ca

From a number theoretic point of view, one of the most striking results in arithmetic geometry, first proved by Faltings, is that a curve of genus at least 2, which from a Riemannian point of view is a *hyperbolic* variety, has only finitely many rational points. It is an example of how geometry dictates arithmetic properties. For surfaces, there is an analogous property: an algebraic surface is called *algebraically quasihyperbolic* if there are only finitely many genus 0 and 1 curves on it. One expects that this has profound implications for the rational points on such a surface. It also suggests a computational task: given an explicit quasihyperbolic surface, determine the genus 0 (or 1) curves on the surface.

One of the primary means to prove quasihyperbolicity is by proving that the surface has regular symmetric differentials. Such forms give rise to differential equations that a genus 0 or 1 curve would have to satisfy. If one can determine such forms explicitly, then this gives a way to find the curves. Vojta [2] does this successfully on surfaces related to Büchi's problem.

Bogomolov and De Oliveira [1] show that the resolution of a surface in 3-space that has many nodal double point singularities (and no others) compared to its degree admit regular symmetric 1-forms, and hence is quasi-hyperbolic. Their result relies on the asymptotics of certain cohomological dimensions, so they do not a priori provide a way to determine such differentials explicitly.

Barth's sextic surface, with 65 nodal singularities, is an example to which the Bogomolov-De Oliveira result applies. We compute the global sections of a sheaf that would contain the symmetric differentials of degree 2 and we find differentials that are regular outside the nodes. We also determine the linear conditions that need to be satisfied for the sections to extend to regular differentials on the entire surface and find only the trivial solution. As a result, we can determine all genus 0 curves passing through only a limited number of nodes.

References

- [1] Fedor Bogomolov, Bruno De Oliveira, *Hyperbolicity of nodal hypersurfaces*. J. Reine Angew. Math. 596 (2006), 89–101.
- [2] Paul Vojta, *Diagonal quadratic forms and Hilbert's tenth problem*. *Hilbert's tenth problem: relations with arithmetic and algebraic geometry* (Ghent, 1999), 261–274, Contemp. Math., 270, Amer. Math. Soc., Providence, RI, 2000.

Divisor Tripling On Genus 2 Hyperelliptic Curves

Sebastian Lindner¹

¹ University of Calgary, Canada, salindne@ucalgary.ca

A hyperelliptic curve (HEC) over a finite field is a mathematical structure of interest in computational number theory and cryptography. Using the divisor class group over a HEC is an efficient and secure setting for standard public-key cryptosystems. The basic operations in this setting are scalar multiplication; adding a divisor to itself a fixed number of times. Explicit formulas described in terms of finite field operations as opposed to polynomial arithmetic, are the most efficient way to perform divisor arithmetic on low-genus HEC's. Improvements in efficiency to arithmetic with the divisors themselves (divisor doubling, addition and tripling), translate directly to faster cryptographic protocols. With our research we assess and improve the computational speed of divisor arithmetic for which a possible protocol for cryptography can be created.

We found improvements to doubling and addition, and created new explicit formulas for tripling in the imaginary model for genus 2 HEC's. The improved doubling and addition formulas reduce computation time for some current scalar multiplication algorithms. We apply the new tripling formulas to scalar multiplication using double-base (bases 2 and 3) expansions. Double-base expansions have a shorter length and weight than usual binary methods[1], so fast tripling is needed to take advantage. The biggest improvements we found were for HEC's over binary fields, reducing the number of finite field operations required to do a tripling by as much as 40 percent in some cases [5].

In order to achieve our results we studied approaches used in existing explicit formulas and adapted them to the cases we were interested in. We studied two main approaches used in literature, the geometric approach[3] and Cantor's algorithm[4], and found new tripling formulas that are a hybrid of the two. We found that for certain scenarios, using our new tripling formulas out performs some binary scalar multiplication algorithms based on the cost of our doubling, addition and tripling formulas. We are currently extending fastest known scalar multiplication algorithms that use GLV decompositions and Kummer surfaces[2] to make use of double-base expansions and our tripling formulas. We analyze the theoretical cost per bit of state of the art scalar multiplication algorithms and our new algorithms to compare our results to previous best.

Reducing the complexity of scalar multiplication algorithms through mathematical and implementational advances creates possibilities for the use of more efficient cryptographic protocols. Specifically, the tripling operation should improve state of the art speed records for genus 2 HEC scalar multiplication. We anticipate that it will be close to or better than current state of the art algorithms. In this growing field, we hope that our research will make advancements towards faster more efficient cryptographic protocols to be used in the future.

References

- [1] J. Adikari, V.S. Dimitrov, and L. Imbert, *Hybrid Binary-ternary number system for elliptic curve cryptosystems*, *Proceedings of EUROCRYPT 2009*, pp. 76-83 (2009).
- [2] J.W. Bo, C. Costello, H. Hisil, and K. Lauter. *Fast cryptography in genus 2*, in *Proceedings of EUROCRYPT 2013*, ed. T. Johansson and P.Q. Nguyen, LNCS **7881**, pp. 194-210 (2013).
- [3] C. Costello and H. Hisil, *Group law computations on Jacobians of hyperelliptic curves*, in *Selected Areas Of Cryptography 2011*, ed. M. and S. Vaudenay, LNCS **7881**, pp. 92-117 (2011).
- [4] T. Lange, *Formulae for arithmetic on genus 2 hyperelliptic curves*, *Applicable Algebra in Engineering, Communications and Computing* **15**, pp. 295-328 (2005).
- [5] S. Lindner, *Fast Divisor Tripling In Genus 2 Hyper Elliptic Curves*, Masters thesis, University of Calgary. <http://theses.ucalgary.ca/handle/11023/1723>, (2014).

Euclid's Algorithm in Multiquadratic Fields

A. Feaver¹

¹ The King's University, Edmonton, Alberta, Canada, amy.feaver@kingsu.ca

A number field is called norm-Euclidean if its ring of integers is Euclidean with respect to the absolute value of its field norm. We will discuss this property in the context of imaginary n -quadratic fields: degree 2^n number fields which can be expressed as $\mathbb{Q}(\sqrt{-a_1}, \dots, \sqrt{-a_n})$ for $a_1, \dots, a_n \in \mathbb{Z}_{>0}$ squarefree.

For quadratic fields, this classification was completed in 1952 [BSD]. In 2011, Lemmermeyer found a complete list of norm-Euclidean imaginary biquadratic fields [Lem].

Extending this work, we will discuss the norm-Euclideanity of imaginary n -quadratic fields with $n \geq 3$. We find that for $n \geq 4$, there are no norm-Euclidean imaginary n -quadratic fields. In the case of imaginary triquadratic fields, there are at least three which are norm-Euclidean. There may be up to nine other imaginary triquadratic fields which are norm-Euclidean, but no more than that. These results have arisen from both theoretical and computational methods, including Lezowski's *euclid* algorithm implemented in Pari/GP [Lez].

We will also discuss the remaining nine imaginary triquadratic fields which have not been classified according to their norm-Euclideanity, and techniques which may be applied to study them.

References

- [BSD] Barnes, E.S., Swinnerton-Dyer, H.P.F. The inhomogeneous minima of binary quadratic forms I, *Acta. Math* **87** (1952), 259–323.
- [Lem] Lemmermeyer, F. Euclid's algorithm in quartic CM-fields, *arXiv:1108.6215v1*. (2011).
- [Lez] Lezowski, P. *euclid* (version 1.0) <http://www.math.u-bordeaux1.fr/~plezowsk/euclid/index.php>.

Fast algorithms for finding a (short) generator of a principal ideal

J.-F. Biasse

University of Waterloo, Canada, biasse@lix.polytechnique.fr

We present recent work on the resolution of the “Principal Ideal problem” (PIP). Given an ideal $\mathfrak{a} \subseteq \mathcal{O}_K$ in the ring of integers of a number field, solving the Principal Ideal Problem consists in finding $\alpha \in \mathcal{O}_K$ such that $\mathfrak{a} = (\alpha)\mathcal{O}_K$, or deciding that \mathfrak{a} is not a principal ideal. This is a fundamental problem in computational number theory and it involves the computation of the ideal class group of \mathcal{O}_K , and its group of units \mathcal{O}_K^* which are two major tasks in computational number theory. Efficient methods to solve these problems allow us to compute relative class groups and unit groups, as well as the S -class group and the S -unit group of a number field. In turn, algorithms to solve these problems are at the heart of generic methods to solve Diophantine equations of the form

$$\mathcal{N}_{L/K}(x) = \theta,$$

where L/K is an extension of number fields, $x \in L$ and $\theta \in K$. Norm equations occur in a lot of problems, and generic methods for their resolution is an essential topic in the study of Diophantine equations.

The principal ideal problem is also relevant in the scope of cryptography. Indeed, many recent cryptosystems rely on the hardness of finding a short generator of a principal ideal $\mathfrak{a} \subseteq \mathcal{O}_K$ where K is typically a cyclotomic field $K = \mathbb{Q}(\zeta_N)$. Recent work from Campbell Groves and Shepherd suggests that finding a short generator easily reduces to the search for an arbitrary generator, thus making the PIP the bottleneck of the cryptanalysis of many cryptographic schemes.

Higher Mahler measure of some n -variable polynomial families

M. N. Lalín¹, J-S. Lechasseur²

¹ Université de Montréal, Montréal, Canada mlalin@dms.umontreal.ca

² Université de Montréal, Montréal, Canada jeansebl777@gmail.com

We prove formulas for the k -higher Mahler measure of a family of rational functions with an arbitrary number of variables. Our formulas reveal relations with multiple polylogarithms evaluated at certain roots of unity.

For k a positive integer, the k -higher Mahler measure of a non-zero, n -variable, rational function $P(x_1, \dots, x_n) \in \mathbb{C}(x_1, \dots, x_n)$ is given by

$$m_k(P(x_1, \dots, x_n)) = \int_0^1 \dots \int_0^1 \log^k |P(e^{2\pi i \theta_1}, \dots, e^{2\pi i \theta_n})| d\theta_1 \dots d\theta_n.$$

We observe that the case $k = 1$ recovers the formula for the “classical” Mahler measure. This function, originally defined as a height on polynomials, has attracted considerable interest in the last decades due to its connection to special values of the Riemann zeta function, and of L -functions associated to objects of arithmetic significance such as elliptic curves as well as special values of polylogarithms and other special functions.

Let

$$R_m(x_1, \dots, x_m, z) := z + \left(\frac{1-x_1}{1+x_1} \right) \dots \left(\frac{1-x_m}{1+x_m} \right).$$

be a rational function in the $m+1$ variables x_1, \dots, x_m, z . Using the techniques of [2] and some results of Akatsuka [1], we prove formulas for $m_k(R_m)$ involving the Riemann zeta function, the Dirichlet L -function in the character of conductor 4, and multiple polylogarithms evaluated at roots of unity.

A big question that remains is when such formulas may be reduced to formulas involving solely polylogarithms of length 1, such as

$$m_2(R_2) = -\frac{31\pi^2}{360} + \frac{28}{\pi^2} \log 2 \zeta(3) + \frac{32}{\pi^2} \text{Li}_4\left(\frac{1}{2}\right) + \frac{4}{3\pi^2} \log^2 2 (\log^2 2 - \pi^2).$$

Looking for such reductions opens the door to identities of colored multizeta values of which not much is known.

References

- [1] Akatsuka, Hirotaka. Zeta Mahler measures. *J. Number Theory* 129 (2009), no. 11, 2713–2734.
- [2] Lalín, Matilde N. Mahler measure of some n -variable polynomial families. *J. Number Theory* 116 (2006), no. 1, 102–139.

Looking for the best ABC triples

A. Akbary¹, J. Silva¹, S. Yazdani²

¹ University of Lethbridge, Lethbridge, AB, Canada, Math and CS department ² Google Inc., Kitchener, ON, University of Waterloo, Pure Math department, Waterloo, ON

The *ABC* conjecture conjecture states that for every $\varepsilon > 0$ there exists $K_\varepsilon > 0$ such that whenever A, B, C are positive coprime integers so that $A + B = C$ then

$$C > K_\varepsilon \left(\prod_{p|ABC} p \right)^{1+\varepsilon}.$$

This conjecture, if true, will have many interesting consequences in Diophantine equations. An immediate corollary to the *ABC* conjecture is that for every $\varepsilon > 0$ there can only be finitely many positive coprime integers A, B, C so that $A + B = C$ and

$$\log(C)/\log(\prod_{p|ABC} p) > 1 + \varepsilon,$$

and in particular there should be an A, B, C triple so that $\log(C)/\log(\prod_{p|ABC} p)$ is as large as possible. In this talk we investigate the question of how large this value can possibly be. We show that under a conjecture of Baker, we can theoretically find this triple.

Picard Curves with Good Reduction away from $p = 3$

B. Malmskog¹, C. Rasmussen²

¹ Villanova University, Villanova, PA, USA, beth.malmskog@villanova.edu

² Wesleyan University, Middletown, CT, USA crasmussen@wesleyan.edu

A Picard curve C over a field k is a smooth, irreducible, projective, cyclic trigonal curve of genus 3. Every Picard curve has an affine model of the form

$$y^3 = f(x),$$

where $f(x)$ is a polynomial in $k[x]$ of degree 4 with distinct roots over \bar{k} . Picard curves are the simplest curves which are neither rational nor hyperelliptic and have been studied from geometric, arithmetic, and computational perspectives. The moduli space of Picard curves is connected with some Hilbert problems [1]. We determine all Picard curves defined over the rationals which have good reduction at all primes except $p = 3$, up to rational isomorphism [2]. Reduction properties of curves are relevant to the study of modular curves, since the modular curve $X_0(N)$ has good reduction except at primes dividing N . This work was inspired by Nigel Smart's enumeration of genus 2 curves over the rationals with good reduction away from $p = 2$ [3]. Several interesting methods are involved in the enumeration, including using Baker's method and the LLL algorithm to find all solutions to the equation $x + y = 1$, where x, y are S -units in a given number field. We prove a result that improves on earlier techniques in special cases of solving the S -unit equation, and define a new type of equivalence of binary forms to adapt Smart's methods to this situation. The computations for this project were carried out in the computer algebra program Sage. A current project is adapting the existing code to create S -unit equation solving capabilities for Sage.

References

- [1] R.-P. Holzapfel, *The ball and some Hilbert problems*. Lectures in Mathematics ETH Zürich. Birkhäuser Verlag, Basel (1995). Appendix I by J. Estrada Sarlabous.
- [2] B. Malmskog, C. Rasmussen, *Picard curves over \mathbb{Q} with good reduction away from 3*, (2014). Unpublished, submitted (<http://adsabs.harvard.edu/abs/2014arXiv1407.7892M>).
- [3] N. P. Smart. *S -unit equations, binary forms and curves of genus 2*, in *Proc. London Math. Soc. (3)*, 75(2) pp. 271–307 (1997).

Radial asymptotics and algebraic independence in Mahler's method

M.Coons¹

¹ University of Newcastle, Australia, michael.coons@newcastle.edu.au

We present a new method for algebraic independence results in the context of Mahler's method. In particular, our method uses the asymptotic behaviour of a Mahler function $f(z)$ as z goes radially to a root of unity to deduce algebraic independence results about the values of $f(z)$ at algebraic numbers. We apply our method to the canonical example of a degree two Mahler function; that is, we apply it to $F(z)$, the power series solution to the functional equation $F(z) - (1 + z + z^2)F(z^4) + z^4F(z^{16}) = 0$. Specifically, we prove that the functions $F(z)$, $F(z^4)$, $F'(z)$, and $F'(z^4)$ are algebraically independent over $\mathbb{C}(z)$. An application of a celebrated result of Ku. Nishioka then allows one to replace $\mathbb{C}(z)$ by \mathbb{Q} when evaluating these functions at a nonzero algebraic number α in the unit disc.

This is joint work with Wadim Zudilin (Newcastle, Australia) and Richard Brent (Australian National University).

Ring-LWE Cryptography for the Number Theorist

Y. Elias¹, K. E. Lauter², E. Ozman³, K. E. Stange⁴

¹ McGill University, Montreal, Canada, yara.elias@mail.mcgill.ca

² Microsoft Research, Redmond, USA, klauter@microsoft.com

³ Bogazici University, Bebek-Istanbul, Turkey, ekin.ozman@boun.edu.tr

⁴ University of Colorado, Boulder, USA, kstange@colorado.edu

I will survey the status of attacks on the *ring and polynomial learning with errors problems* in lattice-based cryptography. Recent work by the authors, as well as work of Eisenträger and Hallgren, on the security of these problems gives rise to interesting connections to number fields. I will survey what is known and suggest some interesting open problems.

Shorter Compact Representations in Real Quadratic Fields

A. K. Silvester, M. J. Jacobson, Jr., H. C. Williams

University of Calgary, Calgary, Canada, {aksilves,jacobs,hwilliams}@ucalgary.ca

Compact representations are explicit representations of algebraic numbers with size polynomial in the logarithm of their height. These representations enable much easier manipulations with larger algebraic numbers than would be possible using a standard representation and are necessary, for example, in short certificates for the unit group and ideal class group. In this paper, we present two improvements that can be used together to reduce significantly the sizes of compact representations in real quadratic fields. We provide analytic and numerical evidence demonstrating the performance of our methods, and suggesting that further improvements using obvious extensions are likely not possible.

References

- [1] A. K. Silvester, M. J. Jacobson, Jr., and H. C. Williams, *Shorter compact representations in real quadratic fields*, in Buchmann Festschrift, Darmstadt, Germany, ed. M. Fischlin and S. Katzenbeisser, Lecture Notes in Computer Science, vol. 8260, Springer-Verlag, pp. 50–72 (2013).

Simple linear relations between conjugate algebraic numbers

A. Dubickas¹, K. G. Hare², J. Jankauskas³

¹ Vilnius University, Faculty of Mathematics and Informatics, Vilnius, Lithuania, arturas.dubickas@mif.vu.lt

² University of Waterloo, Department of Pure Mathematics, Waterloo, Canada, ON kghare@uwaterloo.ca

³ Vilnius University and Waterloo University, jonas.jankauskas@gmail.com

In this talk, we present our recent results from papers [1, 2] on the solutions on simplest 3 and 4-term linear equations in conjugates of a Pisot number and also about the solutions to 3-term equation in arbitrary algebraic numbers of low degree.

We show that the number $\alpha = (1 + \sqrt{3 + 2\sqrt{5}})/2$ with minimal polynomial $x^4 - 2x^3 + x - 1$ is the only Pisot number whose four distinct conjugates $\alpha_1, \alpha_2, \alpha_3, \alpha_4$ satisfy the additive relation $\alpha_1 + \alpha_2 = \alpha_3 + \alpha_4$. This implies that there exists no two non-real conjugates of a Pisot number with the same imaginary part and also that at most two conjugates of a Pisot number can have the same real part. On the other hand, we prove that similar four term equations $\pm\alpha_1 + \alpha_2 + \alpha_3 + \alpha_4 = 0$ cannot be solved in conjugates of a Pisot number α . We also show that the roots of the Siegel's polynomial $x^3 - x - 1$ are the only solutions to the three term equation $\alpha_1 + \alpha_2 + \alpha_3 = 0$ in conjugates of a Pisot number. In addition to this, we prove that there exists no Pisot number whose conjugates satisfy the relation $\alpha_1 = \alpha_2 + \alpha_3$.

Finally, we consider the three term equations $\alpha_1 = \alpha_2 + \alpha_3$ and $\alpha_1 + \alpha_2 + \alpha_3 = 0$ in conjugate algebraic numbers (not necessarily Pisot) of low degree ($4 \leq d \leq 8$). We prove that solutions exist only for $d = 6$ and find the minimal polynomials of such algebraic numbers in the parametrized form.

References

- [1] A. Dubickas, K. G. Hare, J. Jankauskas, *No two non-real conjugates of a Pisot number have the same imaginary part*, (submitted), arXiv preprint: <http://arxiv.org/abs/1410.1600>.
- [2] A. Dubickas, J. Jankauskas, *Simple linear relations between conjugate algebraic numbers of low degree*, preprint (available on request).

Some Primality Tests that Eluded Lucas

H. Williams¹

¹ University of Calgary, Canada, williams@math.ucalgary.ca

In his extensive memoir on the sequences that now bear his name, Lucas provided some primality tests for numbers N , where either $N+1$ or $N-1$ is divisible by a large prime power. No proofs were provided for these tests, and they are not correct as stated. Nevertheless, it is possible to correct these tests and even make them more general. In this talk we first show how to make these corrections and then show how the ideas behind these tests can be extended to numbers N , where either N^2+1 or N^2-1 is divisible by a large prime power. In order to do this we develop some properties of a certain pair of sequences which satisfy a linear recurrence relation of order 4.

Sums of Digits in q-ary Expansions

J.C. Saunders¹

¹ University of Waterloo, Waterloo, Canada, j8saunde@uwaterloo.ca

We let $s_q(n)$ denote the sum of the digits of a number n expressed in base q . For example, $s_2(n)$ denotes the number of 1's in the binary expansion of n . The study of the distribution of $s_q(n)$ has had a number of significant results. One of these results comes from Stolarsky who proved an asymptotic relationship for

$$\frac{s_2(n^2)}{s_2(n)}, \quad (1)$$

using an explicit construction, Ref. [1]. The result gives the bounds

$$\{\lfloor \log n \rfloor\}^{-1} \leq \frac{s_2(n^2)}{s_2(n)} \leq \frac{(4 \log \log n)^2}{\log n}. \quad (2)$$

where the left inequality always holds, and the right inequality holds for an infinite number of n and

$$c(h)(\log n)^{1-1/h} < \frac{s_2(n^h)}{s_2(n)} \leq 2(h \log n)^{1-1/h} \quad (3)$$

where the right inequality always holds, and the left inequality holds for an infinite number of n where $c(h)$ depends only on h . In particular, this shows that the ratio

$$\frac{s_2(n^2)}{s_2(n)} \quad (4)$$

can get both arbitrarily large and arbitrarily small.

We show that for

$$\alpha = 2 \quad \text{and} \quad q \geq 2, \quad (5)$$

the ratio

$$\frac{s_q(n^\alpha)}{s_q(n)} \quad (6)$$

can in fact be any positive rational number, again using explicit constructions, Ref. [2]. If time permits, we will also study what happens when α is a rational number that is not an integer, terminating the resulting expression by using the floor function.

References

- [1] K. Stolarsky, *The binary digits of a power*, Proceedings of the American Mathematical Society 71.1, pp. 1-5 (1978).
- [2] J.C. Saunders, *Sums of Digits in q-ary Expansions*, to appear in International Journal of Number Theory, DOI:10.1142/S1793042115500311, 17 pgs (2014).

The explicit formula and zeros of L -functions

M. Rubinstein¹, P. Sarnak²

¹ University of Waterloo, Waterloo, ON, Canada

² Princeton University, Princeton, NJ, USA

I will discuss algorithms, based on Weil's explicit formula, for computing zeros of L -functions, and also describe natural limitations to these algorithms.

Unconditional Class Group Tabulation of Imaginary Quadratic Fields to $|\Delta| < 2^{40}$

A. S. Mosunov¹, M. J. Jacobson, Jr.²

¹ University of Waterloo, Waterloo, Canada, {amosunov}@uwaterloo.ca

² University of Calgary, Calgary, Canada, {jacobs}@cpsc.ucalgary.ca

We present an improved algorithm for tabulating class groups of imaginary quadratic fields of bounded discriminant [1]. Our work is inspired by the previous result of Hart, Tornaría and Watkins, who used an out-of-core polynomial multiplication technique to compute all congruent numbers up to 10^{12} [2]. Our method uses classical class number formulas involving theta-series to compute the group orders unconditionally for all $\Delta \not\equiv 1 \pmod{8}$ [3]. The group structure is resolved using the factorization of the group order. The $1 \pmod{8}$ case was handled using the technique of Jacobson, Ramachandran and Williams [4], which involves the batch verification method based on the Eichler-Selberg trace formula to remove dependence on the Extended Riemann Hypothesis [5]. Our new method enabled us to extend the previous bound of $|\Delta| < 2 \cdot 10^{11}$ to 2^{40} [6]. Statistical data in support of a variety conjectures is presented, including Littlewood's bounds on $L(1, \chi_\Delta)$ and the Cohen-Lenstra heuristics, along with new examples of class groups with exotic structures.

References

- [1] A. S. Mosunov, M. J. Jacobson, Jr., *Unconditional Class Group Tabulation of Imaginary Quadratic Fields to $|\Delta| < 2^{40}$* , Mathematics of Computation (to appear).
- [2] W. B. Hart, G. Tornaría, M. Watkins, *Congruent number theta coefficients to 10^{12}* , Algorithmic Number Theory — ANTS-IX (Nancy, France), Lecture Notes in Computer Science **6197**, Springer-Verlag, Berlin, pp. 186 – 200 (2010).
- [3] E. T. Bell, *The class number relations implicit in the Disquisitiones arithmeticæ*. Bulletin of the American Mathematical Society **30** (5-6), pp. 236 – 238 (1924).
- [4] M. J. Jacobson, Jr., S. Ramachandran, H. C. Williams, *Numerical results on class groups of imaginary quadratic fields*, Algorithmic Number Theory - ANTS-VII (Berlin, Germany), Lecture Notes in Computer Science **4076**, Springer-Verlag, Berlin, pp. 87 – 101 (2006).
- [5] R. Schoof, M. van der Vlugt, *Hecke operators and the weight distributions of certain codes*, Journal of Combinatorial Theory **57**, pp. 163 – 186 (1991).
- [6] S. Ramachandran, *Numerical Results on Class Groups of Imaginary Quadratic Fields*, Master's thesis, University of Calgary, Calgary, Canada (2006).

SS-CP Computational Physics

A Single-Stage High-Resolultion Constrained Transport Method for Magnetohydrodynamic Equations

X. Feng¹, A.J. Christlieb², D.C. Seal³, Q. Tang⁴

¹ Michigan State University, East Lansing, USA, fengxia2@msu.edu

² Michigan State University, East Lansing, USA, christlieb@math.msu.edu

³ Michigan State University, East Lansing, USA, seal@math.msu.edu

⁴ Michigan State University, East Lansing, USA, tangqi@msu.edu

Most existing Adaptive-Mesh-Refinement(AMR) frameworks are designed for single-step single-stage methods [1, 2]. The goal of the current work is to develop a high-resolution numerical scheme for magnetohydrodynamic equations that is single-step single-stage, thus amenable to embed in an AMR framework.

We base the scheme on the Picard-Integral-Formulation WENO (PIF-WENO) methods [3]. By using a Taylor-type discretization of the time-averaged flux, we are able to make our scheme single-step single-stage, while being high-resolution.

A further challenge peculiar to magnetohydrodynamic equations is the necessity to maintain a divergence-free magnetic field. Failure to do so is known to cause numerical instabilities [4, 5]. Since our goal is a scheme amenable for AMR, we choose to use the unstaggered constrained transport method first proposed in [6]. This method evolves a magnetic potential and correct the magnetic field to be the curl of this potential. The evolution equation of the magnetic potential is a Hamilton-Jacobi equation [7]. To meet the single-step single-step challenge, we use a method inspired by the Lax-Wendroff WENO scheme for Hamilton-Jacobi equations [8] to numerically evolve the magnetic potential.

Our numerical experiments show that our scheme is third order in time and fourth order in space, and is able to resolve complex features of several classical test problems.

References

- [1] Enzo code, <http://enzo-project.org>
- [2] ForestClaw code, <http://math.boisestate.edu/calhoun/ForestClaw/>
- [3] D.C. Seal, Y. Güclü, and A.J. Christlieb, *The Picard integral formulation of weighted essentially non-oscillatory schemes* (accepted), SIAM J. Numer. Anal.
- [4] J.U. Brackbill and D.C. Barnes, *The effect of nonzero $\nabla \cdot B$ on the numerical solution of the magnetohydrodynamic equations*, J. Comput. Phys. **35**, pp.426-430 (1980)
- [5] G. Tóth, *The $\nabla \cdot B = 0$ constraint in shock-capturing magnetohydrodynamics codes*, J. Comput. Phys. **161**, pp. 605-652 (2000)
- [6] J.A. Rossmanith, *An unstaggered, high-resolution constrained transport method for magnetohydrodynamic flows*, SIAM J. Sci. Comput. **28**, 5, pp. 1766-1797 (2006)
- [7] A.J. Christlieb, J.A. Rossmanith, and Q. Tang, *Finite difference weighted essentially non-oscillatory schemes with constrained transport for ideal magnetohydrodynamics*, J. Comput. Phys. **268**, pp. 302-325 (2014)
- [8] J. Qiu, *WENO schemes with Lax-Wendroff type time discretizations for Hamilton-Jacobi equations*, J. Comput. Appl. Math. **200**, 2, pp. 591-605 (2007)

New accurate reduced mathematical model for particle beam simulation

F. Assous¹, J. Chaskalovic²

¹Ariel University, Israel, franckassous@netscape.net

²D'alembert, University Pierre and Marie Curie, Paris, France

The numerical simulation of charge particle beams or plasma physics problems often needs to solve the time-dependent coupled Vlasov-Maxwell system [1, 2]. However, the numerical solution of such models requires a large computational effort and resources. Therefore, whenever possible, it is worthwhile to take into account the physical and/or geometrical properties of the physical problem to derive approximate simpler models, that allow to cheaper simulations [3, 4].

During the two last decades, several models have been proposed like the gyrokinetic models with application to magnetic fusion or the paraxial models useful for particle accelerators ones. The static or quasi static models can also be interpreted in this framework, assuming that partial or total part of the time-dependent aspect can be neglected. A relevant method to comparison these asymptotic models can be based on data mining techniques, as introduced in [5].

In this talk, we are interested in the transport of high energy short beams. A typical example could be the transport of a bunch of relativistic particles in the interior of a perfectly hollow tube. We propose a new asymptotic model based on an approximation of the Vlasov-Maxwell equations. We first introduce a frame which moves along the optical axis, so that the bunch is evolving slowly in this frame. We then define a scaling of the equations that reflects the characteristics of the beam. This enables the introduction of a small parameter. Using asymptotic expansions techniques, we finally derive a new model which is accurate up to the order four.

Despite its accuracy, the simplicity of the model allows to use a Particle-In-Cell approach to derive an accurate and fast algorithm. Natural applications of the model are particle accelerators or free-electron lasers. Applications to fusion problems may also be envisaged, considering particle accelerators as an alternative to lasers for inertial fusion problems.

References

- [1] C.K. Birdsall and A.B. Langdon, *Plasmas Physics via Computer Simulation* (New York: Mac.Graw-Hill, 1985).
- [2] F. Assous, P. Degond, E. Heintzé, P.A. Raviart, J. Segré, On a finite element method for solving the three dimensional Maxwell equations, *J. Comput. Physics*, 109(2), 222–237, (1993).
- [3] P. Degond,P.-A. Raviart, On the paraxial approximation of the stationary Vlasov-Maxwell. *Math. Mod. Meth. Appl. Sci.*, 3(4) 513–562 (1993).
- [4] G. Laval, S. Mas-Gallic, P.-A. Raviart, Paraxial approximation of ultrarelativistic intense beams, *Numer. Math.*, 69(1), 33–60 (1994).
- [5] F. Assous, J. Chaskalovic, Data mining techniques for scientific computing: Application to asymptotic paraxial approximations to model ultra relativistic particles, *J. Comput. Physics*, 230 (2011) 4811-4827.

Numerical simulation of Stimulated Brillouin Scattering instability in LPI

Hu xiaoyan, Hao liang, Zheng chunyang and Liu zhanjun

Institute of Applied Physics and Computational Mathematics, Beijing, hu_xiaoyan@iapcm.ac.cn

In the process of laser fusion, which uses a high power laser as a drive to implode capsules filled with fuel, and produces thermonuclear energy, laser-plasma interaction (LPI) plays an important role, because the instabilities in LPI not only influence the laser energy absorbed in the target plasma, but also destroy the symmetry of implosion. Commonly, these instabilities consist of filamentation, stimulated Brillouin backscattering (SBS), stimulated Raman backscattering (SRS), and etc., which are nonlinear multi-scale physical processes. Modeling the coexistence of these instabilities in real-size experiments scale is a significative but arduous task, which will be the tools to simulate the LPI processes and provides guidance in the design of laser-driven fusion experiments.

Stimulated Brillouin Scattering (SBS) is deleterious to the realization of laser driven inertial confinement fusion (ICF), and it is one of the instabilities which take the energy away from the incident laser. For studying the physical mechanism of SBS, we establish the three-wave mathematic models of SBS(see Refs.[1]).

$$\left(\frac{\partial}{\partial t} + v_B + v_{gB} \frac{\partial}{\partial z} + \frac{1}{2} \frac{\partial v_{gB}}{\partial z} - \frac{ic^2}{2w_0} D_\perp^2 \right) A_B = - \frac{i\pi e^2}{m_e \omega_0} \delta n_A^* A_0, \quad (1)$$

$$\left[\left(\frac{\partial}{\partial t} + 2ik_0 \vec{u}_z + \vec{u} \cdot \nabla + v_{iaw} \right)^2 - v_{iaw}^2 + c_s^2 \left(4k_0^2 - 4ik_0 \frac{\partial}{\partial z} - \nabla^2 \right) \right] \delta n_A = - \frac{2Zn_{ef}e^2 k_0^2}{m_e m_i c^2} A_0 A_B^*, \quad (2)$$

According to the characteristic of equations, operator splitting method is used for solving the equation(1) of the light wave propagation, where the Fast Fourier translation (FFT) is applied to compute the diffraction operator, and the acoustic wave equation (2) is solved by the coordinate transfer and the finite difference methods. We have simulated the reflectivity of SBS, In Fig. 1, the dotted line shows how the reflectivity of SBS increases along with the incident intensity and the simulated length in theory, and they are consistent with the theoretical curves accurately(see Refs.[2]). In order to simulate the SBS processes in large-scale computers well, several parallel techniques are used. Scalability is demonstrated with a parallel efficiency above 81.6% on 4096 processors.

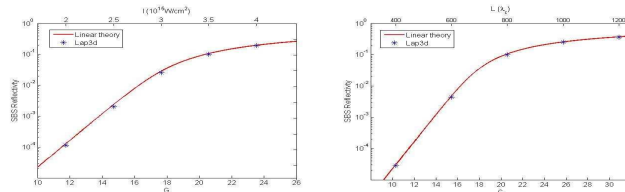


Figure 1: The reflectivity of SBS increases along with the incident intensity and the simulated length.

References

- [1] R. L. Berger, B.F.Lasinski and HT.B.Kaiser, Theory and three-dimensional simulation of light filamentation in laser-produced plasma. *Phys. Fluids B* 5(7), 2243-2258 (1993).
- [2] C.L.Tang. Saturation and Spectral characteristics of the Stokes Emission in the Stimulated Brillouin Process. *Journal of Applied Physics* 37,2945(1966).

Performance study of an optimum SLW model in solution of non-gray radiative heat transfer problems

Masoud Darbandi¹, Bagher Abrar¹, Gerry E. Schneider²

¹ Department of Aerospace Engineering, Center of Excellence in Aerospace Systems, Sharif University of Technology, Tehran, P.O. Box 11365-8639, Iran

² Department of Mechanical and Mechatronics Engineering, University of Waterloo, Waterloo, ON, N2L 3GI, Canada
Email: darbandi@sharif.edu

ABSTRACT

In this study, we present an optimum SLW model and combine it with FV method to solve RTE in non-gray medium. In our optimum SLW, non-gray gas is modeled by proper combination of only 3 gray gases (SLW3-opt). However, the accuracy is guaranteed by optimizing the discretization of absorption coefficient in frequency domain. We evaluated the performance of our SLW3-opt model by solving two test cases in which, non-isothermal and non-homogeneous medium of CO₂ and H₂O participates in radiation. Results of SLW3-opt model are very close to benchmark data in both test cases, which indicates the accuracy of our proposed model. Furthermore, comparison between conventional SLW and SLW3-opt models indicates much reduction in computational costs by using SLW3-opt model, despite the same level of accuracy. Therefore, the SLW3-opt model along with FV method performs accurately and efficiently in solving RTE in non-gray gases medium.

1. INTRODUCTION

Nowadays, CFD tools play a crucial role in many applications. In this regards, lots of research activities have focused on proper simulation of physical phenomena such as radiation in combination with solution of basic fluid flow equations. In most applications, radiation occurs in non-isothermal and non-homogeneous media of non-gray gases, which complicate the problem. In recent years, several models have been developed for solving radiation problems in such medium. A proper radiation model should be accurate and computationally efficient. Furthermore, radiation model should be compatible with conventional CFD solvers. Among radiation

models, LBL is recognized as the most accurate one, but its computationally cost is very high. Besides that, there are some band models such as SNB which are comparable with LBL in accuracy and computationally more efficient. But, these models are still computationally very expensive and only used for benchmark solutions. Researchers recognize the SLW model as a suitable choice between accuracy and computational cost. But application of this model needs further improvement for application in CFD simulation.

In conventional SLW, Non-gray gas is modeled with 10 (SLW10) or more gray gases, which means that RTE should be solved 10 times or more. This would increase the computational costs and make the comprehensive CFD simulations infeasible. Reducing the number of gray gases would cause the loss of accuracy in conventional SLW model. Here, we present an optimum SLW model. In our optimum SLW, non-gray gas is modeled by proper combination of only 3 gray gases (SLW3-opt). However, the accuracy is guaranteed by optimizing the discretization of absorption coefficient in frequency domain.

2. RESULTS AND DISCUSSION

In the following, we provide some results. Detailed discussion about these results will be provided in full paper.

Table 1 - Temperature distribution and species concentration.

Mole fraction: non-homogeneous	$c_0[4(1 - 2 x - 0.5)(1 - 4 y - 0.25) + 1]$
Temperature: non- isothermal	$T_0[0.3333(1 - 2 x - 0.5)(1 - 4 y - 0.25) + 1]$

Table 2 - CPU time for each solution iteration of RTE with different SLW models and grid resolution of $N_x \times N_y = 200 \times 100$ and $N_\theta \times N_\varphi = 10 \times 10$.

Model	Number of equations	CPU time (sec)
SLW ₂₀	21	30.9
SLW ₁₀	11	16.1
SLW ₃	4	6.5
SLW ₂	3	4.7
SLW ₁	2	3.1
grey	1	1.3

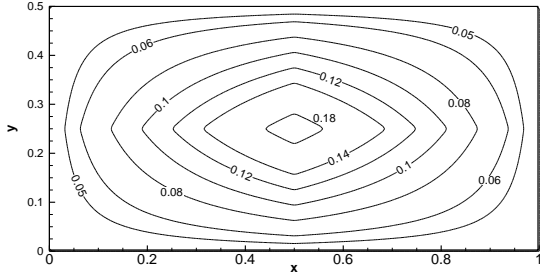


Figure 1- non-homogeneous H2O mole fraction field in test case 2.

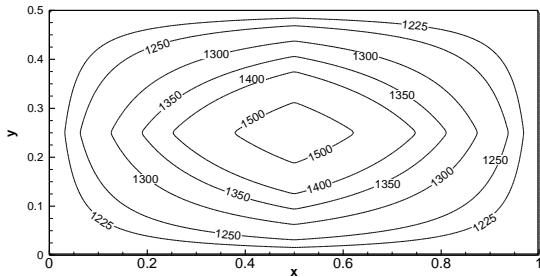


Figure 2- non-isothermal temperature field in test case 1 and 2.

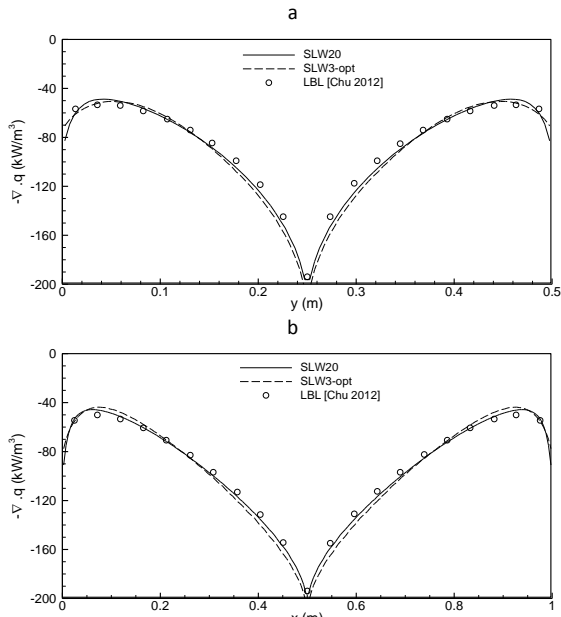


Figure 3- Predicted profiles of radiative heat source in case 1 (CO2 field) calculated by SLW₃-opt and SLW₂₀ and comparison with LBL benchmark data [2], a) data along the $x = 0.5$ m centerline, b) data along the $y = 0.25$ m centerline.

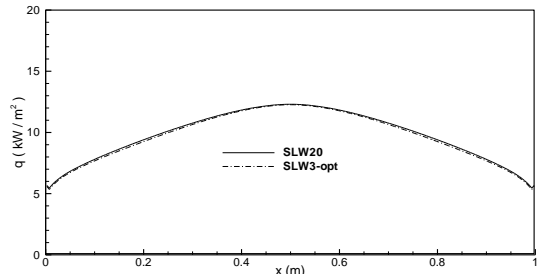


Figure 4- Predicted profiles of radiative heat flux in case 1 (CO2 field) calculated by SLW₃-opt and SLW₂₀, data along the top wall.

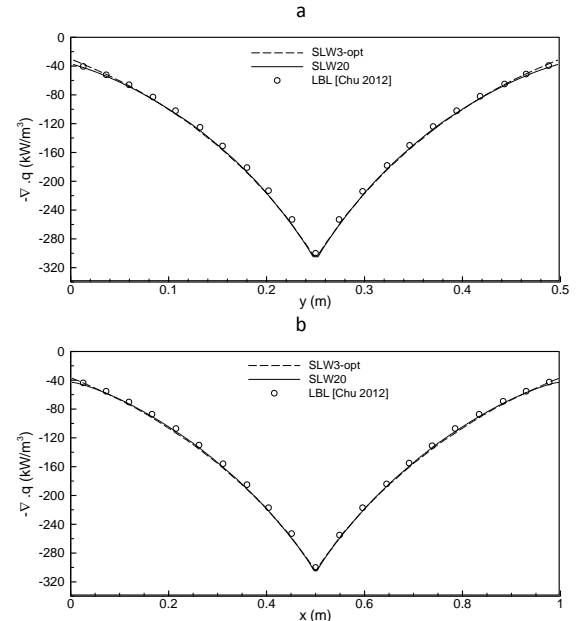


Figure 5- Predicted profiles of radiative heat source in case 2 (H2O field) calculated by SLW₃-opt and SLW₂₀ and comparison with LBL benchmark data [2], a) data along the $x = 0.5$ m centerline, b) data along the $y = 0.25$ m centerline.

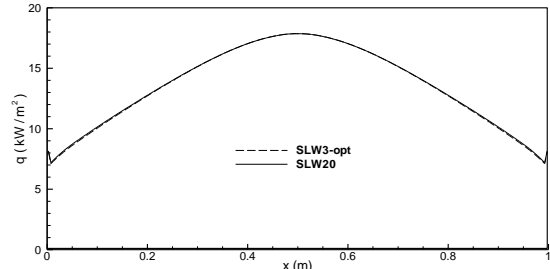


Figure 6- Predicted profiles of radiative heat flux in case 2 (H2O field) calculated by SLW₃-opt and SLW₂₀, data along the top

REFERENCES

- [1] J.T. Pearson, B.W. Webb, V.P. Solovjov, J. Ma, Efficient representation of the absorption line blackbody distribution function for H2O, CO2, and CO at variable temperature, mole fraction, and total pressure, *JQSRT*, 138:82–96, 2014
- [2] H. Chu, F. Liu, H. Zhou, Calculations of gas radiation heat transfer in a two-dimensional rectangular enclosure using the line-by-line approach and the statistical narrow-band correlated-k model, *Int. J. of Thermal Sciences*, 59:66–74, 2012

Two dimensional nodal Riemann solver based on one dimensional Riemann solver for a cell-centered Lagrangian scheme

Yan Liu¹, Dekang Mao², Baolin Tian³, Weidong Shen⁴

¹ Key Laboratory of Computational Physics, Institute of Applied Physics and Computational Mathematics, Beijing, China, yan_liu_zh@163.com

² Department of Mathematics, Shanghai University, Shanghai, China, dkmao@staff.shu.edu.cn

³ Key Laboratory of Computational Physics, Institute of Applied Physics and Computational Mathematics, Beijing, China, tian_baolin@iapcm.ac.cn

⁴ Key Laboratory of Computational Physics, Institute of Applied Physics and Computational Mathematics, Beijing, China, wei_dongshen@iapcm.ac.cn

We develop a new and more general formula for the construction of two dimensional nodal Riemann solver for a cell-centered Lagrangian scheme[1-2] developed by Maire and his co-workers which allows us to use general one dimensional Riemann solvers that have intermediate velocity and pressure in the construction. The old formula for the scheme used in the papers of Maire et al is only a special case of our new formula. We present an entropy discussion, which indicates that the schemes with nodal solvers constructed following the old formula, which can only use the 1D Riemann solvers satisfying our strong entropy condition, are usually numerically very dissipative. To develop numerically less dissipative schemes we introduce a so-called weak entropy condition, and present a one dimensional Riemann solver[3] that satisfies the weak entropy condition but not the strong entropy condition. Analysis shows that the scheme using this 1D solver is numerically less dissipative than the schemes using solvers satisfying the strong condition. Finally, several numerical examples are presented to show that our new formula works well and the scheme using the one dimensional solver satisfying the weak entropy condition improves the accuracy in smooth region, resolution around rarefaction waves and two dimensional symmetry; however it sometime produces small velocity oscillations and mesh distortions.

References

- [1] P.H. Maire, R. Abgrall, J. Breil, J. Ovadia, A cell-centered lagrangian scheme for two-dimensional compressible flow problems, SIAM J. Sci. Comput., 2007, 29: 1781-1824 .
- [2] P.-H. Maire, A high order cell-centered lagrangian scheme for two dimensional compressible fluid flows on unstructured meshes, J. Comput. Phys., 2009, 228: 2391-425.
- [3] Baolin Tian, Weidong Shen, Yan Liu, et. al., Numerical study on several Godunov-type shemes with ALE formulation, Chinese Journal of Computational, 2007, 24(5): 537-542.

SS-DASO Data Analytics for System Optimization

An Advanced Data Analytic Tool: Okapi System and Its Easy Adaption

Sherry Zhu, Tian Yang, Jimmy Huang

Information Retrieval and Knowledge Management Research Lab, York University, Toronto, Canada, {sherryzh}@yorku.ca
 Information Retrieval and Knowledge Management Research Lab, York University, Toronto, Canada, {timyang}@yorku.ca
 Information Retrieval and Knowledge Management Research Lab, York University, Toronto, Canada, {jhuang}@yorku.ca

We describe the easy adaption and development of a highly complex and very robust IR system, Okapi BM25 system [1]. Historically, it is very difficult to migrate the Okapi system from one operating system to another or from one machine to another [2, 3]. The easy adaption process will allow academic researchers to easily adapt the system, and to present and share research results. We present an experiment for learning. We see three main benefits from our re-defined system and workflow. First, the new system could manage Okapi source code by using source code version to control system, to refactor Okapi C and Java source code, and to build structure; second, it will support inverted index reuse and raw data reuse; third, it will allow duplication and easy setup of the Okapi environment.

We start our experiment by improving the workflow of the creation of a better source control management. The Okapi source code is managed by using GitHub. The new commits can be pushed to GitHub, and create Pull Requests to merge development into master for stable builds. We then create a Dockerfile which contains steps to build a complete Okapi system in DockerHub. Any new changes made to Dockerfile (including changes from Okapi) from GitHub will be automatically captured by DockerHub and will start a new build, that push to DockerHub repository (see Fig. 1).

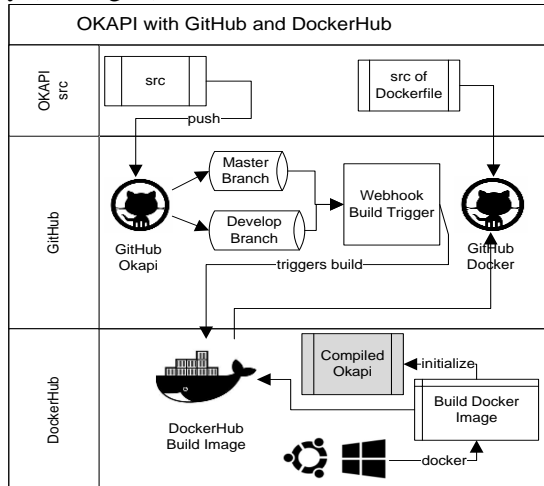


Figure 1: System Overview

References

- [1] Stephen E. Robertson, Steve Walker, Susan Jones, Micheline Hancock-Beaulieu, and Mike Gatford 1994. Okapi at TREC-3. Proceedings of the Third Text Retrieval Conference (TREC 1994). Gaithersburg, USA.
- [2] Huang, X., Wen, M., An, A., and Huang, Y. R. 2006b. *A platform for Okapi-based contextual information retrieval*. In Proceedings of the 29th Annual International ACM SIGIR Conference on Research and Development in Information Retrieval. ACM, New York, NY, 728.
- [3] Zhao, J., Huang, X. J. and Ye, Z. *Modeling Term Associations for Probabilistic Information Retrieval*, ACM Transactions on Information Systems (TOIS). ACM Publisher. Vol 32, No. 2, Article 7, 47 pages.

Analysis and Detection of Coalition Attacks for Online Advertising

Q. Zhang¹, W. Feng¹

¹ Trent University, {qzhang,wfeng}@trentu.ca

With accordance to the recent report of Zenithoptimedia [1], online advertising in 2014 is at \$ 121 billion, which accounts for nearly one-quarter of the global ad spend. While publishers can apply legitimate methods to attract more traffic to their websites, dishonest publishers attempt to generate invalid traffic to make more money. Coalition attacks recently becomes one of the most popular fraud attacks that can be launched with lower cost while still working effectively. Due to its popularity and the difficulty to be detected, we take our efforts to analyze coalition attacks in this paper. In particular, we simulate the attacking mechanism and develop new algorithm to detection them.

The classical way of discarding low quality traffic for fraud detection is too aggressive that the malicious intents of fraudsters are not identified directly. The fraudsters can easily comprise the classical detection tools by mimicking the validity metrics. The detection of coalition attacks is even more challenge than the detection of non-coalition ones, since coalition attacks blur the strong correlation between the fraudulent sites and machines. The key to identify the malicious intend of fraudsters is to identify the correlations of multiple publishers instead of merely focusing on the pattern of a single publisher. Only several attempts [2, 3] in the literature haven been proposed recently to detect such sophisticated attacks. They define the correlations between fraudsters from different perspectives and evaluate the effectiveness of their techniques using different measurements. Due to the lack of benchmarked dataset in the literature for coalition attacks, it is hard to compare the effectiveness of those different methods. Furthermore, more advanced techniques that identify the correlations from different perspectives should improve the detection rate of the coalition attacks.

Different metrics have been proposed for link prediction problems, such as Jaccard coefficient, Adamic, etc. To compare the effective of different metrics in our context, we simulate the generic mechanism of coalition attacks and generate a synthetic dataset. With the comparison of different metrics according to different parameters (e.g., number of the coalition groups, size the coalition groups, etc.), we propose a new metric to identify the correlation between different publishers from different perspectives. Finally, we develop a clustering algorithm to detect the coalition groups. The primary result indicates that the proposed technique overperforms those existing techniques in the literature. With the proposed technique, we compare the effectiveness of different detection techniques in the literature and develop a new algorithm to detect coalition attacks. With the motivation of real world problems in the online advertising, the result of this project will significantly reduce the cost on invalid traffic and improve the ROI (return of investment) for the industry.

References

- [1] http://techcrunch.com/2014/04/07/internet-ad-spend_to_reach_121b_in_2014-23-of-537b_total_ad-spend_ad-tech_gives-display_a_boost_over_search/. Last visited on 2014-11-11.
- [2] A. Metwally, D. Agrawal, and A. Abbadi, *DETECTIVES: DETEcting Coalition hit Inflation attacks in advertising networks streams*, in Proceedings International Conference on Software Engineering, 2007.
- [3] C. Kim, H. Miao, and K. Shima *CATCH: A detecting algorithm for coalition attacks of hit inflation in internet advertisings*, in Information Systems, Volume 36, Issue 8, December 2011, Pages 1105–1123.

Can We Do a Better Job in Ranking than BM25?

S. Wang¹, T. Feng², J. X. Huang³

¹ York University, Toronto, Canada, sarinaw@yorku.ca

² York University, Toronto, Canada, twade.feng@utoronto.ca

³ York University, Toronto, Canada, jhuang@yorku.ca

The probability model BM25 is a widely used ranking function for matching documents based on relevance to a search query. It scores documents based on term frequency, document frequency and document length. BM25 is considered to be the benchmark model for information retrieval, but has much room for improvements. Some of the drawbacks are its inability to determine the contextual relevance of query terms, the significance of query term locations in documents, and the effect of document length on retrieving relevant documents.

Several approaches have been taken to improve BM25. Proximity is a commonly explored approach that calculates the contextual relevance of term proximity using the top ranked documents. [1] Another method assumes that parts of a document such as the beginning are more important and therefore query terms in those locations receive more weight in the ranking function. [2] The relationship between document length and relevance is also further studied by applying various probability density functions to document length. [3]

In this talk, we will address some challenging issues with BM25 and provide some ideas to further improve the BM25 model. The objective is to develop a new technique that will produce more relevant and accurate ranking results than the BM25 model.

References

- [1] J. Zhao and J. X. Huang, *An enhanced context-sensitive proximity model for probabilistic information retrieval*, in *Proceedings of the 37th international ACM SIGIR conference on Research and development in Information Retrieval* (ACM), pp. 1131-1134 (2014).
- [2] J. Zhao, J. X. Huang, and S. Wu, *Rewarding term location information to enhance probabilistic information retrieval*, in *Proceedings of the 35th international ACM SIGIR conference on Research and development in Information Retrieval* (ACM), pp. 1137-1138 (2012).
- [3] X. Zhou, J. X. Huang, and B. He, *Enhancing ad-hoc relevance weighting using probability density estimation*, in *Proceedings of the 34th international ACM SIGIR conference on Research and development in Information Retrieval* (ACM). pp. 175-184 (2011).

Denoising-AutoEncoder with Modified Elliot Function and a Sparsity term.

H. Burhani¹, W. Feng¹

¹ Trent University, *{hashamburhani,wfeng}@trentu.ca*

Recent successes in the deep learning field have been attributed to early unsupervised layer wise pre-training algorithms. These algorithms helped deep architectures learn layer wise representations [2, 1], and more interestingly these unsupervised networks learned abstract features of its input. This was particularly clear in RBM models, but Denoising AutoEncoders were soon discovered to also learn similar features [5]. Since then, various new regularization methods have been discovered to help deep networks learn well; even without unsupervised pre-training. An interesting result of many of these regularization methods is the increased sparsity in the hidden layer representations of the networks they were applied on. For instance, dropout which has been explained to do well due to the averaging of thinned networks, it can also be seen as a sparse large network. This is especially evident when looking at the increased sparsity in hidden neuron activations of networks trained with dropout [4]. More traditional regularization methods have also focused on increasing sparsity. For instance L1 and L2 norm of the weights is a popular method not just in neural netwrks. Both L1 and L2 regularization prefer high sparsity in the weights of the neural network[3].

It can also be seen that the choice of activation functions will have major affects on convergence time and more importantly classification accuracy. Recently ReLU, or rectified linear units have been successfully implemented in various models. In light of new research, in this paper we introduce a model that uses a Denoising Autoencoder with a modified elliot function as a new activation. We also further enforce sparsity in the hidden layer by adding a log-penalty term of the hidden neuron activations to MSE. The model generates competing results when compared with the conventional sigmoidal and ReLU based models. We test this algorithm on image classification problems of MNIST and on document classification problem of newsgroup20. Two-layer networks with unconventionally small layer sizes of 200 are used to test the effectiveness of the model in small networks.

References

- [1] G. E. Hinton, S. Osindero, and Y.-W. Teh. A fast learning algorithm for deep belief nets. *Neural Comput.*, 18(7):1527–1554, July 2006.
- [2] H. Larochelle, Y. Bengio, J. Louradour, and P. Lamblin. Exploring strategies for training deep neural networks. *J. Mach. Learn. Res.*, 10:1–40, June 2009.
- [3] J. Rudy, W. Ding, D. J. Im, and G. W. Taylor. Neural network regularization via robust weight factorization. *CoRR*, abs/1412.6630, 2014.
- [4] N. Srivastava, G. Hinton, A. Krizhevsky, I. Sutskever, and R. Salakhutdinov. Dropout: A simple way to prevent neural networks from overfitting. *Journal of Machine Learning Research*, 15:1929–1958, 2014.
- [5] P. Vincent, H. Larochelle, Y. Bengio, and P.-A. Manzagol. Extracting and composing robust features with denoising autoencoders. pages 1096–1103, 2008.

Viral Information Propagation

J. McVittie¹, J. Wu²

¹ University of Toronto, Toronto, Canada, james.mcvittie@mail.utoronto.ca

² York University, Toronto, Canada, wujh@mathstat.yorku.ca

The analysis of social networks and the propagation of information has applications to the distribution of information within medical networks as well as the effective dispersal of emergency information to a large population. During this talk, we will be examining how a variant of an epidemiological SIR model can be used to accurately describe the diffusion of content over the online social network Digg.com. This system, found below, models the total number of individuals at time t that have become “susceptible” (S), “infected” (I) or have “recovered” (R) from a particular piece of online content [1].

$$S'(t) = -(\beta_0 e^{\alpha t} + c_0) I(t) \quad (1)$$

$$I'(t) = (\beta_0 e^{\alpha t} - \delta) I(t) \quad (2)$$

$$R'(t) = \sigma I(t) \quad (3)$$

where β_0 , c_0 , σ , $\delta = \sigma - c_0$ are positive constants with $c_0 < \sigma$ and α is a negative constant. Using this model, we will examine the qualitative properties of the viral information propagation model over the voting period of 50 hours. We will comment on particular properties such as peak time, turning point, viral period and final size (total number of votes) for particular online stories and we will show that this approach gives much improved prediction of user voting behaviour than other previously established models [2, 3].

References

- [1] M. Freeman, J. McVittie, I. Sivak, J. Wu, *Viral Information propagation in the Digg online social network*, Physica A. Vol. 415, pp. 87-94 (2014).
- [2] F. Wang, H. Wang, and K. Xu, *Diffusive logistic model towards predicting information diffusion in online social networks*, Proceedings of IEEE ICDCS Workshop on Peer-to-Peer Computing and Online Social Networking (HOTPOST), 2012.
- [3] F. Wang, H. Wang, K. Xu, J. Wu, and X. Jia, *Characterizing Information Diffusion in Online Social Networks with Linear Diffusive Model*, Proceedings of International Conference on Distributed Computing Systems (ICDCS), 2013.

Weighted integrative AICs criterion to perform model selection.

Y. Xu¹, X. Gao², S. Wang³, A. Wong⁴, J. Wu⁵

¹ Department of Mathematics and Statistics, York University, Toronto, Canada, yvonnexu@yorku.ca

² Department of Mathematics and Statistics, York University, Toronto, Canada, xingao@mathstat.yorku.ca

³ Department of Mathematics and Statistics, York University, Toronto, Canada, stevenw@mathstat.yorku.ca

⁴ Department of Mathematics and Statistics, York University, Toronto, Canada, august@yorku.ca

⁵ Laboratory for Industrial and Applied Mathematics, York University, Toronto, Canada, wujh@mathstat.yorku.ca

Models are essential in complex data analysis. Once a model has been established, various forms of inference, such as information extraction, model validation, risk assessment and prediction can be performed. Due to model uncertainty, a true model is often out of reach. Therefore, we have to choose an approximate model in order to conduct statistical inference. How to choose a suitable approximate model among a class of competing models by suitable model evaluation criteria becomes a crucial issue. Akaike's entropy information criterion (AIC) is one of the commonly used model evaluation criteria. AIC selects the best model based on information containing one single data set. However, information could come from multiple data sets that are too different to be merged into one. How to effectively perform model selection by integrating information from different data sets is the main focus of the talk.

We propose a weighted integrative AICs as a model evaluation criterion. This proposed method combines AICs across multiple data sets with different weights that minimize the variance of the integrative AICs. Simulation studies show that, in the context of variable selection, our method has the lowest false negative numbers and false detected numbers comparing with the individual test and the equal weights combining test.

References

- [1] H. Akaike. *Information theory as an extension of the maximum likelihood principle*. Second International Symposium on Information Theory (B. N. Petrov, and F. Csaki, Eds.) Akademiai Kiado, Budapest, (1973).
- [2] D.A.S. Fraser *Probability and Statistics: Theory and Applications* DAI, University of Toronto Bookstore, pp.382 (1976)
- [3] C. Varin and P. Vidoni *A Note on Composite Likelihood Inference and Model Selection*, Biometrika, 3:519-528, (2005).

SS-DDEMM Delay Differential Equations as Mathematical Models of Real World Phenomena

An SEI Model with Age-of-Infection and Immigration

Connell McCluskey

Wilfrid Laurier University, Waterloo, Canada
ccmcc8@gmail.com

We consider an SEI model of disease transmission with age-in-class structure for the exposed and infectious classes. The starting point for this is the model in [1]. To that, we add immigration of individuals into all three classes. In particular, we allow that individuals may enter the exposed or infectious classes, with a positive age-in-class. We get the following equations:

$$\begin{aligned} \frac{dS(t)}{dt} &= W_S - \mu_S S(t) - \int_0^\infty \beta(a) S(t) i(t, a) da \\ \frac{\partial e}{\partial t} + \frac{\partial e}{\partial a} &= W_e(a) - (\nu(a) + \mu_e(a)) e(t, a) \\ \frac{\partial i}{\partial t} + \frac{\partial i}{\partial a} &= W_i(a) - \mu_i(a) i(t, a), \end{aligned} \tag{1}$$

with boundary conditions

$$\begin{aligned} e(t, 0) &= \int_0^\infty \beta(a) S(t) i(t, a) da \\ i(t, 0) &= \int_0^\infty \nu(a) e(t, a) da \end{aligned} \tag{2}$$

for $t > 0$. The age-in-class specific immigration rates are given by $W_e(a)$ and $W_i(a)$; other terms are standard.

Due to the immigration of infected individuals, there is no disease-free equilibrium and hence there is no basic reproduction number. Elimination of the disease is impossible under the model assumptions. The only equilibrium is a unique endemic equilibrium.

By proving certain results on boundedness and asymptotic smoothness of the flow, we establish the existence of an attractor. Then, using a Lyapunov functional, we prove global asymptotic stability of the endemic equilibrium.

The model and its results are applicable to the analysis of an infectious disease within a single country or region. The model explicitly accounts for the fact that in the modern world all countries are connected and therefore disease is continually travelling across boundaries. We reach the conclusion that local control of a disease requires global action.

References

- [1] C. McCluskey, *Global stability for an SEI epidemiological model with continuous age-structure in the exposed and infectious classes*, Math. Biosci. Eng. **9**, pp. 819–841 (2012).

Delay Stochastic Models in Finance

A. Swishchuk¹

¹ University of Calgary, Calgary, Canada, aswish@ucalgary.ca

The volatility process is an important concept in financial modeling. This process can be stochastic or deterministic. In quantitative finance, we consider the volatility process to be stochastic as it allows to fit the observed market prices under consideration, as well as to model the risk linked with the future evolution of the volatility, which deterministic model cannot. Heston model [1], e.g., is one of the most popular stochastic volatility models in the industry as semi-closed formulas for vanilla option prices are available, few (five) parameters need to be calibrated, and it accounts for the mean-reverting feature of the volatility. In this talk we will focus on newly developed so-called delayed Heston [7] model that significantly improve classical Heston model with respect to the market volatility surface fitting by 44%. In this model, we take into account not only current state of volatility at time t but also its past history over some interval $[t - \tau, t]$, where $\tau > 0$ is a constant and is called the delay. In this way, our model incorporates path-dependent history for volatility. Significance of path-dependency (a.k.a. delay) may be seen from Figure 1 below: the price of variance swap crucially depends on delay, where we used S&P60 Canada Index as our real data. We will show how to model and price variance and volatility swaps (forward contracts on variance and volatility) for the delayed Heston model and how to hedge volatility swaps using variance swaps. Review of some other delay stochastic models in finance will be given as well (see [2, 3, 4, 5, 6]).



Figure 1: Dependence of variance swap price on delay and jump intensity for S&P60 Canada Index.

References

- [1] S. Heston, *A closed-form solution for options with stochastic volatility with applications to bond and currency options*, Review of Finan. Stud. **6**, 2, pp. 327-343 (1993).
- [2] Y. Kazmerchuk, A. Swishchuk and J. Wu, *A continuous-time GARCH model for stochastic volatility with delay*, Canadian Appl. Math. Quart. **13**, 2, pp. 123-150 (2005).
- [3] A. Swishchuk *Modeling and pricing of variance swaps for stochastic volatilities with delay*, Wilmott Magazine. **September Issue**, 2, pp. 64-72 (2005).
- [4] A. Swishchuk *Modeling and pricing of variance swaps for multi-factor stochastic volatilities with delay*, Canadian Appl. Math. Quart. **14**, 4, pp. 439-459 (2006).
- [5] A. Swishchuk and X. Li *Pricing variance swaps for stochastic volatilities with delay and jumps*, Intern. J. Stoch. Anal. **2011**, Article ID 435145, pp. 1-27 (2011).
- [6] A. Swishchuk and K. Malenfant *Variance swap for local L'evy-based stochastic volatility with delay*, Intern. Rev. Appl. Fin. Ass. Econ. **3**, 2, pp. 432-441 (2011).
- [7] A. Swishchuk and N. Vadòri *Smiling for the delayed volatility swaps*, Wilmott Magazine. **November Issue**, 4, pp. 1-12 (2014).

Distributed delays in a model of chemotherapy-induced myelosuppression

A. Rimbu¹, J. Bélair^{1,2}

¹ Université de Montréal, Montréal, Canada

² McGill University, Montreal, Canada

{rimbu,belair}@dms.umontreal.ca

Myelosuppression is a severe side effect of chemotherapy, to such an extent that for many clinical protocols, neutropenia is a dose-limiting component of the design. Friberg *et al.* [1] developed a pharmacokinetic-pharmacodynamic model that describes chemotherapy-induced myelosuppression using drug-specific and system-related parameters. Their model contains one compartment of proliferative cells, three transit compartments of maturing cells and one compartment of circulating observed blood cells. The drug concentration is assumed to stimulate cell loss following a function E_D yielding the modeling equations:

$$\begin{aligned}\frac{dx}{dt} &= k_p x (1 - E_D) (z_0/z)^\gamma - k_t x \\ \frac{dy_1}{dt} &= k_t (x - y_1) \\ \frac{dy_2}{dt} &= k_t (y_1 - y_2) \\ \frac{dy_3}{dt} &= k_t (y_2 - y_3) \\ \frac{dz}{dt} &= k_t y_3 - k_c z\end{aligned}$$

in which x represent the proliferative cells, y_i denote the maturing cells in one of the three subcompartments, z stand for the circulating cells and γ is a parameter adjusted to the data sets.

We consider two extensions of this model to better understand the influence of the structure of the transit compartments on the behaviour of the solutions, concentrating on the asymptotic stability of the equilibrium solution. We study first an arbitrary increase in the number of transit compartments, leading to a system that is well-known [2] to correspond to a distributed delay with a gamma distribution $g_{k_t}^n$,

$$\begin{aligned}\frac{dx}{dt} &= k_p x (1 - E_D) \left(\frac{z_0}{z} \right)^\gamma - k_t x \\ \frac{dz}{dt} &= k_t \int_0^\infty g_{k_t}^n x(t - \tau) d\tau - k_c z\end{aligned}$$

Secondly, we investigate a distributed delay in the form of a bimodal distribution and compare the relative destabilizing influence of these distribution of delays, as a function of the degree n of the gamma distributions. Our results suggest that the delta function (discrete delay) yields the smallest stability region in parameter space.

Supported by NSERC(Canada), FRQNT (Québec) and Université de Montréal

References

- [1] L.E. Friberg, A. Heningsson, H. Mass, L. Nguyen, and M.O. Karlsson. Model of Chemotherapy-Induced Myelosuppression With parameter Consistency Across Drugs. *J. Clinical Oncology*, **20**:4713–4721, 2002.
- [2] H. Smith *An Introduction to Delay Differential Equations with Applications to the Life Sciences*. Springer, New York, 2011.

Effect of treatment on the global dynamics of delayed pathological angiogenesis models

L. Berezansky¹, E. Braverman², L. Idels

¹ Ben-Gurion University of Negev, Beer-Sheva 84105, Israel, brznsky@cs.bgu.ac.il

² University of Calgary, 2500 University Dr. NW, Calgary, AB, Canada T2N1N4, maelena@ucalgary.ca

³ Dept. of Math, Vancouver Island University (VIU),

900 Fifth St. Nanaimo, BC, Canada V9S5J5, lev.idels@viu.ca

In 1971, J. Folkman has pioneered the hypothesis that tumor growth is angiogenesis-dependent and that inhibition of angiogenesis could be therapeutic, i.e. tumors fail to progress in the absence of angiogenesis. Pathological angiogenesis is the cause of more than 85% of cancer mortality. The following two-compartmental model for cancer cells and vascular endothelial cells was developed by P. Hahnfeldt et.al. in [1]

$$\frac{dx}{dt} = \alpha x(t) \ln \frac{K(t)}{x(t)}, \quad \frac{dK}{dt} = -\mu K(t) + S(x(t), K(t)) - I(x(t), K(t)) - a(t)K(t), \quad (1)$$

We study several cancer-induced angiogenesis models including

$$\begin{aligned} \frac{dx}{dt} &= \alpha x(t) \ln \left(\frac{K(t)}{x(t)} \right) - p_0 x(t), \\ \frac{dK}{dt} &= \beta x(t - h(t)) - \gamma K(t) - \delta x^{2/3}(t - g(t))K(t) - c_0 K(t). \end{aligned} \quad (2)$$

with the initial condition

$$x(t) = \varphi(t), \quad t \leq 0, \quad K(0) = K_0. \quad (3)$$

An example of the results obtained is

Theorem 1. Assume that $\lim_{t \rightarrow \infty} (t - h(t)) = \lim_{t \rightarrow \infty} (t - g(t)) = \infty$, and $\theta := \frac{\beta e^{-p_0/\alpha}}{\gamma + c_0} < 1$. Then a solution of problem (2),(3) converges to zero. If in addition $h(t) \leq \sigma$, $t \geq 0$ then for any initial conditions (3) there exist $C_1 > 0$ and $C_2 > 0$ such that $|x(t)| \leq C_1 e^{-mt}$, $|K(t)| \leq C_2 e^{-mt}$, where $m = -\frac{1}{2\sigma} \ln \left(\mu + (1-\mu)e^{-\sigma(\gamma+c_0)} \right)$, $\mu := \theta^{1-e^{-\alpha\sigma}} < 1$.

In addition to continuous treatment (corresponding to the terms $p_0 x(t)$ and $c_0 K(t)$), we consider the impulsive treatment

$$x(\tau_j^+) = d_j x(\tau_j), \quad K(\tau_j^+) = D_j K(\tau_j), \quad j = 1, 2, \dots,$$

where $0 = \tau_0 < \tau_1 < \dots < \tau_n < \tau_{n+1} < \dots$ are treatment times satisfying $\lim_{n \rightarrow \infty} \tau_n = \infty$, $0 < d_j \leq 1$, $0 < D_j \leq 1$.

The talk is based on the results recently published in [2].

References

- [1] P. Hahnfeldt, D. Panigraphy, J. Folkman and L. Hlatky, *Tumor development under angiogenic signaling: a dynamical theory of tumor growth, treatment response, and postvascular dormancy*, Cancer Res. **59** 4770–4775 (1999).
- [2] L. Berezansky, E. Braverman and L. Idels, *Effect of treatment on the global dynamics of delayed pathological angiogenesis models*, J. Theoret. Biol. **363**, C, 13–21 (2014).

Existence and stability of hybrid systems with time delay

Xinzhi Liu

University of Waterloo, Waterloo, Canada, xzliu@uwaterloo.ca

There has been a growing interest in hybrid dynamical systems in recent years. Such systems often undergo vector field switching and/or state jumps due to sudden changes in model characteristics. Hybrid dynamical systems arise from a wide variety of applications such as switching circuits in power electronics, mechanical systems subject to impacts, multimedia switching communication networks, orbital transfer of space crafts. This talk will discuss some of the recent results on existence, stability and control of hybrid dynamical systems with time delays.

Investigating the impact of pharmacokinetic variability on physiological models with delays: A case study of neutrophil development, zalypsis, and filgrastim.

M. Craig¹, M. Gonzalez-Sales², A.R. Humphries³, J. Bélair⁴, J. Li⁵, M.C. Mackey⁶, F. Nekka⁷

¹ Université de Montréal, Montréal, Canada, morgan.craig@umontreal.ca

² Université de Montréal, Montréal, Canada, mario.gonzalez.sales@umontreal.ca

³ McGill University, Montréal, Canada, tony.humphries@mcgill.ca

⁴ Université de Montréal, Montréal, Canada, belair@dms.umontreal.ca

⁵ Université de Montréal, Montréal, Canada, li@crm.umontreal.ca

⁶ McGill University, Montréal, Canada, michael.mackey@mcgill.ca

⁷ Université de Montréal, Montréal, Canada, fahima.nekka@umontreal.ca

The development of chemotherapeutic treatments in oncological settings has greatly improved the outcome of those diagnosed with cancer. While anti-cancer drug therapy is increasingly successful at stemming the spread of cancer cells within the body, its undesired effects upon other cells limits patients' tolerance to the medications. A common side-effect of chemotherapy drugs is neutropenia, or low neutrophil counts, leaving the body particularly susceptible to infections. Accordingly, mathematical modelling of the hematopoietic system with a focus on neutrophil development can help to answer important questions about chemotherapy administration. Beyond the oncological setting, neutrophils are particularly well-suited to mathematical study because of their multi-phasic development in the bone marrow. Further, they are implicated in oscillatory, congenital diseases the origins of which are still not well understood. As such, having a model to describe neutrophil dynamics is a valuable tool to not only address a multitude of pathology scenarios but to motivate and/or eliminate hypotheses related to the basic physiology of the system. Building from the models of [1] and [3], we developed a three-dimensional system of delay differential equations (DDEs) with variable aging rate which was derived from an age-structured PDE model of neutrophil development. This model was shown to reproduce clinical data of periodic chemotherapy administered with a recombinant human (rh) form of granulocyte colony-stimulating factor (G-CSF), a myelostimulative hormone of which the exogenous form is administered during chemotherapy to bolster neutrophil counts. We then used the model to determine optimal dosing regimens of rhG-CSF during 14-day periodic chemotherapy treatment [2]. This was accomplished by combining the physiological model of neutrophil development with pharmacokinetic and pharmacodynamic (PKPD) models of a chemotherapeutic drug (Zalypsis) and rhG-CSF (filgrastim).

In [2] and our previous studies, no interindividual variability (IIV) was included in the analysis even though between subject variability is an important issue in the physiological and pharmacometric (PKPD) domains, owing to the complexity of the human organism. In this talk, I will begin by detailing the previously mentioned physiological model and briefly highlighting the rhG-CSF dose optimisation. I will then demonstrate that the impact of IIV on physiological models is not a significant consideration when the PKs of a drug are short-lived in comparison to their PDs (as is the case of Zalypsis and filgrastim).

References

- [1] G. Brooks, G.P. Langlois, J. Lei, and M.C. Mackey. *Neutrophil dynamics after chemotherapy and G-CSF: The role of pharmacokinetics in shaping the response.*, Journal of Theoretical Biology **315**, pp. 97-109 (2012).
- [2] M. Craig, A.R. Humphries, J. Bélair, J. Li, F. Nekka, M.C. Mackey *Neutrophil dynamics during concurrent chemotherapy and G-CSF administration: Mathematical modelling guides dose optimisation to minimise neutropenia*, Journal of Theoretical Biology **Under review-JTB-D-14-00842R1**, (2012).
- [3] C. Foley and M.C. Mackey. *Mathematical model for G-CSF administration after chemotherapy.*, Journal of Theoretical Biology **257**, pp. 27-44 (2009).

Modelling virus dynamics with both virus-to-cell infection and cell-to-cell transmission by a DDE system

Xiulan Lai¹, Xingfu Zou²

¹ Renmin University of China, Beijing, China xiulanlai@ruc.edu.cn

² University of Western Ontario, London, Canada, xzou@uwo.ca

Direct cell-to-cell transfer of HIV-1 is found to be a more potent and efficient means of virus propagation than virus-to-cell infection. In this talk, I present a mathematical model to consider these two modes of viral infection and spread, in which infection age is also incorporated. By a rigorous analysis of the model, I show that the model demonstrates a global threshold dynamics, fully described by the basic reproduction number, which is identified explicitly. The formula for the basic reproduction number of our model reveals that the basic reproduction number of a model that neglects either cell-to-cell spread or virus-to-cell infection might be underevaluated

Oscillations and driving mechanism in models of West Nile virus with time delay

Huaiping Zhu

LAMPS and Department of Mathematics and Statistics, York University, Canada
huaiping@mathstat.yorku.ca

West Nile virus is a typical vector-borne disease which is transmitted to humans or other animals by culex mosquitoes. For the virus, avian birds serve as amplification hosts, yet vector mosquitoes play a critical role in the transmission and spread of the virus. To investigate the role of vector mosquitoes and the transmission dynamics of West Nile virus, I will present two models of delay differential equations with different demographics and similar standard incidence functions for vector mosquitoes and host birds. Bifurcation and dynamics analysis suggest that the incidental interaction between mosquitoes and birds would not cause sustainable oscillations (multiple peaks) in the model systems, only the population of vector mosquitoes is the fundamental driving factor for the oscillation in disease transmission when consider the impact of temperature. This talk is based on two papers in the reference.

References

- [1] Guihong Fan, Huaiping Zhu *Oscillation and driving mechanism in a model of West Nile virus with time delay.*, To appear in Journal of Dynamics and Differential Equations.
- [2] Weihua Jiang, Guihua Li, Yonghui Xia and Huaiping Zhu., *The effect of temperature on a vector-borne disease model: via stability and bifurcation analysis of a model with time delay.* Preprint.

Periodic Solutions of a Singular Delay Differential Equation

A.F. Ivanov¹, Z.A. Dzalilov²

¹ Pennsylvania State University, Lehman, USA, aivanov@psu.edu

² CIAO, Federation University Australia, Ballarat, Australia, z.dzalilov@federation.edu.au

Scalar delay differential equation of the form

$$\varepsilon x'(t) = -x(t) + f(x(t-1)), \quad \varepsilon > 0 \quad (1)$$

appears in a wide variety of applications in physics, mathematical biology, engineering, and other fields (see e.g. [1, 2] and further references therein). It also results as an exact reduction of nonlinear boundary value problems for hyperbolic partial differential equations modelling various wave phenomena [2].

We study problems of existence and asymptotic shape of periodic solutions of equation (1), in particular as $\varepsilon \rightarrow 0+$. The limit case $\varepsilon = 0$ formally results in a continuous time difference equation of the form

$$x(t) = f(x(t-1)), \quad (2)$$

which dynamical properties are largely determined by the one-dimensional dynamical system $x \mapsto f(x)$ [2]. Further connections between equations (1) and (2) are established for small values of ε . Several particular cases of the nonlinearity f appearing in specific applications are considered and treated in detail. Theoretical considerations and results are supported by numerical simulations.

References

- [1] A.F. Ivanov and A.N. Sharkovsky, *Oscillations in singularly perturbed delay equations*, Dynamics Reported (New Series) **1**, pp. 165-224 (1991).
- [2] A.N. Sharkovsky, Yu.L. Maistrenko, and E.Yu. Romanenko, *Difference Equations and Their Perturbations*, Kluwer Academic Publishers **250**, 1993, 358 pp.

Phase models and clustering in networks of oscillators with delayed, all-to-all coupling

Zhen Wang¹, S.A. Campbell²

¹ Department of Applied Mathematics, University of Waterloo, Canada., zhen.wang@uwaterloo.ca

² Department of Applied Mathematics and Centre for Theoretical Neuroscience, University of Waterloo, Canada,
sacampbe@uwaterloo.ca

We consider a general model for a network of global coupled oscillators with time-delayed connections. We reduce the system of delay differential equations to a phase model where the time delay enters as a phase shift. By analyzing the phase model, we study the existence and stability of cluster solutions. These are solutions where the oscillators divide into groups; oscillators within a group are fully synchronized, while oscillators in different groups are phase-locked with a fixed phase difference. Finally, analytical results are compared with numerical studies of the full system of delay differential equations.

Post-Newtonian Gravitation

Erik I. Verriest¹,

¹ Georgia Institute of Technology
 Atlanta, GA 30332-0250, USA, erik.verriest@ece.gatech.edu

The *retarded potentials* appearing in electrodynamics [1] lead to a system with state dependent delay. Analogously, Newton's law of gravitation may be generalized. We assume that at time t' the mass distribution is represented by a scalar density field $\rho(\vec{r}', t')$. As this requires a notion of simultaneity, it can only lead to an approximation of the theory of relativity. We postulate that this density field generates a gravitational field, which assumes at a fixed position \vec{r} and time t the value due to the superposition of the fields of all infinitesimal contributions. Because of propagation at speed c , only the past value, $\rho(\vec{r}', t - \tau(\vec{r}'))$, will contribute to the field at \vec{r} at time t . The following will be approximately valid for weak fields and small speeds relative to c , the speed of light. **Assumption:** Given the time varying mass density $\rho(\vec{r}', t')$, the gravitational potential at a fixed point \vec{r} and time t is given by the linear superposition

$$\phi(\vec{r}, t) = G \int_{\mathbb{R}^3} \frac{\rho(\vec{r}', t - \tau(\vec{r}'))}{|\vec{r} - \vec{r}'|} dV(\vec{r}'), \quad (1)$$

where G is the gravitational constant. This equation is coupled with

$$c\tau(\vec{r}') = |\vec{r} - \vec{r}'|. \quad (2)$$

For a unit point mass in motion, prescribed by its trajectory, $\vec{r}_p(t)$, the gravitational potential is shown to be

$$\phi(\vec{r}, t) = \frac{G}{|\vec{r} - \vec{r}_p(t_b)| \left| 1 - \frac{(\vec{r} - \vec{r}'_p(t_b))^\top \dot{\vec{r}}_p(t_b)}{c|\vec{r} - \vec{r}_p(t_b)|} \right|}. \quad (3)$$

We investigate the rectilinear motion of two equal masses due to separation of a single mass point. This leads to coupled equations

$$\ddot{x}(t) = -\frac{Gm}{\left(1 + \frac{\dot{x}(t-\tau(t))}{c}\right)c^2\tau^2(t)} \quad (4)$$

$$c\tau(t) = x(t) + x(t - \tau(t)). \quad (5)$$

Lagrange's inversion technique and a perturbation expansion [2] shed light on the solution, and the effect on the escape velocity is discussed. We show also that the simple use of truncated Taylor expansions in terms of the instantaneous delay do not yield solutions that are consistent with the Newtonian limit.

References

- [1] G.S. Smith, *An Introduction to Classical Electromagnetic Radiation*, Cambridge University Press, (1997).
- [2] E.I. Verriest, *Inversion of State Dependent Delay*, in Recent Results on Nonlinear Delay Control Systems, I. Karafyllis, M. Malisoff, F. Mazenc, and P. Pepe (Eds.), Springer-Verlag, 2014.

Transmission Dynamics of Multiple Species of Malaria Parasites with Time Delay

Matthias Ngwa¹, Ephraim Agyingi², Tamas Wiandt³

¹*Rochester Institute of Technology, Rochester, USA, mxnsma@rit.edu*

²*Rochester Institute of Technology, Rochester, USA, eoasma@rit.edu*

³*Rochester Institute of Technology, Rochester, USA, tiwsma@rit.edu*

We present a model for the transmission dynamics of multiple species of malaria parasites in a community using delay differential equations. The population of the community serves as the incidental host. The model is based on the assumption that there is no immunity to the disease. The reproduction number of the model is constructed and used as a threshold parameter to study the persistence or extinction of a species. Numerical computations that confirm the analytical results are provided.

Zero-Hopf Bifurcation in the Van der Pol Oscillator with Delayed Feedback

J. Bramburger¹, B. Dionne², V. G. LeBlanc³

¹ University of Ottawa, Ottawa, Canada, jbram084@uottawa.ca

² University of Ottawa, Ottawa, Canada, bdionne@uottawa.ca

³ University of Ottawa, Ottawa, Canada, vleblanc@uottawa.ca

The classical Van der Pol oscillator is one of the most well-studied paradigms for nonlinear oscillators. It originated as a model for an electrical circuit with a triode valve, but today has applications in almost every area of the physical sciences. Wei and Jiang [2] studied the general case of a delayed position feedback forcing of the oscillator

$$\ddot{x}(t) + \epsilon(x^2(t) - 1)\dot{x}(t) + x(t) = g(x(t - \tau)), \quad (1)$$

where $\epsilon > 0$ is a parameter, $\tau > 0$ is a delay and g is an arbitrary forcing function. It was shown that under certain conditions, single-, double- and triple-zero eigenvalues were possible as well as a purely imaginary pair with a zero eigenvalue.

In this talk, we consider the more general case of a feedback forcing, which is dependent on both delayed position and delayed velocity

$$\ddot{x}(t) + \epsilon(x^2(t) - 1)\dot{x}(t) + x(t) = g(x(t - \tau), \dot{x}(t - \tau)), \quad (2)$$

and work to understand its dynamics. We find that under certain conditions, the linearization about $x(t) = 0$ of equation (2) can have single-, double-, triple-, and now quadruple-zero eigenvalues as well as a purely imaginary pair with a zero eigenvalue. Using Faria and Magalhaes's methods of normal form reduction on the centre manifold [1], we study the complete unfolding of the Zero-Hopf bifurcation in the delayed oscillator. We compare and contrast our results with the results found for Wei and Jaing's system to fully understand how the additional delayed forcing effects the dynamics near the singularity.

A particularly unique aspect to our work is that we numerically project the solutions onto the centre manifold allowing us to draw a connection between the dynamics of the given delay-differential equation near the singularity and the three-dimensional phase portraits given for the Zero-Hopf bifurcation. To the best our knowledge this undertaking is unique to our work, giving the audience a unique perspective on the relationship between delay equations and their ordinary differential equation counterparts.

References

- [1] T. Faria and L. T. Magalhaes, *Normal forms for retarded functional differential equations and applications to Bogdanov-Takens singularity*, J Differ. Equ. 122, pp. 201-224 (1995).
- [2] J. Wei and W. Jaing, *Stability and bifurcation analysis in Van der Pol's oscillator with delayed feedback*, J. Sound Vib. 283, pp. 801-819 (2005).

SS-DDMDS Data-Driven Methods for Dynamical Systems

Analog Forecasting with Dynamics-Adapted Kernels

Z. Zhao¹, D. Giannakis²

¹ Courant Institute of Mathematical Sciences, NYU, USA, jzhao@cims.nyu.edu

² Courant Institute of Mathematical Sciences, NYU, USA, dimitris@cims.nyu.edu

Analog forecasting is a non-parametric technique introduced by Lorenz in 1969 [1] which predicts the evolution of states of a dynamical system (or observables defined on the states) by following the evolution of the sample in a historical record of observations which most closely resembles the current initial data. Here, we introduce a suite of forecasting methods which improve traditional analog forecasting by combining ideas from state-space reconstruction for dynamical systems and kernel methods developed in harmonic analysis and machine learning. The first improvement is to augment the dimension of the initial data using Takens' delay-coordinate maps to recover information in the initial data lost through partial observations. Then, instead of using Euclidean distances between the states, weighted ensembles of analogs are constructed according to similarity kernels in delay-coordinate space, featuring an explicit dependence on the dynamical vector field generating the data [2]. The eigenvalues and eigenfunctions of associated kernel operators define diffusion coordinates and diffusion distances [3] on the data manifold, improving the identification of skillful analogs compared to the Euclidean distance. Moreover, forecasts based on kernel-weighted ensembles have significantly higher skill than the conventional approach following a single analog. We discuss alternative approaches for kernel-weighted ensemble forecasting based on the Nyström method for out-of-sample extension of functions, as well as multiscale methods based on Laplacian pyramids [4]. We illustrate these techniques in applications to forecasting in a low-order deterministic model for atmospheric dynamics with chaotic metastability, and interannual-scale forecasting in the North Pacific sector of a comprehensive climate model [5].

References

- [1] E. N. Lorenz, *Atmosphere predictability as revealed by naturally occurring analogues*, J. Atmos. Sci., **26**, pp. 636-646 (1969).
- [2] D. Giannakis, *Dynamics-adapted cone kernels*, SIAM. J. Appl. Dyn., accepted (2014).
- [3] R. R. Coifman and S. Lafon, *Diffusion maps*, Appl. Comput. Harmon. Anal., **21**, pp. 5-30 (2006).
- [4] N. Rabin and R. R. Coifman *Heterogeneous datasets representation and learning using diffusion maps and Laplacian pyramids*, in *12th SIAM International Conference on Data Mining*, pp. 189-199 (2012).
- [5] Z. Zhao and D. Giannakis, *Analog forecasting with dynamics-adapted kernels*, submitted (2014).

Data-driven forecasting without a model and with a partially known model

T. Berry¹, J. Harlim¹, D. Giannakis²

¹ Pennsylvania State University, University Park, PA, USA, thb11@psu.edu

² Courant Institute of Mathematical Sciences, New York University, New York, NY, USA

Nonparametric forecasts based on local linearization of the shift map using a training data set were originally developed for low-dimensional chaotic systems. In this research, jointly developed with Dimitris Giannakis and John Harlim, we make a rigorous connection between the shift map and the forward operator for ergodic stochastic differential equations on manifolds. Estimating the forward operator gives us the ability to forecast full probability densities, and by representing these densities in a basis of smooth functions the forward operator becomes a matrix. We show that the diffusion maps algorithm approximates the optimal basis for representing the forward operator. However, the curse-of-dimensionality continues to restrict this nonparametric model to low-dimensional systems. To address this issue we introduce two methods of lifting the nonparametric approach to high-dimensional problems. In the first case, we assume that we have no knowledge of the model, but that we know the spatial structure of the data, allowing us to decompose the dynamics into Fourier modes for which nonparametric models can be built. In the second case, we assume that a partial model is available, and that the unknown ‘model error’ is low-dimensional in an appropriate sense. We show that it is possible to extract and learn the unknown component of the model resulting in significantly improved forecasting.

Data-driven Reduction for Multiscale Stochastic Dynamical Systems

C. J. Dsilva¹, R. Talmon², C. W. Gear¹, R. R. Coifman³, I. G. Kevrekidis¹

¹ Princeton University, Princeton, New Jersey, USA

² Technion - Israel Institute of Technology, Israel

³ Yale University, New Haven, Connecticut, USA

Dynamical systems often contain several disparate time scales. This typically poses problems for analysis, modeling and simulation, as the dynamical modes are highly coupled, and therefore, resolving all relevant scales is computationally challenging. Reducing the model to only contain the slow modes is often based on *a priori* knowledge or analytic transformations of the variables [1, 2], which may not be explicitly given or immediately obvious for complex systems.

To automatically uncover the slow variables from data, we present a manifold-learning based approach, which is specifically designed to accommodate nonlinear structures in high-dimensional data. In manifold learning, the key idea is to define a notion of similarity between data points, and then, to integrate the similarities into a global parametrization of the data through the solution of an eigenvector problem [3, 4]. Standard “off-the-shelf” manifold learning techniques, which typically utilize the Euclidean distance, are not appropriate for analyzing data from multiscale dynamical systems, since the Euclidean distance does not account for the underlying dynamics or the multiple time scales. Recently, research effort has been dedicated to constructing more informative distance metrics, which are less sensitive to noise, can encode dynamics, and can better recover the true underlying structure in the data by suppressing the additional structures arising from unimportant sources of variability, e.g. [5, 6]. In particular, it was shown in [5] that a metric based on the Mahalanobis distance can remove the effect of observing data through a nonlinear function.

In this work, we show the analogy between inverting nonlinear observation functions used in the context of data analysis [5], and reducing dynamical systems by removing the effects of the fast variables. Our method builds a parameterization of the data which is consistent with the slow variables. Because the proposed method is data-driven, no explicit description of the model is required, and it can extract the underlying slow variables from either simulation or experimental data, even when the fast and slow variables are nonlinearly coupled. Furthermore, it implicitly identifies the slow variables within the data and does not require any *a priori* knowledge of the fast or slow sources. We will present analysis for our method and provide conditions under which it attains successful recovery of the slow variables. In addition, we will show how to utilize data to set the parameters of our method appropriately.

References

- [1] V. Sotiropoulos, M. N. Contou-Carrere, P. Daoutidis, and Y. N. Kaznessis, *Model reduction of multiscale chemical langevin equations: a numerical case study*, IEEE/ACM Trans. Computational Biology and Bioinformatics **6**, 3, pp. 470-482 (2009).
- [2] M. Bruna, S. J. Chapman, and M. J. Smith, *Model reduction for slow-fast stochastic systems with metastable behaviour*, The Journal of Chemical Physics **140**, 7, 174107 (2014).
- [3] M. Belkin, and P. Niyogi, *Laplacian eigenmaps for dimensionality reduction and data representation*, Neural Computation, **15**, 6, pp. 1373-1396 (2003).
- [4] R. R. Coifman, and S. Lafon, *Diffusion maps*, Applied Comput. Harmon. Anal., **21**, 1, pp. , 5-30 (2006).
- [5] A. Singer, and R. R. Coifman, *Non-linear independent component analysis with diffusion maps*, Applied Comput. Harmon. Anal., **25**, 2, pp. 226-239 (2008).
- [6] D. Giannakis, and A. J. Majda, *Nonlinear Laplacian spectral analysis for time series with intermittency and low-frequency variability*, Proc. Natl. Acad. Sci., **109**, 7, pp. , 2222 (2012).

Geometric Methods for the Approximation of High-dimensional Dynamical Systems

M. Maggioni, M. Crosskey

Duke University, U.S.A., *{mauro.maggioni,miles.crosskey}@duke.edu*

We discuss a geometry-based statistical learning framework for performing model reduction and modeling of stochastic high-dimensional dynamical systems. We consider two complementary settings. In the first one, we are given long trajectories of a system, e.g. from molecular dynamics, and we discuss new techniques for estimating, in a robust fashion, an effective number of degrees of freedom of the system, which may vary in the state space of the system, and a local scale where the dynamics is well-approximated by a reduced dynamics with a small number of degrees of freedom. We then use these ideas to produce an approximation to the generator of the system and obtain, via eigenfunctions, reaction coordinates for the system that capture the large time behavior of the dynamics. We present various examples from molecular dynamics illustrating these ideas. In the second setting we only have access to a (large number of expensive) simulators that can return short simulations of high-dimensional stochastic system, and introduce a novel statistical learning framework for learning automatically a family of local approximations to the system, that can be (automatically) pieced together to form a fast global reduced model for the system, called ATLAS. ATLAS is guaranteed to be accurate (in the sense of producing stochastic paths whose distribution is close to that of paths generated by the original system) not only at small time scales, but also at large time scales, under suitable assumptions on the dynamics. We discuss applications to homogenization of rough diffusions in low and high dimensions, as well as relatively simple systems with separations of time scales, and deterministic chaotic systems in high-dimensions, that are well-approximated by stochastic differential equations.

References

- [1] M. Crosskey and M. Maggioni *ATLAS: A geometric approach to learning high-dimensional stochastic systems near manifolds*, arXiv:1404.0667, submitted, 2014.

High Order Kernels for Data Extensions

N. Rabin¹, D. Fishelov²

¹ Afeka - Tel Aviv Academic College of Engineering, Israel, {netar}@afeka.ac.il

² Afeka - Tel Aviv Academic College of Engineering, Israel, {daliaf}@afeka.ac.il

Kernel based dimensionality reduction techniques, such as Diffusion Maps [1], have become a common tool for modeling high dimensional datasets. The main advantage of these methods is that the resulting low dimensional representation preserves important features of the data, such as the geometry of the original set. Typically, the low dimensional embedding representation is constructed from a given training set. The embedding coordinates, which capture the underlying process that drives the data, are then used for evaluating a continuous or a discrete function on the data. The next step is to extend the embedding coordinates for evaluating the function on the new data points.

In some applications there is a need to lift embedded data back to the ambient space. Since the dimensionality reduction technique is not linear, there is no natural procedure for inverting data from the low dimensional coordinates back into the original space. A number of papers address this problem. In [2] the authors proposed a Gaussian-based point-wise adaptive approach, which requires adjustment of the kernel width for every particular point. Recently, in [3], a scale-free radial basis function approach was proposed. The latter uses cubic interpolation for inverting Diffusion Maps to synthesize new points in the ambient space. An multi-scale high-order approach was suggested in [4, 5]. This method requires several iterations in order to relax the error.

In this work we propose a kernel, to be used within the Nyström framework, for lifting embedded data and for extending multi-scale functions for data regression. We construct high-order kernels that satisfy several moments conditions and then convolve these kernels with the embedded data. As a result one obtains a higher order (fourth or sixth order) approximations to the extended functions. In particular, the proposed kernels manage to better capture a multi-scale structure in cases where the target function contains several scales. This is compared to the standard Gaussian kernel, which is second order accurate and therefore it has a limited ability to capture multi-scale phenomena.

We demonstrate the efficiency of the newly proposed method on several datasets for extending and lifting the embedded data back to the ambient space. The results are compared to the standard second order Gaussian kernel. The higher-order kernels represent more accurately the geometry of the target functions and the ambient space, thus the errors committed in the lifting procedure are reduced.

References

- [1] R. R. Coifman and S. Lafon, *Diffusion Maps*, Applied and Computational Harmonic Analysis: Special issue on Diffusion Maps and Wavelets, **21**, pp. 5-30 (2006).
- [2] S.M. Buchman and A.B. Lee and C.M. Schafer, *High-dimensional Density Estimation via SCA: An Example in the Modelling of Hurricane Tracks*, in *Statistical Methodology*, **8**, pp. 18-30 (2011).
- [3] N.D. Monnig and B. Fornberg and F.G. Meyer, *Inverting nonlinear dimensionality reduction with scale-free radial basis function interpolation*, in *Applied and Computational Harmonic Analysis*, pp. 162-170 (2014).
- [4] N. Rabin and R.R. Coifman, *Heterogeneous Datasets Representation and Learning using Diffusion Maps and Laplacian Pyramids*, in *Proceedings of the 12th SIAM International Conference on Data Mining (SDM-2012)*, Anaheim, CA, USA, pp. 189-199 (2012).
- [5] Á. Fernández, N. Rabin, D. Fishelov, J. R. Dorronsoro, *Auto-adaptative Laplacian Pyramids for High-dimensional Data Analysis*, arXiv preprint arXiv:1311.6594.

Nonparametric Uncertainty Quantification Methods for Gradient Flows with Isotropic Diffusions

J. Harlim¹, T. Berry².

¹ Dept. of Mathematics and Dept. of Meteorology, The Pennsylvania State University, USA, jharlim@psu.edu

² Dept. of Mathematics, The Pennsylvania State University, USA, thb11@psu.edu

This talk presents a nonparametric statistical modeling method for quantifying uncertainty in stochastic gradient systems with isotropic diffusion. The central idea is to apply the diffusion maps algorithm on a training data set to produce a stochastic matrix whose generator is a discrete approximation to the backward Kolmogorov operator of the underlying dynamics. The eigenvectors of this stochastic matrix, which we will refer to as the diffusion coordinates, are discrete approximations to the eigenfunctions of the Kolmogorov operator and form an orthonormal basis for functions defined on the data set.

Using this basis, we consider representing three uncertainty quantification (UQ) problems (prediction, filtering, and response) into the diffusion coordinates. In these coordinates, the nonlinear prediction and response problems reduce to solving systems of infinite-dimensional linear ordinary differential equations. Similarly, the continuous-time nonlinear filtering problem reduces to solving a system of infinite-dimensional linear stochastic differential equations. Solving the UQ problems then reduces to solving the corresponding truncated linear systems in finitely many diffusion coordinates. By solving these systems we give a model-free algorithm for UQ on gradient flow systems with isotropic diffusion.

References

- [1] T. Berry and J. Harlim, *Variable Bandwidth Diffusion Kernels*, Appl. Comput. Harmon. Anal. (in press).
- [2] T. Berry and J. Harlim, *Nonparametric Uncertainty Quantification for Stochastic Gradient Flows*, SIAM/ASA J. of Uncertainty Quantification (under reviewed).

Spectral clustering with local scaling

T. Berry¹, T. Sauer²,

¹ Penn State University thb11@psu.edu

² George Mason University tsauer@gmu.edu

Methods depending on diffusion dynamics have developed into convenient approaches for the solution of general clustering problems. When the clusters represent connected components, for example, it is important to reproduce the Laplace-Beltrami operator of the manifold of points as closely as possible. Since the zero-eigenspace of this operator is isomorphic to the zero-homology of the manifold containing the points, a basis for the eigenspace exists in terms of indicator functions of the clusters, and the latter can be extracted from the eigenvalue computation.

The theory of diffusion maps due to Coifman and collaborators shows one way to reproduce the Laplace-Beltrami operator. Based on this work, we developed a more general category of “local” kernels whose diffusion operators also can be used for the same purpose. While a wide variety of local kernels construct discrete operators that converge to the Laplace-Beltrami operator in the limit of large data, some converge faster than others when densities vary throughout the point set and data is sparse. In particular, we find that variable-bandwidth kernels are superior to fixed-bandwidth diffusion operators for general clustering problems. In addition, we discuss a simplified approach to the final “unmixing” step in spectral clustering where the indicator functions of individual clusters are located in the zero-eigenspace of the operator.

Timescale Separation and Forecasting with Dynamics-Adapted Kernels

D. Giannakis¹

¹ New York University, New York, USA, dimitris@cims.nyu.edu

We discuss methods for extracting intrinsic timescales of dynamical systems and nonparametric forecasting based on a family of kernels for analysis of time-ordered data. These so-called cone kernels feature a dependence on the dynamical vector field operating in the phase-space manifold (the generator of the dynamics), estimated empirically through temporal finite differences of the data. In particular, cone kernels assign strong affinity to pairs of samples whose relative displacement vector lies within a narrow cone aligned with the dynamical vector field. The outcome of this explicit dependence on the dynamics is that, in a suitable asymptotic limit, the diffusion operators for data analysis constructed from cone kernels generate diffusions along the integral curves of the dynamical vector field. This property is independent of the observation modality, and endows these operators with invariance under a weakly restrictive class of transformations of the data (including conformal transformations), while it also enhances their capability to extract intrinsic dynamical timescales via eigenfunctions. We discuss these features with reference to the Riemannian geometry induced on the data by cone kernels. We find that the corresponding Dirichlet energy is governed by the directional derivative of functions along the dynamical vector field, giving rise to a measure of roughness of functions that favors slowly-varying observables. We present applications in toy dynamical systems and comprehensive climate models. We also discuss applications of these kernels in non-parametric forecasting.

References

- [1] D. Giannakis, *Dynamics-adapted cone kernel*, SIAM. J. Appl. Dyn. Sys. In press (2015).

Variable –Free and Equation-Free Computation

Yannis G. Kevrekidis,

CBE and PACM, Princeton University, USA

I will discuss the interplay of data mining (through manifold learning techniques, and, in particular, diffusion maps) with equation-free computation for complex/multiscale systems. Macroscopic computational tasks for fine-scale simulators (e.g. MD or MC ones) can be accelerated through the design and processing of the results of brief bursts of appropriately initialized fine scale simulation (the equation-free approach). The task is assisted by the detection of good coarse observables (coarse variables) in terms of which the macroscopic dynamics can be modeled (the variable-free component) through data mining. Computational issues arising in linking these two components will be discussed and illustrated.

Objective coordinate change for anisotropic covariance modelling in high dimension

O. Pannekoucke^{1,2}, E. Emili¹, O. Thual^{1,3}

¹ CERFACS/CNRS URA 1875, Toulouse, France, olivier.pannekoucke@cerfacs.fr

² CNRM/GAME, Météo-France/CNRS UMR 3589, Toulouse, France,

³ Université de Toulouse, INPT, CNRS, IMFT, Toulouse, France

Covariance modelling in high-dimension is one of the most challenging issue in geophysical data-assimilation. The goal is to produce covariance model able to represent spatial variation of correlation functions over the Earth.

Among existing covariance models, the use of a coordinate change – able to produce anisotropic correlation function from specified isotropic correlation – is one of the most attractive approach. The principal difficulty is to objectively deduce an appropriate coordinate system from the data. Recent development of ensemble methods in weather forecasting offers new possibilities to objectively construct the setting of covariance model. But the question of how to construct a coordinate change remains open.

A geometrical Riemannian framework, able to construct such a coordinate change, has been introduced in Ref. [1]. In this talk, a generalization is proposed that takes into account a prescribe metric of a given manifold. It relies on the ensemble diagnostic of the local metric tensor that features the shape of local correlation functions. We show that the coordinate change is solution of the harmonic map equation, which can be solved e.g. by using a pseudo-diffusion scheme (Fig. 1). Numerical experiments illustrate the ability of this approach to objectively estimate the coordinate change within simple situation.

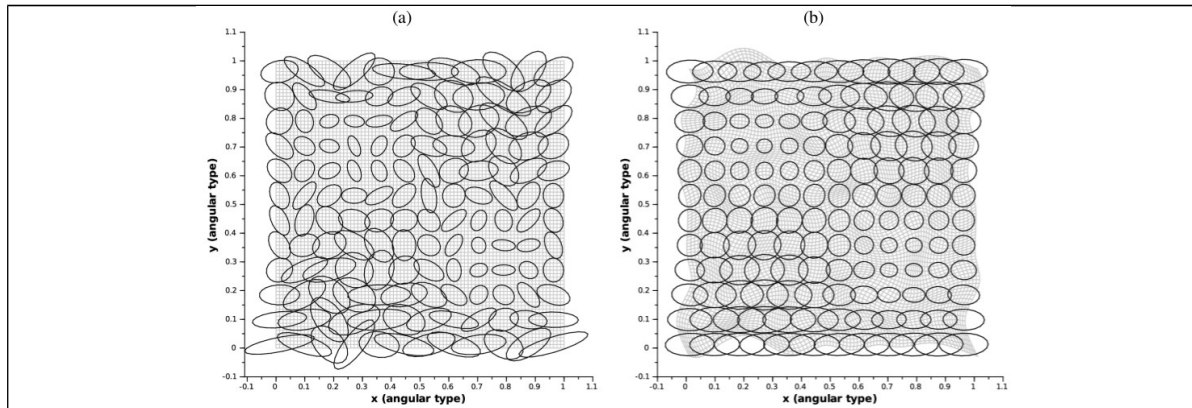


Figure 1: Illustration of coordinate change that transforms anisotropic correlations (a) into locally isotropic one (b) with respect to a prescribe metric.

References

- [1] Pannekoucke, O.; Emili, E. & Thual, O. Modeling of local length-scale dynamics and isotropizing deformations *Quarterly Journal Royal Meteorological Society*, **140**, 1387-1398 (2014)

SS-EBMSAHS Equation-Based Modeling: Structural Analysis and Hybrid Systems

A graphical view of reducing a DAE to an ODE by dummy derivatives

J.D. Pryce¹, R. McKenzie¹

¹ University of Cardiff, Wales, {prycejd1,mckenzie1}@cardiff.ac.uk

The dummy derivatives (DD) method of Mattsson and Söderlind [1] goes in stages, introducing new variables into a differential-algebraic equation (DAE) system to produce a larger system that is equivalent to the original but has index 1, so that it can be solved as an implicit ordinary differential equation (ODE). Indeed some simulation tools, such as Cydesign's Modelica compiler, find it advantageous to reduce the DAE to an explicit ODE system. The second author has shown [2] that the DD stages, and their variables, have a natural one to one correspondence with the stages of the Σ -method [3] for DAE structural analysis (SA), and the derivatives of variables that are solved for at each SA stage. The exposition of DDs in [1] makes it intuitively clear that its result does indeed have index 1, but does not make obvious how the enlarged system should be organised for systematic reduction to an implicit or explicit ODE. We describe a simple approach to this reduction that can be described diagrammatically by a directed graph, and clarifies the role played by the condition-numbers of the Jacobian matrices found during the DD process.

References

- [1] Mattsson, S.E. and Söderlind, G. Index reduction in differential-algebraic equations using dummy derivatives. *SIAM J. Sci. Comput.*, 14(3), 677–692 (1993).
- [2] McKenzie, R. PhD Thesis. Cardiff University, Wales, UK. In preparation.
- [3] Pryce, J.D. A simple structural analysis method for DAEs. *BIT*, 41(2), 364–394 (2001).

Regularization and Numerical Integration of DAEs Based on the Signature Method

A. Steinbrecher¹

¹ TU Berlin, Berlin, Germany, anst@math.tu-berlin.de

The complete virtual design of dynamical systems, e.g., mechanical systems, electrical circuits, flow problems, or whole production processes, plays a key role in our technological progress. Therefore, the interconnection of automatic modeling tools with efficient and robust simulation tools is of growing interest. Automatized modeling of dynamical processes usually leads to systems of *differential-algebraic equations (DAEs)* of the form

$$0 = F(t, x(t), \dot{x}(t)) \quad \text{with } x(t_0) = x_0 \text{ for } t \in [t_0, t_f], \quad (1)$$

where x are the unknown variables. In general, those DAEs are of high index. Therefore, the direct numerical integration usually leads to instabilities, non-convergence, or an order reduction of the numerical methods. These difficulties in the numerical integration occur due to so-called *hidden constraints* which are contained in the DAE but not explicitly stated as equations. Therefore, a regularization or remodeling of the model equations is required which preserves the set of solutions and explicitly contains all formerly hidden constraints.

In modern simulation environments often a structural analysis is used to obtain required information of necessary derivatives of certain equations to determine the hidden constraints. These derivatives can be added to the DAE and then, usually, dynamical state variables are selected for which the occurring derivatives are replaced by newly introduced algebraic variables (so-called dummy derivatives). The advantage of a structural analysis is that fast algorithms based on graph theory can be applied. Here, often the Pantelides algorithm in combination with the Dummy Derivative Method is used.

In this talk we discuss the efficient and robust numerical integration of DAEs (1) of high index.

First, we present an approach for the remodeling of dynamical systems that is based on the *Signature method (Σ -method)* [2]. We describe a regularization technique for structurally well-posed problems that combines the regularization by minimal extension [1] with the information provided by the Σ -method. For more details we refer to [3]. Such a regularization may be valid only locally since the state selection can vary with the dynamical behavior of the system. The obtained regularization can then be solved piecewisely using stiff ODE-solvers.

To avoid this varying state selection, secondly, we will propose an approach which strongly combines a regularization with an efficient numerical integration. This regularization approach also uses the information obtained from the Σ -method to construct a regularized overdetermined formulation. This overdetermined system can be solved using specially adapted integrators without the need of the introduction of new algebraic variables.

Based on that regularization approaches we present the software package **QUALIDAES**. This software package is suited for the direct numerical integration of both of the proposed regularizations and uses adapted discretization methods based on the Runge-Kutta method of type RADAU IIa of order 5.

References

- [1] Kunkel, P. and Mehrmann, V. (2004). Index reduction for differential-algebraic equations by minimal extension. *Zeitschrift für Angewandte Mathematik und Mechanik*, 84(9), 579–597.
- [2] Pryce, J.: A simple structural analysis method for DAEs. *BIT Numerical Mathematics* **41**, 364–394 (2001).
- [3] Scholz, L., Steinbrecher, A.: A Combined Structural-Algebraic Approach for the Regularization of Coupled Systems of DAEs. Institut für Mathematik, TU Berlin, Preprint 30-2013 (2013).

Solving Differential-Algebraic Equations Using The Signature Matrix Method To Exploit Underlying Structures

R. McKenzie¹, J. Pryce², N. Nedialkov³, G. Tan⁴

¹ Cardiff university, UK, mckenzierl@cardiff.ac.uk

² Cardiff University, UK, prycejdl@cardiff.ac.uk

³ McMaster University, Canada nedialk@mcmaster.ca

⁴ McMaster University, Canada tgn3000@msn.com

Differential algebraic equations (henceforth DAEs), arise from the equation based modelling of physical systems, with problems arising in areas such as chemical engineering, electronic circuits and robotics. Models are now frequently built interactively using different components from large libraries in environments such as GPROMS, MAPLESIM, SIMULINK and an assortment of tools that use the Modelica language. This way of modelling systems can lead to large scale DAEs. A common notion in DAE theory is the *differentiation index*—which is equal to the number of times all or part of the system has to be differentiated in order to identify the *hidden constraints* and solve the problem as an ODE. It is well known that solving a high index (larger than one) DAE directly is numerically difficult, hence modelling tools usually perform some structural analysis to determine the index of the problem and then perform an index reduction algorithm. This structural analysis is usually based on Pantelides' algorithm [2], although we will be using the Signature Matrix method [1] for this talk, as it applies to DAEs of arbitrary order and provides us with extra structural information we wish to exploit. After finding a DAE's index different packages handle high index DAEs very differently, DYMOLA for example performs an index reduction algorithm (specifically dummy derivatives [3]) to form a new equivalent index 1 DAE, which it then solves. The talk will give a brief outline the Signature Matrix and Dummy Derivative methods and then proceed to describe a new approach whereby non-canonical Signature Matrix offset vectors are used after modifying the system to remove the difficulty of switching index 1 systems found in the Dummy Derivative method. This approach adds extra hidden constraints to the system in order to find an index 1 system that does not require the dynamic pivoting of states required in the Dummy Derivative method, replacing it with a scheme where a vector of parameters is periodically adjusted.

References

- [1] J. Pryce *A Simple Structural Analysis Method for DAEs*, BIT, textbf{41}, 2, pp. 364–394 (2001).
- [2] C. Pantelides *The consistent initialization of differential-algebraic systems*, SIAM J. Sci. Stat. Comput., **9**, pp. 213–231 (1988).
- [3] S. Mattsson and G. Söderlind *Index reduction in differential-algebraic equations using dummy derivatives* SIAM K. Sci. Comput., **14**, 3, pp. 677–692 (1993).

Symbolic-Numeric Techniques for Improving Structural Analysis of DAEs

G. Tan¹, N. Nedialkov¹, J. Pryce²

¹ McMaster University, Canada, {tang4,nedialk}@mcmaster.ca

² Cardiff University, UK, PryceJD1@cardiff.ac.uk

Systems of differential-algebraic equations (DAEs) are routinely generated by simulation environments. Various algorithms are applied in the steps from creating a model to a final mathematically solvable set of equations. Typically, some form of analysis on the structure of the DAE is performed to determine its index and constraints. This is followed by index reduction for higher-index problems.

The structural analysis (SA) method of Pantelides [4] is widely used, and recently Pryce's SA [6], or the Σ -method, is becoming popular. When they succeed, both methods produce the same information, but the Σ -method is simpler and more direct, and is applicable to DAEs of any order.

Experience shows that these SA methods succeed on most DAEs encountered in practice. However, they can also fail on simple, solvable DAEs [7]. Such a problem would have an identically singular system Jacobian, resulting in SA failure, while there may exist an equivalent problem formulation with a nonsingular system Jacobian that guarantees SA's success. Hidden cancellations are one of the simplest sources of failure [3], but it can also occur due to common subexpressions [5] or intricate relations between equations and/or between variables.

Chowdhry et al. [1] propose a symbolic-numeric index analysis method that deals with linear constant coefficient DAEs and some nonlinear ones. Scholz et al. [7] show how to remedy SA failure for coupled systems of semi-explicit index-1 DAEs.

We have developed general symbolic-numeric techniques for transforming a DAE, on which the Σ -method fails, into an equivalent DAE on which the method succeeds. Our techniques are based on replacing a particular equation by a suitable combination of equations and derivatives of them or introducing new variables as a combination of original variables and derivatives of them. In both cases, the goal is to reduce the value of the associated signature matrix, which value also gives the number of degrees of freedom of the problem. We derive conditions under which our transformations result in a provably solvable (at least locally) DAE.

References

- [1] S. Chowdhry, H. Krendl, and A. A. Linniger. *Symbolic numeric index analysis algorithm for differential algebraic equations*. Ind. Eng. Chem. Res., 43(14):3886–3894, 2004.
- [2] S. E. Mattsson and G. Söderlind. *Index reduction in differential-algebraic equations using dummy derivatives*. SIAM J. Sci. Comput., 14(3):677–692, 1993.
- [3] N. S. Nedialkov and J. D. Pryce. *Solving differential-algebraic equations by Taylor series (I): Computing Taylor coefficients*. BIT Numerical Mathematics, 45(3):561–591, 2005.
- [4] C. C. Pantelides. *The consistent initialization of differential-algebraic systems*. SIAM J. Sci. Stat. Comput., 9:213–231, 1988.
- [5] J. D. Pryce. *Solving high-index DAEs by Taylor Series*. Numerical Algorithms, 19:195–211, 1998.
- [6] J. D. Pryce. *A simple structural analysis method for DAEs*. BIT Numerical Mathematics, 41(2):364–394, 2001.
- [7] L. Scholz and A. Steinbrecher. *A combined structural-algebraic approach for the regularization of coupled systems of DAEs*. Technical Report 30, Reihe des Instituts für Mathematik Technische Universität Berlin, Berlin, Germany, 2013.

The Numerical Solution of Reduced Differential Algebraic Equations

John Ernsthausen, Nedalko Nedialkov

McMaster University, Hamilton, Ontario, Canada, ernsthjm@mcmaster.ca

A reduced differential equation results from applying any reduction procedure to a differential equation. We do not follow the often applied dummy derivative with projection technique to numerically solve the reduced differential equation. Instead we investigate a geometric construction.

A Rabier and Rheinboldt reduced differential equation leads to a tangent vector field on the core manifold. We show the strangeness reduction of Kunkel and Mehrmann as well as the sigma method of Pryce also lead to a tangent vector field on the core manifold.

Modern approaches to numerically solve an ODE on a manifold (ODEM) include stabilization techniques to the invariant manifold and projection techniques. We construct and solve the local ODE to solve the ODEM applying Rheinboldt's algorithms to evaluate local parametrizations.

References

- [1] Abraham, R., Marsden, J.E., Ratiu, T.S.: Manifolds, Tensor Analysis, and Applications, *Applied Mathematical Sciences*, vol. 75, second edn. Springer-Verlag, New York (1988)
- [2] Ascher, U.M., Chin, H., Reich, S.: Stabilization of DAEs and invariant manifolds. *Numer. Math.* **67**, 131–149 (1994)
- [3] Kunkel, P., Mehrmann, V.: Differential-Algebraic Equations. Analysis and Numerical Solutions. Textbooks in Mathematics. European Mathematical Society, Zürich (2006)
- [4] Kunkel, P., Mehrmann, V., Stöver, R.: Multiple shooting for unstructured nonlinear differential-algebraic equations of arbitrary index. *SIAM J. Numer. Anal.* **42**(6), 2277–2297 (2005)
- [5] Pantelides, C.C.: The consistent initialization of differential-algebraic systems. *SIAM J. Sci. Stat. Comput.* **9**(2), 213–231 (1988)
- [6] Pryce, J.D.: A simple structural analysis method for DAEs. *BIT* **41**(2), 364–394 (2001)
- [7] Pryce, J.D., Nedialkov, N.S., Tan, G.: DAESA-a matlab tool for structural analysis of differential-algebraic equations: Theory. *ACM Trans. Math. Software* (2014). To be submitted
- [8] Rabier, P.J., Rheinboldt, W.C.: A geometric treatment of implicit differential-algebraic equations. *J. Diff. Eq.* **109**, 110–146 (1994)
- [9] Rabier, P.J., Rheinboldt, W.C.: Nonholonomic Motion of Rigid Mechanical Systems from a DAE Viewpoint. SIAM, Philadelphia (2000)
- [10] Rabier, P.J., Rheinboldt, W.C.: Theoretical and numerical analysis of differential-algebraic equations. In: P.G. Ciarlet, J.L. Lions (eds.) Solution of Equations in R^n (Part 4), Techniques of Scientific Computing (Part4), *Handbook of Numerical Analysis*, vol. 8, pp. 183–540. Elsevier, Amsterdam (2002)
- [11] Rheinboldt, W.C.: Core manifolds of daes (1994). Lecture Notes
- [12] Rheinboldt, W.C.: MANPAK: A set of algorithms for computations on implicitly defined manifolds. *Computers Math. Applic.* **32**(12), 15–28 (1996)
- [13] Rheinboldt, W.C.: Solving algebraically explicit DAEs with the MANPAK-Manifold-Algorithms. *Computers Math. Applic.* **33**(3), 31–43 (1997)
- [14] Scholz, L., Steinbrecher, A.: A combined structural-algebraic approach for the regularization of coupled systems of daes (2013). Preprint 2013/30, Technische Universität Berlin, Berlin

SS-FCP Fractional Calculus and Probability

Exactly-solvable non-Markovian dynamic network

N. Georgiou¹, I. Z. Kiss¹, E. Scalas¹

¹ University of Sussex, UK, *{n.surname}@sussex.ac.uk*

Non-Markovian processes are widespread in natural and human-made systems, yet explicit modelling and analysis of such systems is underdeveloped. In this letter we consider a dynamic network with random link activation and deletion (RLAD) with non-exponential inter-event times. We study a semi-Markov random process when the inter-event times are heavy tailed Mittag-Leffler distributed, thus considerably slowing down the corresponding Markovian dynamics and study the system far from equilibrium. We derive an analytically and computationally tractable system of forward equations utilizing the Caputo derivative for the probability of having a given number of active links in the network. As an example showing the effects of non-Markovianity, the dynamic network is coupled with a susceptible-infected-susceptible (SIS) spreading dynamics leading to more persistent epidemics. The convergence to equilibrium is discussed in terms of the mixing time of the embedded chain and the difference with the Markovian case is highlighted [1].

References

- [1] The full paper is available at <http://arxiv.org/abs/1502.04072>.

Ground state properties of non-local Schrödinger operators and jump processes

J. Lőrinczi¹

¹ Department of Mathematics, Loughborough University, UK, J.Lorinczi@lboro.ac.uk

Non-local operators and the related random processes with jump discontinuities have recently come to the forefront of pure and applied research. While they pose intriguing problems at the interface of at least three vast fields of mathematics (functional analysis, probability and PDE), they also have an immediate interest in modern scientific modelling and engineering.

In this talk I will discuss some spectral problems of non-local Schrödinger operators by using stochastic methods. Such an operator has the form $H = -L + V$, where the kinetic term $-L$ is a pseudo-differential operator and V is a multiplication operator called potential. A much studied case is the fractional Laplacian $-L = (-\Delta)^{\alpha/2}$, $0 < \alpha < 2$, however, I will consider a large class $-L = \Psi(-\Delta)$ given by so-called Bernstein functions Ψ of the Laplacian [2]. From a probabilistic point of view, $-L$ is the Markov generator of a Lévy process with jump discontinuities $(X_t)_{t \geq 0}$, and the Feynman-Kac formula

$$e^{-tH} f(x) = \mathbf{E}^x[e^{-\int_0^t V(X_s) ds} f(X_t)]$$

establishes a strong and deep link between the operator H and the random process $(X_t)_{t \geq 0}$ [6]. (Here \mathbf{E}^x means expectation over the paths of the process starting from $x \in \mathbf{R}^d$.) When the potential is chosen from a suitable class, H may have a discrete component in its spectrum and a ground state exists, i.e., an L^2 eigenfunction φ lying at the bottom of its spectrum $\lambda = \inf \sigma(H)$. The Feynman-Kac representation then implies

$$\varphi(x) = \mathbf{E}^x[e^{\lambda t - \int_0^t V(X_s) ds} \varphi(X_t)]$$

and thus the properties of the ground state can be analysed by averaging certain functionals over the paths of the associated process.

First I will discuss special cases of H for which the eigenvalue problem can be solved explicitly [5, 1]. Then I will address the problem of spatial decay of φ for confining potentials (V growing to infinity at infinite) and decaying potentials (V tending to zero at infinity), and offer an explanation of the mechanisms of decay [3, 4]. These results are established by a systematic control of the jumps, and reveal a phase transition-like phenomenon in the behaviour of the decay rates as the parameters of the Lévy process vary.

References

- [1] S.O. Durugo and J. Lőrinczi: *Spectral properties of the massless relativistic quartic oscillator*, 2014, submitted for publication.
- [2] F. Hiroshima, T. Ichinose and J. Lőrinczi: *Path integral representation for Schrödinger operators with Bernstein functions of the Laplacian*, Rev. Math. Phys. **24**, pp. 1250013-1250053 (2012).
- [3] K. Kaleta and J. Lőrinczi: *Pointwise estimates of the eigenfunctions and intrinsic ultracontractivity-type properties of Feynman-Kac semigroups for a class of Lévy processes*, Ann. Probab., to appear (2015).
- [4] K. Kaleta and J. Lőrinczi: *Fall-off of eigenfunctions for non-local Schrödinger operators with decaying potentials*, arXiv:1503.03508, 2015.
- [5] J. Lőrinczi and J. Małecki: *Spectral properties of the massless relativistic harmonic oscillator*, J. Diff. Equations **253**, pp. 2846-2871 (2012).
- [6] J. Lőrinczi, F. Hiroshima and V. Betz: *Feynman-Kac-Type Theorems and Gibbs Measures on Path Space. With Applications to Rigorous Quantum Field Theory*, de Gruyter Studies in Mathematics **34**, Walter de Gruyter, Berlin-New York (2011); 2nd ed. vols 1-2 (2015).

Integro-differential operators and non-decreasing processes with independent increments

B. Toaldo¹

¹ Department of Statistical Sciences, Sapienza - University of Rome, Rome - Italy, bruno.toaldo@uniroma1.it

The relationship between fractional Cauchy problems and time-changed processes has been ascertained in [1] and can now be considered a classical result. In order to obtain the stochastic process associated with a time-fractional Cauchy problem, a time-change must be performed via the inverse of a stable subordinator: let $L^\alpha(t)$, $t \geq 0$ be the inverse of an α -stable subordinator $\sigma^\alpha(t)$, $t \geq 0$, let $X(t)$, $t \geq 0$, be a Lévy process with generator A , the one-dimensional marginal of the time-changed process $X(L^\alpha(t))$ solves the fractional Cauchy problem $\partial^\alpha u = Au$. This type of relationship has been then extended in [2] and [4] to a general subordinator $\sigma^f(t)$, in different ways. In [4] integro-differential operators of the form

$$b \frac{d}{dt} u + \frac{d}{dt} \int_0^t u(s) \bar{v}(t-s) ds \text{ where } b \geq 0, \bar{v}(s) = a + v(s, \infty), a \geq 0 \text{ and } v(\cdot) \text{ is a Lévy measure on } (0, \infty) \quad (1)$$

have been introduced. Such operators specialize in the fractional derivative for a suitable choice of \bar{v} and permit to extend the results in [1] to a general subordinator. This approach include also as particular case the distributed-order derivative: in particular in [5] an approach to distributed calculus based on Lévy mixing has been proposed. This implies that subordinators with Lévy measure of the form $\int_W v(ds, y) p(dy)$, $p(\cdot)$ a suitably defined measure, must be considered. The last developments (see [3]) concerns instead variable order calculus. Operators of the form (1) may be generalized as

$$b(t) \frac{\partial}{\partial x} u(x, t) + \frac{\partial}{\partial x} \int_0^x u(s, t) \bar{v}(x-s, t) ds \quad (2)$$

and in [3] it is explored the relationship of (2) with non-decreasing stochastic processes with independent and non-stationary increments.

References

- [1] B. Baeumer and M.M. Meerschaert, *Stochastic solutions for fractional Cauchy problems*, Fractional Calculus and Applied Analysis **4**(4), pp. 481-500 (2001).
- [2] M.M. Meerschaert and H.P. Scheffler, *Triangular array limits for continuous time random walks*, Stochastic Processes and their Applications **118**(9), pp. 1606-1633 (2008).
- [3] E. Orsingher, C. Ricciuti and B. Toaldo, *Non-decreasing processes and variable order calculus*, In preparation.
- [4] B. Toaldo, *Convolution-type derivatives, hitting-times of subordinators and time-changed C_0 -semigroups*, Potential Analysis **42**(1), pp. 115-140 (2015).
- [5] B. Toaldo, *Lévy mixing related to distributed order calculus, subordinators and slow diffusions*, In Revision, 2015. arXiv:1406.4669

Source solution for the fractal Burgers equation with the critical exponent

T. Jakubowski

Wroclaw University of Technology, Poland, tomasz.jakubowski@pwr.edu.pl

Let $d \in \mathbb{N}$ and $\alpha \in (1, 2)$. We consider the following pseudo-differential equation

$$\begin{cases} u_t - \Delta^{\alpha/2} u + b \cdot \nabla (u|u|^{(\alpha-1)/d}) = 0, & t > 0, x \in \mathbb{R}^d, \\ u(0, x) = M\delta_0(x), \end{cases} \quad (1)$$

where $M > 0$ is arbitrary constant and $b \in \mathbb{R}^d$ is a constant vector. The existence and some basic properties of the solution $u_M(t, x)$ of this equation were proved in [1]. In [2] the authors proved that for sufficiently small M there is a constant $C = C(d, \alpha, M, b)$ such that

$$u_M(t, x) \leq Cp(t, x), \quad t > 0, x \in \mathbb{R}^d.$$

I will present a new method which allows to show pointwise estimates of solutions to the nonlinear problem (1) without the smallness assumption imposed on M . This method has been inspired by the proof of [3, Theorem 1]. The main result is

Theorem 1 *Let $d \geq 1$, $\alpha \in (1, 2)$ and $M > 0$. Let $u_M(t, x)$ be the solution of the equation (1). There exists a constant $C = C(d, \alpha, M, b)$ such that*

$$C^{-1}p(t, x) \leq u_M(t, x) \leq Cp(t, x), \quad t > 0, x \in \mathbb{R}^d.$$

The talk is based on the paper [4]

References

- [1] P. Biler, G. Karch, and W. A. Woyczyński. Critical nonlinearity exponent and self-similar asymptotics for Lévy conservation laws. *Ann. Inst. H. Poincaré Anal. Non Linéaire*, 18(5), pp. 613–637 (2001).
- [2] L. Brandoles and G. Karch. Far field asymptotics of solutions to convection equation with anomalous diffusion. *J. Evol. Equ.*, 8(2), pp. 307–326 (2008).
- [3] K. Bogdan and T. Jakubowski. Estimates of the Green function for the fractional Laplacian perturbed by gradient. *Potential Anal.*, 36(3), pp. 455–481 (2012).
- [4] T. Jakubowski and G. Serafin. Stable estimates for source solution of critical fractal Burgers equation. Preprint (2015)

Spectral representation of the solution to the Cauchy problem associated to fractional operators

P. Patie¹, Y. Zhao²

¹ Cornell University, Ithaca, USA, pp396@cornell.edu

² Cornell University, Ithaca, USA, yz645@cornell.edu

The aim of this talk is to present an original methodology to derive a spectral representation and smoothness properties for the solution to the following Cauchy problem

$$\begin{cases} \frac{d}{dt}u(t,x) = L_\alpha u(t,x), & t, x > 0, \\ u(0,x) = f(x) \in \mathcal{D}, & x > 0, \end{cases} \quad (1)$$

where, for $1 < \alpha < 2$, L_α (resp. \mathcal{D}) is the infinitesimal generator (resp. its L^2 -domain) of two strongly continuous contraction semigroups, and, for a smooth function f , expressed in terms of the fractional operators

$$L_\alpha f(x) = D_+^\alpha f(x) = \frac{d^2}{dx^2} \int_0^x \frac{f(y)}{(x-y)^{\alpha-1}} \frac{dy}{\Gamma(2-\alpha)} \quad (2)$$

$$L_\alpha f(x) = {}^C D_+^\alpha f(x) = \int_0^x \frac{f''(y)}{(x-y)^{\alpha-1}} \frac{dy}{\Gamma(2-\alpha)} \quad (3)$$

with D_+^α and ${}^C D_+^\alpha$ being the left-sided Riemann-Liouville (RL) derivative of index α and the Caputo α -fractional derivative respectively. Although fractional operators play a tremendous role in many fields on applied mathematics and sciences, their spectral representation in Hilbert space does not seem to have been studied in the literature, something which is probably due to the lack of a spectral theorem for non-local and non-normal operators. Another motivation underlying our study relies on recent developments, see e.g. [2] and [4], which have shown that these fractional operators are the infinitesimal generators of substantial Markov semigroups, namely the reflected at its infimum and killed α -stable Lévy processes.

Our approach relies on an intertwining relationship that we establish between these semigroups and the one of the squared Bessel, which is a self-adjoint contraction semigroup with a continuous point spectrum, see [3]. We also use techniques borrowed from non-harmonic analysis, such as the theory of (continuous) frame which has been introduced recently in [1]. The spectral representation, which is based on the continuous point spectrum of the operators, turns out to be very useful to also provide smoothness properties of the associated heat kernel. We also provide an explicit series expansion for the heat kernel which can be useful for numerical purposes. The numerical performances of this representation is investigated in depth.

References

- [1] Jean-Pierre Antoine and Peter Balazs, *Frames and Semi-frames*. J. Phys. A, 44(47):479501, 2 (2011).
- [2] Boris Baeumer, Mihály Kovács, Mark M. Meerschaert, René L. Schilling and Peter Straka, *Reflected Stable Subordinators for Fractional Cauchy Problems*, Transaction of American Math. Soc., to appear, (2015).
- [3] Jorge J. Betancor, Eleonor Harboure, Adam Nowak, and Beatriz Viviani. *Mapping properties of fundamental operators in harmonic analysis related to Bessel operators*. Studia Math., 197(2):101-140 (2010).
- [4] Pierre Patie and Thomas Simon. *Intertwining certain fractional derivatives*. Potential Anal., 36(4):569-587 (2012).

**SS-GAMCCM Geometric and Analytic
Methods in Classical and Celestial Mechanics**

A continuation theorem in classical mechanics

C. Stoica¹

¹ Wilfrid Laurier University, Waterloo, Canada, cstoica@wlu.ca

A theorem by K. Meyer and D. Schmidt [2] states that *The reduced three-body problem in two or three dimensions with one small mass is approximately the product of the restricted problem and a harmonic oscillator.*

Specifically, in the three-body problem with one small mass, after the reduction of translational and rotational symmetries, the first order approximation dynamics is given by the sum of the Hamiltonian of the restricted circular three body in the rotating coordinates of the primaries, and the linearized Hamiltonian of the primaries at a relative equilibrium (circular motion). This theorem was used to proving that many of the known results for the restricted problem (existence of non-degenerate periodic solutions, generic bifurcations, Hamiltonian-Hopf bifurcations) continue in the reduced three-body problem.

We examine the analogue statement in a broader class of Lie symmetric mechanical systems and prove it by employing suitable scalings and a Hamiltonian symplectic slice theorem. Examples of other mechanical systems where dynamical features on the restricted problem continue in the non-restricted case will be given.

References

- [1] J.E. Marsden, *Lectures on Mechanics*, London Math. Soc. Lecture Note Ser., **174**, Cambridge University Press, (1992)
- [2] K. Meyer K. and D. Schmidt, *From the restricted to the full three-body problem*, Transactions AMS **352**, 5, pp. 2283?2299, (2000)
- [3] C. Stoica and T. Schmah, *Normal forms for Lie symmetric cotangent bundle systems with free and proper actions*, in *Geometry, Mechanics, and Dynamics: The Legacy of Jerry Marsden*, Fields Institute Communications **73**, Chang, D.E., Holm, D.D., Patrick, G., Ratiu, T. (Eds.) (2015)

A Separating Surface for Sitnikov-like $(n+1)$ -Body Problems

L. Bakker¹, S. Simmons²

¹ Brigham Young University, Provo, USA, bakker@mathematics.byu.edu

² Brigham Young University, Provo, USA, simmons@mathematics.byu.edu

We consider the generalized Sitnikov problem of Newtonian mechanics. For periodic, planar motions of n -bodies which are symmetric under a rotation by a fixed angle, the z -axis is invariant. We consider the effect of placing a massless particle on the z -axis. The study of the motion of this particle can then be modeled as a one degree-of-freedom time-dependent Hamiltonian system. We give a geometric construction of a surface in the three-dimensional phase space separating orbits for which the massless particle escapes to infinity from those which it does not. A procedure for removing the periodicity condition of the planar configuration is outlined. The construction of the separating surface is demonstrated numerically in a few examples.

We will discuss an extended notion of entropy, introduced by Panchenkov as the measure of perfection of the virtual continuous medium and its structures, leading to a new variational principle - the principle of maximum entropy. The resulting differential equations can be used to model various phenomena arising in econometrics, theory of monitoring and other areas. We will also discuss how this new principle interacts with Hamiltonian mechanics.

Aspects and Applications of Quasi-homogeneous Potentials

John A. Arredondo¹

¹ Universidad Konrad Lorenz of Bogota, Colombia, alexander.arredondo@konradlorenz.edu.co

A quasi-homogeneous potential, is a function of the form

$$U(r) = -\frac{A}{r^\alpha} - \frac{B}{r^\beta}, \quad (1)$$

where r is the relative distance between two bodies and $A, B > 0$ are constants related with physical aspects of the bodies. This type of functions models different physical, chemical and stellar dynamics systems in a classical context, i.e., using Newton's law of motion. The principal subject of this talk, is present a qualitative study of different system of particles where the mutual interaction correspond to a quasi-homogeneous potential (Schwarzschild, Manev, Lennard-Jones...). As principal subjects we present a discussion of relative equilibria, central configurations and the collision manifold. Emphasising the distinct features of the quasi-homogeneous models when are compared to its Newtonian counterpart.

We present several classical facts, that differ from the Newtonian case,

- On any level of energy the measure of the set on initial conditions leading to triple collision is positive.
- Whereas in the Newtonian problem triple collision is asymptotically reached only for zero angular momentum, in the quasi-homogeneous problem, triple collision is possible for non-zero total angular momenta (e.g. when two of the mass points spin infinitely many times around the centre of mass). This phenomenon is known in celestial mechanics as the *black-hole effect* and it is understood as an analogue in the classical context of the behaviour near a Schwarzschild black hole.
- While in the Newtonian problem all triple collision orbits are necessarily homographic (in fact, homothetic), quasi-homogeneous problems exhibits triple collision orbits which are not homographic; in particular, that there exist asymptotic geometric configurations at triple collision which are not central configurations.

The aspects above, have been observed by the authors in previous investigations of dynamics and stability in systems of particles governed by some quasi-homogeneous potential function. Some of them are collected in the references.

References

- [1] J. Arredondo, E. Perez-Chavela and C. Stoica, *Dynamics in the Schwarzschild isosceles three body problem*, Journal of Nonlinear Sciences. **24**, 6, pp. 997-1032 (2014).
- [2] J. Arredondo and E. Perez-Chavela, *Central configurations in the Schwarzschild three body problem*, Qualitative theory of Dynamical System. **12**, 1, pp. 183-206 (2013).
- [3] J. Arredondo, H. Gwan, C. Tamayo and C. Stoica, *On the restricted three body problem with oblate primaries*, Astrophysics and Space Science. **341**, 2, pp. 315-322 (2012).
- [4] J. Arredondo, *Relative equilibria in quasi-homogeneous three body problems*, under review, (2015)

Aspects of the Finsler geometry behind Lagrangian mechanical systems

T. Mestdag¹

¹ Ghent University, Belgium, tom.mestdag@ugent.be

We generalize a theorem from Lagrangian mechanics that is sometimes attributed to Jacobi or referred to as "Maupertuis' Principle" (see e.g. [1, 2]). We show that the solutions of the Euler-Lagrange equations of a strongly convex autonomous Lagrangian which lie on a specific energy level can be thought of as geodesics of an associated Finsler metric. For that purpose, we apply a new method based on a Lagrangian symmetry reduction method known as Routh's procedure and a homogenization trick. Routh reduction is a method that takes full advantage of the close relation between symmetries and conserved quantities. The homogenization method enables one, roughly speaking, to go back and forth between a time-dependent Lagrangian framework and a Finslerian one. The proof of our theorem relies on a Routh-reduced 1-homogeneous function on the tangent bundle which, under appropriate conditions, will be a Finsler function.

References

- [1] R. Abraham and J.E. Marsden, Foundations of mechanics, Benjamin/Cummings Publishing Co. (1978).
- [2] V.I. Arnold, Mathematical methods of classical mechanics, Springer (1978).
- [3] T. Mestdag, Finsler geodesics of Lagrangian systems through Routh reduction, accepted for publ. in Mediterranean Journal of Mathematics, arXiv:1412.3526

Canonoid and Poissonoid Transformations, Symmetries and Bi-Hamiltonian Structures

G. Rastelli¹, M. Santoprete²

¹ Universitá di Torino, Torino, Italy, giovanni.rastelli@unito.it

² Wilfrid Laurier University, Waterloo, Canada, msantoprete@wlu.ca

Canonoid transformations are transformations that send a Hamiltonian system (defined on a symplectic manifold) to another Hamiltonian system. Symplectic (or canonical) transformations are special cases of canonoid transformations. The term “canonoid” was introduced by Saletan and Cromer in 1971 in [2], but a description of these transformations can already be found in the 1904 edition of Wittaker’s celebrated book of mechanics [3]. A modern coordinate-free definition of canonoid transformation was given by Marmo.

Let (M, π) be a Poisson manifold, and let (M, π, H) an Hamiltonian system defined by $X_H = \pi^\sharp \cdot dH$, where π^\sharp is the bundle map associated to π . In this talk we will present some result we obtained in [1], in particular we will generalize the coordinate-free definition of canonoid transformations to the Poisson setting. We call this new type of transformations Poissonoid. If f is a Poissonoid transformation the pull-back of the Poisson tensor $\pi_1 = f^*\pi$ is also a Poisson tensor and there is a function K such that $X_H = \pi_1^\sharp \cdot dK$. If π and π_1 are compatible, that is $\pi + \pi_1$ is a Poisson tensor, then Poissonoid transformations give a bi-Hamiltonian structure to the Hamiltonian vector field. Furthermore, Casimirs of the Poisson bivector π_1 are integrals of motion of the original system. Infinitesimal Poissonoid transformations are also connected to Hamiltonian symmetries and Master symmetries. Explicit Poissonoid transformation were obtained in some examples, as for instance, the multidimensional rigid body, namely Euler’s equations on $so^*(4)$ and some integrable cases of the Kirchhoff’s equations for a rigid body in an ideal fluid.

References

- [1] G. Rastelli, M. Santoprete, *Canonoid and Poissonoid Transformations, Symmetries and BiHamiltonian structures*, preprint, 2015
- [2] E. J. Saletan, A.H. Cromer, *Theoretical Mechanics*, Wiley, 1971.
- [3] E. T. Whittaker, *A Treatise on the Analytical Dynamics of Particles and Rigid Bodies*, Cambridge University Press, 1904.

Compatible quadratic Poisson brackets related to a family of elliptic curves

Alexander Odesskii¹, Thomas Wolf²

¹ Brock University, St. Catharines, Canada, aodesski@brocku.ca

² Brock University, St. Catharines, Canada, twolf@brocku.ca

Two Poisson brackets $\{\cdot, \cdot\}_0$ and $\{\cdot, \cdot\}_1$ defined on the same finite dimensional vector space are said to be compatible if

$$\{\cdot, \cdot\}_u = \{\cdot, \cdot\}_0 + u\{\cdot, \cdot\}_1 \quad (1)$$

is a Poisson bracket for any constant u . Note that if $\{\cdot, \cdot\}_{u_1, \dots, u_k} = \{\cdot, \cdot\}_0 + u_1\{\cdot, \cdot\}_1 + \dots + u_k\{\cdot, \cdot\}_k$ is a Poisson bracket for arbitrary u_1, \dots, u_k , then all brackets $\{\cdot, \cdot\}_0, \dots, \{\cdot, \cdot\}_k$ are Poisson and pairwise compatible. Compatible Poisson structures play an important role in the theory of integrable systems [1, 2] and in differential geometry [3, 4]. Many examples of compatible Poisson structures are known [2]. Most of these are linear in certain coordinates. However, quadratic Poisson structures are also interesting. While the theory of linear Poisson structures is well-understood and possesses a classification theory¹, the theory of quadratic Poisson algebras is more complicated. If the dimension of a linear space is larger than four, then no classification results for quadratic Poisson structures on this space are available. All known examples can be divided into two classes: rational and elliptic.

In the work to be described we construct nine pairwise compatible quadratic Poisson structures such that a generic linear combination of them is associated with an elliptic algebra in n generators. Explicit formulas for Casimir elements of this elliptic Poisson structure have been obtained.

References

- [1] F. Magri, A simple model of the integrable Hamiltonian equation, *J. Math. Phys.*, **19**, 1156–1162, 1978.
- [2] A.V. Bolsinov, Compatible Poisson brackets on Lie algebras and the completeness of a family of functions in involution, *Izvestiya of AN SSSR. Ser: Math.*, **55**(1), 69–89, 1991.
- [3] I.M. Gelfand and I.W. Zakharevich, Webs, Lenard schemes, and the local geometry of bi-Hamiltonian Toda and Lax structures, *Selecta Math. (N.S.)*, **6**, no. 2, 131–183, 2000.
- [4] I.M. Gelfand and I.W. Zakharevich, Webs, Veronese curves, and bi-Hamiltonian systems, *J. Funct. Anal.*, **99** (1991), no. 1, 150–178.
- [5] A.V. Odesskii, Elliptic algebras, *Russian Math. Surveys*, **57**(6), 1127–1162, 2002.
- [6] A.V. Odesskii, Bihamiltonian elliptic structures, *Mosc. Math. J.*, **4**(2004), no. 4, 941–946.
- [7] B.L. Feigin and A.V. Odesskii, Functional realization of some elliptic Hamiltonian structures and bozonization of the corresponding quantum algebras, *Integrable Structures of Exactly Solvable Two-Dimensional Models of Quantum Field Theory* (S.Pakuliak et al, eds.), *NATO Sci. Ser. II Math. Phys. Chem.*, *Kluwer, Dordrecht*, **35**, 109–122, 2001.
- [8] D. Mumford, Tata Lectures on Theta I, *Progress in Mathematics*, 28, Birkhauser Verlag, 1983.

¹The theory of linear Poisson structures coincides with the theory of Lie algebras.

Index theory in Celestial Mechanics: recent results and new perspectives

V. L. Barutello¹, X. Hu², A. Portaluri³, S. Terracini⁴

¹ Università degli Studi di Torino, Italy, It vivina.barutello@unito.it

² Shandong University, Jinan, Shandong, China xjhu@sdu.edu.cn

³ Università degli Studi di Torino, Italy, It alessandro.portaluri@unito.it

⁴ Università degli Studi di Torino, Italy, It susanna.terracini@unito.it

In the last decades a zoo of new symmetric periodic collision-less orbits for the n-body problem appeared in the literature as critical points of the Lagrangian action functional. Certainly one of the important features of such orbits, for a better understanding of the dynamics, is the knowledge of the Morse index as well as their linear (in)stability properties. Index theory revealed its tremendous importance in computing this index through a Morse-type index theorem (cfr. [3]) and a refined computation of a popular symplectic invariant, known in literature as *Maslov index*. Although for solutions parametrised by a compact interval the theory is well established, very few results are known on the real line and even worse on the half-line [2].

Motivated by the challenge problem of characterizing colliding trajectories in Celestial Mechanics (which play a key role in order to penetrate the intricate dynamics of this singular problem) and pushing forward the analysis started by authors in [1] through a variational regularisation of the Lagrangian action functional, we introduce the notion of *spectral index* for an important class of total collision solutions, by means of a homotopy invariant associated to a path of bounded Fredholm quadratic forms. By taking into account the underlying Hamiltonian structure and the hyperbolicity of the colliding trajectories (under a suitable spectral condition) a new notion of Maslov index is introduced and a delicate index theory is developed.

In this talk, after a presentation of a new variational regularisation of the Lagrangian action functional, we will show how to define a suitable index theory for a special class of colliding trajectories.

References

- [1] V. Barutello and S. Secchi, *Morse index properties of colliding solutions to the N-body problem*, Ann. Inst. H. Poincaré Anal. Non Linéaire **25**, 3, 539-565 (2008) *Cluster-titled algebras are Gorenstein and stably Calabi-Yau*, Adv. Math. **211**, 1, pp. 123-151 (2007).
- [2] C.N., Chen and X. Hu, *Maslov index for homoclinic orbits of Hamiltonian systems*, Ann. Inst. H. Poincaré Anal. Non Linéaire **24**, 4, 589-603 (2007).
- [3] M. Musso and J. Pejsachowicz and A. Portaluri, *A Morse index theorem for perturbed geodesics on semi-Riemannian manifolds* Topol. Methods Nonlinear Anal. **25**, 1, 69-99 (2005).

Morse index and linear stability of some equivariant solutions for N -body-type problem via index theory

V. Barutello¹

¹ University of Turin, Italy, vivina.barutello@unito.it

In this talk I present some aspects of a research project that I conduct, mainly, with Riccardo Jadauza and Alessandro Portaluri ([1, 2]).

We consider some classes of solutions for the (generalized) N -body problem and we study their linear stability properties, their Morse index (as critical points of the lagrangian action functional) and the, possible, link between them. We start discussing a sufficient condition to detect spectral (hence linear) instability for relative equilibrium motions (a class of equivariant periodic orbits). Then, focusing on the family of Lagrangian circular orbits, we provide the computation of the Morse index of these trajectories and of their iterates and we show that the boundary of the stability region is the envelope of a family of curves on which the Morse index of the iterates jump.

In order to conduct our analysis we rely, for the first problem, on some refined formulæ for computing the spectral flow, whereas, for the second one, on a Maslov-type index theory devised and developed by Y. Long, X. Hu and S. Sun; a key role is played by the Bott-iteration formula, by an appropriate index theorem, and by some precise computations of suitable Maslov-type indices.

We will also present some works in progress on the development on an index theory for solutions interacting with the singularity set.

References

- [1] Barutello V., Jadauza R., Portaluri A., *Linear instability of relative equilibria for n -body problems in the plane*, J. Diff. Eq. 257, (2014), 1773–1813.
- [2] Barutello V., Jadauza R., Portaluri A., *Morse index, Maslov index and linear stability of the Lagrangian circular orbit in 3-body-type problems*, Arch. Rat. Mec. Anal., accepted December 2014.

Nosé–Hoover Thermostats

Leo T. Butler¹

¹ North Dakota State University, leo.butler@ndsu.edu

Statistical mechanics attempts to predict the macroscopic behaviour of many-particle systems. On the other hand, the microscopic behaviour is governed by classical mechanics. The predictions of the two models may or may not coincide.

A thermostat is a system that models a particle system immersed in a heat bath. A fundamental question about such a system is whether it reaches statistical equilibrium with the heat bath. Even for the harmonic oscillator this question is non-trivial, and an answer is only known in the simplest case by work of Legoll, Luskin and Moeckel.

In this talk, I will extend this work to show that in the high-temperature limit, equilibrium is often not attained.

References

- [1] W. Hoover, *Canonical dynamics: equilibrium phase space distributions*, Phys. Rev. A. **31** (1985), 1695–1697.
- [2] W. Hoover, *Nosé-Hoover nonequilibrium dynamics and statistical mechanics*, Mol. Simul. **33** (2007), 13–19.
- [3] Legoll, Frédéric, Luskin, Mitchel, and Moeckel, Richard, *Non-ergodicity of Nosé-Hoover dynamics*, Nonlinearity **22** (2009), no. 7, 1673–1694. 2519685 (2010c:37141)
- [4] Legoll, Frédéric, Luskin, Mitchell, and Moeckel, Richard, *Non-ergodicity of the Nosé-Hoover thermostatted harmonic oscillator*, Arch. Ration. Mech. Anal. **184** (2007), no. 3, 449–463. 2299758 (2008d:82068)
- [5] S. Nosé, *A unified formulation of the constant temperature molecular dynamics method*, J. Chem. Phys. **81** (1984), 511–519.

On the Problem of Similar Motions of a Chain of Coupled Heavy Rigid Bodies

D. Chebanov

City University of New York - LAGCC, USA, dchebanov@lagcc.cuny.edu

One of the classical directions of investigations in the theory of motion of a system of several coupled rigid bodies is concerned with particular cases of integrability of the equations of a system's motion [1, 2, 3]. In comparison with the Euler and Poisson equations describing the dynamics of a single rigid body about a fixed point, the analytical study of mathematical models for a system of hinge-connected rigid bodies is a much more complicated problem; as a consequence, there are very few known cases of integrability in the dynamics of many-body systems [4, 5].

This paper contributes to the study of dynamic properties of a mechanical system S consisting of n heavy rigid bodies B_1, B_2, \dots, B_n . The bodies B_i and $B_{i+1}(i = 1, 2, \dots, n-1)$ are coupled by an ideal spherical joint at a common point O_{i+1} so that (i) the system S constitutes a chain of rigid bodies, and (ii) the line $l_i(i = 1, 2, \dots, n-1)$ connecting the attachment points O_i and O_{i+1} of the body B_i passes through its center of mass C_i . One of the chain's end links, B_1 , is fixed at one of its points $O_1(\neq O_2)$.

The paper constructs a class of particular solutions of the equations of motion of system S that describes a rotational motion of S with the following property: while the system S is in motion, its skeleton $O_1O_2\dots O_nC_n$ composed of the segments of axes l_i bounded by the corresponding attachment points belongs to a vertical plane Π rotating about the vertical axis passing through O_1 while the skeleton's segments change their position with respect to Π identically in time, i.e., all the bodies move similarly. The similar motions of system S were first discovered for a chain of n heavy Lagrange tops [6, 7]. Recently, paper [8] suggested a generic approach for establishing the existence of such motions under no initial assumption regarding the mass distribution in the bodies B_i .

This paper presents a new particular solution of the described above problem that is analogous to the solution of the Euler and Poisson equations found by Hess [9]. The paper describes the structure of the new solution, establishes conditions for its existence, proves compatibility of these conditions, and reduces the equations of motion of system S to quadratures in the case when the conditions are fulfilled. Then, it explores some aspects of the geometry of the motion described by the new solution.

References

- [1] E. Leimanis, *The General Problem of the Motion of Coupled Rigid Bodies about Fixed Point*, Springer, Berlin (1965).
- [2] A.V. Borisov and I.S. Mamaev, *Dynamics of a Rigid Body. Hamiltonian Methods, Integrability, Chaos*, Institute of Computer Science, Moscow – Izhevsk (2005).
- [3] I.N. Gashenenko, G.V. Gorr, and A.M. Kovalev, *Classical Problems of the Rigid Body Dynamics*, Naukova Dumka, Kyiv (2012).
- [4] E.I. Kharlamova, *A survey of exact solutions of problems of the motion of systems of coupled rigid bodies*, Mekh. Tverd. Tela, **26**, pp. 125-138 (1998).
- [5] I.A. Bolgrabskaya, M.E. Lesina, and D.A. Chebanov, *Dynamics of Systems of Coupled Rigid Bodies*, Naukova Dumka, Kyiv (2012).
- [6] P.V. Kharlamov, *Some classes of exact solutions of the problem of the motion of a system of Lagrange gyroscopes*, Mat. Fiz., **32**, pp. 63-76 (1982).
- [7] D. Chebanov, *Exact solutions for motion equations of symmetric gyros system*, Multibody Syst. Dyn., **6**, pp. 39-57 (2001).
- [8] D. Chebanov, *New class of exact solutions for the equations of motion of a chain of n rigid bodies*, Discrete Cont. Dyn. S., Supplement, pp. 105-113 (2013).
- [9] W. Hess, *Über die Eulerschen Bewegungsgleichungen und über eine neue particulare Lösung des Problems der Bewegung eines starren Körpers un einen festen Punkt*, Math. Ann., **37**, 2, pp. 178-180 (1890).

Orthogonal separation of the Hamilton-Jacobi equation on Spaces of Constant curvature

K. Rajaratnam¹, R. McLenaghan²

University of Waterloo, Waterloo, Canada, ¹ k2rajara@uwaterloo.ca
University of Waterloo, Waterloo, Canada, ² rgmclena@uwaterloo.ca

The talk will present the theory of orthogonal separation of the Hamilton-Jacobi equation on spaces of constant curvature, with examples in Euclidean space. The theory is based on results of Eisenhart [Eis34], which connect orthogonal separation of the Hamilton-Jacobi equation to the existence of special types of Killing tensors known as characteristic Killing tensors.

We use geometrical properties of Killing tensors to classify separable coordinates and develop an algorithm to separate the Hamilton-Jacobi equation [RM14a]. In particular, the theory includes a recursive classification of characteristic Killing tensors by way of the warped product decompositions [Nol96] of the Riemannian manifold they induce. This classification is built upon Benenti's theory of a special but important class of characteristic Killing tensors [Ben05].

The theory has been successfully applied to spaces of constant curvature [RM14b]; in the case of Euclidean space and the n -sphere, other authors have arrived at the solution using elementary methods [Kal86, WW03]. We will present some applications of the algorithm for well known Hamiltonians in 3-dimensional Euclidean space. Current work involves extending the algorithm to Hamiltonians with vector potentials. In addition to being a viable method for solving Hamilton's equations for some existing natural Hamiltonians, the method allows us to find new integrable systems defined on these spaces as well.

References

- [Ben05] S Benenti. Special Symmetric Two-tensors, Equivalent Dynamical Systems, Cofactor and Bi-cofactor Systems. *Acta Applicandae Mathematicae*, 87(1-3):33–91, May 2005.
- [Eis34] L P Eisenhart. Separable systems of Stackel. *Annals of Mathematics*, 35(2):284–305, 1934.
- [Kal86] E. G. Kalnins. *Separation of variables for Riemannian spaces of constant curvature*. Longman Scientific & Technical, 1 edition, 1986.
- [Nol96] Stefan Nolker. Isometric immersions of warped products. *Differential Geometry and its Applications*, 6(1):1–30, March 1996.
- [RM14a] Krishan Rajaratnam and R G McLenaghan. Killing tensors, warped products and the orthogonal separation of the Hamilton-Jacobi equation. *Journal of Mathematical Physics*, 55(1):013505, January 2014.
- [RM14b] Krishan Rajaratnam and Raymond G. McLenaghan. Concircular tensors in Spaces of Constant Curvature: With Applications to Orthogonal Separation of The Hamilton-Jacobi Equation. April 2014.
- [WW03] Claes Waksjö and Stefan Wojciechowski. How to Find Separation Coordinates for the Hamilton-Jacobi Equation: A Criterion of Separability for Natural Hamiltonian Systems. *Mathematical Physics, Analysis and Geometry*, 6(4):301–348, April 2003.

Stability and Bifurcation of the Hip-Hop orbit

P-L. Buono¹, M. Kovacic², M. Lewis³, D. Offin⁴

¹ University of Ontario Institute of Technology, ONT, Canada, *{luciano.buono}@uoit.ca*

² Simon Fraser University, BC, Canada, *mitchell.kovacic@sfu.ca*

³ St-Lawrence College, ONT, Canada, @

⁴ Queen's University, ONT, Canada, *offind@mast.queensu.ca*

I will present recent results about the Hip-Hop of the four-body problem. The Hip-Hop orbit was found by Chenciner and Venturelli [1] by minimizing the Lagrangian action functional over a set of loops with the so-called Italian symmetry. By restricting further using an order four symmetry linking the four bodies, they show the existence in a reduced configuration space of only one body. In this talk, I will first present a theorem about the instability of the Hip-Hop orbit where the proof relies on the variational structure and controlling the focal points along the orbit. Second, I will discuss bifurcations of the Hip-Hop orbit as the energy is varied. Numerical simulations of the Poincaré map near the Hip-Hop orbit exhibit pitchfork bifurcations. We explain the appearance of the symmetry-broken solutions by using a classification of possible bifurcating branches and show using index theory that those are the only possible bifurcations possible.

References

- [1] A. Chenciner and A. Venturelli, *Minima de l'intégrale d'action du Problème newtonien de 4 corps de masses égales dans \mathbb{R}^3 : orbites "hip-hop"*, Celestial Mechanics, **77**, 1, pp. 139-152 (2000).

SS-GLS Geocomputational Landscapes and Spaces

Geocomputational Spaces of Social Media: User-level patterns and processes

C. Robertson¹, R. Feick²

¹ Wilfrid Laurier University, Waterloo, Canada

² University of Waterloo, Waterloo, Canada

The advent of social media and other forms of user-generated content that increasingly include geographic references has provided a rich new resource to understand socio-spatial processes, especially in cities. Individual expressions and interactions with online resources create repositories of digitally encoded geo-traces, that in aggregate, mirror contours of how individuals collectively create and characterize places in their environment. There is significant research interest in developing methods of analysis to exploit these digital repositories for a wide array of applications related to understanding urban function (i.e., smart-cities technologies), urban planning (e.g., how people are using spaces over time) and urban design (how people perceive and are influenced by the composition and configuration of city elements).

The objectives of this research were to map the use of space as sensed through social media posts, and to identify locations and spatial patterns of individual spatial expressions obtained from social media messages in an urban setting. Ultimately, our aim was to develop a computational approach to identifying activity centres and movement signatures from georeferenced social media streams. Our secondary objective was to analyze these patterns in relation to the broader environment within which they occurred.

Georeferenced Twitter messages posted within the City of Toronto were collected over the period of a year. Individual-based activity centres were derived using three methods: density surface thresholding, buffering, and the DBSCAN spatial clustering algorithm. Consistency of clustering methods were compared for quantitative and qualitative similarities. Individual clusters were organized as $k - \text{order}$ ranks based on density, and visualized at different times of the day and year. Movement signatures were detected using simple trajectory clustering methods.

Results indicate that geographically encoded social media traces provide interesting insight into the use of urban space on daily and seasonal time scales and show promise for aiding understanding of how urban design affects activity in urban spaces.

Maritime Anomaly Detection Via a Shape Based Local Association Measure

S. A. Roberts¹

¹ Wilfrid Laurier University, Waterloo, Canada, sroberts@wlu.ca

Recently global marine Automatic Identification System (AIS) messages have been captured in a large database allowing for tracking of global shipping traffic. We present an analysis methodology for detecting anomalous trajectories (see Martineau and Roy, 2011) in the Northern Pacific shipping lanes. This is part of a larger effort to develop a maritime tracking and surveillance system based on AIS messages and other data sources. The primary new contribution of this work is the development of a variant of a local spatial autocorrelation measure. In this new measure we replace the traditional attribute difference measure with the Small-Le metric (Small and Le, 2002), a signed measure of turning angle on a parameterized curve representation, that provides a distance measure explicitly for shape, as described in the following sketch. Signed measures $\alpha_0 = 0, \alpha_1, \dots, \alpha_m$ at points with parameters, s_0, s_1, \dots, s_m , where, $0 = s_0 < s_1 < \dots < s_m < s_{m+1} = \ell$. Then $z(s)$ is a polygonal path defined by the union of line segments of length $s_{j+1} - s_j$ meeting at angles α_j . Then we let,

$$\theta(s) = \sum_{k=0}^j \alpha_k , \quad s_j \leq s < s_{j+1} , \quad j = 0, 1, \dots, m \quad \text{and standardizing the parameter get} \quad \theta^*(s) = \theta(s \cdot \ell) . \quad (1)$$

Next we define,

$$\Delta_j^*(s) = \theta^*(s) - \int_0^1 \theta^*(u) du , \quad 0 \leq s \leq 1 \quad (2)$$

Finally defining the shape distance ρ between curves z_1 and z_2 as,

$$\rho^2(z_1, z_2) = \int_0^1 [\Delta_1^*(u) - \Delta_2^*(u)]^2 du . \quad (3)$$

Adjacencies are calculated via discrete Fréchet distances, δ_{dF} (Eiter and Mannila, 1994), calculated pairwise between trajectories. A clustering technique defines the neighbourhood structure, N_i . So we have a metric for comparing morphological similarity independent of absolute position and a metric for similarity in absolute position. This measure may be summarized below as,

$$s_i = \sum_{N_i} \frac{\rho^2(z_i, z_j)}{\delta_{dF}(z_i, z_j)} . \quad (4)$$

Note that we approximate distance calculations in the above metric with geodesics on a sphere. We show discrimination between similarly shaped trajectories close in space (normal traffic), differently shaped trajectories close in space (potential anomaly), similar trajectories separated in space (potential anomaly) and differently shaped trajectories separated in space (normal - different traffic).

References

- [1] T. Eiter and H. Mannila, *Computing discrete Fréchet distance*, Report CD-TR 94/64 Christian Doppler Labor für Expertensysteme, Technische Universität Wien, Austria (1994).
- [2] E. Martineau and J. Roy, *Maritime Anomaly Detection: Domain Introduction and Review of Selected Literature*, Report TM 2010-460, Defense Research and Development Canada, Valcartier, Quebec, Canada (2011).
- [3] C.G. Small and H. Le, *The statistical analysis of dynamic curves and sections*, Pattern Recognition, **35**, pp. 1597-1604 (2002).

Modelling the Risk Landscape of Japanese Encephalitis in the Kathmandu Valley, Nepal

J Metelka¹, C. Robertson²

¹ Wilfrid Laurier University, Waterloo, Canada

² Wilfrid Laurier University, Waterloo, Canada

Japanese Encephalitis (JE) is a vector-borne, zoonotic disease that is transmitted by mosquitoes of the genus *Culex*. JE is the leading cause of viral encephalitis in Southeast and East Asia with an estimated 68,000 clinical cases occurring each year causing approximately 20,400 deaths [1]. About 30-50% of survivors experience permanent neurologic or psychiatric sequelae [1]. The disease is more likely to occur in children and is traditionally more common in rural and agricultural areas [2]. Like other vector-borne diseases, the transmission of the JE virus is highly dependent on landscape factors. Such factors include rice paddy fields, which supply breeding habitat for *Culex* mosquitoes, the geographic distribution of pig farms, which supply the virus's amplifying hosts, and the movement of wading birds from the family *Ardeidae*, which are also hosts of the virus and generally more mobile than pigs. The placement and interactions of these landscape factors compose the risk landscape of the JE virus [3]. Developing prevention and control policies for JE therefore requires understanding how landscape risks interact.

The objectives of this research were to develop a computer model for landscape risks of JE in the Kathmandu Valley in Nepal. Previous research has outlined the major risk factors that contribute to JEV transmission. The aim of this study was to combine previous research on landscape risk into a single modelling framework that would allow exploration of the underlying risk landscape. Landscape risk models can be used to examine various scenarios that may affect the epidemiology of JE.

An agent-based model (ABM) was developed to represent landscape-level risk for JE in the Kathmandu Valley. A large number of datasets were obtained to parameterize model variables, including demographic data, landcover classifications, climate normals and daily precipitation, and WHO surveillance data describing cases of AES and JE from 2007 to 2012. The ABM was implemented in NetLogo v.5.0.5.

Results indicate that the ABM representation of landscape JE risk supports deeper understanding of human/landscape interactions for JE, and subsequent policy development and planning. Although agent-based modelling techniques have been used in many studies to examine disease spread, they have rarely been used to represent human/landscape interactions on vector-borne disease risk in a given population. These results provide evidence that ABMs may be a new tool available for health promotion and control of vector-borne diseases that have strong landscape components.

References

- [1] World Health Organization, *Media Centre: Fact Sheet*, Japanese Encephalitis, [Online: Accessed 11 March 2015]
- [2] J. S. Mackenzie, D. J. Gubler, and L. R. Petersen, *Emerging Flaviviruses: The Spread and Resurgence of Japanese Encephalitis, West Nile and Dengue Viruses*, Nature Publishing Group, 10, pp. S98–S109 (2004)
- [3] E. F. Lambin, A. Tran, S. O. Vanwambeke, C. Linard, and V. Soti, *Pathogenic Landscapes: Interactions Between Land, People, Disease Vectors, and Their Animal Hosts*, International Journal of Health Geographics, 9, pp. 1–13 (2010)

New metrics for new datasets: A comparison of a local spatial analysis methods for homogenous patch extraction in user-generated content.

H. Lawrence¹, C. Robertson², R. Feick¹

¹ University of Waterloo, Waterloo, Canada

² Wilfrid Laurier University, Waterloo, Canada

Geographic data is often collected as a series of observations and measurements (e.g. bird counts, census data) and is frequently aggregated for analysis at modifiable grains and extents. These grains and extents are generally chosen at the discretion of the researcher, sometimes based on arbitrary criteria where there appear to be ‘enough data’. Given a source of geographically referenced spatial data, methods are required to identify sub-areas of the dataset with properties suitable for more in-depth analysis – a task we call homogeneous patch extraction. This paper will describe the properties of a new method for the extraction of homogenous patches in irregular lattice data that explicitly handles features, while common to most datasets, are especially accentuated with user generated content (UGC), such as variable coverage, density, and user-heterogeneity. Coverage is defined as the ratio of the number of cells that contain a minimum threshold of observations to the total number of cells within the study area. Density is assessed by calculating the areas of the four quadrants of a Moran’s scatterplot and finding the difference between the largest area and the smallest area, normalized by patch size. The final component of the metric, user-heterogeneity, quantifies evenness in user-level contributions of UGC over the candidate patch. The component-wise metric is included in an iterative algorithm which identifies groups of adjacent units which maximize the statistic. In this paper we explore the properties of the iterative adjacency algorithm relative to the metric by comparing the highest ranking patch to those found by other methods of spatial analysis, including local Moran’s I, local Geary’s C, and the Kulldorff spatial scan statistic on simulated data and several well-known datasets. Through this analysis, we show that including extra dimensions of data quality are important for homogenous patch extraction tasks, which are missing from other methods, and are particularly important for UGC.

Prediction Model of Ship Movement Resulting from the Effects of Environmental Covariates

B. Friedrich¹

¹ Wilfrid Laurier University, Waterloo, Canada, bfriedrich@wlu.ca

This study will look at a stochastic model created to predict the varying drift patterns of large ships off the coast of North America. This model will be produced by analyzing the effects of environmental covariates (wind & wave) on anchored ships and generates a predicted location of a ship since its last known location. The predicted location will then be compared to the real location of the ship and then analyzed to determine the error of the model.

The data to be used consists of 3 data sets for the year 2013: AIS (Automatic Identification System) data, HF (High Frequency) radar for determining wave velocity, and HF radar for determining wind direction. AIS data is a tracking system installed on large ships that provides information such as ship velocity, size, and geographic position. AIS data will be used to view the drift paths created from a group of anchored ships over a certain time span. The HF radar data can provide data on the wave velocity and wind direction in an area for a given time and space in a multidimensional data set.

To determine the effects of environmental covariates the HF radar data will be compared against the AIS data of the large ships. By generating vector paths for large tanker ships and comparing them to the velocities of wind and waves a relation can be evaluated. By applying the relation, a predicted location can be determined on a ship given the velocities of the covariates and a time span. By using a method such as Kalman Filtering, a comparison of the predicted location and the real location will illustrate the error in the model.

If found to be of high enough accuracy, this information could be applied to multiple applications in ship path prediction and for search and rescue purposes.

We look forward to welcoming you in Waterloo, Canada at the AMMCS-2013 Conference!

References

1. Pallotta, G., Vespe, M., & Bryan, K. (2013). Vessel pattern knowledge discovery from AIS data: A framework for anomaly detection and route prediction. *Entropy*, 15, 2218–2245. doi:10.3390/e15062218
2. Gurgel, K. W., Schlick, T., Horstmann, J., & Maresca, S. (2010). Evaluation of an HF-radar ship detection and tracking algorithm by comparison to AIS and SAR data. 2010 International Waterside Security Conference, WSS 2010. doi:10.1109/WSSC.2010.5730246
3. Pérez Arribas, F. (2007). Some methods to obtain the added resistance of a ship advancing in waves. *Ocean Engineering*, 34, 946–955. doi:10.1016/j.oceaneng.2006.06.002

Using geosocial media to aid understanding of place sensing

Shanqi Zhang¹, Robert Feick²

¹ Department of Geography and Environment Management, University of Waterloo, Waterloo, Canada, s72zhang@uwaterloo.ca

² School of Planning, University of Waterloo, Waterloo, Canada, robert.feick@uwaterloo.ca

Increasingly, social media generated through Twitter, YouTube, Facebook and similar socio-technological communities, is linked to locations through embedded GPS coordinates. Often referred to as geosocial media, these data sources provide real-time and firsthand data from citizens and therefore draw attention from government officials as these data can become potential sources of monitoring public sentiments, collecting public input and sensing public opinions toward urban places. Nonetheless, using geosocial media to obtain local knowledge and understand place sensing is still challenging because geosocial media includes as much noise as useful information and how to automatically harvest information from geosocial media that is related to specific places or development plans remains underexplored. Moreover, although text messages sent through social media may have associated locations, the actual content of the message may refer to other locations, which increases the difficulty for determining the relevance of a text to a particular place. In this paper, we propose a geo-computational method to automatically determine: 1) the thematic relevance of a text message to a local planning topic and 2) the spatial relevance of a text message to a specific location. We first build a local planning vocabulary from authoritative documents, such as official minutes from city meetings and online news by identifying keywords and their importance levels. We then apply algorithms to calculate the thematic and spatial relevance of each text message based on language modeling methods. By considering each text message as a language model and each planning-related topic as a query, the relevance score of a message to a topic was calculated using a Bayes likelihood estimate. The spatial relevance of a text message is then calculated according to both its thematic relevance to planning topics and the occurrence of the place name in the sentence. A case study was carried out in Region of Waterloo, Ontario, using Twitter Tweets collected through March 2014 to March 2015, to show the efficiency of the proposed method. Our empirical study shows the capability of geosocial media in mining public opinions toward urban places and provides insights on the potential of geosocial media as an aid to understand place sensing outside of the traditional arenas of public engagement processes.

SS-GTA Game Theory: Applications and Evolutionary Games

An Evolutionary Game Approach for Dynamic Resource Allocation Problems

Ashkan Pashaie¹, Lacra Pavel², Christopher J. Damaren³

¹ Electrical and Computer Engineering Department, University of Toronto, Toronto, Canada

² Electrical and Computer Engineering Department, University of Toronto, Toronto, Canada pavel@control.utoronto.ca

³ UTIAS, University of Toronto, Toronto, Canada

In this work we consider the distribution and supply of resources in allocation problems by using an evolutionary game-theoretic approach. These challenging engineering problems can include distribution of labor, water, fuel, energy, etc.. As an example we consider a water distribution system (WDS). We use a novel game-theoretic approach, based on modelling WDS control as a population game. A population game is typically defined via a memoryless mapping from the population state to a set of static payoff functions,[1]. To specify the process of a game play, the agents are given opportunities to change their choices by using a revision protocol, which describes how and when the agents switch their strategies. Specific protocols lead to specific mean dynamics, which can be analyzed to predict the game evolution and possible convergence to Nash equilibria. Inspired by [2], in this work we consider a more general class of games played over dynamical systems. This is an extension in that the evolutionary dynamics act on dynamically modified payoffs instead of static payoff functions. This modification can be interpreted as a coupling between a set of evolutionary dynamics and a population game with dynamic dependencies. We consider a water distribution system (WDS) as a population game with dynamic dependencies, [3]. A WDS consists of a number of storage tanks that need to supply water such that customer demands are satisfied while a certain pressure at the tanks output is maintained. We consider that a large number of artificial agents or players fill the tanks by allocating a certain amount of resources to each tank. We assume that each tank is a possible action choice. When a player picks a tank, he dedicates a small portion of the resource to fill that tank. We assign a payoff to each strategy or tank and design different revision protocols. Using these protocols agents can model the game evolution in time as an interconnection between the corresponding evolutionary dynamics and the dynamical system modelling the tanks. We utilize a game-theoretic approach along with a convex-optimization-based controller. Unlike [3] where only the replicator dynamics was used to control the game, we consider different evolutionary dynamics with better properties. Specifically, it is well-known that by using the replicator dynamics a potential problem of nonNash convergence can occur. To address this issue, we consider Brown-von Neumann-Nash (BNN) dynamics and the Smith dynamics, that discard the non-Nash equilibrium points. Furthermore, we add the total input flow controller to enhance the behavior of the system. We characterize convergence to a Nash equilibrium as stability of the closed-loop system. We present sufficient conditions that ensure stability of the negative feedback interconnection of the corresponding evolutionary dynamics and the dynamical system modelling the tanks. These are based on powerful passivity results and Lyapunov stability theorem. Furthermore, we provide an improvement to controllers that achieves a degree of robustness for the system, by rejecting a certain type of disturbances. We consider a generalization to a class of distribution problems that maintains the same stability properties as for the WDS application. The effectiveness of our approach is verified by simulations.

References

- [1] W. H. Sandholm, *Population games and evolutionary dynamics*. MIT press, 2010.
- [2] M. J. Fox and J. S. Shamma, *Population games, stable games, and passivity*, Games, vol. 4, no. 4, pp. 561–583, 2013.
- [3] E. Ramirez-Llanos and N. Quijano, *A population dynamics approach for the water distribution problem*, International Journal of Control, vol. 83, no. 9, pp. 1947–1964, 2010.

Coalitional operating room planning and scheduling

V. Roshanaei¹, D. Aleman², D. Urbach³

¹ University of Toronto, Toronto, Canada, vroshana@mie.utoronto.ca

² University of Toronto, Toronto, Canada, aleman@mie.utoronto.ca

³ University Health Network, Toronto, Canada, david.urbach@uhn.ca

We extend the operating room planning and scheduling problem from a single independent hospital to a coalition of multiple hospitals in a strategic network, where a pool of patients, surgeons, and operating rooms (ORs) are collaboratively planned. We incorporate various patient-to-surgeon allocation flexibilities into our study, and also introduce a new coefficient to determine the tightness of a surgeon's schedule among his/her surgeries, leading to increased surgeon throughput. To solve the resulting mixed-integer dual resource constrained model, we develop a novel logic-based Benders' decomposition (LBB) that employs a multi-objective allocation master problem (MP), multiple scheduling sub-problems (SPs), and novel Benders' cuts. Collaborative OR scheduling with traditional dedicated patient-to-surgeon allocation flexibility results in 11.79% cost savings, on average, while semi-flexible and flexible patient-to-surgeon allocation flexibility increase cost savings to 17.11% and 30.12%, on average, respectively.

To assess each hospital's benefit from collaborative planning, we use a game theoretic approach to fairly redistribute the payoff acquired from a coalition of hospitals via Shapley value [1] and to show the coalitional stability among hospitals by illustrating the convexity [2] of the coalition. The Shapley value captures the average marginal contributions of hospital h , averaging over all possible sub-coalitions from which the grand coalition could be built. Additionally, we show how much each hospital has benefited from the coalition. After forming a coalition among $|H|$ hospitals, the payoff should be distributed among them based on their contribution. Real-valued payoffs associated with sub-coalitions S and the grand coalition of $|H|$ hospitals are denoted $v(S)$ and $v(|H|)$, respectively. Given a coalitional game $(|H|, v)$, there is a unique payoff division $x(v) = \phi(|H|, v)$ that divides the acquired payoff of the grand coalition among its members. The payoff division $\phi_h(|H|, v)$ for each hospital $h \in H$ is computed via the Shapley value as follows:

$$\phi_h(|H|, v) = \frac{1}{|H|!} \sum_{S \subseteq |H| \setminus \{h\}} |S|!(|H| - |S| - 1)! [v(S \cup \{h\}) - v(S)].$$

Our cooperative game $G = (|H|, v)$ is convex because it satisfies the definition of convexity: $v(S \cup T) \geq v(S) + v(T) - v(S \cap T)$, $\forall S, T \subset H$. Convexity states that the grand coalition has the highest payoff and no member of a coalition can profitably deviate the coalition with the hope of forming a more cost-effective coalition [2]. Since our game involves costs instead of rewards, we use the negative of the objective function value to show the convexity of our coalitional game. Due to the convexity of our coalition, our game has a non-empty core. Experimentally, coalitional operating room planning and scheduling is stable under semi-flexible and flexible patient-to-surgeon allocation flexibility. We use these game theoretic observations to provide managerial insights and motivate cooperative behavior among hospitals.

References

- [1] L.S. Shapley, *A value for n-person games*, In Kuhn, H. W., and Tucker, A. W., eds., Contributions to the Theory of Games, Annals of Mathematics Studies **2**, pp. 307-317, Princeton University Press (1953).
- [2] LS. Shapley, *Cores of convex games*, Int. J. of Game Theory **1**, 1, pp. 11-26 (1971).

Deck Based Versions of Mathematical Games

D. Ashlock¹, E. Wild¹

¹ University of Guelph, Guelph, Canada *{dashlock|ewild}@guelph.ca*

If we consider two player simultaneous mathematical games such as prisoner's dilemma or rock-paper-scissors, players may make any move they like. There is a well developed theory for understanding such games and these games are examples of Nash games. In this presentation we consider the impact of using decks of cards with moves for the games printed on them. This moves these games into the realm of generalized Nash games [1]. For prisoner's dilemma [2] it has been found that the deck-based version of the game is actually two games, neither of which is similar to the unlimited move version of iterated prisoner's dilemma. One is a coordination game, the other an anti-coordination game with the two games neatly segmented by the line

$$C + D = T + S \tag{1}$$

where these are the cooperation, defection, temptation, and sucker payoffs. When strategies are considered under replicator dynamics then the coordination game is exponentially dominated by whatever strategy is most common in the initial game. The anti-coordination game induces a situation that, in biology, is called *negative density dependent selection* [3].

This presentation extends an initial investigation in deck-based versions of mathematical games beyond the initial work in prisoner's dilemma, working out how the transformation into the space of generalized Nash games imposed by using the limited spectrum of moves represented by the cards affects game character and dynamics. An evolutionary algorithm is used to investigate strategies that arise under two-parent reproduction when negative density dependent selection is used. The types of strategies that arise are constrained not only by the need to perform well but to maximize the probability their children will be unlike them. This situation yields a novel evolutionary dynamic.

References

- [1] P. T. Harker, *Generalized Nash Games and Quasi-variational Inequalities*, European Journal of Operational Research **54**, pp. 81-94 (1991).
- [2] D. Ashlock and E. Knowles, *Deck-Based Prisoner's Dilemma*, Proceedings of the IEEE 2012 Conference on Computational Intelligence in Games, pp. 17-24, (2012).
- [3] M. Hixon, *Density Dependence and Independence*, Chichester: John Wiley & Sons Ltd, (2009).

Evolution of cooperation in a multidimensional phenotype space

D. Kroumi¹, S. Lessard²

¹ Département de mathématiques et statistiques, Université de Montréal, Canada, {kroumid}@dms.umontreal.ca

² Département de mathématiques et statistiques, Université de Montréal, Canada, {lessards}@dms.umontreal.ca

The emergence of cooperation in populations of selfish individuals is a fascinating topic that has inspired much theoretical work. An important model to study cooperation is the phenotypic model, where individuals are characterised by phenotypic properties that are visible to others. The phenotype of an individual can be represented for instance by a vector $\mathbf{x} = (x_1, \dots, x_n)$, where x_1, \dots, x_n are integers. The population can be well mixed in the sense that everyone is equally likely to interact with everyone else, but the behavioral strategies of the individuals can depend on their distance in the phenotype space. A cooperator can choose to help other individuals exhibiting the same phenotype and defects otherwise. Cooperation is said to be favored by selection if it is more abundant than defection in the stationary state. This means that the average frequency of cooperators in the stationary state strictly exceeds 1/2. Antal *et al.* 2009 found conditions that ensure that cooperation is more abundant than defection in a one-dimensional (i.e. $n = 1$) and an infinite-dimensional (i.e. $n = \infty$) phenotype space in the case of the Prisoner's Dilemma under weak selection. However, reality lies between these two limit cases. In this paper, we derive the condition for the evolution of cooperation in the case of a phenotype space of any finite dimension. This is done by applying a perturbation method to study a mutation-selection equilibrium under weak selection. This condition is obtained in the limit of a large population size by using the ancestral process. The best scenario for cooperation to be more likely to evolve is found to be a high population-scaled phenotype mutation rate, a low population-scaled strategy mutation rate and a high phenotype space dimension. The biological intuition is that a high population-scaled phenotype mutation rate reduces the quantity of interactions between cooperators and defectors, while a high population-scaled strategy mutation rate introduces newly mutated defectors that invade groups of cooperators. Finally it is easier for cooperation to evolve in a phenotype space of higher dimension because it becomes more difficult for a defector to migrate to a group of cooperators. The difference is significant from $n = 1$ to $n = 2$ and from $n = 2$ to $n = 3$, but becomes small as soon as $n \geq 3$.

References

- [1] T. Antal, H. Ohtsuki, J. Wakeley, P.D. Taylor and M.A. Nowak, *Evolution of cooperation by phenotypic similarity*, Proc. Natl. Acad. Sci. USA. **106**, 8597–8600 (2009).

Evolutionary game theory under time constraint

Ross Cressman¹

¹ Department of Mathematics, Wilfrid Laurier University, Waterloo, Canada, rcressman@wlu.ca

Evolutionary game theory was developed under a number of simplifying assumptions. One that is not often explicitly stated is that each interaction among individuals takes the same amount of time no matter what strategies these individuals use. When interaction time is strategy-dependent, it is more realistic to take individual fitness as the payoff received per unit time. For instance, two Hawks interacting in the standard two-player Hawk-Dove game are assumed to engage in a fight, implying that they will be involved in fewer interactions than Doves since they avoid such contests.

Such effects have been taken into account in classical foraging theory models of optimal predator behavior. I will briefly explain how optimization results for classical diet choice and patch choice models (including those that involve the effects of simultaneously encountering different types of prey and of prey recognition effects) can be reinterpreted as Nash equilibrium solutions of time-constrained evolutionary games. I will also explore how interaction times affect the evolutionary outcome (e.g. the evolutionarily stable strategy (ESS) and stability of the replicator equation) in the Hawk-Dove game. If time permits, I will show that cooperation can evolve in the repeated Prisoner's Dilemma game when the number of rounds is under the players' control.

Spatial Spread of an Epidemic through Public Transportation Systems with a Hub

F. Xu¹, C. C. McCluskey², R. Cressman³

¹ Wilfrid Laurier University, Waterloo, Canada, fxu.feixu@gmail.com

² Wilfrid Laurier University, Waterloo, Canada, ccmcc8@gmail.com

³ Wilfrid Laurier University, Waterloo, Canada, rcressman@wlu.ca

In this talk, we investigate an epidemic spreading among several locations through a transportation system, with a hub connecting these locations. Public transportation is not only a bridge through which infections travel from one location to another but also a place where infections occur since individuals are typically in close proximity to each other due to the limited space in these systems. A mathematical model is constructed to study the spread of an infectious disease through such systems. A variant of the next generation method is proposed and used to provide upper and lower bounds of the basic reproduction number for the model. Our investigation indicates that increasing transportation efficiency, and improving sanitation and ventilation of the public transportation system decrease the chance of an outbreak occurring. Moreover, discouraging unnecessary travel during an epidemic also decreases the chance of an outbreak. However, reducing travel by infectives while allowing susceptibles to travel may not be enough to avoid an outbreak.

The Emergence of Cooperative Breeding Systems with Resource Allocation

J. D. Dunn¹, T. Vujicic², G. Wild³

¹ Department of Applied Mathematics, The University of Western Ontario, London, Canada, jdunn45@uwo.ca

² Department of Economics, The University of Western Ontario, London, Canada, tvujicic@uwo.ca

³ Department of Applied Mathematics, The University of Western Ontario, London, Canada, gwild@uwo.ca

Cooperative breeding is a social system in which individuals (helpers) forego reproduction to increase the reproductive success of another. Several hypotheses have been presented to explain the evolution of this counter-intuitive behaviour, but none have investigated how helper resource allocation alters the conditions under which cooperative breeding can emerge. In this study, we investigate helper resource allocation within the confines of benefits of philopatry, which are the direct benefits realized by helpers through delayed dispersal. Benefits of philopatry has previously been shown to promote the emergence of cooperative breeding [1].

To better reflect the biology in cooperative breeding systems we extend an existing model [2] by incorporating self-fertilization and sex allocation for breeders, as well as resource allocation for helpers. Sex allocation is simply how resources are divided between female and male components of reproductive fitness. Initially, the population is composed of two classes: floaters and breeders. Floaters are sexually inactive and seek vacant territories to begin reproduction. Breeders are sexually active and in the extended model are able to either self-fertilize or outbreed with some probability. Sex allocation imposes a trade-off between the allotment of resources towards female and male components of reproductive fitness. This, together with self-fertilization, influences the evolutionarily stable sex allocation strategy in the absence of help. Offspring dispersal strategies also evolve, such that when the probability of dispersal is not equal to unity, helpful behaviour exists within the population. Both of these evolutionary arguments are constructed using inclusive fitness and linear stability analyses. We compare the results of two models, one where offspring cannot inherit their natal breeding territory, and another where they can.

The evolutionarily stable breeder sex allocation strategy recovers classical results in the limits when breeders are resource deprived, and when breeders are resource saturated. In the former, a breeder's sex allocation strategy follows Hamilton's local mate competition result [3]. In the latter, a breeder's sex allocation strategy follows Fisher's theory of equal investment in the sexes [4]. We find that the breeder sex allocation at evolutionary equilibrium effectively balances the marginal gains from investment in reproduction through male and female function. As a result, helpers that optimally allocate their resources always act as if they were breeders who had unlimited resources.

This study shows that resource allocation only has a significant role in the evolution of cooperative breeding systems when breeders and helpers have an intermediate amount of resources. When individuals are resource saturated or resource deprived, varying a helper's resource allocation has negligible effects on the emergence of these systems. Since optimal helper resource allocation can cause cooperative breeding to emerge where it otherwise could not, it provides motivation to search for genetic remnants of this phenomenon.

References

- [1] P. B. Stacey and J. D. Ligon, *The benefits-of-philopatry hypothesis for the evolution of cooperative breeding: variation in territory quality and group size effects*, Am. Nat. **1137**, pp. 831-846 (1991).
- [2] G. Wild and C. Koykka, *The inclusive-fitness logic of cooperative breeding with benefits of natal philopatry*, Phil. Trans. R. Soc. B. **369**, 20130361 (2014).
- [3] W. D. Hamilton, *Extraordinary sex ratios*, Science **156**, pp. 477-488 (1967).
- [4] R. A. Fisher, *The genetical theory of natural selection*, Oxford, United Kingdom: Clarendon (1930).

The Emergence of Equilibrium Help Strategies in a Model of Competitive Helping

E. Wild¹, M.-G. Cojocaru¹

¹ University of Guelph, Guelph, Canada {ewild,mcojocar}@uoguelph.ca

We investigate and generalize a model of competitive helping within a biological market started by Barclay in [1]. In this generalized model, two groups of *mutant* and *non-mutant* individuals provide some amount of help and their fitness function is dependent on this level of help, the cost of providing the help, and the fact that help is proportionally reciprocated by other individuals. Competitive helping occurs when individuals actively try to outdo each other by helping more than other individuals. To account for deviations from proportional matching, Barclay introduces the parameter z to represent the degree to which one receives help in proportion to the relative amount of help one provides, drawn from literature in operant conditioning on the matching law (see [2, 3]) which predicts a quantitative relationship between the relative rates of response and relative rates of reinforcement.

In order to assess the emergence of equilibrium help strategies as adopted by proportions of the population, we examine the competition over available help within three settings: the first is that of replicator dynamics equations, which gives us insight into the complexity of the model; the second is a heuristic approach in which the amount of help provided by the individuals in each group evolves over time; finally, the third approach is that of a heterogeneous agent-based model which allows us to examine the results of autonomous individuals making decisions without the knowledge that being part of one of two groups afforded them previously.

In [1], the author claims that the evolutionary stable level of helping increases with the size of the biological market and the degree of matching, z . Our results show that helping does not increase with the population size, and while there are some instances of an increase in help provided as a result of competition when z increases, this competition is actually a detriment to both groups and in most cases, one group simply gives up. As z increases further, competition actually occurs less often as individuals prefer to give and receive nothing than to compete for an increasingly negative payoff. This finding contradicts the idea that as z approaches infinity we should see a winner-take-all system where the most generous individual receives all of the help produced. In particular, future biological models of this sort need to more carefully define the effects of matching and partner choice so as to construct a model that properly describes this behaviour.

References

- [1] P. Barclay, *Competitive helping increases with the size of biological markets and invades defection*, Journal of Theoretical Biology. **281**, pp. 47-55 (2011).
- [2] W. M. Baum, *Matching, undermatching, and overmatching in studies of choice*, Journal of the Experimental Analysis of Behavior. **32**, pp. 269-281 (1979).
- [3] J. H. Warden and I. S. Burgess, *Matching since Baum*, Journal of the Experimental Analysis of Behavior. **38**, pp. 339-348 (1982).

The evolution of body size in ecological food web networks

R. Rael¹

¹ Tulane University, New Orleans, LA, USA rrael@tulane.edu

To understand how ecosystems respond to both natural and human-caused environmental changes, it is crucial to consider evolutionary processes. Food webs are network models of who eats whom in an ecosystem. Recent studies have led to advancements in understanding how dynamic ecological interactions such as omnivory, competition, and mutualism affect ecological structure and stability. However, as species evolve, the composition of species traits and interaction strengths within a food web change and it is not yet well understood how such adaptation influences the network properties and stability of food webs. Many current evolutionary food web models utilize a speciation process for building the networks, though species traits are static once they enter the web. In order to study the relationship between trait adaptation, network structure, and extinction, I build food webs using a stochastic speciation process while applying Darwinian dynamics, whereby populations and their traits continuously change through time. Because body size is an important factor in determining feeding relationships, consumption rates, and energy efficiency, I consider it as an adaptive strategy. I track the properties of the network along with species biomasses and traits through time and will discuss how strategies and network properties correlate with the likelihood of survival and of causing secondary extinctions. Knowing how traits influence structural properties in dynamic ecosystems will help provide a better understanding of their resilience to both natural and human caused environmental changes.

The evolution of inequity aversion under local competition

P. Barclay¹, B. Stoller²

¹ University of Guelph, Canada, barclayp@uoguelph.ca

² Toronto, Canada, benstoller203@gmail.com

Empirical research in psychology and experimental economics has repeatedly shown that people reject uneven divisions of resources, even at personal cost. Mathematical models in evolutionary game theory have sought to understand the origins of this “inequity aversion”, and the selective pressures that would cause it to evolve. We suggest that the scale of competition is crucial: under local competition with few competitors, it pays to reject inequity – even at cost – if doing so will cost one’s competitor(s) more. When competing against the broader population (“global competition”), absolute payoffs are more important than payoffs relative to one’s immediate group, so inequity aversion is not as beneficial. I will present a game theoretical model of inequity aversion, using the well-known “Ultimatum Game” as a model situation. In an Ultimatum Game, a “Proposer” proposes a division of a resource to a “Responder”: if the offer is accepted then the resource is divided as proposed, but if it is rejected then both players earn zero from the transaction. I vary the scale of competition as the number of people with whom the Responder competes: under pure local competition, life is a zero-sum competition between Proposer and Responder, whereas under global competition the Responder competes with others in the population as well. The results of my mathematical model are that as competition becomes more local, the equilibrium level of demands gets higher. We empirically verify the predictions of this mathematical model using two behavioural experiments using the Ultimatum Game under local and global competition. Together, this supports the idea that local competition may have been responsible for the evolution of people’s demands for fairness and aversion to inequity within relationships.

We look forward to welcoming you in Waterloo, Canada at the AMMCS-2013 Conference!

Figure 1: The AMMCS-CAIMS-2015 Congress is organized in cooperation with SIAM and AIMS.

References

The Maximum Number of Coexisting Species in Evolutionary Dynamics

J. van den Hoogen¹, J.S. Brown² J. Apaloo³

¹ Queen's University, Kingston, Canada, josee.van.den.hoogen@queensu.ca

² University of Illinois, Chicago, USA, squirrel@uic.edu

³ St. Francis Xavier University, Antigonish, Canada, japaloo@stfx.ca

In the evolutionary games literature, statements have been made regarding the maximum number of species that can coexist in the ecological equilibrium phases of an evolutionary game. More specifically, it has been noted that when the strategy has just one component, at most two species can coexist in the neighbourhood of a peak [1]. It has also been shown that a single species with m -dimensional trait space can have at most $m + 1$ alleles or species coexisting at equilibrium [2]. However, no detailed analyses of evolutionary game models have been carried out to provide deeper understanding of these results. Using computer simulations based on faunal build-up algorithm and invasive species ecology, we explore this question of an upper bound on the number of species that can coexist in an evolutionary game. Evolutionary dynamics in the neighbourhood of a strategy that is an evolutionarily stable neighbourhood invader strategy (ESNIS), and of a strategy that is a neighbourhood invader strategy (NIS) [3] but not an evolutionarily stable strategy (ESS) [4] are considered. For an n -species ($n = 1, 2$) evolutionary game with m -dimensional ($m = 1, 2$) trait space, our simulation results revealed an upper bound of the form

$$n(m + 1) \tag{1}$$

for the two cases of evolutionary dynamics in a small neighbourhood of an ESNIS, and in a small neighbourhood of the NIS that is not an ESS. However, this result may not apply when we consider the evolutionary dynamics in an extended neighbourhood of a NIS that is not an ESS.

References

- [1] J.S. Brown, Y. Cohen and T.L. Vincent, *Adaptive dynamics with vector-valued strategies*, Evolutionary Ecology Research **9**, pp 719-756 (2007).
- [2] F. Christiansen and V. Loeschcke, . *Evolution and intraspecific competition. III. One- locus theory for small additive gene effects and multidimensional resource qualities*, Theoretical Population Biology **31**: pp. 33-46 (1987).
- [3] J. Apaloo, *Revisiting strategic models of evolution: The concept of neighbourhood invader strategies*, Theoretical Population Biology **52**, pp. 71-77 (1997).
- [4] J. Maynard Smith and G.R. Price, *The Logic of Animal Conflict*, Nature **246**, pp. 15-18 (1973).

The world's biomes and primary production as a foraging game played by plants

G.G. McNickle¹, M.A. Gonzalez-Meler², D.J. Lynch², J.L. Baltzer¹, and J.S. Brown²

¹ Wilfrid Laurier University, Waterloo, Canada, gmcnickle@wlu.ca, jbaltzer@wlu.ca

² University of Illinois at Chicago, Chicago, USA, mmeler@uic.edu, dlynch3@uic.edu, squirrel@uic.edu

Vegetation is one of the major players in the global climate system. For example, photosynthesis by plants in the northern hemisphere results in intra-annual atmospheric CO₂ fluctuations of ~8ppm [1,2]. Additionally, observed climate change has been less severe than predicted by early models, in part because plants have fixed more CO₂ biomass than expected [3-5]. Unlike many components of the global climate system, vegetation has been difficult to model because it responds to changing conditions on short and long timescales through a combination of short-term plasticity and longer-term ecological and evolutionary dynamics [6]. Here, we describe a model of vegetation growth that captures this complexity in plant dynamics assuming plant reproductive output depends simultaneously on three components of a foraging game to achieve an Evolutionarily Stable Strategy (ESS). Plants in this model have a vector strategy composed of leaf, stem and root production in response to resource competition. We will show that a model composed of just 5 parameters is able to predict global patterns in primary production. Interestingly, the model is also able to predict the global distribution of the world's major biome classifications (e.g. tropical forest vs arctic tundra), and the basic body plans of plants found in those biomes (e.g. trees vs shrubs vs herbs).

The use of evolutionary game theory permits vegetation to evolve to an ESS dynamically within the model without specifying the type of vegetation *a priori*. Thus the model not only accurately predicts production, but predicts how biomes will change from one type to another with changing climate. We expect the general modeling framework presented here to be a starting point for the development of vegetation models that capture the full complexity of vegetation eco-evolutionary dynamics. Vegetation in climate modeling has often been inappropriately approached in the same way as the modeling of geophysical processes; however, plants are alive, and ecologically and evolutionarily dynamic. Our results suggest that capturing this eco-evolutionary dynamic is critical to understanding biome distributions and NPP.

References

- [1] RB Myneni, CD Keeling, CJ Tucker, G Asrar, RR Nemani: *Increased plant growth in the northern high latitudes from 1981 to 1991*. Nature, **386**, 6626, pp. 698-702. (1997)
- [2] CD Keeling, TP Whorf, M Wahlen, J Vanderplicht: *Interannual extremes in the rate of rise of atmospheric carbon-dioxide since 1980*. Nature, **375**, 6533, pp. 666-670. (1995)
- [3] RJ Norby, DR Zak: *Ecological lessons from free-air co₂ enrichment (face) experiments*. Annu Rev Ecol Evol Syst, **42**, pp. 181-203. (2011)
- [4] BB Stephens, KR Gurney, PP Tans, C Sweeney, W Peters, L Bruhwiler, P Ciais, M Ramonet, P Bousquet, T Nakazawa et al: *Weak northern and strong tropical land carbon uptake from vertical profiles of atmospheric CO₂*. Science, **316**, 5832, pp. 1732-1735. (2007)
- [5] RR Nemani, CD Keeling, H Hashimoto, WM Jolly, SC Piper, CJ Tucker, RB Myneni, SW Running: *Climate-driven increases in global terrestrial net primary production from 1982 to 1999*. Science, **300**, 5625, pp. 1560-1563. (2003)
- [6] GG McNickle, R Dybzinski: *Game theory and plant ecology*. Ecol Lett, **16**, 4, pp. 545-555. (2013)

Time-dependent casual encounters games and HIV spread

S.Athar¹, M. Cojocaru²,

¹ University of Guelph, Canada, sathar@uoguelph.ca

² University of Guelph, Canada, mcojocar@uoguelph.ca

In [1] the authors model and investigate casual sexual encounters between two members of a population with two possible HIV states: positive and negative, using a Nash game framework in which players try to maximize their expected payoff resulting out of a possible encounter. Each player knows their own HIV status, but do not know the HIV status of a potential partner. They do however have a personal assessment of the risk that the potential partner may be HIV positive. Last but not least, each player has a ranked list of preferences of potential types of sexual outcomes: unprotected, protected, or no sexual outcome. In [1], the game model is studied via 1- and 2-dimensional sensitivity analyses on parameters such as the utility values of unprotected sex of an HIV negative individual with an HIV positive, and values of personal risk (of encountering an HIV positive partner) perception.

In this work, we introduce time as a variable which affects players' risk perceptions, and thus their strategies. Given that HIV transmission happens when an HIV positive player has a non-zero probability (strategy) of having unprotected sex with a HIV negative player, we are also able to keep track of the time evolution of the overall fraction of HIV positive individuals in the population, as reflected as an outcome of repeated casual encounters.

We model the time-dependence in two ways: first we play a repeated game a discrete, finite number of times, to mimic possible repeated encounters of 1 individual with others in the population; second, we model a continuous time dynamic game (as in [3]) where we compute the stable strategies of each player based on a dynamical system defined on a set of functions. In the cases where (depending on model parameter values) the encounter games have a unique solution, we expect the two techniques to lead to the computation of the same time-dependent Nash equilibrium curve. In cases where uniqueness is not guaranteed, then the continuous time model gives a much better understanding of how players' strategies adapt over time to a time-dependent Nash equilibrium curve.

References

- [1] Tully, S., Cojocaru, M.-G., Bauch, C. , *Multiplayer games and HIV transmission via casual encounters*, submitted to: Mathematical Biosciences and Engineering, AIMS. (2015).
- [2] Cojocaru, M.-G., Daniele, P., Nagurney, A. *Projected dynamical systems and evolutionary variational inequalities via Hilbert spaces and applications*, JOTA 127 No. 3 , 549 - 563. (2005)
- [3] Cojocaru, M.-G., Greenhalgh, S. , *Dynamic games and hybrid dynamical systems* , Optimization and Engineering, Applications of Variational Inequalities Issue, Volume 13 Issue 3, 505 - 517.(2011)

Truncation selection and the ESS

B. Morsky¹, C. T. Bauch²

¹ University of Guelph, Canada, bmorsky@uoguelph.ca

² University of Waterloo, Waterloo, Canada, cbauch@uwaterloo.ca

There is significant conflict between the ESS, and agent-based simulations of replicators, which incorporate more realistic natural conditions. This conflict has focussed on several assumptions of the replicator equation, namely: complete mixing, an infinite population, asexual reproduction, proportional selection, and mean payoffs. Here, we relax the conditions of mean payoffs and proportional selection by incorporating payoff distributions and truncation selection into our models. Truncation selection occurs when replicators below a threshold are culled from the population. Our first equation uses fitness proportional selection and payoff distributions; we show that it is equivalent to the replicator equation. We explore stochastic and deterministic agent-based truncation selection simulations. Our second and third equations use payoff distributions and two different types of truncation selection, dependent and independent, to model the deterministic agent-based models. We analyze these models to show where the equilibria for these systems differ from the ESS of the replicator equation. Further, we show that our models can foster cooperation in the prisoner's dilemma.

Understanding the Dynamics of Infinite Niche Packing through Simulations

R. Cressman¹, A. Halloway², G.G. McNickle¹, J. Apaloo³, J.S. Brown²

¹ Wilfrid Laurier University, Waterloo, Canada

² University of Illinois at Chicago, Chicago, USA

³ St. Francis Xavier University, Antigonish, Canada

Often the questions on the creation and persistence of biodiverse systems can be summed up into a single question: Why are there so many species? [1] Mathematical analysis of a simple, game-theoretic Lotka-Volterra system below has shown that a large number of species can be generated and exist in stable ecosystem, with the model allowing, theoretically, for a continuum of species [2]. While mathematical analysis has proven to be helpful in understanding the system, it is hard pressed to retrieve any analytical results beyond 2 species. Computational simulation of the system, though, can help overcome the hurdles analytical calculations.

$$\frac{dN_i}{dt} = N_i G(v, u, N) \Big|_{v=u_i} \quad \text{and} \quad \frac{du_i}{dt} = \frac{\partial G(v, u, N)}{\partial v} \Big|_{v=u_i}, \quad i = 1, \dots, n,$$

where

$$G(v, u, N) = r \left(1 - \frac{\sum_{j=1}^n a(v, u_j) N_j}{K(v)} \right).$$

Our simulations of this system have shown that a large number of species, 1024 to be precise, is possible. As the number of species increases, the range over which their strategies exist grows in a sub-linear fashion. The simulations point to the existence of large number of species when the niche space is infinite. As the number of species increase from one to a large number, the distance between the extant strategies declines. Thus the niche space is continually divided as species number grows. Despite the growth of the number of species in the system, the total productivity of the system, as measured by total population size, goes to a constant, thereby reducing population size for individual species down to 0.

Simulations also help us understand what leads to and the dynamics of a system with a finite number of species. A finite species system will occur if there is a minimum constant basal level of competition or if the niche axis occurs over a finite range. Simulating the system has shown that the minimum level competition and finite niche space affects the both number of species and range of traits; as minimum competition increases or niche space shrinks, the number of species decreases and the range of traits shrinks.

References

- [1] G.E. Hutchinson, *Homage to Santa Rosalia or Why Are There So Many Kinds of Animals?*, Am. Nat. **93**, 870, pp. 145-159 (1959).
- [2] J. Roughgarden, *Theory of Population Genetics and Evolutionary Ecology: An Introduction*, Macmillan, New York, (1979).

Using Heritage To Determine Strategy In Multi-Agent Systems

A.W. Hlynka¹, Z. Kobti¹

¹ University of Windsor, Windsor, Canada {hlynkaa,kobti}@uwindsor.ca

“History” is a common word used for a type of knowledge, and is defined by the British dictionary as “all that is preserved or remembered of the past” [1]. In comparison, “heritage” is a word defined by the British dictionary as “anything that has been transmitted from the past or handed down by tradition” [1]. These two words may appear very similar, but can have different effects on strategies and behaviour in agent systems. For example, an agent might use history to recall past actions and outcomes, but would use heritage both to remember the past and also define current state of an individual, which might lead to greater likelihood of cooperation (if two agents had a similar heritage) or competition (if two agents had competing heritages) in certain situations. Heritage can also be viewed as an appropriate extension to “cultural algorithms,” a evolutionary algorithm designed to use belief spaces to represent the knowledge gained by individuals. Past work has effectively used cultural algorithms in game theory and evolution simulation [2], but only by letting an individual belong to a single population at a time that determines strategy and behaviour, when real systems might contain more complex assignments of populations.

This concept is placed into a “Heritage-Dynamic” agent system, using a basic model inspired by the “side-blotted lizard” and “rock-paper-scissors” models in evolutionary game theory. This model assumes three different populations with an equal number of agents, with population A overtaking B, B overtaking C, and C overtaking A. Agents are paired randomly to mate, the winning agent of the pair passing their immediate population ID to the offspring that takes the place of the parents. Additionally, the populations of both agents are added to the children as their heritage. For example, a child Z from agents X (A) and Y (B), where X won, would adopt a tree structure A <- A + B, that symbolizes the total weight each original population has in an agent. After several generations, individual agents would have large tree structures symbolizing their heritage, made up of multiple populations.

To apply the use of heritage against the example test model, different strategies are deployed: a competitive strategy, a cooperative strategy, and a cunning strategy (which would either be competitive or cooperative based on personal gain), first with one strategy shared amongst all populations, then with each population starting with one of the three strategies, then with the ability for the populations to adopt a new strategy based on the heritage of its related agents. The use of heritage in this system produces more interesting cyclic patterns overtime compared to the standard computer simulation of the “rock-paper-scissors” game. The use of heritage can be applied to evolutionary algorithms, such as genetic or cultural algorithms, for more varied behaviour and also allows researchers to better understand the effect different populations can have on individuals.

References

- [1] Collins English Dictionary – Complete & Unabridged 10th Edition, 2015.
- [2] R. G. Reynolds, Z. Kobti, T. Kohler and L.Y. Yap, *Unraveling ancient mysteries: reimagining the past using evolutionary computation in a complex gaming environment*, in *IEEE Transactions on Evolutionary Computation*, 9, 6, pp. 707-720 (2005).

SS-MACHS Modeling, Analysis and Control in Hybrid Systems

A new measure of robust stability for impulsive differential equations

K.E.M. Church

University of Ottawa, Canada

Impulsive differential equations are frequently employed as models of biological, chemical, and physical systems, among others. The property of these equations that makes them attractive in applications is the impulse effect, which allows for the inclusion of fast dynamics that might otherwise complicate the analysis of the model, were they to be included in a continuous, as opposed to discrete, manner [1].

The majority of monographs on impulsive differential equations state that they are reasonable approximations of continuous models with perturbations if the perturbations themselves occur quickly, relative to the overall dynamics. In practice, this is often taken as an assumption of the model in question. Methods to determine how quickly these perturbations must occur for the model to be a good “fit” to the associated continuous models have yet to be seen in the literature. Using the recently introduced concept of *impulse extensions*, we have identified impulsive differential equations that provide poor approximations of associated continuous models with perturbations, no matter how small the time-scale on which they occur is [1, 2]. On the more constructive side, under very mild regularity conditions, we have developed methods to determine a correct perturbative time-scale on which the qualitative dynamics of a stable, linear, periodic impulsive differential equation will be preserved in the associated continuous models. The correct time-scale is captured in what we call the *time-scale tolerance* of an impulsive differential equation. This construction has applications to any field where impulsive differential equations are used as models, since it provides a measure of robust stability with respect to what is, essentially, the time-scale separation assumption built into the model: that the duration of impulse effect is negligible.

The time-scale tolerance is not unique, but is, rather, defined with respect to a chosen family of parameterized mean-zero perturbations, denoted \mathcal{E} . The choice of the family \mathcal{E} is analogous to the choice of ϵ in linear robust stability analysis by ϵ -pseudospectra. Moreover, the pseudospectral radius is, indeed, central to the definition of the time-scale tolerance.

During the presentation, a brief introduction to impulse extension equations will be given, followed by an overview and definition of the time-scale tolerance, its usefulness, and how it can be computed in practice. We conclude with an illustrative example.

References

- [1] K. Church, *Applications of impulsive differential equations to the control of malaria outbreaks and introduction to impulse extension equations: a general framework to study the validity of ordinary differential equation models with discontinuities in state*, M.Sc Thesis, University of Ottawa (2014)
- [2] K.E.M. Church and R.J. Smith?, *Analysis of piecewise-continuous extensions of periodic linear impulsive differential equations with fixed, strictly inhomogeneous impulses*, in *Dynamics of Continuous, Discrete and Impulsive Systems Series B: Applications & Algorithms*, Vol. 21, 101-119 (2014).

Input-to-State Stability and H_∞ Performance for Stochastic Control Systems with Piecewise Constant Arguments

M.S. Alwan¹, X.Z. Liu²

¹ University of Waterloo, Waterloo, Canada, malwan@uwaterloo.ca

² University of Waterloo, Waterloo, Canada, xinzhi.liu@uwaterloo.ca

The stochastic control system with piecewise constant arguments considered in the research work has the form

$$dx(t) = (Ax(t) + Bu(t) + Gw(t) + f(x(t), x(\gamma(t))))dt + g(x(t), x(\gamma(t)))dW(t), \quad (1a)$$

$$z(t) = Cx(t) + Fu(t), \quad (1b)$$

$$x(t_0) = x_0, \quad (1c)$$

where $x \in \mathbb{R}^n$ is the system state, $u \in \mathbb{R}^p$ is the control input, $w \in \mathbb{R}^q$ is an external disturbance, $f \in \mathbb{R}^n$ and $g \in \mathbb{R}^{n \times m}$ represent lumped uncertainties, W is an m -dimensional Wiener process, and A, B, G, C , and F are known matrices with proper dimensions. The argument γ which is a piecewise constant function taking values in the infinite set $\Xi = \{\xi_k\}_{k=0}^\infty$ represents the switching signal of system (1); that is, $\gamma : [t_k, t_{k+1}) \rightarrow \Xi$ for any k . So that, the role of this function is to switch among the the values of the state x at some $t \in [t_k, t_{k+1})$.

Since the dynamics in (1) has both continuous and discrete components, the system can be adequately embedded under the hybrid system umbrella [1]. Moreover, the system can also be viewed as a special type of functional differential equations, where the state history is given at certain individual points, rather than intervals.

The primary objective of this work is to establish the problems of input-to-state stabilization (ISS) and H_∞ performance of system (1), where Lyapunov-Razumikhin technique and a dwell-time type switching signal are used to analyze these properties. We should remark that in this work system (1) is being viewed as a hybrid (particularly switched) system with differential equations of Itô type.

Assuming that a full access to the all system states is available, it has been found that under a feedback control law of the form $u = Kx$, for some control gain matrix $K = -\frac{1}{\varepsilon}B^TP$ with ε being a positive tuning parameter and P being a positive-definite matrix, the ISS in mean square (m.s.) of system (1) is achieved if the switching moments are governed by dwell-time type switching signal. Furthermore, if the external system disturbance has a bounded energy, then the controlled output is also bounded in m.s. with an H_∞ -norm bound $\bar{\gamma}$. To further illustrate the proposed results, a numerical example with simulations is presented. For more studies about systems of differential equations with piecewise constant argument, readers may refer to [1, 2].

References

- [1] M.S. Alwan, X.Z. Liu, and W.-C. Xie. Comparison principle and stability results for nonlinear differential equations with piecewise constant arguments, *Journal of the Franklin Institute*, **350**, pp. 211-230, 2013.
- [2] J. Wiener. *Generalized Solutions of Functional Differential Equations*. World Scientific, Singapore, 1993.

New master-slave synchronization criteria of chaotic Lur'e systems with time-varying-delay feedback control

Kaibo Shi^{1,2}, Xinzhi Liu², Hong Zhu¹, Shouming Zhong³

¹ School of Automation Engineering, University of Electronic Science and Technology of China, China, skbs111@163.com

² Department of Applied Mathematics, University of Waterloo, Canada, xinzhi.liu@uwaterloo.ca

³ School of Mathematical Sciences, University of Electronic Science and Technology of China, China, zhongsm@uestc.edu.cn

This study focuses on the problem of designing an effective state-feedback controller for master-slave synchronization issues of chaotic Lur'e systems with time-varying delay. The time delay is assumed to be a time-varying continuous function which is bounded below and above by positive constants. By constructing an appropriate Lyapunov-Krasovskii functional (LKF), novel delay-dependent synchronization conditions are obtained. Besides, by employing a new free-matrix-based inequality via introducing a set of slack variables and compassing the Wirtinger based inequality as a special case, the wishful controller gain matrix are achieved in terms of linear matrix inequalities (LMIs) that can be solved easily.

First, consider the following master-slave synchronization scheme of two identical chaotic Lur'e systems with time-varying delay feedback control:

$$\mathbf{M} : \dot{x}(t) = Ax(t) + B\varphi(Dx(t)), \quad p(t) = Hx(t), \quad (1)$$

$$\mathbf{S} : \dot{y}(t) = Ay(t) + B\varphi(Dy(t)) + u(t), \quad q(t) = Hy(t), \quad (2)$$

$$\mathbf{C} : u(t) = K(p(t - d(t)) - q(t - d(t))), \quad (3)$$

which consists of master system M , slave system S and controller C . M and S with $u(t) = 0$ are identical chaotic time-delay Lur'e systems with state vectors $x(t), y(t) \in R^n$, outputs of subsystems $p(t), q(t) \in R^l$, respectively, $u(t) \in R^n$ is the slave system control input, and $A \in R^{n \times n}$, $B \in R^{n \times n_d}$, $D \in R^{n_d \times n}$, $H \in R^{l \times n}$ are known real matrices, $K \in R^{n \times l}$ is the time-varying delay controller gain matrix to be designed. It is assumed that $\varphi(\cdot)$ is the nonlinear function in the feedback path.

Assumption A. Time-varying delay $d(t)$ is differential function and satisfies the following condition:

$$0 < d_L \leq d(t) \leq d_U, \quad \dot{d}(t) \leq \mu < 1. \quad (4)$$

where d_L, d_U and μ are constants.

Assumption B. The nonlinear function $\varphi_s(\alpha)$ satisfies the following sector condition:

$$\varphi_s(\alpha) \in K_{[k_s^-, k_s^+]} = \{\varphi_s(\alpha) \mid \varphi_s(0) = 0, k_s^- \alpha^2 \leq \alpha \varphi_s(\alpha) \leq k_s^+ \alpha^2, \alpha \neq 0\} \quad (5)$$

Next, given the synchronization schemes (1-3), the synchronization error is defined as $r(t) = x(t) - y(t)$, and we can get the following synchronization error system:

$$\dot{r}(t) = Ar(t) + B\zeta(Dr(t), y(t)) - KHR(t - h(t)), \quad (6)$$

where $\zeta(Dr(t), y(t)) = \varphi(Dr(t) + Dy(t)) - \varphi(Dy(t))$. Let $D = [d_1, d_2, \dots, d_{n_d}]^T$ with $d_s \in R^n$, $s = 1, 2, \dots, n_d$. Under Assumption B, it is easy to obtain that $\zeta_s(d_s^T r, y)$ satisfies the following condition

$$k_s^- \leq \frac{\zeta_s(d_s^T r, y)}{d_s^T r} = \frac{\varphi_s(d_s^T(r+y)) - \varphi_s(d_s^T y)}{d_s^T r} \leq k_s^+, \quad \forall r, y \in R, d_s^T r \neq 0. \quad (7)$$

Finally, one numerical simulation example of Chua's circle is given to illustrate adequately the effectiveness and advantages of the proposed results.

On a Topological Obstruction in the Reach Control Problem

M. Ornik¹, M.E. Broucke²

¹ University of Toronto, Canada, melkior.ornik@scg.utoronto.ca

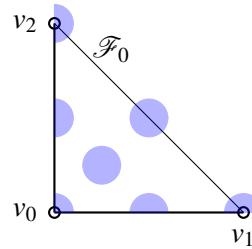
² University of Toronto, Canada, broucke@control.utoronto.ca

The reach control problem (RCP) considers the affine system

$$\dot{x} = Ax + Bu + a, \quad x \in \mathcal{S} \quad (1)$$

where $x \in \mathbb{R}^n$ is the state, $u \in \mathbb{R}^m$ is the input, and $\mathcal{S} \subset \mathbb{R}^n$ is an n -dimensional simplex. The goal is to find a state feedback control $u = u(x)$ that drives the states of the system to exit \mathcal{S} through a predetermined *exit facet* \mathcal{F}_0 , without first leaving through other facets. Recent efforts have been focused on characterizing the appropriate class of feedback to solve the problem, with significant attention paid to affine feedback. For an overview, see [1]. When affine feedback fails, a natural next step is to consider continuous state feedback.

A necessary condition for a feedback control to solve RCP is that the closed-loop system have no equilibria in \mathcal{S} . It can be shown that closed-loop equilibria lie in the set $\mathcal{O}_{\mathcal{S}} = \{x \in \mathcal{S} \mid Ax + a \in \text{Im}(B)\}$. Furthermore, in order to not leave simplex \mathcal{S} through facets other than the exit facet \mathcal{F}_0 , the velocity vectors $Ax + Bu + a$ at points on other facets must point inside \mathcal{S} . This results in an *invariance condition* at every point, depicted by the blue cones in the figure below.



This paper shows that, as a consequence of the above conditions, there is a *topological obstruction* to solving RCP by continuous state feedback. This notion can be interpreted as analogous to the topological obstruction to continuous feedback stabilization for nonlinear control systems [2]. The problem we consider is as follows: *Does there exist a nonvanishing continuous function $f : \mathcal{O}_{\mathcal{S}} \rightarrow \mathcal{B}$ such that $f(x)$ satisfies the invariance conditions at every point $x \in \mathcal{O}_{\mathcal{S}}$?*

The above problem is fully solved in this paper for the case of two- and three-dimensional simplices. Our solution method is novel and uses topological retractions. An appealing geometric condition is identified as the necessary and sufficient condition for existence of a topological obstruction, i.e., as the necessary condition for solvability of RCP using continuous feedback. In addition, the affine analogue to the above problem is completely solved in two and three dimensions. Interestingly, the necessary conditions for solvability by affine feedback are no more restrictive than the necessary conditions for solvability by continuous state feedback.

References

- [1] G. Ashford and M.E. Broucke. Design of reach controllers on simplices. *IEEE Conf. Decision and Control*. December 2013.
- [2] R.W. Brockett. Asymptotic Stability and Feedback Stabilization. In *Differential Geometric Control Theory*. Birkhäuser, Boston, R.W. Brockett, R.S. Millman and H.J. Sussmann, eds., pp. 181-191 (1983).

On Pinning Control, Synchronization and Controllability of Complex Networks

Guanrong (Ron) Chen
City University of Hong Kong

Abstract

In this presentation, we will address some new issues and challenges faced by the conventional control theory in a complex dynamical network environment. After introducing the network science background, we will discuss some research problems regarding pinning control and pinning synchronization of complex dynamical networks, as well as pinning controllability of directed networks. We will show that the coupling structure of a network is essential; therefore, how to utilize the topological features of a complex network to benefit control is of ultimate importance. This also raises some interesting and yet challenging technical questions for control theory and practice under the framework of weighted and directed dynamical networks.

Biography [\[In case needed\]](#)

The speaker received the M.Sc. degree in Computer Science from Sun Yat-sen University, China and the Ph.D. degree in Applied Mathematics from Texas A&M University, USA. Currently he is a Chair Professor and the Founding Director of the *Centre for Chaos and Complex Networks* at the City University of Hong Kong, prior to which he was a tenured Full Professor in the University of Houston, Texas, USA. Prof. Chen is a Fellow of the IEEE and a Member of the Academia Europaea.

Passivity analysis of the stochastic system with time delay

Yuanhua Du^{1,2}, Xinzhi Liu², Shouming Zhong¹

¹ School of Mathematical Sciences, University of Electronic Science and Technology of China, China,
duyuanhua@126.com,zhongsm@uestc.edu.cn

² Department of Applied Mathematics, University of Waterloo, Canada, xzliu@uwaterloo.ca

This paper focus on the passivity analysis issue for stochastic system. The essence of the passivity theory is that the passive properties of a system can keep the system internally stable. The stochastic differential equation is Itô type, in which the random noise is approximated by a Brownian motion process. Based on the Itô formula and Lyapunov functionals, a set of novel sufficient conditions are obtained to guarantee the exponential passivity for the considered system. We also present a numerical example to verify the obtained result.

That we consider the stochastic systems as follows.

$$dx(t) = [Dx(t) + W_0 f(x(t)) + W_1 f(x(t - d(t))) + u(t)]dt + g(t, x(t), x(t - d(t)))d\omega(t),$$

$$y(t) = f(x(t)) + f(x(t - d(t))) + u(t),$$

where $x(t) = [x_1(t), x_2(t), \dots, x_n(t)] \in R^n$ is the state vector, $y(t) \in R^n$ is the output vector, $f(x(t)) \in R^n$ denotes the activation function, D , W_0 and W_1 are real constant matrices of appropriate dimensions, $u(t) \in R^n$ is an external input vector. $\omega(t) = (\omega_1(t), \dots, \omega_m(t))$ is m-dimensional Brownian motion defined on a complete probability space (Ω, P) with a natural filtration $\{\mathcal{F}_t\}_{t \geq 0}$ generated by $w(s) : 0 \leq s \leq t$, where we associate Ω with the canonical space generated by $w(t)$, and denote by the associated σ -algebra generated by $w(t)$ with the probability measure P , and satisfying $E\{d\omega(t)\} = 0$, $E\{d\omega^2(t)\} = dt$; the noise perturbation $g : R^n \times R^n \rightarrow R^{n \times m}$. $\tau(t)$ is time-varying delay satisfying $0 \leq d_1 \leq \tau(t) \leq d_2$, $0 \leq \dot{d}(t) \leq \tau < 1$.

Pinning Stabilization of Cellular Neural Networks with Time-Delay Via Delayed Impulses

Kexue Zhang¹, Xinzhi Liu², Wei-Chau Xie³

¹ Department of Applied Mathematics, University of Waterloo, Waterloo, Canada, k57zhang@uwaterloo.ca

² Department of Applied Mathematics, University of Waterloo, Waterloo, Canada, xzliu@uwaterloo.ca

³ Department of Civil and Environmental Engineering, University of Waterloo, Waterloo, Canada, xie@uwaterloo.ca

Cellular neural networks (CNNs) have been investigated extensively due to their wide applications in image processing, and pattern recognition [1]. Recently, many stability criteria of impulsive CNNs have been reported, and impulsive controllers have been designed accordingly to stabilize the CNNS. However, to our best knowledge, no pinning delayed-impulsive controller has been considered for the stabilization problem of CNNs.

Therefore, in this talk, we will introduce the stabilization problem of CNNs with time-delay. A novel pinning impulsive controller with delays will be proposed, and the pinning algorithm will be introduced. Based on the Razumikhin-type stability results in [2], sufficient conditions will be established to guarantee the designed pinning impulsive controller stabilize the unstable CNNs. It will be shown that the CNNs can be successfully stabilized by pinning a small portion of CNNs' nodes at certain discrete instants. Moreover, it worth noting that the pinning control strategy is also applicable to stabilization and synchronization problems of various dynamical systems, such chaotic systems, Cohen-Grossberg neural networks [3], Hopfield neural networks [4], and neural networks with reaction-diffusion terms.

Numerical examples will be given to illustrate the main results. In order to observe the pinning control process, CNN with two nodes will be considered. Two types of simulation results will be given: pinning control one node at each impulsive instant, and pinning control two nodes at the impulsive times. Comparison of these simulation results will also be discussed.

References

- [1] L.O. Chua and L. Yang, *Cellular neural networks: applications*, IEEE Trans. Circuits Syst. **35**, 10, pp. 1273-1290 (1998).
- [2] P. Cheng, F. Deng, and F. Yao, *Exponential stability analysis of impulsive stochastic functional differential systems with delayde impulses*, Commun. Nonlinear Sci. Numer. Simulat. **19**, 6, pp. 2104-2114 (2014).
- [3] T. Li, A. Song, and S. Fei, *Synchronization control for arrays of coupled discrete-time delayed Cohen-Grossberg neural networks*, Neurocomputing **74**, 1-3, pp. 197-204 (2010).
- [4] S. Guo, L. Huang, and L. Wang, *Exponential stability of discrete-time Hopfield neural networks*, Comput. Math. Appl. **47**, 8-9, pp. 1249-1256 (2004).

Stability Properties of Singular Systems Subject To Impulsive Effects

M.S. Alwan¹, H. Kiyak², X.Z. Liu³

¹ University of Waterloo, Waterloo, Canada, malwan@uwaterloo.ca

² University of Waterloo, Waterloo, Canada, hkiyak@uwaterloo.ca

³ University of Waterloo, Waterloo, Canada, xinzhi.liu@uwaterloo.ca

In this work, we consider the impulsive singular systems of the form

$$\begin{aligned} Ex(t) &= Ax(t) + g(t, x), & t \neq t_k \\ \Delta x(t) &= B_k x(t), & t = t_k, \quad k \in \mathbb{N} \\ x(t_0) &= x_0, \end{aligned} \tag{1}$$

where $x \in \mathbb{R}^n$ is the system state variable, and $A, B_k, E \in \mathbb{R}^{n \times n}$ are known matrices with E being singular and the matrix pair (E, A) being regular. $\{t_k\}_{k=1}^\infty$ are the impulsive times which form an increasing sequence satisfying $t_{k-1} < t_k$ and $\lim_{k \rightarrow \infty} t_k = \infty$. $\Delta x = x(t^+) - x(t^-)$ where $x(t^-)$ (and $x(t^+)$) is the state just before (and just after) the impulsive action with $x(t^+) = \lim_{s \rightarrow t^+} x(s)$. The solution x is assumed to be left-continuous, i.e., $x(t_k^-) = x(t_k)$. $g(t, x)$ represents the system perturbation which is assumed to be bounded by a linear growth bound.

The interest here is to address the stability and stabilization problems of system (1) where the impulses occur at fixed times t_k for all $k \in \mathbb{N}$. To achieve these results, we use the method of Lyapunov function and differential inequalities.

It has been noticed that if the underlying continuous system is exponentially stable and the impulses are viewed as a perturbing force, then the impulsive system (1) maintains its stability property if the impulses act slowly. On the other hand, if the continuous system is unstable, impulses can play as a stabilizer to the system provided that the impulsive effects are applied frequently. To illustrate the effectiveness of these results, numerical examples with simulation are presented. For more studies about singular systems, readers may refer to [1, 2, 3].

References

- [1] S. L. Campbell, *Singular systems of differential equation*, Toronto, Copp Clark Pitman (1980).
- [2] S. L. Campbell, *Singular systems of differential equation II*, Toronto, Copp Clark Pitman (1982).
- [3] G. Duan, *Analysis and design descriptor linear systems*, D. Y. Geo, R. W. Ogden and R.C. Batra (eds), New York, Spring (2011).

Switched singularly perturbed systems with reliable controllers

M.S. Alwan¹, X.Z. Liu², T.G. Sugati³

¹ Department of Applied Mathematics, University of Waterloo, Waterloo, Canada, malwan@uwaterloo.ca

² Department of Applied Mathematics, University of Waterloo, Waterloo, Canada, xinzhi.liu@uwaterloo.ca

³ Department of Applied Mathematics, University of Waterloo, Waterloo, Canada, tsugati@uwaterloo.ca

In this work, we consider the switched control singularly perturbed systems of the form

$$\begin{cases} \dot{x} &= A_{11\sigma(t)}x + A_{12\sigma(t)}z + B_{1\sigma(t)}u, \\ \varepsilon_{\sigma(t)}\dot{z} &= A_{21\sigma(t)}x + A_{22\sigma(t)}z + B_{2\sigma(t)}u, \end{cases} \quad (1)$$

where $x \in \mathbb{R}^m$, $z \in \mathbb{R}^n$ are the system slow and fast states, respectively. σ is the switching law which is a piecewise constant function defined by $\sigma : [t_0, \infty) \rightarrow \mathcal{S} = \{1, 2, \dots, N\}$. The role of σ is to switch among the system modes. For each $i \in \mathcal{S}$, and $j, k = 1, 2$, A_{jk_i} and B_{ji} are known real constant matrices with A_{22_i} being a nonsingular, Hurwitz matrix, and $0 < \varepsilon_i \ll 1$ is a small perturbation parameter. $u \in \mathbb{R}^l$ is the system input, which is a feedback control law. Due to dominant behaviour of the slow state, the control law is assumed to take the form of $K_i x$, for some control gain K_i . We also assume that a full access to all the system modes is available, though the mode-dependent, slow-state feedback controllers experience faulty actuators of an outage type.

The focus here is to address the problem of exponential stability of the above system not only when all the control actuators are operational, but also when some of them experience failures.

The novelty of this work, then, is to write some new sufficient conditions that guarantee the exponential stability property of system (1), where the methodology of multiple Lyapunov function and the average dwell-time (ADT) switching signal are used to achieve this goal. Also, system (1) is viewed as an interconnected system that has been decomposed into isolated, lower order, slow and fast subsystems, and the interconnection between them.

It has been observed that if the degree of stability of each isolated mode is greater than the interconnection between them, the i th interconnected mode is exponentially stable, and, then, the switched singularly perturbed system in (1) is also exponentially stable for all admissible switching signals with ADT. The stability analysis adopted in this work, in turn, results in evaluating the range of the perturbation parameter ε_i . A numerical example with simulations is presented to further clarify the proposed results. For more studies about the switched singularly perturbed systems, readers may consult [1, 2].

References

- [1] M.S. Alwan, *Stability of Hybrid Singularly Perturbed Systems with Time Delay*, Master's Thesis, University of Waterloo, Ontario, Canada, 2006.
- [2] P.V. Kokotovic, H.K. Khalil and J. O'Reilly, *Singular Perturbation Methods in Control: Analysis and Design*. Academic Press, Inc., London, 1986.

Switching controlled synchronization of nonlinear systems with time-delays

P. Stechlinski¹, X.Z. Liu²

¹ Massachusetts Institute of Technology, Cambridge, USA, pstechli@mit.edu

² University of Waterloo, Waterloo, Canada, xzliu@uwaterloo.ca

The synchronization of nonlinear systems, which has important applications in areas like secure communications, is possible using switching control when a continuous control law is inadequate or cannot be found. Motivated by how frequently time-delays arise in physical and biological phenomena, the focus of this work is on studying the synchronization of systems composed of integro-differential equations under various switching control strategies. The modeling framework is a switched system formulation, which are systems that evolve according to mode-dependent dynamics and experience abrupt changes between modes triggered by threshold events. Using Razumikhin-like theorems, classes of switching rules (e.g. average dwell-time satisfying, periodic, state-dependent) are determined which guarantee the stabilization of switched systems with bounded or unbounded time-delays (and hence synchronization in the original context).

SS-MFMCR Mathematical Finance - Modeling, Computation and Risk Management

A Framework for Efficient Valuation of Large Portfolios of Unit-Linked Insurance Products

Amir Hejazi¹ and Ken Jackson²

¹ Computer Science Department, University of Toronto, Toronto, ON, M5S 3G4, Canada. amir@cs.toronto.edu

² Computer Science Department, University of Toronto, Toronto, ON, M5S 3G4, Canada. krj@cs.toronto.edu

Because of unique features of unit-linked insurance products with embedded guarantees, insurance companies have been successful in selling large volumes of these products and hence they have accumulated large portfolios of these financial instruments. The embedded guarantees, which are the attractive features of these products for consumers, expose insurers to substantial risk. In the fear of a market crash and to meet regulatory requirements, insurance companies have started hedging programs to manage their risk exposures. As part of these hedging programs, insurers have to value large portfolios of insurance products to compute the Greeks associated with their portfolios. Because of embedded guarantees in these products, conventional Monte Carlo simulations are computationally expensive. In this talk, we will introduce a novel method to approximate the Greeks that is based on ideas in spatial functional data analysis that can reduce the computational load while achieving high accuracy.

Accurate Operator Splitting Approximation for Pricing CEV Spread Options

C.F. Lo¹ and X.F. Zheng²

¹ The Chinese University of Hong Kong, Hong Kong SAR, cflo@phy.cuhk.edu.hk

² The Chinese University of Hong Kong, Hong Kong SAR, xfzheng@phy.cuhk.edu.hk

Spread options whose payoff is contingent upon the price difference of two underlying assets are very popular in a wide range of financial markets. Unlike pricing single-asset options, pricing spread options is a very challenging task because the distribution of the spread of two correlated lognormal variables is not available. The simplest approach is to evaluate the expectation of the final payoff over the joint probability distribution of the two correlated lognormal underlying assets by means of numerical integration. However, practitioners often prefer to use analytical approximations rather than numerical methods because of their computational ease. Among various analytical approximations, Kirk's approximation seems to be the most popular and is the current market standard, especially in the energy markets [1]. The aim of our paper is to present a new closed-form approximation based upon the Lie-Trotter operator splitting method [2,3] to value spread options for underlying assets following the constant-elasticity-of-variance (CEV) processes:

$$dS_i = \mu_i S_i dt + \sigma_i S_i^{\beta/2} dZ_i \quad \text{for } i = 1, 2 . \quad (1)$$

(Note: the limiting case $\beta \rightarrow 2$ yields the lognormal process.) Since the joint probability distribution function of the two correlated CEV underlying assets does not exist in closed form, one must resort to numerical approaches like Monte Carlo simulation or finite-difference method. Unfortunately, there is a trade-off between computational efficiency and accuracy in these techniques. The approximate price formula derived by our operator splitting method closely resembles Kirk's formula for Black-Scholes spread options and has the same favourable properties. The proposed approach can also be straightforwardly extended to pricing the multi-asset CEV spread options. Unlike the numerical approaches, the high dimensionality does not compromise the efficiency and accuracy of the operator splitting method. In fact, numerical results show that our approximation gives very accurate estimates of the spread option prices efficiently.

References

- [1] E. Kirk, "Correlation in the Energy Markets" in *Managing Energy Price Risk* (Risk Publications, 1995).
- [2] H.F. Trotter, "Approximation of Semi-groups of Operators", *Pacific J. Math.* vol.8, pp.887-919 (1958).
- [3] H.F. Trotter, "On the Product of Semi-groups of Operators", *Proceedings of the American Math Society* vol.10, no.4, pp.545-551 (1959).

Algorithms for Finding Copulas Minimizing Convex Functions of Sums and Applications to Finance and Risk Management

C. Bernard¹, D. McLeish²

¹ Grenoble Ecole de Management, carole.bernard@grenoble-em.com

² University of Waterloo, dlmcleis@uwaterloo.ca

We propose improved rearrangement algorithms to find the dependence structure that minimizes a convex function of the sum of dependent variables with given margins. We develop a multivariate dependence measure that can assess the convergence of the rearrangement algorithms and can be used as a stopping rule. Using MCMC techniques, we are able to design an algorithm that converges to the global optimum. We finally show how to apply these algorithms for example to finding the dependence among variables for which the marginal distributions and the distribution of the sum are known. As an example, we can find the dependence between two uniformly distributed variables that makes the distribution of the sum of two uniform variables indistinguishable from a normal distribution.

This algorithm has important applications in finance and risk management in dealing with model uncertainty on risk aggregation and risk assessment. A typical example of application is in credit risk measurement with the assessment of the risk of a large portfolio of risky loans. Other examples can be found in Embrechts et al. (2013).

References

- [1] Embrechts, P., Puccetti, G., Rüschendorf, L.: *Model uncertainty and VaR aggregation*. Journal of Banking and Finance **37**(8), 2750-2764 (2013).

Bond and CDS Pricing with Recovery Risk: The Stochastic Recovery Black-Cox Model

A. Cohen¹, N. Costanzino²

¹ Michigan State University, USA, albert@math.msu.edu

² RiskLab, Toronto, Canada, nick.costanzino@gmail.com

Building on recent work incorporating recovery risk into structural models [2], we consider the Black-Cox model [1] with an added recovery risk driver. The recovery risk driver arises naturally in the context of imperfect information implicit in the structural framework. This leads to a two-factor structural model we call the Stochastic Recovery Black-Cox model, whereby the asset risk driver A_t defines the default trigger and the recovery risk driver R_t defines the amount recovered in the event of default. We then price zero-coupon bonds and credit default swaps under the Stochastic Recovery Black-Cox model. Introducing separate but correlated risk drivers leads to a decoupling of the default and recovery risk premiums in the credit spread. Finally, we compare our results with the classic Black-Cox model and give explicit expressions for the recovery risk premium in the Stochastic Recovery Black-Cox model.

References

- [1] F. BLACK & J.C. COX, *Valuing Corporate Securities: Some Effects of Bond Indenture Provisions*, Journal of Finance 31, 1976, pp 351-367.
- [2] A. COHEN & N. COSTANZINO, *Bond and CDS Pricing with Recovery Risk I: The Stochastic Recovery Merton Model*, available on SSRN as a preprint. Submitted to IJTAF, 2015.

Comparative Analysis of Warrants Pricing Models

Alan Xinghua Zhou¹, Mark Reesor²

¹ Western University, London, Canada, xzhou68@uwo.ca

² Western University, London, Canada, mreesor@uwo.ca

Pricing warrants with a dilution-adjusted Black-Scholes model is first introduced by Galai and Schneller[1]. Using structural models, Crouhy and Galai[2] extended Galai-Schneller's framework to incorporate the leverage effects in pricing warrants by including zero-coupon debt in the firm's capital structures. Empirical studies on how dilution affects warrant pricing have been done by many authors. However, studies on whether to include the leverage effect when pricing warrants is limited. In this paper we review the current warrant pricing models by conducting a comparative analysis. Our study focuses on how firm leverage/capital structures affects warrants pricing. Moreover, by comparing different models, we discuss how dilution-adjustment and leverage affect the hedge ratios for warrants.

References

- [1] D. Galai and M. Schneller, *Pricing of warrants and the value of the firm*, The Journal of Finance. **33**, 5, pp. 1333-1342 (1978).
- [2] M. Crouhy and D. Galai, *The interaction between the financial and investment decisions of the firm: The case of issuing warrants in a levered firm*, Journal of Banking & Finance. **18**, 5, pp. 861-880 (1994).

Correlated Poisson Processes

A.Kreinin¹

¹ IBM,Risk Analytics, Canada, {alex.kreinin}@ca.ibm.com

Poisson processes have many important applications in Finance and Insurance. The theory of Poisson processes is very well developed in the single-dimensional case, but the multivariate Poisson processes are less studied. In this talk we address the simulation problems for correlated Poisson processes and discuss conditions providing solution to the calibration problem for the parameters of the model. Our approach is based on the idea of Backward Simulation leading to the construction of the Poisson Bridge, similar in spirit to the well-known Brownian Bridge process.

This research was motivated by Operational Risk and Credit Risk modeling problems [1], [2].

References

- [1] K. Duch, Y. Jiang, A. Kreinin, *New Approaches to Operational Risk Modeling*, IBM Journal Res. Dev. **58**, 3, pp. 123-132 (2014).
- [2] A. Kreinin, *Correlated Poisson processes and their applications*, Financial signal processing and machine learning, Wiley, accepted for publication. (2015)

Cumulative prospect theory with skewed return distribution

M. Kwak¹, T. A. Pirvu²

¹ Hankuk University, Gyeonggi-do, S. Korea, mkwak@hufs.ac.kr

² McMaster University, Hamilton, Canada, tpirvu@math.mcmaster.ca

We investigate a one-period portfolio optimization problem of a cumulative prospect theory (CPT) investor with multiple risky assets and one risk-free asset. The returns of multiple risky assets follow multivariate generalized hyperbolic (GH) skewed t distribution. We obtain a three-fund separation result of two risky portfolios and risk-free asset. Furthermore, we reduce the high dimensional optimization problem to two 1-dimensional optimization problems and derive the optimal portfolio. We show that the optimal portfolio composition changes as some of *investor-specific* parameters change. It is observed that the consideration of skewness of stock return distribution has considerable impact on the distribution of CPT investor's wealth deviation, and leads to less total risky investment.

Dimension and Variance Reduction for Monte Carlo Methods for High-Dimensional Models in Finance

Duy-Minh Dang¹, Ken Jackson² and Mohammadreza Mohammadi³

¹ School of Mathematics and Physics, The University of Queensland, Brisbane, QLD 4072, Australia. duyminh.dang@uq.edu.au

² Computer Science Department, University of Toronto, Toronto, ON, M5S 3G4, Canada. krj@cs.toronto.edu

³ Statistical Sciences Department, University of Toronto, Toronto, ON, M5S 3G3, Canada. m.mohammadi@mail.utoronto.ca

One-way coupling often occurs in multi-dimensional models in finance. In this paper, we present a dimension reduction technique for Monte Carlo (MC) methods, referred to as drMC, that exploits this structure for pricing plain-vanilla European options under a N-dimensional one-way coupled model, where N is arbitrary. The dimension reduction also often produces a significant variance reduction.

The drMC method is a dimension reduction technique built upon (i) the conditional MC technique applied to one dimension and (ii) the derivation of a closed-form solution for the conditional Partial Differential Equation (PDE) that arises via Fourier transforms. In the drMC approach, the option price can be computed simply by taking the expectation of this closed-form solution. Hence, the approach results in a powerful dimension reduction from N to one, which often results in a significant variance reduction as well, since the variance associated with the other N-1 factors in the original model are completely removed from the drMC simulation. Moreover, under the drMC framework, hedging parameters, or Greeks, can be computed in a much more efficient way than in traditional MC techniques.

If time permits, a variance reduction analysis of the method will be provided. Numerical results illustrating the method's efficiency will be presented.

Disorderly hedge fund liquidation under asymmetric information and market impact

C. Hillairet¹, C. Hyndman², Y. Jiao³, R. Wang⁴

¹ Centre de Mathématiques Appliquées, École Polytechnique, France, hillaire@cmap.polytechnique.fr

² Department of Mathematics and Statistics, Concordia University, Montréal, Canada, cody.hyndman@concordia.ca

³ Institut de Science Financière et d'Assurances, Université Claude Bernard Lyon 1, ying.jiao@univ-lyon1.fr

⁴ Department of Mathematics and Statistics, Concordia University, Montréal, Canada, ren_wa@live.concordia.ca

We study the case of a hedge fund or trader with a large position in an asset that must be liquidated when the asset price crosses a barrier. The disorderly liquidation of the position will have an impact on the market price of the asset that cannot be anticipated by ordinary investors. We consider the problem from the perspective of an insider, or rival trader, with some knowledge of the liquidation barrier. The insider wishes to trade in such a way as to benefit from his or her, possibly incomplete, information about the existence and level of the liquidation barrier and market impact of liquidation. We compare the optimal investment problem of the informed and uninformed investors.

Efficient Convergent Lattice Method for Asian Options Pricing with Superlinear Complexity

Ling Lu¹, Wei Xu² and Zhehui Qian³

^{1,3} Department of Mathematics, Tongji University, Shanghai, China, 200092.

² Department of Mathematics, Tongji University, Shanghai, China, 200092; Faculty of Mathematics, University of Waterloo, Waterloo, Ontario, Canada.

Asian options have payoffs that depend strongly on the historical information of the underlying asset price. Although approximated closed form formulas are available with various assumptions, most them do not guarantee the convergence. Thus, binomial tree and PDE methods are two popular numerical solutions for pricing. However, either the PDE method or binomial tree method has the complexity of $O(N^2)$ at least, where N is the number of time steps. In this paper, we propose a first convergent lattice method with the complexity of $O(N^{1.5})$ based on the willow tree method [1, 2]. The corresponding convergence rate and error bounds are also analyzed. It shows that our proposed method can provide the same accuracy as the PDE and binomial tree methods, but requires much less computational time. When a quick pricing is required, our method can give the price with precision in a penny less than half second. Finally, numerical results support our claims.

References

- [1] Curran, M, *Willow power: optimizing derivative pricing trees*, ALGO RESEARCH QUARTERLY, 4, 15-24, 2001.
- [2] Xu, W. and Hong, Z. and Qin, C., *A new sampling strategy willow tree method with application to path-dependent option pricing*, Quantitative Finance, 13(6), 861–872, 2013.

Exponentially affine pricing kernels: from GARCH to diffusions

A. Badescu¹, Z. Cui², J.P. Ortega³

¹ University of Calgary, Calgary, Canada, abadescu@math.ucalgary.ca

² Brooklyn College of the City University of New York, Brooklyn, United States, zhenyucui@brooklyn.cuny.edu

³ Université de Franche-Comté, Besançon, France, juan-pablo.ortega@univ-fcomte.fr

This paper investigates the weak convergence of a general non-Gaussian GARCH model together with an application to the pricing of variance swaps. Since the market is incomplete, we consider the family of exponential affine stochastic discount factors as our pricing kernel candidates. Applying this change of measure to a discretized version of asymmetric GARCH models, we first derive its diffusion limit and link the market prices of variance risk in both discrete and continuous time. We show that some of the already existing limits of GARCH models risk-neutralized via an the extended Girsanov principle, conditional Esscher transform or a variance dependent pricing kernel can be obtained as special cases of our result. Using different assumptions on the GARCH innovation distribution, we investigate the convergence of the fair strikes of discrete variance swaps computed on the GARCH models to their continuous time counterparts. In several cases the fair strike of the variance swap can be obtained in closed-form, while in other cases the convergence can be showed only numerically.

Financial Modeling with multivariate mixed Fractional Brownian motion

A. Alvarez¹

¹ Ryerson University, Toronto, Canada
alexander.alvarez@ryerson.ca

In this work I introduce multivariate mixed models of the form

$$x_t^{(i)} = x_0^{(i)} \exp \left((\mu_i - \sigma_i^2/2)t + \sigma_i W_t^{(i)} + s_i B_t^{(i)} \right), \quad i = 1, 2, \dots, n \quad (1)$$

where for every $1 \leq i \leq n$, $W^{(i)}$ is a Brownian motion and $B^{(i)}$ is a Fractional Brownian Motion with Hurst index $H_i > 1/2$. The process $W^{(i)}$ is assumed to be independent of $B^{(j)}$, for all $1 \leq i, j \leq n$. However it is assumed that $W^{(i)}$ and $W^{(i)}$ are correlated, as well as $B^{(i)}$ and $B^{(j)}$.

These models may reproduce complex dependence structures, and at the same time are analytically tractable. I derive some statistical properties of this model. In particular, it can be proved that the correlation structure of the returns is scale dependent. This means that these models could explain, at least partially, a well known stylized fact known as the Epps effect.

I also study the pricing problem under these models for the bivariate case, using the Non Probabilistic formalism introduced in [1]. The replication of bivariate European derivatives, like spread options, is derived using Föllmer's Non Probabilistic version of Ito's formula [2]. It is worth noticing that, in general, these mixed models are not semimartingales, so the risk neutral approach for derivatives pricing is not always possible.

I discuss the implications of these results for the modelling of the dependence structure in the financial markets, and the possibility of using other processes with zero quadratic variation instead of the Fractional Brownian motion in (1).

References

- [1] A. Alvarez, S. Ferrando and P. Olivares (2012), Arbitrage and Hedging in a non probabilistic framework, *Mathematics and Financial Economics*, Vol 7, Issue 1, 1–28.
- [2] H. Föllmer (1981), Calcul d'Itô sans probabilité, *Séminaire de Probabilité XV. Lecture Notes in Math.* bf 850, Springer Berlin, 143–150.

Modelling Default Risk with Occupation Times

R. Makarov¹, A. Metzler²

¹ Wilfrid Laurier University, Waterloo, Canada, rmakarov@wlu.ca

² Wilfrid Laurier University, Waterloo, Canada, ametzler@wlu.ca

Structural models based on occupation times or excursion times allow for a temporal separation between the default event and liquidation. As such, they allow for a more faithful representation of actual bankruptcy proceedings. We develop a semi-analytic pricing formula, easily implemented via quadrature, for a structural model based on occupation times that contains both the Merton and Black–Cox models as limiting cases. We introduce a process that keeps track of the cumulative amount of time that the firm’s asset value spends below the default barrier, and assume that liquidation is triggered when this occupation time first reaches a predefined upper threshold. In keeping with the aforementioned literature we may interpret this parameter as the length of a grace period granted by the bankruptcy court, during which reorganization is possible and beyond which liquidation is enforced. The Merton and Black–Cox models are obtained by sending this threshold parameter to its upper and lower limit, respectively. Surprisingly, we find that the value of the firm’s debt (i) need not be monotone in the threshold parameter and (ii) need not lie between the Merton and Black–Cox values.

On Optional Processes and Financial Market Modelling

M. Abdelghani¹ & A. Melnikov²

¹ University of Alberta, Edmonton, Canada, mnabdelghani@gmail.com

² University of Alberta, Edmonton, Canada, melnikov@ualberta.ca

Stochastic analysis and mathematical finance have been comprehensively studied under the usual conditions. Nevertheless, two great experts in Stochastic analysis Doob (1975) and Dellacherie (1975) initiated studies of stochastic processes without these common and convenient assumptions. Further developments were done by Lepingle (1977), Horowitz (1978), Lenglart (1980), and most notably by Galtchuk in several papers published in the period 1975-1985. In these publications, a parallel theory of stochastic analysis of optional processes was constructed. In this theory, the stochastic basis is defined as, $(\Omega, \mathcal{F}, \mathbf{F} = (\mathcal{F}_t)_{t \geq 0}, \mathbf{P})$ a complete probability space – \mathcal{F} contains all \mathbf{P} null sets. However, the family \mathbf{F} is not assumed to be complete, right or left continuous. The spaces $\mathcal{O}(\mathbf{F})$ and $\mathcal{P}(\mathbf{F})$ are the optional and predictable σ -algebras on \mathbf{F} . A random process X is said to be *optional* if it is $\mathcal{O}(\mathbf{F})$ -measurable. Optional processes have right and left limits but are not necessarily continuous. Most notable properties of optional processes are the right, $\Delta X_t = X_t - X_{t-}$ and left $\Delta^+ X_t = X_{t+} - X_t$ jumps. An optional semimartingale $X = (X_t)_{t \geq 0}$ can be decomposed to an optional local martingale and an optional finite variation processes, which, in turn can be decomposed to a sum of right continuous and left continuous processes. A stochastic integral with respect to optional semimartingale X is the bilinear form $(\varphi, \phi) \circ X_t$ defined as

$$Y_t = (\varphi, \phi) \circ X_t = \int_{0+}^t \varphi_s dX_s^r + \int_0^{t-} \phi_s dX_{s+}^g.$$

where Y_t is again an optional semimartingale $\varphi_- \in \mathcal{P}(\mathbf{F})$, and $\phi \in \mathcal{O}(\mathbf{F})$. The existence of a theory of optional processes calls for its further development and application to mathematical finance as a natural and promising reserve for further studies.

It is necessary to mention that up to now there are no fundamental papers devoted to the further development of the calculus of optional process or its applications to mathematical finance. However, we can mention here a recent development in pricing and hedging of derivative contracts with transaction costs Czichowsky and Schachermayer (2014) not treated with the calculus of optional semimartingales but show some relevance to the problem we are studying now.

The goal of this work is to develop previous results in the calculus of optional processes and provide new findings. Also, working in the framework of optional semimartingale we extend the stochastic exponents technique, which, we successfully exploited in several areas of research. Using this technique we introduce a general financial market model based on optional semimartingales. Following Melnikov et al (2002), we derive a very helpful methodology of finding local martingale measures and show how it works in this general setting. Furthermore, we illustrate our results in a generalized Black-Scholes market with the possibility of simultaneous left right jumps, and discuss pricing and hedging of a European call option in this market.

Risk Measurement of Variable Annuity Under Stochastic and Correlated Risk Factors

H. Gao¹, R. Mamon², S. Provost³

¹ Bank of Montreal, Toronto, Canada, huangeorgia.gao@bmo.com

² University of Western Ontario, London, Canada, rmamon@stats.uwo.ca

³ University of Western Ontario, London, Canada, provost@stats.uwo.ca

Lapse rate is a key factor in the pricing and risk management of a variable annuity (VA). It impacts financial outcome in two respects: the guaranteed payoff and fee income. We propose a stochastic modelling framework to evaluate risk measures in which the lapse rate with affine structure is incorporated, and the risk factors affecting VA have a correlation structure. Moment-based density approach is employed in the approximation of the loss distribution facilitating immediate risk measure determination. A sensitivity analysis of VA's risk measures provides a demonstration of the utmost importance of reliable model parameter estimation.

References

- [1] M. Hardy, *Investment Guarantees*, Wiley & Sons, New Jersey, 2003.
- [2] S. Provost, *Moment-based density approximants*, Mathematica Journal, 9:4, pp. 729-756 (2005).

SS-MMNN Mathematical Models for Nanoscience and Nanotechnology

Boundary conditions for quantum hydrodynamic model of electron gas

Naijing Kang¹, Z. L. Mišković^{1,2}

¹ Department of Applied Mathematics, University of Waterloo, Waterloo, Ontario, Canada, n7kang@uwaterloo.ca

² Waterloo Institute for Nanotechnology, University of Waterloo, Waterloo, Ontario, Canada, zmiskovi@uwaterloo.ca

Recent achievements in studying the electric field enhancement in plasmonic nanostructures pointed to the need of including nonlocal effects in modeling of the collective, or plasma oscillations of the electron gas (EG) in metallic nanoparticles [1]. This may be achieved by using a standard hydrodynamic model (SHD), which includes quantum pressure in EG at the level of a Thomas-Fermi (TF) approach [2, 3]. We extend this approach to modeling nonlocal effects by adopting quantum hydrodynamic model (QHD), which includes the quantum Bohm (QB) potential, in addition to the TF pressure in the dynamic response of electrons in metallic nanoparticles [4].

Studying the effects of the QB potential on plasmon excitations in a metal slab in the nonretarded regime [5], we have shown that, after Fourier transforming the time dependence, the spatial distribution of the induced charge density in the EG, ρ , satisfies a fourth-order partial differential equation (PDE), given by $\hat{\mathcal{L}}\rho = k_s^2 \rho_{\text{ext}}$, where ρ_{ext} is the external charge density, and the operator $\hat{\mathcal{L}}$ is defined by

$$\hat{\mathcal{L}} = \nabla^2 (1 - \ell_c^2 \nabla^2) - k_s^2 (1 - \omega^2 / \omega_p^2). \quad (1)$$

Here, ω_p is the plasma frequency of the EG, k_s its inverse TF screening length, and $\ell_c = \sqrt{3} / (2k_F)$ (with the Fermi wavenumber k_F) is a characteristic length brought into the QHD model due to the QB potential. Notice that the SHD model is obtained by letting $\ell_c \rightarrow 0$ in Eq. (1), which reduces the problem to a second-order PDE for ρ [5].

Assuming that the EG occupies a region with an impenetrable boundary \mathcal{B} , one needs to impose a physically motivated boundary condition (BC) that the normal component of the charge flux density in the EG vanishes on \mathcal{B} , giving [2, 3]

$$\frac{\partial}{\partial n} [(1 - \ell_c^2 \nabla^2) \rho] = -\frac{k_s^2}{4\pi} \frac{\partial \phi}{\partial n}, \quad (2)$$

where $\frac{\partial}{\partial n}$ is the normal derivative, and ϕ is the electrostatic potential on the inner surface of \mathcal{B} . While this BC suffices for the SHD model, one also needs an additional BC (ABC) in order to solve the equation $\hat{\mathcal{L}}\rho = k_s^2 \rho_{\text{ext}}$ in the QHD model. We have shown in Ref. [5] that, keeping the operator $\hat{\mathcal{L}}$ Hermitian, or self-adjoint, there are two equally valid possibilities for the ABC, namely $\nabla^2 \rho = 0$ or $\frac{\partial}{\partial n} (\nabla^2 \rho) = 0$, to be imposed on the induced charge density ρ in conjunction with the BC in Eq. (2). In this work we further explore the significance of having *two* physically plausible sets of BCs for plasmon eigenfrequencies in a metal slab described with the QHD model.

References

- [1] C. Ciraci, R. T. Hill, J. J. Mock, Y. Urzhumov, A. I. Fernández-Domínguez, S. A. Maier, J. B. Pendry, A. Chilkoti, and D. R. Smith, *Probing the Ultimate Limits of Plasmonic Enhancement*, Science **337**, pp. 1072-1074 (2012).
- [2] C. Ciraci, J. B. Pendry, and D. R. Smith, *Hydrodynamic Model for Plasmonics: A Macroscopic Approach to a Microscopic Problem*, Chem. Phys. Chem. **14**, pp. 1109-1116 (2013).
- [3] Naijing Kang, Z. L. Mišković, Y.-Y. Zhang, Y.-H. Song, and Y.-N. Wang, *Analyzing nonlocal effect in the plasmon spectra of a metal slab by the Green's function technique for hydrodynamic model*, Nanoscale Syst.: Math. Model. Theory Appl. **3**, pp. 44-54 (2014).
- [4] F. Haas, *Quantum Plasmas: an Hydrodynamic Approach*, (Springer, New York, 2011).
- [5] Y.-Y. Zhang, S.-B. An, Y.-H. Song, N. Kang, Z. L. Mišković, and Y.-N. Wang, *Plasmon excitation in metal slab by fast point charge: The role of additional boundary conditions in quantum hydrodynamic model*, Phys. Plasmas. **21**, pp. 102114 (2014).

Coupling Electromagnetic wave to Dirac Electrons in Graphene: A Hydrodynamic Modelling

N. Ghafarian¹, A. H. Majedi², S. Safavi³

¹ University of Waterloo, Waterloo, Canada, n2ghafar@uwaterloo.ca

² University of Waterloo, Waterloo, Canada, ahmajedi@uwaterloo.ca

³ University of Waterloo, Waterloo, Canada, safavi@uwaterloo.ca

The interaction between the electromagnetic wave and the drifting carrier plasma wave in graphene is investigated. Graphene is a 2D symmetric honeycomb lattice of carbon atoms. It is a semimetal material that can carry a large two-dimensional density of electrons. The electrons in doped graphene is modelled as two dimensional Fermi liquid.

We analyse graphene in collision dominate regime $\hbar\omega \ll k_B T$ where collisions establish local equilibrium and the fluid is strongly correlated. The assumption of the local equilibrium allows to reduce the Boltzmann kinetic equation for the distribution function to the hydrodynamic equations for macroscopic variables: local density and velocity.

The response of graphene to an external electric field is determined by the electron-electron elastic scattering. For samples on substrate even at room temperature, in the linear-response regime the contribution of the electron-phonon and the electron-impurity scattering on the graphene response is negligible. The Coulomb interactions between electrons are included in the viscosity of the fluid.

Electrons in graphene behave like a Dirac fluid of massless quasi-particles, propagating at a Fermi speed of about $v_f \simeq 10^6 m/s$. Therefore, electrons in graphene mimic zero mass relativistic particles with an effective light speed of $v_f = c/3000$. The maximum drift velocity of graphene is around $0.3v_f$. Therefore, to analyse graphene with drifting carriers we use the hydrodynamic description derived from relativistic fluid approach [1]. Based on this hydrodynamic model, the induced current is calculated for a harmonic perturbation of both stationary and uniformly moving charged carriers and the conductivity is obtained in the linear region. For small drift velocities at low frequency the relativistic correction term can be neglected and non-relativistic Navier-Stokes hydrodynamics equation is recovered.

The obtained conductivity relation shows that for a coupled slow electromagnetic field with phase velocity smaller than the drift velocity of carriers, graphene changes from a lossy propagating medium to a gain medium that transfers power from the DC power to the electromagnetic field. The conductivity equation is augmented by Maxwell's equations relating the electric field to the current. The graphene is modelled as a surface current density in the Maxwell's equations. To find the dispersion equation and gain we apply the self consistency condition to combine the relations between the electric field and current obtained separately from the hydrodynamic analysis of graphene and electromagnetic analysis of the waveguide.

References

- [1] M. Muller, J. Schmalian and L. Fritz, *Graphene: A Nearly Perfect Fluid*, PRL **103**, 1, 025301 (2009).

Feasibility of single electron spin control with gate potential in III-V semiconductor quantum dots without magnetic field

Sanjay Prabhakar, and Roderick Melnik

The MS2Discovery Interdisciplinary Research Institute, M²NeT Laboratory, Wilfrid Laurier University, Waterloo, ON, N2L 3C5 Canada

We present results on how to obtain the spin splitting energy in the absence of magnetic field by transporting quantum dots slowly in the plane of two dimensional electron gas. We show that the spin splitting energy of moving quantum dots can be achieved in the absence of the magnetic field and can be manipulated with the application of the gate controlled electric field that might consider to make next generation spintronic devices. Such spin splitting energy is highly dependent on the material properties of semiconductor. We provide examples of spin splitting behaviors in GaAs, InAs, GaSb and InSb. It turns out that this energy is in the range of meV and can be further enhanced with increasing pulse frequency. In particular, we confirm that neither for the pure Rashba nor pure Dresselhaus cases, oscillations in spin-flip behaviors can be observed.

In Fig. 1, we plot the spin splitting energy difference vs rotation angle of III-V semiconductor quantum dots. Such spin splitting energy is highly dependent on the Rashba-Dresselhaus spin-orbit coupling coefficients and on the control frequency ω . For the case of $\omega = 0.1\text{GHz}$, the spin splitting energy is comparable to the Landau energy levels and might be utilized to break the in-plane rotational symmetry (see Fig. 1). The splitting of s- and p-states of quantum dots without magnetic field allows us to investigate the several physics phenomena such decoherence, robustness of spin manipulation through Berry phase for topological quantum computing and other spintronics devices. [1, 2]

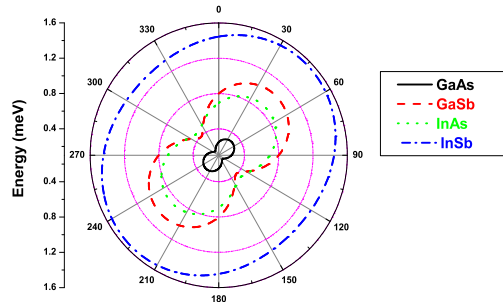


Figure 1: Spin splitting energy difference vs rotation angle in III-V semiconductor quantum dots. Here we chose $r_0 = 1.5\text{ }\mu\text{m}$, $\omega = 0.1\text{ GHz}$, $\ell_0 = 32\text{ nm}$ and $E = 10^5\text{ V/cm}$.

References

- [1] S. Prabhakar, R. Melnik, L. Bonilla, and A. Inomata, *Gate control of Berry phase in III-V semiconductor quantum dots*, Phys. Rev. B **89**, 245310 (2014).
- [2] S. Prabhakar, R. Melnik and A. Inomata, *Geometric spin manipulation in semiconductor quantum dots*, Applied Physics Letters, **104**, 142411 (2014).

Ionic screening of charged impurities in electrolytically gated graphene using Green's function approach

P. Sharma¹ and Z. L. Miskovic^{1,2}

¹ Department of Applied Mathematics, University of Waterloo, Waterloo, Ontario, Canada, p36sharm@uwaterloo.ca

² Waterloo Institute for Nanotechnology, University of Waterloo, Waterloo, Ontario, Canada, zmiskovi@uwaterloo.ca

Carbon nanostructures, in terms of wide range of applications for biological and chemical sensors, have become the cynosure of all eyes in the scientific communities all over the world [1]. While experimental investigation of graphene based biochemical sensors is rapidly accelerating area [1,2], theoretical modeling of electrochemistry of graphene is still in its infancy [3,4]. Graphene operates in such applications in the configuration of a field-effect transistor (FET) with its surface exposed to an electrolyte containing mobile ions [2]. By applying a gate potential through the electrolyte, one may achieve a control of graphene's conductivity that is extremely sensitive to the presence of adsorbed molecules, ion concentration, or the pH in an aqueous solution. However, graphene is usually supported by an insulating substrate, such as SiO₂, which may contain large density of charged impurities that also affect graphene's conductivity [5].

We have recently investigated the ability of mobile ions in the solution to screen the effects of charged impurities in the regime of a low potential drop across electric double layer by using a linearized Poisson-Boltzmann (PB) model of the electrolyte [6]. However, typical applications of graphene FETs require high doping densities of charge carriers that are achieved by applying relatively large electrolytic gate potentials, of the order of 1 V [2], which render the linearized PB model insufficient. To remedy this situation, we develop a partially-linearized PB model for ionic screening of charged impurities underneath graphene, which is based on the Green's function (GF) approach presented in Ref.[7]. In order to include the effect of finite ion size, at least at a qualitative level, we derive a GF for the partially-linearized PB model that includes Stern layer and allows modeling of ionic screening in the regime of a dually-gated single-layer graphene FET.

References

- [1] Y. Liu, X. Dong, and P. Chen, *Critical Review: Biological and chemical sensors based on graphene materials*, Chem. Soc. Rev. **41**, pp. 2283-2307 (2012).
- [2] F. Chen, J. Xia, and N. Tao, *Ionic screening of charged-impurity scattering in graphene*, Nano Lett. **9**, 4, pp. 1621-1625 (2009).
- [3] M. Z. Bazant, M. S. Kilic, B. D. Storey, and A. Ajdari, *Towards an understanding of induced-charge electrokinetics at large applied voltages in concentrated solutions*, Advances in Colloid and Interface Science **152**, pp. 48-88 (2009).
- [4] P. Sharma and Z. L. Miskovic, *Capacitance of graphene in aqueous electrolytes: The effects of dielectric saturation of water and finite size of ions*, Phys. Rev. B **90**, p. 125415 (2014).
- [5] S. Adam, E. H. Hwang, V. M. Galitski, and S. D. Sarma, *A self-consistent theory for graphene transport*, Proceedings of the National Academy of Sciences, USA, **104**, pp. 18392-18397 (2007).
- [6] Z. L. Miskovic, P. Sharma, and F. O. Goodman, *Ionic screening of charged impurities in electrolytically gated graphene*, Phys. Rev. B **86**, p. 115437 (2012).
- [7] A. W. C. Lau, *Fluctuation and correlation effects in a charged surface immersed in an electrolyte solution*, Phys. Rev. E **77**, p. 011502 (2008).

Modeling of Coupled Surface and Diffusion Forces for the Transport and Retention of Nanoparticles in Porous Media

F. Javadpour¹, A. Hosseini¹

¹ University of Texas at Austin, USA, farzam.javadpour@beg.utexas.edu

Nanoparticle transport in porous media is modeled using a hierarchical set of differential equations corresponding to pore scale and macroscale. At the pore scale, movement and interaction of a single particle with a solid matrix is modeled using the advection-dispersion equation. A single nanoparticle entering the space encounters diffusion and surface forces. Surface forces (electrostatic and van der Waals forces) between nanoparticles and grains are measured directly using an atomic force microscope (AFM). Measured surface forces appear as an additional force term in the velocity field equation of a microparticle in the interstitial space [1]. These local events are then transformed into a macroscale continuum by imposing periodic boundary conditions for contiguous unit cells and using a scheme of moment analysis. At the macroscale, propagation and capture of particles are characterized by three position-independent coefficients: mean nanoparticle velocity vector U^* , macroscopic dispersion coefficient D^* , and mean nanoparticle retention rate constant k^* . Model results validated with a set of nanoparticle transport tests in porous microchip [2]. Decrease in advective velocity increases particle retention. Short distance attractive surface forces play an important role in particle retention.

References

- [1] F. Javadpour, A. Jeje, *Modeling filtration of platelet-rich plasma in fibrous filters*, Transp. Porous Med. **91**, pp. 677-696 (2012).
- [2] S. Sajjadi, F. Javadpour, A. Jeje, *Trajectory and transit patterns of isolated nanoparticles in structured micromodels*, Austin J. Chem. Eng. **1** (2), pp. 1-9 (2014).

Pattern Analysis Using Shapelets for Nanoscale Self-Assembly Imaging

R. Suderman¹, D. J. Lizotte², N. M. Abukhdeir¹

¹University of Waterloo, Canada, nmabukhdeir@uwaterloo.ca; ²University of Western Ontario, Canada, dlizotte@uwo.ca

Pattern formation resulting from nanoscale self-assembly has been an area of intense research for the past few decades. Recent advances in microscopy and imaging of surface at nanoscale resolution have produced a sizable set of high-quality images of self-assembled materials. Analysis of these images and, subsequently, determination of relations between self-assembled pattern structure and desired physicochemical properties has not advanced at an equally rapid pace. Frequently, researchers have rely on qualitative techniques (*e.g.* visual inspection) to interpret imaging data for determining these relations. Robust quantitative analysis is required to determine meaningful relationships but existing theory, such as bond-orientational order (BOO) theory, are limited in their robustness in the presence of measurement noise and generality.

In this work, an analysis method for two-dimensional self-assembled surface imaging is presented that is fundamentally different from past approaches [3]. It is based upon the use of a family of localized functions called “shapelets” [2], which were originally developed to characterize images of galaxies ($\approx 10^{20}$ m). Here they are used quantitatively characterize images of nano-patterned surfaces ($\approx 10^{-9}$ m) in a robust and general way. The method is applied to simulation data of self-assembled surfaces resulting from heteroepitaxial pattern formation and shown to robustly and efficiently determine local pattern characteristics using an appropriate subset of shapelets [2] and steerable filter theory [1]. Local pattern metrics including pattern strength and orientation are determined which enable researchers to quantitatively determine whether or not a pattern is present in the image and its orientation. Furthermore, the method is robust in the presence of measurement noise and pattern degeneracies (defects) along with being compatible for implementation on graphics processing units (GPUs).

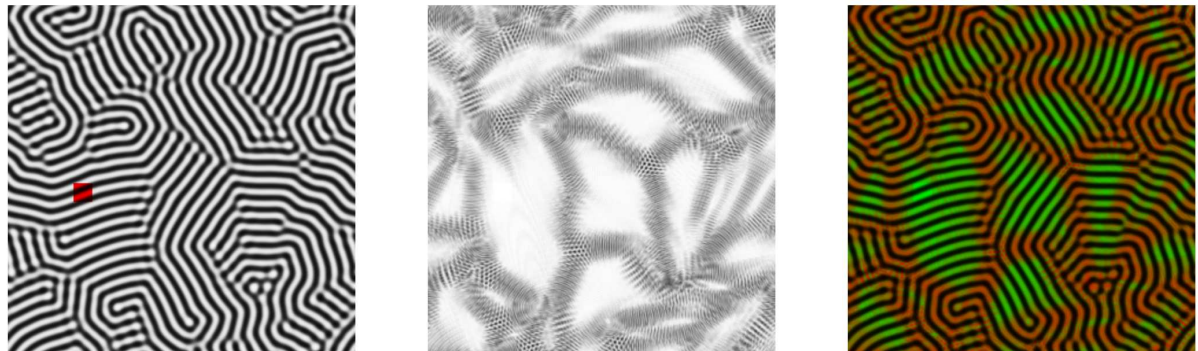


Figure 1: Examples of shapelet-based pattern analysis of a (left) self-assembled surface image with a stripe pattern; (centre) computed local pattern strength; (right) overlay of pattern strength on the original image. Images taken from ref. [3].

References

- [1] W. T. Freeman and E. H. Adelson. The design and use of steerable filters. *IEEE Transactions on Pattern Analysis and Machine Intelligence*, 13:891–906, 1991.
- [2] A. Refregier. Shapelets – i. a method for image analysis. *Monthly Notices of the Royal Astronomical Society*, 338(1):35–47, 2003.
- [3] R. Suderman, D. Lizotte, and N. Abukhdeir. Theory and application of shapelets to the analysis of surface self-assembly imaging. *Phys. Rev. E*, 2015.

Photoluminescent Decay Dynamics in Nanocrystals

Brian Fernandes¹, Zoran L. Miskovic², Pavle V. Radovanovic³

¹ Department of Applied Mathematics, University of Waterloo, Waterloo, Canada, blfernand@uwaterloo.ca

² Department of Applied Mathematics, University of Waterloo, Waterloo, Canada zmiskovic@uwaterloo.ca

³ Department of Chemistry, University of Waterloo, Waterloo, Canada, pavler@uwaterloo.ca

In the past it was assumed that nanocrystals were largely defect free, because their small volume allowed defects to migrate to the surface and be expelled. However, growing evidence has suggested that defects play an important role in the properties of nanocrystals. Ga_2O_3 has a very large band gap (4.9 eV), high electrical conductivity, and strong blue photoluminescence. This combination of properties, arising from the presence of native defects makes Ga_2O_3 interesting for opto-electronic applications.

We studied size-dependent decay dynamics of defect-based photoluminescence of colloidal $\gamma\text{-}\text{Ga}_2\text{O}_3$ nanocrystals [1, 2]. In this talk we will discuss progress in theoretical modelling of this decay in the framework of the donor-acceptor pair (DAP) model. We have adapted the original DAP model, which was developed for a large volume of bulk material, to include the influence of the geometry of the nanocrystal [3]. Furthermore, we will discuss the connection to the stretched exponential as a fit for our model [4].

References

- [1] T. Wang, S. S. Farvid, M. Abulikemu, P. V. Radovanovic, *Size-tunable phosphorescence in colloidal metastable $\gamma\text{-}\text{Ga}_2\text{O}_3$ nanocrystals*, Journal of the American Chemical Society, **132**, (2010).
- [2] M. Hegde, T. Wang, Z. Miskovic, P. Radovanovic, *Origin of size-dependent photoluminescence decay dynamics in colloidal $\gamma\text{-}\text{Ga}_2\text{O}_3$ nanocrystals*, Appl. Phys. Lett. **100**, (2012).
- [3] A. Blumen, J. Klafter, G. Zumofen, *Influence of restricted geometries on the direct energy transfer*, J. Chem. Phys. **84**, (1986).
- [4] G. Dattoli, K. Górska, A. Horzela, K.A. Penson, *Photoluminescence decay of silicon nanocrystals and Lévy stable distributions*, Physics Letters A **378**, (2014).

Quantum Field Modelling of Nonlinear Optical Response in Graphene

B.Semnani ^{1,2},S. Safavi-Naeini¹, A.H. Majedi ^{1,2,3,4}

¹ Department of Electrical & Computer Engineering, University of Waterloo, Waterloo, ON, Canada ,

² Waterloo Institute for Nanotechnology, University of Waterloo, Waterloo, ON, Canada

³ Department of Physics & Astronomy , University of Waterloo, Waterloo, ON, Canada

⁴Perimeter Institute for the Theoretical Physics (PI) , Waterloo, ON, Canada

Graphene is a monolayer of carbon atoms sitting in a hexagonal lattice. Owing to the special symmetries of the crystalline structure, the band structure of graphene differs substantially from the other condensed matter systems. The effective Hamiltonian describes quasirelativistic massless Dirac fermions. The Dirac fermions introduced by the low energy Hamiltonian are dominantly chiral [1]. Moreover, the band structure of graphene is scale-invariant in the low energy limit [2]. It has been shown that the chirality of the charged carrier leads to several unconventional transport properties such as minimum conductivity, Klein paradox and Zitterbewegung [1]. The impact of the chirality on the optical response of graphene has not been investigated so far.

We have shown that the chiral nature of the charged carriers in conjunction with the scale invariance of the band structure results in a strong nonlinear optical response. The time evolution of the quasiparticles in the presence of the electromagnetic field can be decomposed into the quasiclassical intraband transport and interband time evolution. Employing Semiconductor Bloch Equations (SBEs) [3] for graphene, we have decoupled the quasiclassical and quantum dynamics. Based on SBEs, the dynamics is governed by a classical theory with quantum fluctuations superimposed. The principle advantage of SBEs is twofold: first they provide a convenient mathematical scheme leading to analytical expressions for arbitrary order of interaction. Secondly, SBEs encode the topological properties of band structure in an effective dipole appearing in the equations. As a matter of fact, the geometrical properties of the band structures affect the intraband contribution of the optical response and interband transitions are influenced by the special topological aspects of the band. We exploit the band renormalizations such as spin-orbit coupling to calculate the nonlinear optical response. We have shown that the nonlinear response function can be expressed as the summation three different contributions: pure-intraband, pure-interband and combination of the both.

References

- [1] A. H. Castro Neto, F. Guinea and N. M. R. Peres, K. S. Novoselov and , A. K. Geim, *The electronic properties of graphene*, *Rev. Mod. Phys.* , Vol 81, pp.109-162 (2009).
- [2] Bácsi, Ádám and A. Virosztek, , *Low-frequency optical conductivity in graphene and in other scale-invariant two-band systems*, in *Phys. Rev. B* , pp.125425 (2013).
- [3] C.Aversa, and J.E. Sipe , *Nonlinear optical susceptibilities of semiconductors: Results with a length-gauge analysis*, in *Phys. Rev. B* , pp.14636–14645 (1995).

Random Telegraph Signal and 1/f Noise in Graphene

L. Daniels¹, M. Scott¹ and Z. L. Mišković^{1,2}

¹ Department of Applied Mathematics, University of Waterloo, Waterloo, Canada, lm2danie@uwaterloo.ca

² Waterloo Institute for Nanotechnology, University of Waterloo, Waterloo, Ontario, Canada, zmiskovi@uwaterloo.ca

Graphene shows great promise for applications in electronics and photonics [2] owing to high mobility of its charge carriers and the tunability of their density by means of the potential applied on external gates. However, electrical conductivity of graphene is often plagued by the presence of charged impurities in an underlaying insulator, such as SiO₂ [2, 1]. Those impurities are often modeled as stationary charges due to electrons or holes from graphene being trapped in the donor- and acceptor-like centers in the substrate, which cause degradation of graphene conductivity due to Coulomb scattering of its charge carriers [1]. However, the dynamic regime of charge trapping and de-trapping, or emission from those defect centers may give rise to a low-frequency noise known as 1/f noise in graphene [3].

We model the 1/f noise in a graphene-based field effect transistor due to charge trapping and de-trapping by a stochastic process known as random telegraph signal (RTS) [4]. This process takes only two states, {a, b}, which correspond to different charge states of each impurity in the substrate, with asymmetric transition rates: $a \xrightarrow{\lambda} b$ and $b \xrightarrow{\mu} a$. Those rates depend on the Fermi energy in graphene [4], which may be varied in quite a broad range of values by the gate potential to achieve high doping densities of charge carriers in graphene [1]. We use the model due to McWhorter [5], where the inverse dependence on frequency f is obtained from a linear superposition of the spectral densities due to individual RTS contributions to the current fluctuations to explain the dependence of the 1/f noise in graphene on its doping density.

References

- [1] S. Adam, E. H. Hwang, V. M. Galitski, and S. D. Sarma, *A self-consistent theory for graphene transport*, Proceedings of the National Academy of Sciences, USA, **104**, pp. 18392-18397 (2007).
- [2] Ph. Avouris and F. Xia, *Graphene applications in electronics and photonics*, MRS Bulletin, **37**, pp. 1225-1234 (2012).
- [3] A. A. Balandin, *Low-Frequency 1/f Noise in Graphene Devices*, Nature Nanotechnology, **8**, pp. 549-555 (2013).
- [4] H. H. Mueller and M. Schultz, *Review: Individual Interface Traps at the Si-SiO₂ Interface*, Journal of Material Science: Materials in Electronics, **6**, pp. 65-74 (1995).
- [5] A. L. McWhorter and R. H. Kingston, *Semiconductor Surface Physics* (Univ. of Pennsylvania Press, 1957).

Topological characterization of phase space manifolds corresponding to collective charge fluctuations in nanoparticle assemblies

Bosiljka Tadić¹, Miroslav Andjelković^{1,2}, Milovan Šuvakov³

¹ Department of Theoretical Physics, Jožef Stefan Institute, Ljubljana, Slovenia, bosiljka.tadic@ijs.si

² Institute of Sciences Vinča, Belgrade, Serbia, andjelkovic@gmail.com

³ Institute of Physics, University of Belgrade, Belgrade, Serbia, milovan.suvakov@ipb.ac.rs

In conducting nanoparticle assemblies, the conduction mechanism with single-electron tunnelings (SET) is provided by Coulomb blockade conditions occurring between neighboring nanoparticles ([1] and references within). It has been recognized that, in a range of voltage values above a threshold V_T , the current–voltage characteristics is nonlinear, $I(V) \sim (V - V_T)^\zeta$ and the exponent $\zeta \in (1, 4)$ robustly correlates with the structure of the assembly [2]. The origin of this phenomenon is in the collective charge fluctuations along the (dynamically established) conduction paths through the assembly. While current fluctuations over time are directly measured at the electrode [2], the tunneling events inside the sample remain a challenging problem to the experimental techniques. In this work, we study collective features of charge transport by simulating SET processes in nanoparticle assemblies of different structure.

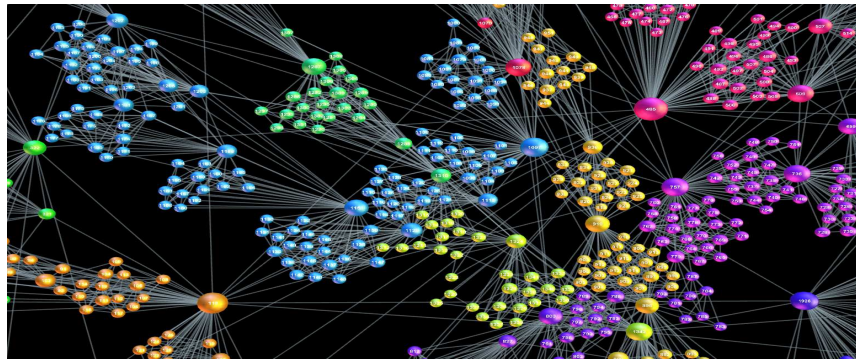


Figure 1: Manifold of connections in phase space analyzed as a graph: Identified groups of nodes contain high-order cliques.

We analyze time series of the number of tunnelings per time unit. Firstly, we show how the quantitative signatures of the collective dynamics vary with the structure of the underlying assembly. Further, considering that each time series represents a particular manifold in phase space, we map such manifolds onto mathematical graphs, Fig. 1, by using one of the established mapping rules. Then, applying algebraic topology methods on these graphs [3], we study simplexes (cliques of different orders) and their agglomerates—simplicial complexes. Computing various topology measures [4] reveals the connection complexity of nodes, i.e. dynamical states of the system.

References

- [1] M. Šuvakov, B. Tadić, *Modeling collective charge transport in nanoparticle assemblies*, J. Phys. Condens. Matt. **22**, 163201 (2010).
- [2] M.O. Blunt, M. Šuvakov *et al.*, *Electronic transport in cellular nanoparticle networks: Meandering through nanoscale mazes*, Nano Lett. **7**, 855-860 (2007).
- [3] J. Jonsson, *Simplicial Complexes of Graphs*, Lecture Notes in Mathematics, Springer-Verlag Berlin Heidelberg, 2008.
- [4] M. Andjelković, B. Tadić, S. Maletić, M. Rajković, *Hierarchical sequencing of online social graphs*, arxiv:1410.7259.

SS-MMPND Matrix Manifold Problems subject to Noisy Data

On higher-order singular value decomposition from incomplete data

Yangyang Xu¹

¹ University of Waterloo, Waterloo, Canada, yangyang.xu@uwaterloo.ca

Higher-order singular value decomposition (HOSVD) [1] is an efficient way for data reduction and also eliciting intrinsic structure of multi-dimensional array data. It has been used in many applications, and some of them involve incomplete data. To obtain HOSVD of the data with missing values , one can first impute the missing entries through a certain tensor completion method and then perform HOSVD to the reconstructed data. However, the two-step procedure can be inefficient and does not make reliable decomposition.

In this work, we formulate an incomplete HOSVD problem and combine the two steps into solving a single optimization problem, which simultaneously achieves imputation of missing values and also tensor decomposition. We also present two algorithms for solving the problem based on block coordinate update. Global convergence of both algorithms is shown under mild assumptions. The convergence of the second algorithm implies that of the popular higher-order orthogonality iteration (HOOI) method [2], and thus we, for the first time, give global convergence of HOOI.

In addition, we compare the proposed methods to state-of-the-art ones for solving incomplete HOSVD and also low-rank tensor completion problems and demonstrate the superior performance of our methods over other compared ones. Furthermore, we apply them to face recognition and MRI image reconstruction to show their practical performance.

References

- [1] L. Lathauwer, B. Moor, and J. Vandewalle, *A multilinear singular value decomposition*, SIAM J. On Matrix Analysis and Applications. **21**, pp. 1253-1278 (2000).
- [2] L. Lathauwer, B. Moor, and J. Vandewalle, *On the best rank-1 and rank-(r1,r2,...,rN) approximation of higher-order tensors*, SIAM J. On Matrix Analysis and Applications. **21**, pp. 1324-1342 (2000).

Modeling protein loops using Frenet frames, inverse kinematics and optimization

Forbes Burkowski¹, Xiao-Bo Li², Henry Wolkowicz³

¹ University of Waterloo, Waterloo, Canada, fjburkowski@uwaterloo.ca

² University of Waterloo, Waterloo, Canada, x22li@uwaterloo.ca

³ University of Waterloo, Waterloo, Canada, hwolkowicz@uwaterloo.ca

Loop modeling is a final step in protein structure prediction. In other applications, understanding alternate conformations of protein loops is important for drug design and any full understanding of protein function. We are given an amino acid sequence for a loop: $a^{(i)} \ i = 1, 2, \dots, n+1$ (for example: TEYKLVVGA where each character names an amino acid). The vector $r^{(i)}$ will be used to represent the coordinates of the alpha carbon atom of residue $a^{(i)}$. We are given the positions of $r^{(0)}$ and $r^{(n+1)}$ in the 3D space. The problem is to predict the positions $r^{(1)}, r^{(2)}, \dots, r^{(n)}$ of all the alpha carbon atoms between $a^{(0)}$ and $a^{(n+1)}$. Over the past several years, many strategies have been used: Inverse kinematics [1] (robotics) and statistical frequency distributions of backbone angles [2]. Our approach involves Frenet frames and the solution of a nonlinear optimization problem that is subject to constraints. We assume a Frenet frame at each alpha carbon position $r^{(i)}$:

$$t^{(i)} = \frac{r^{(i+1)} - r^{(i)}}{\|r^{(i+1)} - r^{(i)}\|} \quad b^{(i)} = \frac{t^{(i-1)} \times t^{(i)}}{\|t^{(i-1)} \times t^{(i)}\|} \quad n^{(i)} = b^{(i)} \times t^{(i)} \quad (1)$$

Each position will have a bond angle and dihedral angle defined for the pseudo bonds of the chain trace:

$$\cos(\theta_i) = t^{(i-1)} \cdot t^{(i)} \quad \cos(\gamma_i) = b^{(i)} \cdot b^{(i+1)} \quad (2)$$

Assuming a constant pseudo bond length for any two consecutive alpha carbon atoms in the chain we use the first equation in (1) to define the $r^{(i)}$ values by deriving all the $t^{(i)}$ tangent vectors. This can be done by solving a nonlinear optimization problem involving constraints that can be extracted from a data base that provides a statistical corelation between $(t^{(i)}, b^{(i)})$ pairs and the related (θ_i, γ_i) pairs. The data base can be generated by scanning high accuracy protein data files containing the coordinates of all atoms in the protein. The optimization problem finds the minimum of the objective function:

$$F(t, b) = \sum_{i=1}^n (b^{(i)} \cdot b^{(i+1)} - \cos(\gamma_i))^2 + \sum_{i=1}^n (t^{(i)} \cdot t^{(i+1)} - \cos(\theta_i))^2 \quad (4)$$

subject to the constraints that all $n^{(i)}, b^{(i)}, t^{(i)}$ vector triplets define orthonormal frames and the $t^{(i)}$ vectors satisfy a loop closure constraint:

$$r^{(k)} - r^{(0)} = \sum_{i=0}^{k-1} \|r^{(i+1)} - r^{(i)}\| \cdot t^{(i)} \quad (5)$$

The paper reports on the accuracy of the predictions.

References

- [1] S.R. Buss and J.-S. Kim. *Selectively damped least squares for inverse kinematics*. J. Graphics Tools, **10**, pp. 37-49 (2005).
- [2] W. Boomsma and T. Hamelryck. *Full cycle coordinate descent: solving the protein loop closure problem in Ca space*. BMC Bioinformatics. Open access: <http://www.biomedcentral.com/1471-2105/6/159>.
- [3] M. Lundgren, A. Krokhutin, and A. Niemi. *Topology and structural self-organization in folded proteins*. Physical Review E, **88**, pp. 042709 1-15 (2013).

Noisy sensor network localization: robust facial reduction and the Pareto frontier

Yuen-Lam Voronin¹, Dmitriy Drusvyatskiy², Nathan Krislock³, Henry Wolkowicz⁴

¹ University of Colorado, Boulder, yuen-lam.voronin@colorado.edu

² University of Washington, Seattle, ddrusv@uw.edu

³ Northern Illinois University, Dekalb, nkrislock@gmail.com

⁴ University of Waterloo, Waterloo, Canada, hwolkowicz@uwaterloo.ca

We consider the localization problem in sensor networks where the inter-sensor distance measurements are inaccurate and incomplete. In this paper, we present two novel algorithms for large-scale sensor localization based on semidefinite programming relaxations. Emerging exoscale networks lead to semidefinite relaxations that are prohibitively large for interior-point methods to handle. Both of our methods are able to efficiently solve the semidefinite programming relaxations without the use of interior-point methods. Our first method works by relating cliques in the graph of the problem to faces of the positive semidefinite cone, allowing us to devise a combinatorial algorithm for the localization problem that is provably robust and parallelizable. Our second algorithm is a first order method for maximizing the trace—a popular low-rank inducing regularizer—in a robust formulation of the localization problem. Namely, we consider the related much easier problem where the trace objective and the robust constraint are interchanged. By solving a sequence of these easier problems, we are able to obtain a solution to the original max-trace problem. Both of our algorithms output a configuration of sensors that can serve as a high-quality initialization for local optimization techniques. We provide numerical experiments on large-scale sensor network localization problems illustrating the development.

Protein Structure Network Models on the Euclidean Distance Matrix Cone

Xiao-Bo Li¹, Forbes Burkowski¹, Henry Wolkowicz¹

¹ University of Waterloo, Canada, {x22li, fburkowski, hwolkowicz}@uwaterloo.ca

Network models were introduced in the late 1990s [1, 2]. They use distances between atoms to model a protein's dynamics and flexibility. However, optimization problems involving proteins are often formulated using distance-squared [3, 4]. The cone of matrices of distance-squared entries, also called the Euclidean distance matrix (EDM) cone, can be mapped to the cone of centered positive semidefinite (PSD) matrices. The set of PSD matrices of fixed rank is also a Riemannian manifold, a natural setting for classical dynamics. Thus, the effect of formulating protein dynamics problems using distance-squared is to study dynamics on this manifold. Furthermore, this switch unifies optimization and dynamics onto the same mathematical space.

I will present an overview of my current research in formulating network models on the EDM cone [5, 6]. The focus will be on normal mode analysis and generating transitional conformations on the EDM cone.

References

- [1] M. Tirion, “Large amplitude elastic motions in proteins from a single-parameter, atomic analysis,” *Physical Review Letters*, vol. 77, no. 9, pp. 1905–1908, August 1996.
- [2] I. Bahar, A. Atilgan, and B. Erman, “Direct evaluation of thermal fluctuations in proteins using a single-parameter harmonic potential,” *Folding and Design*, vol. 2, no. 3, pp. 173–181, 1997.
- [3] N. Krislock, “Semidefinite facial reduction for low-rank euclidean distance matrix completion,” Ph.D. dissertation, School of Computer Science, University of Waterloo, 2010.
- [4] B. Alipanahi, N. Krislock, A. Ghodsi, H. Wolkowicz, L. Donaldson, and M. Li, “Determining protein structures from noesy distance constraints by semidefinite programming,” *Journal of Computational Biology*, vol. 20, no. 4, pp. 296–310, 2013.
- [5] X.-B. Li and F. J. Burkowski, “Conformational transitions and principal geodesic analysis on the positive semidefinite matrix manifold,” in *Bioinformatics Research and Applications*, ser. Lecture Notes in Computer Science, M. Basu, Y. Pan, and J. Wang, Eds. Springer International Publishing, 2014, vol. 8492, pp. 334–345.
- [6] X. Li and F. Burkowski, “Generating conformational transitions using the euclidean distance matrix.” *IEEE transactions on nanobioscience*, 2015.

Scalable Manifold Learning by Isometric Patch Alignment

We propose a novel dimensionality reduction method that is scalable and has low computational cost. This method is inspired by two key observations: (i) the structure of reasonably large patches of high-dimensional data can be preserved as a whole, rather than divided into small neighborhoods; and (ii) attaching two neighboring patches will align them such that the overall rank does not increase. In the proposed approach, the data is divided into smaller clusters (and can be distributed to different machines). Each cluster (on a different machine) is embedded into a low-dimensional patch and then all of the patches are rearranged such that their border points are matched. We show that the rearrangement can be computed by solving a relatively small semidefinite program. The embedding computed by this optimization is provably low-rank. The proposed method is stable, fast, and scalable; experimental results demonstrate its capability for dimensionality reduction data visualization, and even complex tasks such as protein structure determination.

SS-MSMB Modeling & Simulation in Medicine and Biology

A hybrid mathematical model of directed endothelial cell motility in angiogenesis

N. Tarfulea¹

¹ *Purdue University Calumet, Hammond USA, ntarfule@purduecal.edu*

In recent years, tumor-induced angiogenesis has become an important field of research because it represents a crucial step in the development of malignant tumors. The process consists of the proliferation of new capillaries from preexisting ones and is regulated by the interactions between various cell types such as endothelial cells and macrophages, and by biochemical factors. These include angiogenic promoters (e.g., vascular endothelial growth factor - VEGF) and inhibitors (angiostatin). Endothelial cells play an important role in this process since they are in direct contact with blood and control the exchanges of material between the bloodstream and the surrounding tissues. Therefore, endothelial cell movement is an essential component of angiogenesis. On one hand, directed movement requires signal detection and force generation by the cells and, on the other hand, it involves mechanical interactions between cells and their surroundings.

We present a discrete cell model for capillary tube formation by endothelial cells (ECs) during *in vitro* tumor induced angiogenesis. In this hybrid discrete/continuous mathematical model, endothelial cells are treated as discrete units in a continuum field of chemoattractant (such as VEGF) which evolves according with a system of reaction-diffusion equations, whereas cells serve as sources/sinks in this continuum field. It incorporates a realistic model for signal transduction and VEGF production and release, and gives insights into the aggregation patterns and the factors that influence stream formation. The model allows us to explore how changes in the microscopic rules by which cells determine their direction and duration of movement affect macroscopic formations. In particular, it serves as a tool for investigating tumor-vessel signaling and the role of mechano-chemical interactions of the cells with the substratum.

Absenteism impact on local economy during an epidemic via constrained hybrid SI dynamics

E. W. Thommes¹, M. G. Cojocaru², S. Athar³

¹ University of Guelph, Guelph, Canada, ethommes@uoguelph.ca

² University of Guelph, Guelph, Canada, mcojocar@uoguelph.ca

³ University of Guelph, Guelph, Canada, sathar@uoguelph.ca

In this paper we would like to optimize (minimize) the cost of missing work during an epidemic/pandemic in a local economy with several geographically distinct locations, and with populations consisting of individuals who live and work in the same city, and individuals who live and work in different locations (they commute to work daily).

The mathematical framework we employ here is that of a hybrid dynamical system, specifically a non-standard continuous time infection model (SIS) and a discrete transition state matrix encapsulating individuals' daily decision making regarding going to or missing work that day. A healthy susceptible individual is considered to have a probability $C \frac{I}{N}$ of missing work, where $\frac{I}{N}$ is the fraction of infected people in the population. An infected individual has a probability of missing work given by the severity of the disease. Susceptible individuals can contract the infection given averaged number of contacts during the work day, at the respective work locations. The infected individuals who choose to miss work are considered to be staying home and are thus removed from the transmission dynamics.

To implement the transmission dynamics, we use a known SIS model inspired by [1], modified further with constraints to reflect daily commuters trips. The total population of the area is held constant. Thus to solve for the trajectories of the continuous time dynamics we use a constraint dynamical system framework; to blend in the daily morning decision making, we use the hybrid dynamics framework widely used in engineering applications, as shown in [2].

We run simulations for 20 weeks of an 8hr work day period, and we study the effects of the parameter C on the number of missed work days in the region. Incorporating prophylactic practices (such as existing vaccination) highlights the effects of these practices on the economic impact on the region.

References

- [1] Sattenspiel, Lisa, and Klaus Dietz. "A structured epidemic model incorporating geographic mobility among regions." Mathematical Biosciences 128.1 (1995): 71-91
- [2] van der Schaft, A. and H. Schumacher, An Introduction to Hybrid Dynamical Systems, LNCIS 251, Springer (2000).

Black-box simulations for vesicle transport

Bryan Quaife¹, Gökberk Kabacaoğlu¹, George Biros¹

¹ University of Texas, Austin, USA *quaife@ices.utexas.edu*

Vesicle suspensions, which are experimental and numerical proxies for red blood cells and other biomembranes, are ubiquitous in various applications such as biological flows. I will present an integro-differential equation that is used to simulate the suspension of vesicles in a Stokesian fluid. This integral formulation has several advantages such as the fact that only the boundary of the vesicles must be discretized rather than the entire computational domain.

Unfortunately, when simulating vesicle suspensions, a user must often use a trial and error procedure to choose appropriate spatial and temporal resolutions. For instance, accurate quadrature must be used to resolve vesicles that come arbitrarily close to one another. Therefore, in our group, we have been developing algorithms that automatically resolve complex dynamics by controlling both the discretization and truncation errors.

Several complications for high concentration flows were first resolved in [1]. Here, we introduced time integrators that resolve several sources of stiffness, introduced quadrature formula that resolves nearly touching vesicles, and developed an accurate collision detection scheme that only requires linear complexity. Then, in [2, 3], a high-order adaptive time integrator was developed. This time integrator allows a user to specify a desired tolerance for the time horizon at the onset of the simulation; then, the method automatically adjusts the time step size based on estimates of the local truncation error.

Now that we have developed a robust solver for vesicle suspensions, we are coupling the velocity field induced by a vesicle suspensions with an advection diffusion equation. The goal is to simulate different transport phenomenon such as oxygen transport and drug delivery.

References

- [1] Bryan Quaife and George Biros, *High-volume fraction simulations of two-dimensional vesicle suspensions*, J. Comput. Phys. **274**, pp. 245–267 (2014).
- [2] Bryan Quaife and George Biros, *Adaptive Time Stepping for Vesicle Simulations*, J. Comput. Phys. *to appear* (2014).
- [3] Bryan Quaife and George Biros, *High-order adaptive time stepping for vesicle suspensions with viscosity contrast*, in *IUTAM Symposium on Dynamics of Capsules, Vesicles and Cells in Flow* (2014).

Computational Simulations of the Onset and Treatment of Hydrocephalus in Infants and Mice Based on a Novel Mesh Warping Algorithm

S.M. Shontz¹ and C.S. Drapaca²

¹ University of Kansas, Lawrence, USA, shontz@ku.edu

² The Pennsylvania State University, University Park, USA, csd12@psu.edu

Hydrocephalus is a serious neurological disorder caused by abnormalities in cerebrospinal fluid (CSF) flow, resulting in large brain deformations and neuronal damage. Treatments drain the excess CSF from the ventricles either via a CSF shunt or an endoscopic third ventriculostomy. However, patients' response to these treatments is poor. Mathematical models of hydrocephalus mechanics could aid neurosurgeons in hydrocephalus treatment planning. Current models and corresponding computational simulations of hydrocephalus are still in their infancy, despite this being a disease with serious long-term implications.

We recently proposed a novel geometric computational approach for tracking the evolution of hydrocephalic brain tissue - ventricular CSF interface via the level set method and an adaptive version of a finite element-based mesh warping technique (FEMWARP) [1]. Our method uses the solution gradient of the PDE in the mesh warping approach as an enrichment indicator to determine where to coarsen/refine the mesh. Previously, in [2], we evolved the ventricular boundary in 2D CT images which required a backtracking line search for obtaining valid intermediate meshes for use with FEMWARP. In [3], we used the level set method to automatically evolve the ventricular boundary deformation for 2D CT images. To help surgeons determine where to implant a shunt, we also computed the brain ventricle volume evolution for 3D MR images using FEMWARP. Our new technique generalizes the results in [2, 3].

We present the results of our computational simulations of the onset and treatment of pediatric hydrocephalus and hydrocephalus in mice based on 2D CT and MR images, respectively. Together, they demonstrate the success of our combined level set/adaptive finite element-based mesh warping approach.

References

- [1] S.M. Shontz and C.S. Drapaca, *Prediction of Ventricular Boundary Evolution via a Combined Level Set and Adaptive Finite Element Mesh Warping Method*, in *Proceedings of the International Conference on Adaptive Modeling and Simulation (ADMOS 2015)*, Nantes, France (2015).
- [2] J. Park, S.M. Shontz, and C.S. Drapaca, *A combined level set/mesh warping algorithm for tracking brain and cerebrospinal fluid evolution in hydrocephalic patients*, in Y. Zhang (ed.), *Image-Based Geometric Modeling and Mesh Generation*, Springer, Lecture Notes in Computational Vision and Biomechanics, **3**, pp. 107-141 (2013).
- [3] J. Park, S.M. Shontz, and C.S. Drapaca, *A Combined Level Set and Mesh Warping Technique: Application to Hydrocephalus*, in *Proceedings of the Mesh Processing in Medical Image Analysis 2012 - MICCAI 2012 International Workshop (MeshMed 2012)*, Nice, France, pp. 122-133 (2012).

Discovery of Principles of Nature from Matrix and Tensor Modeling of Large-Scale Molecular Biological Data

Orly Alter

*Scientific Computing and Imaging Institute and Departments of Bioengineering and Human Genetics, University of Utah, USA,
orly@sci.utah.edu*

I will describe the use of matrix and tensor decompositions in the simultaneous modeling of different types of large-scale molecular biological data, from different studies of cell division and cancer [1, 2] and from different organisms [3], to computationally predict previously unknown physical [4], cellular and evolutionary mechanisms that govern the activity of DNA and RNA [5]. I will present novel multi-matrix [6, 7] and multi-tensor generalizations of the singular value decomposition as well as experimental verification and validation of some of the computational predictions [8]. These models bring physicians a step closer to one day being able to predict and control the progression of cell division and cancer as readily as NASA engineers plot the trajectories of spacecraft today [9].

References

- [1] P. Sankaranarayanan,* T. E. Schomay,* K. A. Aiello, and O. Alter, *Tensor GSVD of Patient- and Platform-Matched Tumor and Normal DNA Copy-Number Profiles Uncovers Chromosome Arm-Wide Patterns of Tumor-Exclusive Platform-Consistent Alterations Encoding for Cell Transformation and Predicting Ovarian Cancer Survival*, to be published in PLoS One 10, article e121396 (2015); <http://dx.doi.org/10.1371/journal.pone.0121396>
- [2] C. H. Lee,* B. O. Alpert,* P. Sankaranarayanan, and O. Alter, *GSVD Comparison of Patient-Matched Normal and Tumor aCGH Profiles Reveals Global Copy-Number Alterations Predicting Glioblastoma Multiforme Survival*, PLoS One 7 (1), article e30098 (January 2012); <http://dx.doi.org/10.1371/journal.pone.0030098>
- [3] O. Alter, P. O. Brown and D. Botstein, *Generalized Singular Value Decomposition for Comparative Analysis of Genome-Scale Expression Datasets of Two Different Organisms*, Proc Nat Acad Sci USA 100 (6), pp. 3351–3356 (March 2003); <http://dx.doi.org/10.1073/pnas.0530258100>
- [4] N. M. Bertagnolli, J. A. Drake, J. M. Tennessen, and O. Alter, *SVD Identifies Transcript Length Distribution Functions from DNA Microarray Data and Reveals Evolutionary Forces Globally Affecting GBM Metabolism*, PLoS One 8 (11), article e78913 (November 2013); <http://dx.doi.org/10.1371/journal.pone.0078913>
- [5] O. Alter, and G. H. Golub, *Integrative Analysis of Genome-Scale Data Using Pseudoinverse Projection Predicts Novel Correlation Between DNA Replication and RNA Transcription*, Proc Nat Acad Sci USA 101 (47), pp. 16577–16582 (November 2004); <http://dx.doi.org/10.1073/pnas.0406767101>
- [6] S. P. Ponnappalli, M. A. Saunders, C. F. Van Loan, and O. Alter, *A Higher-Order Generalized Singular Value Decomposition for Comparison of Global mRNA Expression from Multiple Organisms*, PLoS One 6 (12), article e28072 (December 2011); <http://dx.doi.org/10.1371/journal.pone.0028072>
- [7] S. P. Ponnappalli, G. H. Golub, and O. Alter, *A novel higher-order generalized singular value decomposition for comparative analysis of multiple genome-scale datasets*, in *Stanford University and Yahoo! Research Workshop on Algorithms for Modern Massive Datasets (MMDS)*, Stanford, CA, USA (June 21–24, 2006).
- [8] L. Omberg, J. R. Meyerson, K. Kobayashi, L. S. Drury, J. F. X. Diffley, and O. Alter, *Global Effects of DNA Replication and DNA Replication Origin Activity on Eukaryotic Gene Expression*, Mol Syst Biol 5, article 312 (October 2009); <http://dx.doi.org/10.1038/msb.2009.70>
- [9] O. Alter, *Discovery of Principles of Nature from Mathematical Modeling of DNA Microarray Data*, Proc Natl Acad Sci USA 103 (44), pp. 16063–16064 (October 2006); <http://dx.doi.org/10.1073/pnas.0607650103>

Dynamics and Bifurcations in Low-Dimensional Models of Intracranial Pressure

D. Evans¹, J. P. Cusumano², C. Drapaca³,

¹ The Pennsylvania State University, USA, dje5104@psu.edu

² The Pennsylvania State University, USA, jpc3@psu.edu

³ The Pennsylvania State University, USA, csd12@psu.edu

Intracranial Pressure (ICP) monitoring has been shown to provide valuable physiological information for patients suffering from brain disorders such as hydrocephalus and traumatic brain injury. Currently, all reliable methods for measuring ICP involve drilling through the skull to place a pressure probe inside the brain [1]. As a result, intracranial pressure is only measured in the most critical cases. Mathematical models that relate ICP to other noninvasive measurements could contribute to better diagnostic and treatment protocols. For instance, such mathematical models could have the capability to predict ICP in real time without the need for invasive direct measurements.

In this paper, we examine in detail the dynamics and stability of the Ursino model [2] that predicts ICP from measurements of arterial blood pressure. We study how the equilibria vary with the model parameters and, aided by numerical simulations, we obtain bifurcation diagrams for the system. Expanding upon the work of Ursino *et al.*, we show that the model exhibits both forward and reverse Hopf bifurcations in certain parameter regimes. We also present global phase portraits of the system in interesting parameter configurations.

Whereas the problem of ICP dynamics is fundamentally (though not entirely) mechanical in nature, the Ursino model was derived using an electrical circuit analogy. Thus, following the work of Marmarou et al. [3], we propose a new low-dimensional mechano-hydraulic model of ICP dynamics that couples the hydraulics of the ventricular cerebrospinal fluid (CSF) system with the brain tissue mechanics. We investigate the dynamics of the new model, and discuss how the model can be expanded to include the cerebral vasculature, as well.

References

- [1] Jose I Suarez, *Critical care neurology and neurosurgery*, Springer (2004).
- [2] M. Ursino, C. Lodi *A simple mathematical model of the interaction between intracranial pressure and cerebral hemodynamics*, in *Journal of Applied Physiology* 82.4 (1997): 1256-1269.
- [3] A. Marmarou, K. Shulman, R. M. Rosende *A nonlinear analysis of the cerebrospinal fluid system and intracranial pressure dynamics*, in *Journal of neurosurgery* 48.3 (1978): 332-344.

Effect of non-Newtonian Rheology on Transition to Turbulence

M. Owais Khan¹, K. Valen-Sendstad¹, D. Steinman¹

¹ University of Toronto, Toronto, ON, Canada, owais/kvs/steinman@mie.utoronto.ca

Recent high-resolution CFD studies have shown turbulent-like flow in cerebral arteries, with the potential ramifications for the understanding of cerebral aneurysm initiation [1]. Although non-Newtonian rheology has shown negligible impact for laminar flows, recent experiments suggest a delay in transition to turbulence Reynolds number (Re) in straight pipes [2]. The aim of the present study was to investigate the effects of non-Newtonian rheology on transition to turbulence in a controlled numerical experiment. We chose the eccentric stenosis model previously published by Varghese et al. [3], i.e., a 50% diameter reduction and a 5% offset in the xz plane. Transient CFD simulations with steady parabolic inflow for $Re=500-1000$ in increments of 100 was performed with Newtonian and Cross shear-thinning viscosity model fitted to the viscosity curve of porcine blood. The non-Newtonian Re was defined based on the corresponding high shear rate viscosity. Figure 1 shows instantaneous vorticity maps where transition to turbulence occurs at $Re=700-800$ for non-Newtonian vs. $Re=600-700$ for Newtonian simulations. Notably, non-Newtonian simulations for $Re=700$ showed only mild vortex-shedding, while the Newtonian simulation at this Re showed jet breakdown and apparent turbulence. These findings indicate that shear-thinning effect, as opposed to viscoelastic or other blood properties, are sufficient to model delay in transition, since they are consistent with experimental results where transition was delayed for blood vs. Newtonian fluid by $\sim 20\%$ [2]. Clinical relevance of these preliminary findings remain in question owing to idealized, rather than patient-specific, geometry. Moreover, it is also possible that a better definition of characteristic non-Newtonian viscosity, rather than common-place high-shear viscosity, to define generalized Re for shear-thinning fluids may cause these differences to disappear.



Figure 1: Instantaneous vorticity maps for Newtonian and non-Newtonian rheology models for various Re .

References

- [1] Valen-Sendstad et al. High-resolution computational fluid dynamics detects flow instabilities in the carotid siphon: Implications for aneurysm initiation and rupture? *Journal of Biomechanics* 47.12 (2014): 3210-3216.
- [2] Biswas, D. Transition to Turbulence in Non-Newtonian Fluids: An In-Vitro Study Using Pulsed Doppler Ultrasound for Biological Flows. *PhD Dissertation. The University of Akron*, 2014.
- [3] Varghese et al. Direct numerical simulation of stenotic flows. Part 1. Steady flow. *Journal of Fluid Mechanics* 582 (2007): 253-280.

Lagrangian Shape Optimization for Segmentation of Multiphase Images

G. Doğan¹

¹ Theiss Research, National Institute of Standards and Technology, USA gunay.dogan@nist.gov

Image segmentation is the problem of identifying homogeneous regions and their boundaries in given images. It is a fundamental task in image processing required for many higher level imaging tasks or analyses. Therefore, an efficient and robust algorithm for image segmentation is crucial. A widely-studied class of images for this are multiphase images, namely, images that can be approximated as piecewise constant images, with applications in medical imaging and material science. An effective approach to multiphase image segmentation is to express it as an energy minimization problem, in which the set of region boundaries Γ is the unknown. Given an image function $I : D \rightarrow \mathbb{R}$, defined on a bounded image domain $D \subset \mathbb{R}^2$, we propose the following the multiphase segmentation energy [2]

$$J(\Gamma) = \frac{1}{2} \sum_{k=0}^{n_\Omega} \int_{\Omega_k} \chi_D(I(x) - c_k)^2 dx + \gamma \int_{\Gamma} dS, \quad \gamma > 0, \quad (1)$$

where $\Gamma = \bigcup_{k=1}^{n_\Omega} \Gamma_k$ is the union of all the region boundaries or curves Γ_k , each of which enclose a region Ω_k . The image function is approximated by an average value c_k within each region Ω_k . The energy (1) is a generalization of the two-phase energy proposed by Chan and Vese in [1].

We propose a shape optimization algorithm to compute the curves Γ^* minimizing the energy (1), thereby providing a segmentation of the image I . For this, we compute the first and second shape derivatives of (1) and formulate an Newton-type minimization scheme that works by deforming a given set of initial curves iteratively to the optimal configuration [3, 4]. As the curves are infinite-dimensional objects, we take care to discretize them in a way that is faithful to the geometry and resolves important features in the image. This is realized with an adaptive Lagrangian representation that dynamically adapts the node distribution of the discretized curves, and handles topological changes, such as splitting or merging of the curves, as well. The differential equations governing each step of the iterative minimization are discretized with the finite element method. This leads to efficient linear systems that can be solved in linear time. Bringing together the shape derivatives, spatial adaptivity and finite element method under the shape optimization framework results in an efficient method that works well in practical scenarios. We demonstrate the effectiveness of our method with several examples.

References

- [1] T.F. Chan, and L.A. Vese, *Active contours without edges*, IEEE Transactions on Image processing, 10(2), pp. 266-277 (2001).
- [2] G. Doğan, *An efficient algorithm for multiphase image segmentation*, Energy Minimization Methods in Computer Vision and Pattern Recognition, Springer Berlin Heidelberg (2015).
- [3] G. Doğan, *Shape calculus for shape energies in image processing*, arXiv:1307.5797.
- [4] G. Doğan, *Fast minimization of region-based active contours using the shape Hessian of the energy*, Scale Space and Variational Methods in Computer Vision, Springer Berlin Heidelberg (2015).

Mathematical Challenges in Medical Image Registration

Mehran Ebrahimi, Lorraine Ma

*Faculty of Science, University of Ontario Institute of Technology, Oshawa, Ontario, Canada
mehran.ebrahimi@uoit.ca, lok.ma@uoit.ca*

In general, many real-world inverse problems are ill-posed, mainly due to the lack of existence of a unique solution. The procedure of providing acceptable unique solutions to such problems is known as regularization. Indeed, much of the recent progress in imaging has been due to advances in the formulation and practice of regularization. This, coupled with progress in optimization and numerical analysis, has yielded much improvement in computational methods of solving inverse imaging problems. Image registration, the process of aligning different sets of data into one coordinate system [5], is a key challenge in many medical imaging applications, e.g., tumour detection and surgery planning, that can be modelled as an inverse problem. Given a template (or moving) image and a reference (or fixed) image, the goal is to find a reasonable transformation that maximizes a predetermined similarity measure between the reference and the transformed template image. Solving this inverse problem is specifically challenging when images of highly deformable tissue, e.g., breast [2] or heart [1] is considered. In this talk, we present a number of current research challenges and plans in this direction.

- Breast Magnetic Resonance Imaging (MRI) is frequently performed prior to breast conserving surgery in order to assess the location and extent of the lesion. Ideally, the surgeon should be able to use the pre-surgery image information during surgery to guide the excision. This requires the prone pre-surgical MR image to be aligned or co-registered to conform to the patient's supine position on the operating table. The future breast Computer Assisted Surgery technology (CAS) will demand novel efficient alignment algorithms that employ the surface information of the breast in the operating room along with the intensity information of the pre-surgical images [2].
- Recently, Dynamic Contrast-Enhanced (DCE) imaging has emerged as a powerful screening tool. Accurate registration of DCE images is valuable for proper identification of the lesions [3, 4]. This requires defining regularization expressions that directly incorporate the underlying physical process of this inverse problem.
- In image registration, we generally rely on smooth transformations to describe the alignment process relating two images. However, in the clinical setting, there are many situations where the deformation may have discontinuities. An open problem is to develop a method that would enable deformable registration in the presence of various types of large-scale discontinuities.

References

- [1] M. Ebrahimi and S. Kulaseharan *Deformable image registration and intensity correction of cardiac perfusion MRI*, Lecture Notes in Computer Science, Statistical Atlases and Computational Models of the Heart-Imaging and Modelling Challenges, Springer, **8896**, pp. 13-20 (2015).
- [2] M. Ebrahimi, P. Siegler, A. Modhafar, C. Holloway, DB. Plewes, and AL. Martel *Using surface markers for MRI guided breast conserving surgery: a feasibility survey*, Physics in Medicine and Biology **59**, 7, pp. 1589-1605 (2014).
- [3] M. Ebrahimi, A. Lausch and AL. Martel *A Gauss-Newton approach to joint image registration and intensity correction*, Computer Methods and Programs in Biomedicine **112**, 3, Elsevier, pp. 398-406 (2013).
- [4] A. Lausch, M. Ebrahimi and AL. Martel *Image registration for abdominal dynamic contrast-enhanced magnetic resonance images*, IEEE International Symposium on Biomedical Imaging (ISBI): From Nano to Macro, IEEE, pp. 561-565 (2011).
- [5] J. Modersitzki *FAIR: flexible algorithms for image registration*, SIAM (2009).

Modeling and forecasting of mosquito abundance and risk of West Nile virus in Great Toronto Area

Huaiping Zhu

LAMPS and Department of Mathematics and Statistics, York University, Canada
huaping@mathstat.yorku.ca

West Nile virus is a mosquito-borne flavivirus typically transmitted between birds and mosquitoes, and can infect humans and other domestic mammals. Like other mosquito-borne or vector-borne diseases, the transmission and dynamics of the West Nile virus can be very complicated due to climate and environmental impact on vector mosquitoes density and biting incidences of the vectors. In this talk, I will present modeling studies of using surveillance data, daily weather (temperature and precipitation) and landscape data to model the mosquito density and distribution, and the transmission of the virus among birds and mosquitoes. I will also present our weekly real-time forecasting of mosquito abundance and minimum infection rate (MIR) for risk assessment of West Nile virus in Great Toronto Area. This is a joint work of Lamps group with Health Units in GTA, Public Health Ontario and Public Health Agency of Canada.

Role of Iron-dependent Oxidative Stress in Breast Cancer

S. Arat^{1,2}, J. Chifman³, C. Lopez⁴, S.V. Torti², R. Laubenbacher^{2,5}

¹ Virginia Tech, Blacksburg, VA, USA, sedag@vt.edu

² University of Connecticut Health Center, Farmington, CT, USA, {arat, storti, laubenbacher}@uchc.edu

³ Wake Forest University, Winston-Salem, NC, USA, jchifman@wakehealth.edu

⁴ Vanderbilt University, Knoxville, TN, USA, c.lopez@vanderbilt.edu

⁵ Jackson Laboratory for Genomic Medicine, Farmington, CT, USA, Reinhard.Laubenbacher@jax.org

Every aerobic organism requires iron for many processes such as energy production, cellular respiration and proliferation. Iron can be toxic due to its ability to exist in various oxidation states. In order to prevent damage, all organisms that require iron have developed a complicated machinery to tightly control iron at both the systemic and the cellular levels. Inappropriately low levels of iron or excess iron are detrimental and can lead to a wide range of diseases. Dysregulation of iron metabolism in cancer is well-documented and it has been suggested that there is interdependence between excess iron and increased cancer incidence [1].

In this study, we build a predictive mathematical model of an expanded iron metabolism with other pathways such as heme biosynthesis, oxidative stress response and oncogenic pathways, which is an extension of our iron metabolism model in a normal breast cell [2]. This expanded protein-protein interaction network consists of free iron (LIP), iron-related proteins (TfR1, Fpn, Ft, IRP1, IRP2, Hep), heme, heme-related proteins (HO-1, ALAS1), H_2O_2 , oxidative stress-related proteins (Cat, Nfr2, Keap1), an immune response protein (IL-6) and oncogenic proteins (Ras, SOS, ERK, c-Myc, GAPS, EGFR). We used a time- and state-discrete mathematical framework, Polynomial Dynamical System (PDS), which allows us to model regulatory networks over a finite field [3]. We run a customized Python script to compute the whole state space and the basin of attraction (long-term behavior) of the system. Our model provides two predictions based on overexpression and knockout simulations. The first hypothesis is that IRP2 overexpression can alter only the iron homeostasis pathway in a way that free iron and the iron-related proteins present a cancer-like behavior. This hypothesis is validated by experimentation (unpublished data). This finding highlights that although IRP2 overexpression disrupts iron homeostasis pathway and other pathways like oncogenic pathways in many cancers, it is not the case in breast cancer. The second hypothesis is related with the fact that breast cancer cells are frequently under persistent oxidative stress. Our model predicts that high oxidative stress response activity can be achieved only when the defense mechanism for oxidative stress is disrupted. This hypothesis is validated by a recent study [4]. To our knowledge, our single-cell model is the only expanded iron metabolism model that can capture a breast cancer phenotype by overexpression and knockout simulations. One motivation for this study is to understand how normal cells become malignant cells and identify key players in the system for therapeutic targets.

References

- [1] S.V. Torti, and F.M. Torti, *Ironing Out Cancer*, Cancer Research **71**, 5, pp. 1511-1514 (2011).
- [2] J. Chifman, A. Kniss , P. Neupane, I. Williams, B. Leung, Z. Deng, P. Mendes, V. Hower, F.M. Torti, S.A. Akman, S.V. Torti and R. Laubenbacher, *The core control system of intracellular iron homeostasis: A mathematical model*, Journal of Theoretical Biology **300**, pp. 91 - 99 (2012).
- [3] A. Veliz-Cuba, A.S. Jarrah, and R. Laubenbacher, *Polynomial algebra of discrete models in systems biology*, Bioinformatics **26**, 13, pp. 1637-1643 (2010).
- [4] S.Sen, B. Kawahara, and G. Chaudhuri, *Maintenance of higher H_2O_2 levels, and its mechanism of action to induce growth in breast cancer cells: Important roles of bioactive catalase and PP2A*, Free Radical Biology and Medicine **53** pp. 1541-1551 (2012).

The Evolution of Group Dispersal with Leaders and Followers

C. Koykka¹, G. Wild²

¹ Department of Applied Mathematics, The University of Western Ontario, London, Ontario, Canada ckoykka@uwo.ca

² Department of Applied Mathematics, The University of Western Ontario, London, Ontario, Canada gwild@uwo.ca

In many animal species, individuals disperse together in groups [1]. Group dispersal often occurs among genetic relatives and is frequently initiated or even coordinated by a subset of individuals (leaders). While this phenomenon is well-documented, previous theoretical work has focused on the consequences rather than the evolutionary origins of this dispersal strategy, and has largely neglected the presence of leader-follower relationships [2]. In this study [3], we create an inclusive fitness model to examine the conditions under which group dispersal can emerge and be maintained. We investigate from an evolutionary perspective why certain individuals are motivated to lead while others follow. We calculate the dispersal rate, propensity to lead, and propensity to follow at evolutionary equilibrium using numerical analysis. Additionally, we use this model to mathematically describe the evolutionary incentives for leading and following in dispersal groups.

We find that high within-group relatedness, significant reductions in the cost of dispersal, and reproductive skew in favour of followers facilitates the emergence of group dispersal. We also show that the incentives for leading can be either selfish or altruistic, depending on social and ecological factors. This is in contrast to lone dispersal [4], which theoretical work has suggested occurs in order to alleviate local kin competition and is therefore an act of altruism. Moreover, we show that leaders of dispersal groups evolve to be neither completely egalitarian nor selfish. Lastly, we illustrate how our model provides further evidence for the theory that individuals may differ in their intrinsic propensity to become leaders and followers, irrespective of their immediate condition. We demonstrate that kin selection is sufficient and individual differences in state and ability are not required for the emergence of leader-follower relationships. Therefore, our work suggests it is possible that leaders and followers evolved to possess different traits only after leader-follower relationships had emerged in order to take advantage of their respective social positions.

These results provide us not only with important insights regarding why certain species exhibit group dispersal, but they also grant greater understanding of the evolution of leadership and followership. Most previous theoretical work deemed leadership as a uniformly selfless (indirect-fitness maximizing) or uniformly selfish (direct-fitness maximizing) strategy [5], but we in fact have shown that leading is a strategy that can be used to maximize either one's direct fitness or one's indirect fitness, depending on the ecological and social conditions.

References

- [1] A. Ridley *Invading together: the benefits of coalition dispersal in a cooperative bird*, Behavioural Ecology and Sociobiology **66** pp. 77-83. (2012).
- [2] M. Nakamaru, T. Takada, A. Ohtsuki, S. Suzuki, K. Miura, and K. Tsujii, *Ecological conditions favouring budding in colonial organisms under environmental disturbance*, PLoS ONE **9** pp. 1-13. (2014).
- [3] C. Koykka and G. Wild, *The evolution of group dispersal with leaders and followers*, J. Theor. Biol. **In press** (2015).
- [4] P. Taylor, *An inclusive fitness model for dispersal of offspring*, J. Theor. Biol. **130** pp. 363-378. (1988).
- [5] S. Gavrilets and L. Fortunato, *A solution to the collective action problem in between-group conflict with within-group inequality*, Nat. Comm. **3526** pp. 1-11. (2014).

**SS-RALSMCL Recent Advances in Lie
Symmetry Methods and Conservation Laws for
Differential Equations and Applications**

Benjamin-Bona-Mahony Equation with Variable Coefficients: Conservation Laws and Exact Solutions

Chaudry Masood Khalique

*International Institute for Symmetry Analysis and Mathematical Modelling,
Department of Mathematical Sciences, North-West University, Mafikeng Campus,
Private Bag X 2046, Mmabatho 2735, Republic of South Africa.*

Masood.Khalique@nwu.ac.za

In this talk we derive conservation laws for a Benjamin-Bona-Mahony equation with variable coefficients [1], which is a third-order partial differential equation. The Noether approach [2] is employed to construct the conservation laws. Finally, a conservation law is used to obtain exact solution [3] of a special case of the Benjamin-Bona-Mahony equation.

References

- [1] K. Singh, R.K. Gupta, S. Kumar, Benjamin-Bona-Mahony equation(BBM) equation with variable coefficients: Similarity reductions and Painlevé analysis. *Appl. Math. Comput.* 2011, 217, 7021–7027.
- [2] E. Noether, Invariante Variationsprobleme. *König. Gesell. Wissen. Göttingen. Math Phys. Klasse* 1918, 2, 235–257.
- [3] A. Sjöberg, Double reduction of PDEs from the association of symmetries with conservation laws with applications. *Appl. Math. Comput.* 2007, 184, 608–616.

Closed-form solutions for the Lucas-Uzawa model with externality via the Partial Hamiltonian Approach

Rehana naz

Centre for Mathematics and Statistical Sciences, Lahore School of Economics, Pakistan-53200, Lahore

This paper studies celebrated Economic growth model of endogenous growth Lucas-Uzawa model with externality. A dynamical system of first order ordinary differential equations (ODEs) is obtained for the control, state and costate variables. The closed-form solutions for this dynamical system are derived by using the newly developed Partial Hamiltonian approach. First, the Partial Hamiltonian approach is applied to construct the first integrals for the system of ODEs and two cases arise. In the first case, two first integrals are obtained whereas the second case yields three first integrals under certain restrictions on the parameters of model. Second, the first integrals for both cases are utilized to obtain closed form solutions for the system of ODEs which have not been previously reported in the known literature. The closed form solutions play a vital role in economic dynamics to assess transition dynamics of endogenous economic growth models. The dynamics properties of this system are studied. The growth rates of physical capital, consumption and human capital are constructed to study several features associated with the transitional dynamics of this model.

References

- [1] H. Uzawa, Optimum technical change in an aggregative model of economic growth. *International Economic Review*, 6 (1965) 18-31.
- [2] R. Lucas, On the mechanics of economic development. *Journal of Monetary Economics*, 22 (1988) 3-42.
- [3] R. Naz, F. M. Mahomed and A. Chaudhry, A Partial Hamiltonian Approach for Current Value Hamiltonian Systems. *Comm. Non-linear. Sci. Numer. Simulat.*, 19 (2014) 3600-3610.
- [4] V. Dorodnitsyn, R. Kozlov, Invariance and first integrals of continuous and discrete Hamiltonian equations. *Journal of Engineering Mathematics*, 66 (2010) 253-270. (2011).

Conservation laws of fluid flow on Riemannian manifolds

S.C. Anco¹, A. Dar², N. Tufail³

¹ Brock University, St Catharines, Canada, sanco@brocku.ca

² Mirpur University of Science and Technology, Mirpur, Pakistan

³ Quaid-e-azam University, Islamabad, Pakistan

All local conservation laws of kinematic type on moving domains and moving surfaces for inviscid compressible fluid flow on curved Riemannian manifolds are derived. In particular, any such conservation laws will be found that hold only for (1) special dimensions of the manifold or the surface; (2) special conditions on the geometry of the manifold or the surface; (3) special equations of state. Importantly, the general form of these kinematic conservation laws will be allowed to depend on the intrinsic Riemannian metric, volume form, and curvature tensor of the manifold or the surface. All kinematic constants of motion that arise from the resulting kinematic conservation laws also will be determined.

These results generalize earlier work on finding all kinematic local conservation laws on moving domains for inviscid compressible fluid flow in n -dimensional Euclidean space.

References

- [1] V.I. Arnold and B.A. Khesin, Topological Methods in Hydrodynamics, Springer-Verlag (1998).
- [2] A.A. Dezin, *Invariant forms and some structure properties of the Euler equations of hydrodynamics*, Zeit. Anal. Anwend. (in Russian) **2** pp. 401–409 (1983).
- [3] D. Serre, *Invariants et dégénérescence symplectique de l'équation d'Euler des fluids parfaits incompressibles*, C.R. Acad. Sci. Paris, Sér. A **298** pp. 349 (1984).
- [4] S.C. Anco and A. Dar, *Classification of conservation laws of compressible isentropic fluid flow in $n > 1$ spatial dimensions*, Proc. Roy. Soc. A **464** pp. 2461–2488 (2009).
- [5] S.C. Anco and A. Dar, *Conservation laws of inviscid non-isentropic compressible fluid flow in $n > 1$ spatial dimensions*, Proc. Roy. Soc. A **466** pp. 2605–2632 (2010).

Exact solutions of semilinear radial Schrödinger equations by group foliation reduction

Stephen Anco¹, Wei Feng², Thomas Wolf³

¹ Brock University, St. Catharines, Canada, sanco@brocku.ca

² Zhejiang University of Technology, Hangzhou, China, fengwei9999@gmail.com

³ Brock University, St. Catharines, Canada, twolf@brocku.ca

In this talk a novel symmetry-group method will be outlined which has been used successfully in recent work to find exact solutions to radial semilinear Schrödinger equations in multi-dimensions [1, 2] and earlier for radial semilinear wave equations and heat equations [3, 4, 5], with power nonlinearities.

The method is based on the geometrical idea of group foliation [7, 6] in which the solution jet space of a given nonlinear PDE is reduced to a quotient space of orbits under the action of a one-dimensional group of symmetries admitted by the PDE. Certain algebraic homogeneity features of the group-invariant equations describing the orbits are used to seek explicit solutions by a relatively simple separation of variables ansatz that involves the solution of a nonlinear overdetermined differential-algebraic system. All solutions of these systems are obtained by using the package CRACK [8].

References

- [1] S.C. Anco, W. Feng, T. Wolf, *Exact solutions of semilinear radial Schrödinger equations by group foliation reduction*, To appear J. Math. Anal. Appl. (2015).
- [2] S.C. Anco and W. Feng, *Group-invariant solutions of semilinear Schrödinger equations in multi-dimensions*, J. Math. Phys. **54** (2013), 121504 (41 pages).
- [3] S.C. Anco and S. Liu, *Exact solutions of semilinear radial wave equations in n dimensions*, J. Math. Anal. Appl. **297** pp. 317–342 (2004).
- [4] S.C. Anco, S. Ali, T. Wolf, *Symmetry analysis and exact solutions of semilinear heat flow in multi-dimensions*, J. Math. Anal. Appl. **379** pp. 748–763 (2011).
- [5] S.C. Anco, S. Ali, T. Wolf, *Exact solutions of nonlinear partial differential equations by the method of group foliation reduction*, SIGMA **7** (2011), 066 (10 pages).
- [6] L.V. Ovsiannikov, Group Analysis of Differential Equations, (New York, Academic) 1982.
- [7] E. Vessiot, *Sur l'intégration des systèmes différentiels qui admettent des groupes continus de transformations*, Acta Math. **28** pp. 307–349 (1904).
- [8] T. Wolf, *Applications of CRACK in the Classification of Integrable Systems*, in CRM Proceedings and Lecture Notes **37** pp. 283–300 (2004).
<http://lie.math.brocku.ca/crack/demo/>

Local Conservation Laws of a Generalized Variable-Coefficient Gardner Equation with Generalized Evolution

M. Bruzón¹, R. de la Rosa²

¹ University of Cádiz, Spain, m.bruzon@uca.es

² University of Cádiz, Spain, rafael.delarosa@uca.es

The phenomenon of shallow water wave engineering experiment is modelled by the Gardner equation, which is basically the Korteweg-de Vries equation with dual power-law nonlinearity [3]. The generalization is based on the same kind as given by the $K(m, n)$ equation, which is a generalization of the Korteweg-de Vries equation [4, 5, 6, 7, 8].

Bluman and Anco devised and developed an effective algorithmic method for finding the local conservation laws for partial differential equations with any number of independent and dependent variables [1, 2], called Direct Construction Method. The method does not require the use or existence of a variational principle and reduces the calculation of conservation laws to solving a system of linear determining equations similar to that for finding symmetries.

In this paper we construct some nontrivial conservation laws for a Generalized Variable-Coefficient Gardner equation with generalized evolution by applying the Direct Construction Method.

References

- [1] S. Anco and G. Bluman, *Direct construction method for conservation laws of partial differential equations. Part I: Examples of conservation law classifications*, Euro. J. Appl. Math. **15**, 5, pp. 547-568 (2001).
- [2] S. Anco and G. Bluman, *Direct construction method for conservation laws of partial differential equations. Part II: General treatment*, Euro. J. Appl. Math., **13**, pp. 567-585 (2002).
- [3] M.S. Bruzón and M.L. Gandarias, *Traveling wave solutions of the $K(m, n)$ equation with generalized evolution*, Math. Meth. Appl. Sci. 2010.
- [4] M. S. Bruzón, M. L. Gandarias, R. de la Rosa, *Conservation laws of a Gardner equation with time-dependent coefficients*, Journal of Applied Nonlinear Dynamics, to appear.
- [5] R. de la Rosa, M. L. Gandarias, M. S. Bruzón, *On symmetries and conservation laws of a Gardner equation involving arbitrary functions*, Appl. Math. Comput, preprint.
- [6] A. G. Johnpillai and C. M. Khalique, *Gruop analysis of KdV equation with time dependent coefficients*, Appl. Math. Comput, 216 (2010), pp. 3761–3771.
- [7] A. G. Johnpillai and C. M. Khalique, *Conservation laws of KdV equation with time dependent coefficients*, Commun Nonlinear Sci Numer Simulat, 16 (2011), pp. 3081–3089.
- [8] H. Kumar, A. Malik and F. Chand, *Soliton solutions of some nonlinear evolution equations with time-dependent coefficients*, J. Phys. **80**, 2, pp. 361-367 (2013).

Nonclassical symmetry analysis of heated two-dimensional flow problems

I. Naeem

Department of Mathematics, School of Science and Engineering, LUMS, Lahore Cantt 54792, Pakistan

This paper analyzes the nonclassical symmetries and group invariant solution of boundary layer equations for two-dimensional heated flows. First, the non classical symmetry determining equations are derived with the aid of computer package SADE. These equations are solved directly to obtain nonclassical symmetries. The standard procedure of computing nonclassical symmetries is adopted and two different scenarios $\xi^1 \neq 0$ and $\xi^1 = 0, \xi^2 \neq 0$ are considered. Several nonclassical symmetries are reported for both scenarios. Furthermore, numerous group invariant solutions for nonclassical symmetries are derived. The similarity variables associated with each nonclassical symmetry are computed. The similarity variables reduce the system of partial differential equations (PDEs) to a system of ordinary differential equations (ODEs) in terms of similarity variables. The reduced ODEs are solved to obtain group invariant solution for governing boundary layer equations for two-dimensional heated flow problems.

References

- [1] P. A. Clarkson and E. L. Mansfield, Algorithms for the nonclassical method of symmetry reductions, SIAM. J. Appl. Math. 55 (1994) 1693-1719.
- [2] R. Naz and D. P. Mason, Conservation laws for heated laminar radial liquid and free jets, J. Non. Math. Phy. 16 (2009) 299-309.
- [3] T. M. R. Filho, A. Figueiredo, [SADE] a Maple package for the symmetry analysis of differential equations, Comput. Phys. Commun. 182 (2011) 467-476.

On conserved quantities and boundary conditions of the 2 + 1-dimensional nonlinear Schrödinger equation

J. Prada,

¹, University of Salamanca, Spain, *prada@usal.es*

In this study a natural integrable generalization of the defocusing cubic nonlinear

Schrödinger equation to two dimensions is considered and the admissible boundary conditions classified. In particular,

it is determined whether the classical physical observables are conserved: mass, momentum, and Hamiltonian. This is the case when a certain integral (the mass constraint) vanishes. The vanishing of the mass constraint, and thus the existence of conserved quantities, is contingent on the boundary conditions adopted. In particular, under decaying boundary conditions, the Hamiltonian is not necessarily conserved.

On Infinite Sub-Symmetries and Infinite Conservation Laws for Euler Equations

V. Rosenhaus¹, R. Shankar²

California State University, Chico, USA,

¹ *vrosenhaus@csuchico.edu,*

² *r.shankar997@gmail.com*

We study local conservation laws of the Euler equations that contain arbitrary functions of dependent variables (velocities or vorticities). A key tool of our study is the method suggested by one of the authors (V.R.) that establishes a correspondence between symmetries and local conservation laws for differential systems without a well-defined Lagrangian function. We develop and employ a generalization of this method based on a concept of a sub-symmetry. For two- and three-dimensional Euler equations with constraints, we find flows with infinite conservation laws containing arbitrary functions of dependent variables. We will discuss the relations between our results and earlier obtained conservation laws for Euler equations.

On the nonlinear self-adjointness of similar equations

R. Traciná¹

¹ University of Catania, Italy, tracina@dmi.unict.it

We show that the property of nonlinear self-adjointness is conserved by an invertible point transformation. We use this property to give necessary conditions for the existence of invertible point transformation which maps a given PDE into a linear PDE [1].

References

- [1] R. Traciná, Nonlinear self-adjointness: a criterion for linearization of PDEs, *J. Phys. A: Math. Theor.*, **48**, 06FT01 (2015).

Solutions and conservation laws for a Kaup-Boussinesq system

Abstract

In this paper we study a Kaup-Boussinesq system, which is used in the analysis of long waves in shallow water. Travelling wave solutions are obtained by using the direct integration and employing the Lie symmetry analysis along with the simplest equation method. Moreover, conservation laws are derived by using the multiplier method.

Solutions and conservation laws of a coupled Korteweg-de Vries modified Korteweg-de Vries system

Abdullahi Rashid Adem

*International Institute for Symmetry Analysis and Mathematical Modelling, Department of Mathematical Sciences, North-West University,
Mafikeng Campus, Private Bag X 2046, Mmabatho 2735, Republic of South Africa.
Abdullahi.Adem@nwu.ac.za*

Lie symmetry analysis is performed on a coupled Korteweg-de Vries modified Korteweg-de Vries (KdV-mKdV) system, which arises in the analysis of various problems in theoretical physics and many scientific applications. The similarity reductions and exact solutions are obtained. The solutions obtained include the solitary waves, cnoidal and snoidal waves. In addition, we derive the conservation laws of the coupled KdV-mKdV system.

Some conservation laws for a Fisher equation with variable coefficients

M.L. Gandarias, M. Rosa

¹, University of Cádiz, Spain, marialuz.gandarias@uca.es

² University of Cádiz, Spain, maria.rosa@uca.es

Fisher's equation is commonly used in biology for population dynamics models and in bacterial growth problems as well as development and growth of solid tumours [9]. Generalizations of the Fisher equation are needed to more accurately model complex diffusion and reactions effects found in many biological systems. There are many models that use nonlinear dispersal to describe the tendency for diffusion to increase due to overcrowding [9]. The physical aspects of this equation are not fully understood without getting deeper into the concept of conservation laws. It is known that conservation laws play a significant role in the solution process of an equation or a system of differential equations. Although not all of the conservation laws of partial differential equations (PDEs) may have physical interpretation they are essential in studying the integrability of the PDEs. Moreover, the conservation laws are used for analysis, particularly, development of numerical schemes, study of properties such as bi-Hamiltonian structures and recursion operators, and reduction of partial differential equations. For variational problems, the Noether theorem can be used for the derivation of conservation laws. For non variational problems there are different methods for the construction of conservation laws In [2], Anco and Bluman gave a general treatment of a direct conservation law method for partial differential equations expressed in a standard Cauchy-Kovalevskaya form. In [7] a general theorem which does not require the existence of Lagrangians has been introduced. This theorem is based on the concept of adjoint equations for nonlinear equations. The concept of strictly self-adjoint equations has been generalized [3, 8]. In this work we study a generalization of the well known Fisher equation with variable coefficients. We determine the subclasses of these equations which are weak self-adjoint and nonlinearly self-adjoint. By using a general theorem on conservation laws proved by Nail Ibragimov and the symmetry generators, we find conservation laws for these partial differential equations without classical Lagrangians. We also derive conservation laws by using the direct method of the multipliers.

References

- [1] M.J. Ablowitz, A. Zeppetella *Explicit solutions of Fisher's equation for a special wave speed*. Bull. Math. Biol., **41**, pp 835-840, (1979).
- [2] S.C. Anco, G. Bluman. *Direct construction method for conservation laws for partial differential equations Part II: General treatment.*, Journal of Applied mathematics, **41**, pp 567-585, (2002).
- [3] M.L. Gandarias *Weak self-adjoint differential equations.*, Journal of Physics A: Mathematical and Theoretical, **44**, pp 262001, (2011).
- [4] M.L. Gandarias *Nonlinear self-adjointness and conservation laws for a generalized Fisher equation.*, Commun. Nonlinear Sci. Numer. Simulat., **18**, pp 1600-1606, (2013).
- [5] M. Rosa, M.S. Bruzón, M.L.Gandarias *Symmetry analysis and exact solutions for a generalized Fisher equation in cylindrical coordinates*, Commun. Nonlinear Sci. Numer. Simulat., In Press, Accepted Manuscript, Available online 29 January 2015 <http://dx.doi.org/10.1016/j.cnsns.2015.01.010>
- [6] M.L. Gandarias, M.S. Bruzón, M.Rosa, *Nonlinear self-adjointness for a generalized Fisher equation in cylindrical coordinates*. Journal of Applied Nonlinear Dynamics, Accepted Manuscript (2015)
- [7] N.H. Ibragimov. *A new conservation theorem.*, J. Math. Anal. Appl., **333**, pp 311-328, (2007).
- [8] N.H. Ibragimov. *Nonlinear self-adjointness and conservation laws*. Journal of Physics A: Mathematical and Theoretical, **44**, pp 432002, (2011).
- [9] J.D. Murray. *Mathematical Biology*. Springer-Verlag, New York, Berlin, Heidelberg, 3rd edition, (2002).

Symmetries and exact solutions for a nonlinear generalization of the Camassa-Holm equation

E. Recio¹, S. C. Anco²

¹ Brock University, Saint Catharines, ON, Canada, ereciorodriguez@brocku.ca

² Brock University, Saint Catharines, ON, Canada, sanco@brocku.ca

In this talk, we use a symmetry method to obtain exact solutions for an interesting family of nonlinear breaking wave equations that depend on an arbitrary nonlinearity power, and generalize the Camassa-Holm equation.

SS-SSMBP Simulations in Soft Matter and Molecular Bio-Physics

A thermodynamic study of Amyloid-beta fibrils using computer simulations.

Cristiano L. Dias¹

¹ New Jersey Institute of Technology, Department of Physics, 07102-1982, Newark, New Jersey, cld@njit.edu

I will discuss recent computer simulations in which we studied the thermodynamic properties of Abeta(16-21) dissociation from an amyloid fibril. Thermodynamics can provide important insights into the molecular mechanisms underlying peptide dissociation. However, quantities like entropy and free-energy of peptide dissociation are not easily measured experimentally. To provide insights into these quantities, we use an umbrella sampling protocol to compute potentials of mean force at seven temperatures as well as changes in enthalpy, entropy and heat capacity upon dissociation. An all-atom model with explicit TIP4P water is used.

We find similarities and differences between the thermodynamics of peptide dissociation and protein unfolding. Similarly to protein unfolding, Abeta(16-21) dissociation is characterized by an unfavorable change in enthalpy, a favorable change in the entropic energy, and an increase in the heat capacity. A main difference is that peptide dissociation is characterized by a weak enthalpy-entropy compensation. The exposure of non-polar residues that are initially buried in the dry core of the fibril and become exposed to water as the peptide dissociates could be associated with the positive change in heat capacity. The increased freedom of the backbone and the loss of native contacts as the peptide dissociates from the fibril can explain the favorable entropy and unfavorable enthalpy, respectively. Furthermore, we characterize dock and lock states of the peptide based on the solvent accessible surface area. We observe that the Lennard-Jones energy of the system increases continuously in lock and dock states as the peptide dissociates. The electrostatic energy in the lock state increases as the peptide dissociates and inter-peptide hydrogen bonds are ruptured while it decreases in the dock state as new peptide-water hydrogen bonds are formed. Implication of these results to fibril growth will be discussed.

Protein aggregation is a medically relevant phenomenon that can lead to protein-folding diseases such as Alzheimer's and Prion's. The aggregation process is largely determined by hydrogen bonds (HB), involving hundreds of peptides, over a period of days or even months. This rules out molecular dynamics (MD) simulations of all-atom protein models in explicit solvents. However, coarse-grained models of protein aggregation must accurately represent HB. This work considers the coarse-grained model used by Head-Gordon and coworkers to study the beta-amyloid ($A\beta$) peptides that forms plaques in Alzheimer's diseases [1]. The model represents one amino-acid residue by a single bead, and used the Mercedes-Benz (MB) model to describes backbone HB. This has been adapted to study residue 25 to 35 of the peptide, $A\beta_{25-35}$, which is believed to be the most toxic stretch of $A\beta$. Preliminary work has obtained data on Langevin dynamics of 100 $A\beta_{25-35}$ in a $100A \times 100A \times 100A$ box. The model peptides will be immersed in the MB water model of Dias and coworkers [2], used previously to study cold denaturation of proteins. The final model will be used to accurately identify the structure of $A\beta$ intermediates believed to the neurotoxin agents in Alzheimer's disease.

[1] Hui, Fawzi, Head-Gordon, *Proteins* **70**, 626 (2008)

[2] Dias, Alla-Nissila, Grant, Kartunnen, *J. Chem. Phys.* **131**, 054505 (2009)

Concentration Dependent Properties of RNA Nanoclusters in Salt-Based Solutions using Molecular Dynamics Simulation

Shyam Badu, Roderick Melnik and Sanjay Prabhakar

MS2Discovery Interdisciplinary Research Institute,

M²Net Laboratory, Wilfrid Laurier University, Waterloo, ON, N2L 3C5 Canada

The flexible nature of RNA nanoclusters, such as nanotubes, allows one to build a variety of secondary structures from them. The motivation behind the study of RNA nanoclusters is due to their potential applications in the field of bionanotechnology. The modeling of RNA nanotubes of variable size and predicting their physical and thermal properties are carried out in this contribution by using the molecular dynamics simulation method [1, 2, 3]. A typical structure of the RNA nanotube consisting of the eight nanorings is shown in Figure 1. For these RNA nanostructures our focus here is on their properties at different concentrations of physiological solutions such as salt-based solutions. Specifically, the salts used here in our simulations are NaCl, KCl and MgCl₂. We report new results on the characteristics defining the structural properties of the corresponding nanotubes such as the root mean square deviation, the radius of gyration, the number of hydrogen bonds per base pairs, and the radial distribution function of RNA nanotubes at different concentrations of the salts in solutions. Furthermore, the numbers of ²³Na⁺, ²⁵Mg²⁺, K⁺ and ³⁵Cl⁻ ions around the nanotubes within the distance of 5 Å at different concentrations have also been analyzed in detail. It has been found that the number of ions accumulated around the nanotubes within the particular distance is growing by small amount while the concentrations of the ²³Na⁺ and ³⁵Cl⁻ ions are substantially increased. The change in the ion concentration around the tube for different ions will influence the physical properties of these systems, including folding characteristics as found in a typical experimental study performed for the RNA hairpin in the presence of different salt solutions. We also present our new results on the elastic properties of the RNA nanotubes in these salt solutions.

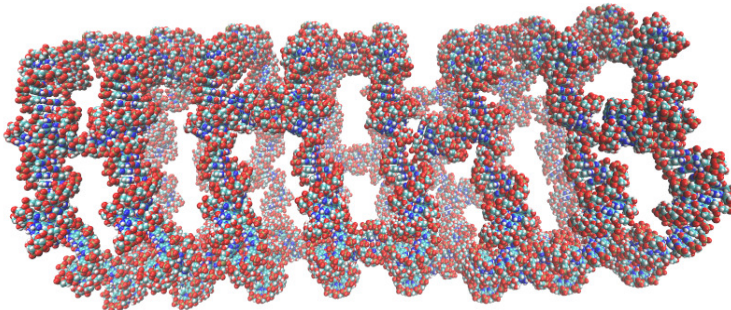


Figure 1: A typical RNA nanotube consisting of eight nanorings.

References

- [1] Paliy, M., Melnik, R., and Shapiro, B. A., "Molecular dynamics study of the RNA ring nanostructure: a phenomenon of self-stabilization," *Phys. Biol.* **6**, 046003 (Dec. 2009).
- [2] Badu, S. R., Melnik, R., Paliy, M., Prabhakar, S., Sebetci, A., and Shapiro, B. A., "Modeling of RNA nanotubes using molecular dynamics simulation," *Eur Biophys J* **43**, 555–564 (Nov. 2014).
- [3] Yingling, Y. G. and Shapiro, B. A., "Computational design of an RNA hexagonal nanoring and an RNA nanotube," *Nano Lett.* **7**, 2328–2334 (Aug. 2007).

Generalizing Euclidean distance to understand polymer uncrossing and knotting: A physicist's foray into protein folding

S. S. Plotkin¹

¹ University of British Columbia, Vancouver, Canada, steve@phas.ubc.ca

Physics often deals quite rightfully with symmetries and conservation laws, while molecular biology has historically retained little of this distinguished standard. Even the simplest biological macromolecules are aperiodic, have disordered energetics, and have enormously vast phase space relevant at biological temperatures. A central biophysical problem capturing all of these aspects is the question of how a protein, once synthesized by a ribosome in the cell, spontaneously folds up to its biologically functional structure. In this context, equilibrium and non-equilibrium statistical mechanics, as formulated in what has been called the energy landscape theory, has been essential in understanding protein folding, function, and evolution. Unfortunately however, geometry, structure, and transformation often fade away into the ensemble of a statistical mechanical description. A fundamental problem which is nevertheless central to protein folding and structural comparison of biomolecules is the notion of what **distance** means for higher-dimensional objects such as a polymer. Here we generalize the notion of distance between points to the distance between non-crossing space curves to uniquely define the Euclidean distance between two biopolymer conformations ([1-4]). We then tackle the conceptual and practical hurdles required to apply this quantity to the problem of protein folding [5]; we find that a simple measure of distance, with no adjustable parameters, predicts folding rates with remarkable accuracy (a correlation of 0.95; see Ref. [6]). We discuss the implications of this finding.

References

- [1] Plotkin, S. S. *Generalization of distance to higher dimensional objects*, Proc. Natl. Acad. Sci. USA. **104**, pp. 14899-14904 (2007).
- [2] Mohazab, A. R. and Plotkin, S. S. *Minimal distance transformations between links and polymers: Principles and applications* J. Phys. Condens. Matter **20** 244133 (24pp) (2008).
- [3] Mohazab, A. R. and Plotkin, S. S. *Minimal folding pathways for coarse-grained biopolymer fragments* Biophys. J., **95** (12) pp. 5496-5507 (2008).
- [4] Mohazab, A. R. and Plotkin, S. S. *Structural alignment using the generalized Euclidean distance between conformations* Int. J. Quant. Chem., **109** (14) pp. 3217-3228 (2009).
- [5] Mohazab A. R., Plotkin S. S. *Polymer Uncrossing and Knotting in Protein Folding, and Their Role in Minimal Folding Pathways* PLoS One **8** (1): e53642 (27 pp) (2013).
- [6] Das A, Sin B K, Mohazab A R, and Plotkin S S *Unfolded protein ensembles, folding trajectories, and refolding rate prediction* J. Chem. Phys. **139**, 121925 (15 pp) (2013).

Mesoscopic simulation method of lipid bilayers and active membrane machines

M.-J. Huang¹, R. Kapral², A. S. Mikhailov³, H.-Y. Chen⁴

¹ University of Toronto, Toronto, Canada, mjhuang@chem.utoronto.ca

² University of Toronto, Toronto, Canada, rkapral@chem.utoronto.ca

³ Fritz-Haber-Institut der Max-Planck-Gesellschaft, Berlin, Germany, mikhailov@fhi-berlin.mpg.de

⁴ National Central University, Jhongli, Taiwan, hschen@phy.ncu.edu.tw

A computationally efficient mesoscopic simulation method for biomembranes will be presented. The method combines molecular dynamics simulations for the lipids, with multiparticle collision dynamics for the solvent [1]. Self-assembled lipid membranes were observed to form in simulations of the dynamics. Macroscopic membrane properties, such as stretching and bending elastic moduli, extracted from the simulations were found to be comparable to those seen in experiments. This mesoscopic method was extended to treat a model molecular machine, described by an elastic-network, which performs active conformational motions induced by ligand binding and product release after reaction [2]. Simulations showed that an active peripheral machine produces hydrodynamic lipid flows, which provide an important mechanism for interactions among active machines.

References

- [1] M.-J. Huang, R. Kapral, A. S. Mikhailov, H.-Y. Chen, *Coarse-grain model for lipid bilayer self-assembly and dynamics: Multiparticle collision description of the solvent*, *J. Chem. Phys.* **137**, 055101 (2012).
- [2] M.-J. Huang, R. Kapral, A. S. Mikhailov, H.-Y. Chen, *Coarse-grain simulations of active molecular machines in lipid bilayers*, *J. Chem. Phys.* **138**, 195101 (2013).

Nanomotor dynamics in a chemically oscillating environment

B. Robertson¹, R. Kapral²

¹ University of Toronto, Toronto, Canada, bryan.robertson@mail.utoronto.ca

² University of Toronto, Toronto, Canada, rkapral@chem.utoronto.ca

In recent years, self-propelled nanomotors have been synthesized that transduce chemical energy from their environment into directed mechanical motion. An important requirement to sustain such motion is the constant supply of fuel in order to break detailed balance and maintain the system in an out-of-equilibrium state.[1] Thus, the chemical environment plays a pivotal role in the resultant dynamics of a nanomotor. In this work, we employ mean-field theory and coarse-grained mesoscopic simulations to study a nanomotor in a chemically-active medium exhibiting natural oscillations in the motor's fuel. The simulations were performed using a hybrid molecular dynamics-reactive multiparticle collision (MD-RMPC) dynamics approach.[2, 3] We show that the oscillating chemical environment and nanomotor influence one another in nontrivial ways. The chemical oscillations couple to the motor's reaction to produce oscillations in the propulsion velocity of the nanomotor. In addition, the reaction at the motor introduces local structure in the concentration fields in the environment, influencing the amplitude and phase of the chemical oscillations; the motor can even destroy the background oscillations altogether. Overall, these results indicate the importance of the chemically active medium when the nanomotor's reaction couples to its surrounding environment. An understanding of such an interaction will be important for real-life applications of nanomotors.

References

- [1] S. Thakur, R. Kapral, *Dynamics of self-propelled nanomotors in chemically active media*, J. Chem. Phys. **135**, 024509 (2011).
- [2] R. Kapral, *Multiparticle Collision Dynamics: Simulation of Complex Systems on Mesoscales*, Adv. Chem. Phys. **140**, pp. 89-146 (2008).
- [3] K. Rohlf, S. Fraser, R. Kapral, *Reactive Multiparticle Collision Dynamics*, Comp. Phys. Commun. **98**, 150603 (2008).

Role of Multilamellar Lipid Matrices in Polymerization of Organic Monomers in the Prebiotic World

Mostafa Nategholeslam¹, Paul Higgs¹

¹ Department of Physics and Astronomy, McMaster University

Initiation of autocatalytic polymerization is an essential spark in any scenario that can lead to emergence of the earliest forms of life. A minimal set of functional polymers is often envisioned to have established a stable population (e.g. in the RNA World model) that through subsequent mutation and selection formed the first cell-like organisms.

Successive hydration-dehydration cycles of the organic monomers in the prebiotic world could have led to condensed monomer colonies. Confinement of such accumulations of monomers between multilamellar lipid matrices, could have vastly facilitated their early, non-catalytic polymerization, through spatially ordering the monomers [1]. Such ordering can indeed take place, e.g., for adenosine monophosphate (AMP) when dehydrated and confined between stacks of DMPC bilayers [2].

Using molecular dynamics simulations, we study the effect of dehydration and confinement between various substrates on ordering of AMP molecules in aqueous environments. While it is established that dehydration and confinement between DMPC bilayers result collectively in ordering of the AMP molecules, many aspects of the underlying process can not be resolved experimentally. These include the specific pattern that is formed, the time-scale of the ordering process, the nature of the AMP-substrate interaction, as well as several dynamical aspects of the emergent pattern and the underlying processes. The confining substrates used in the simulations include DMPC bilayers, silicon dioxide membranes and artificial potentials that act as invisible confining surfaces, enabling us to study the effect of confinement alone, without involvement of molecular substrates. Together with the existing and in-progress experimental work on these systems, our results give a more detailed view of the spontaneous polymerization through the dehydration-confinement process.

References

- [1] F. Olasagasti et al, Biochimie 93.3 (2011): 556-561
- [2] L. Toppozini et al, PloS one 8.5 (2013): e62810

Simulated force spectroscopy of superoxide dismutase (SOD1) protein

M. Habibi¹, J. Rottler², S. Plotkin³

¹ Department of Physics and Astronomy, University of British Columbia, Canada, mhabibi@phas.ubc.ca

² Department of Physics and Astronomy, University of British Columbia, Canada, jrottler@phas.ubc.ca

³ Department of Physics and Astronomy, University of British Columbia, Canada, steve@phas.ubc.ca

We used single-molecule pulling molecular dynamic simulations to capture the detailed structural mechanism of the unfolding process for proteins linked to neurodegenerative diseases. In these simulations, a loop-truncated variant of superoxide dismutase (SOD1) was stretched from the N- and C-termini. Force-extension curves (FECs) of the protein were obtained for all-atom models, and the results compared to several coarse-grained (CG) models in common use, including AWSEM, AMH-Gō, and Calpha-based Gō models. AWSEM is an associative memory Hamiltonian model with several physico-chemical based terms using a three-bead per amino-acid residue representation. AMH-Gō model is a more specific, non-additive structure based model using a three-bead representation, and Calpha is the simplest available CG model in common use, wherein each residue is represented by only one bead.

Spatial organization of a chain molecule in a crowded and confined space

Bae-Yeun Ha¹ et al

¹ Department of Physics and Astronomy, University of Waterloo, Waterloo, Ontario, N2L 3G1, byha@uwaterloo.ca

It has been known for some time that a long chain molecule in a crowded space can be entropically phase-separated into a compact state. Using molecular dynamics simulations, we study the effects of crowder size and poly-dispersity on the entropic compaction of a polymer chain under cylindrical confinement. Our results suggest that doubling crowder size is equivalent to increasing their concentration fourfold. Intriguingly, the effect of poly-dispersity can be correctly mimicked by adjusting the size of crowders in a homogeneous system. Under different conditions, however, crowding particles can promote chain adsorption onto the cylinder wall, stretching the chain, which would otherwise remain condensed. Finally, we discuss the relevance of our results for understanding chromosome organization in elongated bacterial cells.

We look forward to welcoming you in Waterloo, Canada at the 2015 AMMCS-CAIMS Congress!

Figure 1: The 2015 AMMCS-CAIMS Congress is organized in cooperation with SIAM and AIMS.

SS-TMN Topics In Mathematical Neuroscience

A computational model of the influence of depolarization block on initiation of seizure-like activity

C. Kim¹, D. Q. Nykamp²

¹ University of Freiburg, Germany, christopher.kim@bcf.uni-freiburg.de

² University of Minnesota, Minneapolis, USA, nykamp@mnmn.edu

The dynamics of networks of excitatory and inhibitory neurons exhibit pathological activity when excessive excitation is not balanced by inhibition. Impairment of inhibitory neurons has been observed to precede the initiation of epileptiform activity in biological neural networks. However, the exact cause of the failure of inhibition is not well understood. We hypothesized that inhibitory neurons become vulnerable to depolarization block when extracellular potassium concentration is increased and investigated different types of pathological dynamics arising from the network. Using a Wilson-Cowan type model, we found that the transition from a physiological to a pathological state can occur via a saddle-node bifurcation or a homoclinic bifurcation. For networks exhibiting the saddle-node bifurcation, transient perturbations switched the network to seizure state, in which inhibitory neurons entered into depolarization block and excitatory neurons fired at their maximum rate. A tonic to clonic phase transition was observed in the network model with a homoclinic bifurcation when the recovery of the extracellular potassium concentration to normal levels shifted the network states. The predictions of the mean field model were tested in network simulations. Our network model with the proposed mechanism for failure of inhibition reproduces network activity observed in brain slices at the onset of seizure-like events and provides an explanation for the tonic to clonic transition as an emergent phenomenon of the network.

Bursting in Networks of Integrate and Fire Neurons

W. Nicola¹, S.A. Campbell^{1,2}

¹ Department of Applied Mathematics, University of Waterloo, Canada, wnicola@uwaterloo.ca

² Department of Applied Mathematics and Centre for Theoretical Neuroscience, University of Waterloo, Canada, sacampbell@uwaterloo.ca

We use mean field analysis to study bursting in networks of all-to-all coupled, pulse-coupled neurons. The individual neurons are represented using a class of two-dimensional integrate and fire model which includes the Izhikevich model [2], the adaptive exponential model [1, 4] and the quartic integrate and fire model [7]. The mean field model is derived using a population density approach [3], moment closure assumptions [3, 6] and a quasi-steady state approximation. The resulting model is a system of switching ordinary differential equations and the transition to bursting involves both standard and nonsmooth bifurcations. We show that the results of the mean field analysis are a reasonable prediction of the behaviour seen in numerical simulations of large networks [5, 6].

References

- [1] R. Brette and W. Gerstner. *Adaptive exponential integrate-and-fire model as an effective description of neuronal activity*, J. Neurophys., **94**(5) pp. 3637–3642 (2005).
- [2] E.M. Izhikevich. Simple model of spiking neurons. *Neural Networks, IEEE Transactions on*, 14(6):1569 – 1572, nov. 2003.
- [3] C. Ly and D. Tranchina. *Critical analysis of dimension reduction by a moment closure method in a population density approach to neural network modeling*, Neural Computation, **19**(8) pp. 2032–2092 (2007)
- [4] R. Naud, N. Marcille, C. Clopath and W. Gerstner. *Firing patterns in the adaptive exponential integrate-and-fire model*, Biological Cybernetics, **99** pp. 335–347 (2008)
- [5] W. Nicola and S.A. Campbell, *Bifurcations of large networks of two-dimensional integrate and fire neurons*, J. Comp. Neurosci., **35**, pp. 87–108 (2013).
- [6] W. Nicola and S.A. Campbell. *Mean-Field Models for Heterogeneous Networks of Two-Dimensional Integrate and Fire Neurons* Front. Comp. Neurosci., **7**, 184 (2013).
- [7] J. Touboul. Bifurcation analysis of a general class of nonlinear integrate-and-fire neurons. *SIAM Journal on Applied Mathematics*, 68(4):1045–1079, 2008.

Exploring firing patterns of stellate cells

Peter Rowat¹

¹ *Institute for Neural Computation, University of California San Diego, California, USA. prowat@ucsd.edu*

The medial entorhinal cortex (MEC) provides an important input to the hippocampus, which plays an a major role in memory and spatial navigation. The primary excitatory cells of the MEC are stellate cells which feed forward to place cells in the hippocampus. Most stellate cells are grid cells, which play an important role in spatial navigation in rats, as well as in bats and humans. Curiously, grid cells fire when the rat crosses points in space that form an hexagonal pattern. It is established that an ionic current known as “ I_h ” plays an important role in the dynamics of grid cells. Using a reduced model of stellate cells we explore the role that I_h -current plays in this phenomenon.

Modeling Populations of Neurons

P. Greenwood¹

¹ University of British Columbia, Canada, pgreenw@math.ubc.ca

We use stochastic Wilson-Cowan like equations to model interacting families of neurons. An approximation to the local stochastic dynamics of Baxendale and Greenwood [1] is used to explain the "gamma bump" in local field potentials and the high rate of phase shift at times when amplitude is low. This is part of a forthcoming chapter from Springer titled "Probability Problems Arising in Models of Stochastic Neural Systems."

References

- [1] P. H. Baxendale and P. E. Greenwood, *Sustained oscillations for density dependent Markov processes*, J. of Math Biol. **63**, pp. 433-457 (2011).

Neuromodulation and heterogeneity in neural networks

S. Knudstrup¹, M. Zochowski², V. Booth³

¹ Dept of Mathematics, University of Michigan, scottknudstrup@gmail.com

² Dept of Physics and Biophysics, University of Michigan, michalz@umich.edu

³ Dept of Mathematics and Anesthesiology, University of Michigan, vbooth@umich.edu

Identifying specific neural mechanisms responsible for the generation of spatiotemporal activity patterning in brain networks is notoriously difficult in part because of experimental limitations in recording activity of all neurons in a network simultaneously and determining the synaptic connectivity structure of a neural network. This task is further stymied by the wide heterogeneity of intrinsic neural properties, of synaptic connectivity structure and of synaptic efficacy in brain networks. To compound the complexity, heterogeneity in all these network components is dynamic in the brain. Intrinsic cellular properties can change significantly due to neuromodulation by key brain modulators, such as acetylcholine (ACh) whose release varies across behavioral state. Synaptic efficacy dynamically changes due to synaptic plasticity mechanisms that respond to neural activity patterning and synaptic structure can change in some neural pathologies. Such mechanisms of dynamic heterogeneity can result in very different spatiotemporal activity patterns being generated by networks with similar properties of synaptic connectivity structure.

In this modeling study, we aim to understand the specific roles that cellular and synaptic heterogeneity play in the generation of network spatiotemporal activity. We focus on synchronous activity in biophysical neural network models with excitatory synapses. In these networks, synchrony occurs in the form of network bursts in which episodes of high-frequency, coincident spiking across all cells in the network alternate with periods of quiescence when few cells fire at low frequency. Our model cells have heterogeneous intrinsic properties, due to nonuniform neuromodulation by ACh. Previous work has shown that ACh modulation increases neural excitability, reflected in changes in the frequency response to applied current (I-f curve), and significantly alters neural firing properties, as measured by the phase response curve (PRC). Specifically, ACh switches PRCs of cortical pyramidal cells from Type II, wherein excitatory perturbations can either delay or advance the timing of cell firing depending on the timing of the perturbation, to Type I, which only responds to perturbations by advancing cell firing regardless of the perturbation timing. Analytical and numerical studies have shown that networks of Type II cells have a higher propensity for synchronization compared to Type I networks due to their ability to either advance or delay their timing of firing in response to input.

Our numerical simulation results show that different network burst patterns can result from variations in the heterogeneous makeup of individual neural firing properties and the resultant heterogeneity in synaptic connectivity of the underlying network. In particular, cells that are strongly (Type I) and weakly (Type II) modulated by ACh contribute differentially to the existence of network bursts as well as to their initiation, maintenance and intraburst synchronization. Generally, as predicted by other studies, Type II neurons promote synchronized activity, while Type I cells are more excitable and provide overall network excitation. However, network activity depended on the distribution of synapses among the two cell types. Our results show that variations in the balance of the interactions between cell types cause dramatic changes in the stereotypic properties of network bursts and can lead to their abolition. These results suggest how nonuniform neuromodulation can affect network dynamics and offer targets for experimental intervention of pathological synchronous activity associated with seizures.

Nonlocal oscillations in membrane potential provoked by a slow current ramp.

L. M. Bilinsky¹, S. M. Baer²

¹ Duke University, Durham, USA, bilinsky@math.duke.edu

² Arizona State University, Tempe, USA, Steven.Baer@asu.edu

We present an example of an excitable system from mathematical neuroscience that features oscillations in membrane potential confined to a location distal from the point of injection of the stimulus current. The continuum model of a spiny cable due to Baer and Rinzel [1] models an electrically passive dendritic shaft studded with many excitable dendritic spines, tiny evaginations of the dendritic membrane. We numerically solved the model equations with boundary conditions chosen to model injection of a slowly increasing linear current ramp at the $X = 0$ end of the cable while the other end is sealed to current. Fig. 1 shows that when oscillations in membrane potential arise, they are confined to a location some distance from the end at which current is injected.

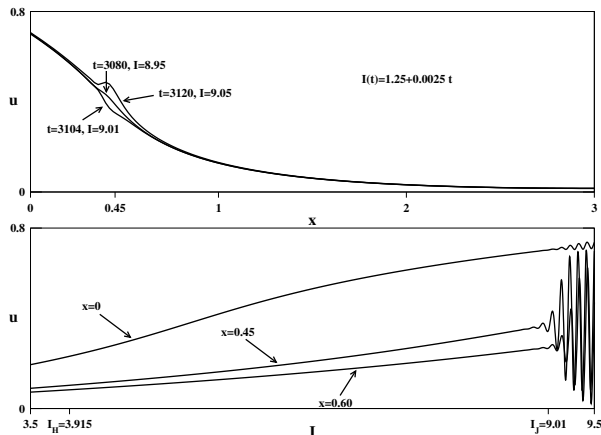


Figure 1: Numerical solution of the spiny cable response to the slow current ramp $I = 1.25 + 0.0025t$ injected at the $X = 0$ end; other end is sealed to current. Cable of electrotonic length 3 studded with 75 uniformly distributed identical FitzHugh-Nagumo spines. *Top:* Spatial profiles of the potential in the spine heads at a few instants of time near the onset of instability. *Bottom:* Time course of the spine head potential at three points along the cable.

We emphasize that this result occurs for a cable with uniform geometrical and electrical properties, studded with identical, uniformly distributed spines with identical stem conductances, and that current is only applied at one end of the cable. We show that dynamic Hopf bifurcation is the mechanism underlying this phenomenon, and that a WKB asymptotic analysis yields both the value of current at which $O(1)$ oscillations arise as well as their location along the cable. It is well-known that dynamic Hopf bifurcation can delay the onset of sustained oscillations as the bifurcation parameter is increased, and this work establishes a spatial parallel.

References

- [1] S. M. Baer and J. Rinzel, *Propagation of dendritic spikes mediated by excitable spines: A continuum theory*, J. of Neurophysiology **65**, 4, pp. 874-890 (1991).

PDEs with stochastically switching boundary conditions and application to the control of neurotransmitter concentration

Sean D. Lawley¹, Janet Best², and Michael C. Reed³

¹*University of Utah, Salt Lake City, UT, USA, lawley@math.utah.edu*

²*The Ohio State University, Columbus, OH, USA, best.82@osu.edu*

³*Duke University, Durham, NC, USA, reed@math.duke.edu*

Motivated by several biological questions, we consider PDEs with stochastically switching boundary conditions and prove statistical properties of solutions. One motivating biological problem is to understand the concentration of neurotransmitters in the extracellular space in the brain. Modulated by the arrival of action potentials, nerve terminals alternate between brief periods of rapid neurotransmitter release and long periods of neurotransmitter absorption. We thus model the concentration of neurotransmitter in the extracellular space by the heat equation with boundary conditions at nerve terminals that randomly switch between absorbing Dirichlet and positive Neumann conditions. In this talk, we will highlight both the mathematical and biological significance of our results.

Projecting Biochemistry Over Long Distances

M. Reed¹, H. H. Nijhout², J. Best³

¹ Duke University, Durham, NC, USA, reed@math.duke.edu

² Duke University, Durham, NC, USA, hfn@duke.edu

³ The Ohio State University, Columbus, OH, USA, best.82@osu.edu

Many neurons change brain function not by communicating in one-to-one fashion with other neurons, but instead by projecting changes in biochemistry over long distances. This is true for some dopamine neurons and may be true for all serotonin neurons. This biochemical network is of crucial importance for brain function and it influences and is influenced by the more traditional electrophysiological networks. This kind of neural transmission, called volume transmission in the biological literature, is important in Parkinson's Disease and may also play a role in depression. Understanding how biochemical networks interact with electrophysiological networks to produce brain function both in health and disease poses new challenges for mathematical neuroscience.

Sleep and Thermoregulation

S. Bañuelos¹, J. Best², G. Huguet³, A. Prieto-Langarica⁴, P. Pyzza⁵, M. Schmidt⁶, S. Wilson⁷

¹ California State University- Channel Islands, CA, USA, selenne.banuelos@csuci.edu

² The Ohio State University, Columbus, OH, USA, best.82@osu.edu

³ Universitat Politècnica de Catalunya, Barcelona, Spain, gemma.huguet@upc.edu

⁴ Youngstown State University, Youngstown, OH, USA, aprietol Langarica@ysu.edu

⁵ Rensselaer Polytechnic Institute, Troy, NY, USA, fullep@rpi.edu

⁶ Ohio Sleep Medicine Institute, Dublin, OH, USA, mschmidt@sleepmedicine.com

⁷ Morehouse College, Atlanta, GA, USA, shelby.wilson@morehouse.edu

The processes of thermoregulation and sleep interact, but the nature of the connection is unknown. To what extent do thermoregulatory needs shape sleep/wake cycling and REM-nonREM cycling? We have developed a mathematical model of human sleep/wake regulation with thermoregulation and ambient temperature effects in order to investigate such questions. The model accounts for several features reported in experimental data such as elongation of REM bouts across the night and the occurrence of awakenings due to deviations of body temperature from thermoneutrality. Analysis of the model leads to an understanding of the mathematical mechanisms, as well as insights into the biological mechanisms underlying the sleep-wake-temperature dynamics.

SS-WDSEE Wealth Distribution and Statistical Equilibrium in Economics

Exploring the origin of inequality in academic background-oriented society

Jun-ichi Inoue

Graduate School of Information Science and Technology, Hokkaido University, Japan, j_inoue@complex.ist.hokudai.ac.jp

Japan is still a conservative academic background-oriented society. In fact, even well-established companies still select the candidates as employees according to their academic background, in particular, the name of their university. Of course, some global enterprises attempt to select the employees on the basis of their own valuation. However, the details are still in a ‘black box’ and this fact might cause a mismatch between students and companies. Hence, to make this issue clear, here we assume that each company $k (= 0, \dots, K - 1)$ possesses their own evaluation base $\mathbf{Y}^{(k)} = (y_1^{(k)}, \dots, y_M^{(k)})$, where $y_l^{(k)}$ obeys a white Gaussian with mean zero and variance $Q^2: \mathcal{N}(0, Q^2)$. On the other hand, each student $i (= 1, \dots, N)$ tries to make up their own skills so as to point their own feature vector $\mathbf{X}^{(i)} = (x_1^{(i)}, \dots, x_M^{(i)})$ toward the company of his choice, say, $\mathbf{Y}^{(k)}$. Namely, $\mathbf{X}^{(i)} = \mathbf{Y}^{(k)} + \mathbf{n}$, where each component of noise vector $\mathbf{n} = (n_1, \dots, n_M)$ follows $\mathcal{N}(0, q^2)$, and feature vectors of students are ‘clustered’ around the valuation bases of companies as shown in Figure 1. The score of student i by the company k is given by $s^{(i,k)} = \mathbf{X}^{(i)} \cdot \mathbf{Y}^{(k)}$, and the student i obtains an informal acceptance from the company k if $s^{(i,k)} = s_{(l \leq v_k^*)} = \max\{s^{(1,k)}, \dots, s^{(v_k,k)}\}$, where v_k^* is a quota of company k and v_k denotes the actual number of application letters the company k obtains. Then, the resulting job-matching is regarded as an equilibrium state of the Gibbs-Boltzmann distribution with the following Hamiltonian (Note: the choice $J = 0$ leads to our previous study [1] as a multivariate Logit model):

$$H(\boldsymbol{\sigma} : \{c_{ij}\}) = -\frac{J}{N} \sum_{ij} c_{ij} \delta_{\sigma_i, \sigma_j} - \gamma \sum_{i=1}^N \sum_{k=0}^{K-1} \epsilon_k \delta_{k, \sigma_i} + \beta \sum_{i=1}^N \sum_{k=0}^{K-1} |v_k^* - v_k(t-1)| \delta_{k, \sigma_i}, \quad \epsilon_k \equiv 1 + \frac{k}{K}$$

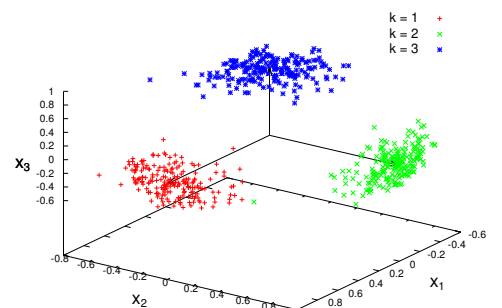
where a Potts spin σ_i can take $0, \dots, K - 1$, and $\sigma_i = k$ implies that student i posts his/her application letter to company k . Thus, the first term causes the collective behavior of students, the second term stands for the ranking preference, and the third is a history effect on the market. We may select the interaction c_{ij} as $\mathbf{X}^{(i)} \cdot \mathbf{X}^{(j)}$, and in the limit of $M \rightarrow \infty$, the c_{ij} follows $\mathcal{N}(Q^2, q^2(q^2 + 2Q^2))$. Thus, the selection of companies by students is described by a variant of the infinite-range Potts spin glasses [2]. We evaluate the informal acceptance rate A by means of

$$A = \ll \frac{\sum_{\boldsymbol{\sigma}} \sum_{k=0}^K \left\{ \delta_{s_{(l \leq v_k^*)}, \max\{s^{(1,k)}, \dots, s^{(v_k,k)}\}} + \left(1 - \delta_{s_{(l \leq v_k^*)}, \max\{s^{(1,k)}, \dots, s^{(v_k,k)}\}}\right) \Theta(v_k^* - v_k) \right\} \delta_{\sigma_i, k} \exp(-H(\boldsymbol{\sigma} : \{c_{ij}\}))}{\sum_{\boldsymbol{\sigma}} \exp(-H(\boldsymbol{\sigma} : \{c_{ij}\}))} \gg$$

where $\ll \dots \gg$ denotes an ensemble average over the realization of interactions $\{c_{ij}\}$, and here we carry it out by using replica method [3]. We investigate to what extent the performance could be improved when one increases the ‘diversities’ of valuation bases through (Q, q) . Obviously, the limit $M/K \rightarrow 0$ means that companies use almost ‘unified’ valuation. With the assistance of computer simulations, we also evaluate the Gini or k -index [4, 5] for the number of acceptances, which might be one of the origins of inequality in our society leading to income gap.

References

- [1] H. Chen and J. Inoue, *Evolutionary and Institutional Economics Review* **10**, 55 (2013).
- [2] H. Nishimori and M.J. Stephen, *Phys. Rev. B* **27**, 5644 (1983).
- [3] M. Mézard G. Parisi, and M.A. Virasoro, *Spin Glass Theory and Beyond* (Singapore: World Scientific 1987).
- [4] N. Sazuka and J. Inoue and E. Scalas, *Physica A* **388**, 2839 (2009).
- [5] J. Inoue, A. Ghosh, A. Chatterjee and B. K. Chakrabarti, *Physica A* **429**, 184 (2015).



Finitary probabilistic methods in Economics

E. Scalas¹

¹ University of Sussex, UK, e.scalas@sussex.ac.uk

Many interesting probabilistic models in Economics can be derived from the problem of allocating n objects into g classes or categories. Specific allocations can be considered as facts (taking place or not) whereas events are propositions (true or not) about facts. Not everything around us is known. Therefore, probability theory naturally enters in our description of the world. Classes or categories can be also be seen as labels. Time is another important label representing subsequent observations of the system under scrutiny. As time passes, objects can change class. In general, the exact laws of change are not known, leading to a description of movement in terms of stochastic processes. This methodology leads to derivations of the distribution of wealth without strong assumptions on the behaviour of human beings [1].

A simple example is given by the so-called Bennati-Dragulescu-Yakovenko (BDY) model [2, 3]. In this model, n tokens of wealth are allocated among g individuals. At each time-step, two individuals are chosen at random: A loser (randomly and uniformly chosen among the agents with at least one token of wealth) and a winner (randomly and uniformly selected among all agents), then the loser gives one of its wealth tokens to the winner and this procedure is repeated at the next time step. The BDY model can be formally described as an irreducible and aperiodic Markov chain whose equilibrium invariant distribution can be analytically derived. It turns out that this model leads to inequality, even if it is based on purely random exchanges of wealth. The model is less unrealistic than one can think. In fact, just due to asymmetry of information, many economic transactions imply wealth transfer from an agent or household to another one. This model indeed suggests that inequality can appear by mere chance with individual merit playing no role.

In this talk, I will present further properties of the BDY model.

References

- [1] U. Garibaldi and E. Scalas, Finitary Probabilistic Methods in Econophysics, Cambridge University Press (2010).
- [2] E. Bennati, La simulazione statistica nell'analisi della distribuzione del reddito. Modelli realistici e metodo di Monte Carlo, ETS Editrice, Pisa (1988).
- [3] A. Dragulescu and V. M. Yakovenko, Statistical mechanics of money, *The European Physical Journal B* **17**, 723–729 (2000).

Kinetic models for wealth distribution

B. Düring¹

¹ University of Sussex, UK, b.during@sussex.ac.uk

The distribution of wealth in simple market economies can successfully be described borrowing mathematical tools from kinetic theory of rarefied gases. In this talk we present a unifying approach to the study of the evolution of wealth in the large-time regime. For a wider range of wealth distribution models from the econophysical literature we are able to classify the most important feature of the steady (or self-similar, respectively) wealth distributions, namely the fatness of the Pareto tail. This allows to characterise the tails' dynamical stability in terms of the model parameters. The results are derived by means of a qualitative analysis of the associated homogeneous Boltzmann equations. The key tools are suitable metrics for probability measures, and a concise description of the evolution of moments. We present results from numerical experiments that confirm the theoretical predictions.

References

- [1] B. Düring and D. Matthes. A mathematical theory for wealth distribution. In: Mathematical modeling of collective behavior in socio-economic and life-sciences, G. Naldi et al. (eds.), pp. 81-113, Birkhäuser, Boston, 2010.
- [2] B. Düring, D. Matthes, and G. Toscani. Kinetic equations modelling wealth redistribution: a comparison of approaches. Phys. Rev. E 78(5) (2008), 056103.

Statistical Mechanics of Inequality in Distributions of Money, Income, Debt, and Energy Consumption

Victor M. Yakovenko

Department of Physics, University of Maryland, College Park, MD 20742-4111, USA

Similarly to the probability distribution of energy in physics, the probability distribution of money among the agents in a closed economic system is also expected to follow the exponential Boltzmann-Gibbs law, as a consequence of entropy maximization [1]. Analysis of empirical data shows that income distributions in the USA, European Union, and other countries exhibit a well-defined two-class structure [2, 3]. The majority of the population (about 97%) belongs to the lower class characterized by the exponential ("thermal") distribution. The upper class (about 3% of the population) is characterized by the Pareto power-law ("superthermal") distribution, and its share of the total income expands and contracts dramatically during booms and busts in financial markets [4, 5]. Globally, data analysis of energy consumption per capita around the world shows decreasing inequality in the last 30 years and convergence toward the exponential probability distribution, in agreement with the maximal entropy principle [6, 7]. Similar results are found for the global probability distribution of CO₂ emissions per capita.

All papers are available on the Web site [8]. See Ref. [9] for a recent popular coverage in the special issue on *The Science of Inequality* in the *Science* magazine.

References

- [1] A.A. Drăgulescu and V.M. Yakovenko, *Statistical mechanics of money*, The European Physical Journal B, **17**, 723–729 (2000). <http://dx.doi.org/10.1007/s100510070114>
- [2] A.A. Drăgulescu and V.M. Yakovenko, *Exponential and power-law probability distributions of wealth and income in the United Kingdom and the United States*, Physica A, **299**, 213–221 (2001). [http://dx.doi.org/10.1016/S0378-4371\(01\)00298-9](http://dx.doi.org/10.1016/S0378-4371(01)00298-9).
- [3] M. Jagielski and R. Kutner, *Modelling of income distribution in the European Union with the Fokker-Planck equation*, Physica A **392**, 2130–2138 (2013). <http://dx.doi.org/10.1016/j.physa.2013.01.028>
- [4] A.C. Silva and V.M. Yakovenko, *Temporal evolution of the ‘thermal’ and ‘superthermal’ income classes in the USA during 1983–2001*, Europhysics Letters **69**, 304–310 (2005). <http://dx.doi.org/10.1209/epl/i2004-10330-3>
- [5] V.M. Yakovenko and J.B. Rosser, *Colloquium: Statistical mechanics of money, wealth, and income*, Reviews of Modern Physics **81**, 1703–1725 (2009). <http://dx.doi.org/10.1103/RevModPhys.81.1703>
- [6] A. Banerjee and V.M. Yakovenko, *Universal patterns of inequality*, New Journal of Physics **12**, 075032 (2010). <http://dx.doi.org/10.1088/1367-2630/12/7/075032>
- [7] S. Lawrence, Q. Liu, and V. M. Yakovenko, *Global inequality in energy consumption from 1980 to 2010*, Entropy **15**, 5565–5579 (2013). <http://dx.doi.org/10.3390/e15125565>
- [8] Econophysics research in Victor Yakovenko’s group, <http://physics.umd.edu/~yakovenk/econophysics/>.
- [9] A. Cho, *Physicists say it’s simple*, Science **344**, 828 (2014). <http://dx.doi.org/10.1126/science.344.6186.828>

The Equilibrium-Seeking Behaviour of a Very Simple Model of Wealth

G. H. Boyle¹

¹ Orrery Software, Richmond, Ontario, Canada, orrery@sympatico.ca

This material arises from a larger ongoing project which explores the dynamics of sustainable economies and seeks to identify some of the necessary and sufficient conditions for sustainability. Agent-based computer models (ABMs) do not just simulate such dynamics, but exhibit them, and so may prove to be a singularly useful testbed for such studies. This project has advanced in three overlapping streams of activity. First, it was inspired by capital exchange models described by Bennati, Drăgulescu and Yakovenko (see Refs [1, 2]). It has been shown that rising entropy clearly plays a role guiding those systems towards equilibrium. Scalas, Garibaldi and Donadio examined the mathematical properties of such models, but without reference to entropy (see Ref [3]). To better understand the role that entropy plays, a similar ABM was constructed with the goal of generating entropy-related data. Second, MS Excel has been used not only to analyse the output of that ABM, but also to construct and analyze a comprehensive union of all state spaces of all those models that differ only in the amount of initial total wealth endowment. Third, the results are translated into mathematical formulae. Analysis of the model's behaviour is ongoing, but the interim results are presented here.

The presentation starts with a description of the computer model, its origins, its basic functioning, and its relation to other similar models. The state space of the model is then described in the context of the comprehensive state space of which it is a part. With some arbitrariness, a formula for the entropy of a state is introduced, and an entropic index of a state is defined on the interval $[0, 1]$. A scatter plot of entropic indices of all possible states in the comprehensive state space is presented, displaying a curious pattern of apparent lines. Mathematical formulae for the apparent lines are presented, the significance of such lines is discussed, and the formula for the virtual enveloping curve of the comprehensive space is presented and discussed.

Then using an extremely small state space as an example, the set of all possible transitions is described for every state, the probability of state-to-state transition is computed for each transition pair, and the relationship between probability of transition and change in entropic index is explored. The source of the “arrow of time” that drives the model towards equilibrium is discussed in the context of edge effects (disallowed transitions) and asymmetric probabilities of transition between members of each transition pair. The weighted average entropic change is then calculated for each state, and the virtual equilibrium state is defined as that state for which the weighted average entropic change is 0.

Finally, using a somewhat larger state space, three characteristic aspects of the model are examined: the density of states is plotted against their entropic indices on the interval $[0, 1]$; the ‘at equilibrium’ density of occupancies of states is also so plotted; and the ‘at equilibrium’ tarry times are examined for consecutively revisited states. Speculative mathematical descriptions of these phenomena are presented.

The presentation ends with a plea for continued research into such ABMs, with the goal of improving our understanding of the dynamics of such ABMs, and, ultimately, hopefully, of sustainable economic systems.

References

- [1] E. Bennati, *Un metodo di simulazione statistica per l'analisi della distribuzione del reddito*, Rivista Internazionale di Scienze Economiche e Commerciali, 35, pp. 735-756 (1988).
- [2] A. Drăgulescu and V. M. Yakovenko, *Statistical mechanics of money*, Eur. Phys. J. B., 17(4), pp. 723-729 (2000).
- [3] E. Scalas, U. Garibaldi and S. Donadio, *Statistical equilibrium in simple exchange games I*, Eur. Phys. J. B., 53(2), pp. 267-272 (2006).

Thermodynamics of Economic Inequalities

Matteo Smerlak

Perimeter Institute for Theoretical Physics, Waterloo, Canada

msmerlak@pitp.ca

Increasingly large social and economic inequalities are observed throughout the world. Theorists after Pareto have studied this phenomenon in terms of the tail structure of the wealth distribution at a given time. Unfortunately, this approach leaves unaddressed the *dynamics* of inequalities in non-equilibrium situations, e.g. under redistribution policies. Here we introduce a thermodynamical theory of inequalities based on the analogy between economic stratification and statistical entropy. Within this framework we identify the combination of *upward mobility* with *precariousness* as a fundamental driver of inequality. We formalize this statement by a “second-law” inequality displaying upward mobility and precariousness as thermodynamic conjugate variables. Our method can be generalized to gain insight into the dynamics of inequalities in any Markovian model of socioeconomic interactions.

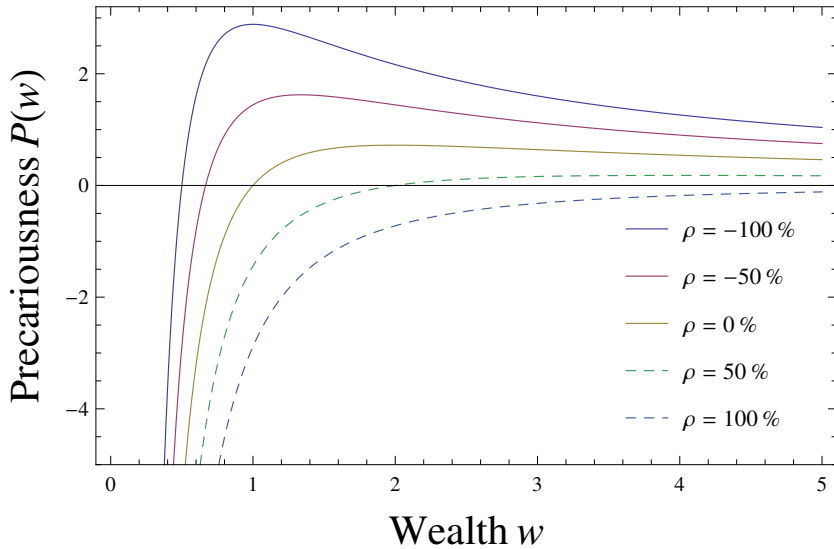


Figure 1: “Precariousness” function in a model of stochastic wealth w for various values of the expected effective interest rate ρ . The product of precariousness P and expected income Δw is a lower bound on the inequality growth rate, for the same reason that the product of inverse temperature β and heat Q is a lower bound on entropy growth in thermodynamics.

References

- [1] M. Smerlak, *Thermodynamics of inequalities*, arXiv:1406.6441, submitted to Physica A.

SS-WPA Wave Propagation and Applications

A generalized Camassa-Holm equation and its peakon solutions

S.C. Anco¹, E. Recio²

¹ Brock University, St Catharines, Canada, sanco@brocku.ca

² Brock University, St Catharines, Canada, er14iq@brocku.ca

A nonlinearly generalized Camassa-Holm equation, depending an arbitrary nonlinearity power $p \neq 0$, is considered. The generalization shares one of the Hamiltonian structures of the Camassa-Holm equation and the equation itself reduces to the Camassa-Holm equation when $p = 1$. Two main results are presented. Local conservation laws and corresponding conserved quantities are obtained, and a peakon solution is derived for all powers $p \neq 0$.

References

- [1] R. Camassa and D. D. Holm, *An integrable shallow water equation with peaked solitons*, Phys. Rev. Lett. **71** pp. 1661–1664 (1993).
- [2] R. Camassa, D.D. Holm, J.M. Hyman, *A new integrable shallow water equation*, Adv. Appl. Mech. **31** pp. 1–33 (1994).
- [3] M. Fisher and J. Schiff, *The Camassa Holm equation: conserved quantities and the initial value problem*, Phys. Lett. A **259** pp. 371–376 (1999).
- [4] A.N.W. Hone and J.P. Wang, *Prolongation algebras and Hamiltonian operators for peakon equations*, Inverse Problems, **19** pp. 129–45 (2003).

A High Order Method for Electromagnetic Scattering from Metallic Gratings

M.C. Haslam¹

¹ York University, Toronto, Canada, mchaslam@mathstat.yorku.ca

The problem of evaluating the electromagnetic response of a periodic surface to an incident plane wave is of great importance in science and engineering. Applications of the theory exist in several fields of study including solar energy research, optical instrument design, and remote sensing. We discuss the extension of our previous methods [1][2] to treat the problem of scattering from metallic surfaces with a complex refractive index. The generalization of our methods is not straight-forward, and involves the careful treatment of certain hyper-singular operators which arise in the formulation of the problem in terms of surface integral equations. We demonstrate the rapid convergence of our methods for classically difficult cases in the optical sciences.

References

- [1] O.P. Bruno and M.C. Haslam, *Efficient high-order evaluation of scattering by periodic surfaces: deep gratings, high frequencies and glancing incidences*, J. Opt. Soc. Am. A **26**(3): 658–668, 2009.
- [2] O.P. Bruno and M.C. Haslam, *Efficient high-order evaluation of scattering by periodic surfaces: vector-parametric gratings and geometric singularities*, Waves in Random and Complex Media **20**(4): 530–550, 2010.

A robust inversion method for quantitative 3D shape reconstruction from coaxial eddy-current measurements

H. Haddar¹, Z. Jiang², M. K. Riahi³

¹ CMAP, Ecole Polytechnique, Route de Saclay, 91128 Palaiseau Cedex FRANCE.

² Centre for Industrial Mathematics, Universitaet Bremen, Germany,

³Department of mathematical science, New Jersey Institute of Technology, University Heights Newark, New Jersey, USA. riahi@njit.edu

This work is motivated by the monitoring of conductive clogging deposits in steam generator at the level of support plates of steam generator in nuclear power plant. One would like to use monoaxial coils measurements to obtain estimates on the clogging volume. We propose a 3D shape optimization technique based on simplified parametrization of the geometry adapted to the impedance measurements and resolution. In eddy current testing (ECT), we introduce in the steam generator (SG) tube a probe composed of two coils. The generator coil creates an electromagnetic field which in turn induces a current flow in the conductive material nearby. The default distorts the flow and change the current in the receiver coil, which is measured as ECT signals (see Figure 1), from which we will estimate the shape of deposits with known electromagnetic parameters.

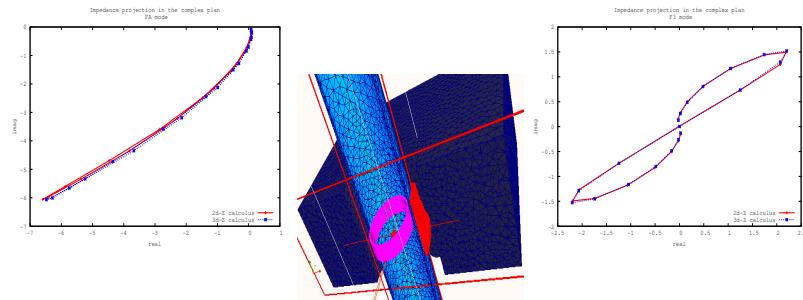


Figure 1: Probing the TSP in steam generator.

For the numerical validation, we consider deposits with conductivity ($\sigma = 1.e+4 S/m$) and constant permeability ($\mu_r = 1$). We present a series of impedance signal measurements, with respect to the iteration of the inversion algorithm, in Figure 2.

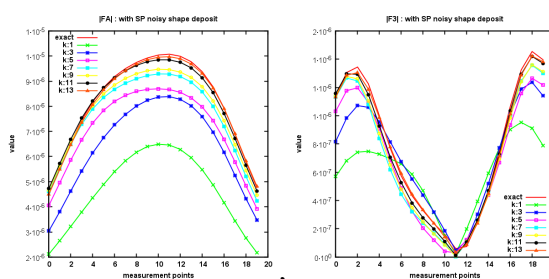


Figure 2: History (on the iteration number) of the impedances in the case of noisy shaped deposit: $|FA|$ measurement (left) and $|F3|$ measurement (right).

Bifurcations and stability of standing waves in the nonlinear Schrödinger equation on the tadpole graph

Diego Noja¹, Dmitry Pelinovsky², and Gaukhar Shaikhova^{2,3}

¹ Dipartimento di Matematica e Applicazioni, Università di Milano Bicocca, via R. Cozzi 55, 20125 Milano, Italy

² Department of Mathematics, McMaster University, Hamilton, Ontario, L8S 4K1, Canada

³ Department of General and Theoretical Physics, Eurasian National University, Astana 010000, Kazakhstan

We develop a detailed analysis of edge bifurcations of standing waves in the nonlinear Schrödinger (NLS) equation on a tadpole graph (a ring attached to a semi-infinite line subject to the Kirchhoff boundary conditions at the junction). It is shown in the recent work [1] by using explicit Jacobi elliptic functions that the cubic NLS equation on a tadpole graph admits a rich structure of standing waves. Among these, there are different branches of localized waves bifurcating from the edge of the essential spectrum of an associated Schrödinger operator.

We show by using a modification of the Lyapunov-Schmidt reduction method that the bifurcation of localized standing waves occurs for every positive power nonlinearity. We distinguish a primary branch of never vanishing standing waves bifurcating from the trivial solution and an infinite sequence of higher branches with oscillating behavior in the ring. The higher branches bifurcate from the branches of degenerate standing waves with vanishing tail outside the ring.

Moreover, we analyze stability of bifurcating standing waves. Namely, we show that the primary branch is composed by orbitally stable standing waves for subcritical power nonlinearities, while all nontrivial higher branches are linearly unstable near the bifurcation point. The stability character of the degenerate branches remains inconclusive at the analytical level, whereas heuristic arguments based on analysis of embedded eigenvalues of negative Krein signatures support the conjecture of their linear instability at least near the bifurcation point. Numerical results for the cubic NLS equation show that this conjecture is valid and that the degenerate branches become spectrally stable far away from the bifurcation point.

References

- [1] C. Cacciapuoti, D. Finco, and D. Noja, Topology induced bifurcations for the NLS on the tadpole graph, arXiv:1405.3465v2 (2014).

Discontinuous Galerkin Schemes for the Relativistic Vlasov-Maxwell System

Pierson Guthrey¹ and James A. Rossmanith²

¹ *Iowa State University, Department of Mathematics, 396 Carver Hall, Ames, IA 50011, USA, pguthrey@iastate.edu*

² *Iowa State University, Department of Mathematics, 396 Carver Hall, Ames, IA 50011, USA, rossmani@iastate.edu*

The Vlasov-Maxwell system describes the evolution of a collisionless plasma, represented through a probability density function (PDF) that self-interacts via the electromagnetic force. One of the main difficulties in numerically solving this system is the severe time-step restriction that arises from parts of the PDF associated with moderate-to-large velocities. The dominant approach in the plasma physics community is the so-called particle-in-cell method. The focus of the current work is on semi-Lagrangian methods. In particular, we develop a method based on high-order discontinuous Galerkin (DG) scheme in phase space, and an operator split, semi-Lagrangian method in time. The method is designed to be (1) high-order accurate, (2) mass conservative, and (3) positivity-preserving. The resulting scheme is applied to laser-plasma acceleration problems.

Efficient high-order integral equation methods for problems of scattering by defects in layered media

O. P. Bruno¹, C. Pérez-Arcibia¹

¹ California Institute of Technology, Pasadena, USA, *{obruno, cperezar}@caltech.edu*

In this talk we present high-order integral equation methods for the evaluation of electromagnetic wave scattering and absorption by dielectric/conducting bumps and cavities on penetrable half-planes and multi-layer structures. In the first part of this talk we present an algorithm based on the accurate and efficient evaluation of layer Green function. The numerical far- and near-fields exhibit excellent convergence as discretizations are refined – even at and around points where singular fields and infinite currents exist [1]. The method presented in this part of the talk is applied to study the power absorption that results from the interaction of electromagnetic waves with defects on flat conducting surfaces. The performance this integral equation solver allows for the accurate evaluation of electromagnetic fields at and around the surface of the conducting material where relevant physical phenomena, such as skin-depth effects, occur [2].

In the second part of this talk we present a novel integral equation method which, unlike the one based on the layer Green function, *does not* require numerical evaluation of computationally expensive Sommerfeld-like integrals. In this method the system of integral equations is obtained by the direct formulation [3] of the transmission problem. Although the integral kernels arising from this formulation are expressed in terms of the fundamental solution of the Helmholtz equation, this representation involves unknown densities defined on infinite interfaces. In order to deal with this issue, the unknown densities are expressed as $\varphi = w\varphi + (1-w)\varphi$, where w is a compactly supported (with support size $\ell > 0$) smooth window function centered at the region of interest. This new method is based upon the observation that, for sufficiently large values of $\ell > 0$, $(1-w)\varphi$ can be accurately approximated by $(1-w)\varphi^{ff}$, where φ^{ff} corresponds to the far-field of φ that can be computed analytically by solving the problem of scattering by the flat layered media. Moving the terms containing $(1-w)\varphi^{ff}$ to right-hand-side of the equation, we arrive to a system that contains unknown densities defined on the support of the window function only, and therefore, existing high-order integral equation solvers, such as [4], can be utilized to numerically approximate such densities. As is shown by numerical experiments, this new method exhibits excellent performance. The numerical error decays exponential fast as the window size ℓ increases, for all angles of incidence, even at grazing angles. Comparison of the application of the aforementioned Green function method and the windowing method to various problems, including problems of scattering by defects on flat dielectric/conducting half-planes and impedance planes, demonstrates that, for a given accuracy, the latter is much more efficient than the former.

References

- [1] C. Pérez-Arcibia, and O. P. Bruno, *High-order integral equation methods for problems of scattering by bumps and cavities on half-planes*. J. Opt. Soc. Am. A, **31**, 8, 1738-1746 (2014).
- [2] C. Pérez-Arcibia, P. Zhang, O. P. Bruno and Y. Y. Lau, *Electromagnetic power absorption due to bumps and trenches on flat surfaces*. Journal of Applied Physics, **116**, 12, 124904.(2014).
- [3] M. Costabel and E. Stephan, *A direct boundary integral equation method for transmission problems*. J. Math. Anal. Appl., **106**, 2, 367-413 (1985).
- [4] Y. Boubendir, O. P. Bruno, D. Levadoux and C. Turc, *Integral equations requiring small numbers of Krylov-subspace iterations for two-dimensional smooth penetrable scattering problems*. In press, Appl. Numer. Math., (2015).

Expansion of a wedge of non-ideal gas into vacuum

M. Zafar¹, V. D. Sharma²

¹ Department of Mathematics, Indian Institute of Technology Bombay, Mumbai, India, {zafar}@math.iitb.ac.in

² Department of Mathematics, Indian Institute of Technology Bombay, Mumbai, India, vsharma@math.iitb.ac.in

We study the problem of expansion of a wedge of non-ideal gas into vacuum and discuss its global smooth solution in a two-dimensional bounded domain. The non-ideal gas is characterized by a van der Waals type equation of state. The problem is modeled by standard Euler equations of compressible flow, which are simplified by a transformation to similarity variables and then to hodograph transformation to arrive at a second order quasilinear partial differential equation in phase space; this, using Riemann variants, can be expressed as a non-homogeneous linearly degenerate system provided that the flow is supersonic. For the solution of the governing system, we study the interaction of two-dimensional planar rarefaction waves, which is a two-dimensional Riemann problem with piecewise constant data in the self-similar plane; the original problem, formulated as a quasilinear system together with the corresponding interaction region in the phase-plane, is a Goursat boundary value problem, which admits a unique smooth solution; however, the shock may appear on the interface of gas and vacuum. The real gas effects, which significantly influence the flow regions and boundaries and which do not show-up in the ideal gas model, are elucidated.

Please Insert the Title of Your Talk Here

N. Boussad¹, H. Hajaiej², S. Ibrahim³, L. Michel⁴

¹ Université de Franche-Comté, Besançon, France, {nbousai}@univ-fcomte.fr

² NYU Shanghai, Shanghai, China, hh62@nyu.edu

³ UVic, Victoria, Canada, ibrahims@uvic.ca

⁴ Université de Nice, Nice, France, Laurent.MICHEL@unice.fr

Consider the non-linear Schrödinger equation with magnetic field in \mathbf{R}^n

$$i\partial_t u = -\Delta_A u - f(x, u) \quad (1)$$

with initial condition

$$u|_{t=t_0} = u_0. \quad (2)$$

Here the unknown function $u : (-T_*, T^*) \times \mathbf{R}^n \rightarrow \mathbf{C}$ and $f : \mathbf{R}^n \times \mathbf{C} \rightarrow \mathbf{C}$ is some non-linear measurable function. The non-autonomous magnetic Laplacian $\Delta_{A(t)}$ is defined by

$$\begin{aligned} -\Delta_{A(t)} &= \sum_{j=1}^n (i\partial_{x_j} - A_j(t, x))^2, \quad t \in \mathbf{R}, x \in \mathbf{R}^n \\ &= -\Delta - 2iA \cdot \nabla - i \div A + |A|^2, \end{aligned} \quad (3)$$

where $A(t, x) = (A_1(t, x), \dots, A_n(t, x))$ denotes the real vector magnetic potential. We sometimes omit the space dependence and write $A(t)$ instead of $A(t, x)$.

The study of the Cauchy problem has a long and rich history especially in the flat case i.e. $A \equiv 0$. In presence of magnetic effect, the problem was less investigated. If the magnetic potential is bounded, the situation is quite similar to the case $A \equiv 0$. When A is allowed to grow at infinity, the analysis is more involved since the operator $u \mapsto Au$ is not bounded anymore on L^2 . One possibility to overcome this difficulty is to consider initial data decaying to 0 at infinity and to solve the Cauchy problem in the corresponding functional space. Recently, the last author managed to solve the local Cauchy problem in the associated energy space (see below for a precise definition) which turns out to be more natural. Using a standard evolution law, he also obtained global wellposedness in the defocusing case. The aim of this paper is to investigate the question of global wellposedness and to give some example (and criterion) for blow up.

We established some important properties of the diamagnetic potential that allows us to obtain a key Gagliardo-Nirenberg inequality in magnetic form. This allows us to study the L^2 subcritical/critical case and establish the existence and uniqueness of the global Cauchy problem even in the non autonomous setting. In the subcritical case, this is achieved in whole generality, whereas the critical case requires a smallness assumption on the initial data.

High order penalty methods: a Fourier approach to solving PDE's on domains with curved boundaries

Penalty methods offer an attractive approach for solving partial differential equations (PDEs) on domains with curved or moving boundaries. In this approach, one does not enforce the PDE boundary conditions directly, but rather solves the PDE in a larger domain with a suitable source or penalty term. The new penalized PDE is then attractive to solve since one no longer needs to actively enforce the boundary conditions. Despite the simplicity, these methods have suffered from poor convergence rates which limit the accuracy of any numerical scheme (usually to first order at best). In this talk I will show how to systematically construct a new class of penalization terms which improve the convergence rates of the penalized PDE, thereby allowing for higher order numerical schemes. I will also show that the new penalized PDE has the added advantage of being solved in a straightforward manner using Fourier spectral methods. Finally, I demonstrate that the method is very general and works for elliptic (Poisson), parabolic (heat), and hyperbolic (wave) equations and can be applied to practical problems involving the incompressible Navier-Stokes equations and Maxwells equations.

Integral equation methods for Laplace eigenvalue problems

E. Akhmetgaliyev, O. Bruno

Computing and Mathematical Sciences, California Institute of Technology, eakhmetg@caltech.edu

In this talk we present a range of numerical methods which, based on use of Green functions and integral equations, can be applied to produce solution of Laplace eigenvalue problems with arbitrary boundary conditions (including, e.g., Dirichlet/Neumann mixed boundary conditions) and in arbitrary domains (including e.g. domains with corners). As part of our presentation we present newly obtained characterizations of the singularities of solutions and eigenfunctions which arise at transition points where Dirichlet and Neumann boundary conditions meet; the numerical methods mentioned above rely on use of these characterizations in conjunction with the novel Fourier Continuation technique to produce solutions with a high order of accuracy. In particular, the resulting method exhibits spectral convergence for smooth domains (in spite of the solution singularities at Dirichlet/Neumann junctions) and prescribed high-order convergence for non-smooth domains.

A point of interest concerns the search algorithm in our eigensolver, which proceeds by searching for frequencies for which the integral equations of the problem admit non-trivial kernels. As it happens, the “minimum-singular-value” objective function gives rise to a challenging nonlinear optimization problem. To tackle this difficulty we put forth an improved objective functional which can be optimized by means of standard root-finding methods.

The methods above were also applied to modal analysis problems in electromagnetics: our calculation of TE and TM modes (eigenfunctions) of the cross sections of specifically designed quadruple-ridged flare horn microwave (astrophysical) antenna have been applied to the problem of optimization of the antenna parameters. The resulting eigensolutions are produced with such high accuracy that it becomes possible to track the eigenvalue/eigenfunction evolution with shape changes even as eigenvalues cross—a capability that is necessary for the antenna-design application, and which existing commercial software packages were not able to deliver.

Other applications will also be mentioned, including methods for evaluation of transmission eigenvalues that arise in the field of inverse problems and computation of Laplace eigenfunctions as a basis for spectral decomposition of functions in the space of square integrable functions—with application to, e.g., highly accurate separation-of-variables solution of time-dependent problems (including diffusion and wave-propagation) in arbitrary, possibly singular spatial domains and with possibly mixed boundary conditions.

Certain aspects of this work have benefited from collaborations with various colleagues, including Ahmed Akgiray, Nilima Nigam and Carlos Perez-Arancibia.

References

- [1] Akhmetgaliyev, Eldar, Oscar Bruno, and Nilima Nigam, *A boundary integral algorithm for the Laplace Dirichlet-Neumann mixed eigenvalue problem.*, arXiv preprint arXiv:1411.0071 (2014).

LOCAL BOUNDARY CONDITIONS IN NONLOCAL WAVE EQUATIONS

BURAK AKSOYLU, HORST R. BEYER, AND FATIH CELIKER

ABSTRACT. We study nonlocal equations from the area of peridynamics on bounded domains. In our companion paper, we discover that, on \mathbb{R}^n , the governing operator in peridynamics, which involves a convolution, is a bounded function of the classical (local) governing operator. Building on this, we define an abstract convolution operator on bounded domains which is a generalization of the standard convolution based on integrals. The abstract convolution operator is a function of the classical operator, defined by a Hilbert basis available due to the purely discrete spectrum of the latter. As governing operator of the nonlocal equation we use a function of the classical operator, this allows us to incorporate local boundary conditions into nonlocal theories.

We present a numerical study of the solutions of the wave equation. For discretization, we employ a weak formulation based on a Galerkin projection and use piecewise polynomials on each element which allows discontinuities of the approximate solution at the element borders. We study convergence order of solutions with respect to polynomial order and observe optimal convergence. We depict the solutions for each boundary condition.

Semilinear Hyperbolic Partial Differential Equations in Curved Spacetimes

Anahit Galstyan

University of Texas-Pan American, Edinburg, TX, U.S.A, agalstyan@utpa.edu

We consider the Klein-Gordon equation in the spacetimes belonging to some family of the Friedmann-Lemaître-Robertson-Walker spacetimes (FLRW spacetimes). In the FLRW spacetime, the metric has the form $ds^2 = -dt^2 + a^2(t)d\sigma^2$. In the case of a massive scalar field, the equation of motion is the semilinear Klein-Gordon equation generated by the metric g :

$$\frac{1}{\sqrt{|g(x)|}} \frac{\partial}{\partial x^i} \left(\sqrt{|g(x)|} g^{ik}(x) \frac{\partial \psi}{\partial x^k} \right) = m^2 \psi + V'_\psi(x, \psi). \quad (1)$$

A typical example of a potential function would be $V(\phi) = \phi^4$. We study the Cauchy problem with the data prescribed at some positive time t_0

$$\psi(t_0, x) = \psi_0, \quad \psi_t(t_0, x) = \psi_1, \quad (2)$$

and we look for the solution defined for all values of $t \in [t_0, \infty)$ and $x \in R^n$. We change the unknown function $\psi = t^{-\frac{ln}{4}} u$, then for the new function $u = u(t, x)$ we obtain the equation

$$u_{tt} - t^{-\ell} \Delta u + M^2(t)u + t^{n\ell/4} V'_\psi(x, t, t^{-\frac{ln}{4}} u) = 0$$

with the “curved mass” $M_{EdS}^2(t) := m^2 - \frac{n\ell(n\ell-4)}{16t^2}$. It is easily seen that for the range $(0, 4/n]$ of the parameter ℓ the curved mass is positive while its derivative is non-positive. This is crucial for the non-increasing property of the energy and in the derivation of the energy estimate.

We obtained global in time existence in the energy class of solutions of the Cauchy problem (1), (2). More precisely, we assumed that $n = 3, 4$ $m > 0$ and there is a positive number c_0 such that the real-valued positive function $a = a(t)$ satisfies

$$a(t) > 0, \quad \dot{a}(t) > 0, \quad M(t) > c_0 > 0, \quad \dot{M}(t) \leq 0 \quad \text{for all } t \in [t_0, \infty), \quad (3)$$

and considered the Cauchy problem for the equation (1) with the derivative of potential function $V'_\psi(s, t, \psi) = -\Gamma(t)F(s, \psi)$ such that F is a Lipschitz continuous with exponent α , $F(s, 0) = 0$ for all $s \in S$, and either $|\Gamma(t)| \leq C_{\Gamma} \frac{\dot{a}(t)}{a(t)}$ for all $t \in [t_0, \infty)$, or, there is α_0 such that $C_{a, \Gamma, \alpha_0}(\infty) < \infty$, $0 < \alpha_0 < 4/n$.

For $\frac{4}{n} \leq \alpha \leq \frac{2}{n-2}$, we proved that for every $\psi_0 \in H_{(1)}(S)$ and $\psi_1 \in L^2(S)$, sufficiently small initial data, $\|\psi_0\|_{H_{(1)}(S)} + \|\psi_1\|_{L^2(S)}$, the problem (1),(2) has a unique solution $\psi \in C([t_0, \infty); H_{(1)}(S)) \cap C^1([t_0, \infty); L^2(S))$ and its norm $\|a^{\frac{n}{2}} \psi\|_{X(\infty)}$ is small.

Furthermore, we proved the local existence with the less restrictive conditions and give an estimate for the lifespan of solution.

References

- [1] K. Yagdjian, A. Galstian, *Fundamental solutions for the Klein-Gordon equation in de Sitter spacetime*, Comm. Math. Phys. 285, pp. 293–344(2009).
- [2] A. Galstian, K. Yagdjian, *Global solutions for semilinear Klein-Gordon equation in FLRW spacetimes*, Nonlinear Analysis Series A: Theory, Methods & Applications, 113, pp. 339-356 (2015) .

Vortex filament dynamics

Walter Craig

The Fields Institute

and

McMaster University

I will describe a problem in mathematical hydrodynamics, in a setting with a strong analogy to Hamiltonian dynamical systems. The analysis addresses vortex filaments for the three dimensional Euler equations, and a system of model equations for the dynamics of near-parallel filaments. These PDEs can be formulated as a Hamiltonian system, and the talk will describe some aspects of a phase space analysis of solutions, including a theory of periodic and quasi-periodic orbits via a version of KAM theory, a brief description of the relevance of Anderson localization, and a topological principle to count multiplicity of solutions. This is ongoing joint work with C. Garcia (Fields Institute and UNAM) and C.-R. Yang (McMaster and the Fields Institute).

CAIMS Scientific Themes

ST-AADS Applied Analysis and Dynamical Systems

The 2015 AMMCS-CAIMS Congress

Waterloo, Ontario, Canada

June 7-12, 2015

A Holistic Framework for Analysing General Failure and Safety Problems

Feifei Sun¹, Kumaraswamy Ponnambalam¹, Shi Cao¹, and Andy Zielinski²

¹ Department of Systems Design Engineering, University of Waterloo, Waterloo, Canada, feifei.sun@uwaterloo.ca

² Ontario Power Generation, Kipling, Canada

In this era with increasing population, fast globalization, and climate change, the failure or safety of many engineering systems such as dam and nuclear power stations are of immediate concern. Failure and safety of engineering systems are multilevel management and multidisciplinary problems. Taking dam safety as an example, traditional methods such as engineering standards, event and fault trees, probabilistic risk assessment are not capable of addressing dam safety issues. Thus, a more holistic understanding of dam safety should be established. This paper presents a new system of systems framework founded on system theories, information theory, and software engineering, specifically, systems analysis, uncertainty modelling, optimization, and agent-based modeling methods.

A modified discrete time nonlinear sliding mode observer with application to diffusion equation

S. Afshar¹, K. Morris², A. Khajepour³

¹ Dept. of Applied Mathematics, University of Waterloo, Waterloo, Canada, safshar@uwaterloo.ca

² Dept. of Applied Mathematics, University of Waterloo, Waterloo, Canada, kmorris@uwaterloo.ca

³ Dept. of Mechanical and Mechatronics Eng., University of Waterloo, Waterloo, Canada, akhajepour@mecheng1.uwaterloo.ca

In this paper, the problem of state estimation or observer design for systems modelled by nonlinear partial differential equations (PDE's) is studied. An observer is constructed using the original system and a output feedback term. The estimation of PDE's can be considered from two points of view. Either the original PDE representation can be used in the design process or the system can be approximated by some finite-dimensional representation first. Although improving an observation technique for a system in PDE representation is much more precise, it is a complicated process and often impossible. However, using an approximation introduces errors.

In this research, the PDE model is approximated with a system of ODE's using a finite element method. In order to compare the performance of different observation methods while transforming the PDE's to ODE's, the analysis is with a simple illustrative PDE, the heat equation. The heat equation is utilized here in three different versions: linear, quasi-linear, and fully nonlinear. Furthermore, as is the case in practice, the dynamics include some disturbance terms. A sliding mode observer (SMO) is suggested as the estimation method due to its robustness to disturbances.

Different types of SMO are introduced in the literature for different system representations [1], [2], and [3]. In most applications, the SMO is combined with a Luenberger observer. At first this usual type of SMO is used to estimate the state of the heat equation. The simulation results shows that SMO loses performance when the system is nonlinear. Moreover, since the measurements are only available at discrete times, a continuous-time observer is not appropriate. The SMO is therefore modified to discrete time application and for nonlinear systems.

The modified SMO is a sampled time prediction-correction method of state observation. The simulation results shows the adequate performance of the modified SMO in compensating the disturbances and also nonlinearities. The estimation error converges to a small error bound for all three types of the heat equation, with error that decreases with the size of finite-dimensional approximation used. Further, since the observer is placed in a prediction-correction form, computation time is much smaller than for a continuous SMO.

References

- [1] K. C. Veluvolu, Y. C. Soh, and W. Cao, *Robust observer with sliding mode estimation for nonlinear uncertain systems*, IET Control Theory Appl., vol. 1, no. 5, pp. 1533-1540 (2007).
- [2] S. Drakunov, and V. Utkin, *Use This Template*, in *Proceedings of the 34th IEEE Conference on Decision and Control*, Vol. 4, pp. 3376-3378 (1995).
- [3] Y. Xiong and M. Saif, *Sliding mode observer for nonlinear uncertain systems*, IEEE Trans. Autom. Control, vol. 46, no. 12, pp. 2012-2017 (2001).

Bifurcations in a system of two coupled delayed feedback loops

A. Rimbu¹, J. Bélair^{1,2}

¹ Université de Montréal, Montréal, Canada

² McGill University, Montreal, Canada

{rimbu,belair}@dms.umontreal.ca

The production and control of human (and, more generally, mammalian) blood cells is regulated through a highly intertwined system of feedback mechanisms involving, among others, differentiation of cell lines from a common pool of stem cells and hormonal interactions between circulating cells and cells at different stages of maturation. In an attempt at modelling, in a physiologically honest fashion, the full haematopoietic system together with its perturbation under pharmaceutical interventions such as chemotherapeutic treatments, we consider the prototypical system of two coupled, negative feedback loops with time delays given by

$$\begin{aligned}\frac{dx}{dt} &= -\alpha x(t) + f_1(x(t - \tau_1)) + f_2(y(t - \tau_2)) \\ \frac{dy}{dt} &= -\beta y(t) + g_1(x(t - \tau_1)) + g_2(y(t - \tau_2))\end{aligned}$$

where the functions f_i and g_k are monotone decreasing in each of their arguments, here taken as Hill's functions. This caricature system mimics the juxtaposition and interaction in the production of erythrocytes (red blood cells) and thrombocytes (platelets), these species being predominantly regulated by, respectively, the hormones erythropoietin and thrombopoietin. Our interest revolves around clinical observations at low levels of either of the hormones and their effective replacement by the other in maintaining the production of the respective cell lines. Stability analysis of the equilibrium solution, which is shown to be unique, and computer-assisted centre manifold computations are used to determine the nature of, and the regulatory rôle played by, Hopf bifurcations in this system of delay-differential equations.

Supported by NSERC(Canada) , FRQNT (Québec) and Université de Montréal

Biological Invasions, Random Walks, and Interfaces

F. Lutscher¹, G. Andreguetto Maciel², J. Musgrave³

¹ University of Ottawa, Canada, flutsche@uottawa.ca

² Universidade Estadual Paulista, São Paulo, Brazil, gabriel.andreguetto@gmail.com

³ University of Ottawa, Canada, musgrave.jeff@gmail.com

The spatial spread of non-native biological populations is one of the greatest risks to biodiversity worldwide. A recent example in North America is the Emerald Ash borer, first detected in 2002 near Detroit, that has by now spread to many US states and Canadian provinces and killed millions of ash trees. Management options against such invasions are often costly if they exist at all. Mathematical models are indispensable to understand such processes of spatial invasion that occur on large temporal and spatial scales.

A common approach to modeling spatial invasions utilizes reaction-diffusion equations that result as scaling limits from random walks. A particular challenge is to include abrupt edges in a landscape and individual response to such interfaces into these models of movement and growth. I will present random-walk based derivations of interface conditions and show that relatively simple assumptions lead to discontinuous densities at interfaces.

The complete model then consists of a system of reaction-diffusion equations for the density of a population (one equation per patch) coupled by discontinuous interface conditions between adjacent patches. I will analyze these equations with regards to persistence conditions and spreading speeds. I will show that the population spread rate depends critically on the assumptions of how individuals behave at patch interfaces.

One option for managing invasive species is to partially remove their main resources, for example Ash trees for the Emerald Ash borer. As a somewhat surprising application of the theory presented, I will outline mechanisms by which such a patchy removal of resources could lead to an increase in spread rate rather than the intended decrease.

I will also consider the scenario that the population has a strong Allee effect on all patches, and I will show that a homogenization approach does provide good approximations to the spreading speed and a surprising non-monotone relationship between the speed and the diffusion rate.

References

- [1] G.A. Maciel and F. Lutscher, *How individual movement response to habitat edges affects population persistence and spatial spread*, American Naturalist **182**, pp. 42-52 (2013)
- [2] J. Musgrave, A. Girard and F. Lutscher, *Population spread in a patchy landscape under an Allee effect* Theor. Ecol. (2015) DOI: 10.1007/s12080-015-0252-1
- [3] J. Musgrave and F. Lutscher, *Integrodifference equations in patchy landscapes I: Dispersal kernels* J. Math. Biol. **69**, pp. 583-615 (2014)
- [4] J. Musgrave and F. Lutscher, *Integrodifference equations in patchy landscapes II: Population level consequences* J. Math. Biol. **69**, pp. 617-658 (2014)

Computability of fixed points in analog systems

D. Poças¹, J. Zucker²

¹ Department of Mathematics and Statistics, McMaster University, Hamilton, Canada, pocasd@math.mcmaster.ca

² Department of Computing and Software, McMaster University, Hamilton, Canada, zucker@cas.mcmaster.ca

Most of the physical processes arising in nature are modeled by differential equations, either ordinary (example: the spring/mass/damper system) or partial (example: heat diffusion). From the point of view of analog computability, the existence of an effective way to obtain solutions (either exact or approximate) of these systems is essential.

We develop a framework in which the solutions can be seen as fixed points of certain operators in continuous data streams. As such, we present a fixed point construction to retrieve these solutions. For the techniques to be reliable, the fixed points should be (a) continuous in the input variables, and (b) stable under small perturbations. We present sufficient conditions on the operators that ensure well-posedness and stability of the corresponding fixed points.

We also present a theory of computability on topological partial algebras, under which we can reason about the computable properties of the corresponding fixed points. We discuss the relationship between the notions of *computability*, *continuity* and *stability* in this setting, in the light of Hadamard's Principle.

References

- [1] J. Hadamard, *Lectures on Cauchy's problem in linear partial differential equations*, Dover (1952).
- [2] J. Tucker and J. Zucker, *Computability of analog networks*, Theoretical Computer Science. **371**, pp. 115-146 (2007).
- [3] J. Tucker and J. Zucker, *Continuity of operators on continuous and discrete time streams*, Theoretical Computer Science. **412**, pp. 3378-3403 (2011).
- [4] N. James and J. Zucker, *A class of contracting stream operators*, The Computer Journal. **56**, pp. 15-33 (2013).

Conservative Plankton Models with Time Delay

M. Kloosterman¹, S.A. Campbell², F. Poulin³

¹ Department of Applied Mathematics, University of Waterloo, Canada, mkloosterman@uwaterloo.ca

² Department of Applied Mathematics and Centre for Theoretical Neuroscience, University of Waterloo, Canada, sacampbell@uwaterloo.ca

³ Department of Applied Mathematics, University of Waterloo, Canada, fpoulin@uwaterloo.ca

We consider a three compartment (nutrient-phytoplankton-zooplankton) model with nutrient recycling. When there is no time delay the model has a conservation law and may be reduced to an equivalent two dimensional model. We consider how the conservation law is affected by the presence of a time delay in the model. We study the stability and bifurcations of equilibria when the total nutrient in the system and the time delay are used as bifurcation parameters [1, 2].

References

- [1] M. Kloosterman, S.A. Campbell and F.J. Poulin. *A closed NPZ model with delayed nutrient recycling.* J. Mathematical Biology, **68**(4) pp. 815-850 (2014).
- [2] M. Kloosterman, S.A. Campbell and F.J. Poulin. *A NPZ model with state-dependent delay due to size-structure in juvenile zooplankton.* Preprint (2014).

Degenerate Hopf Bifurcations in DDEs and Endemic Bubbles

V.G. LeBlanc

*Department of Mathematics and Statistics
 University of Ottawa
 Ottawa ON Canada
 vleblanc@uottawa.ca*

We consider the Banach space $C = C([-\tau, 0], R)$ of continuous functions from $[-\tau, 0]$ into R , endowed with the supremum norm. For $(\lambda, \mu) \in R^2$, let

$$\dot{x}(t) = \mathcal{L}(\lambda, \mu)x_t + \mathcal{F}(x_t, \lambda, \mu) \quad (1)$$

denote a smoothly parametrized family of nonlinear retarded functional differential equations, with linear part \mathcal{L} and nonlinear terms \mathcal{F} . We will suppose that the equilibrium solution $x = 0$ for (1) has a pair of complex conjugate eigenvalues

$$\xi(\lambda, \mu) \pm i\omega(\lambda, \mu), \quad \text{such that } \xi(0, 0) = 0, \quad \omega(0, 0) = \omega_0 > 0$$

and

$$\xi_\lambda(0, 0) = 0, \quad (2)$$

and when $(\lambda, \mu) = (0, 0)$, all other eigenvalues have strictly negative real part.

Condition (2) means that the crossing condition of the classical Hopf bifurcation theorem [5] is violated. Using an approach based on results from [1, 2, 3], we then give a classification and unfolding of the degenerate Hopf bifurcation diagrams for (1) near $(\lambda, \mu) = (0, 0)$ assuming certain non-degeneracy conditions are satisfied.

These theoretical results are then applied to the following susceptible-infected-susceptible (SIS) model incorporating delayed behavioral response [4]

$$\dot{y}(t) = -y(t) + R_0 h(y(t - \tau), p)y(t)(1 - y(t)) \quad (3)$$

where $y(t)$ represents the proportion of infected individuals in the population, R_0 is the basic reproduction number (expressing the expected number of secondary infections generated by a single infectious agent introduced into a wholly susceptible population), and the smooth behavioral function $h : [0, 1] \times R \rightarrow (0, 1]$ is such that $h_y(y, p) \leq 0$, $h(0, p) = 1$ and $h(1, p) < 1$. We show that the phenomenon of *endemic bubbles* which was displayed in [4] for this model is a consequence of a degenerate Hopf bifurcation which occurs in the (R_0, p) parameter space from the endemic equilibrium of (3).

References

- [1] T. Faria and L.T. Magalhães. *Normal forms for retarded functional differential equations and applications to Bogdanov-Takens singularity*. J. Differential Equations **122**, 201–224 (1995).
- [2] T. Faria and L.T. Magalhães. *Normal forms for retarded functional differential equations with parameters and applications to Hopf bifurcation*. J. Differential Equations **122**, 181–200 (1995).
- [3] M. Golubitsky and W.F. Langford. *Classification and unfoldings of degenerate Hopf bifurcations*. J. Differential Equations **41**, 375–415 (1981).
- [4] M. Liu, E. Liz and G. Röst. *Endemic bubbles generated by delayed behavioral response: global stability and bifurcation switches in an SIS model*. SIAM J. Appl. Math. **75**, 75–91 (2015).
- [5] J.E. Marsden and M.F. McCracken. *The Hopf Bifurcation and Its Applications* Springer-Verlag, New York, 1976.

Ecological models with multiple stable states.

Hongying Shu¹, Hu Xi², Lin Wang² and James Watmough²

¹ Department of Mathematics, Tongji University, Shanghai 200092, P. R. China.

² University of New Brunswick, Canada, watmough@unb.ca

Many important questions in ecology and immunology involve dynamical systems with multiple stable states. We present a simple example of intra-guild predation which exhibits a variety of bi- and tri-stabilities. Intra-guild systems can be viewed as a coupling of two predator-prey systems by allowing one predator to additionally prey on the other. The two predators and the resource can coexist in equilibrium, in periodic solutions, and in chaotic solutions. One basic model of intra-guild predation is the system

$$\begin{aligned} R'(t) &= rR(t) \left(1 - \frac{R(t)}{K}\right) - c_1 R(t)N(t) - c_2 R(t)P(t), \\ N'(t) &= e_1 c_1 R(t-\tau)N(t-\tau) - c_3 N(t)P(t) - m_1 N(t), \\ P'(t) &= e_2 c_2 R(t)P(t) + e_3 c_3 N(t)P(t) - m_2 P(t). \end{aligned}$$

Here R is a prey species, N and P are predator species, and P additionally preys on N . In contrast with the simple predator-prey model, where delay tends to destabilize the dynamics, we show in [1] that the delay in the intra-guild predation model can have both stabilizing and destabilizing effects. In [2] we study the appearance and disappearance of an invariant torus in a related model without delay, but with saturating functional and numerical responses.

$$\begin{aligned} R'(t) &= rR(t) \left(1 - \frac{R(t)}{K}\right) - c_1 R(t)N(t) - c_2 R(t)P(t), \\ N'(t) &= e_1 c_1 R(t)N(t) - \frac{c_3 N(t)P(t)}{1 + b_3 N(t)} - m_1 N(t), \\ P'(t) &= \frac{e_2 c_2 R(t)P(t)}{1 + b_2 R(t)} + \frac{e_3 c_3 N(t)P(t)}{1 + b_3 N(t)} - m_2 P(t). \end{aligned}$$

Both models illustrate the wide variety of alternate steady-states that are possible in even simple ecological models.

References

- [1] Shu, Hongying, Hu, Xi, Wang, Lin and Watmough, James *Delay induced stability switch, multitype bistability and chaos in an intraguild predation model*, J. Math. Biol. , X, pp. 123-151 (2015).
- [2] Hu, Xi, Wang, Lin and Watmough, James *Torus Like attractor induced by intraguild predation*, in preparation.

Modeling informed optimal and adaptive public health information for emerging infection risk control

Jianhong Wu

Laboratory for Industrial and Applied Mathematics, York University, Toronto, Canada, wujh@mathstat.yorku.ca

We summarize progress of some on-going projects at the Laboratory for Industrial and Applied Mathematics in modelling media impact on emerging infectious disease outbreak control [1, 2, 3], with particular focus on the collaborative work with Yanni Xiao and Sanyi Tang which was recently featured by the Globe and Mail [4]. We proposed to model media impacts using a piecewise smooth function depending on both the case number and its rate of change. We showed that the model can be converted into a switching system, with the switching surface determined by a functional relationship between susceptible populations and different subgroups of infectives. We demonstrated that during a 2009 A/H1N1 influenza outbreak, media impact switched off almost as the epidemic peaked. The finding suggests attention to both the rate of change of case numbers and the absolute number of cases in order to alter behavioral changes of the population, through a self-adaptive media impact switching on and off, for better control of disease transmission. We will discuss the relevant challenges to quantify, evaluate and design media impact on the control of emerging infectious diseases. It is true that *Information should be transparent, but there are different ways of interpreting that information to the public*, so the challenge faced by the modellers is how to derive optimal ways for informing the public.

References

- [1] Y. Xiao, S. Tang & J. Wu, Media impact switching surface during an infectious disease outbreak, *Scientific Report*, 5: 7838, 1-9, 2015.
- [2] Q. Wang, L. Zhao, R. Huang, Y. Yang & J. Wu, Interaction of media and disease dynamics and its impact on emerging infection management, *DCDS (B)*, 20:1, 215 Ð 230, 2015.?
- [3] R. Liu, J. Wu & H. Zhu, Media/psychological impact on multiple outbreaks of emerging infectious diseases, *J. Computational & Mathematical Methods in Medicine*, 8:3, 153-164, 2007.
- [4] I. Semeniuk, Media can help slow spread of disease, study finds, *The Globe and Mail*, Published Sunday, Jan. 18 2015, 8:43 PM EST.

Non-radial multi-vortex solutions to the magnetic Chern-Simon-Higgs equations

W. Ao¹, F. Pacard², F. Ting³, J. Wei¹

¹ Department of Mathematics, University of British Columbia, Vancouver, Canada

² Center de Mathématiques Laurent Schwartz, École Polytechnic, France

³ Department of Applied Mathematics, Hong Kong Polytechnic University, Hung Hom, Hong Kong

We show that there exists multi-vortex, non-radial, finite energy solutions to the magnetic Chern-Simon-Higgs equations on the plane close to the self-dual regime.

Oscillations in Phytoplankton Growth due to Limitation by Light and Nitrogen

Gail S. K. Wolkowiz¹, Yuan Yuan²

¹ McMaster University, Canada wolkowic@mcmaster.ca

² Memorial University, Canada, yyuan@mun.ca

A mathematical model of growth of two types of phytoplankton: non-nitrogen-fixing and nitrogen-fixing phytoplankton that compete for light and nutrients is modeled and analyzed. We consider stability and persistence of the different populations and discuss the qualitative behavior of the system under different environmental conditions. In particular, we compare the predictions of the model when the assumption of constant water depth is relaxed to allow the water depth to vary in an annual cycle due to natural seasonal forcing.

Relaxation Oscillations in an SIR Epidemic Model

Michael Y. Li¹, Weishi Liu², Chunhua Shan³, Yingfei Yi⁴

¹ University of Alberta, Canada, mli@math.ualberta.ca

² University of Kansas, Lawrence, USA, wliu@math.ku.edu

³ University of Alberta, Canada, chunhuashan@gmail.com

⁴ University of Alberta, Canada, yingfei@ualberta.ca

Investigation of oscillations in disease incidence is of fundamental importance in mathematical epidemiology. Earlier investigations in the literature rely on Hopf bifurcation analysis, which requires certain degree of complexity in the transmission process to produce instability of the endemic equilibrium, and often leads to parameter regimes that are biologically unrealistic.

In this study, using the growth rate of the susceptible population as a small parameter, we apply geometric singular perturbation analysis to a simple SIR epidemic model, and show the existence of large amplitude periodic solutions of relaxation oscillation type. Mathematically, key to the analysis is a general centre manifold theorem and the phenomenon of delay of stability loss due to turning point.

Biologically, our results show that when the intrinsic growth rate of the susceptible population is small, the disease dynamics tend to be oscillatory and relaxation oscillation cycles can exist. This is comparable to the relaxation oscillation cycles in the predator-prey dynamics which are known to occur when the growth rate of the prey is small.

Some partial results on the dynamics of a nonlinear wave equation

Jorge A. Esquivel-Avila

Universidad Autónoma Metropolitana, Mxico

E-mail: jaea72@gmail.com

Abstract. A nonlinear wave equation without damping and with a super-linear source term is considered. Qualitative behavior of solutions is studied. In particular, the dynamics around the ground state is analyzed. Partial results for blow up, boundedness, convergence, and rates of decay to the set of nonzero equilibria as $t \rightarrow \infty$ are proved. Several invariant and positive invariant sets are defined.

Keywords: Nonlinear wave equation. Asymptotic behavior. Blow up.
Invariant sets.

Strong convergence and stability of Kirk-multistep-type iterations for contractive-type operators with Applications *

Hudson Akewe[†]

Department of Mathematics, University of Lagos, Akoka,
Yaba, Lagos, Nigeria

Abstract: In this paper, we introduce Kirk-multistep and Kirk-multistep-SP iterative schemes and prove their strong convergences and stabilities for contractive-type operators in normed linear spaces. By taking numerical examples, we compare the convergence speed of our schemes (Kirk-multistep-SP iterative schemes) with the others (Kirk-SP, Kirk-Noor, Kirk-Ishikawa, Kirk-Mann and Kirk iterative schemes) for this class of operators. Our results generalize and extend most convergence and stability results in the literature.

Keywords and Phrases: Kirk-multistep, Kirk-multistep-SP and multistep-SP iterative schemes, strong convergence results, contractive-type operators.

*2000 Mathematics Subject Classification: 47H09; 47H10.

[†]hakewe@unilag.edu.ng

Studies of Annular Smectic Electroconvection

S.W. Morris¹, M.C. Pugh²

¹ Physics, University of Toronto, Ontario, Canada, smorris@physics.utoronto.ca

² Mathematics, University of Toronto, Ontario, Canada, mpugh@math.utoronto.ca

We discuss electroconvection in a free submicron-thick liquid crystal film in an annular geometry. The film is flat in the xy plane; seen from above it looks like a DVD. (Seen from above, it has two boundaries: concentric circles.) A voltage is applied across the film, from the inner boundary to the outer boundary; this voltage provides a convective forcing. Because of the annular geometry, the dynamics are periodic in the azimuthal direction and the only boundaries are those at which the convective forcing is applied. The liquid crystal is in smectic A phase, forming a nearly-perfect two-dimensional fluid because the film does not change thickness, even while flowing. Also, the inner electrode can be rotated and so the experiment can be used to study the interplay between a stabilizing force applied via the boundary (Couette shear) and convection. We present numerical simulations of special solutions such as convection cells, oscillatory convection cells, undulating convection cells, and localized vortex solutions. New results involving time-dependent driving are presented. This is joint work with Stephen Morris (Physics, University of Toronto).

The Slow Dynamics of Localized Spot Patterns for Reaction-Diffusion Systems on the Sphere

Phillipe Trinh¹, Michael J. Ward²

¹ Oxford University, United Kingdom; trinh@maths.ox.ac.uk

² Univ. of British Columbia, Vancouver, Canada; ward@math.ubc.ca

In the singularly perturbed limit corresponding to large a diffusivity ratio between two components in a reaction-diffusion (RD) system, many such systems admit quasi-equilibrium spot patterns, where the solution concentrates at a discrete set of points in the domain. In this context, we derive and study the differential algebraic equation (DAE) that characterizes the slow dynamics for such spot patterns for the Brusselator RD model on the surface of a sphere. Asymptotic and numerical solutions are presented for the system governing the spot strengths, and we describe the complex bifurcation structure and demonstrate the occurrence of imperfection sensitivity due to higher order effects. Localized spot patterns can undergo a fast time instability and we derive the conditions for this phenomena, which depend on the spatial configuration of the spots and the parameters in the system. In the absence of these instabilities, our numerical solutions of the DAE system for $N = 2$ to $N = 8$ spots suggest a large basin of attraction to a small set of possible steady-state configurations. We discuss the connections between our results and the study of point vortices on the sphere, as well as the problem of determining a set of elliptic Fekete points, which correspond to globally minimizing the discrete logarithmic energy for N points on the sphere.

ST-ACM Applied and Computational Mechanics

A dynamic perspective of viscoelastic turbulence: new insights into a decades-old question

L. Xi

McMaster University, Hamilton, Canada, xili@mcmaster.ca

Low levels of flexible polymer additives are known to drastically reduce the turbulent friction drag, leading to significant energy saving in fluid transportation applications. Among many unsolved problems in this area, the most prominent one is the origin of the maximum drag reduction (MDR), an asymptotic upper limit of DR that is universal with respect to changing polymer solutions. We numerically isolated and analyzed the life cycle of typical turbulent structures and their interaction with polymer molecules [1]. The results lead to a new framework [2, 3] of understanding viscoelastic turbulence which consistently addresses all qualitative features of MDR. It is revealed that dynamics at MDR are likely dominated by a class of weak turbulent states. These states exist in both Newtonian and viscoelastic turbulence and polymer additives do not seem to alter their behaviors. The nature of these states however remains unknown. Our further study [4] takes an a priori approach and explores the domain of weak turbulence near the boundary separating laminar and turbulent states. Dynamical trajectories along this boundary can be numerically computed through a pair of direct numerical simulation (DNS) solutions that tightly pinch the boundary. Trajectories on this boundary converge to an asymptotic “edge state”. Edge states are found for Newtonian and viscoelastic systems at a range of parameters. It is observed that viscoelasticity has a negligible effect on the statistics of these solutions. This confirms the existence of weak turbulent states that cannot be suppressed by polymer additives, explaining why polymer-induced drag reduction must be bounded by an upper limit. Dependence of these states on the Reynolds number (Re) is more complex: although at one low Re the mean velocity profiles correspond closely to experimental observations for polymer solutions in the MDR regime, at higher Re , these profiles are higher than that of MDR. The quantitative origin of MDR may lie in a domain between the edge state and the turbulent basin.

References

- [1] L. Xi and M.D. Graham, *Turbulent drag reduction and multistage transitions in viscoelastic minimal flow units*, J. Fluid. Mech. **647**, pp. 421-452 (2010).
- [2] L. Xi and M.D. Graham, *Active and hibernating turbulence in minimal channel flow of Newtonian and polymeric fluids*, Phys. Rev. Lett. **104**, 218301 (2010).
- [3] L. Xi and M.D. Graham, *Intermittent dynamics of turbulence hibernation in Newtonian and viscoelastic minimal channel flows*, J. Fluid. Mech. **693**, pp. 433-472 (2012).
- [4] L. Xi and M.D. Graham, *Dynamics on the laminar-turbulent boundary and the origin of the maximum drag reduction asymptote*, Phys. Rev. Lett. **108**, 028301 (2012).

A Feasibility Study on Yazd Solar Trough Parabolic Powerplant to Improve the Efficiency by Tilting its Solar Collectors

M. Darbandi¹, M. Atarodi², K. Dastjani-Farahani³, M. Khodadadi-Yazdi⁴, G. E. Schneider⁵

¹ Department of Aerospace Engineering, Sharif University of Technology, Tehran, Iran, darbandi@sharif.edu

² Department of Aerospace Engineering, Sharif University of Technology, Tehran, Iran, mahmood_atarodi@yahoo.com

³ IPDC, Iran Power Development Company, Tehran, Iran

⁴ Center for Developing Modern Energy Systems, Sharif University of Technology, Tehran, Iran, mohsen.khodadadiyazdi@gmail.com

⁵ Department of Mechanical and Mechatronics Engineering, University of Waterloo, Waterloo, Ontario, Canada, gerry.schneider@uwaterloo.ca

The solar trough parabolic powerplant is one major type of solar powerplant, which has been widely used in solar power generation. They are made of mirrors with parabolic shapes having in-line assortments. The amount of energy produced by these solar power is directly related to the cosine of angle of incidence for the incoming solar radiation [1]. Therefore, these mirrors should suitably trace the sun motion to reduce the incidence angle and thus to increase the cosine of incidence angle. In real applications, the trace of sun is performed in one axis of freedom. Typically, they trace the sun in the north-south axis direction. In commercial cases, the mirror planes are parallel to the ground level. In this paper, we properly investigate the effect of mirror plane tilting with respect to the ground level. We also try to evaluate this consideration on the amount of perture normal irradiance. The study is performed for Yazd in Iran, with the latitude and longitude of 32 and 55 degrees, respectively. The sunlight is simulated using the model presented by Daneshyar [2]. Using this model and applying suitable cosine of incidence angle, we calculate the amount of aperture normal irradiance during one full year. To enrich the study, this value is calculated for different tilted angles and that they are compared with the case in which there is no tilting angle with respect to the ground surface. Figure 1 shows the variation in the percentages of aperture normal irradiance during a year with the tilted angle. This figure indicates that an increase in the tilt angle magnitude up to 2 degrees will cause an increase of about 1% in aperture normal irradiance over a full year. The figure also shows that a tilted-angle increase to 25 degrees can enhance the amount of energy absorption about 7%. However, this angle is relatively too large and requires major changes in the attributed solar powerplant and its cost effective optimization.

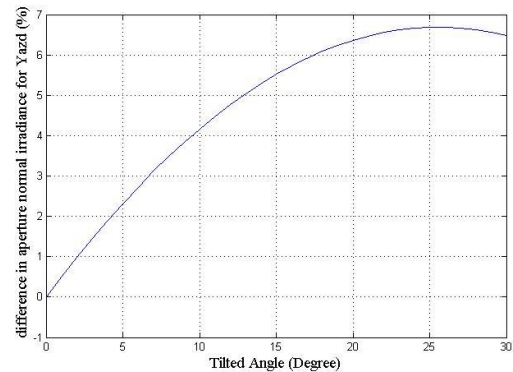


Figure 1: The chart of increasing the percentage of aperture normal irradiance over a full year.

References

- [1] M. A. Mokheimer, N. Dabwan, A. Habib, A. M. Said, and A. Al-Sulaiman, *Techno-economic performance analysis of parabolic trough collector in Dhahran, Saudi Arabia*, Energy Conversion and Management. **86**, pp. 622-633 (2014).
- [2] M. Daneshyar, *Solar radiation statistics for Iran*, Solar Energy. **21**, pp. 345-349 (1978).

A moving-mesh method for spectral collocation solutions of partial differential equations

Christopher J. Subich¹

¹ Environment Canada, Dorval, Québec
Christopher.Subich@ec.gc.ca

This presentation discusses the application of the moving mesh partial differential equation (MMPDE, Ref. [1]) method to time-varying partial differential equations discretized with a spectral collocation method.

Spectral collocation methods typically feature exponential convergence with increasing resolution. Asymptotically, this allows spectral methods to dominate lower-order methods in accuracy, permitting the most accurate possible solution of partial differential equations within a fixed memory limit. Unfortunately, this asymptotic behaviour is only seen after the solution is already well-resolved. For domains with no coordinate mapping (or a fixed mapping that does not adapt to the solution), this means that a locally sharp feature requires high resolution throughout the domain.

Moving-mesh methods seek to avoid this problem by optimally-allocating a fixed number of grid points in order to minimize discretization error, increasing grid density near areas where the solution undergoes rapid change. They accomplish this by creating a time-varying mapping from a computational coordinate ($x = x(\xi, t)$ in one dimension), where the grid movement is defined by an ancillary equation (MMPDE6 from Ref. [1]), solved alongside the physical PDE:

$$\frac{\partial^2}{\partial \xi^2} x_t(\xi, t) = -\frac{1}{\tau} \frac{\partial}{\partial \xi} \left(M(u(x, t)) \frac{\partial x(\xi, t)}{\partial \xi} \right), \quad (1)$$

where τ is a timescale parameter and $M(u(x, t))$ is an error monitor function, which estimates discretization error.

Unfortunately, straightforward application of the method, originally developed for finite-difference methods, fails for spectral collocation discretizations because the latter are extremely sensitive to grid smoothness and regularity. Current approaches have had limited success at creating a suitably regular mapping based on smoothing a lower-resolution finite-difference approximation.

This work presents a more robust method of calculating grid movement, through the use of two modified error monitor functions. The first is the conventional arclength monitor function ($M(u(x, t)) \propto \sqrt{1 + u_x^2}$), low-pass filtered in the spectral representation.

The second, qualitatively different monitor function is derived algorithmically from the envelope of high-frequency content of the PDE solution $u(x, t)$, providing a direct estimate of where discretization error is likely to be larger than the background (near-roundoff) level. This results in a monitor function that is more robust to non-smooth solution features that do not themselves involve an abnormally large derivative, such as in a rarefaction shock. Additionally, the filtering approach minimizes grid movement when the underlying solution is already well-resolved and not in need of grid refinement.

References

- [1] Weizhang Huang, Yuhe Ren, and Robert D. Russell. Moving mesh methods based on moving mesh partial differential equations. *Journal of Computational Physics*, 113(2):279–290, August 1994. ISSN 00219991. doi: 10.1006/jcph.1994.1135.

A New Numerical Approach for Linear and Non-Linear Advection

Jean-Christophe Nave¹

¹ McGill University, Montreal, jcnav@math.mcgill.ca

In this talk I will present a new numerical method for the advection of arbitrary sets. The approach is based on evolving the underlying flow map using the Gradient-Augmented Level Set Method (GALSM). The method is unique in the sense it retains both geometric information (diffeomorphism) and integrated quantities (e.g. densities). I will present several examples, including linear advection and 2D incompressible Euler flow.

A quadrilateral spectral multidomain penalty method model for the simulation of environmental stratified flow processes: towards an efficient pressure solver

S.M. Joshi¹, G. Thomsen², P.J. Diamessis³

¹ Center for Applied Mathematics, Cornell University, Ithaca, NY, U.S.A., smj96@cornell.edu

² Applied Research Laboratories, University of Texas, Austin, TX, U.S.A., gthomsen@arlut.utexas.edu

³ School of Civil and Environmental Engineering, Cornell University, Ithaca, NY, U.S.A., pid38@cornell.edu

This presentation will outline the salient features of a 2-D deformed quadrilateral spectral multidomain penalty method² model for the simulation of incompressible environmental stratified flows at high Reynolds numbers in domains with variable bathymetry. Particular emphasis will be placed on the numerical solver of the pressure Poisson equation (PPE). An efficient and accurate solution of this equation is critical for the reproduction of the highly non-hydrostatic dynamics of strongly nonlinear phenomena in stratified waters such as internal solitary waves² (ISWs) and localized turbulence. ISW propagation occurs in long and relatively shallow stratified wave-guides requiring simulations with high-aspect ratio (lepticity) elements, which pose significant challenges to the conditioning of the discretized PPE and its numerical solution.

The computational problems at hand involve a very high number of degrees of freedom. Hence, we rely on a parallel matrix-free Householder-based GMRES algorithm to solve the PPE. To minimize the number of iterations in the Poisson solver, an iterative substructuring approach is employed to assemble and solve the Schur problem of the Poisson matrix. For high-order methods, this Schur problem is far smaller and better conditioned than the original operator. Then, a block-diagonal preconditioner is used to mitigate the effects of domain aspect ratio, and a deflation technique bounds the number of GMRES iterations required as the number of subdomains grows. We will demonstrate the use of these techniques on several benchmark problems to assess the performance and accuracy of the SMPM and the preconditioned iterative substructuring method we employ. Finally, we will outline a possible avenue for extension to three dimensions, along with a discussion on the scalability of these methods in a practical distributed parallel computing environment.

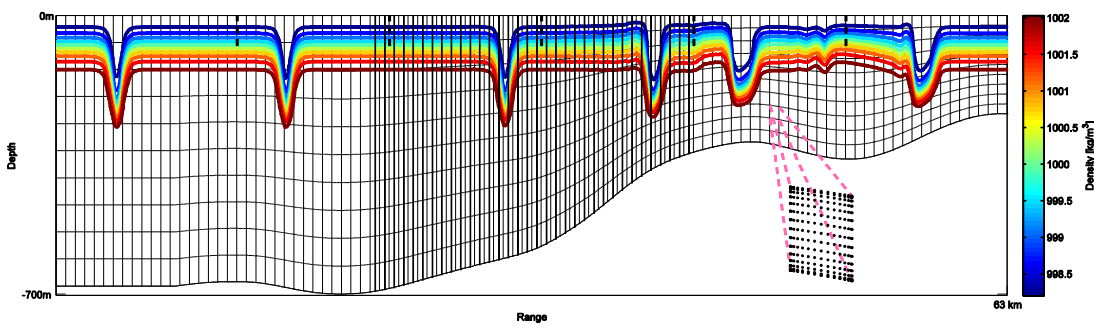


Figure 1: Successive snapshots from the SMPM-based simulation of a shoaling internal wave over realistic bathymetry. Also shown are outlines of subdomain interfaces and an exploded view of the internal Gauss-Lobatto-Legendre grid.

References

- [1] J.A. Escobar-Vargas, J.A. , P.J. Diamessis and T. Sakai. *A spectral quadrilateral multidomain penalty method model for high Reynolds number incompressible stratified flows*. Int. J. Num. Methods Fluids, **75**, 403–425 (2014).
- [2] K.R. Helfrich and W.K. Melville, *Long nonlinear internal waves*. Annual Review Fluid Mech. **38**, 395–425 (2006).

Application of a Genetic Algorithm to Optimize Work Hardening Parameters Used in Plasticity Modelling of a Zirconium Alloy

T. Skippon¹, M.R. Daymond²

¹ Queen's University, Kingston, Canada, travis.skippon@queensu.ca

² Queen's University, Kingston, Canada, mark.daymond@queensu.ca

The elasto-viscoplastic self-consistent (EVPSC) model has been shown to be effective in predicting the stress-strain behaviour of polycrystalline metals subjected to various types of thermomechanical loading [1]. However, the model requires several parameters to be entered as an input, including parameters that describe the work hardening of the material (i.e. how its strength changes with applied plastic strain). In general, these parameters are obtained through trial and error by varying them until the model produces results in good agreement with well established experimental data. Doing this by hand is very labour intensive and can involve running the model hundreds of times to observe how the goodness of fit changes with each iteration. At Queen's we have implemented a genetic algorithm to automate the process and have found that it gives results comparable to those obtained by a highly skilled individual performing the optimization by hand, and in a fraction of the time [2].

A genetic algorithm is an optimization technique that is modelled after Darwin's theory of evolution by natural selection. In nature, many living organisms share an environment and compete for resources in order to survive. Natural selection states that the organisms possessing traits that are most advantageous for survival will produce more viable offspring than those with less advantageous traits. Over many generations this leads to the "survival of the fittest" where undesirable traits become progressively less common and more desirable traits progressively more common. This same principle can be applied to solving a numerical optimization problem, which in this case involves fitting the output of a plasticity model to experimental data from tensile tests performed on samples of Zircaloy-2, a Zirconium based alloy used frequently in the nuclear industry.

Until now, the experimental data used in the fitting process has consisted only of simple uniaxial tensile tests performed on the material. The present study adds some complexity in the form of two-stage deformation, as well as changes in loading direction. Tensile specimens of rolled Zircaloy-2 sheet were prepared and deformed to various plastic strains along a single direction and then unloaded. The deformed material was then made into smaller tensile specimens which were deformed again in directions either parallel, perpendicular, or at 45 degrees to the original direction of loading. The entire set of experiments is then modelled in EVPSC and the genetic algorithm is used to arrive at a set of hardening parameters that best represent the material's response to this more complex set of loading conditions. Since hardening parameters obtained from single-stage uniaxial tests alone are known to be non-unique solutions (i.e. there are multiple sets of hardening parameters that give equally valid results) adding a second stage of loading are thought to add additional constraints and give more physically meaningful results.

References

- [1] C. Mareau and M.R. Daymond, *Study of internal strain evolution in Zircaloy-2 using polycrystalline models: Comparison between a rate-dependent and a rate-independent formulation* Acta Materialia. **58**, 9, pp. 3313-3325 (2010)
- [2] T. Skippon, C. Mareau, and M.R. Daymond, *On the determination of single-crystal plasticity parameters by diffraction: optimization of a polycrystalline plasticity model using a genetic algorithm* J. Appl. Crystallography. **45**, 4, pp. 627-643 (2012)

Coriolis forces control the secondary circulation and erosion patterns in large submarine turbidity currents.

M. G. Wells¹, R. Cossu^{1,2}, & J. Peakall³

¹ Department of Physical & Environmental Sciences, University of Toronto Scarborough, 1265 Military Trail, Toronto, ON M1C 1A4, Canada

² Present address: Australian Maritime College, University of Tasmania, Launceston 7250 Tasmania, Australia

³ School of Earth and Environment, University of Leeds, Leeds LS2 9JT, UK

Turbidity currents are large scale flows driven by suspended sediment that transport sediments on the ocean floor. As they flow from the continental margin to deep ocean they erode large submarine channels, which are of considerable interest to geologists. The driving mechanisms for submarine channel evolution are highly complex, reflected by recent debates about the formation and global distribution of sinuosity in turbidite channels (see ref [1,2,3]). We present recent laboratory experiments on channelized gravity currents running over an erodible bed, where the magnitude of Coriolis forces is changed to reproduce conditions at low and high latitudes (see ref [4,5]). We find a striking systematic change in deposition and erosion patterns as Coriolis forces become dominant at high latitudes so that erosion and deposition occur only on opposite sides of channels; in contrast, at low latitudes significant inner-bank intra-channel bars form on alternate sides of sinuous channels. Our observations show very good agreement with sedimentation patterns in Coriolis-dominated contourite drift systems and with deposits in modern and ancient turbidity current channels. We hypothesize that Coriolis forces are a key parameter for submarine channel evolution and sedimentary architecture at high latitudes but not at low latitudes; this proposal offers a new approach to interpret deep-sea architectural features at high latitudes.

References

- [1] Peakall, J., Kane, I. A., Masson, D. G., Keevil, G., McCaffrey, W., & Corney, R. *Global (latitudinal) variation in submarine channel sinuosity*. Geology, 40(1), 11-14. (2012)
- [2] Sylvester, Z., Pirmez, C., Cantelli, A., & Jobe, Z. R. (2013). *Global (latitudinal) variation in submarine channel sinuosity: Comment*. Geology, 41(5), e287-e287. (2013)
- [3] Peakall, J., M.G. Wells, R. Cossu, I. A. Kane, D. G. Masson, G. M. Keevil, W. McCaffrey, and R. Corney. *Global (latitudinal) variation in submarine channel sinuosity: Reply*. Geology 41, no. 5 e288-e288. (2013):
- [4] Wells, M., & Cossu, R. *The possible role of Coriolis forces in structuring large-scale sinuous patterns of submarine channel-levee systems*. Philosophical Transactions of the Royal Society A: Mathematical, Physical and Engineering Sciences, 371(2004), 20120366. (2013).
- [5] Cossu, R., Wells, M. G., & Peakall, J. *Latitudinal variations in submarine channel sedimentation patterns: the role of Coriolis forces*. Journal of the Geological Society, 2014-043. (2015).

Distinguishing Double Diffusive Processes from Convective Instability in Laboratory Experiments

S. Davarpanah Jazi¹, M.G. Wells²

¹ University of Toronto, Toronto, Canada, sh.davarpanahjazi@mail.utoronto.ca

² University of Toronto, Toronto, Canada, Wells@utsc.utoronto.ca

When a sediment-laden flow of a river enters into a stratified lake or the coastal ocean, it is of great interest to geologists to know how fast the sediment settles from the resulting surface or sub-surface intrusion. Although the resulting sediment laden intrusion can be stable with respect to density, a double diffusive instability may arise due to the diffusion of salt being much faster than the Brownian diffusion of sediment [1]. Such instability results in the “sediment fingering” transport phenomena: a double diffusive sedimentation associated with vertical sediment concentration and salt gradient. Sediment fingering is governed by similar mechanism as salt fingering, but there is a paucity of solid experimental or theoretical descriptions of the process, which motivates the present study.

Our new quantitative experimental investigation of double diffusive sedimentation makes direct measurements of different flow characteristics associated with such sedimentation process. A series of experiments are used to make the first direct velocity measurements of sediment fingering convection using a high resolution Nortek Acoustic Doppler Velocimeter (ADV) to measure turbulent convection above and below the density interface. Previous experiments on sediment fingering estimate the velocities of the sediment fingers using series of photos. They showed that the velocities for these fingers could be an order of magnitude higher than the Stokes settling velocity of the particles [1, 2, 3, 4, 5, 6]. However these visual methods could only measure mean velocities, and were limited to the lower optically clear layer. Our new experiments will also be compared to the results with the recent DNS numerical simulations [7, 8].

Our new results quantitatively confirm that the velocity of the sediment fingers in the lower layer are always larger than their Stokes settling velocity, in some cases by several orders of magnitudes. Our measurements also show an asymmetry in the turbulent velocity between the upper and lower convective layers. This suggests that sediment fingering is acting in concert with the mean settling velocity, so that the velocity of the convection in the upper layer is much smaller than the velocity of sediment fingers.

References

- [1] J. D. Parsons and M. H. Garcia, *Enhanced sediment scavenging due to double-diffusive convection*. Journal of Sedimentary Research, Vol. 70, No. 1, pp. 47-52 (2000).
- [2] C. F. Chen, *Particle flux through sediment fingers*. Deep-Sea Research, Vol. 44, No. 9-10, pp. 1645-1654 (1997).
- [3] T. Green, *The importance of double diffusion to the settling of suspended material*. Sedimentology, Vol. 34, pp. 319-331 (1987).
- [4] D. C. J. D. Hoyal, M. I. Bursik and J. F. Atkinson, *The influence of diffusive convection on sedimentation from buoyant plumes*. Marine Geology, Vol. 159, pp. 205-220 (1999a).
- [5] D. C. J. D. Hoyal, M. I. Bursik and J. F. Atkinson, *Settling-driven convection: A mechanism of sedimentation from stratified fluids*. Journal of Geophysical Research, Vol. 104, No. C4, pp. 7953-7966 (1999b).
- [6] J. D. Parsons, J. W. M. Bush and J. P. M. Syvitsky, *Hyperpycnal plume formation from riverine outflows with small sediment concentrations*. Sedimentology, Vol. 48, pp. 465-478 (2001).
- [7] P. Burns and E. Meiburg, *Sediment-laden fresh water above salt water: linear stability analysis*. Journal of Fluid Mechanics, Vol. 691, pp. 279-314 (2012).
- [8] P. Burns and E. Meiburg, *Sediment-laden fresh water above salt water: non linear stability analysis*. Journal of Fluid Mechanics, Vol. 762, pp. 156-195 (2015).

Dynamics of vortex Rossby waves in tropical cyclones

Lucy Campbell¹, Lidia Nikitina²

¹ Carleton University, Ottawa, Canada campbell@math.carleton.ca

² Geomagnetic Laboratory, Natural Resources Canada, Ottawa, Canada lidia.nikitina@nrcan-rncan.gc.ca

Observational analyses of hurricanes in the tropical atmosphere indicate the existence of spiral rainbands which propagate outwards from the eye and affect the structure and intensity of the hurricane. These disturbances may be described as vortex Rossby waves. It has been suggested that vortex Rossby waves may play a role in the eyewall replacement cycle observed in tropical cyclones in which concentric rings of high-intensity wind develop and propagate in towards the centre of the cyclone. In this presentation we discuss analytical and numerical simulations to investigate the dynamics of vortex Rossby waves in a cyclonic vortex in a two-dimensional configuration on a beta-plane.

Eulerian modelling of air-droplets flow: Perspectives and numerical solutions

S. Keita¹, Yves Bourgault²

University of Ottawa, Canada, ¹skeit085@uottawa.ca, ²ybourg@uottawa.ca

Air flows charged with particles or droplets occurs in many biomedical, industrial and environmental applications. A common approach to simulate such flows is to solve Navier-Stokes equations coupled with a second set of partial differential equations for the volume fraction, average velocity and energy of the particles at each point in the domain. A complete hierarchy of these so-called Eulerian models of air-particle flows have been derived [3]. A main issue for these models arises with the handling of the pressure terms, whether one or two pressures are needed or if each momentum equation for the air and particles should include a pressure gradient. Moreover, some of these Eulerian models cannot be written in a conservative form, in the spirit of hyperbolic conservation laws, or even worst strict hyperbolicity is lost.

In [1], an Eulerian model was proposed for air-droplets flows. This model is successfully used for the prediction of droplets impingement on airfoils and ice accretion on airplane wings during in-flight icing events. Extension to particle flows in airways was more recently attempted [2]. A main advantage of this model is its simplicity, its expression in conservative form and the fact that it is hyperbolic (with only one multiple eigenvalue) as opposed to other models which completely loose hyperbolicity for some flow regimes. In our talk we will explain how our Eulerian model fits in the hierarchy of models for two-phase flows presented in [3] and under which flow regimes our simpler model is valid. Numerical results comparing different models will be presented. We will also cover methods and issues for numerically solving these Eulerian models.

References

- [1] Y. Bourgault, J. Dompierre, W.G. Habashi and G.S. Baruzzi, *A finite element method study of Eulerian droplets impingement models*, International Journal for Numerical Methods in Fluids **29**, pp. 429-449 (1999).
- [2] Y. Bourgault, *Computing Gas-particle flows in airways with an Eulerian model*, In European Conference on Computational Fluid Dynamics-ECCOMAS CFD, (2006).
- [3] J. Cortes, F. Bouchut, Y. Brenier and J.F. Ripoll, *A hierarchy of models for two-phase flows*, Journal of Nonlinear Science, **10**, pp. 639-660, (2000).

Formation and Switching Dynamics of Nematic Liquid Crystalline Domains

P. Khayyatzadeh, F. Fu, N. M. Abukhdeir

University of Waterloo, Canada, nmabukhdeir@uwaterloo.ca

Liquid crystalline materials are used pervasively in display technology, specifically liquid crystal displays (LCDs). The majority of LCD technology utilizes the nematic liquid crystal (LC) phase which has translational disorder as in a liquid, but some degree of orientational order at the molecular level. Materials exhibiting a nematic phase exhibit birefringence which can be manipulated through the application of an external field. Subsequently, the vast majority of liquid crystal-based display technology utilizes this coupled electro-optical property of nematics in order to “switch” or tune the optical properties of a nematic domain to a desired optical state. Current LCD technology utilizes a rectangular domain, or pixel, within which the nematic is confined and is exposed to surface anchoring conditions that preclude the possibility of defects forming.

In this work, a fundamentally different type of liquid crystal domain is studied which is formed through “bottom-up” manufacturing techniques, such as phase separation of a liquid crystal/polymer mixture to form a polymer-dispersed liquid crystal (PDLC) composite. These domains are spheroidal and under most conditions require the formation of defects within the LC domain. Thus they exhibit substantially different behaviour in the presence of an external field. The dynamics of these domains are studied using the phenomenological continuum Landau-de Gennes model [1]. The results of this study [3] show the main dynamic pathways through which the nematic domains transition from relaxed and field-driven states. These pathways are found to be governed by the motion and interaction of defects and not by bulk reorientation.

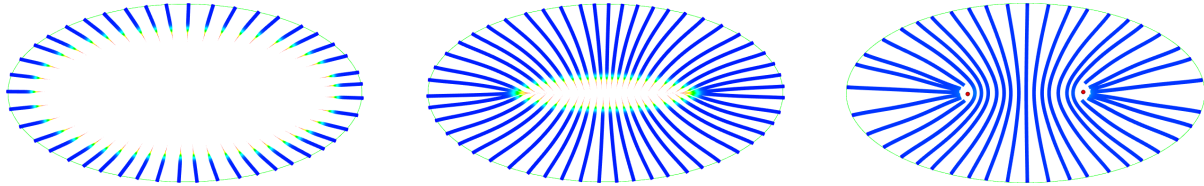


Figure 1: Hyperstreamline visualizations [2] of nematic tensor order parameter simulation results of the formation of nematic liquid crystalline order in an elliptic cylinder domain: (left) post-nucleation of nematic order at the boundaries (heterogeneous nucleation); (centre) growth of the nematic domain into the unstable isotropic central region; (right) the fully-formed nematic domain with orientational defects formed in the central region. Images taken from ref. [3].

References

- [1] P. de Gennes and J. Prost. *The Physics of Liquid Crystals*. Oxford University Press, New York, second edition, 1995.
- [2] F. Fu and N. Abukhdeir. A topologically-informed hyperstreamline seeding method for alignment tensor fields. *Visualization and Computer Graphics, IEEE Transactions on*, 21(3):413–419, March 2015.
- [3] P. Khayyatzadeh, F. Fu, and N. Abukhdeir. Geometry and anchoring effects on switching dynamics of nematic elliptic cylinder domains. 2015. submitted to Physical Review Applied.

Internal Wave Boundary Layer Interaction: a novel instability over broad topography

S. Harnanan¹, N. Soontiens², M. Stastna³

¹ University of Waterloo, Waterloo, Canada, *{sharnanan}@uwaterloo.ca*

² University of British Columbia, Vancouver, British Columbia, Canada, *nsoontie@eos.ubc.ca*

³ University of Waterloo, Waterloo, Canada, *mmstastn@uwaterloo.ca*

It has been known for some time that internal wave-induced currents can drive near bed instabilities in the bottom boundary layer over a flat bottom. However, when the bottom is not flat the situation can become quite complicated, with a diverse set of mechanisms responsible for the near bed instabilities. Using numerical simulations, we demonstrate the existence of a mode of instability due to internal solitary wave propagation over broad topography. This instability takes the form of a roll up of vorticity near the crest of the topography, and is fundamentally different from the two dominant paradigms of flow separation over sharp topography and the global instability in the wave footprint that occurs over a flat bottom observed at high Reynolds number. We will discuss both the two and three-dimensional evolution of the instability on experimental scales, and contrast it to the classical flow separation over sharp topography. As the near bed region is unstratified in the simulations, little three-dimensionalization is observed. We will also demonstrate that the instability-induced currents provide an efficient means to modulate across boundary layer transport. Extensions to the field scale will also be discussed, which will be compared and contrasted to the experimental scales. Finally, we will compare this instability to the instabilities which result from having a stratified near bed region.

Large eddy simulation of stratified turbulence

S. Khani¹, M. L. Waite²

¹ University of Waterloo, Waterloo, Canada sinakhani@uwaterloo.ca

² University of Waterloo, Waterloo, Canada mwaite@uwaterloo.ca

Direct numerical simulation (DNS) of stratified turbulence is computationally challenging because of the wide range of length scales present. When vortical motion dominates at large scales, quasi-horizontal “pancake” vortices, with small aspect ratios, develop. Between these vortices, there are Kelvin–Helmholtz (KH) instabilities and patches of more isotropic three-dimensional turbulence. Capturing these features in DNS requires fine grid spacings to resolve the different structures at various scales: the thin vertical layers, which have thickness given by the buoyancy scale $L_b = u_{rms}/N$; the smaller-scale turbulence below the Oztmidov scale L_o ; and ultimately molecular dissipation at the Kolmogorov scale. This resolution requirement can be demanding, or impossible, in realistic geophysical flows. Here u_{rms} is the rms velocity, and N is the buoyancy frequency.

As a result of this challenge, there is increasing interest in using large eddy simulations (LES) for stratified turbulence. LES resolves only the large scales and parameterizes the subgrid scale (SGS) motions. In this talk, we evaluate the ability of three commonly-employed LES approaches – the Kraichnan spectral eddy viscosity model [1], the Smagorinsky model [2], and the dynamic Smagorinsky model [3] – to simulate stratified turbulence when the Oztmidov scale is not resolved.

Simulations of stratified turbulence forced by large-scale vortical motion will be presented. For each SGS model, a number of simulations with different stratifications N and grid spacings Δ are considered. We investigate the threshold grid spacing, below which the simulations are able to capture some of the fundamental features of stratified turbulence. These features are: a cascade of kinetic energy to small horizontal scales; a horizontal wavenumber kinetic energy spectrum with a slope around $-5/3$; and KH instabilities. These features are known to be suppressed when resolution is too low. Here, we show that they are captured when Δ/L_b is sufficiently small, i.e. when the buoyancy scale is adequately resolved. The critical resolution depends on the SGS models: it is around $\Delta/L_b \approx 0.47$ for the Kraichnan model, $\Delta/L_b \approx 0.17$ for the Smagorinsky model, and $\Delta/L_b \approx 0.24$ for the dynamic Smagorinsky model. The Kraichnan model can be run with the coarsest grid, but is only applicable for spectral models with idealized boundary conditions. The dynamic Smagorinsky model shows a significant improvement over the regular Smagorinsky model. This improvement is explained by analysis of the spatial structure and statistics of the dynamic Smagorinsky coefficient c_s .

References

- [1] Kraichnan R. H. *J. Atmos. Sci.* 33: 1521-1536, 1976.
- [2] Smagorinsky J. *Mon. Weather Rev.* 91(3): 99-164, 1963.
- [3] Germano M., Piomelli U., Moin P. & Cabot W. H. *Phys. Fluids A* 3(7): 1760-1765, 1991.

Modeling the behavior of confined colloidal particles under shear flow

C. Denniston

Dept. of Applied Mathematics, University of Western Ontario, London, ON N6A 5B7

We investigate the behavior of colloidal suspensions with different volume fractions confined between parallel walls under a range of steady shears. We model the particles using molecular dynamics (MD) with full hydrodynamic interactions implemented through the use of a lattice-Boltzmann (LB) fluid. A quasi-2d ordering occurs in systems characterized by a coexistence of coupled layers with different densities, order, and granular temperature. We present a phase diagram in terms of shear and volume fraction for each layer, and demonstrate that particle exchange between layers is required for entering the disordered phase[1].

References

- [1] F.E. Mackay, K. Pastor, M. Karttunen, and C. Denniston, *Soft Matter* **10**, 8724 (2014).

Multiscale computational mechanics for non-linear behavior of lattice materials

D. Pasini¹, A. Vigliotti²

¹ McGill University, Montreal, Canada, damiano.pasini@mcgill.ca

² Cira, CIRA, Italian Aerospace Research Centre, A.Vigliotti@cira.it

This work presents a multiscale homogenisation method to capture the non-linear constitutive laws of lattice materials. In particular, we focus on geometric non linearity undergone by lattice members as a result of a macroscopic load applied to the lattice. We study lattices with dissimilar cell topologies, obtain their homogenized (effective) properties, and examine the impact that the size of the representative volume element has on them. To capture the non-linear behaviour, we calculate the macroscopic stress via the gradient of the strain energy density with respect to the components of the macroscopic displacement gradient. The results are validated via a comparison of the homogenized properties with those obtained from a discrete analysis, where each single element of the lattice is individually modelled.

References

- [1] Vigliotti A., Deshpande V. S., Pasini, D., Non linear constitutive models for lattice materials, *Journal of the Mechanics and Physics of Solids*, Vol. 64, pp. 44–60, 2014.
- [2] Vigliotti A., Pasini, D., Stiffness and Strength of Tridimensional Periodic Lattices, *Journal of Computer Methods in Applied Mechanics and Engineering*, Vol. 229-232, pp. 27-43, 2012.

Numerical evaluation of the near-wall convection velocity and Kolmogorov constants for use in the inertial dissipation method

A. Jabbari¹, L. Boegman², U. Piomelli³

¹ Environmental Fluid Dynamics Laboratory, Department of Civil Engineering, Queen's University, Kingston, Ontario, Osaj@queensu.ca

² Environmental Fluid Dynamics Laboratory, Department of Civil Engineering, Queen's University, Kingston, Ontario, leon.boegman@queensu.ca

³ Turbulence Simulation and Modelling Laboratory, Department of Mechanical and Materials Engineering, Queen's University, Kingston, Ontario, ugo@queensu.ca

The inertial dissipation method (IDM) is commonly applied to wall-bounded flows in environmental flow studies for calculation of the dissipation of the turbulent kinetic energy. Since the flow within boundary layers does not have homogeneous isotropic turbulence conditions, using the IDM for the prediction of the dissipation may result in inaccuracies due to converting frequency spectra into wavenumber ones and applying the theoretical Kolmogorov constants for isotropic flows. To address this issue, we evaluated the IDM within boundary layers by performing well-resolved direct numerical simulation and large eddy simulation of turbulent channel flows.

The convection velocity, commonly used to convert frequency spectra into wavenumber spectra, is found to be larger than the local mean velocity by approximately a factor of 2 near the wall, and by ~10% in the logarithmic layer and beyond. Comparing the dissipation calculated directly from the numerical data with that deduced from the frequency spectra, shows that usage of the standard Kolmogorov constants (particularly in the vertical and spanwise directions) leads to errors of 50% or more in computation of the dissipation. Including both optimal convection velocities and modified values of the Kolmogorov constants, that account for the anisotropy of the flow, results in significantly more accurate calculation of the dissipation rate in environmental flows, specifically in the vicinity of boundaries.

Self-similar reversing interfaces (contact lines) for the porous medium equation with absorption

J. M. Foster¹ & D. Pelinovsky²

¹ McMaster University, Canada. jamie.michael.foster@gmail.com

² McMaster University, Canada. dmpeli@math.mcmaster.ca

This talk considers the following family of one-dimensional porous medium (nonlinear diffusion) equations with ‘strong’ absorption:

$$\frac{\partial h}{\partial t} = \frac{\partial}{\partial x} \left(h^m \frac{\partial h}{\partial x} \right) - h^{1-q}. \quad (1)$$

In particular, solutions that have interfaces (contact lines) that change their direction of propagation are examined. Although this phenomenon of reversing interfaces has been seen in numerical solutions to the PDE, and some special exact solutions have been obtained, there was previously no analytical insight into how this occurs in the general case. The approach taken here is to seek self-similar solutions local to the moving interface and local to the reversing time. The analysis is split into two parts, one for the solution prior to the reversing time and the other for the solution after the reversing time. In each case the governing PDE can be reduced to a second order, non-linear, non-autonomous ODE using a suitable self-similar reduction. These ODEs do not readily admit any nontrivial exact solutions and so the asymptotic behavior of solutions near the singular points are studied. By doing this the number of adjustable parameters, or degrees of freedom, which may be used in a numerical shooting scheme are determined. A numerical algorithm is then proposed, based on the reformulation of the ODE problems to dynamical systems in \mathbb{R}^3 and the ‘blow-up’ technique, to furnish meaningful solutions to the ODEs and hence the PDE in the limit of interest. Finally, some physically motivated examples are presented.

References

- [1] J. M. Foster, C. P. Please, A. D. Fitt & G. Richardson, *The reversing of interfaces in slow diffusion processes with strong absorption*, SIAM J. Appl. Math. **72**, 1, pp. 144–162 (2012).

The influence of bottom topography on energy transfer between length scales

Marek Stastna¹

¹ Department of Applied Mathematics, University of Waterloo, Waterloo, Canada, mmstastn@uwaterloo.ca

Naturally occurring bodies of water exhibit energetic motions on a wide range of length scales. For moderate sized lakes (e.g. Lake Simcoe north of Toronto), energy is imparted by the winds at scales similar to the areal extent of the lake. This energy is subsequently spread across length scales by a variety of instabilities in a process widely referred to as the turbulence cascade. Often the classical theory of isotropic, homogeneous turbulence due to Kolmogorov is used as a heuristic for predicting the shape of the kinetic energy spectrum. However, during the ice free seasons most lakes are temperature stratified and the temperature stratification serves as a wave guide for a variety of internal waves. Hence classical turbulence theory has to be modified to account for the presence of stratification. However, the presence of stratification, especially when combined with bottom topography, leads to other nonlinear phenomena including nonlinear waves of various type. I will discuss numerical simulations that consider the evolution of a long internal wave as it interacts with a bottom slope. I will demonstrate two distinct mechanisms by which non-local interactions in wavenumber space occur, and will contrast the picture in kinetic energy-wave number space and physical space. Finally, I will discuss past measurements in Lake Simcoe and will speculate on future directions.

The 2015 AMMCS-CAIMS Congress is organized in cooperation with SIAM and AIMS.

The Interaction Between Swimming Plankton and Internal Waves

J. Shaw¹, M. Stastna²

¹ University of Waterloo, Waterloo, Canada, j9shaw@uwaterloo.ca

² University of Waterloo, Waterloo, Canada, mmstastna@uwaterloo.ca

While their small size ensures that zooplankton are primarily advected by ambient fluid currents, many are capable of organized swimming. We examine stochastic models of the run and tumble type [1] for plankton moving in a velocity field induced by internal waves in a channel. Ensembles of pairs of plankton are released into time-dependent flows and the results under the different swimming models and different background flows are compared. Some limiting cases of the motion, which allow mathematical analysis, are discussed. Based on the simulations, the statistics of the inter-particle distance of each pair of plankton is examined as a function of time. Finally, we provide a discussion of what would be required to make the swimming behaviour as realistic as possible and how this might be achieved in future work.

References

- [1] A. W. Visser, *Lagrangian modelling of plankton motion: From deceptively simple random walks to Fokker-Planck and back again*, Journal of Marine Systems **70** pp. 287-299 (2008).

Topology optimization and its applications in aerospace design and planetary vehicle design

IY. Kim¹, B. Taylor², R. Pitre³

¹ Queen's University, Kingston, Canada, kimi@queensu.ca

² Queen's University, Kingston, Canada, bradley.taylor@queensu.ca

³ Queen's University, Kingston, Canada, ryan.pitre@queensu.ca

Throughout the design process engineers are often faced with the problem of determining the most effective tradeoff of performance characteristics for their design. Whether due to budget constraints, time constraints, or indifference, this problem is often given relatively limited consideration. However, rigorous analysis and design optimization can yield tremendous benefits in performance optimization and cost minimization. This is particularly true for disciplines which have extreme performance requirements. The general approach to design optimization considers a variety of parameters, which represent different design characteristics, and comprise a “design vector.” In its most general sense, the practice of design optimization is the process of determining the design vector (or combination of design characteristics) which provides the best performance.

Topology optimization is a specific type of design optimization, wherein the design variables are the density of each individual element within a finite element model. An initial (large) design space is defined as the area for refinement, the model is meshed, and any applicable load cases are defined. The optimization problem is then set up to optimize performance, based on any number of performance metrics desired, and subject to any necessary constraints. A typical example of a topology optimization problem structure may be minimizing compliance while subject to a maximum weight, or minimizing the mass of a component while subject to a maximum allowable deformation. The optimization process then removes material from unnecessary areas within the design space – represented by a decreased density in these elements – in order to determine the optimum design for the prescribed load case.

Given the extreme performance requirements, and increasing emphasis on efficiency within the aerospace industry, the demand for topology optimization within this area is growing rapidly. Many individual components within aircraft present excellent opportunities through weight reduction through topology optimization, though some of them are subject to particularly complicated load cases. One such case which was investigated revolves around optimizing the performance of an engine bracket, which is regularly subjected to a wide range of coupled thermal and structural loads. This presents a particularly complicated problem for the optimization process because of the increased complexity of the finite element analysis, and the ability of existing software to accurately predict material properties for such coupled problems for intermediate and low element densities.

Another industry which has particular interest in minimizing mass while maintaining strict performance requirements is spacecraft design. The recursive relationship associated with increased mass and fuel requirements means that minimizing mass of spacecraft payloads or structural components can have immense repercussions when it comes to the size and cost of a launch. Through the use of topology optimization, the mass of a proposed lunar rover chassis was reduced by 38.7% while maintaining or exceeding all structural or thermal performance benchmarks.

Water Quality modeling of storm-water ponds for eutrophication management

N. Nakhaei¹, L. Boegman², M. Loewen³

¹ Queen's University, Kingston, Ontario, Canada, 11nn6@queensu.ca

² Queen's University, Kingston, Ontario, Canada, leon.boegman@queensu.ca

³ University of Alberta, Edmonton, Alberta, Canada, mrloewen@ualberta.ca

Storm water ponds receive significant streamflow, runoff and wastewater discharges. These loads include nutrients, that cause eutrophication and algae blooms in urban environments, which pose a threat to public health. Management of stormwater pond waterquality becomes problematic, due to the complex nature of these systems. In the present study, stormwater pond management is investigated using a numerical modelling approach. Four ponds in the city of Edmonton (Mactaggart 2, South Terwillegar 2, Silverberry 4, Terwillegar Towne 2) have been chosen to model eutrophication, algae blooms, nutrient load impacts and general water quality. A three-dimensional (3-D) model ELCOM-CAEDYM is applied to determine the causes of eutrophication and examine different nutrient control based remediation plans. This approach is motivated by other studies demonstrating that the reduction in external nutrient loading may have significant impacts on improving water quality, especially in shallow lakes [1, 2].

ELCOM is a 3-D hydrodynamic model for lakes and reservoirs, and is used to predict water volume, cuurrents, temperature and salinity in space and time. It solves the unsteady 3-D Reynolds-averaged Navier-Stokes (RANS) and scalar (heat and salinity) transport equations for incompressible flow using the hydrostatic assumption for pressure. CAEDYM, an aquatic biogeochemical model that can couple with the hydrodynamic model, is a complex model that uses a series of differential equations to simulate the major biogeochemical processes influencing water quality. The models are forced with observed meterological and boundary condition flow data. Calibration and validation of the models have been undertaken using goodness of fit metrics against observed water level, temperature, current and biogoechemical data. A sensitivity analysis is applied to investigate the source of the nutrients and limiting factor for eutrophication. In this study, the goal was to determine a common set of biogeochemical calibration parameters to demonstrate the generality of the models in application to stormwater systems.

References

- [1] B. Kronvang, E. Jeppesen, D. J. Conley, M. Søndergaard, S. E. Larsen, N. B. Ovesen, and J. Carstensen, , *Nutrient pressures and ecological responses to nutrient loading reductions in Danish streams, lakes and coastal waters*, Journal of Hydrology. **304**, pp. 274-288 (2005).
- [2] D.T. Van der Molen and R. Portielje, *Multi-lake studies in The Netherlands: trends in eutrophication*, Hydrobiologia. **408**, pp. 359-365 (1999).

ST-IM Industrial Mathematics

A Multiscale Model for Maple Sap Exudation

John M. Stockie¹ and Isabell Graf¹

¹ Department of Mathematics, Simon Fraser University, Burnaby, Canada, {jstockie,imgraf}@sfu.ca

The sugar maple tree (*Acer saccharum*) has a peculiar ability to generate unusually high stem pressure when in a leafless state. This elevated pressure is what permits sap to be extracted in large enough quantities that make maple syrup production a viable industry. This phenomenon of *sap exudation* has been studied for well over a century, and although many possible biophysical explanations have been proposed, it is only recently that a complete and consistent mathematical model has been developed for the exudation process [2, 4].

Our model is based on a freeze-thaw hypothesis proposed by Milburn and O’Malley [5], who were inspired by observations showing stem pressure builds up only after temperatures repeatedly cycle above and below the freezing point. We also incorporate the ideas in Cirelli et al. [3], who recognized the essential role of osmotic pressure generated by sugar concentration differences between various sapwood compartments. We capture these cell-level processes using a coupled system of nonlinear differential-algebraic equations that govern mass and heat conservation in a multiphase mixture consisting of gas, liquid and ice.

This talk focuses on the development of a macroscale (tree level) model by applying the method of periodic homogenization to upscale the microscale (cell level) equations [4]. Our approach relies on an essential separation in time scales between slow and fast diffusing temperature variables. The corresponding homogenized model consists of the microscale model equations, coupled to an equation for the global temperature that includes a source term containing a suitably averaged contribution from the microscale variables. Numerical simulations demonstrate that this model reproduces exudation pressures observed in actual experiments on maple trees and the closely-related species black walnut [1].

References

- [1] T. Améglio, F. W. Ewers, H. Cochard, M. Martignac, M. Vandame, C. Bodet, and P. Cruiziat. Winter stem xylem pressure in walnut trees: effects of carbohydrates, cooling and freezing. *Tree Physiol.*, 21:387–394, 2001.
- [2] M. Ceseri and J. M. Stockie. A mathematical model for sap exudation in maple trees governed by ice melting, gas dissolution and osmosis. *SIAM J. Appl. Math.*, 73(2):649–676, 2013.
- [3] D. Cirelli, R. Jagels, and M. T. Tyree. Toward an improved model of maple sap exudation: the location and role of osmotic barriers in sugar maple, butternut and white birch. *Tree Physiol.*, 28:1145–1155, 2008.
- [4] I. Graf and J. M. Stockie. Homogenization of the Stefan problem, with application to maple sap exudation. Submitted for publication, Nov. 2014, arXiv:1411.3039 [math.AP].
- [5] J. A. Milburn and P. E. R. O’Malley. Freeze-induced sap absorption in *Acer pseudoplatanus*: a possible mechanism. *Can. J. Bot.*, 62(10):2101–2106, 1984.

A novel heat transfer switch

I. Karimfazli¹, I.A. Frigaard², A. Wachs³

¹ Mechanical Engineering, University of British Columbia, Canada [ida.karimfazli@gmail.com](mailto:id.a.karimfazli@gmail.com)

² Mathematics, University of British Columbia, Canada frigaard@math.ubc.ca

³ IFP Energies nouvelles, Solaize, France, anthony.wachs@ifpen.fr

We explore the feasibility of a novel method for the regulation of heat transfer across a cavity, by using a controllable yield stress in order to suppress the convective heat transfer. Practically, this type of control can be actuated with electro-rheological or magneto-rheological fluids. From a hydrodynamic perspective, the feasibility of the proposed idea depends not only on existence of a static regime at sufficiently high yield stress and the stability of the static state, but also on the transition characteristics between conductive and convective flows.

We demonstrate that above a given critical yield stress value only stationary steady flows are possible, i.e. a purely conductive unyielded fluid fills the cavity. We show that this limit is governed by a balance of yield stress and buoyancy stresses, here described by B . With proper formulation the critical state can be described as a function of the domain geometry, and is independent of other dimensionless flow parameters (Rayleigh number, Ra , and Prandtl number, Pr).

We focus on the hydrodynamic characteristics of Bingham fluids in transition between conductive and convective limits. We use computational simulations to resolve the Navier-Stokes and energy equations for different yield stresses, and for different imposed controls. We show that depending on the initial conditions, a yield stress less than the critical value can result in temporary arrest of the flow. The temperature then develops conductively till the fluid yields and the flow restarts. We provide estimates of the hydrodynamic timescales of the problem and examples of flow transitions.

Finally, we explore the effect of Pr on steady and transient flow characteristics. We show that the steady state characteristics vary negligibly with Pr for $Pr \geq 1$. We present scaling analysis and give examples of flow development to illustrate that the prime effect of Pr is on transient characteristics. These results may seem to be in contradiction with those of [2, 3] and [1]. We establish that this apparent discrepancy is due to the different definitions of dimensionless variables and comment on the effect of choice of the dimensionless variables on the role of certain dimensionless groups in the analysis.

References

- [1] R. R. Huilgol and G. . R. Kefayati. Natural convection problem in a bingham fluid using the operator-splitting method. *J. non-Newtonian Fluid.*, 2014.
- [2] O. Turan, N. Chakraborty, and R. J. Poole. Laminar natural convection of Bingham fluids in a square enclosure with differentially heated side walls. *J. non-Newtonian Fluid.*, 165(15-16):901–913, 2010.
- [3] O. Turan, R. J. Poole, and N. Chakraborty. Aspect ratio effects in laminar natural convection of Bingham fluids in rectangular enclosures with differentially heated side walls. *J. non-Newtonian Fluid.*, 166(3-4):208–230, 2011.

Conditioning of uneven boreholes in primary cementing

A. Roustaei¹, I.A. Frigaard²

¹ Mechanical Engineering, University of British Columbia, Canada ali.rostaei@gmail.com

² Mathematics, University of British Columbia, Canada frigaard@math.ubc.ca

We perform a detailed computational study of the flow of a Bingham fluid along a narrow channel, with one locally uneven wall. This uneven section of the channel represents a washed out section of an oil well about to be cemented. In our previous work [1] we have studied the effects of washout shape, but in Stokes flow. We found that in the limit of large washout depth h and large Bingham number B , regardless of the washout geometry, the area of the channel that contains moving fluid is the same for each length L . Uneven and distant parts of the washout become full of static fluid, while the flow self-selects its own unique flowing geometry.

Here we extend our previous study into the regime of non-zero Reynolds number Re . The results are somewhat surprising. For small/moderate Re we observe that the amount of fluid that is mobilized in the washout increases with Re at fixed B , but beyond a critical value this trend is reversed as the flow essentially by-passes the washout section. We also study the progression of increasing Re with ReB fixed, which again implies increasing flow rate. Again we find the non-monotone behaviour in flowing area. On closer inspection we see that the loss of monotonicity is compensated by the emergence of zones within the washout within which the fluid simply recirculates, albeit weakly. A selection of computational results and analysis is presented.

References

- [1] A. Roustaei, I.A. Frigaard, *Residual drilling mud during conditioning of uneven boreholes in primary cementing. Part 1: Rheology and geometry effects in non-inertial flows*, J. non-Newt. Fluid Mech., <http://dx.doi.org/10.1016/j.jnnfm.2014.09.019>.

Coulomb Explosions as a Molecular Imaging Technique

C.S. Bohun¹

¹ University of Ontario Institute of Technology, Oshawa, Canada, sean.bohun@uoit.ca

Pixel Imaging Mass Spectrometry is an exciting new molecular imaging technique that relies on femtosecond laser pulses to strip molecules of their valence electrons, causing them to explode. By pre-aligning the molecules and using fast cameras, it is possible to concurrently detect of all of the ionic fragments of the resulting coulomb explosion and to use this information to reconstruction the structure of the parent molecule. Some of the key mathematics aspects of this problem will be discussed and a comparison of the forward model predictions with experimental data for the imaging of 3,5-dibromo-3',5'-difluoro-4'-cyanobiphenyl molecules that are pre-aligned in space will be presented. An update on the current state of the art and where the research is progressing will also be presented.

Estimating fugitive emissions of metallic particulates using a Gaussian plume model

Bamdad Hosseini*,¹ and John M. Stockie*,²

* Simon Fraser University, Burnaby, Canada. ¹ bhossein@sfu.ca, ² stockie@math.sfu.ca

In this project we consider estimating emissions of particulate matter from an industrial site using measurements of concentration and particulate depositions away from the sources. We are particularly interested in fugitive emissions of metallic particles such as lead. Fugitive emissions refer to emissions from sources that are not directly measurable or identifiable. For example, emissions from vents and stacks can be measured by installing sensors. However, emissions from piles of material, moving trucks or small windows cannot be measured directly.

Dispersion of pollutants into the atmosphere can be modelled by the advection-diffusion partial differential equation (PDE) which consists our forward model. One can choose to solve this equation numerically using Finite Volume or Finite Element methods. This often involves choosing appropriate models for the wind profile and eddy diffusion coefficients and solving a variable coefficient PDE. Another approach, which we choose in this work, is to approximate the solution using the Green's function of a simplified version of the PDE.

With the forward problem identified we can move on to solution of the inverse problem. We construct a model for measurement devices and formulate the inverse problem in the Bayesian perspective. Different choices of the prior measure on the sources are considered and the posterior mean is taken as an estimate of the actual emission rates. At this stage we utilize the linearity of the forward problem in the source term to improve the performance of our method.

Finally, we apply our method to estimate the emissions of lead particulates from an industrial site in Trail, BC, Canada. We discuss various practical aspects of the problem such as regularization of wind data and dealing with data from multiple measurement devices. After solution of the inverse problem we substitute the estimated emission rates back into the forward model to assess the impact of the sources on the surrounding environment (see Figure 1 below).

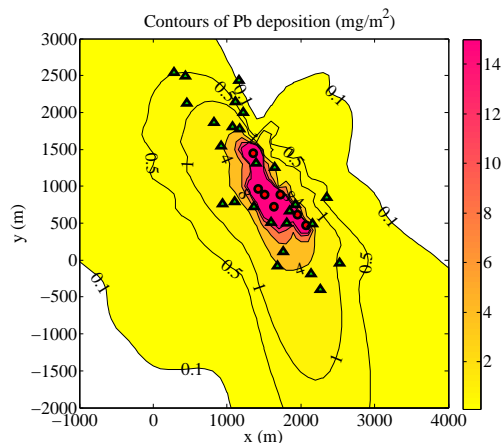


Figure 1: Assessing the impact of the estimated sources of lead for an industrial site in Trail, BC, Canada. Red dots indicate point sources that approximate all emissions from a section of the industrial site. Green triangles indicate the position of nearby sensors.

Estimating parameter sensitivity in a spatially continuous model of fermentation and transport processes in the human colon

Arun S. Moorthy and Hermann J. Eberl

University of Guelph, Guelph, Canada {amoorthy,heberl}@uoguelph.ca

Transport processes, anaerobic digestion and microbial complexity observed in the human colon is modeled as a spatially continuous pipe with both fluid and attached media [1]. The model is an extension of the 3-stage model of colon processes developed in [2] where the microbial representation is refined to accommodate greater exploration of microbial interaction, using the diversity methods of [3], and the colon is represented as a spatially continuous biochemical reactor to accommodate greater spatial specificity in simulation experiments, a follow up of our assessment of reactor system design criteria in [4]. The resulting model is a variable-sized system of first-order Partial Differential Equations with stiff, non-linear source terms.

The non-linearity of the anaerobic digestion process and size of parameter space make it difficult to form intuition of biochemical reaction parameter sensitivity. Additionally, the model extensions (increased microbial refinement and spatial continuity) introduce additional physical and simulation/operation parameters. Thus we employ a combination of simulation methods and qualitative techniques to estimate model sensitivity. This include monte carlo model simulation to assess stochastically chosen biochemical reaction and component exchange parameters, perturbation analysis of diet and flow parameters, full-factorial experimentation of microbial complexity parameters, and qualitative inspection of model structure and identification of special case solutions.

Using these methods, it was found that model behaviour is sensitive to biochemical reaction, component exchange, and microbial complexity parameters associated with the enzymatic hydrolysis sub-process within the anaerobic digestion chain of processes. Cross-examining with our qualitative assessment of the model structure, we can verify that enzymatic hydrolysis is the preliminary and reaction/digestion limiting step in the hierarchy of anaerobic digestion steps, and so conclude that the identified parameters are valuable in discerning the overall model behaviour. However, we were unable to rank/categorize the entire model parameter space quantitatively, thus treat our results as qualitative estimations.

References

- [1] A.S. Moorthy, S.P.J. Brooks, M. Kalmokoff and H.J. Eberl, *A spatially continuous model of carbohydrate digestion and transport processes in the human colon*, In preparation (2015).
- [2] R. Muñoz-Tamayo, B. Laroche, E. Walter, J. Dore, and M. Leclerc, *Mathematical modelling of carbohydrate degradation by human colonic microbiota*, *J. Theor. Biol.* **266**, 1, pp. 189-201 (2010).
- [3] I. Ramirez, E.I. Volcke, R. Rajnikanth, and J.P. Steyer. *Modeling microbial diversity in anaerobic digestion through an extended ADM1 model*, *Water Res.* **43**, 11, pp. 2787-2800 (2009).
- [4] A.S. Moorthy and H.J. Eberl, *Assessing the influence of reactor system design criteria on the performance of model colon fermentation units.*, *J. Biosci. Bioeng.* **117**, 4, pp. 478-484 (2014).

Flow currents and ventilation in Langstroth beehives due to brood thermoregulation efforts of honeybees

R. Sudarsan^{1,2}

¹ Department of Mathematics and Statistics, University of Guelph, Guelph, Ontario, Canada N1G 2W1, (rsudarsa@uoguelph.ca)

² Biophysics Interdepartmental Graduate Program, University of Guelph, Guelph, Ontario, Canada N1G 2W1

Beekeepers universally agree that ensuring sufficient ventilation is vital for sustaining a thriving, healthy honeybee colony. Despite this fact, surprisingly little is known about the ventilation and flow patterns in bee hives. We take a first step towards developing a model-based approach that uses computational fluid dynamics to simulate natural ventilation flow inside a standard Langstroth beehive. A 3-D model of a Langstroth beehive with one brood chamber and one honey super was constructed and inside it the honeybee colony was distributed among different clusters each occupying the different bee-spaces between frames in the brood chamber. For the purpose of modeling, each honeybee cluster was treated as an air-saturated porous medium with constant porosity. Heat and mass transfer interactions of the honeybees with the air, the outcome of metabolism, were captured in the porous medium model as source and sink terms appearing in the governing equations of fluid dynamics. The temperature of the brood that results from the thermoregulation efforts of the colony is applied as a boundary condition for the governing equations. The governing equations for heat, mass transport and fluid flow were solved using Fluent[©], a commercially available CFD program.

The results from the simulations indicate that (a) both heat and mass transfer resulting from honeybee metabolism play a vital role in determining the structure of the flow inside the beehive and mass transfer cannot be neglected, (b) at low ambient temperatures, the non-uniform temperature profile on comb surfaces that results from brood incubation enhances flow through the honeybee cluster which removes much of the carbon-dioxide produced by the cluster resulting in lower carbon-dioxide concentration next to the brood, (c) increasing ambient (outside) air temperature causes ventilation flow rate to drop resulting in weaker flow inside the beehive. Flow visualization indicates that at low ambient air temperatures the flow inside the beehive has an interesting 3-D structure with the presence of large recirculating vortices occupying the space between honey super frames above the honeybee clusters in the brood chamber and the structure and strength of the flow inside and around the honeybee clusters changes as we increase the ambient air temperature outside the beehive.

Full waveform inversion in seismic imaging

M.P. Lamoureux¹, G.F. Margrave², V.N. Zubov³

¹ University of Calgary, Canada, mikel@ucalgary.ca

² University of Calgary, Canada, margrave@ucalgary.ca

³ Pinnacle/Halliburton, vnzubov@gmail.com

Seismic imaging is a key technology in the oil and gas industry for locating and managing hydrocarbon resources buried deep within the earth. Traditionally, images of the subsurface are created by applying digital signal processing algorithms to recorded data representing seismic vibrations at, or near, the surface of the earth. Seismic energy, reflected off subsurface geological boundaries, produce a clear signature in the data recording that can be migrated into a good image of the geological structures in the earth.

Recently, progress has been made in applying mathematical inverse theory to the problem of directly estimating physical parameter values (rock density, elasticity, porosity, fluid content) from the seismic data [1, 2]. Advances in these methods will produce more than just an image of the subsurface, but also details about reservoir properties such as the character of the oil-bearing reservoir rocks, and the nature and quantity of the fluids in the reservoir.

We will report our work on modelling 2D seismic inversion using multi-grid methods, including a exploration of the problems that arise when the source data is unknown, and low frequency data is absent from the seismic experiment. A simulated numerical wavefield is propagated using finite difference code on a fine, bounded grid, while parameter values are determined on a coarse grid using a local optimization algorithm to produce a best fit to the data. Results for both density and elasticity inversions are considered. Iterations that focus the optimization on a layer-by-layer construction is shown to be more successful than a blind, full field inversion. These results are a continuation of work presented earlier in [3].

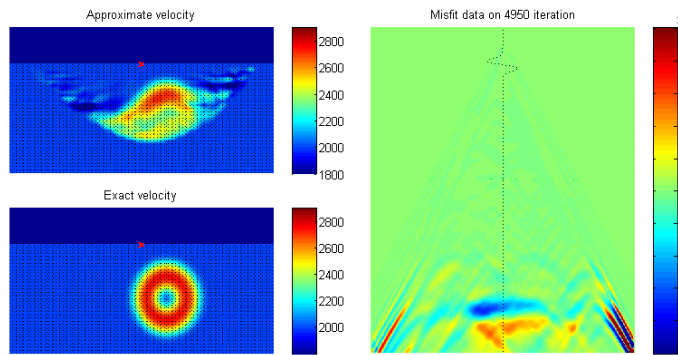


Figure 1: Sample output of parameter estimation and data fit.

References

- [1] C.M. Hogan, K.J. Hedlin, G.F. Margrave, and M.P. Lamoureux, *Feasibility Testing of Time-Lapse Seismic Monitoring with Full Waveform Tomography*, Canadian Society of Exploration Geophysicists Expanded Abstracts (2009).
- [2] R.G. Pratt, *Seismic waveform inversion in the frequency domain, Part 1: Theory and verification in a physical scale model*, Geophysics, Vol. 64, No. 3, pp. 888–901 (1999).
- [3] V.N. Zubov, M.P. Lamoureux, G.F. Margrave, *Multi-scale 2D acoustic full waveform inversion with high frequency impulsive source*, Canadian Society of Exploration Geophysicists Proceedings (2013).

Mathematical Modeling of Cellulose Degradation by *Clostridium thermocellum*

A. Dumitache¹, H.J. Eberl², E. Jalbert³, G.M. Wolfaardt⁴

¹ Oak Ridge National Laboratories, USA

² University of Guelph, Canada; heberl@uoguelph.ca

³ University of Guelph, Canada

⁴ Stellenbosch University, South Africa

Recent years have seen an increased interest in using abundantly available, biodegradable, and renewable resources to produce liquid ethanol as an alternative to petroleum based fuels, e.g. in transportation. The raw material for this bioenergy is to a large extent provided in form of agricultural products, by-products and waste products. An attractive route of ethanol production is cellulose based, which has little or no contribution to the greenhouse effect and potentially higher yield than corn based ethanol production. A key player in the cellulose to ethanol conversion process is the cellulolytic anaerobic thermophilic bacterium *Clostridium thermocellum*, which is able, for example to solubilize crystalline sources of cellulose, such as cotton.

In this talk we present two mathematical models for the cellulolytic activity of *C. thermocellum*, on different length scales.

The first model is a (laboratory) reactor scale ordinary differential equation. It is compared against online CO₂ data as measurements of microbial activity. Although the mathematical model is conceptually very simple the quantitative fits are excellent.

The second model is a spatial description of the carbon utilization by *C. thermocellum* on the length scale of the cellulosic material. The bacteria are modeled by a degenerate partial differential equation, coupled with an ODE for the degradation of the immobile carbon substrate. The strong nonlinearities, so far, prevent an analytical treatment, wherefore the model is studied numerically. To this end we extend a previous semi-implicit numerical scheme for a similar problem to a fully implicit method. Our simulations suggest the formation of travelling waves.

Optimal Backward Error and the Dahlquist Test Problem

Robert M. Corless¹

¹ University of Western Ontario, London, Canada. rcorless@uwo.ca

The Dahlquist test problem is the simple linear first order ODE $\dot{y} = \lambda y$, $y(t_n) = y_n$, to be solved on $t_n \leq t \leq t_n + h$. Taking $\lambda \in \mathbb{C}$ gives rise to the classical theory of stiffness (when $\operatorname{Re}\lambda \ll 0$). Several mathematical theories emerged from study of this equation: A-stability, L-stability, and the so-called theory of “order stars”. These theories connected approximation theory over \mathbb{C} with the theory of stability of numerical methods.

Recently, we have made some progress understanding numerical methods for initial-value problems (IVP) $\dot{y} = f(y)$, $y(0) = y_0$ from the point of view of “optimal backward error”. That is, a numerical method, say $y_{n+1} = y_n + h\Phi$, produces a *skeleton* $\{(t_n, y_n)\}_{n=0}^N$ of a solution, which is usually interpolated by a piecewise polynomial to give a continuously differentiable solution. By interpolating instead with the solution of either

$$\dot{z} = f(z) + \Delta(t) \quad t_n \leq t_{n+1}$$

or

$$\dot{z} = f(z)(1 + \delta(t)) \quad t_n \leq t_{n+1}$$

we ask for the “smallest” Δ (or δ) that still has both $z(t_n) = y_n$ and $z(t_{n+1}) = y_{n+1}$. This computational *a posteriori* analysis can be applied to any problem and any method. For the Dahlquist test problem, the results are surprising. This talk uses the calculus of variations and optimal control theory. But only just.

Post-Harvest Diseases of Apples: From Spore Dispersal to Epidemiology

R.C. Tyson¹, L. Nelson¹, K.A. Williams¹, M. Dutot¹

¹ University of British Columbia Okanagan, Kelowna, Canada

Postharvest diseases, especially those caused by fungi, can cause considerable damage to harvested apples in controlled atmosphere storage. Fungicides are used to control the disease, but resistance to fungicides is increasing and there is pressure by consumers and ecologists to reduce reliance on chemical controls. There is some evidence that physical conditions related to orchard management are predictive of postharvest disease incidence, and so the first line of defense against postharvest disease should involve best practices in orchards. In this work, we develop and analyse mathematical models to understand the dispersal of spores in the orchard, the initial infection level of fruit entering storage, and the epidemiology of the disease once the apples are in storage. We focus on conditions in the Okanagan Valley, where summers are dry and fungal spore presence is generally low. This leads to a mathematical problem where we are attempting to quantitatively and deterministically evaluate conditions surrounding rare events, that is, infection of fruit, and the fundamental stochasticity of the problem is crucial.

Recent results on scattering in layered media

P. Gibson

York University, Toronto, Canada, pcgibson@yorku.ca

The classical model for scattering in piecewise constant layered media is fundamental in seismic imaging [1],[9]—historically the main driver of research into the subject—as well as in acoustic and electromagnetic imaging [5], and the design of optical coatings [3], for example. At the same time, from the theoretical point of view, it serves as a case study in hyperbolic PDEs with rough coefficients: the governing equations comprise a basic example of a wave equation with discontinuous coefficients, a feature that is incompatible with a wide swath of established theory (e.g., [2], [8], [6], [7]). In imaging applications, the impulse response at the boundary for these equations, or boundary Green’s function, corresponds to measured data, which can be recorded only for a finite length of time. A central theoretical difficulty stems from the combination of discontinuous coefficients with finite time duration; indeed, despite the extensive literature on layered media, an explicit closed-form formula for the time limited Green’s function was discovered only recently [4]. Consequently, the way measured data depends on physical parameters, encoded as coefficients of the governing equations, has remained obscure, allowing only a partial understanding of the associated inverse problem. In this talk we present a novel perspective on piecewise constant layered media that resolves the central theoretical difficulty and reveals an underlying mathematical structure not previously known.

References

- [1] N. Bleistein, J. K. Cohen, and J. W. Stockwell, Jr. *Mathematics of multidimensional seismic imaging, migration, and inversion*, volume 13 of *Interdisciplinary Applied Mathematics*. Springer-Verlag, New York, 2001. Geophysics and Planetary Sciences.
- [2] R. Burridge. The Gelfand-Levitan, the Marchenko, and the Gopinath-Sondhi integral equations of inverse scattering theory, regarded in the context of inverse impulse-response problems. *Wave Motion*, 2(4):305–323, 1980.
- [3] S. A. Furman and A. V. Tikhonravov. *Basics of Optics of Multilayer Systems*. Basics of. Editions Frontières, Gif-sur-Yvette, France, 1992.
- [4] P. C. Gibson. The combinatorics of scattering in layered media. *SIAM J. Appl. Math.*, 74(4):919–938, 2014.
- [5] D. Kurrant and E. Fear. An improved technique to predict the time-of-arrival of a tumor response in radar-based breast imaging. *Biomedical Engineering, IEEE Transactions on*, 56(4):1200 –1208, april 2009.
- [6] Rakesh. An inverse problem for a layered medium with a point source. *Inverse Problems*, 19(3):497–506, 2003.
- [7] Rakesh. Inverse problems for the wave equation with a single coincident source-receiver pair. *Inverse Problems*, 24(1):015012, 16, 2008.
- [8] W. W. Symes. Impedance profile inversion via the first transport equation. *J. Math. Anal. Appl.*, 94(2):435–453, 1983.
- [9] O. Yilmaz. *Seismic data analysis : processing, inversion, and interpretation of seismic data*. Number 10 in Investigations in Geophysics. Society of Exploration Geophysicists, Tulsa, OK, 2nd edition, 2001. Edited by Stephen M. Doherty.

Some novel circle-packing algorithms devised for the construction of tubular networks in \mathbf{R}^3

W. Jiang¹, T. Qiao¹, F. Mendivil², S. D. Peterson¹ and E.R. Vrscay¹

¹ University of Waterloo, Waterloo, Ontario, Canada, {w53jiang,t2qiao,peterson,ervrscay}@uwaterloo.ca

² Acadia University, Wolfville, NS, Canada, franklin.mendivil@acadiau.ca

We describe a new set of circle-packing (“CP”) algorithms and procedures developed as part of our work on the construction of networks of tubes with a range of diameters to fit into arbitrary 3D regions. (The algorithms for the construction of these tubular networks will be described in another paper at this conference.) A significant simplification of the packing problem exists for 3D regions which may be considered as “quasi two-dimensional,” i.e., having a principal direction along which the cross-section varies. In this case, the tubular network is formed by connecting together a series of blocks B_i composed of parallel tubular assemblies. Each block B_i exhibits no variation in the principal direction; that is, its cross section C_i (approximated as a polygon) remains constant. The packing of tubes of prescribed diameters then becomes a 2D CP problem over region C_i .

Our basic CP algorithm uses methods from [1]. Features of our problem have required some new strategies for packing and rearranging. Here we mention a few:

1. It may be desirable that larger tubes be situated primarily in interior regions. We have developed a CP scheme which starts in the center of a region and packs outwardly. At first, this scheme may be supplied with circles of largest diameter. Various strategies may then be employed to provide circles of smaller diameter as the outer boundary is approached.

In order to minimize misalignments at boundaries of neighbouring blocks, we consider an interior region R that is common to several, if not all, blocks. This region is packed first using the methods described in 1. above. The resulting packing is then employed in all blocks. In this way, it is possible that a tube will extend continuously from one end of the network to the other through all blocks.

2. The remainder of the unpacked area in each block B_i is then packed starting from the packed region and working outward to its boundary using the methods outlined in 1.

3. The greedy packing from 1. or 2. might produce suboptimal packings (in terms of packing efficiency). As shown in [1], some mild rearrangement of the packing – using a fictitious gravitational force – can often make some space(s) available for the packing of additional circles. We have developed a scheme to produce such arrangements according to fictitious forces that may be directed in any direction, in particular toward the center, with the primary purpose of increasing the packing efficiency near the boundary.

4. It is possible that there are “hard to reach” regions near the boundary of a 2D region. In such cases, the schemes devised in [1] will not work. We have devised some alternate packing methods, e.g., packing against a single packed circle over a prescribed set of angles.

5. We have also studied the problem of how a circle packing in a 2D region will change with small changes in the outer boundary.

References

- [1] J.A. George, J.M. George and B.W. Lamar, *Packing different-sized circles into a rectangular container*, Eur. J. Op. Res. **84**, 693-712 (1995).

The barbecue pool heater: An algorithm to construct tubular networks that occupy arbitrary regions in \mathbf{R}^3

W. Jiang¹, B. Kettlewell¹, T. Qiao¹, F. Mendivil², S. D. Peterson¹ and E.R. Vrscay¹

¹ University of Waterloo, Waterloo, Ontario, Canada, {w53jiang,brian.kettlewell,t2qiao,peterson,ervrscay}@uwaterloo.ca

² Acadia University, Wolfville, NS, Canada, franklin.mendivil@acadiau.ca

We describe some preliminary, yet novel, algorithms for constructing a network of tubes with a range of diameters into an arbitrary three-dimensional region. Though other industrial applications exist, this work is primarily motivated by the “barbecue pool heater” [1], which uses a branched tubular network as a heat exchanger to warm pool water using a propane barbecue. A simplification in our approach occurs if the arbitrary region possesses a principal direction along which the cross-section varies; that is, the region can be considered to be quasi-two dimensional. In this case, our tubular network is formed by connecting together a series of blocks B_i composed of parallel tubular assemblies. Each block B_i exhibits no variation in the principal direction; that is, its cross section (approximated as a polygon) remains constant. The variation of the entire tubular network along the principal direction occurs at the block junctions in the form of discontinuous jumps.

Packing: Each block B_i is packed with a set of parallel tubes by means of some rather novel circle-packing algorithms (variations of those found in, e.g., [2]) that were developed for the current problem. (The details of this algorithm will be reported in another paper in this conference.) Packing the blocks independently may cause problems at boundaries between neighbouring blocks since it is not guaranteed that tubes are aligned, making connections difficult. As such, we first consider an interior region R that is common to several, if not all, blocks. This region is packed first and the resulting packing is employed in all blocks. In this way, it is possible that a tube will extend continuously from one end of the network to the other through all blocks. The remainder of the unpacked area in each block B_i is then packed starting from the packed region and working outward to its boundary.

Connecting: There are three fundamental connection schemes employed at present in order to construct a continuous tubing network with one entrance and one exit, though the network can be locally parallel: (i) endcap connection - a 180-degree bend that connects two neighbouring tubes at their ends, (ii) a “merge” operation in which a tube flows into a neighbouring tube, and (iii) a “shift” operation in which a tube is shifted into a vacant neighbouring position.

Tubes at the extreme ends of the network must be connected via endcap connections. As well, it is possible that there are tubes in given block B_i that cannot enter neighbouring block B_{i+1} (and B_{i-1}). Such tubes must either be turned back into block B_i or merged into a neighbouring tube.

For very small numbers of blocks and tubes, it may well be possible to arrive at connections manually. But in more realistic situations, an algorithm is necessary. We have adapted “minimum degree matching” to generate all possible endcap and merge-shift configurations. As well, it must be checked that there are no “dead ends” or isolated loops in which continuous flow of fluid may not be possible.

References

- [1] <http://www.readneckpoolheater.com>.
- [2] J.A. George, J.M. George and B.W. Lamar, *Packing different-sized circles into a rectangular container*, Eur. J. Op. Res. **84**, 693-712 (1995).

The effects of cycling on the ‘connectedness’ of the binder in lithium-ion cathodes

J. M. Foster¹, A. Gully², H. Liu³, S. Krachkovskiy⁴, Y. Wu⁵, S. Schougaard⁶, M. Jiang⁵, G. Goward⁴, G. A. Botton³ & B. Protas⁷.

¹ Department of Mathematics & Statistics, McMaster University, Canada. {jamie.michael.foster@gmail.com}

² Department of Mathematics & Statistics, McMaster University, Canada.

³ Materials Science & Engineering, McMaster University, Canada.

⁴ Department of Chemistry, McMaster University, Canada.

⁵ R&D Department, General Motors of Canada.

⁶ Department of Chemistry, Universite du Quebec a Montreal.

⁷ Department of Mathematics & Statistics, McMaster University, Canada. {bprotas@mcmaster.ca}

We will present some recent results from a collaborative research effort which has been focussed on using novel mathematical modelling, homogenisation, image acquisition and image processing to elucidate the effects of cycling on the ‘connectedness’ of the (carbon black/polymer) binder matrix in lithium-ion battery cathodes. The aim of doing so has been to understand whether, and to what extent, the ageing of the polymer binder is responsible for battery fading.

In the first part of the talk we will discuss a state-of-the-art ‘nested’ homogenisation technique [1] which has been developed to determine effective transport coefficients, e.g., the effective (or macro-scale) electronic/ionic conductivity or porosity, of composite electrodes comprised of three material phases, namely: binder, electrolyte and active material. The effective transport properties are defined such that the homogeneous material carries the same flux as the original composite material under the same imposed gradients. This approach is indispensable when formulating device scale models of electrochemical cells, and, it offers two advantages over the commonly used Bruggeman formula: (i) it explicitly accounts for the micro-scale geometry of the composite material, and; (ii) gives exact (rather than approximate) values for the effective transport coefficients.

In the second part of the talk we will show how this homogenisation technique has been utilised to compute the effective electronic conductivity of two pairs of commercial NMC-based cathodes both before and after cycling. There are two key prerequisites for applying the technique to real electrodes: (i) a series of high-resolution FIB/SEM images of the cathodes, and; (ii) an image processing algorithm which can digitally segmenting each image into its three constituent phases. These two prerequisites will be discussed. By computing the effective electronic conductivity of the two pairs of cathodes we will show that, even after a fairly modest number of cycles: (i) there is an appreciable decrease of the ‘effective’ conductivity of the electrode, and; (ii) that the binder tends delaminate from the surfaces of the particles of active material.

Motivated by these findings, in the final part of the talk, we will present a poroviscoelastic model for these electrodes. We demonstrate that, in the physically relevant regime, there is a small dimensionless parameter that can be exploited in a systematic asymptotic analysis of the model to derive a wholly analytical description of the mechanical evolution of the binder matrix under operating conditions. Finally, the solution of the model is interpreted to make some recommendations on what can be done to prevent binder ageing and delamination, thus improving electrode longevity.

References

- [1] A. Gully, H. Liu, S. Srinivasan, A. K. Sethurajan, S. Schougaard & B. Protas, *Effective transport properties of porous electrochemical materials - a homogenization approach*, J. Electrochem. Soc. **161**(8):E3066-E3077, 2014.

ST-MB Mathematical Biology

A Fully Spatially Structured Metapopulation Model for Predator-Prey Dynamics

M.R. Garvie¹, J. Morgan², V. Vandana³

¹ Department of Mathematics & Statistics, University of Guelph, ON Canada N1G 2W1, mgarvie@uoguelph.ca

² Department of Mathematics, The University of Houston, Houston, USA, TX 77204-3008, jmorgan@math.uh.edu

³ Department of Mathematics, The University of Houston, Houston, USA, TX 77204-3008, vandanav@math.uh.edu

This paper is devoted to the study of a fully spatially structured PDE metapopulation model for predator-prey dynamics in $d \leq 3$ space dimensions. A nonlinear reaction-diffusion system of the Rosenzweig-MacArthur form models predator-prey dynamics in two ‘high’ quality patches embedded in a ‘low’ quality subdomain, where species can diffuse, convect and die. Our model substantially generalizes and improves earlier fully spatial metapopulation models which were formulated in one space dimension. We establish the existence of unique, global, uniformly bounded weak solutions. Furthermore, we present a nondimensionalization procedure and a fully discrete Galerkin finite element method in two space dimensions, which is a generalization of the finite element method analyzed in a previous single patch predator-prey model. The numerical solutions are illustrated for some test cases using MATLAB and independently verified with Comsol. Numerical experiments demonstrate that the initial local extinction in one patch gives rise to waves of recolonization from another patch.

A Local Optimization Approach to Resolving Conservation Conflicts in Mosaic Ecosystems

S. Nowack¹, C. T. Bauch², M. Anand³

¹ University of Guelph, ON, Canada, spnowack@gmail.com

² University of Waterloo, ON Canada, cbauch@uwaterloo.ca

³ University of Guelph, ON, Canada, anand.madhur@gmail.com

The introduction of sustainable land-use practices often leads to conflicts between the agriculture sector and conservationists [1]. A successful conflict resolution is one that ensures both the livelihood of human inhabitants and the persistence of healthy and biologically diverse ecosystems. Identifying and implementing proposed resolutions is a difficult task due to the demand for land heavily outweighing the supply. One promising strategy that has been introduced, and has the potential to compensate for this imbalance, is to identify alternative spatial arrangements of the vegetative states on the landscape that improve both biodiversity and agricultural productivity [2, 3]. Multi-objective, global optimization approaches have been developed to achieve this goal, and although global solution techniques can be effective at identifying the best solution, they are inherently ineffective at identifying alternative solutions and implementation strategies.

Here we introduce a local optimization method that complements global approaches. Species-area relationships constructed from data collected from forest-grassland mosaics in Rio Grande do Sul, Brazil were used to parameterize an objective function that models plant species biodiversity. Landsat images were then used to characterize the land use and land cover of areas in this region, and the optimization algorithm was initiated from landscapes with these attributes.

Via a local search algorithm applied to the objective function, spatially rearranged landscapes were identified that improve biodiversity without having an adverse affect on agricultural activities. The new methodology resulted in several incremental improvements on previous approaches, including: (i) its ability to provide multiple, viable options to decision-makers for resolving conservation conflicts, (ii) its ability to provide an implementation strategy to obtain each of the viable options, and (iii) an evaluation system for comparing and contrasting the list of candidates. The method is presented in the context of a forest-grassland mosaic ecosystem, but is flexible by design in that it can be applied to any ecosystem, and easily adapted to fit the needs of decision-makers.

Local optimization approaches can be an effective planning tool, both on their own and in tandem with other approaches. Identifying the best possible global solution may be ideal, but it is not always possible to implement. Thus, alternative, good solutions that result from local approaches should be considered, especially when those solutions sustain more biodiversity than the initial landscape and provide a flexible implementation strategy.

References

- [1] C. Margules, S. Sarkar, and C. R. Margules, *Systematic Conservation Planning*, Cambridge University Press (2007).
- [2] S. Polasky, E. Nelson, J. Camm, B. Csuti, P. Fackler, E. Lonsdorf, et al., *Where to put things? Spatial land management to sustain biodiversity and economic returns*, *Biol. Conserv.* **141**, pp. 1505-1524 (2008).
- [3] K. Cao and X. Ye, *Coarse-grained parallel genetic algorithm applied to a vector based land use allocation optimization problem: the case study of Tongzhou Newtown, Beijing, China*, *Stoch. Env. Res. Risk A.* **27**, pp. 1133-1142 (2013).

A matrix population model for the abundance of Culex mosquitoes with temperature in different seasons

L. Chen¹, S. Wang¹, H. Zhu¹

¹ LAMPS, Department of Mathematics and Statistics, York University, Toronto, Canada, {lbchen, stevenw, huaiping}@mathstat.yorku.ca

The reproduction and development of Culex mosquitoes are closely related to temperature in spring and summer. The mosquito overwintering process also has an impact on the mosquito abundance in spring and therefore effects the mosquito abundance in the summer. In this work, we subdivide one year into four different periods and a specific model is developed for each period to better describe the mosquito development. We also consider the mosquitoes into aquatic and adult stages and incorporate the summer daily mean temperature and average temperature of other seasons. In this presentation, I will first introduce the four different periods for Culex mosquitoes in Southern Ontario, and then define the mathematical conditions to represent the start and end of different seasons for a given year. Finally a matrix model with age and stages will be presented. Our simulation results show that the model captures well the trend of mosquito abundance and matches well with the surveillance data in Peel region, Ontario, Canada. The model can be used for forecasting the Culex mosquitoes abundance.

This is a joint work with Prof. Huaiping Zhu and Prof. Steven Wang, supported by CIHR, PHAC and NSERC.

References

- [1] J. Cushing and Y. Zhou, *The net reproductive value and stability in matrix population models*, Natural Resource Modeling, **8**, 4 (1994).
- [2] J. Wang, N.H. Ogden and H. Zhu, *The impact of weather conditions on Culex pipiens and Culex restuans (Diptera: Culicidae) abundance: A case study in Peel region*, Journal of medical entomology, **48**, 2, pp. 468-475 (2011).

A Metapopulation Cholera Model

Pauline van den Driessche¹

¹ University of Victoria, B.C. Canada. pvdd@math.uvic.ca

Cholera is an infectious human disease caused by the aquatic bacterium *Vibrio cholerae*. Spatial heterogeneity of both humans and water may influence the spread of cholera. To incorporate spatial effects, a metapopulation cholera model for several patches is proposed that includes direct (rapid) and indirect (environmental/water) transmission and explicitly incorporates both human and water movement between patches. Mathematical tools from graph theory are used to understand the dynamics of this spatially heterogeneous cholera model, and to show that (under certain assumptions) it satisfies a sharp threshold property [1]. The model is used to investigate the dependence of the disease threshold on the patch connectivity and water movement [2], as well as to consider control strategies to eliminate cholera from all patches.

References

- [1] M.C. Eisenberg, Z. Shuai, J.H. Tien and P. van den Driessche, *A cholera model in a patchy environment with water and human movement*, Mathematical Biosciences, **246**, pp. 105-112 (2013).
- [2] J.H. Tien, Z. Shuai, M.C. Eisenberg and P. van den Driessche, *Disease invasion on community networks with environmental pathogen movement*, Journal of Mathematical Biology, in press, DOI 10.1007/s00285-014-0791-x.

A Model of Microtubule Organization in the Presence of Motor Proteins

Diana White¹, Gerda de Vries², Adriana Dawes³

¹ University of Aix-Marseille, Marseille, France, dtwhite@ualberta.ca

² University of Alberta, Edmonton, AB, Canada, gerda.devries@ualberta.ca

³ Ohio State University, Columbus, OH, USA, dawes.33@osu.edu

Microtubules and motor proteins interact in vivo and in vitro to form higher-order structures such as bundles, asters, and vortices. In vivo, the organization of microtubules is connected directly to cellular processes such as cell division, motility, and polarization. To address questions surrounding the mechanism underlying microtubule organization, we have developed a system of integro-partial differential equations that describes the interactions between microtubules and motor proteins [1, 2]. Our model takes into account motor protein speed, processivity, density, and directionality, as well as microtubule treadmilling and re-organization due to interactions with motors. Our model is able to provide a quantitative and qualitative description of microtubule patterning. Simulations results show that plus-end directed motor proteins form vortex patterns at low motor density, while minus-end directed motor proteins form aster patterns at similar densities. Also, a mixture of motor proteins with opposite directionality can organize microtubules into anti-parallel bundles such as are observed in spindle formation.

References

- [1] D. White, G. de Vries, and A. Dawes, *Microtubule patterning in the presence of stationary motor distributions*, Bull. Math. Biol. **76**, pp. 1917-1940 (2014).
- [2] D. White, G. de Vries, J. Martin, and A. Dawes, *Microtubule patterning in the presence of moving motor proteins*, J. Theor. Biol. (submitted, in review).

A Social Contact Model With Applications to Choice Disability, HIV Transmission, and Sexual Assault

R. deBoer¹

¹ University of Ottawa, Canada, rdeboer@uottawa.ca

The concept of choice disability includes a number of different factors, such as poverty and a lack of education, that may limit an individual's ability to make choices that might be beneficial. In particular, choice disability has been identified as an important driver of HIV transmission in contexts where many people cannot make choices to reduce their HIV risk [1]. Some choice disability factors occur only within relationships. For example income and educational disparities between sexual partners may reduce the power of one partner to negotiate safer sex practices such as condom use.

With this in mind, a mathematical model of choice disability focusing on social or sexual contacts is developed. The two sex population based model is a discretized version of a generalized kinetic model. Choice disability factors are accumulated through heterosexual contacts. The resulting social contact model is general enough to describe a number of different phenomena. Two different applications of the basic social contact model will be discussed. In addition describing the accumulation of choice disability factors for HIV transmission, the social contact model may also be used to model the incidence of sexual assault.

To model HIV transmission in the presence of choice disability, the social contact model is used as a setting for a multigroup SI model of disease transmission. The disease is transmitted through the same heterosexual contacts involved in the accumulation of choice disability factors with disease incidence dependant on choice disability status. Numerical simulations of this HIV model can be used to illustrate that intervention programs designed to prevent HIV by improving the choice disability status of some segments of the population may have unintended side effects in other segments of the population. These side effects may be either beneficial or detrimental to the success of an intervention program.

When used as a model of sexual assault, the model compartments describe the lifetime history of sexual assault focusing on female victims and male perpetrators. The sexual assault model can be used to compute estimates of the number of sexual assaults that go unreported provided that appropriate values for the model parameters are found. The extent to which the required parameters can be estimated using police report data will be discussed.

References

- [1] N. Andersson and A. Cockcroft, *Choice-Disability and HIV Infection: A Cross Sectional Study of HIV Status in Botswana, Namibia and Swaziland*, AIDS Behav. **16**, 1, pp. 189-198 (2012).

An interplay between division of labour and disease in a honeybee colony

V. Ratti¹, P. G. Kevan², H. J. Eberl³

¹ University of Guelph, Guelph, vratti@uoguelph.ca

² University of Guelph, Guelph, pkevan@uoguelph.ca

³ University of Guelph, Guelph, heberl@uoguelph.ca

The western honeybees are vanishing. Recent years have seen honeybees in distress, with up to 35% of colonies breaking down annually. These losses are usually associated with the Colony Collapse Disorder (CCD) or wintering losses. The main culprits causing colony collapse are the varroa mites and the deadly viruses they carry. The common symptoms of CCD are the absence of adult bees and their corpses in the collapsed colony. This indicates that the foragers that leave the colony never return back to the hive. Focussing on these causes and symptoms, we formulate a mathematical model for the honeybees-varroa mites-virus complex in which, based on division of labour, the bee population is divided into two categories: hive bees and forager bees. Hive bees are the bees that stay in the hive and take part in the tasks such as cleaning the comb, taking care of the brood and the queen etc. Foragers are the bees that leave the hive depending upon their age and other hive requirements to collect nectar, pollen etc. The model consists of ordinary differential equations for the dependent variables: uninfected hive bees, uninfected foragers, infected hive bees, number of mites overall, and of mites carrying the virus. The main objective of the model is to study the interplay between disease propagation and division of labour in a honeybee colony. The model focuses on Acute Bee Paralysis Virus and is studied with analytical and computational techniques. We use well established methods for autonomous systems to study the stability of equilibria. Using computer simulations, we investigate whether the results of the autonomous case carry over to the case where the coefficients are functions of time.

Backward Bifurcation in an Mathematical Model for HIV Infection in vivo with Anti-Retroviral Treatment

Michael Y. Li¹, Liancheng Wang²

¹ University of Alberta, Canada, mli@math.ualberta.ca

² Kennesaw State University, Atlanta, USA, lwang5@kennesaw.edu

Anti-retroviral treatments (ART) such as HAART have been used to control the replication of HIV virus in HIV-positive patients. In this study, we study an in-host model of HIV infection with ART and carry out mathematical analysis of the global dynamics and bifurcations of the model in different parameter regimes. Among our discoveries is a parameter region for which backward bifurcation can occur. Biologically, the catastrophic behaviors associated with backward bifurcations may explain the sudden rebound of HIV viral load when ART is stopped, and possibly provide an explanation for the viral blips during ART suppression of HIV.

Compartmental modeling for the transmission of Dengue in Guangzhou, China

Wenjing Zhang¹, Huaiping Zhu²

Department of Mathematics and Statistics, L.A.M.P.S., York University, Toronto, Canada

¹ Email: zhang.wenjing14@gmail.com

² Email: huaiping@mathstat.yorku.ca

Dengue, a mosquito-borne viral disease, hit a Chinese metropolis capital city Guangzhou in 2014, and caused the worst outbreak in two decades. Epidemiological and serological studies reveal three main reasons, which are unusual hot and warm weather, subsequent infection caused by co-circulation of multiple serotypes of dengue viruses, and imported infected cases from international travelling. Compartmental model is formulated to express the subsequent infection and imported cases, and then associated with a predictive statistic model [1] to describe the impact of weather conditions on mosquito abundance. The basic reproduction number [2, 3], R_0 , is derived to measure the ability of dengue outbreak in human population. Incorporating the local weather conditions and travelling cases, our simulation results demonstrate the complex dynamics of the dengue transmission, in particular, reveal the triggering factors responsible for the Guangzhou dengue outbreak in 2014.

References

- [1] J. Wang and N. H. Ogden and H. Zhu *The impact of weather conditions on Culex pipiens and Culex restuans (Diptera: Culicidae) abundance: A case study in Peel region* J. Med. Entomol. **48**, 2, pp. 468-475 (2011).
- [2] M. J. Wonham and T. de-Camino-Beck and M. A. Lewis *An epidemiological model for West Nile virus: invasion analysis and control applications*, Proc. R. Soc. Lond. B. **271**, pp. 501-507 (2004).
- [3] P. Van den Driessche and J. Watmough *Reproduction numbers and sub-threshold endemic equilibria for compartmental models of disease transmission*, Math. biosci. **180**, 1, pp. 29-48 (2002).

Coupling Fishery Dynamics, Human Health and Social Learning in a Model of Fish-borne Pollution Exposure

M. Yodzis¹, C.T. Bauch², M. Anand³

¹ University of Guelph, Canada, myodzis@uoguelph.ca

² University of Waterloo, Canada, cbauch@uwaterloo.ca

³ University of Guelph, Canada, manand@uoguelph.ca

Pollution-induced illnesses are caused by toxicants that result from human activity and should be entirely preventable. However, social pressures and misperceptions can undermine efforts to limit pollution, and vulnerable populations can remain exposed for decades. This talk presents a human-environment system model for the effects of water pollution on the health and livelihood of a fishing community. Such problems lie at the interface of biological ecosystem dynamics and human behaviour modelling. We incorporate dynamic social feedbacks that determine how effectively the population recognizes the injured and acts to reduce the pollution exposure. The model is motivated by an incident from 1949-1968 in Minamata, Japan where methylmercury effluent from a local factory poisoned fish populations and humans who ate them. We will discuss the conditions that allow for the outbreak of a pollution-induced epidemic, and explore the sensitivity of the model with respect to its parameters.

Disease extinction and re-emergence in differential-equation models

S.W. Greenhalgh¹, M.L. Ndeffo-Mbah², A.P. Galvani³, J. Medlock⁴

¹ Yale University, New Haven, USA, scott.greenhalgh@yale.edu

² Yale University, New Haven, USA, martial.ndeffo-mbah@yale.edu

³ Yale University, New Haven, USA, alison.galvani@yale.edu

⁴ Oregon State University, Corvallis, USA, jan.medlock@oregonstate.edu

Traditional differential equation models of disease transmission are often used to predict disease trajectories and evaluate the effectiveness of alternative intervention strategies. However, such models cannot account explicitly for probabilistic events, such as those that dominate dynamics when prevalence numbers are low. Here we present a novel approach, to account for the dynamics at low prevalence, i.e. extinction and re-emergence of infection, without the added analytical and computational complexity of a stochastic model. We apply our approach to analyze measles outbreaks from 1923 to 1938 in Iceland, providing insight on the temporary extinction of measles and the risk of re-emergence.

Dispersal Under Recolonization of Regenerating Landscape

R.C. Tyson¹, K. Larsen², S.M. Krone³

¹ University of British Columbia Okanagan, Kelowna, Canada, rebecca.tyson@ubc.ca

² Thompson Rivers University, Kamloops, Canada, klarsen@tru.ca

³ University of Idaho, Moscow, USA, krone@uidaho.edu

We present a study of the process whereby juveniles of a species disperse out of their natal landscape and recolonize rejuvenating landscapes nearby. This involves a significant number of long-distance dispersal events, which must occur, but which are difficult to measure in practise. Much previous research has used logical arguments coupled with mathematical models to derive plausible dispersal kernels for a variety of dispersal hypotheses. We turn this process on its head, developing an agent-based model incorporating well-studied dispersal behaviour, and then observe the dispersal kernel that results under various landscape configurations. We find that while the decision rules of the dispersing agents does not change, the dispersal kernel changes significantly under different landscape configurations and agent densities. In particular, as the recolonization invasion proceeds, the dispersal kernel varies across the landscape and across time.

Modelling Avian Influenza using Filippov Systems to determine Culling of Infected Birds and Quarantine

Nyuk Sian Chong¹, Robert Smith²

¹ Universiti Malaysia Terengganu, Malaysia. nchon077@uottawa.ca

² The University of Ottawa, Ottawa, Canada, rsmith43@uottawa.ca

The growing number of reported avian influenza cases has prompted awareness of the effectiveness of pharmaceutical or/and non-pharmaceutical interventions that aim to suppress the transmission rate. We propose two Filippov models with threshold policy: the avian-only model with culling of infected birds and the SIIR (Susceptible-Infected-Recovered) model with quarantine. The dynamical systems of these two models are governed by nonlinear ordinary differential equations with discontinuous right-hand sides. The solutions of these two models will converge to either one of the two endemic equilibria or the sliding equilibrium on the discontinuous surface. We prove that the avian-only model achieves global stability. Moreover, by choosing an appropriate quarantine threshold level I_c in the SIIR model, this model converges to an equilibrium in the region below I_c or a sliding equilibrium, suggesting the outbreak can be controlled. Therefore a well-defined threshold policy is important for us to combat the influenza outbreak efficiently.

Information Theory and the Evolvability of Biological Populations

Troy Day

Department of Mathematics and Statistics

Department of Biology

Queen's University, Kingston, Canada

tday@mast.queensu.ca

The term ‘evolvability’ refers to the ability of a population to evolve in response to novel environments and selective pressures. There is growing interest in quantifying evolvability in the context of both pure and applied evolutionary biology. For example, high evolvability is often desirable in bioengineering because one seeks to experimentally evolve new proteins or organisms. But high evolvability is undesirable in the context of invasive species because evolutionary change can enhance the invasion success of foreign species. In this talk I will show how some simple considerations from evolutionary biology lead naturally to ideas from information theory. In particular, I will show how the genetic information entropy of a population provides a general measure of its evolvability. Time permitting I will also discuss how these ideas lead to novel ways of quantifying pleiotropy as well as the dimensionality of organismal phenotypes.

Interactions Between Simultaneous Behaviourally-Driven Disease Interventions in a Model of Seasonal Influenza

M.A. Andrews¹, C.T. Bauch^{1,2}

¹ University of Guelph, Canada, {mandre04}@uoguelph.ca

² University of Waterloo, Canada, {cbauch}@uwaterloo.ca

The spread of infectious diseases can be inhibited by both vaccines and non-pharmaceutical interventions (NPIs) such as hand washing, respiratory etiquette, and social distancing. Theoretical models of disease spread have incorporated how individuals make decisions concerning these interventions in the face of disease risks and intervention costs [1]. However, previous models have generally considered these two intervention strategies separately from one another. Here, we utilize an agent-based simulation model on a contact network to simultaneously incorporate decision making processes for both of these intervention strategies with respect to seasonal influenza.

The choices of whether or not to vaccinate and practice NPIs in our model are driven by concepts from decision field theory [2]. This method allows us to capture the decision-making processes of individuals in an uncertain environment. These decisions are based on previous experience with the disease, the current state of infection amongst one's contacts, and the personal and social impacts of the choices they make.

We find that when considering these two major disease interventions as behaviourally-driven decisions, measures taken to increase the uptake of one intervention can alter transmission patterns, thus reshaping perceived risks which in turn reduce the uptake of the other intervention. The effectiveness of the interventions also play an important role in the level of interference each receives from the other. As a result, measures that support expansion of only vaccination (such as reducing vaccine cost), or measures that simultaneously support vaccination and NPIs (such as emphasizing harms of influenza infection, or satisfaction from preventing infection in others through both interventions) can significantly reduce influenza incidence, whereas measures that only support expansion of NPI practice (such as making hand sanitizers more available) have little net impact on influenza incidence. (However, measures that improve NPI efficacy may fare better.)

We conclude that the impact of interference on programs relying on multiple interventions should be carefully studied, for both influenza and other infectious diseases.

References

- [1] S. Funk and M Salathé and V.A. Jansen, *Modelling the influence of human behaviour on the spread of infectious diseases: a review*, Journal of the Royal Society: Interface **7**, pp. 1247-1256 (2010).
- [2] J.R. Busemeyer and J.T. Townsend, *Decision Field Theory: A Dynamic-Cognitive Approach to Decision Making in an Uncertain Environment*, Psychological Review **100**, pp. 432-459 (1993).

Mathematical Analysis of a Quorum Sensing Induced Biofilm Dispersal Model

B.O. Emerenini¹, S. Sonner², H.J. Eberl³

¹ University of Guelph, Canada, buzor@uoguelph.ca

² University of Kaiserslautern, Germany, sonner@mathematik.uni-kl.de

³ University of Guelph, Canada, heberl@uoguelph.ca

Biofilms are dense accumulations of microbial cells on biotic or abiotic surfaces (called substratum) in aqueous environment. Once the microbial cells become sessile, they produce extracellular polymeric substances (EPS), which provide mechanical stability and protection against antibiotic attacks and mechanical washout. Biofilm accumulation is determined by the balance of attachment, growth and detachment (or dispersal) processes [4]. Among these phenomenon, there is a growing interest in the study of detachment which is a release of microbial cells from the biofilm into the aqueous environment. One of the triggers of cell dispersal from biofilm is quorum sensing [5]. This is a cell-cell communication that arise among bacterial cells that produce chemically signalling molecules called autoinducers. The detection of an apparent threshold stimulatory concentration of an autoinducer leads to an alteration in gene expression and this is called quorum sensing.

Presently, we are concerned with a mathematical description and analysis of a quorum sensing induced detachment model which was proposed in [3]. This is a system of non-linear, density-dependent diffusion-reaction equations. The model for the sessile biomass consists of non-linear diffusion effect, a degeneracy - as in the porous medium equation; and a fast diffusion. The quorum sensing induced biofilm detachment model [3] is an extension of a prototype model that was proposed for a single species biofilm. In fact, in the absence of the production of the quorum sensing signal molecule and the dispersed cells, the model reduces to a prototype growth model for the biomass and a single substrate. Such mono-species single-substrate biofilm models have been studied both analytically and numerically. Albeit the inclusion of the signal molecule production and the dispersal makes it complex having multi-component for a mono species.

We prove the existence of a unique bounded solution of the degenerate problem proposed in [3] by studying a system of non-degenerate auxiliary equation and passing to the limits using the results obtained for a single-species model in [2] and that of multi-component model [1]

We present analytical results to show the well-posedness of the quorum sensing controlled detachment model. The existence results are formulated assuming homogeneous Dirichlet boundary conditions for the sessile biomass, dispersed cells and the signal molecule, which results in a microfloc (i.e. biofilm without a substratum). The well-posedness carries over to the biofilm case. The simulation results also reveal hollowing in microfloc, which is a dynamic feature that changes in size and depth over time. We also use numerical simulations to illustrate the behavior of the solution.

References

- [1] Eberl HJ, Effendiev MA, Sonner S: *On the Well-Posedness of Mathematical Models for Multicomponent Biofilms* Math. Meth. Appl. Sc., 2013 submitted
- [2] Efendiev MA, Eberl HJ, Zelik SV: *Existence and Longtime Behavior of a Biofilm Model* Communications on Pure and Applied Mathematics 2009 8(2), pp. 509-531.
- [3] Emerenini BO, Eberl HJ, Kuttler C, Hense BA : *A Mathematical Model of Quorum Sensing Induced Detachment* 2014, submitted.
- [4] Trulear MG, Characklis WG: *Dynamics of biofilm processes*. J.Water Pollut. Control Fed. 1982 54:1288-1301.
- [5] Webb JS: *Differentiation and dispersal in biofilms*, Book chapter in "The Biofilm Mode of Life: Mechanisms and Adaptations", Horizon Bioscience, Oxford 2007, pp. 167-178

Mathematical Approach to Reduce the Enzymatic Inhibition for Maximum Production of Biodiesel through J.C. Oil

Priti Kumar Roy*, Jahangir Chowdhury and Fahad Al Basir

*Centre for Mathematical Biology and Ecology
Department of Mathematics, Jadavpur University
Kolkata - 700032, India*

*Corresponding Author Email:pritiжу@gmail.com
Research is supported by UGC, Government of India.

An enormous importance for the production of biodiesel has increased significantly in recent years. The needs for an alternative fuel from renewable resources like Jatropha Curcas Oil which can produce Triglyceride have been employed as feedstocks for biodiesel production. In order to a sustainable biodiesel production, a proper understanding of the inhibition reaction process through the factors like concentration of enzyme, alcohol (methanol/ ethanol), and glycerol is to be needed. In this research article, a mathematical model of enzymatic process is formulated to describe the kinetics of the transesterification and inhibition of enzyme by methanol and glycerol. Our results contemplated the effect of ethanol and enzyme concentrations towards the system. Using control theoretic approach we have also reformed to produce maximum biodiesel production with minimum inhibition of the enzyme. Our analytical results validate our numerical results.

Keywords: Biodiesel, Jatropha Curcas Oil, Enzymatic Inhibition, Transesterification, Control Theoretic Approach.

References

- [1] P. K. Roy, S. Datta, S. Nandi and F. A. Basir, *Effect of Mass Transfer Kinetics for Maximum Production of Biodiesel from Jatropha Curcas Oil: A Mathematical Approach*, Fuel, **134**, pp. 39-44 (2014).
- [2] F. A. Basir and P. K. Roy, *Production of Biodiesel using Enzymatic Transesterification of Jatropha Curcas Oil: A Mathematical Study*, Mathematics in Engineering, Science and Aerospace, **5**, 1, pp. 175-184 (2014)

Modeling dynamic changes in immune tolerance during type 1 diabetes progression: Investigating the contribution of pancreatic beta-cell suicide and homicide in type 1 diabetes

Majid Jaber-Douraki¹

¹ Department of Physiology, McGill University, Montreal, QC, Canada, Majid.Jaber-Douraki@Mail.Mcgill.ca

It has been suggested that disease progression in type 1 diabetes, an autoimmune disease mediated by autoreactive effector T-cells (Teffs) that target and kill insulin-secreting pancreatic beta-cells, may additionally involve protective mechanisms to impede such auto-destructive mechanisms. Regulatory T cells (Tregs) for example play a crucial role in immunomodulation by suppressing effector T cells. Furthermore, metabolic stress caused by beta-cell loss triggers a series of signal transduction cascades, commonly termed the adaptive unfolded protein response, in surviving beta cells to restore normal insulin synthesis required for maintaining glucose homeostasis. Mathematical and computational methods are powerful techniques to investigate the interactions of these components in this system and decipher the mechanisms regulating their dynamics. In this talk, I will present a summary of our most recent findings of how this system behaves quantitatively under various conditions.

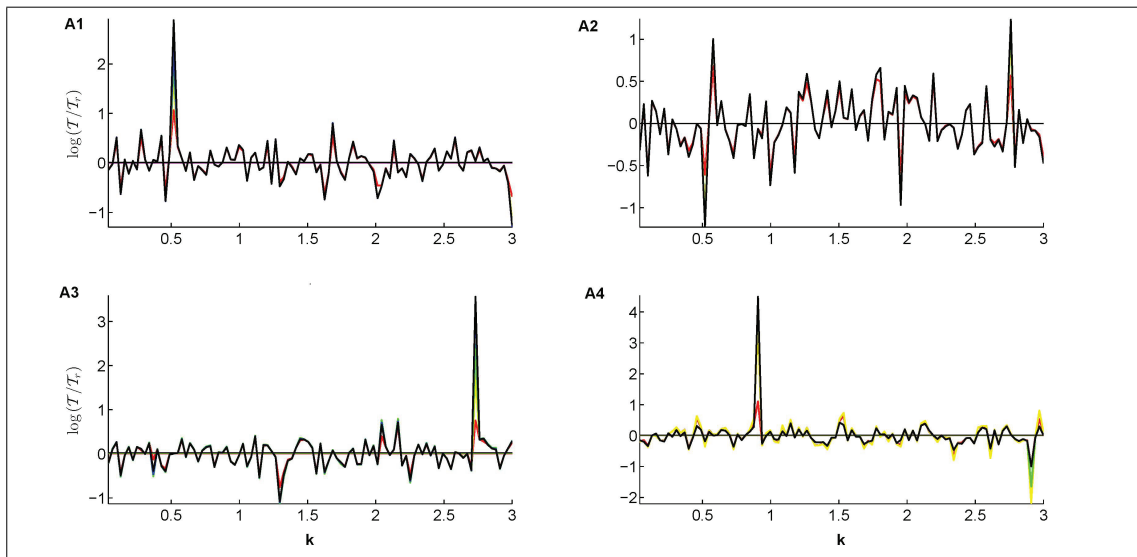


Figure 1: The ratios of effector-to-regulatory T-cells (each averaged over 10 years) for 4 distinct cases listed are displayed in logarithmic scale at 5 different points in time. The presence of very pronounced negative (positive) peaks at specific values of k (T-cell avidity) reflects Treg-dominance (Teff-dominance) over Teffs (Tregs).

References

- [1] Jaber-Douraki M. Khadra A. Pietropaolo M. *Continuum Model of T-cell Avidity: Understanding Autoreactive and Regulatory T-Cell Responses in Type 1 Diabetes*. Immunology & Cell Biology. Nature Publishing Group. In review.
- [2] Jaber-Douraki. M. Pietropaolo M. Schnell S. Khadra A. *Unraveling the contribution of pancreatic beta-cell suicide in autoimmune type 1 diabetes*. Journal of Theoretical Biology, In press (2015).
- [3] Jaber-D. M. Liu SW. Pietropaolo M. Khadra A. *Autoimmune Responses in T1DM : Quantitative Methods to Understand Onset, Progression and Prevention of Disease*. Pediatric Diabetes. 15(3)(2014) : 162-174.
- [4] Jaber-D. M. Pietropaolo M. Khadra A. *Predictive Models of Type 1 Diabetes Progression : Understanding T-Cell Cycles and Their Implications on Autoantibody Release*. PLoS ONE 9(4)(2014) : e93326.

Modeling, analysis, and simulation of a chemostat with wall attached and suspended bacterial growth, with an application to nitrification in a wastewater biofilm reactor

H.J. Eberl¹, A. Masic²

¹ University of Guelph, Canada; heberl@uoguelph.ca

² EAWAG, Switzerland

Bacteria tend to form bacterial biofilms, i.e. aggregates of microbes on immersed surfaces. In these biofilms rate controlling dissolved substrates, such as oxygen or carbon sources are subject to diffusion and reaction, leading to substrate gradients. As a consequence, bacteria in different layers of a biofilm experience different growth conditions.

While many biological wastewater technologies are designed as pure biofilm processes there is indeed a continuous exchange of biomass between wall attached biofilms and the suspended bacteria. A simple well-known mathematical model for such systems with wall-attached and suspended growth is the Freter model, which however neglects the diffusion gradients in the biofilm and assumes an implicitly predefined maximum biofilm thickness. We will overcome this limitation by replacing the simplified biofilm description with the standard Wanner-Gujer biofilm model from the engineering literature. In the simple case of a single biomass type and a single growth limiting substrate this can formally cast as a system of three ODEs, the evaluation of the right hand side of which, however, requires the solution of a two-point boundary value problem. We will study this model with a mix of analytical and numerical techniques.

We will then extend the model concept to a more involved system that describes nitrification in a biofilm reactor. In this scenario two active and one inert biomass fraction are accounted for and four types of dissolved substrates. The biofilm in this cases is modeled by a hyperbolic free boundary value problem with nonlocal reactions for the biomass fractions, coupled with two-point boundary values problems for the dissolved substrates in the biofilm. This biofilm model is embedded in a system of reactor-level mass balances, formulated as ordinary differential equations. This extended model is too involved to lend itself to insightful mathematical analysis, wherefore we investigate it in extensive numerical simulations.

Modelling and analysis of the relapse-remission behavior in autoimmune diseases

Wengjing Zhang¹, Lindi M. Wahl², Pei Yu³

¹ Department of Mathematics and Statistics, L.A.M.P.S., York University, Toronto, Canada, zhang.wenjing14@gmail.com

² Applied Mathematics, Western University, London, Canada, lwahl@uwo.ca

³ Applied Mathematics, Western University, London, Canada, pyu@uwo.ca

Relapse-remission behavior occurs in many autoimmune diseases, even in the absence of treatment, such as multifocal osteomyelitis, eczema, subacute discoid lupus erythematosus, and psoriasis. Although the phenomenon attracts much attention in recent research [1, 2], its etiology is still not well understood. Thus, an improved understanding of relapse-remission dynamics in autoimmune disease is crucial to promote correct diagnosis, patient management and treatment decisions. In this project, we present a 4-dimensional ODE autoimmune model to investigate the relapse-remission pattern. This model incorporates a newly discovered class of terminally differentiated regulatory T cells, HLA-DR⁺ T_{Reg} cells, into an established T cell-mediated autoimmune disease model [3]. Moreover, the relapse-remission behavior is preserved in the reduced and scaled 3- and 4-dimensional models. Qualitative analysis is carried out for the 3- and 4-dimensional models based on dynamical systems theory and bifurcation theory with the help of the symbolic computation program, Maple. The normal form of Hopf bifurcation is computed via an established Maple program developed in [4]. We proved that the relapse-remission behavior (or oscillation) arises due to a Hopf bifurcation or a persistent oscillation rather than homoclinic orbits. Numerical simulations are given to verify the analytical results and identify the relapse-remission parameter region.

References

- [1] W. Zhang and L. M. Wahl and P. Yu *Viral blips may not need a trigger: How transient viremia can arise in deterministic in-host models*, SIAM Rev., **56**, pp. 127-155 (2014).
- [2] N. V. de Mendizábal and J. Carneiro and R. V. Solé and J. Goñi and J. Bragard and I. Martínez-Forero and S. Martínez-Pasamar and J. Sepulcre and J. Torrealdea and F. Bagnato and J. García-Ojalvo and P. Villoslada, *Modeling the effector - regulatory T cell cross-regulation reveals the intrinsic character of relapses in Multiple Sclerosis*, BMC Systems Biology, **5**, 114, pp. 1-15 (2011).
- [3] H. K. Alexander and L. M. Wahl, *Self-tolerance and Autoimmunity in a Regulatory T Cell Model*, Bull. Math. Biol. **73**, 1, pp. 33-71 (2010).
- [4] P. Yu, *Computation of normal forms via a perturbation technique*, J. Sound Vibration, **211**, pp. 19-38 (1998).

Modelling Contact Tracing in Control of Epidemic Diseases

X. Huo^{1,2}, K. Lan¹, J. Wu²

¹ Ryerson University, Toronto, Canada

² York University, Toronto, Canada

Aside from identified case isolation, vaccination and quarantine are additional control measures in preventing an epidemic disease transmission at the beginning of the outbreak. In many cases, there are two alternative ways to conduct such controls, namely targeted control or mass control. For example, vaccinating or quarantining the close contacts of known infectives is a typical targeted control method; mass vaccination (such as flu shots) or school closing is categorized as mass control method. Targeted control methods, which rely on the process of contact tracing, are essential interventions in controlling outbreaks of emerging or re-emerging infectious diseases, such as Ebola, SARS (Severe Acute Respiratory Syndrome), H1N1, smallpox, etc. We will present a mathematical model that could help predict the outcomes and assess the effectiveness of the two major public health interventions in epidemic outbreak controls: (1) identifying and isolating symptomatic cases, and (2) tracing of their contacts, followed by isolation, quarantine, or vaccination. Applications on the control of SARS, smallpox, or Ebola Virus Disease will be discussed and presented if time permits.

Modelling human-environment interactions and their impact on conservation incentive effectiveness in forest ecosystems

C.T. Bauch¹, K. Henderson², A. Cecile³, L. Barlow⁴, M. Anand⁵

¹ University of Waterloo, Waterloo, Canada, cbauch@uwaterloo.ca

² University of Guelph, Guelph, Canada, hendersk@uoguelph.ca

³ University of Guelph, Guelph, Canada, alice.i.cecile@gmail.com

⁴ University of Guelph, Guelph, Canada, leann.barlow@gmail.com

⁵ University of Guelph, Guelph, Canada, manand@uoguelph.ca

On shorter timescales, it is possible to treat human impacts on ecosystems as fixed, and likewise to treat ecosystem impacts on humans as fixed. However, on sufficiently long timescales, both ecosystems and human systems respond to one another, forming a single, fully coupled human-environment system (HESs). In this talk I will describe two recent models concerning the effectiveness of forest conservation incentives in the face of human-environment feedbacks, in the context of (1) firewood movement restrictions for preventing the spread of forest pest infestations in Canada, and (2) forest conservation incentives and penalties to promote afforestation in Brazil. We find that social processes can fundamentally alter ecosystem dynamics. For instance, introducing human-environment feedback can increase the number of stable system states. It can also mitigate conservation strategies, by reducing their effectiveness through negative feedbacks, or by causing instabilities in the form of oscillations. We conclude that HES models can help us entertain possibilities that we might not otherwise have thought of, and in the future may also have some predictive power. Human-environment feedbacks should be more extensively analyzed during the design and implementation of forest conservation policies. This work is conducted jointly with Madhur Anand, Kirsten Henderson, Alice Cecile, and Lee-ann Barlow.

Modelling RNA Replication in the RNA World

Paul G. Higgs

McMaster University, Hamilton, Canada. higgsp@mcmaster.ca

The RNA World is a period thought to have existed in the early evolution of life on Earth when RNA sequences acted as both genes and catalysts. A key component of the RNA world would have been a polymerase that acts on a template strand to make a complementary strand to the template. Sustained replication is possible by this means if the polymerase is able to deal with templates that are at least as long as itself and if the accuracy of replication is sufficient to preserve the sequence against accumulation of mutations. A polymerase is a co-operator in the sense that it copies other strands and requires other strands to copy it [1]. As in many areas of evolutionary biology, co-operators are vulnerable to being destroyed by parasites. In the RNA World, any strand that can act as a template is potentially a parasite of the polymerase. A polymerase would first arise in a prebiotic world that must have already contained many random non-functional sequences, so it would be born into a world full of parasites.

In previous studies using mathematical and computational models, we have shown that a polymerase can indeed survive and spread if diffusion is relatively slow and spatial clustering of strands arises [2]. In this case, co-operative strands tend to interact with other co-operative strands and help one another. In contrast, if the system is well mixed, encounters between strands occur at random, and parasites tend to invade and destroy the polymerases. Spatial clustering also greatly facilitates the origin of life in models that consider the transition from a non-living to a living state [3].

Currently we are developing these spatial models of RNA replication to investigate the conditions in which other ribozymes having useful functions can coexist with a polymerase. A nucleotide synthase could help a polymerase by increasing the monomer concentration but it would be dependent on the polymerase for its own replication. However, a synthase also takes time and resources away from the polymerase itself. In well mixed systems, we find that the synthase either replicates more slowly than the polymerase, in which case it dies out, or it replicates faster than the polymerase, in which case it behaves like a parasite and destroys the system. However, in spatial models there is a possibility of stable coexistence of the two catalysts, and there are parameter ranges where the two can survive together but neither could survive on its own. This is relevant to understanding the way a single component polymerase system could have evolved towards a complex metabolism involving many different mutually dependent catalysts with different functions.

References

- [1] P.G. Higgs, and N. Lehman, *The RNA World: molecular co-operation at the origin of life*. Nature Rev. Genet. **16**, 7-17 (2015).
- [2] J.A. Shay, C. Huynh and P.G. Higgs, *The origin and spread of a cooperative replicase in a prebiotic chemical system*. J. Theor. Biol. **364**, 249-259 (2015).
- [3] M. Wu and P.G. Higgs, *The origin of life is a spatially localized stochastic transition*. Biology Direct **7**: 42 (2012).

Multitype Branching Processes in Continuous Time Predict Adaptation Rates in Bacteria

L. M. Wahl¹ and A. D. Zhu²

¹ Western University, London, Canada, lwahl@uwo.ca

² Western University, London, Canada, azhu4@uwo.ca

The extinction probability of a branching process is sensitive to both the mean and variance of the offspring distribution. For rare beneficial mutations that arise during adaptation, many approaches accurately approximate the mean number of offspring in the mutant lineage, but the variance in this number is sensitive to the details of the model. Here we develop a life-history model for bacterial populations in experimental settings, and predict the survival of mutations that increase the mean number of offspring through their effects on specific traits: lag time, fission time, viability and the timing of stationary phase. We proceed by deriving, from first principles, a partial differential equation describing the time evolution of a multitype probability generating function. The multitype approach allows us to generate realistic gamma-distributed lifetimes for daughter cells in the lineage, using a chain of exponentials. Repeated population bottlenecks, which are imposed both in laboratory and natural settings, are also considered. Our results demonstrate that mutations that have the same effect on growth rate, once established, can have very different probabilities of escaping extinction when rare, depending on the trait affected. We further predict that approximately five-fold population growth between bottlenecks will optimize the adaptation rate.

New reaction kinetics for models of disinfection of microbial biofilms by antibiotics

Kazi A. Rahman¹, Otini Kroukamp², Gideon M. Wolfaardt^{2,3}, Hermann J. Eberl¹

¹*Dept. Mathematics and Statistics, University of Guelph, Guelph, Canada, {krahman,heberl}@uoguelph.ca*

²*Dept. Chemistry and Biology, Ryerson University, Toronto, Canada, {mkroukam,gwolfaar}@ryerson.ca*

³*Water Institute, Stellenbosch University, Stellenbosch, South Africa*

Recent laboratory experiments showed increased metabolic activity, measured in terms of carbon dioxide production during periods of exposure of bacterial biofilms to antibiotics, a phenomenon that is not reflected by current biofilm models. In order to incorporate this observation in models of disinfection of microbial biofilms we introduce extended reaction kinetics based on carbon consumption during disinfection. We implement this extension in a 0-dimensional simplified reactor scale model (ODE) where carbon substrates and antibiotics are well mixed but biomass is attached to the wall and not washed out, and in a highly nonlinear 2-dimensional density dependent cross-diffusion model (PDE), that considers spatial effects, such as substrate gradients and heterogeneous biofilm architectures. Our simulations show that the extended model captures the experimental observation, and suggest that the consumption of carbon substrates during inactivation due to antibiotics helps biofilms to survive and re-grow. Not accounting for this effect in a model might lead to false negatives, over-predicting the efficacy of antibiotic disinfection.

Nilpotent Singularities and Dynamics in an SIR Type of Compartmental Model with Hospital Resources

Chunhua Shan

University of Alberta, Canada, cshan@ualberta.ca

An SIR type of compartmental model with a standard incidence rate and a nonlinear recovery rate was formulated to study the impact of available resources of public health system especially the number of hospital beds. Cusp, focus and elliptic type of nilpotent singularities of codimension 3 were discovered and analyzed in this three dimensional model. Complex dynamics of disease transmission including multi-steady states and multi-periodicity were revealed by bifurcation analysis. Large-amplitude oscillations found in our model provide a more reasonable explanation for disease recurrence. With clinical data, our studies have practical implications for the prevention and control of infectious diseases.

Non-standard numerical schemes for approximating predator-prey dynamics

B.D. Corbett¹

¹ University of Guelph, Guelph, corbettb@uoguelph.ca

We examine a non-standard finite-difference scheme constructed to simulate a predator-prey model of Gause-type with a generalized functional response. It is shown that the scheme preserves the physical properties of the model and gives results that are qualitatively equivalent to the dynamics of the model. In particular the nonstandard scheme preserves the model's non-negative feasibility region, its equilibrium points, and their bifurcations. It is also shown that the scheme undergoes supercritical Hopf bifurcation for a specific value of the bifurcation parameter. This leads to a stable limit cycle created by the scheme when the bifurcation parameter passes through the same value found in the continuous model.

References

- [1] S.M. Moghadas, M.E. Alexander, and B.D. Corbett, *A nonstandard numerical scheme for a generalized Gause-type predator-prey model.* in *Phys. D : Nonlinear Phenomena.* **188**(12) (2004), 134-151.
- [2] S.M. Moghadas, M.E. Alexander, B.D. Corbett, and A.B. Gumel, *A positivity-preserving Mickens-type discretization of an epidemic model.* in *Journal of Difference Equations and Applications* **9**(11) (2003), 1037-1051.

On a reaction diffusion system for the sterile insect release method in a bounded domain

Xin Li¹, Weihua Jiang¹, Xingfu Zou²

¹ Harbin Institute of Technology, Harbin, China

² University of Western Ontario, London, Canada, xzou@uwo.ca

In this talk, I will present some recent results on a reaction diffusion system a bounded domain which describes the interaction of fertile and sterile insects. Two releasing strategies for the sterile strain will be be discussed, one is domain-wise release and the other is release only on the boundary. By analyzing the models, we obtain some conditions that ensure the success of the sterile release method in eradicating the insects.

On the co-infection of malaria and schistosomiasis

K.O. Okosun

Vaal University of Technology, South Africa, kazeemo@vut.ac.za

Malaria and schistosomiasis often overlap in tropical and subtropical countries and impose tremendous disease burdens. In this paper, a mathematical model for malariaschistosomiasis co-infection is formulated in order to investigate their synergistic relationship in the presence of treatments. The single infection steady states is analyze, and also calculate the basic reproduction number and then investigate the existence and stability of equilibria. Then the co-infection model, is analyze. The single and co-infection models are found to exhibit backward bifurcations. The impact of schistosomiasis and its treatment on the dynamics of malaria is further investigated. It is also found that malaria infection may be associated with an increased risk of schistosomiasis and also schistosomiasis infection is associated with an increased risk for malaria.

References

- [1] Doumbo S, Tran TM, Sangala J, Li S, Doumtabe D, et al. 2014. Co-infection of Long-Term Carriers of Plasmodium falciparum with Schistosoma haematobium Enhances Protection from Febrile Malaria: A Prospective Cohort Study in Mali. *PLoS Negl Trop Dis* 8(9): e3154. doi:10.1371/journal.pntd.0003154
- [2] Semenya, A.A., Sullivan, J.S., Barnwell, J.W., Secor, W.E., 2012. Schistosoma mansoni Infection Impairs Antimalaria Treatment and Immune Responses of Rhesus Macaques Infected with Mosquito-Borne Plasmodium coatneyi. *Infection and Immunity*. 80(11): 38213827
- [3] Chiyaka, E.T., Garira, W., 2009. Mathematical analysis of the transmission dynamics of schistosomiasis in the human-snail hosts. *Journal of Biological Systems*. 17(3): 397423

Refining a theory for the alternative life history strategies of a freshwater fish

M. Zhou¹, G. Wild²

¹ Department of Applied Mathematics, The University of Western Ontario, London, Canada mzhou224@uwo.ca

² Department of Applied Mathematics, The University of Western Ontario, London, Canada gwild@uwo.ca

The *life history strategy* of an organism refers to its schedule of reproductive development, as well as various aspects of its morphology and behaviour related to reproduction. Life history strategies provide biologists with many examples of the remarkable variety that is possible within natural populations. For example, certain male sunfish (*Lepomis macrochirus*) mature late, are large in size, construct nests for spawning, and provide parental care to eggs and larvae, whereas other male sunfish, mature early, are small in size, and achieve reproductive success by cuckolding their larger counterparts [1].

Examples like those provided by male sunfish raise important questions [2]. Why might selection give rise to different solutions to, ostensibly, the same problem? What ecological conditions influence the coexistence of these different solutions? Charnov and Gross [1] have provided a partial answer to these questions, as they apply to sunfish. These authors argued that strategies coexist when their respective fitness returns are equal. Furthermore, they used a continuous-time age-structured model to predict that selection will favour those males for whom the likelihood of developing into the smaller type is equal to the fraction of paternity they steal from others.

Although it is straightforward mathematically, the prediction made by Gross and Charnov [1] relies on important, tacit assumptions. Importantly, these assumptions do not reflect key aspects of sunfish biology. The purpose of our work, then, is to make biologically relevant refinements to Gross and Charnov's basic model, and evaluate the extent to which these refinements alter their prediction. We build a dynamical model of a sunfish population, then apply adaptive dynamics [3] to develop new predictions about the male life-history strategies. In particular, we investigate the effects that spatial clumping of nests, and interference competition among small males have, respectively, on the likelihood of using one life-history strategy or another. We conclude that our refinements do change the original predictions, but the extent to which this improves our understanding of data remains equivocal.

References

- [1] M. Gross and E. L. Charnov, *Alternative male life histories in bluegill sunfish*, Proc. Natl. Acad. Sci. USA **77**, 11, pp. 6937–6940 (1980).
- [2] M. Taborsky and H. J. Brockman, *Alternative reproductive tactics and life history phenotypes*, in P. Kappeler (ed.) *Animal Behaviour: Evolution and Mechanisms*, Springer, pp. 537–586 (2010) Adv. Math. **211**, 1, pp. 123–151 (2007).
- [3] U. Dieckmann and R. Law, *The dynamical theory of coevolution: a derivation from stochastic ecological processes*, J. Math. Biol. **34**, 579–612 (1996).

Seasonality and predation: what happens when hunting behavior changes?

F. Lutscher¹, R. Tyson²

¹ University of Ottawa, Canada, flutsche@uottawa.ca
² University of British Columbia rebecca.tyson@ubc.ca

Predators are typically categorized as either specialists or generalists, depending on whether they solely rely on a single focal prey for their survival or not. This difference is reflected in the mathematical formulation of the predation term, most commonly as a type II or type III functional response. There is, however, strong evidence that some predators change their behavior from generalist in the summer season when alternative prey is plentiful to specialist in the winter season when alternative prey is scarce.

In this talk, I will present a two-season model for a focal prey and a predator, whose behavior changes from specialist to generalist. Accordingly, the functional response will switch between seasons. I will illustrate the qualitative behavior of the system and compare it with a temporally averaged model. It turns out that the averaged system describes the dynamics of the seasonally varying system quite well for realistic parameter values of the Great horned owl and snowshoe hare system in Western Canada. The qualitative dynamics of the system are much more interesting than those typically found in two-species predator-prey models; they include global bifurcations of limit cycles, and a stable limit cycle coexisting with a stable equilibrium.

I will discuss the results in the light of latitudinal and elevational gradients as well as under a global change scenario.

Sensitivity of the General Rosenzweig–MacArthur Model to the Mathematical Form of the Functional Response: a Bifurcation Theory Approach

Gunog Seo¹, Gail S. K. Wolkowicz²

¹ Colgate University, USA, gseo@colgate.edu

² McMaster University, Canada, wolkowic@mcmaster.ca

The equations in the Rosenzweig–MacArthur predator-prey model have been shown to be sensitive to the mathematical form used to model the predator response function even if the forms used have the same basic shape: zero at zero, monotone increasing, concave down, and saturating. Here, we revisit this model to help explain this sensitivity in the case of Holling type II, Ivlev, and Trigonometric response functions. We consider both the local and global dynamics and determine the possible bifurcations with respect to variation of the carrying capacity of the prey, a measure of the enrichment of the environment. We give an analytic expression that determines the criticality of the Andronov-Hopf bifurcation, and prove that although all three forms can give rise to supercritical Andronov-Hopf bifurcations, only the Trigonometric form can also give rise to subcritical Andronov-Hopf bifurcation and has a saddle node bifurcation of periodic orbits giving rise to two coexisting limit cycles, providing a counterexample to a conjecture of Kooij and Zegeling. We also revisit the ranking of the functional responses, according to their potential to destabilize the dynamics of the model and show that given data, not only the choice of the functional form, but the choice of the number or position of the data points can influence the dynamics predicted.

Spatially Structured Neural Systems

P. Greenwood¹

¹ University of British Columbia, Vancouver, Canada, pgreenw@math.ubc.ca

Stochastic reaction diffusion equations can express the local dynamics of neuron populations together with the coupling of neighboring populations of neurons. We specialize ideas from a 2014 paper on pattern formation of McKane, Biancalani, and Rogers. We recall well-known conditions for Turing patterns of deterministic systems and introduce conditions for stochastically sustained neural patterns. We attempt to interpret an approximation result for oscillations sustained by noise (quasi-cycles) of Baxendale and G., 2011, in this setting. A goal is to model spatial neural phenomena such as patterned visual hallucinations.

Strategies for Early Vaccination During Novel Influenza Outbreaks

Yanyu Xiao

University of Alberta, Edmonton, yanyuxiao@gmail.com

In this work, we attempted to evaluate the potential benefits of early vaccination from both public health and socioeconomic perspectives. Given the availability of a strain-specific vaccine during the early stages of a pandemic, we sought to examine the effectiveness of different vaccination strategies in reducing attack rates in the population. For this evaluation, we developed an agent-based simulation model considering the effect of vaccination based on previously established frameworks. We present the results of this model and place the findings in the context of public health policy for immunization. This is a collaboration work with Drs. Laskowski and Moghadas.

Target Reproduction Numbers in Population Biology

Zhisheng Shuai¹

¹ University of Central Florida, Orlando, USA. shuai@ucf.edu

There are several important threshold parameters in the literature on population dynamics that determine the population persistence and disease invasibility. For example, the population growth rate and the net reproductive ratio are often derived in matrix population models to determine whether the population persists or goes to extinction. In mathematical epidemiology, the basic reproduction number often serves as a sharp threshold parameter determining whether or not a disease dies out; type reproduction numbers [1, 3] and target reproduction numbers [2, 4] recently are introduced for measuring disease control strategies in a heterogeneous host population. In this talk the concept of the target reproduction number is extended to a more general setting so that it unifies all the above threshold parameters and resolves confusions about their connections.

This is a preliminary report on joint work with Mark Lewis and Pauline van den Driessche.

References

- [1] J.A.P. Heesterbeek and M.G. Roberts, *The type-reproduction number T in models for infectious disease control*, Math. Biosci. **206**, pp. 3–10 (2007).
- [2] J.W. Moon, Z. Shuai and P. van den Driessche, *Walks and cycles on a digraph with application to population dynamics*, Linear Algebra Appl. **45**, pp. 182–196 (2014).
- [3] M.G. Roberts and J.A.P. Heesterbeek, *A new method for estimating the effort required to control an infectious disease*, Proc. R. Soc. Lond. B **270**, pp. 1359–1364 (2003).
- [4] Z. Shuai, J.A.P. Heesterbeek and P. van den Driessche, *Extending the type reproduction number to infectious disease control targeting contacts between types*, J. Math. Biol. **67**, pp. 1067–1082 (2013).

The Birth-Death-Diversification Model of Mobile Genetic Elements in Prokaryotes: A Location-Based Model Using Mobile Promoter Data from Sequenced Prokaryotic Genomes

M. Rabbani¹, Lindi M. Wahl²

¹ Western University, London, Canada, mrabbani@uwo.ca

² Western University, London, Canada, lwahl@uwo.ca

The role of mathematical modelling and scientific computing in the progress of biological sciences is unquestionable. Without a doubt, genetics is one of the fields most impacted by these approaches, and recent remarkable achievements in this area couldn't be accomplished without the benefits of modelling and computation.

The field of genetics has typically focused on coding DNA, and the non-coding regions were considered to be "junk DNA" which has no function. In more recent years however, there has been a growing interest in the importance of non-coding DNA, such as mobile genetic elements, also known as "selfish DNA". Mobile or transportable elements (TEs) are DNA sequences which are able to link themselves into new sites of the genome(s) and are considered as the key source of alteration in genome architecture. Because of their crucial influence in genome plasticity, various mathematical and statistical models have been developed to describe the dynamics of these mobile elements during genome evolution.

In this study, we extend previous work on birth-death-diversification model [1] of a class of MGEs known as mobile promoters, and propose a novel location-based model for the evolution of these elements. The new model incorporates two biologically meaningful regions of the genome: inside promoter regions, and other sites of the genome. When applied to real data, obtained by scanning all available sequenced prokaryote genomes with the aid of sequence searching programs (e.g. BLAST), differences between these two regions are compared with regards to the rates of four key factors in the genome evolution: gene duplication, gene loss, gene diversification and horizontal gene transfer (HGT).

References

- [1] Mark WJ van Passel, Harm Nijveen, and Lindi M Wahl. Birth, death, and diversification of mobile promoters in prokaryotes. *Genetics*, 197(1):291–299, 2014.

The importance of cell-to-cell transmission during the acute stage of HIV infection

C. Wells¹, A. Perelson², A. Galvani^{1,3}

¹ Center for Infectious Disease Modeling and Analysis, Yale School of Public Health, CT, USA, chad.wells@yale.edu

² Theoretical Biology and Biophysics, Los Alamos National Lab, NM, USA

³ Epidemiology of Microbial Diseases, Yale School of Public Health, CT, USA

HIV can infect cells through cellular conjugates, which is a process known as cell-to-cell transmission. Cell-to-cell transmission reduces the neutralizing effects of antibodies and some therapeutic drugs. HIV can also infect cells through free virus transmission, but the virus is exposed to the neutralizing effects of antibodies and therapeutic drugs. Both cell-to-cell transmission and free virus transmission occur during the acute stage of infection. However, it is unclear as to what their relative contributions are to the establishment and persistence of HIV within the host. The establishment of persistent HIV infection is highly dependent on the early stages of infection. Once infection is established, HIV disseminates to various lymphatic tissues, such as the lymph nodes, spleen, and gut. One of the most successful approaches in treating HIV infection is through the administration of therapeutic drugs, such as protease inhibitors and reverse transcriptase inhibitors. However, one of the main challenges in HIV treatment is the heterogeneity of drug concentrations in underlying tissues and organs. In addition, the immune response is heterogeneous among the various tissues, thereby clearing HIV at different rates. Therefore, we have developed a spatial within-host model for HIV infection that stratifies the peripheral blood and lymphatic tissue to quantify the role of cell-to-cell transmission in early HIV infection and evaluate the different classes of therapeutic drugs. Specifically, we used empirical concentrations of reverse transcriptase inhibitors and protease inhibitors from various tissues to evaluate the effectiveness of a combination antiretroviral therapy. Our model tracks the assembly and disassembly of cellular conjugates to quantify the role of cell-to-cell transmission in HIV infection. This approach allows us to explicitly estimate the frequency in which HIV is transmitted along a cellular conjugate, the distribution of conjugates among infected cells, and the average number of conjugates per cell. We found that the contribution of cell-to-cell transmission fluctuates over the course of early HIV infection, with the contribution ranging between 45%—75% of new infections. On average, cell-to-cell transmission accounted for 61% of new infections over the course of acute infection. However, the contribution of cell-to-cell transmission was heterogeneous among the underlying tissues. We estimated that the contribution of cell-to-cell transmission was 57% in the lymph nodes, 52% in the spleen, and 62% in the gut. As a result of this heterogeneity, our model suggests that the success of combination antiretroviral therapy is dependent on its ability to inhibit cell-to-cell transmission, primarily within the gut. Based on the results of our model, a slight decrease in the effectiveness of a therapeutic drug's ability to inhibit cell-to-cell transmission may result in a noticeable decrease in the CD4 cell count and an increase in the viral load.

The MIRACLE project: Tools and analysis methods for output from agent-based models of coupled human-natural systems

D. Parker¹, M. Barton², T. Dawson³, T. Filatova⁴, X. Jin¹, A. Lee², J. Lee⁴, L. Milazzo³, G. Polhill⁵, K. Robinson¹, A. Voinov⁴

¹ University of Waterloo, Waterloo, Canada, {dcparker; x37jin}@uwaterloo.ca, kirsten.robinson@gmail.com

² Arizona State University, Tempe, United States, {michael.barton, allen.lee}@asu.edu

³ University of Dundee, Dundee, United Kingdom, t.p.dawson@dundee.ac.uk, lorenzo.milazzo@hutton.ac.uk

⁴ University of Twente, Enschede, Netherlands, {t.filatova, j.s.lee-1}@utwente.nl, aavoinov@gmail.com

⁵ The James Hutton Institute, Aberdeen, United Kingdom, gary.polhill@hutton.ac.uk

Motivated by a desire to explore research questions related to the dynamics and consequences of human-environment interactions that can not be investigated using traditional equilibrium-based and statistical modeling approaches, a generation of environmental scientists have developed computational modeling methods. In particular, agent-based models (ABMs), which create virtual worlds of social agents and their interaction environments in computer code, have been developed to explore the dynamics of coupled human-natural systems. While researchers have made substantial progress in model framing, design, construction, and parameterization, less progress has been made with respect to sensitivity analysis, hypothesis generation, and hypothesis testing. Since these models have stochastic elements and many potential parameter combinations, multiple model runs that sweep parameters are conducted, creating large quantities of computationally generated, hyper-dimensional, “big data” from which we hope to extract answers to research questions on coupled socio-ecosystems. Yet we lack appropriate methods to mine, analyze, visualize, and synthesis large-scale model output data in order to answer our questions. Traditional analysis methods for mapping relationships between input parameters and output data - in both real-world and computational data - are designed for data that are linear, continuous, and normally distributed. However, data from models of complex socio-ecological systems can be non-linear, discontinuous, and power-law distributed.

In response to this gap, the MIRACLE team, funded through the international Digging into Data initiative, is working to develop a cloud based community platform that presents prototype examples of output and analysis methods for agent-based models of coupled human-natural systems. The platform will allow users to view, download, and analyze output data from models of urban development, agriculture and biodiversity, flood risk and coastal development, and development of early agrarian civilizations. Each project provides examples of novel data visualization and analysis methods. The platform should facilitate improved communication within research groups, as its design allows users to save, share, and comment on computational experiments within the group. It also allows users outside the group to explore new parameter spaces of the existing output data and to download, modify, and apply analysis algorithms.

We will present the design for the new platform and will also highlight novel analysis methods being implemented by the research team.

The potential impact of vaccination on the dynamics of dengue infections

D. Knippl

Agent-Based Modelling Laboratory, York University, Toronto, Canada, knipl@yorku.ca

We develop a serotype-specific, vector-host compartmental model to evaluate the effect of vaccination on the dynamics of dengue infection. The ODE model incorporates the phenomena of antibody-dependent enhancement and cross-protection following recovery from primary infection, and is able to reproduce the reported multi-annual patterns of dengue infection. Our model projects that vaccination can dramatically reduce the overall incidence of the disease. However, vaccination can potentially increase the incidence of severe infection of dengue hemorrhagic fever following the vaccine introduction due to the effects of antibody-dependent enhancement. The magnitude and timelines for this increase depend strongly on the efficacy and duration of the vaccine-induced protection. Corresponding to the current estimates of vaccine efficacy, we show that dengue eradication is infeasible using an imperfect vaccine. Furthermore, for a vaccine that induces lifetime protection, a nearly full coverage of infant vaccination is required for dengue elimination. Our findings suggest that other vector control measures may still play a significant role in dengue prevention even when a vaccine with high protection efficacy becomes available. This is based on the joint work with S. M. Moghadas (Agent-Based Modelling Laboratory, York University).

Modelling human-environment interactions and their impact bistability in forest-grassland mosaics

M. Anand¹, C.T. Bauch², K. Henderson³, C. Innes⁴

¹ School of Environmental Sciences, University of Guelph, Guelph, Canada, manand@uoguelph.ca

² Department of Applied Mathematics, University of Waterloo, Waterloo, Canada, cbauch@uwaterloo.ca

³ School of Environmental Sciences, University of Guelph, Guelph, Canada, hendersk@uoguelph.ca

⁴ Department of Mathematics and Statistics, University of Guelph, Guelph, Canada, clintoni@sfsu.ca

We present a fully coupled human-environment system (HESs) in which ecological dynamics responds in a two-way feedback with human dynamics. Coexistence of vegetation in forest-grassland mosaics is characterized by the existence of alternative stable states, known as bistability. The dominant vegetation in a bistable system often maintains stability when faced with small disturbances; however once a threshold is crossed large state shift occurs. Such catastrophic shifts are difficult to predict and can have devastating environmental impacts that are even harder to reverse. We used empirical data to model ecosystem state shifts and stability in the Atlantic forest-Campos grassland mosaics of southern Brazil influenced by human behaviour and interventions such as carbon incentives. Large incentives increase stability in the region, while increasing the likelihood of being in a forested state. The strength of coupling of human interactions affects bistability, such that the largest phase space for occurrence of bistability occurs at intermediate levels of human coupling. Very high levels of coupling leads to highly unstable dynamics. Afforestation of degraded lands and carbon sequestration incentives to mitigate climate change are examples of large-scale shifts in ecosystems that have the potential to alter landscapes. We examined the influence of carbon sequestration incentives on the stability of forest-grassland mosaic system. Large incentives restore stability in the region, compared to other land management behaviours. Large incentives also increase the probability of being bistable or in the forest dominant state. We conclude that human interactions with natural systems should be viewed as a dynamic entity with the role of human behaviour to be key to environmental sustainability. This work is conducted jointly with Chris Bauch, Clinton Innes and Kirsten Henderson.

To a Predictive Model of Pathogen Die-off in Soil Following Manure Application

A. Skelton, A.R. Willms

*University of Guelph, Guelph, Canada,
skelton@uoguelph.ca, awillms@uoguelph.ca*

Producing fruits and vegetables in field conditions typically requires significant application of manure, compost and other biosolids. In order to ensure food safety and protect the environment, the application of such fertilizers is subject to strict regulations. These regulations include mandatory waiting periods following application before livestock are allowed to graze or crops can be harvested. Current regulations are derived from data obtained in laboratory settings. It is valuable to obtain field-derived data that can provide scientific information leading to policies and regulations that optimize crop production while continuing to guard food safety.

A number of studies have been conducted in an attempt to determine the factors that affect the survival of bacteria under field conditions. In [4], the authors provide a nice survey of a number of studies investigating factors that can potentially affect survival of E.Coli in open environments. In [1], the authors consider the effect of manure application method on survival of Salmonella in soil columns. A recent study [2] considers a diverse array of factors such as soil and water quantities, bacteria type, experimental location, soil type, water type, temperature, soil pH and quantities of various chemicals. It was found that temperature and soil pH were the most significant factors affecting die-off rates of E.Coli. This study took the form of a stepwise regression analysis in which the die-off rate was predicted from subsets of explanatory variables. Other studies look at genetic, instead of environmental, factors that contribute to survivability of bacteria in unpredictable environments [3].

Data for our study were collected in field trials by a research team led by Dr. Ann Huber from the Soil Research Group. Trials were conducted to measure the die-off rates of E.Coli, Salmonella and Listeria on two types of soils prevalent in Southern Ontario. They also recorded measurements of environmental factors such as air and soil temperature, precipitation, soil pH and soil nutrient levels. The study found that die-off rates were correlated most strongly with soil temperature and moisture. Data were collected from June 2011 to May 2012 and from June 2013 to May 2014, however both years featured unseasonably cool and wet weather conditions. As a result, additional field and laboratory trials are planned in order to obtain data from drier and warmer conditions.

Our goal was the development of a predictive model for pathogen die-off in soil following manure application. We have developed a family of ordinary differential equation models to analyze the effect temperature and soil moisture have on soil pathogen levels. In this talk, we will discuss our model, show how it can be calibrated to our field data and test its predictive capabilities. We will discuss the various difficulties faced in modelling pathogen die-off rates, including "viable, but non-culturable bacteria", that is, bacteria in a dormant state that cannot be easily cultured and counted from samples, but are still present in the soil as viable and potentially harmful cells.

References

- [1] T. Bech, *Leaching of Salmonella enterica in Clay Columns Comparing Two Manure Application Methods*, Ground Water, 49 (1), pp. 32-42 (2011).
- [2] E. Franz et al., *Meta-Regression Analysis of Commensal and Pathogenic Escherichia coli Survival in Soil and Water*, Environmental Science and Technology, 48, pp. 6763-6771 (2014).
- [3] C. Saint-Ruf et al., *Massive Diversification in Aging Colonies of Escherichia coli*, Journal of Bacteriology, 196 (17), pp. 3059-3073 (2014).
- [4] J. D. van Elsas et al., *Survival of Escherichia coli in the environment: fundamental and public health aspects*, International Society for Microbial Ecology, 5, pp. 173-183 (2011).

Wave Blocking Phenomena in Periodic Landscapes

J. Dowdall¹, F. Lutscher², V. LeBlanc³

¹ University of Ottawa, Canada, jdowd044@uottawa.ca

² University of Ottawa, Canada, flutsche@uottawa.ca

³ University of Ottawa, Canada, vleblanc@uottawa.ca

The growing flow of people and goods around the globe has allowed new, non-native species to establish and spread in already fragile ecosystems. The introduction of invasive species can have a detrimental impact on the already established species. Thus, it is important that we understand the mechanisms that facilitate or prevent invasion. Since reaction-diffusion invasion models produce travelling waves we can study invasion by looking at the mechanisms that allow for wave propagation failure, or wave-blocking. The object of this talk is to provide an approach to predicting propagation failure for species invasion in a fragmented landscape. We begin by considering the parameterized equation

$$\frac{\partial u}{\partial t} = D \frac{\partial^2 u}{\partial x^2} + ru \left(1 - \frac{u}{K}\right) \left(\frac{u}{K} - \alpha\right) \quad (1)$$

where the parameters r, K and D vary periodically in space. Adopting a homogenization approach outlined by ([1]) we are able to approximate the speed of invasion. However, we observe wave-blocking phenomena where our approximation predicts successful propagation. Thus, we alter our approach and consider the prototype equation

$$u_t = u_{xx} + u(1-u)(u-\alpha) + \varepsilon g(u_x, u, x; \varepsilon) \quad (2)$$

with a symmetry breaking perturbation g . When $\varepsilon = 0$ we know that (2) admits a family of travelling wave solutions parameterized by its speed c . Extending the results in ([2]) we are able to show that wave-blocking occurs in a cone in the (c, ε) parameter space.

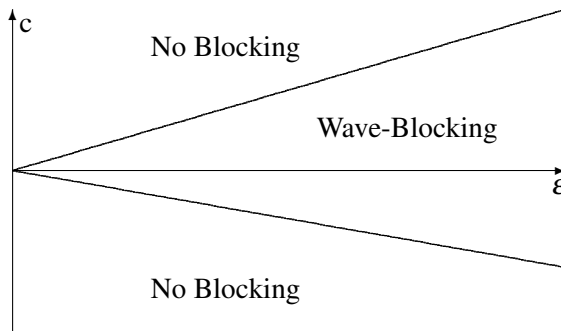


Figure 1: Wave-blocking occurs for (c, ε) belonging to the region above.

References

- [1] G. Maciel and F. Lutscher, *Allee Effects and Population Spread In Patchy Landscapes*, J Biol. Dynamics (submitted). (2015).
- [2] LeBlanc, V.G. and Roy, C. *Forced translational symmetry-breaking for abstract evolution equations*, J. Abs. Diff. Eqns. 4, pp. 16-43 (2013).

**ST-SCNA The 2nd Canadian Symposium on
Scientific Computing and Numerical Analysis**

A Fast Solver for Dense Linear Systems: The Inverse Fast Multipole Method

P. Coulier^{1,2 *}, H. Pouransari², E. Darve²

¹ KU Leuven, Department of Civil Engineering, Belgium

² Stanford University, Department of Mechanical Engineering, USA

*pcoulier@stanford.edu

Linear systems of equations involving dense matrices arise in a variety of applications in science and engineering (e.g., in boundary element methods). Many of these dense matrices can be represented in a hierarchical format, where matrix blocks corresponding to well-separated interactions are replaced by low-rank approximations. Such hierarchical representations facilitate matrix–vector multiplications, hence enabling the use of iterative solvers. The precarious convergence behavior (and thus the number of iterations) is a major disadvantage of this type of solvers, however, depending on the spectral properties of the matrix. This necessitates the incorporation of a preconditioning strategy to improve the latter, which is often a difficult and case-dependent problem.

In this talk, the inverse fast multipole method (IFMM) is presented as a robust and efficient preconditioner for iterative schemes involving dense matrices. The preconditioner is essentially a fast direct solver with low accuracy, where "direct" refers to the use of an approximate LU factorization. The solver is inexact, although the error can be controlled and made as small as needed (with an increase in computational cost). The IFMM was originally discussed in [1] and relies on two key ideas. First, the dense hierarchical matrix is converted into an extended sparse matrix, introducing additional unknowns (which can be interpreted as local and multipole coefficients at different levels in the framework of the fast multipole method). Second, fill-ins arising during the elimination of the extended sparse matrix are compressed as low rank matrices if they correspond to well-separated interactions. As a result, the sparsity pattern of the extended sparse matrix is maintained throughout the elimination, resulting in a very efficient algorithm with nearly linear complexity (strictly linear if the rank is bounded independent of the matrix size). The proposed preconditioning strategy shows similarities to multigrid methods [2] (as it uses a hierarchical decomposition of the domain), as well as to the incomplete LU factorization and its variants [3] (as the sparsity pattern is preserved). The IFMM can also be used as an accurate direct solver, although a much higher accuracy for approximating the well-separated interactions is required in that case.

References

- [1] S. Ambikasaran and E. Darve, *The inverse fast multipole method*, arXiv:1407.1572, 2014.
- [2] W. Hackbusch, *Multi-grid methods and applications*, Springer, 1995.
- [3] Y. Saad, *Iterative methods for sparse linear systems*, PWS Publishing, Boston, 1996.

A fast-marching method for non-monotonically evolving fronts

J.-C. Nave¹, A. Tcheng²

¹ McGill University, Montreal, QC, Canada, jcnave@math.mcgill.ca

² McGill University, Montreal, QC, Canada, alexandra.tcheng@mail.mcgill.ca

Front propagation is a time-dependent phenomenon occurring when the boundary between two distinct regions of space is evolving. It is possible to make the distinction between *monotone* and *non-monotone* motion of fronts. For example, a fire evolves monotonically in that, if a point \vec{x} of space belongs to a burnt region, then it cannot belong to an unburnt region at a later time [1]. Given an initial front \mathcal{C}_0 as a codimension-one C^1 subset of R^n , let each point of the front evolve with a given speed $F : R^n \times [0, T] \rightarrow R$ in the direction of the outward normal to the front. Numerical algorithms tracking interface propagation aim to recover the front \mathcal{C}_t at later times $t > 0$.

On the one hand, a robust but computationally expensive numerical method for tracking either kind of evolution is the Level-Set Method (LSM) [1]. On the other hand, the Fast Marching Method (FMM) [2, 3] may be used when $F(\vec{x}) \geq \delta > 0$, and is therefore suited for monotone propagation. This approach builds the *first arrival time function* ψ , i.e., $t = \psi(\vec{x})$ gives the unique time at which the front reaches the point $\vec{x} \in R^n$. The FMM finds ψ by marching the front at a computational speed that is *optimal*. This talk will discuss an algorithm able to handle speed functions changing sign while featuring a computational complexity comparable to that of the FMM.

Consider the set $\mathcal{M} := \{(\vec{x}, t) : \vec{x} \in \mathcal{C}_t\}$ consisting of the surface traced out by the fronts as they evolve. We describe \mathcal{M} locally with functions of the form $\psi(\vec{u})$ where the n variables $\vec{u} = (u_1(\vec{x}, t), \dots, u_n(\vec{x}, t))$ parameterise *some hyperplane* lying in $R^n \times [0, T]$. We show that $\psi : R^n \rightarrow R$ solves a Dirichlet problem of the form:

$$\begin{cases} H(\vec{u}, \psi(\vec{u}), \nabla \psi(\vec{u})) = 0 & \text{in } \mathcal{U} \subset R^n \\ \psi(\vec{u}(\vec{x}, t)) = u_{n+1}(\vec{x}, t) & \text{on } \vec{x} \in \mathcal{C}_t \cap \mathcal{V} \end{cases} \quad (1)$$

for appropriate neighbourhoods \mathcal{U} and \mathcal{V} , where u_{n+1} is normal to the plane. Points sampling \mathcal{M} are no longer required to lie on any grid. Rather, to compute each new point $p \in \mathcal{M}$, the algorithm first finds an appropriate hyperplane before solving a finite-difference discretization of (1). The location of the new point is determined by the solution of a non-linear optimisation problem. This talk will elaborate on this problem, as well as on the global constraints imposed on the evolution in order to capture the singularities of \mathcal{M} .

References

- [1] S. Osher and J. Sethian., *Fronts propagating with curvature dependent speed: algorithms based on Hamilton-Jacobi Formulations*, J. Comp. Phys., pp.12–49, Volume 79, (1988).
- [2] J. Sethian, *A fast marching level set method for monotonically advancing fronts*, Proc. Natl. Acad. Sci., pp.1591–1595, Volume 93, (1996).
- [3] J.N. Tsitsiklis, *Efficient algorithms for globally optimal trajectories*, IEEE Trans. Automat. Control, pp. 1528–1538, Volume 40, Number 9, (1995).

A high-order solution-adaptive simulation framework for hyperbolic conservation laws on cubed-sphere grids

L. Ivan¹, H. De Sterck², C. P. T. Groth²

¹ Department of Applied Mathematics, University of Waterloo, Waterloo, Canada, livan@uwaterloo.ca

² Department of Applied Mathematics, University of Waterloo, Waterloo, Canada, hdesterck@uwaterloo.ca

³ University of Toronto Institute for Aerospace Studies, Toronto, Canada, groth@utias.utoronto.ca

High-order accurate and efficient computational methods are highly desirable in many fields of computational physics, especially in the study of problems characterized by a wide range of temporal and length scales on which the interesting physics occurs. A particular case of interest is the numerical simulation of large-scale space-physics problems, which requires the discrete computation of plasma fluid flows and the associated complex multiphysics phenomena that occur at a variety of scales relative to the domain size. High-order discretizations and solution-driven adaptive mesh refinement (AMR) techniques are major classes of approaches capable of resolving the wide range of dynamic scales of such simulations at reduced computational cost.

This talk describes a high-order central essentially non-oscillatory (CENO) finite-volume scheme in combination with a block-based adaptive mesh refinement (AMR) algorithm for solution of hyperbolic conservation laws on three-dimensional cubed-sphere grids. In particular, the fluid flows of interest are governed by the compressible form of Euler and ideal magnetohydrodynamics (MHD) equations and pertain to space-physics applications. The CENO scheme [1] is based on a hybrid solution reconstruction procedure that provides high-order accuracy in smooth regions, even for smooth extrema, and non-oscillatory transitions at discontinuities. The scheme is applied in combination with a divergence correction technique to enforce the solenoidal condition for the magnetic field as proposed in [2]. Figure 1 depicts an instance of the solution predicted by the time-accurate, fourth-order, CENO scheme in conjunction with dynamic, solution-driven AMR to the translation of an iso-density MHD vortex. Additional results to demonstrate the accuracy and capability of the computational framework are also discussed.

References

- [1] L. Ivan and H. De Sterck and A. Susanto and C. P. T. Groth *High-Order Central ENO Finite-Volume Scheme for Hyperbolic Conservation Laws on Three-Dimensional Cubed-Sphere Grids*, J. Comput. Physics, **282**, pp. 157-182 (2015).
- [2] A. Susanto and L. Ivan and H. De Sterck and C.P.T. Groth, *High-order central ENO finite-volume scheme for ideal MHD*, J. Comput. Physics, **250**, pp. 141-164 (2013).

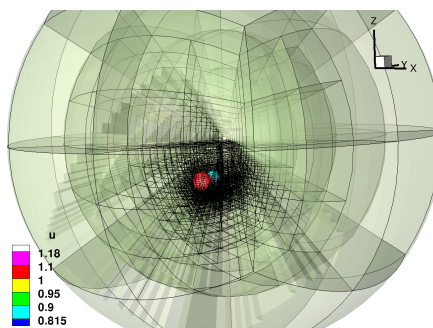


Figure 1: Adapted cubed-sphere grid generated by the CENO AMR algorithm for an unsteady MHD problem.

A multirate accelerated Schwarz Waveform Relaxation Method

Ronald D. Haynes¹, Khaled H. Mohammad¹

¹ Memorial University of Newfoundland, Newfoundland, Canada, {rhaynes, km2605}@mun.ca

In this talk we describe an approach which combines a multirate method and domain decomposition in space and time. This approach uses the multirate splitting provided by Savcenco's multirate method to locate an appropriate interface for the Schwarz Waveform relaxation method. We show that this initial guess has a dramatic effect – reducing the number of Schwarz Waveform relaxation iterations to recover the single domain solution. In fact, in many cases only one SWR iteration is required to recover the global accuracy of the solution at the final time saving a lot of work and making the Multirate Schwarz Waveform relaxation (MR-SWR) algorithm efficient. The performance of the MR-SWR algorithm can be improved by increasing the number of subdomains resulting in a multi-domain multirate Schwarz Waveform relaxation algorithm (MD-MR-SWR). A corrected variant is possible using subsequent refinements of the interfaces between the fast and slow components.

References

- [1] Hundsdorfer, Willem; Savcenco, Valeriu Analysis of a multirate theta-method for stiff ODEs. *Appl. Numer. Math.* 59 (2009).
- [2] Savcenco, V.; Hundsdorfer, W.; Verwer, J. G. A multirate time stepping strategy for stiff ordinary differential equations. *BIT* 47 (2007)
- [3] Constantinescu, Emil M.; Sandu, Adrian Multirate timestepping methods for hyperbolic conservation laws. *J. Sci. Comput.* 33 (2007), no. 3, 239–278.
- [4] M. J. Gander and A. M. Stuart, Space-time continuous analysis of waveform relaxation for the heat equation, *SIAM J. Sci. Comput.*, 19 (1998), pp. 2014–2031.
- [5] Gander, Martin J. A waveform relaxation algorithm with overlapping splitting for reaction diffusion equations. *Czech-US Workshop in Iterative Methods and Parallel Computing, Part 2* (Milovy, 1997). *Numer. Linear Algebra Appl.* 6 (1999), no. 2, 125–145.

A New Penalization Method for the Shallow Water Equations with Applications to Global Ocean Flow

N.K.-R. Kevlahan¹, T. Dubos², M. Aechtner²

¹ McMaster University, Hamilton, Canada, kevlahan@mcmaster.ca

² Ecole Polytechnique, France, dubos@lmd.polytechnique.fr

We propose a new mass and energy conserving Brinkman boundary condition penalization for the rotating shallow water equations. This penalization does not lead to higher wave speeds in the solid region. The error estimates for the penalization are derived analytically and verified numerically for linearized one dimensional equations. The penalization is implemented in a conservative dynamically adaptive wavelet method for the rotating shallow water equations on the sphere with bathymetry and coastline data from NOAA's ETOPO1 database. This code could form the dynamical core for a future global ocean model. The potential of the dynamically adaptive ocean model is illustrated by using it to simulate the 2004 Indonesian tsunami and wind-driven global ocean circulation.

A Nonlinearly Preconditioned Conjugate Gradient Algorithm for Rank- R Canonical Tensor Approximation

H. De Sterck¹, M. Winlaw²

¹ University of Waterloo, Waterloo, Canada, hdesterck@uwaterloo.ca

² University of Waterloo, Waterloo, Canada, mwinlaw@uwaterloo.ca

Alternating least squares (ALS) is often considered the workhorse algorithm for computing the rank- R canonical tensor approximation, but for certain problems its convergence can be very slow. The nonlinear conjugate gradient (NCG) method was recently proposed as an alternative to ALS [1], but the results indicated that NCG is usually not faster than ALS. To improve the convergence speed of NCG, we consider a nonlinearly preconditioned nonlinear conjugate gradient (PNCG) algorithm. Our approach uses ALS as a nonlinear preconditioner in the NCG algorithm. We demonstrate numerically that the PNCG convergence acceleration mechanism often leads to important pay-offs for difficult tensor decomposition problems, with convergence that is significantly faster and more robust than for the stand-alone NCG or ALS algorithms. We consider several approaches for incorporating the nonlinear preconditioner into the NCG algorithm that have previously been described in the literature and have met with success in certain application areas. However, it appears that the PNCG approach has received relatively little attention in the broader community and remains underexplored both theoretically and experimentally. Thus, we provide a concise overview of several PNCG variants and their properties, and systematically compare the performance of these PNCG variants for the tensor decomposition problem, and draw further attention to the usefulness of nonlinearly preconditioned NCG as a general tool. We also briefly discuss the convergence of the PNCG algorithm. In particular, we obtain a new convergence result for one of the PNCG variants under suitable conditions.

References

- [1] A. Acar, D.M. Dunlavy and T.G. Kolda, *CA scalable optimization approach for fitting canonical tensor decompositions*, Journal of Chemometrics **25**, 1, pp. 67-86 (2011).

A Novel Approach for a Coupled Fire-Atmosphere Model with Application to the Propagation of Wildfires

L. Proulx¹

¹ Université de Montréal, Canada, louis-xavier.proulx@umontreal.ca

Current models in use to predict the spread of wildfires neglect some physical aspects in order to decrease the computational time of the numerical model. A new approach has been taken in order to develop a coupled model, where the local wind flow: (1) takes into account the geometry of the topography and (2) satisfies a divergence constraint with a source term which accounts for the effects of the heat released by the fireline. The aim of this new model is to identify the regimes with nondimensional parameters, where our suggested coupling may achieve better predictions of the spread of wildfires than coupled models relying on full Navier-Stokes equations for the atmospheric flow.

In predictive models, the fireline is represented by an interface, a manifold of codimension two, that circumscribes the boundaries of the burned regions on the topography. The level-set method is used for the time evolution of this interface whose rate of spread depends on the geometry of the terrain, fuel and the surrounding wind. The Cartesian grid embedded boundary method and projection methods are used to compute the wind flow satisfying a divergence constraint with the fire heat source represented by a delta function centered at the interface. This singular source changes the local wind flow which in turn contributes to the spread of the fire.

We will first discuss a regularization technique for the singular delta function supported on a codimension two manifold, itself lying on an irregular boundary of the computational domain. A necessary condition for the convergence of the solutions of the Poisson equation with this singular source term will be given. Then, we will present the derived coupled model including the divergence constraint. Some numerical experiments with the coupled model will give us some insight on the possible regimes of propagation.

A numerical framework for tracking interfaces in generalized Mullins-Sekerka dynamics

Iain Moyles¹, Brian Wetton²

¹ Mathematics, UBC, imoyles@math.ubc.ca

² Mathematics, UBC, wetton@math.ubc.ca

We present a numerical framework for computing the evolution of curves subject to a class of generalized singular interface conditions from nonlocal elliptic problems. A classic example is Mullins-Sekerka dynamics, which comes as the sharp interface limit of the Cahn-Hilliard equations from materials science. The motivating example for the current work is a particular, singular, asymptotic limit of a system of reaction-diffusion equations: the saturated Gierer-Meinhardt system. Using fully implicit time-stepping and a finite difference approximation of the curve points, which are constrained to remain parameterized by scaled arc length, we solve a suitably discretized singular boundary integral formulation of the elliptic problem. The resulting approach can be used on a wide class of problems with little additional effort.

Adaptive Time-stepping in the Numerical Solution of the Reaction-Diffusion Master Equation

S. Ilie¹, J.M.A. Padgett²

¹ Ryerson University, Toronto, Canada, silvana@ryerson.ca

² Ryerson University, Toronto, Canada, jill.padgett@ryerson.ca

Stochastic modelling and simulation are essential tools for studying important biological processes at the level of a single cell, when some molecular species are in low amounts. The random fluctuations due to small population numbers of certain biochemically reacting species have been observed experimentally. Mathematically, the dynamics of these biochemical systems may be modelled using Markov processes. The evolution of spatially heterogeneous biochemical systems with some species in low amounts is accurately described by the mesoscopic model of the Reaction-Diffusion Master Equation. This discrete stochastic model has been successfully employed to analyze key cellular processes, such as signaling chemical pathways or morphogenesis, where the spatial distribution of the reacting species may have a strong influence on the system behaviour. For most biochemical systems, this model is intractable, therefore numerical methods must be used to approximate its exact solution. The Inhomogeneous Stochastic Simulation Algorithm [1], provides an exact strategy to numerically solve the Reaction-Diffusion Master Equation, but it is prohibitively slow as it simulates every chemical reaction and diffusion event in the system [2]. To overcome this difficulty approximation techniques, such as the tau-leaping scheme [3], were developed that step over multiple reactions and diffusion events.

The objective of this work is to design effective and accurate numerical methods for approximating the solution of the stochastic discrete model of the Reaction-Diffusion Master Equation. Often, biochemical systems arising in applications evolve on multiple time-scales, thus their mathematical models exhibit stiffness. Stochastic models which, in addition, are stiff are computationally challenging, and the existing numerical strategies for them are quite intensive. We propose an adaptive time-stepping scheme for the tau-leaping method for approximating the solution of the Reaction-Diffusion Master Equation. This technique combines effective strategies for variable time-stepping with post-leap checking [4] to reduce the computational cost, while maintaining the desired accuracy. This strategy is compared to the existing schemes, including the Inhomogeneous Stochastic Simulation Algorithm, for several models of practical interest. The numerical results show that the proposed adaptive technique significantly speeds-up the simulation, while maintaining an excellent accuracy of the numerical solution. Our method will allow to efficiently and accurately solve some difficult mathematical models of cellular processes.

References

- [1] A.B. Sturzia, C.J. Lumsden, *Stochastic simulation of coupled reaction-diffusion processes*, J. Comput. Phys., **127**, pp. 196-207 (1996).
- [2] D.T. Gillespie, A. Hellander, L.R. Petzold, *Perspective: stochastic algorithms for chemical kinetics*, J. Chem. Phys. **138**, pp. 170901 (2013).
- [3] D.T. Gillespie, *Approximate accelerated stochastic simulation of chemically reacting systems*, J. Chem. Phys., **115**, pp. 1716-1733, (2001).
- [4] D.F. Anderson, *Incorporating postleap checks in tau-leaping*, J. Chem. Phys., **128**, pp. 054103 (2008).

An embedding method for the numerical approximation of partial differential equations on moving surfaces

A. Petras¹, S. Ruuth²

¹ Simon Fraser University, Burnaby, Canada, apetras@sfsu.ca

² Simon Fraser University, Burnaby, Canada, sruuth@sfsu.ca

Partial differential equations (PDEs) on moving surfaces arise in a variety of application areas. In this talk, we consider the combination of a recent grid based particle method [1] (for geometric interface motions) with the closest point method [2] (for the evolution of PDEs on stationary surfaces). In this context, we find that the standard grid based particle method has a relatively strict stability time stepping restriction. A modified particle method for geometric motion is proposed, yielding an improved coupling with the closest point method. Numerical experiments are provided.

References

- [1] S. Leung and H.-K. Zhao, *A grid based particle method for moving interface problems*, J. Comput. Phys. **228**, 8, pp. 2993-3024 (2009).
- [2] S.J. Ruuth and B. Merriman, *A simple embedding method for solving partial differential equations on surfaces*, J. Comput. Phys. **227**, 3, pp. 1943-1961 (2008).

An Immersed Boundary Method for Mass Transfer Cross Permeable Interfaces

Huaxiong Huang, York University

In this talk, we present an immersed boundary method for mass transfer across permeable deformable moving interfaces interacting with the surrounding fluids. One of the key features of our method is the introduction of the mass flux as an independent variable, governed by a non-standard vector transport equation. The flux equation, coupled with the mass transport and the fluid flow equations, allows for a natural implementation of an immersed boundary algorithm when the flux across the interfaces is proportional to the jump in concentration. As an example, the oxygen transfer from red blood cells in a capillary vessel is used to illustrate the applicability of the proposed method. We show that our method is capable of handling multi-physics problems involving fluid-structure interaction with multiple deformable moving interfaces and (interfacial) mass transfer simultaneously. If time permits, extension of the current method will be discussed.

This is joint work with X. Gong and Z. Gong.

An integral equation method for flow in porous media

Bryan Quaife¹, George Biros¹, Pietro de Anna², Ruben Juanes²

¹ University of Texas, Austin, USA, *quaife@ices.utexas.edu*

² Massachusetts Institute of Technology, Cambridge, USA

Integral equations are a powerful method to simulate certain complex flows. One such example is a two-dimensional incompressible Stokesian flow in a porous media. After formulating an integral equation representation, I will apply it to several geometries and compare the results to experimental data of collaborators at MIT.

To compare the results, I will resort to statistical methods. For instance, the probability density function of the numerical and experimental velocity fields will be compared. Future work includes comparing more sophisticated statistics and developing analytic methods for finding the velocity distribution.

Auto Insurance Fraud Detection Using Unsupervised Spectral Ranking for Anomaly

K. Nian¹, H. Zhang², A. Tayal³, T.F. Coleman⁴, Y. Li⁵

¹ University of Waterloo, Canada, knian@uwaterloo.ca

² University of Waterloo, Canada, haofan.zhang@uwaterloo.ca

³ University of Waterloo, Canada, amtayal@uwaterloo.ca

⁴ University of Waterloo, Canada, tfcoleman@uwaterloo.ca

⁵ University of Waterloo, Canada, yuying@uwaterloo.ca

For many data mining problems, obtaining labels is costly and time consuming, if not practically infeasible. In addition, unlabeled data often includes categorical or ordinal features which, compared with numerical features, can present additional challenges. Inspired by the spectral clustering techniques, we propose a new unsupervised spectral ranking method for anomaly (SRA). We illustrate that the spectral optimization in SRA can be viewed as a relaxation of an unsupervised SVM problem. We demonstrate that the first non-principal eigenvector of a Laplacian matrix is linked to a bi-class classification strength measure which can be used to rank anomalies. Using the 1st non-principal eigenvector of the Laplacian matrix directly, the proposed SRA generates an anomaly ranking either with respect to the majority class or with respect to two main patterns. The choice of the ranking reference can be made based on whether the cardinality of the smaller class (positive or negative) is sufficiently large. Using an auto insurance claim data set but ignoring labels when generating ranking, we show that our proposed SRA significantly surpasses existing outlier-based fraud detection methods. Finally we demonstrate that, while proposed SRA yields good performance for a few similarity measures for the auto insurance claim data, notably ones based on the Hamming distance, choosing appropriate similarity measures for a fraud detection problem remains crucial.

B-spline Adaptive Gaussian Collocation for Error Controlled Numerical Solutions of ODEs and PDEs

Paul Muir¹

¹ Saint Mary's University, Halifax, Nova Scotia, Canada, muir@smu.ca

Boundary value ordinary and (time-dependent) partial differential equations arise in a wide variety of applications. Software based on B-spline adaptive Gaussian collocation (a type of orthogonal collocation) has had a long history of success in the numerical solution of such equations over the last (approximately) 40 years. In this approach, the spatial dependence of the approximate solution is represented in the form of a linear combination of B-spline basis functions with unknown coefficients. Equations for the determination of these coefficients are obtained by requiring the approximate solution to satisfy the differential equation at certain points (the collocation points) within each element into which the spatial domain is partitioned. The choice of these points is related to the images of the well-known Gaussian quadrature points mapped on to each element. The approximate solution is also required to satisfy the boundary conditions. (For the ODE case, the collocation process gives a set on nonlinear algebraic equations; for the PDE case, we obtain a set of differential-algebraic equations.) The important feature of adaptive spatial error control, i.e., the adaptation of the computation (typically through the adaptation of the spatial mesh) in order to ultimately obtain an approximate solution for which the corresponding spatial error estimate satisfies a given user tolerance, requires the efficient computation, through an auxiliary process, of a high quality estimate of the spatial error.

In this talk we discuss a number of software packages, based on B-spline adaptive Gaussian collocation, for the error controlled numerical solution of systems of nonlinear boundary value ODEs, systems of nonlinear parabolic 1D PDEs, and systems of nonlinear parabolic 2D PDEs. The talk will consider, in particular, our recent work in the development of software of this type for 1D PDEs and our progress to date for 2D PDEs.

Data mining and probabilistic models for error estimate analysis of finite element method

J. Chaskalovic¹, F. Assous²,

¹ D'alembert, University Pierre and Marie Curie, Paris, France jch1826@gmail.com

² Ariel University, Israel, franckassous@netscape.net

In previous papers [1-3], we proposed to extend the scope of data mining techniques to scientific computing. In particular, we used data mining as a tool to compare and evaluate different asymptotic models. Our idea started from the observation that numerical methods produce today a huge quantity of numerical results, especially with the availability of parallel computers. We also relied on the fact that data mining techniques have already proved to be efficient in other contexts which deal with massive data, like in biology, medicine, marketing, advertising and communications.

In this paper, we open a new chapter of this research by extending and generalizing this idea to error estimate evaluation in numerical approximations of partial differential equations. We will consider finite elements error estimates, and will seek a way to identify and qualify more precisely, that is locally in space and time, these errors by exploratory data mining and probabilistic models. We will also show the limits of the approach, mainly due to the lack of absolute reference solution.

Then, for illustrative purpose, we will consider a paraxial Vlasov-Maxwell system of equations, that model charged particle beams and plasma physics problems. We will then derive two approximation methods based on a P₁ and P₂ finite element method. Then, we will investigate the accuracy between the two implemented methods by modeling the dependency of the odds with physical predictors, which characterizes when P₁ and P₂ finite elements produce equivalent results.

Among other, we will see that it is sometimes possible to precise the classical Bramble Hilbert's theorem, that gives, in a certain sense, a *global deterministic* error estimate, whereas our approach is based on a *local and probabilistic* analysis.

Let us emphasize that, beyond this particular study, this novel approach could operate in other sources of errors (see a description in [2]) which appear in the process of modeling, where approximations are implemented for simulations which take a central part to understand the features of a given real and complex system.

References

- [1] F. Assous, J. Chaskalovic, Data mining techniques for scientific computing: Application to asymptotic paraxial approximations to model ultra-relativistic particles, *J. Comput. Phys.* 230 (2011) 4811-4827.
- [2] F. Assous, J. Chaskalovic, Error estimate evaluation in numerical approximations of partial differential equations: A pilot study using data mining methods, *C. R. Mecanique* 341 (2013) 304-313.
- [3] F. Assous, J. Chaskalovic, Indeterminate constants numerical approximations of PDE's: A pilot study using data mining techniques, *J. Comput. and Appl. Math* 270 (2014) 462-470.

Derivation and some asymptotic estimates of the convergence rate of a Schwarz waveform relaxation domain decomposition method for some quantum wave equations

X. Antoine¹, E. Lorin²

¹ University of Lorraine, France

² Carleton University, Canada

This presentation is dedicated to the derivation of Schwarz waveform relaxation domain decomposition methods using high order pseudodifferential transmission conditions. The methods will be applied to linear and nonlinear Schroedinger equations in real time for laser-molecule interaction problems, as well as imaginary time for nonlinear eigenvalue problems. Some numerical and analytical convergence rate estimates will be presented.

Eye Tracking Studies of Category Learning: Fitting Complex Models to Individuals

P. F. Tupper¹

¹ Simon Fraser University, Burnaby, BC. pft3@sfsu.ca

The Cognitive Science Lab at SFU conducts experiments in which human subjects are asked to categorize a series of images based on criteria that are not initially specified to the subject. At the beginning of a trial, a subject must simply guess the correct category, but is given feedback on performance. Within an hour, most subjects learn the correct rule for categorization. The data collected includes the guesses of the subjects, the timing of the guesses, and eye tracking data, i.e. where on a video screen the subject's gaze is fixated at every point in time. We have constructed a model that is able to reproduce many features of this data set, while trying to maintain neuropsychological plausibility. I'll talk about some of the challenges of fitting this model to individual subjects (rather than averages over subjects, as is usually done) and in interpreting the resulting distribution of parameters. This is joint work with Jordan Barnes and Mark Blair (SFU, Psychology).

Implicitly Padded Convolutions on Hybrid Parallel Architectures

John C. Bowman¹, Malcolm Roberts²

¹ University of Alberta bowman@ualberta.ca

² University of Strasbourg malcolm.i.w.roberts@gmail.com

Convolutions are widely used in many areas of science and engineering, including data analysis, signal and image processing, and pseudospectral simulations of fluids. The most efficient convolution algorithms are based on the discrete fast Fourier transform (FFT). While the desired convolutions in most applications are linear, the discrete Fourier transform is inherently periodic. The convolution theorem requires that these unwanted aliases be removed. Conventionally, this dealiasing has been accomplished by zero padding the data in an extended buffer, wasting a significant amount of memory and computer time. A much more efficient and compact method accounts for this excess padding implicitly. In the transformed space, the inputs to the convolution are multiplied together as they are produced, without ever computing the entire FFT image all at once. In three dimensions, the resulting method of *implicitly dealiasing* runs roughly twice as fast as explicit zero padding, with only 44% of the storage requirements.

In this work, we discuss the parallelization of implicit dealiasing on distributed multicore architectures running in a hybrid OpenMP/MPI configuration. Unrolling the original serial algorithm [1] for centered Hermitian convolutions allows loop independence to be achieved, significantly improving performance in both the serial and parallel contexts. As a result, even in one dimension, implicit dealiasing of pseudospectral convolutions is now significantly faster than explicit zero padding.

In higher dimensions, implicit dealiasing vastly outperforms conventional zero padding by decoupling the data and temporary work arrays. We have optimized our convolution algorithm for modern high-performance parallel computer architectures, consisting of distributed networks of multicore processors. A key component of convolutions in higher dimensions is the matrix transpose used to localize the computation of the FFT in each direction onto individual processors.

We present an adaptive matrix transposition algorithm designed for hybrid architectures. Significant boosts in speed are observed relative to the distributed transpose used in the state-of-the-art adaptive FFTW library. In some cases, a hybrid configuration allows one to reduce communication costs by reducing the number of MPI nodes, and thereby increasing message sizes. This also allows for a more slab-like than pencil-like domain decomposition for multidimensional FFTs, reducing the cost of, or even eliminating the need for, a second distributed transpose. Nonblocking all-to-all transfers enable user computation and communication to be overlapped.

We apply our adaptive matrix transposition algorithm to the parallelization on hybrid architectures of implicitly dealiased pseudospectral convolutions used to simulate turbulent flow. These algorithms are publically available in the open-source library FFTW++ [2].

References

- [1] John C. Bowman and Malcolm Roberts, *Efficient Dealiased Convolutions without Padding*, SIAM J. Sci. Comput. **33**, 1, pp. 386-406 (2011).
- [2] John C. Bowman and Malcolm Roberts, FFTW++: A fast Fourier transform C++ header class for the FFTW3 library, <http://fftwpp.sourceforge.net>, 2010.

Infinite-dimensional ℓ^1 minimization techniques for multivariate function interpolation

B. Adcock¹

¹ Simon Fraser University, Burnaby, Canada, ben_adcock@sfu.ca

Many computational tasks in science and engineering, such as uncertainty quantification, require the approximation of smooth, multivariate functions from finite sets of pointwise samples. A common feature of such problems is their high dimensionality and limited availability of data, which makes accurate approximation a challenging task. Spurred by the advent of compressed sensing, there has been an increasing focus in the last several years on the use of convex optimization techniques for this problem. Smooth, multivariate functions possess increasing sparsity in higher dimensions; that is, their coefficients in certain orthogonal expansions, e.g. multivariate Legendre polynomials, are increasingly sparse. Hence the expectation is that such techniques will yield substantial gains over more standard approaches such as discrete least squares and interpolation, at least when the dimension is sufficiently high and the data points arise from appropriate random sampling distributions.

In this talk, I will introduce a new technique for this problem based on infinite-dimensional weighted ℓ^1 minimization. The advantages of this approach over existing optimization-based method are the following. First, it provides exactly interpolating approximations in the absence of noise. Second, it does not require impractical *a priori* bounds on the expansion tail in order to be implemented. In particular, the truncation strategy we introduce as part of this framework is completely independent of the function being approximated. Third, it allows one to understand the crucial roles weights play in the optimization problem; namely, that of regularizing and removing so-called aliasing phenomena, rather than matching smoothness of the underlying function.

Next, I will present a number of different approximation results. In particular, I will show that these techniques achieve the best of two worlds. First, they achieve near-optimal approximation rates for linear function models (e.g. smooth functions) for arbitrary scattered data points. Second, for appropriately randomized data points, they give near-optimal nonlinear approximation rates for classes of functions that are sparse or compressible with respect to an appropriate orthogonal basis (e.g. Legendre polynomials). Hence weighted ℓ^1 minimization techniques are guaranteed under broad conditions to perform at least as well as classical techniques, and will offer increasing performance gains as the dimension (and therefore the amount of sparsity) grows.

References

- [1] B. Adcock, *Infinite-dimensional ℓ^1 minimization and function approximation from pointwise data*, Preprint, 2015.

Matrix Manifold Optimization Methods for Tucker Tensor Approximations

H. De Sterck¹, A. Howse²

¹ University of Waterloo, Waterloo, Canada, hdesterck@waterloo.ca

² University of Waterloo, Waterloo, Canada, ahowse@waterloo.ca

Two algorithms are presented for computing higher order singular value decomposition (HOSVD) Tucker format tensor approximations by minimizing the distance to a given target tensor in the Frobenius norm. The HOSVD Tucker format expresses a d -dimensional tensor as a multilinear product of a d -dimensional core tensor with d matrices, such that the core tensor has orthogonal subtensors (i.e. tensors obtained by fixing one index at particular values) and the matrices have orthonormal columns, which has applications in multilinear principal component analysis. In a given dimension, the core tensor is no larger than the original tensor, and is typically much smaller. For instance, approximating a tensor with dimensions of length n by a core tensor with dimensions of length $r \ll n$ and d matrices in $\mathbb{R}^{n \times r}$, the storage cost is reduced from n^d to $r^d + rnd$.

To avoid complications arising from the invariance of the Frobenius norm under orthogonal transformations, and to maintain the orthonormality of these matrix variables without the use of equality constraints, minimization is carried out over the Cartesian product of Grassmann manifolds. A Grassmann manifold $\text{Gr}(n, p)$ is the set of all p -dimensional subspaces of \mathbb{R}^n , and a given element may be represented by an orthonormal matrix.

The first method considered is a nonlinearly preconditioned conjugate gradient (NPCG) algorithm [1], wherein a nonlinear preconditioner is used to generate a direction to play the role of the gradient in the standard nonlinear CG iteration. The second method is a nonlinear generalized minimal residual (N-GMRES) algorithm [2], in which a linear combination of past iterates and a tentative new iterate, generated by a nonlinear optimization method, is minimized to produce an improved search direction. Both algorithms have been adapted to the context of optimization over manifolds. The higher order orthogonal iteration (HOOI), a standard method for computing approximate Tucker decompositions, is used as the nonlinear preconditioner in NPCG and the optimization method in N-GMRES.

Several variants are provided for the update parameter β in NPCG, two for each of the Fletcher–Reeves, Polak–Ribière and Hestenes–Stiefel formulae. Variations are also discussed for the N-GMRES method, based on how to approximate the Hessian operator applied to a vector. Numerical results show that the N-GMRES algorithm, with the Hessian-vector result approximated by a difference of gradients, and the NPCG algorithm, with Polak–Ribière and Hestenes–Stiefel based update parameters, may significantly outperform the HOOI for large tensors, in cases where there is significant amounts of noise in the data, and when high accuracy results are required.

References

- [1] Hans De Sterck and Manda Winlaw, *A nonlinearly preconditioned conjugate gradient algorithm for rank- r canonical tensor approximation*, Numerical Linear Algebra with Applications, Wiley Online Library, 2014.
- [2] Hans De Sterck, *A nonlinear GMRES optimization algorithm for canonical tensor decomposition*, SIAM Journal on Scientific Computing, 34(3):A1351–A1379, 2012.

Monolithic Multigrid Methods for Two-Dimensional Resistive Magnetohydrodynamics

J.H. Adler¹, T.R. Benson¹, E.C. Cyr², S.P. MacLachlan³, R.S. Tuminaro⁴

¹ Tufts University, Medford, USA, {james.adler,thomas.benson}@tufts.edu

² Sandia National Laboratories, Albuquerque, USA, eccyr@sandia.gov

³ Memorial University of Newfoundland, St. John's, Canada, smaclachlan@mun.ca

⁴ Sandia National Laboratories, Livermore, USA, rstumin@sandia.gov

Magnetohydrodynamic (MHD) representations are used to model a wide range of plasma physics applications and are characterized by a nonlinear system of partial differential equations that strongly couples a charged fluid with the evolution of electromagnetic fields. The resulting linear systems that arise from linearization and discretization of the nonlinear problem are generally difficult to solve. In this talk, we investigate multigrid preconditioners for this system.

Design of effective multigrid preconditioners requires appropriately complementary relaxation and coarse-grid correction processes. In this study, we consider linearized finite-element discretizations and, as such, take advantage of geometric finite-element interpolation operators and Galerkin coarsening for the coarse-grid correction process. To complement this, we extend two well-known relaxation techniques from the literature on incompressible fluid dynamics, Braess-Sarazin relaxation and Vanka relaxation. Braess-Sarazin relaxation [1] follows from a classical matrix-splitting view of the saddle-point problem in incompressible fluid flow, with a simple (diagonal) approximation of the nonzero (1,1) block of the system, and a point smoother used in place of solves with the resulting approximate Schur complement. In contrast, Vanka relaxation [3] can be viewed as an overlapping block Gauss-Seidel method, where the blocks are chosen according to the structure of the incompressibility constraints. While both are readily extended to the linear systems that arise in this context, and both offer scalable performance, we see clear differences in the overall computational efficiency using the two relaxation methods [2].

References

- [1] D. Braess and R. Sarazin, *An efficient smoother for the Stokes problem*, Applied Numerical Mathematics, **23**, pp. 3-19 (1997).
- [2] T.R. Benson, J.H. Adler, E.C. Cyr, S.P. MacLachlan, and R.S. Tuminaro, *Monolithic multigrid methods for two-dimensional resistive magnetohydrodynamics*, submitted, 2015.
- [3] S.P. Vanka, *Block-implicit multigrid solution of Navier-Stokes equations in primitive variables*, Journal of Computational Physics, **65**, pp. 138-158 (1986).

Multigrid Method for Oligopolistic Competition Modelled by Stochastic Differential and Mean-Field Games

S. Amarala¹, P. Tan², J. Wan³

¹ University of Waterloo, Waterloo, Canada, samarala@uwaterloo.ca

² University of Waterloo, Waterloo, Canada, p8tan@uwaterloo.ca

³ University of Waterloo, Waterloo, Canada, jwlwan@uwaterloo.ca

In economics, oligopoly is a market structure in which a small number of firms producing substitutable goods compete by setting quantities (Cournot model) or prices (Bertrand model) strategically. For example, Pepsi and Coca-Cola in the soft drink industry, Apple and Samsung in the smart phone industry. Firms choose quantities or prices to maximize expected profit in the sense of Nash Equilibrium. The oligopolistic competition can be modelled as nonzero sum differential games. By applying the dynamic programming principle, oligopoly under uncertain demand can be formulated as a system of Hamilton-Jacobi-Bellman (HJB) equations. More precisely, let V_i be the value functions, which represent the expected discount lifetime profit. Then for the special Bertrand model case where there are only two players (duopoly), the unknowns V_i satisfy:

$$\frac{\partial V_i}{\partial t} = LV_i - D_M(p_j) \frac{\partial V_i}{\partial x_j} + \sup \left\{ D_i(p_i, p_j) \left[p_i - \left(\frac{\partial V_i}{\partial x_i} - \frac{\gamma}{\beta} \frac{\partial V_i}{\partial x_j} \right) \right] \right\} - rV_i,$$

where p_i is the price for goods produced by firm i , and L is the differential operator:

$$L = \frac{1}{2} \sigma_1^2 \frac{\partial^2}{\partial x_1^2} + \rho \sigma_1 \sigma_2 \frac{\partial^2}{\partial x_1 \partial x_2} + \frac{1}{2} \sigma_2^2 \frac{\partial^2}{\partial x_2^2}.$$

For the case of N -player games where N is large, the models can be formulated as mean-field games where the system is much smaller than N . In this talk, we will present numerical methods for solving the system of HJB PDEs. We will discuss the discretization of the nonlinear equation, the issues of viscosity solutions, and present a monotone finite difference scheme. We will then solve the resulting discrete systems by a multigrid method. We will present a relaxation scheme as a smoother, and a prolongation method for the system case. Finally, numerical results will be presented for duopoly and N -player examples.

Nonrecourse stock loans

P. Azimzadeh¹, P. A. Forsyth¹, K. R. Vetzal¹

¹ University of Waterloo, Canada, *{pazimzad,paforsyt,kvetzal}@uwaterloo.ca*

We consider nonrecourse stock loans, an extremely popular financial product. These were first studied in [1], where it was shown that a (perpetual) stock loan giving the holder the right to redeem the stock at any time is equivalent to a perpetual American option with a time-dependent strike price. This has since been extended to allow for more industry-standard features such as margin calls, in which the writer is allowed to request that the holder pay back part of the loan when the stock price drops too low. More recently, [2] characterized optimal strategies in a finite-maturity model. We study a finite-maturity formulation in which at any point in time, either the holder or the bank are allowed to lapse, yielding a stochastic differential game between the holder and the writer.

References

- [1] J. Xia and X. Y. Zhou, *Stock loans*, Mathematical Finance 17.2 pp. 307-317 (2007).
- [2] M. Dai and Z. Q. Xu, *Optimal redeeming strategy of stock loans with finite maturity*, Mathematical Finance 21.4 pp. 775-793 (2011).

Numerical methods for parameter identification of cardiac electrophysiology models

D.V. Pongui-Ngoma¹, Y. Bourgault², H. Nkounkou³

¹ Département de mathématiques, Université Marien Ngouabi, République du Congo, diogene.ponguingoma@umng.cg

² Department of Mathematics and Statistics, University of Ottawa, Canada, ybourg@uottawa.ca

³ Département de mathématiques, Université Marien Ngouabi, République du Congo, hnkounkou@yahoo.fr

Ionic models are used to describe the evolution of the electrical potential across cardiac cell membranes. These models usually read as a systems of coupled highly nonlinear first order ordinary differential equations (ODE). The right-hand-side of these ODEs is not always continuous, for instance to model instantly closing ionic gates controlled by the trans-membrane potential. This results in solutions that are less regular and difficulties in adjusting the model parameters, in particular using optimal control and differentiable optimization methods.

Our talk will address numerical methods to optimally adjust the parameters in such ionic models. We will illustrate the method for the Mitchell-Schaeffer model [1], which is a simple two variables ionic model with a limited set of parameters and one discontinuity in r.h.s. of the ODE for the gating variable. This model can still capture the main features of the cardiac action potential (AP), namely the action potential duration (APD), the conduction velocity (CV), depolarization time (DT), recovery time (RT), etc. A one-to-one relation exists between the model parameters and the AP main characteristics, but the adjustment of the parameters based on asymptotic formulae is not yet automatics [2]. We will present optimal control problems, in particular one where the cost functional is related to the characteristics of the AP. In this problem, the state variable is the solution the ODEs of the ionic model. Numerical methods are used to solve the ODEs, within the loop of a non-differentiable optimization method. Any attempts at differentiable optimization methods, for instance with gradient methods, did not work. Looking at a regularized version of the Mitchell-Schaeffer model, we showed that the sensitivities of the solution with respect to the model parameters grows rapidly with the regularization parameter, explaining the difficulties with gradient methods even with the regularized model. We will show that our non-differentiable optimization method can easily recover the ADP, DT, RT and so on, by identifying the values of the four parameters $\tau = [\tau_{in}, \tau_{out}, \tau_{open}, \tau_{close}]$ of the Mitchell-Schaeffer model. The method is general and can easily be applied to other ionic models.

References

- [1] Colleen C. Mitchell and David G. Schaeffer, *A two-current model for the dynamics of cardiac membrane*, Bulletin of Mathematical Biology, **65**, pp. 767–793 (2003).
- [2] M. Rioux and Y. Bourgault, *A predictive method allowing the use of a single ionic model in numerical cardiac electrophysiology*, ESAIM: Mathematical Modelling and Numerical Analysis (M2AN), **47**, pp. 987–1016 (2013).

Numerical solution of the Kuramoto-Sivashinsky initial-boundary value problem

Lennaert van Veen¹

¹ University of Ontario Institute of Technology, Canada, lennaert.vanveen@uoit.ca

The Kuramoto-Sivashinsky (KS) equation models interface growth, flame propagation and similar physical processes (see, e.g. [1] for an introduction). Most analysis of the KS equation has been done assuming periodic boundary conditions. In this setting, the Fourier decomposition of the solution is central to many theoretical ideas, such as renormalization group arguments, as well as to numerical solution, allowing for the use of standard pseudo-spectral methods. Fixed boundary conditions, in contrast, induce boundary layers and necessitate the use of non-uniform grids. On such grids, numerical differentiation is ill-conditioned and can potentially lead to a catastrophic blow-up of round-off error. In this paper, we use ideas recently explored by Viswanath *et al.* to completely eliminate numerical differentiation from the time-stepping algorithm [2].

We study the KS initial-boundary value problem (IBVP) given by

$$u_t + uu_x + u_{xx} + vu_{xxxx} = 0 \quad u(-1) = l, \quad u(1) = r, \quad u_{xx}(-1) = u_{xx}(1) = 0$$

The time-stepping scheme is based on an implicit-explicit scheme of order up to four in time and avoids numerical differentiation by analytically “inverting” the spatial differential operator by use of Green’s function. In this scheme, only memory requirements and CPU time set the limits of the spatial resolution. We present simulations on Chebyshev grids with up to 20,000 points, resolving dynamics for a viscosity v in the range 10^{-1} – 10^{-8} .

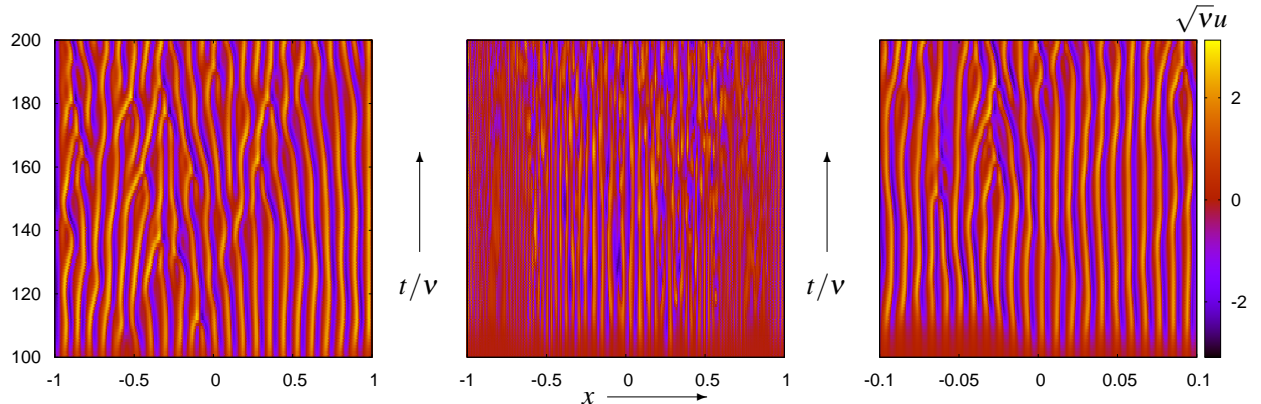


Figure 1: A hint of self-similar behaviour in the KS IBVP. Time series over $t/v \in (0, 200]$ with transients discarded, starting from random perturbations to the equilibrium solution $u \equiv 0$. Left: $v = v_1 = 10^{-4}$, 1001 grid points. Middle: $v = v_2 = 10^{-6}$, 4001 grid points. Right: enlargement of a fraction of $\sqrt{v_2/v_1} = 1/10$ of the spatial domain for $v = v_2$.

It is expected that the solutions, scaled as $\sqrt{v}u(\sqrt{v}x', vt')$ will become statistically independent of v and x' away from the boundaries and for small enough v . This is demonstrated in Fig. 1.

References

- [1] R. W. WITTENBERG AND P. HOLMES, *Scale and space localization in the Kuramoto-Sivashinsky equation*, Chaos, 9 (1999), pp. 452–465.
- [2] D. VISWANATH AND I. TOBASCO, *Navier-Stokes solver using Green’s functions I: Channel flow and plane Couette flow*, J. Comput. Phys., 251 (2013), pp. 414–431.

Padé Time Stepping Method of Rational Form for PDEs

S. Algarni¹

¹ King Fahd University of Petroleum and Minerals, Saudi Arabia, garnis@kfupm.edu.sa

One of the difficulties of the numerical solution of time-dependent ordinary and partial differential equations is the severe restrictions on time-step sizes for stability in explicit methods. Otherwise, challenging, generally nonlinear systems of equations in implicit schemes would be imposed to solve such problem.

A class of explicit methods based on use of Padé approximation, [3], is introduced [1]. They are inexpensive per time-step and they possess stability restrictions similar to the one offered by implicit schemes. Due to the rationality form of PTS, some numerical error occurs and then some a kind of control is imposed [2]. We find that the Padé time stepping (PTS) showed a preferable behaviour when reaction diffusion equations are considered. We also notice that the PTS schemes have less computational time than the compared ones. Finally, numerical runs are conducted to obtain the optimal local error control threshold.

References

- [1] D. Amundsen and O. Bruno, *Time stepping via one-dimensional Padé approximation*, J. of Scientific Computing, **30**, pp. 83-115 (2007).
- [2] S. Algarni, *Numerical Evolution Methods of Rational Form for Reaction Diffusion Equations*, PhD Thesis, (2012).
- [3] Baker and P. Graves-Morris, *Padé Approximants Part 1: Basic Theory*, Encyclopaedia of Mathematics and Its Applications, Vol. 13, Addison-Wesley, (1981).

Particle settling in yield stress fluids: limiting time, distance and applications

I.A. Frigaard¹, A. Wachs²

¹ University of British Columbia, Canada frigaard@math.ubc.ca

² IFP Energies nouvelles, Solaize, France, anthony.wachs@ifpen.fr

Yield stress fluids occur widely in industrial and natural settings [1], exhibiting the unique property that the fluids do not deform unless a critical stress threshold is exceeded. As industrial fluids it is common that particles and/or bubbles are immersed in such fluids and a natural fluid dynamics problem to study therefore concerns the balance between buoyancy stresses and the yield stress. In the simplest case, this amounts to the statement that a sufficiently small bubble or particle may be held in suspension indefinitely by the yield stress of the fluid, e.g. [2].

The above described problem concerns stationary static flows. Here we present new analytical and computational results concerning associated transient flows. For a single particle in an unbounded domain we show that the static flow criterion defines a critical stress ratio for the stability of the transient flow. When the yield stress exceeds this critical ratio, initially moving particles come to rest in a finite time, which also means that they migrate only a finite distance.

For symmetric particles, particle orientation does not affect the stability criterion. However, asymmetric particles have a stability criterion that depends on orientation. For Newtonian fluids, it is known that settling with constant drift is possible at zero Reynolds number, Re , but for small $Re > 0$ inertial effects act to move particles to stable orientations. This leads to an interesting possibility, for yield stress fluids with small $Re > 0$; namely an initial orientation may be statically unstable, but the particle may then change orientation to a statically stable orientation.

References

- [1] N.J. Balmforth, I.A. Frigaard and G. Ovarlez, *Yielding to Stress: Recent Developments in Viscoplastic Fluid Mechanics*, Ann. Rev. Fluid Mech., **46**, pp. 121-146 (2007).
- [2] A. Beris, J. Tsamopoulos, R. Armstrong, R. Brown *Creeping motion of a sphere through a Bingham plastic.*, J. Fluid Mech., **158**, pp. 219-244 (1985).

Reconstruction of Dynamic SPECT Images

A. Celler¹, T. Humphries², S. Nakano³, M. Trummer⁴

¹ University of British Columbia and Vancouver Coastal Health Research Institute, Vancouver, Canada, aceller@physics.ubc.ca

² Oregon State University, Corvallis, USA, humphrit@science.oregonstate.edu

³ Simon Fraser University, Burnaby, Canada, snakano@sfu.ca

⁴ Simon Fraser University, Burnaby, Canada, trummer@sfu.ca

Single photon emission computed tomography (SPECT) is a diagnostic functional imaging modality wherein the distribution of a radioactive tracer inside the body is estimated based on data acquired from around the patient by a slowly rotating camera. Conventional SPECT image reconstruction assumes that this distribution remains constant during acquisition. In this talk we investigate imaging of a time-varying distribution of radiotracer, which results in a highly underdetermined reconstruction problem. Recovery of an accurate dynamic image from this data requires the use of additional constraints, including temporal regularization. We use simple inequality constraints to restrict the temporal behaviour of the reconstructed image. Since dynamic tracer behavior in the human body arises as a result of continuous physiological processes, changes in tracer concentration should follow a smooth time activity curve (TAC). Our algorithm promotes smoothness by constraining the concavity of the TAC in every voxel of the reconstructed image. Digital phantom simulations show that the algorithm yields more accurate images, with smoother, more consistent TACs within dynamic regions of interest. We will also describe some recent results obtained with a pinhole camera which allows for data acquisition from all directions simultaneously. In this case we again obtain much smoother TACs.

Relaxation method for the nonlinear p -curl problem in applied superconductivity : a relaxed Yee scheme

Y.-M. L.-K. Cio¹, M. Laforest¹

¹ École Polytechnique de Montréal, Montréal, Canada, yann-meing.law-kam-cio@polymtl.ca

² École Polytechnique de Montréal, Montréal, Canada, marc.laforest@polymtl.ca

The power law model of magnetic resistivity

$$\rho(\nabla \times \mathbf{B}) = \alpha_0 |\nabla \times \mathbf{B}|^{p-2}$$

is the main model used by engineers to predict propagating magnetic fronts inside so-called high-temperature superconductors (HTS). This macroscopic model leads to a nonlinear form of eddy-current problem

$$\partial_t \mathbf{B} + \nabla \times (\rho(\nabla \times \mathbf{B}) \nabla \times \mathbf{B}) = 0$$

which, for the optimal design of new classes of HTS devices, still cannot be solved cost-effectively in 3D using traditionnal finite element methods (FEM) adapted to the nonlinearity. Moreover, traditionnal FEM also possess unphysical oscillations near the front which impact the propagation speed of the front, and hence the accuracy of quantities of interest. The similarity between this model and the p -Laplacian explain why this problem is sometimes referred to as the p -curl problem.

Recent work by Naldi and his collaborators for degenerate parabolic problems [1], specifically for the porous media equation, and work of Jin and Xin on the Hamilton-Jacobi equation [2], has been combined to produce a relaxation model and scheme of the nonlinear Maxwell equations from applied superconductivity. The scheme involves a splitting into a convective part, handled explicitly and a relaxation step, handled implicitly. As Naldi had noticed, the implicit nonlinearity is in fact solved explicitly, and with a staggered discretization over a uniform mesh, the convective part is discretized in a manner similar to the well-known Yee scheme [3]. This new scheme belongs to a larger class of cost-effective high-order schemes with an implicit treatment of the nonlinearity, a significant innovation. Most important of all, these schemes control the numerical oscillations near the magnetic front. Other relaxation schemes for this model are the subject of ongoing work with H. J. Kim.

References

- [1] F. Cavalli, G. Naldi, G. Puppo, and M. Semplice, *High-order relaxation schemes for nonlinear degenerate diffusion problems*, SIAM J. Numer. Anal., **45**, 5, pp. 2098-2119 (2007).
- [2] S. Jin and Z. Xin, *Numerical passage from systems of conservation laws to Hamilton-Jacobi equations, and relaxation schemes*, SIAM J. Numer. Anal., **35**, 6, pp. 2385-2404 (1998).
- [3] K. Yee, *Numerical solution of initial boundary value problems involving Maxwell's equations in isotropic media*, IEEE Transactions on Antennas and Propagation, **14**, 3, pp. 302-307, (1966).

Smooth regularizations of the Dirac delta distribution

Bamdad Hosseini, Nilima Nigam and John Stockie¹

¹ Simon Fraser University, Burnaby, BC {bhossein, nigam, jstockie}@sfu.ca

In this talk we discuss regularizations of the Dirac delta distribution with applications to prototypical elliptic and hyperbolic partial differential equations (PDEs). We consider the convergence of a sequence of distributions \mathcal{S}_H to a singular term \mathcal{S} as a parameter H (associated with the support size of \mathcal{S}_H) shrinks to zero. We characterize this convergence in both the weak-* topology of distributions, as well as in a weighted Sobolev norm. These notions motivate a framework for constructing regularizations of the delta distribution that includes a large class of existing methods in the literature. We also discuss various practical issues concerning numerical solution of PDEs with singular source terms. For example, using the well known tensor product regularizations of the the delta distribution in the second order wave equation results in a non-symmetric solution while a radial regularization maintains this qualitative behavior.

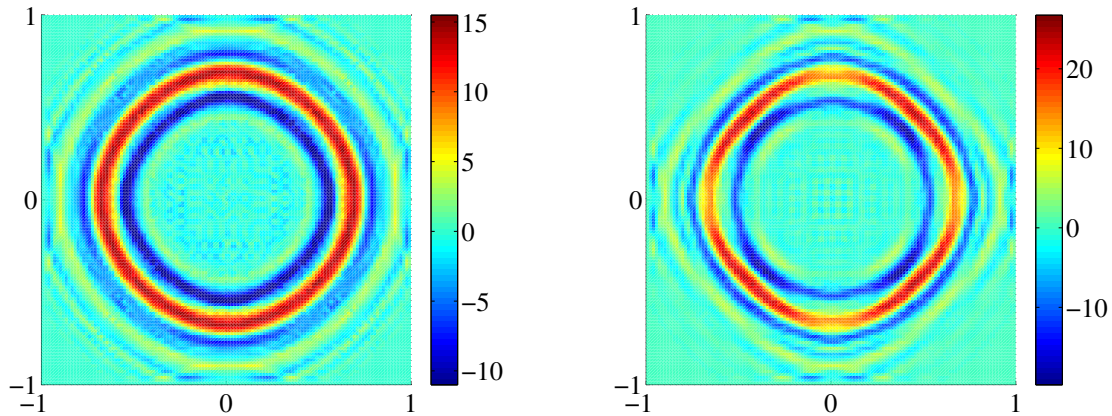


Figure 1: Comparing solution of the second order wave equation on unit square with impulse initial conditions. On left the solution is computed using a radial regularization of the delta distribution and on right the solution is computed using a tensor product regularization.

Some optimal and optimized Schwarz iterations for Nonlinear BVPs

R. Haynes¹, F. Kwok², A. Sarker¹

¹ Memorial University of Newfoundland, {rhaynes,ans363}@mun.ca

² Hong Kong Baptist University, felixk80@gmail.com

Motivated by the grid generation problem via the equidistribution principle, we consider various domain decomposition methods for a class of nonlinear boundary value problems. Classical Schwarz type methods are known to converge slowly, hence we design and analyze families of optimal and optimized Schwarz methods. These iterations leads us to a beautiful class of nonlinear Peaceman–Rachford iterations and the theory of M -functions popularized by Ortega and Rheinboldt. We demonstrate and motivate our theory with numerical examples.

Sparse Jacobian Matrix Determination using Two-sided Compressions

Daya R. Gaur¹, Shahadat Hossain¹, Anik Saha¹

¹ University of Lethbridge, Lethbridge, Alberta, Canada.
 daya.gaur@uleth.ca
 shahadat.hossain@uleth.ca
 anik.saha@uleth.ca

We consider the problem of determining the Jacobian matrix $J \equiv F'(x)$ of a mapping $F : \mathbb{R}^n \mapsto \mathbb{R}^m$. Using differences, the product of the Jacobian matrix with a vector s may be approximated as

$$\frac{\partial F(x+ts)}{\partial t} \Big|_{t=0} = F'(x)s \approx \hat{J}s = \frac{1}{\varepsilon}[F(x+\varepsilon s) - F(x)] \equiv b, \quad (1)$$

where $\varepsilon > 0$ is a small increment and \hat{J} is the finite difference approximation of matrix J , using one extra function evaluation. Algorithmic Differentiation (AD) [3] *forward mode* and *reverse mode* give $b = Js$ and $c = w^\top J$, respectively, for suitable vectors s, w without incurring any truncation error, at a cost which is a small multiple of the cost of one function evaluation. In many applications, the sparsity structure (i.e., location of nonzero entries) of the Jacobian matrix is known a priori. If a group of columns, say columns j and k , are structurally orthogonal i.e. no two columns have nonzero entries in the same row position, only one extra function evaluation

$$J_j + J_k \approx \hat{J}(:, j) + \hat{J}(:, k) = \frac{1}{\varepsilon}[F(x + \varepsilon(e_j + e_k)) - F(x)]$$

is sufficient to read off the nonzero entries from the vector $b = \hat{J}s, s \equiv e_j + e_k$. Here, e_j and e_k are the j th and the k th unit coordinate vectors. Partitioning the columns of a matrix A (A^\top) into structurally orthogonal groups, an observation first made in [2], can be viewed as a compression of the rows of $A(A^\top)$ and can be computed as products of matrix A and A^\top with vectors s as shown above. The classical arrow-head matrix example demonstrates that one-sided compression (i.e., row compression of A or A^\top) may not yield full exploitation of sparsity [4]. Hossain and Steihaug [4], and Coleman and Verma [1] independently proposed techniques for two-sided compression (i.e. row compression of A and A^\top) for the sparse Jacobian determination problem. Finding a two-sided compression that minimizes the number of matrix-vector products has been shown to be NP-Hard [1, 4]. In this paper, we present a new algorithm for computing a two-sided compression of a sparse matrix. We also give new lower bounds on the number of matrix-vector products needed to determine the matrix. Our algorithm exploits the synergy between sparse matrices and graphs. We extend the notion of direct cover of [4] and consider the columns of A and A^\top based on a new ordering criteria. The columns are then included in the least numbered group. On a set of test problems considered in [5] our algorithm saves, on average, about 20% matrix-vector products over the coloring algorithm of [5].

References

- [1] T. F. Coleman and A. Verma. The efficient computation of sparse Jacobian matrices using automatic differentiation. *SIAM J. Sci. Comput.*, 19(4):1210–1233, 1998.
- [2] A. R. Curtis, M. J. D. Powell, and J. K. Reid. On the estimation of sparse Jacobian matrices. *J. Inst. Math. Appl.*, 13:117–119, 1974.
- [3] A. Griewank and A. Walther. *Evaluating Derivatives: Principles and Techniques of Algorithmic Differentiation*. (2nd ed.) Number 105 in Other Titles in Applied Mathematics. SIAM, Philadelphia, PA (2008)
- [4] A. S. Hossain and T. Steihaug. Computing a sparse Jacobian matrix by rows and columns. *Optimization Methods and Software*, 10:33–48.
- [5] D. Juedes and J. Jones. Coloring Jacobians revisited: a new algorithm for star and acyclic bicoloring. *Optimization Methods and Software*, 27(2):295–309, 2012.

Stability and dynamics of liquid threads and annular layers in a corrugated tube

Qiming Wang

York University, Canada {qmwang}@yorku.ca

We study the stability and breakup behavior of an axisymmetric liquid thread which is surrounded by another viscous fluid layer. The two fluids are immiscible and confined in a concentrically placed cylindrical tube. We first derive a reduced model through a long wave approximation, where the effect of the tube wall corrugation is taken into account in the model, allowing the access of the interaction between the wall shape and the thread interfacial dynamics. The linearized system is studied by the Floquet theory due to the presence of non-constant coefficients in the equation and the spectrum is computed numerically via the *Fourier-Floquet-Hill* method. The resulting features agree qualitatively with those obtained based on a lubrication model in the thin annulus limit, where the short-wave disturbances that would be stabilizing owing to the capillarity in the absence of wall corrugation, can excite some unstable long waves. Those results from the linear theory are also confirmed numerically by the direct numerical simulation on the evolution equations. Meanwhile, a transition on the dominant modes from the one for a tube without corrugation to the one with wall shape included is found. The drop formation is shown in the nonlinear regime when the pinch off of the core thread is obtained. The annular film drainage regime is also approached slowly along with pinching when the tube wall is close to the thread interface. In addition, our results demonstrate the possibility to suppress pinching, depending on the averaged annular layer thickness and the variation in tube radius. Finally we numerically solve the full axisymmetric problem by using a boundary-integral method, where a periodic version of the Green's functions (Stokeslets) for the Stokes flow that satisfies no slip boundary condition on tube wall, is used. The results qualitatively agree with the prediction of the asymptotic model.

The Double Exponential Sinc Collocation Method for Singular Sturm-Liouville Problems

Hassan Safouhi

Campus Saint-Jean, University of Alberta

8406, 91 Street, Edmonton, Alberta T6C 4G9, Canada

hsafouhi@ualberta.ca

<http://www.csj.ualberta.ca/safouhi/>

Joint work with:

Philippe Gaudreau and Richard M. Slevinsky

Abstract. The Sinc collocation method (SCM) has been used extensively during the last three decades to solve many problems in numerical analysis [1]. Their applications include numerical integration, linear and non-linear ordinary differential equations. The double exponential transformation [2] yields optimal accuracy for a given number of function evaluations when using the trapezoidal rule in numerical integration. Recently, combination of the SCM with the double exponential (DE) transformation has sparked great interest [3].

Sturm-Liouville (SL) equations are abundant in the numerical treatment of scientific and engineering problems. For example, SL equations describe the vibrational modes of various systems, such as the energy eigenfunctions of a quantum mechanical oscillator, in which case the eigenvalues correspond to the energy levels. SL problems arise directly as eigenvalue problems in one space dimension. They also commonly arise from linear PDEs in several space dimensions when the equations are separable in some coordinate system, such as cylindrical or spherical coordinates.

In this talk, we present a method based on the double exponential Sinc collocation method (DESCM) for singular SL problems. Implementing the DESCM transformed the problem into a generalized eigenvalue problem where the matrices are symmetric and positive definite. This leads to an extremely efficient computation of eigenvalues of singular SL problems. We also show that the DESCM has exponential convergence. Three singular SL problems are treated and comparisons with the single exponential transformation are presented for each example clearly illustrating the superiority of the DESCM.

Keywords

Sinc-collocation method. Double exponential transformation. Sturm-Liouville eigenvalue problems.

References

- [1] F. Stenger. Summary of Sinc numerical methods. *J. Comput. Appl. Math.*, 121:379–420, 2000.
- [2] H. Takahasi and M. Mori. Double exponential formulas for numerical integration. *RIMS*, 9:721–741, 1974.
- [3] K. Tanaka, M. Sugihara, and K. Murota. Function classes for successful DE-Sinc approximations. *Math. Comput.*, 78:1553–1571, 2009.

The multiplier method to construct conservative finite difference schemes for ordinary and partial differential equations

A. Wan¹, A. Bihlo², J.C. Nave³

¹ McGill University, Montréal, Canada, andy.wan@mcgill.ca

² Memorial University of Newfoundland, St. John's, Canada, abihlo@mun.ca

³ McGill University, Montréal, Canada, jcnav@math.mcgill.ca

Structure-preserving discretizations are numerical methods which preserve important structure of differential equations at the discrete level. For system derived from a Hamiltonian or Lagrangian, symplectic and variational integrators are a class of discretizations which can preserve symplectic and variational structure at the discrete level. In this talk, we introduce the multiplier method of constructing conservative finite difference schemes for ordinary and partial differential equations. The proposed discretization is shown to be consistent for any order of accuracy and that by construction, the discrete densities can be exactly conserved. In particular, the multiplier method does not require the system to possess a symplectic or variational structure. Examples, including dissipative problems, are given to illustrate the method. Moreover, stability for such conservative methods are discussed. This is joint work with Alexander Bihlo at Memorial University and Jean-Christophe Nave at McGill University.

References

- [1] A. Wan, A. Bihlo and J.C. Nave, *The multiplier method to construct conservative finite difference schemes for ordinary and partial differential equations*, arxiv.org/abs/1411.7720, (currently in review).

The Sphere Decoding Approach for Mixed Integer Least Squares Problems

Xiao-Wen Chang¹, Jiequn Shen², Xiaohu Xie³

¹ McGill University, Montreal, Canada, chang@cs.mcgill.ca

² McGill University, Montreal, Canada, jiequn.shen@mail.mcgill.ca

³ IBM, Toronto, Canada, xiaohu.xi@mail.mcgill.ca

Given $\mathcal{X} \subseteq \mathbb{R}^p$, $\mathcal{Z} \subseteq \mathbb{Z}^q$, $y \in \mathbb{R}^m$, $A \in \mathbb{R}^{m \times p}$ and $B \in \mathbb{R}^{m \times q}$ with $[A, B]$ being of full column rank, we consider the following general mixed integer least squares (MILS) problem:

$$\begin{aligned} & \min \|y - Ax - Bz\|_2^2 \\ & \text{s.t. } x \in \mathcal{X}, z \in \mathcal{Z} \end{aligned} \tag{1}$$

Some special cases of this general MILS problem arise from many applications, including GPS, wireless communications, and cryptograph etc.

There are a few approaches to solving the ordinary ILS problem, which is also referred to as the closest vector problem, a special case of (1), where A does not exist and $\mathcal{Z} = \mathbb{Z}^q$. The most efficient one used in practice is the so called sphere decoding approach, which enumerates integer points in an ellipsoid (or equivalently lattice points in a sphere) to find the optimal solution [5] [7]. This approach is a branch and bound approach and has been extended to some constrained ILS problems, see, e.g., [2] and [3]. In this work, we extend the approach to the more general MILS problem (1) and we also show how to find a good initial search radius, which determines the size of the initial search space. To prune the search space, we give a simple and unified way to derive a class of lower bounds, from which the typical lower bounds used in the literature for the ordinary or box-constrained ILS problems (see, e.g., [6], [8], [4], and [1]) can be obtained.

References

- [1] C. Buchheim, A. Caprara, and A. Lodi, *An effective branch-and-bound algorithm for convex quadratic integer programming*, Mathematical Programming, **135**, pp. 369-395 (2012).
- [2] X.-W. Chang and Q. Han, *Solving box-constrained integer least squares problems*, IEEE Transactions on Wireless Communications, **7**, pp. 277-287 (2008).
- [3] X.-W. Chang and G. Golub, *Solving ellipsoid-constrained integer least squares problems*, SIAM Journal on Matrix Analysis and Applications, **31**, pp. 1071-1089 (2009).
- [4] V. M. Garcia, S. Roger, R. A. Trujillo, A. M. Vidal, and A. Gonzalez, *A deterministic lower bound for the radius in sphere decoding search*, in *Proceedings of the International Conference on Advanced Technologies for Communications*, pp. 11-16 (2010).
- [5] U. Fincke and M. Pohst, *Improved methods for calculating vectors of short length in a lattice, including a complexity analysis*, Mathematics of Computation, **44**, pp. 463-471 (1985).
- [6] A. Kamath and N. Karmarkar, *A continuous method for computing bounds in integer quadratic optimization problems*, Journal of Global Optimization, **2**, pp. 229-241 (1992).
- [7] C. Schnorr and M. Euchner, *Lattice basis reduction: Improved practical algorithms and solving subset sum problems*, Mathematical Programming, **66**, pp. 181-199 (1994).
- [8] M. Stojnic, H. Vikalo, and B. Hassibi, *Speeding up the sphere decoder with h^∞ and SDP inspired lower bounds*, IEEE Transactions on Signal Processing, **56**, pp. 712-726 (2008)

Three tales of success for numerical methods in heart simulation

R.J. Spiteri¹, S. Torabi Ziaratgahi²

¹ University of Saskatchewan, Saskatoon, Canada, raymond.spiteri@usask.ca

² University of Saskatchewan, Saskatoon, Canada, saeed.torabi@usask.ca

Cardiac electrophysiology can be mathematically modelled by the bidomain equations, a multi-scale reaction-diffusion system of nonlinear ODEs describing the ionic currents at the cellular scale coupled with a set of PDEs describing the propagation of the electrical activity at the tissue scale. On a spatial domain $\Omega \subset \mathbb{R}^d$ of dimension d and time interval $[t_0, t_f]$, the bidomain model can be written as [3]

$$\frac{\partial \mathbf{s}}{\partial t} = \mathbf{f}(\mathbf{s}, v, t), \quad (1a)$$

$$\chi C_m \frac{\partial v}{\partial t} + \chi I_{\text{ion}}(\mathbf{s}, v, t) + I_{\text{stim}}(\mathbf{x}, t) = \nabla \cdot (\sigma_i \nabla v) + \nabla \cdot (\sigma_e \nabla u_e), \quad (1b)$$

$$0 = \nabla \cdot (\sigma_i \nabla v) + \nabla \cdot ((\sigma_i + \sigma_e) \nabla u_e), \quad (1c)$$

subject to boundary conditions on $\partial\Omega \times [t_0, t_f]$ given by

$$\begin{aligned} \hat{\mathbf{n}} \cdot (\sigma_i \nabla v + \sigma_e \nabla u_e) &= 0, \\ \hat{\mathbf{n}} \cdot (\sigma_e \nabla u_e) &= 0, \end{aligned} \quad (2)$$

where, at location $\mathbf{x} \in \Omega$ and time $t \in [t_0, t_f]$, $\mathbf{s} = \mathbf{s}(\mathbf{x}, t)$ is a vector related to the cellular states such as gating variables and ionic concentrations, $v = v(\mathbf{x}, t)$ is the transmembrane potential, and $u_e = u_e(\mathbf{x}, t)$ is the extracellular potential. The terms $\mathbf{f}(\mathbf{s}, v, t)$ and $I_{\text{ion}}(\mathbf{s}, v, t)$ are non-linear functions related to the cell model; $I_{\text{stim}}(\mathbf{x}, t)$ is an applied stimulus current; σ_i and σ_e are conductivity tensors related to the intracellular and extracellular potentials, respectively. Finally, χ is the area of cell membrane per unit volume, C_m is the capacitance of the cell membrane per unit area, and $\hat{\mathbf{n}}$ is the unit outward normal to $\partial\Omega$. The boundary conditions represent the non-conductivity of the heart boundary.

To solve the bidomain equations and produce clinically useful data via simulation, billions of variables must be evolved. Even with modern-day computing hardware, the efficiency of the numerical methods employed is critical in determining the viability of a simulation.

In this presentation, I tell the tale of three successful time-integration methods for the bidomain equations. The first is a partitioned type-insensitive method for solving only the cell model equations (1a). The second is an L-stable method to suppress spurious oscillations in the solution of (1b)–(1c). The third is a fast operator-splitting method to solve (1). Full details can be found in [1, 4, 2].

References

- [1] M.E. Marsh, S. Torabi Ziaratgahi, and R.J. Spiteri, *The secrets to the success of the Rush–Larsen method and its generalizations*, IEEE Trans. Biomed. Eng. **59**, 9, pp. 2506–2515 (2012).
- [2] R.J. Spiteri and S. Torabi Ziaratgahi, *Lickety-split operator splitting for the bidomain model*, under review.
- [3] J. Sundnes, G.T. Lines, X. Cai, B.F. Nielsen, K.A. Mardal, and A. Tveito, *Computing the electrical activity in the heart*, Berlin: Springer-Verlag (2006).
- [4] S. Torabi Ziaratgahi, M.E. Marsh, J. Sundnes, and R.J. Spiteri, *Stable time integration suppresses unphysical oscillations in the bidomain model*, Front. Phys. **2**, 40 (2014).

Three-dimensional effects in miscible pipe displacement flows in the viscous regime

S. Yoon¹, K. Alba², I.A. Frigaard^{1,3}

¹ Mathematics, University of British Columbia, Canada. sungho.yoon5@gmail.com

² Department of Engineering Technology, University of Houston, US. kalba@uh.edu

³ Mechanical Engineering, University of British Columbia, Canada. frigaard@math.ubc.ca

We study the displacement flow of two Newtonian fluids in an inclined pipe. The fluids have the same viscosity but different densities. The displacing fluid is denser than the displaced fluid and is placed above the displaced fluid (i.e., a density unstable configuration). Three dimensionless groups describe these flows: a densimetric Froude number Fr , a Reynolds number Re , and the pipe inclination β . For strongly inclined pipes and with suitable combinations of Fr and Re , these flows tend to adopt a stratified structure in which the heavier layer advances along the bottom of the pipe in a structured slumping pattern; see the experimental study reported in [1].

Here we report the results of a computational study of the same flows, using a 3-dimensional finite element method and modeling the different fluids using a scalar concentration. We first benchmark the code against the viscous experiments, producing surprisingly good comparisons. We then use the numerical simulations to study the structure of the flow. In particular we find interesting secondary flows that recirculate fluid within the pipe cross-section and are responsible for squeezing the residual wall layer around the sides of the pipe. Comparisons with the results from the latter part of the experiments are made more difficult by the long computational domains required. We give an overview of the numerical strategy employed and explain the limitations of our current method.

References

- [1] S. M. Taghavi, K. Alba, T. Seon, K. Wielage-Burchard, D. M. Martinez, I.A. Frigaard, *Miscible displacement flows in near-horizontal ducts at low Atwood number* J. Fluid. Mech. **696**, 175–214 (2012).

Time-Stepping Methods in Cardiac Electrophysiology

T. Roy¹, Y. Bourgault²

¹ University of Ottawa, Canada, troy068@uottawa.ca

² University of Ottawa, Canada, ybourg@uottawa.ca

Modelling in cardiac electrophysiology results in a complex system of partial differential equations (PDE) describing the propagation of the electrical wave in the heart muscle coupled with a highly nonlinear system of ordinary differential equations (ODE) describing the ionic activity in the cardiac cells. This system forms the widely accepted bidomain model or its slightly simpler version, the monodomain model. To a large extent, the stiffness of the whole model depends on the choice of the ionic model, which varies in terms of complexity and realism. These simulations require accurate and, depending on the ionic model used, possibly very stable numerical methods. At this time, solving these models numerically requires CPU time of around one day per heartbeat. Therefore, it is necessary to use the most efficient method for these simulations.

This research focuses on the comparison and analysis of several time-stepping methods: explicit or semi-implicit, operator splitting and Rush-Larsen methods [1, 2, 3]. The goal is to find the optimal method for the ionic model used. For our analysis, we used the monodomain model but our results apply to the bidomain model as well. We compare the methods for three ionic models of varying complexity and stiffness: the Mitchell-Schaeffer models with only 2 variables, the more realistic Beeler-Reuter model with 8 variables, and the stiff and very complex TNNP models with 17 variables. For each method, we derived absolute stability criteria of the spatially discretized monodomain model and verified that the theoretical critical time steps obtained closely match the ones in numerical experiments. Convergence tests were also conducted to verify that the numerical methods achieve an optimal order of convergence on the model variables and derived quantities (such as speed of the wave, depolarization time), and this in spite of the local non-differentiability of some of the ionic models. We looked at the efficiency of the different methods by comparing computational times for similar accuracy. Conclusions are drawn on the methods to be used to solve the monodomain model based on the model stiffness and complexity, measured respectively by the most negative eigenvalue of the model's Jacobian and the number of variables, and based on strict stability and accuracy criteria.

References

- [1] M. Ethier and Y. Bourgault, *Semi-implicit time-discretization schemes for the bidomain model*, SIAM J. Numer. Anal., **46**, 5, pp. 2443-2468 (2008).
- [2] M.E. Marsh, S.Z. Torabi, and R.J. Spiteri, *The secrets to the success of the Rush-Larsen method and its generalizations*, IEEE, BME-**59**, 9, pp. 2506-2515 (2013).
- [3] J. Sundnes, G.T. Lines, B.F. Nielsen X. Cai, K.-A. Mardal, and A. Tveito, *Computing the Electrical Activity in the Heart*, Monogr. Comput. Sci. Eng., vol.1, Springer (2006)

Utilizing Support Vector Machines to Improve Graph Transduction

Edward Cheung, Yuying Li

University of Waterloo, Canada, {eycheung, yuying}@uwaterloo.ca

Graph diffusion has become a popular approach for many semi-supervised problems due to computational efficiency and strong experimental results. A common issue that plagues many existing semi-supervised algorithms is that performance degrades when the underlying data has imbalanced class proportions. This is of particular concern in the imbalanced class setting where the labels are expected to be disproportionate. While there has been work done to address imbalanced label issues, we have found experimentally that most existing graph algorithms can only perform well under balanced label settings or when the true proportions are known beforehand.

In this paper, we propose an iterative support vector machine (SVM) based graph diffusion algorithm. We use the optimal values from the SVM dual problem to assign diffusion weights, allowing us to balance weights only on informative nodes. The algorithm is made efficient by training only on a small subset of nodes created from the previous set of support vectors and the most recently introduced set of labeled nodes. We demonstrate that this reduced set is sufficient to describe the manifold, reducing computation time and improving binary classification performance on imbalanced datasets.

**ST-CFDSC The 23rd Conference of the CFD
Society of Canada**

2.5-D CFD Simulation of Swept High-Lift Wing Configurations

Hong Yang¹ and Kurt Sermeus²

^{1,2}Bombardier Aerospace
2351 boul. Alfred-Nobel (BANI), Ville Saint-Laurent, Québec, H4S 2A9

Email: hong.yang@aero.bombardier.com

ABSTRACT

The prediction of high-lift flows is a challenge of practical interest to aerospace industry. For configurations that include multiple elements such as leading edge slats and trailing edge flaps, the flow physics can be particularly challenging for current generation CFD codes and turbulence models. These challenges include wakes in pressure gradients, wake/boundary layer merging, curvature effects, separated flow, possible unsteadiness, wing-tip vortical flow and laminar/turbulent transition, etc. The full 3D RANS modeling of high-lift flows is still time consuming even on present High Performance Computing (HPC) platforms, hence for quick design or analysis purpose, two-dimensional CFD modeling of high-lift devices is very popular in industrial practice. However, for swept wings, the 2D modeling by ignoring crossflow in spanwise direction may result in considerable discrepancy in aerodynamic force prediction than the one extracted from the 3D modeling. To relieve the restriction of the 2D modeling, the so-called 2.5-D CFD modeling capability was developed recently in Bombardier in-house 3D unstructured CFD package DRAGON with the hypothesis of infinite swept wing. The 2.5-D model was created by extruding a 2D planar grid in spanwise direction followed by shearing one side plane to take into account wing sweep angle and then associating the two side planes with periodicity (see Figure 1). The validation of the 2.5-D modeling on the 2nd AIAA high lift prediction workshop test case is to be presented, along with demonstration of its advantages over the 2D modeling.

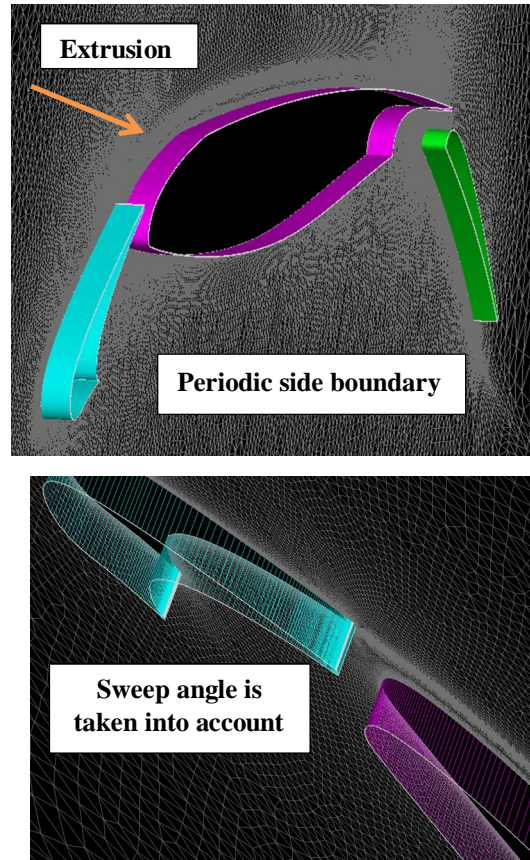


Figure 1 2.5-D model of a high-lift section built from a 2D grid

2D Analysis of a Flow Past a Square Cylinder Using the Spectral Element Method

Pradeep Jha and Catherine Mavriplis

*Department of Mechanical Engineering
University of Ottawa, 161 Louis Pasteur, Ottawa, ON, K1N6N5, Canada*

Email: *pjha@uottawa.ca*

ABSTRACT

The flow past a square cylinder has not been as extensively studied in the literature as compared to the circular cylinder. There is general agreement in the literature that, for low Reynolds (Re) number flows, there is a smooth line correlation between the Re number and the vortex shedding frequency, which ends at around a Re of 200 – 300. The exact number is not agreed upon. In the present communication, we compare the results obtained by a high-order spectral element solver with existing results.

1 INTRODUCTION

Many studies have been reported on the flow past a circular cylinder. Relatively, the flow past a square cylinder has not been investigated as thoroughly. The flow properties of the wake behind the square cylinder as a function of the flow Reynolds number, Re , are a subject of interest for practical applications such as flow past tall buildings and have been studied in some detail [8, 7, 4].

The Strouhal number, St , is a dimensionless quantity which gives the vortex shedding frequency behind the cylinder. The variation of St with Re , gives an indication of the flow behavior in the wake as a function of Re . The separation Re , Re_{sep} , indicates the Re at which flow separation begins at the sharp edges. While Okajima [5] reports this critical Re to be around 70, later studies by Klekar et al. [3] have predicted this number to be around 54. A smooth variation has been observed in the literature in St as a function of Re , from the critical Re to a value of around 300. For this range, some investigations report that the flow determined by sharp corners can be considered two-dimensional. However, beyond this range, the onset of three-dimensional structures can be seen in the wake



Figure 1: The vortex shedding seen behind the square cylinder for a grid with $K = 1204$ elements and Re of 150 shown as pressure contours.

of the cylinder [6, 10].

The flow behind the square cylinder depends on several parameters such as the inflow profile, the blockage ratio of the cylinder defined as the ratio of its side and the distance between the wall boundaries, and the outflow conditions. In the present report, we investigate the flow past a square cylinder for a flow configuration previously studied by Breuer et al. [1].

2 NUMERICAL SCHEME

The open-source computational fluid dynamics solver based on the spectral element method (SEM), Nek5000 [2], was used as the computational tool for the simulation of the flow. The code is written in Fortran77/C and employs the MPI standard for parallelism. The simulations were carried out on the High Performance Computing Virtual Laboratory (HPCVL) (<http://www.hpcvl.org>) facility at Ontario, Canada.

3 SAMPLE RESULTS

Figure 1 shows the pressure contours of a flow past a square cylinder. The total number of elements in the

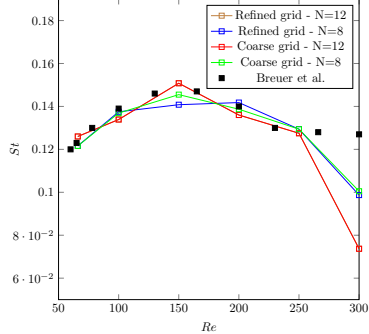


Figure 2: Strouhal number, St , vs Reynolds number, Re , variation seen for flow past a square cylinder using the Nek5000 computational tool.

grid is $K = 1204$. The number of elements in the x -direction is 61 and the number of elements in the y -direction is 20. For the refined grid $K = 2484$. The orders of the polynomial, N , for the SEM used are 8 and 12. For $N = 8$, there are 4 elements on each side of the square. The finest collocation point spacing at the corner of the square is around $0.014D$, where D is the side of the square. The pressure contours of Figure 1 show a slight drop in pressure behind the cylinder.

Figure 2 shows the variation of the St with the Re obtained for the present flow configuration. It shows good agreement with the earlier computational data obtained by Breuer et al. [1]. However there is a difference between the data for values of Re above 250. While the present simulations show a sharp drop in the St value, the earlier data shows a constant value for Re higher than 250. Some earlier works [9] mention the formation of some secondary instabilities in the wake of the cylinder around Re of 250. These secondary instabilities are found to cause a discontinuity in the St - Re graph.

4 CONCLUSION

The flow past a square shows some very interesting properties near the Re_{cr} . The instabilities for low Re are two-dimensional in nature, and slowly transform to three-dimensional structures at higher Re around $250 - 300$. This communication will investigate the change in the nature of the instabilities for the flow past a square cylinder, and analyze how the sharp corners affect the instabilities.

REFERENCES

- [1] M. Breuer, J. Bernsdorf, T. Zeiser, and F. Durst. Accurate computations of the laminar flow past

a square cylinder based on two different methods: Lattice-Boltzmann and Finite-Volume. *International Journal of Heat and Fluid Flow*, 21(2):186–196, 2000.

- [2] P. F. Fischer, J. W. Lottes, and S. G. Kerkemeier. Nek5000 Web page, 2008. <http://nek5000.mcs.anl.gov>.
- [3] K. M. Klekar and S. V. Patnakar. Numerical prediction of vortex shedding behind square cylinders. *International Journal of Numerical Methods in Fluids*, 14:327–341, 1992.
- [4] R. Mittal and S. Balachandar. Generation of streamwise vortical structures in bluff body wakes. *Phys. Rev. Lett.*, 75:1300, 1995.
- [5] A. Okajima. Strouhal number of rectangular cylinders. *Journal of Fluid Mechanics*, 123:379–398, 1982.
- [6] F. R. Rodi and W. Schonung. Numerical calculation of laminar vortex shedding past cylinders. *Journal of Wind Engineering and Industrial Aerodynamics*, 35:237–257, 1990.
- [7] A. Roshko. On the development of turbulent wakes from vortex streets. *NACA report*, page 1191, 1954.
- [8] C. H. K. Williamson. The existence of two stages in the transition to three-dimensionality of a cylinder wake. *Physics of Fluids*, 31:3165, 1988.
- [9] C. H. K. Williamson. Mode-a secondary instability in wake transition. *Physics of Fluids*, 8:1680–1682, 1996.
- [10] C. H. K. Williamson. Vortex dynamics in the cylinder wake. *Annual Review of Fluid Mechanics*, 82:477–539, 1996.

A Characteristic-based CFL Number for the Discontinuous Galerkin Method on Triangular Meshes

Noel Chalmers¹ and Lilia Krivodonova²

Department of Applied Mathematics, University of Waterloo, 200 University Avenue West, Waterloo, ON N2L 3G1

Email: *bnachalm@uwaterloo.ca*¹, *lgk@uwaterloo.ca*²

1 INTRODUCTION

The discontinuous Galerkin (DG) finite element method is a high-order adaptive numerical scheme which has gained popularity in recent years and has been developed into a robust method in computational fluid dynamics. When applied to convection problems in one dimension and with a standard pairing with an explicit Runge-Kutta method, it is well-known that an effective CFL condition is $\Delta t \leq \frac{1}{2p+1} \frac{h}{|a|}$, where h is the smallest element size and $|a|$ is the largest wave speed. On triangular grids in higher dimensions, however, an exact CFL condition is not known. Instead, the stability condition

$$\Delta t \leq \frac{1}{2p+1} \min_j \frac{r_j}{\|\mathbf{a}_j\|},$$

has been proposed and supported with numerical evidence [1], where r_j is the radius of the inscribed circle in each element and $\|\mathbf{a}_j\|$ is the largest wave speed. While this CFL condition provides a stable time step, it is known to not be a tight bound [2] and in some cases a much larger stable time step exists. In this talk we propose a CFL condition which is scaled not by the radius of the inscribed circles, but by a parameter h_j which depends on the characteristic flow directions in each cell. We provide several numerical examples which demonstrate the efficacy of this CFL condition.

2 ANALYSIS OF SPECTRUM

We provide an analytic justification for the proposed CFL condition through the analysis of the spectrum of the DG method in 2D for a particularly simple problem and mesh. We consider the linear advection equation

$$u_t + au_x + bu_y = 0,$$

and apply the DG discretization. We then derive a PDE which is satisfied by the numerical solution itself and through classical Fourier analysis we derive solutions to this PDE. We then use these solutions on a simple uniform mesh with periodic boundary conditions to derive a condition which must be satisfied by every spectral value of the DG spatial operator. The analysis reveals that the spectrum is scaled by a parameter h_j which geometrically can be seen to be the width of the each cell in the direction of the flow vector $\mathbf{a} = [a, b]$. The spectrum can also be seen to depend on a parameter $\theta \in [0, 1]$ which can be viewed as giving a measure of the flow direction in each cell. Numerical computations of the spectrum of the DG discretization has indicated that the size of the spectrum is only weakly influenced by this parameter θ , and therefore we propose a CFL condition of the form

$$\Delta t \leq CFL \min_j \frac{h_j}{\|\mathbf{a}\|}.$$

By pairing the spatial discretization with an explicit Runge-Kutta-($p+1$) time integration, we propose that taking

$$CFL = \frac{1}{(2p+1) \left(1 + \frac{4}{(p+2)^2} \right)},$$

provides a fairly tight bound on the time step Δt . We then generalize the conclusions from this scalar linear problem to non-linear systems of conservation laws.

3 COMPUTED EXAMPLES

We present several numerical examples to verify the stability of the proposed CFL condition and to observe the increase in efficiency of the method gained by allowing larger time steps. We present two linear examples, the first demonstrating that the proposed CFL condition allows us to take stable time steps over 65%

larger than given by the usual CFL condition for the $p = 1$ scheme, and over 100% larger for the $p = 3$ scheme.

The second linear example presents a special case of the proposed CFL condition. Since geometrically h_j is the width of a cell along the direction of flow, it will have no dependence on the size of the cell's other dimension. We therefore consider a mesh which is much more refined along the y axis than the x axis, and we consider the linear advection equation with a flow direction of $\mathbf{a} = [1, 0]$. We show that because the parameter h_j will have no dependence on the refinement in y in this case, we are able to take time steps over eight times larger than usually taken. We note that the disparity in time step size can increase without bound as the mesh is continually refined in the y dimension.

We finally present two non-linear examples to show the application of the proposed CFL condition to non-linear problems. We show an example with Burgers' equation where we observe a similar improvement over the usual time step size as in the linear case. We also show an example with the 2D Euler equations and show significant improvements in the size of time steps we are able to take.

4 CONCLUSION

We propose a new CFL condition for the DG method on triangular meshes which is scaled by a parameter h rather than the usual inscribed radius in each cell. The h parameter can be seen geometrically to be the width of the cell in the direction of the characteristic flow directions. We present several numerical examples which show the efficacy of this new CFL condition.

REFERENCES

- [1] B. Cockburn, S. Hou, and C.-W. Shu. The Runge-Kutta local projection discontinuous Galerkin finite element method for the conservation laws IV: The multidimensional case. *Mathematics of Computation*, 54: 545-581, 1990.
- [2] E.J. Kubatko, C. Dawson, and J.J. Westerink. Time step restrictions for Runge–Kutta discontinuous Galerkin methods on triangular grids. *Journal of Computational Physics*, 227 (23):9697-9710, 2008.

A comparison between two-dimensional (2D) and three-dimensional (3D) simulations of finite amplitude sound waves in a trumpet using the discontinuous Galerkin method

Janelle Resch¹ and Lilia Krivodonova²

Department of Applied Mathematics, University of Waterloo, 200 University Avenue West, Waterloo, Ontario Canada, N2L 3G1

Email: *jresch@uwaterloo.ca*¹, *lgk@uwaterloo.ca*²

1 INTRODUCTION

In order to accurately model the sound propagation in brass musical instruments, higher amplitude propagating waves must be taken into account. Assuming the pressure disturbance entering the narrow tubing of the bore is large enough, the crest of the wave will travel fast than the trough causing the wave to steepen. Wave steepening will excite the higher harmonic components of the sound pressure waves influencing the timbre of the sound by giving it a more ‘brassy’ effect. Such wave propagation can be modeled using the equations of motion found in gasdynamics. In order to incorporate nonlinear wave propagation and compressibility effect, we consider the compressible Euler equations and solved them numerically by using the discontinuous Galerkin method (DGM).

Previously, in [1], we modeled nonlinear wave propagation for a trumpet in 2D. In addition, we considered the consequences of neglecting the third spatial dimension. We calculated that the 2D - 3D dimensionality difference in our results would be approximately 14 dB. Here we present some of our preliminary results for considering the analogous problem in 3D.

2 EXPERIMENTAL AND SIMULATION DATA

The experimental data that we collected from a B^b Barcelona BTR-200LQ trumpet shown in Fig. 1 is discussed in detail in [1]. We took one period of the sound pressure measurements obtained from a quarter-inch microphone carefully mounted at the shank of the trumpet mouthpiece, and applied Fourier analysis to the data to reconstruct the waveform as a sum of sinusoidal waves. This experimental data obtained at

the mouthpiece was then used as a boundary condition on the pressure for our simulations. The musical notes recorded and then simulated were the B_3^b and B_4^b notes played at forte. For our simulations, the first 30 harmonics was taken into account. A half-inch microphone was also placed on the central axis of the trumpet around 16 cm - 17 cm outside the bell. We compared our simulation results with the pressure measurements obtained from this microphone outside the bell.



Figure 1: Placement of microphones on the Barcelona BTR-200LQ trumpet.

For the simulations, we assumed initially that the flow was at rest and related pressure and velocity through the 1D expression derived from linear acoustic theory. For the boundary conditions, we prescribed reflecting boundary conditions on the inner and outer walls of the trumpet mesh (excluding the mouthpiece). Since we modeled a trumpet in a box, we used pass-through boundary conditions on the computational domain. The 2D trumpet mesh we will be discussing has 8028 cells whereas the 3D mesh has 40,473 cells. Details of the mesh construction can be found in [1] and [2].

3 COMPUTED EXAMPLE

Several numerical simulations have been carried out to determine if the model we considered is adequate. Some such computational experiments are discussed in [1]. Others, specifically the 3D simulations, will soon be submitted for publication [2]. The simulations were carried out on trumpet mesh that is 1.48 m in total length. The diameter of the tube is constant with a radius of 0.58 cm, except near the end where it slowly increases and then flares rapidly at the bell. To properly account for the bell geometry, special software was used to carefully trace out the shape of the bell. Further details can be found in [1]. The 3D trumpet mesh with constant cylindrical bore was made directly by rotating the upper half of the 2D mesh around the x-axis.

The frequency spectrum of the measured B_3^b and B_4^b pressure waveforms outside the trumpet bell can be seen in Fig. 2 and 3 respectively. The 2D (blue lines) and 3D (green lines) simulation results for the B_3^b and B_4^b notes are also depicted in Figs. 2 and 3 respectively.

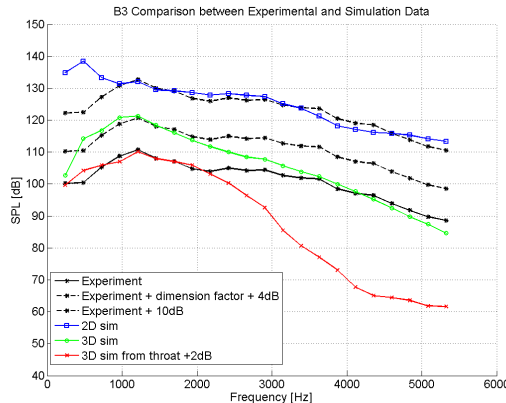


Figure 2: Numerical results for B_3^b

In reality, the tube of the trumpet near the mouthpiece is not cylindrical. One thing we are examining is how the taper from the mouthpiece to the first bend influences the wave propagation being modeled. Thus, we constructed several other 3D trumpet meshes: e.g., one where the diameter at the mouthpiece is set to the radius of the mouthpiece's throat (0.155 cm) and another which is set to the radius of the shank (0.45 cm). The B_3^b note was simulated in the 3D mesh that starts from the throat diameter, and the B_4^b note was simulated in the 3D mesh that starts from the shank diameter. These results can also be seen in Figs. 2 and 3 respectively. Additional commentary of these results as well as additional simulations will be presented at the conference.

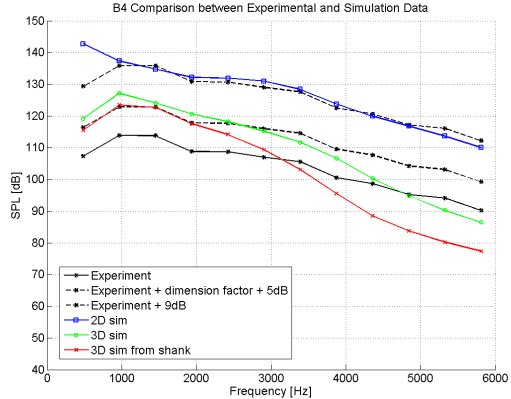


Figure 3: Numerical results for B_4^b

4 CONCLUSION

We have outlined the 2D and 3D simulation results of modeling nonlinear wave propagation in a trumpet. It is evident that neglecting the third spatial dimension, and thus the spreading of the wave in all directions, is too significant to dismiss. The 3D simulation results presented here illustrate that the tapper near the mouthpiece end is also important to consider. Although the shape of the harmonic distribution for components less than 2000 Hz match the experimental data if a tapper is considered, the amplitude is still off by 3 - 9 dB. However, according to [3], losses could account for this. If the tapper at the mouthpiece is neglected, the higher harmonic components of the notes match the experimental data rather well. However, there is this odd transition phase between the upper and lower harmonic components that we will be further exploring.

REFERENCES

- [1] J. Resch, L. Krivodonova, and J. Vanderkooy. A two-dimensional study of finite amplitude sound waves in a trumpet using the discontinuous Galerkin method. *Journal of Computational Acoustics*, 22(3): 27 pages, 2014.
- [2] J. Resch, L. Krivodonova, and J. Vanderkooy. A three-dimensional study of finite amplitude sound waves in a trumpet using the discontinuous Galerkin method. *Soon to be submitted*.
- [3] W. Kausel, and T. Moore. Influence of wall vibrations on the sound of brass wind instruments. *Universitat fur Musik und darstellende Kunst Wien* 1-46, 2010.

A Dual-Rotor Horizontal Axis Wind Turbine In-House Code (DR_HAWT)

K. Lee Slew¹, M. Miller¹, P. Tawagi², G. El-Hage², M. Hou², and E. Matida¹

¹*Department of Mechanical and Aerospace Engineering, Carleton University,
1125 Colonel By Drive, Ottawa, ON, Canada, K1S 5B7*

²*ZEC Wind Power, 1800 Woodward Drive, Ottawa, ON, Canada K2C 0P7*

Email: KennyLeeSlew@cmail.carleton.ca, MikeMiller@cmail.carleton.ca, patrickt@zecwindpower.com,
georgesh@zecwindpower.com, michaelh@zecwindpower.com, Edgar.Matida@carleton.ca

1. INTRODUCTION

With the recent increase in oil prices, wind energy has become one of the leading green energy solutions worldwide [1]. In an attempt to maximize the energy extraction capability of wind turbines, a Dual-Rotor, Contra-Rotating Horizontal Axis Wind Turbine has been proposed. By having both an upwind and a downwind rotor on a single tower, a medium sized wind turbine is able to produce more energy at a lower cost.

Blade Element Momentum theory (BEM) is widely used in industry to design wind turbines [1]. BEM is a computationally inexpensive method used to predict wind turbine rotor forces such as torque and power. However, it cannot accurately account for the wake produced by the wind turbine, and hence cannot be used for a dual rotor configuration where the wake interaction is important. Existing CFD programs, such as ANSYS, can be used to accurately simulate any wind turbine configuration with a high degree of accuracy. Unfortunately, these CFD simulations are computationally expensive relative to BEM based methods.

In an attempt to accurately predict the power and interacting wake produced by a dual rotor configuration, and to reduce computation runtimes compared to CFD, an in-house code was created and implemented. The resulting code produced more accurate results than BEM, while achieving greater efficiency than existing commercial CFD programs.

2. THEORY

BEM is a numerical method in which a given wind turbine blade is discretized along its span into

multiple elements at which the geometric data is known. Using the flow conditions at each point, lift and drag forces can be calculated based on data obtained from XFOIL for each airfoil profile. The forces at each element can then be integrated along the blade to determine the total resulting torque, thrust, and power of the rotor. Additionally, induction factors, which provide an approximation for the effects of the wake, can be included in BEM [1].

To represent the wake more accurately, a vortex filament method can be implemented in place of the induction factors in BEM. The strength of the vortex attached to the blade can be determined based on the Kutta-Joukowski theorem [1]. These bound vortices, and their related strengths, can then be shed from the blade to form the wake. The vortex filament method provides a suitable representation of the wake [2].

3. DR_HAWT

Fortran95 was used to create a Dual Rotor Horizontal Axis Wind Turbine program (DR_HAWT), which is a combination of BEM and the vortex filament method, based on Ref. [2, 3]. DR_HAWT allows for simulation of either a single rotor or dual rotor configuration. With regard to the latter, the wake created by the upwind rotor is convected downstream and interacts with the downwind rotor's wake. The combination of the upwind and downwind wakes result in an induced velocity on each blade element of each rotor. This in turn gives a more accurate representation of the true aerodynamic performance, which is the result of having a dual rotor configuration.

Figure 1, showing a dual rotor configuration with blades discretized into 24 elements, demonstrates DR_HAWT's ability to create visualizations of the

wake with each point representing the centroid of a shed vortex filament. DR_HAWT also has the ability to be run in serial (one CPU) or parallelized using multiple CPUs with one shared memory, which reduces runtimes significantly.

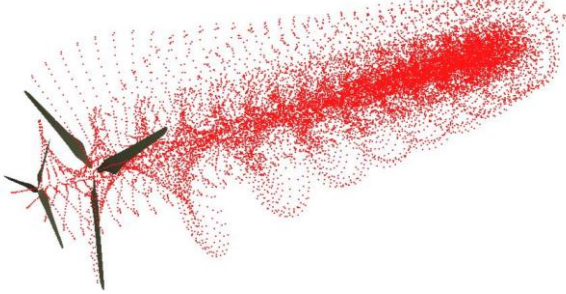


Figure 1: Wake Visualization generated by DR_HAWT

4. SINGLE ROTOR VALIDATION

The current work is to validate DR_HAWT with the National Renewable Energy Laboratory (NREL) Unsteady Aerodynamics Experiment (UAE) Phase VI experiment, which is one of the most data-rich wind turbine experiments in a steady and controlled environment.

In accordance with NREL UAE Phase VI Test Sequence S [4], the two-bladed rotor was configured and simulated for wind speeds ranging from 5 m/s to 25 m/s. As Figure 2 illustrates, the power curve produced by DR_HAWT (solid line) is in agreement with experimental data (points) and shows an improvement over the BEM method (dashed line). DR_HAWT resulted in an average error of about 20% when compared to experimental data at all wind speeds. This error is on the lower end of the range of 25%-175% produced by 30 industrial and academic experts using CFD methods of their choice in a blind comparison study [5].

DR_HAWT required approximately 1 hour of computation time, whereas some other methods required upwards of several days [5]. The closely matched power curve produced by DR_HAWT is indicative of its ability to accurately simulate a wind turbine under steady conditions. However, the present error indicates that certain flow physics are not accounted for. Since BEM is the foundation of DR_HAWT, and uses 2D airfoil data, one of the primary variables that DR_HAWT cannot account for are the 3D flow effects occurring over the blade. Due to the rotational nature of the wind turbine, the airflow over the top of the blade airfoils is not exactly parallel to the airfoil chord. In reality, the flow direction is a combination of the relative velocity of the oncoming wind as well as any velocities in the

radial direction caused by the rotation of the rotor. Other variables that are not currently simulated or accounted for include aero-elasticity, the losses around the hubs and tips of the rotors as well as losses due to the presence of a nacelle and tower.

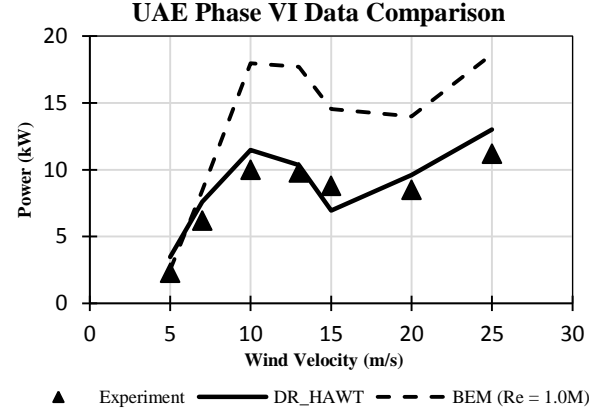


Figure 2: Data comparison for UAE Phase VI experiment

5. CONCLUSIONS

A horizontal axis wind turbine in-house code using BEM and vortex filaments was created and the results agreed with the NREL UAE Phase VI experiment. Future work will include further validation and sensitivity analyses as well as the implementation of aero-elastic interactions between the air and the wind turbine and correction factors to account for hub, tip, nacelle, and tower losses. CFD modeling of a dual rotor wind turbine will be performed and compared to DR_HAWT and wind tunnel results.

REFERENCES

- [1] M. O. Hansen, *Aerodynamics of Wind Turbines*, London, UK: EARTHSCAN, 2008.
- [2] J. Strickland et al., "A Vortex Model of the Darrius Turbine- an analytical and experimental study," Sandia Nation Laboratories, Lubbock, TX, 1980.
- [3] A. Fereidooni, "Numerical Study of Aeroelastic Behaviour of a Troposkiien Shape Vertical Axis Wind Turbine," Ottawa, ON, 2013.
- [4] D. Simms et al., "Unsteady Aerodynamics Experiment Phase VI: Wind Tunnel Test Configurations and Available Data Campaigns," NREL, Golden, CO, 2001.
- [5] D. Simms et al., "NREL Unsteady Aerodynamics Experiment in the NASA-Ames Wind Tunnel: A Comparison of Predictions to Measurements," NREL, Golden, CO, 2001.

A Dynamic Subfilter-scale Stress Model for Large Eddy Simulations Based on Physical Flow Scales

Amirreza Rouhi¹, Ugo Piomelli¹ and Bernard J. Geurts²

¹ Department of Mechanical and Materials Engineering, Queen's University, Kingston, Ontario, Canada

² Department of Applied Mathematics, University of Twente, Enschede, The Netherlands

Email: amirreza.rouhi@queensu.ca

ABSTRACT

We propose an eddy viscosity approach independent of the simulation grid for Large Eddy Simulations (LES). The model extends a previous proposal (Piomelli *et al.*[1]), in which the LES length-scale was associated with the intergal length-scale of turbulence based on flow characteristics, decoupling LES parameters from the grid, arriving at an Integral Length-Scale Approximation (ILSA) model. In the original ILSA, the model parameter was determined as a constant value based on a desired contribution of unresolved, subfilter scales (SFS) to the global transport. Here we propose a dynamic reformulation for ILSA (local ILSA) in which the model parameter is calculated dynamically in space, maintaining a desired level of subfilter activity in a local manner. Application of the new formulation on channel flow and backward-facing step indicates a robustness of local ILSA similar to the original model with the advantage of higher flexibility, making it well suited for complex problems.

1 FORMULATION

In Large Eddy Simulation (LES), the large, energy-containing eddies are resolved while the small, unresolved ones are modelled. This separation is performed through a filtering operation with an assigned filter width Δ , which determines the physical size of the smallest retained eddies. Thus the term subfilter scales (SFS) is associated with those eddies smaller than Δ . Having the large scales to account for most of the momentum transport requires Δ to be a fraction of the local integral length-scale. In current-day LES models however, the filter width is assigned based on the grid size h , *i.e.*, $\Delta \propto h$. This choice is in disagreement with the physical implication of the filter width, causing several undesirable characteris-

tics for the modelled eddies. Piomelli *et al.*[1] proposed to link the filter width to an approximation of the integral length-scale, based on the resolved turbulent kinetic energy $\mathcal{K}_{\text{res}} = 1/2\bar{u}_i^l\bar{u}_i^l$ and its dissipation rate $\varepsilon_{\text{tot}} = 2(\mathbf{v} + \mathbf{v}_{\text{sfs}})\bar{s}'_{ij}\bar{s}'_{ij}$, where \bar{s}'_{ij} is the fluctuating part of the strain-rate tensor. The integral length-scale is estimated as $L_{\text{est}} = \mathcal{K}_{\text{res}}^{3/2}/\varepsilon_{\text{tot}}$ and was called Integral Length-Scale Approximation (ILSA). Parametrizing subfilter eddies in an eddy viscosity context with a filter width associated with ILSA yields

$$\mathbf{v}_{\text{sfs}} = (C_m\Delta)^2 |\bar{\mathbf{S}}| = C_k^2 \frac{\langle \mathcal{K}_{\text{res}} \rangle^3}{\langle \varepsilon_{\text{tot}} \rangle^2} |\bar{\mathbf{S}}| \quad (1)$$

where C_k is the only parameter. In the original formulation[1], C_k was adjusted such that a certain level of dissipation rate was represented by the SFS. In more detail, s_ε (Meyers *et al.*[2]), quantifies this measure of subfilter activity:

$$s_\varepsilon^V = \frac{\langle \varepsilon_{\text{sfs}} \rangle_{V,t}}{\langle \varepsilon_{\text{tot}} \rangle_{V,t}} = \frac{\langle 2\mathbf{v}_{\text{sfs}}\bar{S}_{ij}\bar{S}_{ij} \rangle_{V,t}}{\langle 2(\mathbf{v}_{\text{sfs}} + \mathbf{v})\bar{S}_{ij}\bar{S}_{ij} \rangle_{V,t}} \quad (2)$$

where volume and time averaging ($\langle \dots \rangle_{V,t}$), denotes the global integration. After assigning a desired value for s_ε^V , the corresponding C_k (as a constant input) was optimized by performing several auxiliary coarse grid calculations. This formulation is named global ILSA. Having s_ε^V a certain value however, the level of SFS activity might differ from the desired s_ε^V value locally. Also s_ε becomes less sensitive to C_k at high Re ; therefore a more sensitive measure of SFS activity is required.

Piomelli *et al.*[1] proposed a new measure of SFS activity based on Reynolds stresses:

$$s_\tau^\Omega = \left[\frac{\langle \tau_{ij}^a \tau_{ij}^a \rangle_\Omega}{\langle (\tau_{mn}^a + R_{mn}^a)(\tau_{mn}^a + R_{mn}^a) \rangle_\Omega} \right]^{1/2} \quad (3)$$

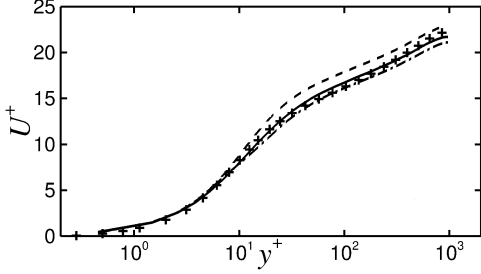


Figure 1: Mean velocity for channel flow, $Re_\tau = 1,000$, $64 \times 97 \times 64$ grid points. — Local ILSA with $s_\tau^\Omega = 0.022$; - - - global ILSA model [1] with $s_\tau = 0.022$; - - - dynamic model [3]; + DNS [4].

$$\tau_{ij}^a = \tau_{ij} - \frac{\delta_{ij}}{3}\tau_{kk} = -2v_{\text{fsf}}\bar{S}_{ij}, \quad R_{ij}^a = \bar{u}'_i\bar{u}'_j - \frac{\delta_{ij}}{3}\bar{u}'_k\bar{u}'_k \quad (4)$$

where τ_{ij}^a and R_{ij}^a are the anisotropic parts of the modelled and resolved Reynolds stresses. $\langle \dots \rangle_\Omega$ indicates averaging in time and, if possible, homogeneous directions. Having a specified value for s_τ^Ω yields a variable C_k . Substituting (1) and (4) into (3), yields a quadratic equation for C_k which can be calculated at each time step and in each grid cell without the need for extra calculations. This new formulation is called local ILSA.

2 RESULTS

Local ILSA was applied to channel flow at $Re_\tau = 1,000$ and 2,000. Fig 1 compares local ILSA, global ILSA[1] and the Dynamic Smagorinsky model (Germano *et al.*[3]) on a relatively coarse grid. The comparison indicates robustness of both ILSA formulations compared to the Dynamic model. On a coarse grid global ILSA produces a relatively high eddy viscosity close to the RANS turbulent-viscosity. Such values are attained near the wall where small, Reynolds dependent scales emerge (Piomelli *et al.*[1]). High values for the eddy viscosity compensate for the momentum deficit due to under-resolution of near-wall eddies. Sensitivity tests established accuracy for $s_\tau^\Omega \leq 0.03$ at both Reynolds numbers.

Local ILSA was also applied to a backward-facing step at $Re_c = 28,000$ based on inflow centreline velocity and step height, consistent with the experiment of Vogel & Eaton[5]. Three levels of coarse ($256 \times 100 \times 64$), intermediate ($384 \times 150 \times 96$) and fine ($512 \times 200 \times 128$) grids were tested. The mean and *rms* velocities were observed to be more accurately predicted by local ILSA than with the Dynamic model. For this flow $s_\tau^\Omega \leq 0.03$ was found to be ap-

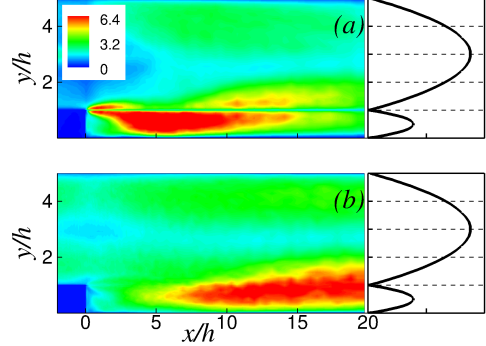


Figure 2: Ratio (v_{fsf}/v) for the backward-facing step on a coarse grid using (a) Dynamic model and (b) local ILSA with $s_\tau^\Omega = 0.022$. The grid size Δy distribution is plotted on the right side.

propriate for accuracy. The main advantage of the proposed model is its detachment from grid; the Dynamic model (Fig 2(a)) has a grid-dependent eddy viscosity, resulting in a sharp drop in model activity at the edge of the step where the grid size is refined while local ILSA (Fig 2(b)) follows the flow structures; according to Vanella *et al.*[6], the resolved solution is less contaminated by modelling and aliasing errors if the eddy viscosity has a more uniform distribution.

REFERENCES

- [1] U. Piomelli, A. Rouhi and B.J. Geurts. A grid-independent length scale for large-eddy simulations. *Journal of Fluid Mechanics*, 766:499–527, 2015
- [2] J. Meyers, B.J. Geurts. and M. Baelmans. Database analysis of errors in large-eddy simulation. *Physics of Fluids*, 15(9):2740–2755, 2003
- [3] M. Germano, U. Piomelli, P. Moin and W. H. Cabot. A dynamic subgrid-scale eddy viscosity model. *Physics of Fluids*, 3(7):1760–1765, 1991
- [4] S. Hoyas and J. Jiménez. Scaling of the velocity fluctuations in turbulent channels up to $Re_\tau = 2003$. *Physics of Fluids*, 18(1):011702, 2006
- [5] J. C. Vogel and J. K. Eaton. Combined heat transfer and fluid dynamic measurements downstream of a backward-facing step. *Journal of heat transfer*, 107(4):922–929, 1985
- [6] M. Vanella, U. Piomelli and E. Balaras. Effect of grid discontinuities on large-eddy simulation statistics and flow fields. *Journal of Turbulence*, 9:2008

A Finite Difference Cut-Stencil Formulation for the Solution of Lid-Driven Cavity Flow

M. Esmaeilzadeh¹, R.M. Barron^{2,1} and R. Balachandar^{3,1}

¹Dept. of Mechanical, Automotive & Materials Engineering, University of Windsor, Windsor, ON N9B3P4 Canada

¹Dept. of Mathematics & Statistics, University of Windsor, Windsor, ON N9B3P4 Canada

³Dept. of Civil & Environmental Engineering, University of Windsor, Windsor, ON N9B3P4 Canada

Email: esmaeilm@uwindsor.ca

ABSTRACT

Application of a new finite difference method, referred to as the Cartesian cut-stencil method, to solve the streamfunction – vorticity equations for 2D steady incompressible flow, is considered in this paper. The cut-stencil method allows a finite difference solution in any arbitrary domain by mapping each 5-point physical stencil, including those cut by a boundary, to a uniform computational stencil. The flow in a lid-driven cavity with aspect ratio 1 and 1.5 is used to investigate some of the key features and implementation of this formulation. Second-order accurate results are in good agreement with other simulation results in the literature. The Cartesian cut-stencil approach can be extended to high-order accuracy using Hermitian compact finite differencing. The implementation of the 4th-order scheme is discussed.

1. INTRODUCTION

Unlike the traditional finite difference method, the cut-stencil finite difference method can be applied on an arbitrarily shaped physical domain by using localized mappings from the physical stencil to a generic computational stencil, as illustrated in Fig. 1. Previous research [1] has demonstrated that this Cartesian cut-stencil formulation can be used to solve model PDEs arising in engineering and applied sciences.

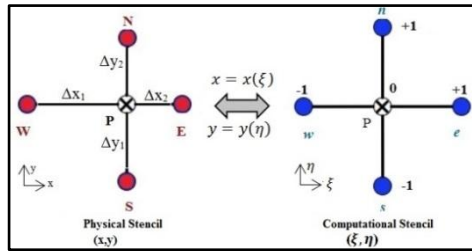


Figure 1: Mapping from arbitrary physical stencil to a computational stencil in 2D

The Cartesian cut-stencil method and some of its unique features for arbitrary complex 2D domains will be discussed in this paper. The streamfunction – vorticity form of the Navier-Stokes equations is used to illustrate the implementation of boundary conditions, error estimates and higher-order discretizations.

2. STREAMFUNCTION – VORTICITY FORMULATION

The mapped form of the streamfunction – vorticity formulation of the 2D Navier-Stokes equations, under the transformation equations $x = x(\xi), y = y(\eta)$, are:

$$\frac{1}{(x')^2} \frac{\partial^2 \psi}{\partial \xi^2} - \frac{x''}{(x')^3} \frac{\partial \psi}{\partial \xi} + \frac{1}{(y')^2} \frac{\partial^2 \psi}{\partial \eta^2} - \frac{y''}{(y')^3} \frac{\partial \psi}{\partial \eta} = -\omega \quad (1)$$

$$\frac{-1}{Re} \left(\frac{1}{(x')^2} \frac{\partial^2 \omega}{\partial \xi^2} - \frac{x''}{(x')^3} \frac{\partial \omega}{\partial \xi} + \frac{1}{(y')^2} \frac{\partial^2 \omega}{\partial \eta^2} - \frac{y''}{(y')^3} \frac{\partial \omega}{\partial \eta} \right) + \frac{u}{x'} \frac{\partial \omega}{\partial \xi} + \frac{v}{y'} \frac{\partial \omega}{\partial \eta} = 0 \quad (2)$$

In these equations ψ, ω, u, v and Re represent streamfunction, vorticity, x and y -components of velocity and Reynolds number, respectively. The metrics of the transformation are denoted by x', x'', y' and y'' . The mapping of a non-uniform stencil, as shown in Fig. 1, possibly created by a boundary cut, can be accomplished with quadratic functions, with coefficients depending on the physical coordinates of the points on the stencil.

For flow in a closed region, the only physical boundary conditions are $u = 0, v = 0$ on the boundaries (no-slip walls). These translate into Neumann conditions for ψ , i.e., $\frac{\partial \psi}{\partial x} = 0, \frac{\partial \psi}{\partial y} = 0$ on all boundaries. The boundary conditions on vorticity, obtained by applying eqn. (2) on the boundaries, are all Dirichlet. Figure 2 gives the boundary conditions on ψ and ω for the cavity flow problem [2].

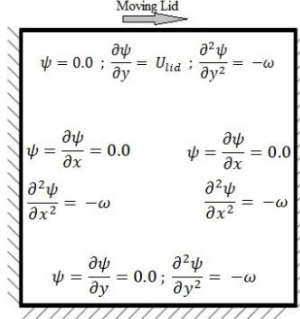


Figure 2: Schematic of the boundary conditions used for the lid-driven cavity flow

3. DISCRETIZATION

The derivatives in the diffusion terms are approximated by central differencing while either upwind or central differencing are used to approximate the derivatives in the convective terms, depending on Reynolds number.

The vorticity on the boundary can be approximated with 1st, 2nd or 3rd-order accuracy using compact finite differencing (Hermitian formulation). For example, the 2nd-order formulation of the vorticity at a node S along a lower horizontal wall can be expressed as

$$\begin{aligned} -\omega|_S &= \frac{1}{(y'_S)^2} \frac{\partial^2 \psi}{\partial \eta^2}|_S \\ &= \frac{-6\psi_S + 6\psi_P}{(y'_S)^2} - \frac{2}{(y'_S)^2} (y'_P u_P) \end{aligned} \quad (3)$$

where P is the interior node immediately above S , and u_P is the horizontal component of velocity evaluated at point P .

4. RESULTS

Comparison of the results obtained using the cut-stencil formulation with results in the literature shows good agreement. Table 1 shows sample results for a square cavity, while Fig. 3 illustrates the flow pattern for a cavity with aspect ratio 1.5. Additional results for a non-uniform mesh and for a skewed cavity with a Cartesian mesh containing cut-stencils will be presented, as well as boundary condition

implementation issues and results using a 4th-order discretization scheme. Accuracy will also be assessed using the local truncation error obtained from the modified PDEs.

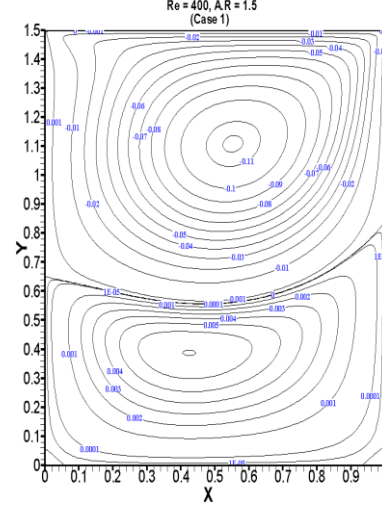


Figure 3: Flow pattern in a cavity with an aspect ratio of 1.5 (Re = 400)

REFERENCES

- [1] R.M. Barron, M. Esmaeilzadeh and S. He. A Cartesian cut-stencil method for the finite difference solution of the convection-diffusion equation in a complex domain. *22nd Ann. Conf. of the CFD Society of Canada*, CFD2014, Toronto, Canada, 2014.
- [2] W.F. Spotz. Accuracy and performance of numerical wall boundary conditions for steady, 2D, incompressible streamfunction vorticity. *Int. Journal for Numerical Methods in Fluids*, 28:737–757, 1998
- [3] U. Ghia, K.N. Ghia and C.T. Shin. High-Re solutions for incompressible flow using the Navier-Stokes equations and a multigrid method. *Journal of Computational Physics*, 48:387-411, 1982
- [4] S. Hou, Q. Zou, S. Chen, G. Doolen and A.C. Cogley. Simulation of cavity flow by the lattice Boltzmann method. *Journal of Computational Physics*, 118:329-347, 1995.

Source	Primary Vortex			Lower Left Vortex			Lower Right Vortex		
	ψ	x	y	ψ	x	y	ψ	x	y
Ghia et al. [3]	0.1139	0.5547	0.6055	1.42e-5	0.0508	0.0469	6.42e-5	0.8906	0.1250
Hou et al. [4]	0.1121	0.5608	0.6078	1.30e-5	0.0549	0.0510	6.19e-5	0.8902	0.1255
Present	0.1132	0.5563	0.6063	1.46e-5	0.0500	0.0500	6.34e-4	0.8875	0.1250

Table 1: Streamfunction value and location of the vortex cores for the square cavity ($Re = 400$)

A Fourth-Order CENO Finite-Volume Scheme for Resistive MHD Equations on Three-Dimensional Multiblock Hexahedral Grids

Lucian Ivan¹, Hans De Sterck¹, and Clinton P. T. Groth³

¹ Department of Applied Mathematics, University of Waterloo, Waterloo, Ontario, Canada N2L 3G1

² University of Toronto Institute for Aerospace Studies, Toronto, Ontario, Canada M3H 5T6

Email: lucian.ivan@uwaterloo.ca

1 RESEARCH OUTLINE

Resistive magnetohydrodynamics (MHD) equations provide a single-fluid description of the macroscopic behavior of a magnetized plasma on time scales much slower relative to the electron collision time, in which case the plasma acquires its electric resistivity and resistive dissipative effects become important. Mathematically, the resistive MHD equations contain flux terms of both hyperbolic (ideal) and elliptic (resistive) nature. In particular for global modelling of space-physics problems, the set of resistive MHD equations describes well the spatio-temporal evolution of various plasma phenomena such as magnetic tearing instabilities, current filamentation and magnetic reconnection, which typically occur in some very limited spatial region where ideal MHD model breaks down. As the spatial scales of global space-physics problems are usually much larger relative to the length scales characterizing the non-ideal resistive modes, accurate and efficient computational methods for solving the resistive MHD equations are highly desirable. However, the development of accurate and efficient algorithms for space-plasma modelling is challenging due to the intricate nature of the MHD equations which require magnetic-monopole-free solutions, the presence of collocated regions of smooth and discontinuous solution variations, the complexities encountered in the discretization of spherical domains associated with celestial bodies, the difficulties in prescribing high-order boundary conditions and the stiffness in the time scales of ideal and non-ideal modes.

In the current work, a high-order central essentially non-oscillatory (CENO) finite-volume scheme [1, 2, 5] is proposed for the discretization of the resistive MHD equations on three-dimensional multiblock hexahedral

grids. The current CENO high-order algorithm extends the recently proposed CENO formulation for hyperbolic conservation laws on three-dimensional hexahedral grids [3] to equations containing resistive (non-ideal) flux terms. The spatial discretization of the ideal (hyperbolic) term is based on a hybrid solution reconstruction procedure that combines an unlimited high-order k -exact least-squares reconstruction following from a fixed central stencil with a monotonicity preserving limited piecewise linear reconstruction algorithm. The unlimited k -exact reconstruction is used for cells in which the solution is fully resolved and the limited lower-order counterpart is applied to computational cells with under-resolved/discontinuous solution content. Switching in the hybrid procedure is determined by a solution smoothness indicator. The hybrid approach avoids the complexity associated with other (W)ENO schemes that require reconstruction on multiple stencils. The high-order resistive (elliptic) fluxes are computed based on a k -order accurate gradient derived from the same unlimited high-order reconstructions.

Since most space physics flows involve spherical objects, a particular multiblock hexahedral grid of interest in this work is the cubed-sphere grid [4], which recently emerged as a technique for discretizing spherical geometry with quasi-uniform grids that are free of strong singularities. The high-order central essentially non-oscillatory (CENO) finite-volume scheme for resistive MHD is implemented in combination with a block-based adaptive mesh refinement (AMR) algorithm on three-dimensional cubed-sphere grids.

2 PRELIMINARY NUMERICAL RESULTS

To demonstrate certain current capabilities of the computational framework, grid convergence studies with a three-dimensional time-dependent manufactured solution to the magnetic diffusion equations are presented. Full details about the analytical solution of this problem will be provided in the final paper. The simulations are performed up to $t = 0.01$ on the three-dimensional sphere of radius $R = 2.2$. A multiblock cubed-sphere grid with seven blocks is used to discretize initially the computational domain of this problem. A series of grids ranging in size from seven $16 \times 16 \times 16$ initial blocks to 3,584 $16 \times 16 \times 16$ cubed-sphere blocks, which corresponds to 28, 672 and 14, 680, 064 total cells, respectively. Figure 1(a) depicts the contour plot of the total magnetic field at the end of the simulation. In Fig. 1(b) the L_1 , L_2 and L_∞ -error norms relative to the exact solution obtained using the fourth-order CENO scheme are compared against the same errors corresponding to a standard limited second-order finite-volume scheme. The results show the capability of the fourth-order CENO scheme to achieve the expected theoretical order of accuracy, and to produce relative to the standard second-order algorithm large savings in the required number of computational elements for a targeted solution accuracy.

The final version of the paper will provide details of the high-order CENO approach and the treatment of boundary conditions. The scheme will be thoroughly analyzed for resistive MHD problems characterized by a full range of magnetic Reynolds numbers, which determine the relative importance of magnetic advection to magnetic diffusion. The ability of the scheme to accurately represent solutions with smooth extrema and yet robustly handle under-resolved and/or non-smooth solution content will be shown. It will also contain additional cases for more complex problems, including a thorough numerical investigation of the proposed scheme on cubed-sphere grids. Furthermore, the final manuscript will present parallel performance studies.

REFERENCES

- [1] L. Ivan and C. P. Groth. High-order solution-adaptive central essentially non-oscillatory (CENO) method for viscous flows. *J. Comput. Phys.*, 257, Part A(0):830 – 862, 2014.
- [2] L. Ivan, H. D. Sterck, S. A. Northrup, and C. P. Groth. Multi-dimensional finite-volume scheme for hyperbolic conservation laws on three-dimensional solution-adaptive cubed-sphere grids.
- [3] L. Ivan, H. D. Sterck, A. Susanto, and C. P. T. Groth. High-order central eno finite-volume scheme for hyperbolic conservation laws on three-dimensional cubed-sphere grids. *J. Comput. Phys.*, 282:157–182, 2015.
- [4] C. Ronchi, R. Iacono, and P. S. Paolucci. The “cubed sphere”: A new method for the solution of partial differential equations in spherical geometry. *J. Comput. Phys.*, 124:93–114, 1996.
- [5] A. Susanto, L. Ivan, H. D. Sterck, and C. Groth. High-order central ENO finite-volume scheme for ideal MHD. *J. Comput. Phys.*, 250(0):141 – 164, 2013.

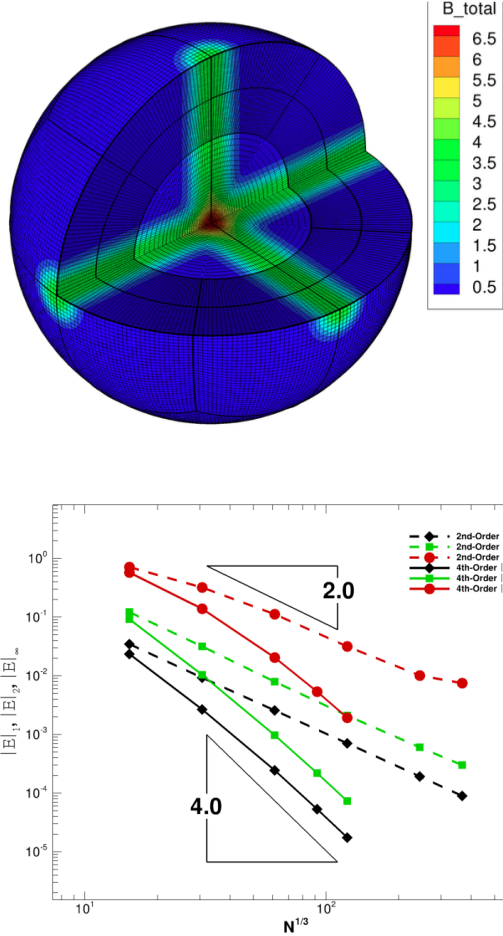


Figure 1: (a) Contour plot predicted by the CENO algorithm for the total magnetic field at $t = 0.01$ and (b) comparison between the error norms obtained using the fourth-order CENO and a limited-second order scheme as a function of mesh density.

J. Comput. Phys., 255:205 – 227, 2013.

- [3] L. Ivan, H. D. Sterck, A. Susanto, and C. P. T. Groth. High-order central eno finite-volume scheme for hyperbolic conservation laws on three-dimensional cubed-sphere grids. *J. Comput. Phys.*, 282:157–182, 2015.
- [4] C. Ronchi, R. Iacono, and P. S. Paolucci. The “cubed sphere”: A new method for the solution of partial differential equations in spherical geometry. *J. Comput. Phys.*, 124:93–114, 1996.
- [5] A. Susanto, L. Ivan, H. D. Sterck, and C. Groth. High-order central ENO finite-volume scheme for ideal MHD. *J. Comput. Phys.*, 250(0):141 – 164, 2013.

A Hybrid Central Solver for Compressible Euler Equations

N.H Maruthi¹ and S.V. Raghurama Rao²

^{1,2} Department of Aerospace Engineering, Indian Institute of Science, Bengaluru, India-560012

Email: maruthi@aero.iisc.ernet.in, raghu@aero.iisc.ernet.in

1 NUMERICAL METHOD

Approximate Riemann solvers [5] use eigen-structure of the system and often they exhibit pathological behaviours like carbuncle phenomena, odd-even decoupling, kinked Mach-stem [3]. In this work, we introduce a hybrid solver which does not depend on the eigen-structure for compressible Euler equations. The MOVERS (Method of Optimal Viscosity for Enhanced Resolution of Shocks) developed by Jaisankar and Raghurama Rao [2] is further improved to capture the flow features devoid of pathological behaviours.

Consider the 1-D Euler equations given by

$$\frac{\partial U}{\partial t} + \frac{\partial F}{\partial x} = 0 \quad (1)$$

where, $U = (\rho \quad \rho u \quad \rho E)^T$ is the conserved variable vector and $F = (\rho u \quad p + \rho u^2 \quad \rho u + \rho u E)^T$ is the inviscid flux vector.

Semi discrete finite volume method on a standard three point stencil is given as below

$$\frac{dU_i}{dt} = -\frac{1}{\Delta x}(F_{i+\frac{1}{2}}^n - F_{i-\frac{1}{2}}^n) \quad (2)$$

where

$$F_{i+\frac{1}{2}}^n = \frac{1}{2}(F_R + F_L) - \frac{1}{2}\alpha_I(U_R - U_L). \quad (3)$$

The coefficient of numerical diffusion α_I as in MOVERS [2] (derived based on R-H condition) with a slight modification is given as follows.

$$s_{j+\frac{1}{2}} = \begin{cases} \left| \frac{F_{j+1} - F_j}{U_{j+1} - U_j} \right| & \text{if } U_j \neq U_{j+1} \text{ and } F_j \neq F_{j+1} \\ 0 & \text{if } U_j \neq U_{j+1} \text{ and } |F_{j+1} - F_j| < \epsilon \\ \lambda_{min} & \text{if } |U_{j+1} - U_j| < \epsilon \end{cases} \quad (4)$$

where ϵ is a small parameter. Wave speed correction is enforced to keep the α_I within eigen-spectrum.

$$s_{j+\frac{1}{2}} = \lambda_{max} \text{ if } s_{j+\frac{1}{2}} > \lambda_{max} \quad (5)$$

$$s_{j+\frac{1}{2}} = \lambda_{min} \text{ if } s_{j+\frac{1}{2}} < \lambda_{min} \quad (6)$$

Here, λ_{max} and λ_{min} are maximum and minimum eigenvalues computed across the interface [2]. This simple central solver captures steady discontinuities exactly, is less diffusive than required and is prone to instabilities.

1.1 Pressure gradient based diffusion

Pressure gradient vanishes across the contact discontinuities, at which numerical diffusion based on MOVERS will be enforced. In other regions of the flow, in addition to MOVERS, diffusion in which pressure gradient scaled by maximum eigenvalue is used. Coefficient of diffusion at the interface is redefined as

$$\alpha_I = \alpha_M + \alpha_P \quad (7)$$

where α_M and α_P are coefficients of diffusion based on MOVERS and pressure gradients. α_P is defined as follows,

$$\alpha_P = \beta |\max(\lambda_1, \lambda_2, \lambda_3)|\phi \quad (8)$$

where β is a small number and is taken as 0.2. ϕ is a pressure based sensor to sense contacts [1].

$$\phi = \begin{cases} 0 & \text{if } |\frac{\Delta p}{2\bar{p}}| \leq \epsilon \\ 1 & \text{otherwise} \end{cases} \quad (9)$$

ϵ is very small number. Δp is difference in left and right states and \bar{p} is average pressure of left and right states.

The sensor $|\frac{\Delta p}{2\bar{p}}|$ becomes zero at contact discontinuities and close to 1 near strong shocks. We also tried another coefficient of diffusion as given below.

$$\alpha_I = \alpha_M - \left| \frac{\Delta p}{2\bar{p}} \right| (\alpha_M - \lambda_{max}) \quad (10)$$

α_I , α_M and λ_{max} are as defined previously. The numerical diffusion is less in case of 10 compared to 7, however, 7 yields more stable scheme. All the results presented here are based on 7. This new scheme is termed as MOVERS-H (H stands for hybrid). Time derivatives are discretized using strong stability preserving Runge-Kutta method [4].

2 RESULTS AND DISCUSSION

The present method is tested on various 1D and 2D benchmark test problems [5, 3]. Figure 1 (a) shows the result of steady contact discontinuity. As expected MOVERS-H captures the steady contact discontinuity exactly. Shock tube Riemann test problem with sonic point is used to assess the numerical method for its entropy satisfying property. As shown in the Figure 1 (b), our method has no sonic point problem. Figure 1 (c) and Figure 1 (d) show the result of the shock tube problem with strong discontinuity. These test cases are used to assess numerical method for robustness.

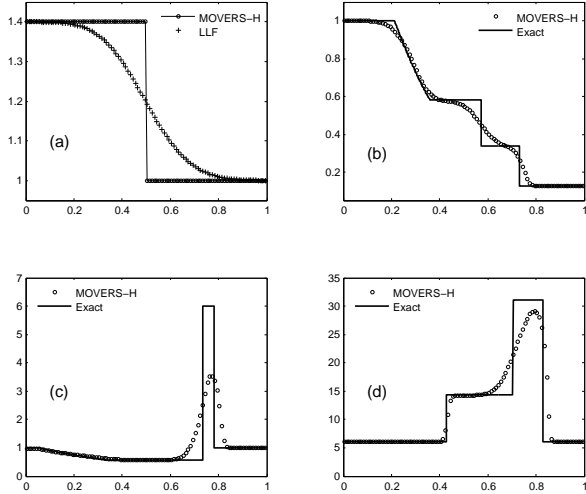


Figure 1: First order solution of shock tube test cases on 100 grid points: (a) steady contact (b) shock tube with sonic point (c) strong shock (d) several strong shocks.

Shock diffraction benchmark test case is a 2D problem, with a strong shock wave of Mach 5.09 diffracting around 90° corner followed by a complicated flow

structure. Many upwind schemes give rise to an expansion shock and distortion of the planar shock. As shown in Figure 2. The present method resolves flow features reasonably well without any shock instabilities. Hypersonic flow over a half-cylinder test case is used to check schemes for carbuncle phenomena. As shown in Figure 2, MOVERS-H encounters no carbuncle problem.

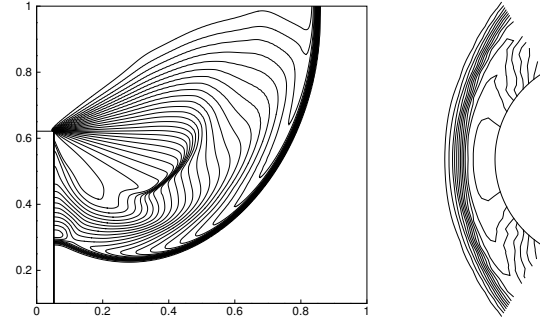


Figure 2: First order result of shock diffraction (left) with MOVERS-H on 400×400 grid points and result of Mach 20 flow over half-cylinder (left) using MOVERS-H on 41×45 grid points.

In conclusion, a pressure gradient based hybrid scheme in combination with MOVERS is presented. This new scheme is free of catastrophic shock instabilities. MOVERS-H being central solver is free of Riemann solvers and can easily be extended to other hyperbolic systems, which is currently being pursued.

REFERENCES

- [1] F. Ismail. Toward a reliable prediction of shocks in hypersonic flow: resolving carbuncles with entropy and vorticity control. 2006.
- [2] S. Jaisankar and S. V. Raghurama Rao. A central rankine-hugoniot solver for hyperbolic conservation laws. *Journal of Computational Physics*, 228(3):770–798, 2009.
- [3] J. J. Quirk. A contribution to the great riemann solver debate. *International Journal for Numerical Methods in Fluids*, 18(6):555–574, 1994.
- [4] R. J. Spiteri and S. J. Ruuth. A new class of optimal high-order strong-stability-preserving time discretization methods. *SIAM Journal on Numerical Analysis*, 40(2):469–491, 2002.
- [5] E. F. Toro. *Riemann solvers and numerical methods for fluid dynamics*. Springer, 1999.

A Modified Discontinuous Galerkin Method with an Improved CFL Number

Noel Chalmers¹ and Lilia Krivodonova²

Department of Applied Mathematics, University of Waterloo, 200 University Avenue West, Waterloo, ON N2L 3G1

Email: *bnachalm@uwaterloo.ca*¹, *lgk@uwaterloo.ca*²

1 INTRODUCTION

The discontinuous Galerkin (DG) spatial discretization applied to convection problems has a Courant-Friedrichs-Lowy (CFL) number that decreases with the order of approximation p as (approximately) $1/(2p + 1)$ when paired with an appropriate order Runge-Kutta scheme. This rather restrictive condition is caused by the growth of the spectrum of the spatial discretization operator of the semi-discrete scheme, which increases slightly slower than $O(p^2)$ [1]. In contrast, finite difference schemes have a stability restriction that grows with the size of the computational stencil as $O(p)$. This makes the DGM a more expensive scheme for the same theoretical order of convergence.

2 ANALYSIS OF SPECTRUM

We propose modifications to the DG method which involve $p+1$ parameters (flux multipliers) α_k , $k = 0, 1, \dots, p$, with the resulting method being called a modified DG (mDG) [2]. A suitable choice of parameters reduces the size of the method's spectrum, i.e. allows us to increase the CFL number. We also show that improvement in the CFL number necessary involves increased numerical diffusion and dissipation. In particular, the accuracy in approximating the exact wave number is $p+k$ for mDG, while the DGM approximates this quantity with a $2p+1$ accuracy. This error manifests itself in an increased rate of error accumulation with time while the formal $p+1$ convergence rate is preserved.

3 COMPUTED EXAMPLES

We present a number of numerical experiments demonstrating the performance of the mDG method. In our examples, the mDG method preserves the con-

vergence rate of the original DG method. For very smooth problems the modified method performs better than the DGM for a fixed computational effort, i.e. the number of cells times the number of time steps, but the improvement is modest. However, when the solution has discontinuities, and especially when limiters are involved, the modified scheme provides a comparable solution on the same mesh, but in less computation time. In particular, for the Euler equations example, the mDG method results in a better solution with the CFL number being three times larger than in the usual DG method.

4 CONCLUSION

We propose a modification to the DG scheme that alters the contribution of the numerical flux to the propagation of the degrees of freedom. Given a simple relation between solution coefficients and derivatives of the solution for one-dimensional problems, the proposed method can be thought of as a modification of a contribution of the interface jumps to propagation of solution derivatives. We prove some properties of this modification for one-dimensional problems and demonstrate extensibility of the approach to multi-dimensional problems.

REFERENCES

- [1] L. Krivodonova and R. Qin. An analysis of the spectrum of the discontinuous Galerkin method, *Applied Numerical Mathematics* 64, 1-18.
- [2] N. Chalmers, L. Krivodonova, and R. Qin. Relaxing the CFL condition of the discontinuous Galerkin method, *SIAM Journal on Scientific Computing* 36 (4), A2047-A2075

A Morphing Blade Design for Vertical-Axis Wind Turbines

David MacPhee and Asfaw Beyene

*Department of Mechanical Engineering, San Diego State University
5500 Campanile Dr., San Diego, CA, 92182*

Email: *davidwmacphee@gmail.com*

ABSTRACT

Wind turbines, like any other engineering device, operate optimally at a certain set of conditions. Conversion efficiency can drop significantly away from these conditions, and as a result, handling varying wind loads is a significant area of research in wind turbine design. Geometric variability has proven to be a useful design tool to mitigate these losses, most notably in the form of pitch control schemes, which can add significant up-front, maintenance and operational costs. As a result, these schemes are rarely implemented for vertical axis wind turbines, where the problem is intensified due an attack angle dependence on armature position.

This project investigates a low-cost, simplistic pitch control mechanism for vertical-axis wind turbines. The blades are built incorporating flexibility as a design parameter, are able to adapt passively to local wind velocities, and achieve similar results as active pitch control schemes. Using a finite-volume fluid-structure interaction algorithm, the aeroelastic behavior and performance of several blades of differing stiffness are compared to a rigidly-designed H-type rotor with known performance characteristics. The results indicate that such morphing blades can increase efficiency, improve start-up, and increase operational ranges when compared to similarly designed rigid turbines.

1 INTRODUCTION

There are two main types of wind turbines, namely Horizontal Axis Wind Turbines (HAWTs) and Vertical Axis Wind Turbines (VAWTs). The vast majority implemented today are HAWTs, which is due in some part to the ease in which off-design loadings are handled through the use of pitch control strategies. This is inherently more difficult for VAWTs, especially since airfoil attack angle depends on not only air and rotor speeds, but also armature (polar) position along

its rotation. There have been many attempts to design pitch control schemes for VAWTs, both active and passive, with varying levels of success. Active schemes, which bring an increased system complexity and up-front costs, have been shown to increase efficiencies by as much as 30% [5]. Passive schemes are generally less successful in terms of performance gains and more difficult to design.

In this study, we investigate a *morphing* VAWT blade, which is purposefully designed to be flexible, and acts as a passive pitch control device to improve turbine performance. In order to assess its viability, a VAWT with known performance is first modeled and validated using traditional Computational Fluid Dynamics (CFD) techniques, after which a geometrically identical (at zero load) morphing turbine is simulated using a similarly designed Fluid-Structure Interaction (FSI) code.

2 COMPUTATIONAL MODELING

The transient FSI routine used herein is built on the OpenFOAM extend project [1], and described in Fig. 1 for one time step. Essentially, the FSI solver requires several iterations in each of the solid and fluid domains, with an added mesh motion solver to allow for an arbitrary Lagrangian-Eulerian description of the fluid governing equations.

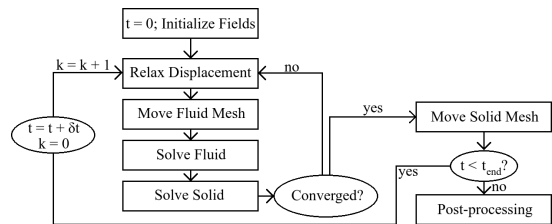


Figure 1: FSI solution procedure for a single time step.

The fluid equations of motion are solved using the

PISO algorithm, assuming an incompressible, Newtonian fluid in a rotating reference frame. Turbulence is handled using the k- ω -SST model. The solid is assumed to be a St. Venant Kirchhoff material undergoing finite strain, using the updated Lagrangian technique [6]. All governing equations are discretized using the cell centered, 2nd order finite volume method, with various interpolation schemes used where required for transferral of traction vectors between domains as well as for fluid and solid mesh update procedures.

3 RESULTS AND DISCUSSION

The FSI routine was slightly modified to allow for rigid-turbine simulation, and after sufficient independence tests were conducted, the algorithm was used to predict the performance of a high-solidity rotor, whose characteristics can be found in [2]. The morphing blade simulations utilized the same fluid discretization as the rigid, but also underwent similar independence tests in the solid domain. The flexible blade includes a small rigid support near the leading edge to facilitate tail-wise bending of the blades, Fig. 2. Both domains were meshed into an assortment of structured hexahedral (fluid domain) and unstructured tetrahedral (solid domain) volumes using gmsh [3].

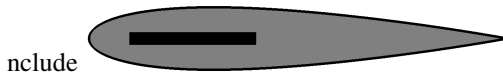


Figure 2: Cross-section of morphing blade, showing airfoil profile (NACA 0015), flexible material (grey) and rigid support (black).

The rigid bladed simulation achieved an average torque value similar to other two-dimensional CFD studies, e.g., [4], while the flexible bladed simulation was seen to have increasing average torque (and hence, power coefficient) with decreased Young's modulus (E). In fact, with four separate values for E ranging from 500kPa to 10MPa, the blades which were most flexible elicited the largest increase in performance, up to 16% for the blade with $E = 500$ kPa.

The reasons for this increased performance are not attributed to any change in maximal torque, but rather to the morphing blades ability to recover regions of separated flow, reducing the severity of vortices and lessening the magnitude of low pressure regions when compared to the rigid-bladed design. As a result, the morphing VAWT is expected to not only increase system efficiency, but also to reduce the amplitude of oscillatory structural loadings, increase operational range,

and perhaps increase the self-starting capabilities of the VAWT.

4 CONCLUSIONS

This paper investigates the behavior of a morphing blade design for use in vertical-axis wind turbines. Using a computational fluid-structure interaction algorithm, the fluid and solid equations of motion are solved using the cell-centered finite volume technique in the OpenFOAM framework. This routine is then used to simulate a turbine with known performance characteristics, with adequate results, after which several flexible blades of differing elasticity modulus are simulated in place of the traditional rigid blade. The results indicate that, compared to the rigid turbine, the morphing blades offer superior performance, with increasing efficiency as elasticity modulus decreases, with up to 16% gain in power generation possible. This novel design technique could make the vertical-axis turbine much more viable going forward, as it is expected to increase energy capture without increasing system costs or complexity.

REFERENCES

- [1] The OpenFOAM ® extend project. <http://www.extend-project.de>.
- [2] R. Bravo, S. Tullis, and S. Ziada. Performance testing of a small vertical-axis wind turbine. In *Proceedings of the 21st Canadian Congress of Applied Mechanics (CANCAM07)*, Toronto, Canada, June, pages 3–7, 2007.
- [3] C. Geuzaine and J. F. Remacle. Gmsh: a three-dimensional finite element mesh generator with built-in pre- and post-processing facilities. *International Journal for Numerical Methods in Engineering*, 79(11):1309–1331, 2009.
- [4] R. Lanzaflame, S. Mauro, and M. Messina. 2d cfd modeling of h-darrieus wind turbines using a transition turbulence model. *Energy Procedia*, 45:131–140, 2014.
- [5] I. Paraschivou, O. Trifu, and F. Saeed. H-darrieus wind turbine with blade pitch control. *International Journal of Rotating Machinery*, 2009.
- [6] Z. Tukovic and H. Jasak. Updated lagrangian finite volume solver for large deformation dynamic response of elastic body. *Transaction of Famaea*, 2007.

Numerical Investigation of Wind Turbine Far Wake and Performance Using the Actuator Disc Model

Ali Behrouzifar¹, Masoud Darbandi², and Gerry E. Schneider³

^{1,2}*Center of Excellence in Aerospace Systems, Department of Aerospace Engineering,
Sharif University of Technology, Tehran, P.O. Box 11365-8639, Iran*

³*Department of Mechanical and Mechatronics Engineering,
University of Waterloo, Waterloo, Ontario, N2L 3G1, Canada*

Email: behrouzifar@ae.sharif.ir

ABSTRACT

In this paper, predicting of wind turbine far wake and performance using an Actuator Disc method are done. This model combines a 3D full Navier-Stokes solver with an AD method in which the loading is distributed along disc representing the blade forces. The loading is obtained iteratively using a Blade Element Momentum Theory (BEMT) and tabulated 3D correction of airfoil data. Based on Weibull distribution, 6 m/s long term flow velocity (Average wind speed) for simulation of wind turbine wake is considered. The Results of induction factors, power and trust were compared with BEM method. There is 11% difference between the output power of our study and BEM method due to the mentioned wind velocity (6 m/s). Therefore, the results of AD models show excellent agreement with BEM for simulation of wind turbine's wake.

1. INTRODUCTION

One of the major problems for prediction of the performance of a wind turbine is correct estimation of the induced velocity generated along blade sections. Several numerical and analytical methods are developed in this field. The aim of all these methods extracts the coefficients of induced velocity. These methods use from a tabulated airfoil data or full blade geometry. Analytical methods can be noted BEM and VWM (Vortex Wake Method). The first method (BEM) uses induction factor convergence for prediction of wind turbine performance. However, numerous studies have been done to improve this method [1, 2]. The second method (VWM) the shed vorticity in the wake is employed to compute the induced velocity field [3, 4]. Numerical solutions are generally divided into two categories: direct methods (full-scale scale simulation) and AD technique. The

direct CFD (full scale), blade details of wind turbine are solved based on full Navier Stokes and turbulence equations. This method is sensitive to the turbulence model and quality of computational grid and usually is used for the final design [5]. There are other numerical techniques such as Actuator disk that is a combination of BEM and CFD methods. The methods used tabulated airfoils data such as 3D correction of lift and drag data. The calculated forces (body force) added to governing equation and created wake region in this area [6-8].

1.1 Geometry of the Wind Turbine Blade and the Applied Computational Grid

In this article, a large wind turbine configuration (NREL 5MW) is used to predict far wake and performance. Figure 1 shows numbering of segments along the blade configuration. As can be seen, most of the turbine power was generated in the tip area by NACA airfoil families.

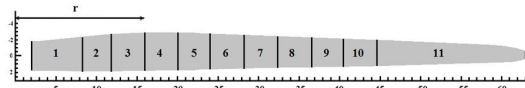


Figure 1 Numbering of segments along the blade configuration

Figure 2 shows the computational grid and solution domain for this wind turbine. Grid-independent solutions have been achieved with a computational domain of 15 and 10 rotor diameters for axial and radial coordinate, respectively. The turbine is located 5R downstream from the inlet boundary. To capture the gradients of the flow field, grid points are concentrated at the rotor position. 70, 60 and 60 points are used to discretize domain for axial, radial and azimuthal direction, respectively.

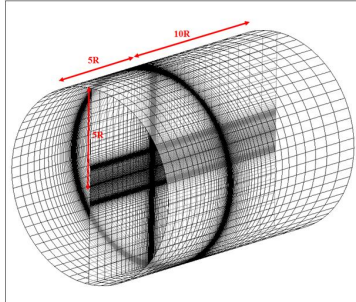


Figure 2 The computational grid and solution domain

2. ACTUATOR DISK MODEL

To determine the body forces acting on the rotor blades, blade-element approach combined with 3D correction of airfoil characteristics is used. In Fig. 3, a cross-sectional element at radius r shows the airfoil in the (θ, z) plane.

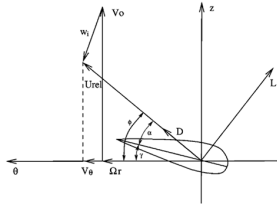


Figure 3 A cross-sectional element on airfoil

Forces extracted along the blades can be applied as sink terms in the governing equations (body force terms). These forces are shown in the Eqs. (1)-(3). It should be noted that the body forces are defined in the secondary cylindrical coordinates for simplify the equations ($(x_1, x_2, x_3) \leftrightarrow (r, \theta, z)$).

$$f_r = 0 \quad (1)$$

$$f_\theta = \frac{1}{4\pi r dz} B \rho V_{rel}^2 c (C_L \sin \phi - C_D \cos \phi) \quad (2)$$

$$f_z = \frac{1}{4\pi r dz} B \rho V_{rel}^2 c (C_L \cos \phi + C_D \sin \phi) \quad (3)$$

3. RESULTS

Finally, the correct prediction of induction factors led to the achievement of the valid wind turbine performance. Figure 4 shows power and trust of turbine versus wind speed for AD model and BEM method. Based on Weibull distribution, 6 m/s long term flow velocity (Average wind speed), the maximum difference between the two methods is less than 11% and 7% for wind turbine power and trust,

respectively. The results show accuracy and excellent agreement between two methods.

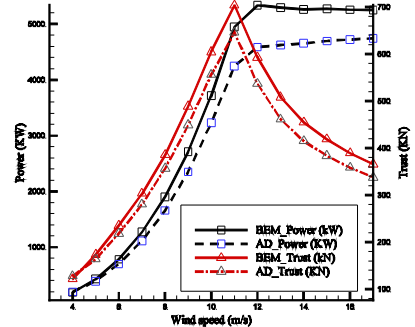


Figure 4 Wind turbine performance versus wind speed

4. CONCLUSION

As it can be seen, there is a very good adaptation between the results of numerical simulation (AD) and BEM methods. As before mentioned, the maximum difference between the two methods is less than 11% and 7% for wind turbine power and trust, respectively. These results against speed of convergence are appropriate.

REFERENCES

- [1] Glauert, H. "Airplane propellers", in W. F. Durand (ed) Aerodynamic Theory", vol 4, Division L, Julius Springer, Berlin, pp169–360, 1935
- [2] Simms, D.; Schreck, S.; Hand, M.; Fingersh, L.J. "NREL Unsteady Aerodynamics Experiment in the NASA-Ames Wind Tunnel: A Comparison of Predictions to Measurements", 2001
- [3] Miller RH. The aerodynamic and dynamic analysis of horizontal axis wind turbines. Journal of Wind Engineering and Industrial Aerodynamics, 1983
- [4] Simoes FJ, Graham J.M.R. Prediction of loading on a horizontal axis wind turbine using a free vortex wake model. Proceeding of the 13th BWEA Conference, Swansea, 247–253, 1991
- [5] Bazilevs, Y., M-C. Hsu "3D simulation of wind turbine rotors at full scale. Part I: Geometry modeling and aerodynamics." International Journal for Numerical Methods in Fluids , 2011
- [6] Madsen, H. Aa., "The Actuator Cylinder Flow Model for Vertical Axis, 1982
- [7] van Kuik, G. A. M. "On the Limitations of Froude's Actuator Disc Concept," Ph.D. thesis, Eindhoven University of Technology, the Netherlands, 1991
- [8] Sørensen, J. N., and Myken, A. "Unsteady Actuator Disc Model for Horizontal Axis Wind Turbines," J. Wind. Eng. Ind. Aerodyn. 39, pp. 139–149, 1992.

A Preliminary DNS Study of the Effect of a Blunt Leading Edge on the Instability of a Separating Laminar Boundary Layer

Joshua R. Brinkerhoff

School of Engineering, University of British Columbia–Okanagan, 3333 University Way, Kelowna, BC V1V 1V7

Email: joshua.brinkerhoff@ubc.ca

To reduce part counts and weight, aeroengine manufacturers have aimed at reducing the number of blades in the low-pressure turbine (LPT) section of a gas turbine engine while maintaining or even increasing the aerodynamic loading on the remaining blades. Such highly-loaded blades are susceptible to flow separation on their suction surfaces, particularly in the adverse pressure-gradient region of the blade, leading to a degradation of the turbine performance through loss of lift and increased drag. Laminar-to-turbulent transition of the flow, either upstream of flow separation via attached viscous instability modes or downstream of separation due to inviscid instability modes, enhances momentum exchange between the separated flow and the free-stream, promoting flow reattachment as a turbulent boundary layer.

The importance of laminar-to-turbulent transition to aeroengine performance and other engineering or environmental flows has made it the focus of numerous experimental or computational investigations. Several computational studies by the present author and others use direct numerical simulation (DNS) to compute all relevant length and time scales in the flow and thereby resolve the transition process, with the aim of developing semi-empirical models that can be used for predicting transition during the engineering design process. Due to the computational cost of DNS, a significant portion of published studies have made geometric simplifications to the LPT blade that include omitting the blunt shape of the leading edge. The typical rationale for omitting the blunt leading edge is that the local Reynolds number at the leading edge is small and thus the laminar boundary layer there is likely very stable and transition does not occur until much further downstream. Although there has been some recent emphasis on the importance of the blunt leading edge in conditions of elevated free-stream tur-

bulence [3] and leading-edge sweep [4], there is a shortage of in-depth analysis of the impact of a blunt leading-edge on the onset of disturbance amplification in the suction-surface boundary layer of LPT blades. Considering that the streamwise pressure gradients on a LPT blade suction-surface results in the potential for interaction between viscous and inviscid instability modes [1], a focused numerical study is required that identifies the influence of leading-edge bluntness on the growth of disturbances within the attached laminar boundary layer and their subsequent influence on flow separation and boundary-layer transition. The aim of the present paper is conduct a preliminary DNS study that establishes the suitability of the computational approach and identifies the impact of leading-edge bluntness on the two-dimensional (2D) formation and growth of disturbances in the separating laminar boundary layer. This preliminary 2D study will lay the groundwork for a more thorough follow-on study in which the three-dimensional growth of disturbances are examined.

The two computational domains used in this 2D study consist of flat, 700-mm-long no-slip test surfaces below a contoured free-slip ceiling that imposes a pressure distribution on the test surfaces approximating a LPT-blade suction surface. Free-slip regions upstream and downstream of the test surfaces are sized to prevent boundary conditions from adversely affecting the flow on the test surfaces. A baseline case has a thin leading edge while the other has a blunt leading edge shaped as an ellipse with a major-to-minor axis ratio of 2 and a thickness of 3.4% of the plate length, which is typical for a modern LPT blade. A steady inflow velocity of 4 m/s is imposed at the inflow to the domains, yielding a Reynolds number based on the test-surface length of 280,000 and kinematic viscosity of 1×10^{-5} m²/s.

A structured curvilinear grid consisting of hexahedral finite-volume cells with 127 nodes in the wall-normal direction, 2 nodes in the spanwise dimension, and 1380 (2076) nodes in the streamwise direction for the thin (and blunt) leading-edge cases; the additional nodes in the blunt case account for the finer spatial resolution required to resolve the leading-edge region. The grid-node spacing resolves the 2D disturbances developing in the boundary layer on the test surface, and was verified through a grid-convergence analysis.

The transient, incompressible continuity and momentum equations were solved in OpenFOAM-2.1 using the finite-volume spatial discretization approach. Discretization employs second-order central differencing and second-order upwind differencing for the spatial and temporal derivatives, respectively. Spurious oscillations intrinsic to second-order methods are prevented by limiting the facial fluxes arising from the convective term in the momentum equation by a total variation diminishing scheme. The continuity equation is solved using a conjugate gradient method with an incomplete-Cholesky preconditioner, while the momentum equation is solved using a Gauss-Seidel method. Integration of the unsteady system of equations is performed by the well-known pressure-implicit splitting operator (PISO) approach described by Ferziger and Perić [2], in which the momentum and continuity equations are solved separately and non-linear terms are lagged. All equations are solved and the lagged terms are updated twice per time step, and one explicit correction loop is performed to correct for the non-orthogonality of the spatial grid that exists near the leading edge. This approach results in a stability constraint based on the Courant-Friedrichs-Lowy (CFL) condition that limits the time step size to 1.5×10^{-5} s, which is also sufficient to resolve high-frequency disturbances that may develop in the boundary layer. The simulation required approximately 30 flow-through times to reach a statistically-steady state, after which approximately 5 flow-through times were collected for analysis.

To verify the numerical approach, a series of parametric studies were performed by varying the spatial resolution, number of non-orthogonal correctors, and simulation duration. The effect of these quantities on the simulation results are established by comparing wall-normal profiles of Reynolds stresses at relevant locations within the boundary layer. The DNS results indicate negligible sensitivity to these parameters, providing verification of the simulation approach.

In the blunt leading-edge case, flow separation occurs right at the leading edge due to the strong adverse pressure gradient occurring there, resulting in the for-

mation of a separated shear layer that is unstable to a Kelvin-Helmholtz mode with a most-amplified frequency of 78 Hz. Due to the strong flow acceleration imposed on the test surface by the contoured ceiling, the K-H instability is damped and the leading-edge separation reattaches (in a time-averaged sense) by 10% of the test-surface length. For the remainder of the test surface, the free stream velocity, streamwise acceleration parameter, and skin-friction coefficient of the thin and blunt leading-edge cases are essentially identical. This is despite much higher disturbance levels in the blunt case, seen in Reynolds stress profiles that are several orders of magnitude larger than thin case. In the adverse gradient region, flow separation occurs in both cases at essentially identical locations, and the lengths of the time-averaged separation bubbles are essentially identical.

Differences between the thin and blunt leading-edge cases become apparent when looking at the power spectra within the separated and reattached boundary layers. The power spectral density in these locations is about 10^3 times larger in the blunt case, and has more several more peaks at higher frequencies than the thin leading-edge case. The Reynolds shear stress ($u'v'$) in the separated region of the blunt case is about six times larger than in the thin case, while the normal stresses ($u'u'$ and $v'v'$) follow very similar distributions. The boundary layer shape factor in the blunt case is substantially larger downstream of flow reattachment than in the thin case. These conclusions suggest that while the blunt leading-edge produces higher disturbance levels in the boundary layer, it does not affect the 2D amplification of disturbances until well into the reattached region, at which point three-dimensional DNS results are required to elucidate their role in the transition process and the growth of the reattached turbulent boundary layer.

REFERENCES

- [1] J. R. Brinkerhoff and M. I. Yaras. Interaction of viscous and inviscid instability modes in separation-bubble transition. *Physics of Fluids*, 23(12):124102, 2011.
- [2] J. Ferziger and M. Perić. *Computational Methods for Fluid Dynamics*. Springer-Verlag, 2002.
- [3] V. Ovchinnikov, M. M. Choudhari, and U. Piomelli. Numerical simulations of boundary-layer bypass transition due to high-amplitude free-stream turbulence. *Journal of Fluid Mechanics*, 613:135–169, 2008.
- [4] L.-U. Schrader, S. Amin, and L. Brandt. Transition to turbulence in the boundary layer over a smooth and rough swept plate exposed to free-stream turbulence. *Journal of Fluid Mechanics*, 646:297–325, 2010.

A Projection Method Based Fast Transient Solver for Incompressible Turbulent Flows

Chris Sideroff¹, Darrin Stephens², and Aleksandar Jemcov³

¹ Applied CCM Canada, Ottawa, ON K1J 6K3, Canada

² Applied CCM Pty Ltd, Dandenong, Victoria 3175, Australia

³ Aerospace and Mechanical Engineering, University of Notre Dame, Notre Dame, IN 46556, USA

Email: c.sideroff@appliedccm.ca

ABSTRACT

We present a fast transient solver suitable for the simulation of transient turbulent flows. The main characteristic of the solver is that it is based on the projection method and requires only one pressure and the momentum solve per time step. Furthermore, using the projection method has the additional advantage that the formulation of the pressure equation is particularly efficient because the Laplacian term depends only on geometric quantities. This improves the parallel scalability of the Algebraic Multigrid Method (AMG) because the coarse agglomeration levels can be cached if the grid is not changing and are consistent throughout each time step. The fractional step error near the boundaries is removed by utilising the incremental version of the algorithm. The solver is implemented for the freely available Caelus computational mechanics library. Accuracy and performance of the solver was investigated through several validation cases. The results indicate the solver is both accurate and has excellent computational efficiency.

1 DISCUSSION

Transient solutions of incompressible, turbulent flows occupy an increasing portion of engineering computations. The majority of solvers that use the finite volume method on unstructured meshes with arbitrary number of faces per cell use either a transient SIMPLE [1] or the PISO algorithm [2]. While these algorithms are known to produce satisfactory spatial and temporal accuracy, they are not particularly efficient due to algorithmic constraints. Typically they require multiple solutions of the pressure equation (PISO algorithm) or multiple solutions of both momentum and pressure per time step (SIMPLE algorithm). In these algorithms,

multiple solutions of the pressure and/or momentum equation per time step are required to remove the fractional step error due to splitting of equations and recover the time accuracy.

Unlike SIMPLE and PISO algorithms, the projection algorithm introduced originally by Chorin [3], does not require multiple pressure and momentum solves per time step. This work describes an efficient implementation of the projection algorithm that utilizes the Algebraic Multigrid (AMG) Method, herein called Semi-Linear Implicit Method (SLIM). It combines two main ingredients:

- Projection-based pressure-velocity coupling method
- Algebraic multigrid method that preserves coarsening strategy throughout solution procedure

Due to the nature of pressure-velocity splitting, SLIM satisfies continuity every time step within the prescribed tolerance level without the need for additional pressure solves. Moreover, the formulation results in a pressure equation with purely geometric coefficients in the Laplacian. This allows for a more efficient pressure computation since the agglomeration can be geometric without any loss of convergence properties.

The basis of the SLIM algorithm consists of the projection method implemented with an incremental pressure in order to decrease the fractional step error on the boundaries. The current implementation is written using the Caelus library and is capable of using the same boundary conditions, solver and discretization types that are valid for use with PISO. Therefore the SLIM algorithm can be directly substituted for the PISO algorithm. The SLIM method is suitable for use with time dependent problems involving

either unsteady RANS, DES or LES computations. In summary, the benefits realized by SLIM are:

- Better spatial and temporal accuracy due to exact pressure-velocity splitting
- Run times typically 25-100% faster (dependent on mesh quality and linear solver settings)
- Better parallel scaling due to geometric coefficients in the pressure Laplacian

[4] J. Frölich, C.P. Mellen, W. Rodi, L. Temmerman and M.A. Leschziner. "Highly resolved large-eddy simulation of separated flow in a channel with streamwise periodic constrictions." *Journal of Fluid Mechanics* 526:19–66, 2005

Results from separated flow in a channel with periodic hills [4] will be presented together with comparison to existing results and data in open literature. In addition, comparisons between SLIM and PISO accuracy, run times and parallel scaling will be provided. An example of parallel scaling results from a 50 million cell pre-cursor simulation used for wind farm analyses is shown in Fig. 1.

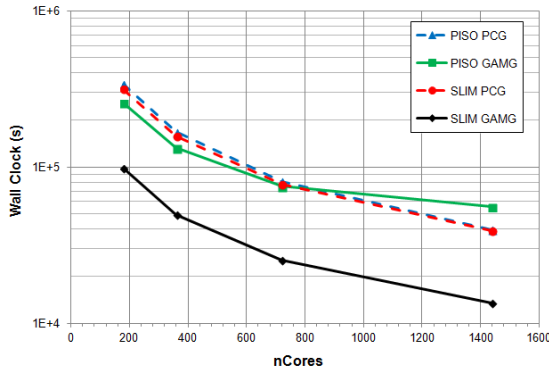


Figure 1: Pararallel scalability of PISO versus SLIM with Preconditioned Conjugate Gradient (PCG) and Algebraic Multigrid (AMG) linear solvers.

REFERENCES

- [1] S.V. Patankar and D.B. Spalding. "A calculation procedure for heat, mass and momentum transfer in three-dimensional parabolic flows." *International Journal of Heat and Mass Transfer* Vol 15, 10:1787–1806, 1972
- [2] R.I. Issa. "Solution of the Implicit Discretized Fluid Flow Equations by Operator Splitting." *Journal of Computational Physics* 62:40–65, 1985
- [3] R.I. Issa. "Numerical Solution of the Navier-Stokes Equations." *Mathematics of Computation* 22:40–65, 1968

An h -adaptive implementation of the discontinuous Galerkin method for nonlinear hyperbolic conservation laws on unstructured meshes for graphics processing units

Andrew Giuliani¹ and Lilia Krivodonova²

Department of Applied Mathematics, University of Waterloo, 200 University Avenue West, Waterloo, ON N2L 3G1

Email: *agiulian@uwaterloo.ca*¹, *lgk@uwaterloo.ca*²

1 INTRODUCTION

The discontinuous Galerkin (DG) method is a high-order method without an extensive stencil that can successfully capture shocks in the numerical solution of hyperbolic conservation laws. The method is predisposed to applications on highly parallel graphics processing unit (GPU) architectures [1]. Indeed, since the introduction of support for double-precision arithmetic, GPUs have become a very attractive platform for scientific computing.

A modern approach to numerical simulation is computational adaptivity. One technique is spatial refinement, or h -adaptivity, which attempts to selectively subdivide or merge mesh cells thereby locally increasing or decreasing solution resolution, see Figure 1.

The DG method naturally supports refined meshes. H -adaptivity on unstructured meshes in the context of GPUs can be difficult due to the inevitable irregularity of memory accesses and operations; in this paper we outline an efficient cell-based h -adaptive DG-GPU algorithm in NVIDIA’s CUDA C on unstructured triangular meshes. We present a computed example demonstrating the implementation’s effectiveness and examine its performance. A detailed overview of the non-adaptive aspects of this software is available in [1].

2 ADAPTIVE MESH REFINEMENT

An h -adaptive solver will execute a refine and coarsen cycle every few time steps. Typically, a cycle is composed of a number of stages: first an error indicator is computed on the current solution for all cells. Cells with too much error are flagged for re-

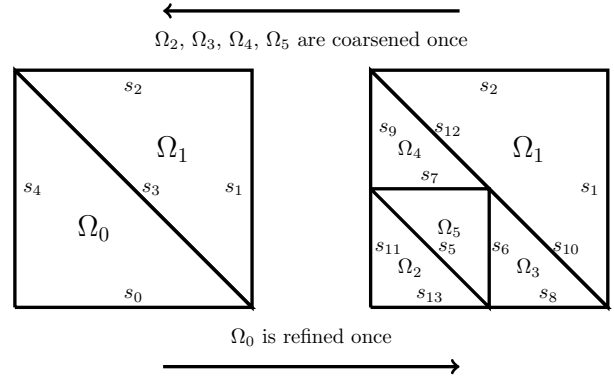


Figure 1: A typical h -adaptive cycle: elements and sides are denoted by Ω_i and s_k respectively.

finement, whereas cells in areas deemed over resolved are flagged for coarsening. Finally, mesh connectivity data are updated accordingly; the simulation is then continued on the refined or coarsened mesh.

In order to compute the numerical solution of a particular cell, knowledge of its adjacent cells is needed. Parent-child relationships for elements and sides are stored in tree structures. This allows for mesh connectivity to be updated after a refinement and coarsening cycle.

Implementing parallel kernels that operate on tree structures can be difficult on the GPU. Tree traversal was done iteratively rather than recursively. Further, great care was taken to ensure performance was not hindered by divergent control structures necessary for tree operations.

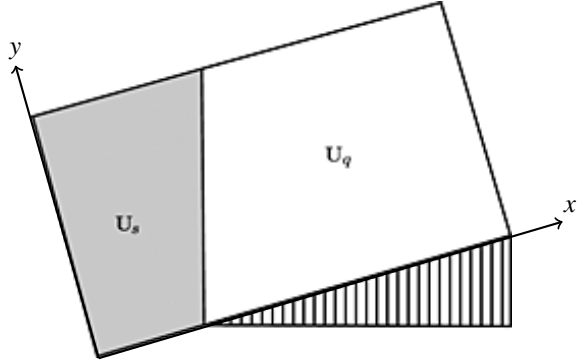


Figure 2: The rectangular computational domain along a triangular reflecting wedge [1]. The initial oblique shock is composed of the pre-shock state \mathbf{U}_q and the post-shock state \mathbf{U}_s .

3 COMPUTED EXAMPLE

For the Euler equations, the double Mach reflection models an oblique rightward moving shock incident on a triangular reflecting wedge. The initial set-up is plotted in Figure 2, and further details of this test case can be found in [1]. The problem is solved on $(x, y, t) \in [0, 4] \times [0, 1] \times [0, 0.2]$. The initial Mach 10 shock forms a 60° angle with the x -axis and separates the pre-shock and post-shock states. We compute the solution using our h -adaptive implementation and display the fluid's filled density isolines in Figure 3 at the final time $t = 0.2$.

The initial unrefined mesh is composed of 58,540 triangular elements. Every 5 timesteps, a refinement and coarsening cycle is performed. We allow at most 5 levels of refinement, i.e. ~ 1024 of the most refined elements can fit inside 1 of the coarsest elements. Further, no more than one level of refinement difference is permitted between adjacent elements. Refinement is indicated based on the gradient of the fluid's density.

The final mesh is composed of 814,951 elements and has the effective resolution of a mesh of approximately 60,000,000 triangles; its configuration near the Mach stem is displayed in Figure 4. We observe that the refinement region near the shocks remains tight; further, we gain substantially in resolution near the contact discontinuity and the flow emanating from it.

4 PERFORMANCE

This implementation performed quite well in light of the effective resolution achieved. The average number of elements present in the mesh was 468,655, with only $\sim 8\%$ of the total runtime spent executing the re-



Figure 3: Filled density isolines of the double mach reflection problem at a final time $t = 0.2$.

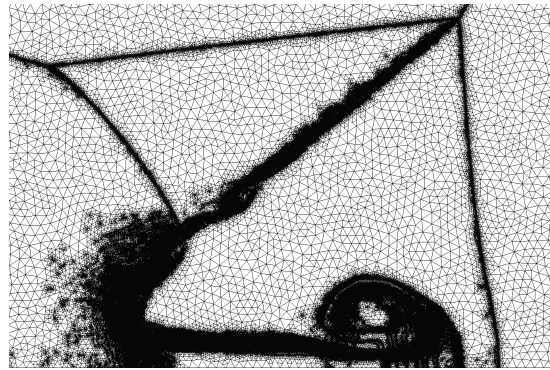


Figure 4: Mesh configuration near the Mach stem.

finement and coarsening subroutines. Overall runtime was negatively influenced by a restrictive timestep defined by the smallest cells in the refined mesh.

5 CONCLUSION

We have presented an efficient h -adaptive DG-GPU implementation on NVIDIA GPUs. Further work that is planned includes the addition of local timestepping, p -adaptivity and finally, an extension to multi-GPU architectures.

REFERENCES

- [1] M. Fuhrer, A. Giuliani and L. Krivodonova. Discontinuous Galerkin Methods on Graphics Processing Units for Nonlinear Hyperbolic Conservation Laws. *International Journal for Numerical Methods in Fluids*, 76 (12):982-1003, 2014.

An Implicit Cartesian Grid Method for CFD using Finite Volume and Finite Difference Discretizations

F. Dierich¹, S. Ananiev², and P. Nikrityuk³

¹ CIC Virtuhcon, Technische Universität Bergakademie Freiberg, Fuchs mühlenweg 9, 09599 Freiberg, Germany

² Institute of Aerospace Engineering, Dresden University of Technology, Mommsenstrasse 13, 01062 Dresden, Germany

³ Department of Chemical and Materials Engineering, University of Alberta, 9107-116 Str; Edmonton T6G 2V4, Canada

Email: nikrityu@ualberta.ca

ABSTRACT

This work describes a methodology to implement an implicit Cartesian grid '*Matrix-Cut*' method to model heat and fluid flow in irregular geometries using any Cartesian grid implicit matrix solver for finite-difference and finite-volume methods. This method allows the precise imposition of Dirichlet, Neumann and Robin boundary conditions in any internal node of the grid. The main idea of this method comes from a finite-element method, where the coefficients of implicit matrix of a discretized equation are modified directly to ensure the boundary conditions at immersed boundaries represented by grid nodes. One of the advantage of this method is its capability to solve a transport equation implicitly in steady and unsteady mode applied to complex geometry immersed into the Cartesian grid.

1 INTRODUCTION

Recently, with the great improvement of computer's computational power, especially applied to multiprocessor-based desktop computers, the immersed-boundary (IB) method originally developed by Peskin [1] and its modifications, see the review [2], became very popular in the numerical modeling of the momentum, heat and mass transfer in different applied engineering problems. Following the classification done by Mittal and Iaccarino [2], basically, IB method has two mainstream approaches. The first one is so called '*continuous forcing approach*', where the forcing is incorporated into the continuous equations before discretization, e.g. see the work of Goldstein et al. [3]. The second approach of IB method is termed

as *discrete forcing approach*, the forcing is included after the equation are discretized, e.g. see the works of Mohd-Yosuf [4], Faldun et al. [5]. The disadvantage of this method in comparison to continuous forcing approach is its unsteady character of solving any problem including steady state one. This issue makes this method computationally more expensive in respect to previous approach. In addition to IB methods, there is another class of methods, usually referred as *Cartesian grid methods* mentioned at the beginning of this section. Basically, Cartesian grid method *does not* utilize a momentum forcing or any force to set up the given values of a variable on the immersed boundary. Most of the contributions in Cartesian grid technique, which is also known as the *cut-cell* method, have been done by Udaykumar and collaborators [6]. It should be noted that *cut-cell* method is somehow similar to the *flag matrix concept* introduced originally by Kuipers et al. [7]. Next variant of *Cartesian grid method* is so-called *implicit fictitious boundary method* introduced by Turek and co-workers [8] using FEM, which main idea is to modify directly the coefficients of implicit matrix of the discretized equations to ensure the boundary conditions at the immersed boundaries. However, basically in the literature only the Dirichlet boundary condition has been highlighted. Ananiev and coworkers[9, 10] adopted this method in finite volume formulation applied to the numerical solution of phase change problems. However, no details on numerical implementation were given. To close the gap in mathematical formulation of an Implicit Cartesian Grid '*Matrix-Cut*' method, in this work we describe the derivation of this method for finite-volume and finite-difference formulations applied to a numerical solution of the heat transfer related problems coupled

with fluid flow.

2 BASIC IDEA

To describe the 'Matrix-Cut' method we consider a generic transport equation in integral form with respect to a conserved variable ϕ :

$$\frac{\partial}{\partial t} \int_{\Omega} \rho \phi d\Omega + \int_S \rho \phi \mathbf{u} \cdot \mathbf{n} dS = \int_S \Gamma \operatorname{grad} \phi \cdot \mathbf{n} dS + \int_{\Omega} q_{\phi} d\Omega \quad (1)$$

After a discretisation of eq. (1) we have the following equation for each control volume of a two-dimensional Cartesian grid:

$$A_W \phi_W + A_E \phi_E + A_P \phi_P + A_S \phi_S + A_N \phi_N = Q_P \quad (2)$$

Considering all CVs the following matrix equation can be written:

$$[A][\phi] = [Q] \quad (3)$$

Fig. 1a shows the matrix structure obtained after FV or FD discretization using 5-point computational stencil. It can be shown mathematically (will be demonstrated in the final paper) that for a case when we set up a boundary condition in one CV located in the center of our domain the matrix has to be modified according to the Fig. 1b. Finally, any matrix solver can be applied to solve modified matrix equation. In this formulation, any boundary condition can be 'implemented' directly. For the validation of this method we use analytical solutions and classical CFD approach utilizing unstructured grid for a heat transfer problem.

REFERENCES

- [1] C.S. Peskin . Flow pattern around heart valves: a numerical method *J. Comp. Phys.*, 10:252-271, 1972
- [2] R. Mittal and G. Iaccarino. Immersed boundary methods. *Annual Rev. Fluid Mech.*, 37:239-261, 2005
- [3] D. Goldstein, R. Handler and L. Sirovich. Modeling a no-slip flow boundary with an external force field. *J. Comp. Phys.*, 105:354-366, 1993
- [4] J. Mohd-Yosuf. Combined immersed boundary/B-spline methods for simulation of flow in complex geometries *Annu. Res. Briefs, Cent. Turbul. Res.*, 317-328, 1997
- [5] E.A. Faldun, R. Verzicco, P. Orlandi, J. Mohd-Yusof. Combined immersed-boundary finite-difference methods for three dimensional complex flow simulations. *J. Comp. Phys.*, 161:30-60, 2000
- [6] H.S. Udaykumar, R. Mittal, W. Shyy. Computation of solid-liquid phase fronts in the sharp interface limit on fixed grids. *J. Comp. Phys.*, 153:535-574, 1999
- [7] J.A.M. Kuipers, K.J. van Duin, F.P.H. van Beckum, W.P.M. van Swaaij. Computer simulation of the hydrodynamics of a two-dimensional gas-fluidized bed *Comp. & Chem. Eng.*, 17:839-858, 1992
- [8] S. Turek and D.C. Wan and L.S. Rivkind The fictitious boundary method for the implicit treatment of Dirichlet boundary conditions with applications to incompressible flow simulations. *Lecture Notes in Computational Science and Engineering*, 35:37-68, 2003
- [9] P.A. Nikrityuk, S. Ananiev, K. Eckert, R. Grundmann. The influence of a direct electric current on the growth of solutal dendrites. *Magnetohydrodynamics J.*, 45:267-276, 2009
- [10] F. Dierich, P.A. Nikrityuk, S. Ananiev. 2D modeling of moving particles with phase-change effect. *Chem. Eng. Sci.*, 66:5459-5473, 2011

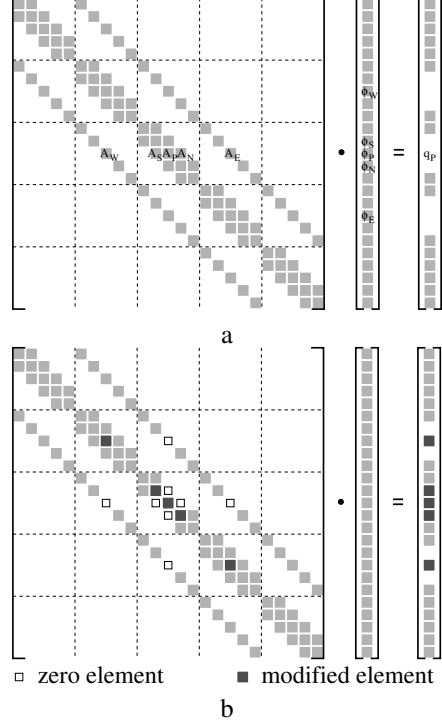


Figure 1: Illustration of the matrix structure obtained after FV or FD discretization using 5-point computational stencil (a), modifications of the matrix elements due to the point-wise immersed object in the center of domain - (b).

- 450

Anisotropic Non-Uniform Block-based Adaptive Mesh Refinement for Three-Dimensional Inviscid and Viscous Flows

L. Freret and C.P.T. Groth

*University of Toronto Institute for Aerospace Studies
4925 Dufferin Street, Toronto, Ontario, M3H5T6, Canada*

Email: *lfreret@utias.utoronto.ca, groth@utias.utoronto.ca*

ABSTRACT

A parallel anisotropic block-based adaptive mesh refinement (AMR) algorithm is proposed and described for the solution of physically complex flow problems with disparate spatial and temporal scales exhibiting highly anisotropic features on three-dimensional multi-block body-fitted hexahedral meshes with non-uniform grid blocks. Instead of using the classical uniform treatment for the cells of each block within the multi-block grids, the proposed anisotropic AMR approach adopts a non-uniform representation of the cells within each block, using directly the neighboring cells as the ghost cells whatever the grid resolution might be. A modified upwind finite-volume spatial discretization scheme is applied in conjunction with the proposed AMR scheme to the solution of Euler and Navier-Stokes equations for inviscid and viscous compressible gaseous flows. The potential flexibility and efficiency of this enhanced anisotropic AMR method is demonstrated by considering various complex flows.

1 INTRODUCTION

One way to decrease the computational burden when solving complex flow problems without simplifying the physics while maintaining solution accuracy consists in using AMR schemes. Parallel block-based AMR methods have been proposed previously by Groth and co-workers [1, 2] for solving complex flow problems on multi-block body-fitted meshes, where both isotropic and anisotropic AMR strategies have been investigated. While such AMR schemes have demonstrated their potential in a broad range of applications, they are suffering from some limitations, typically when a high-order spatial discretization method is used such as those developed by Ivan et al. [3].

2 ANISOTROPIC AMR

In block-based AMR scheme, a mesh adaptation is accomplished by refining and coarsening predefined grid blocks. A hierarchical tree data structure is used for tracking block connectivity and mesh refinement history. A classical strategy for adapting the mesh to key physical features of the flow consists in using physics-based indicators such as the flow density gradient. This work is based on the 3D anisotropic AMR scheme [4]; we also refer the reader to [5] for a detailed description of the previous 2D implementation.

In the previous implementation of the block-based AMR method, each block contains a structured mesh with $N_i \times N_j \times N_k$ number of cells and N_g ghost cell layers that allow solution information transfer from neighboring blocks. This requires prolongation and restriction procedures in one or more directions to fill the neighboring ghost cells. One scenario of mesh resolution change is particularly problematic when using high-order schemes [5], that is, coarse-to-fine in one direction along with fine-to-coarse in the other direction. Not accounting for this configuration results in a significantly reduced effectiveness of the anisotropic AMR. It was found in [5] that the optimal solution is to modify the definition of the block and its related ghost cells so that high-order spatial discretizations can be treated in a similar fashion to second-order schemes.

2.1 Non-Uniform Block-Based Approach

In the proposed implementation of anisotropic AMR, the ghost cells are directly provided by the adjacent blocks. All the information (solution and geometry) is used to determine the ghost cells and their solu-

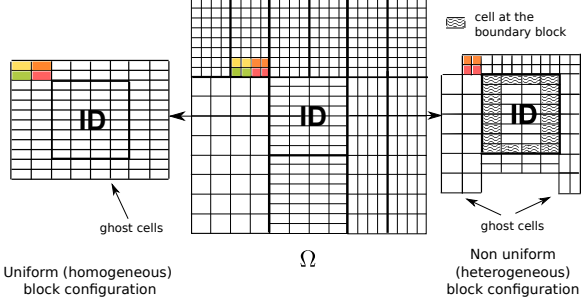


Figure 1: Configuration of a uniform structured mesh block (left) and non-uniform structured mesh block (right) from a common block-based anisotropic AMR grid mesh (center).

tion values (see Figure 1 where a 2D representation is used for clarity). In Figure 1 the domain Ω is decomposed into 11 blocks. On the left side we represent the uniform structured block geometry provided by the original implementation which corresponds to the block itself (ID) extended by 2 layers of ghost cells. The new non-uniform block is composed of an interior block (ID) enlarged by 2 layers of ghost cells keeping the neighbor's mesh resolution. On the right side, the non-uniform heterogeneous block consists of 10 sub-elements: the block itself (ID) and 9 block boundary elements (5 edges and 4 corners) arising from the surrounding blocks. In a 3D configuration, the resultant heterogeneous block will contain the interior domain (ID) and at least 26 block boundary elements (6 faces, 12 edges and 8 corners). While a uniform block can simply be represented by one array of values, a non-uniform block is represented by at least 27 arrays of information. This represents an additional layer of complexity; however, it also brings two major advantages. First, the prolongation and restriction procedures are no longer required to determine the solution content with the ghost cells at grid block resolution changes (these procedures represent a blocking point in the uniform block representation). Secondly, it simplifies the implementation of message passing between adjacent blocks since conservative flux corrections are entirely eliminated by naturally handling the non-conforming cells in the finite-volume method. As a matter of fact, when using uniform blocks, a natural consequence of refining and coarsening is to have non-conforming cells where the faces of both blocks meet. To maintain the conservation properties of the finite-volume scheme, the flux through these non-conforming faces must be corrected. Typical procedures for flux correction involve correcting the solution flux through the coarse cell faces to be equal to

that of the total flux through the faces of the cells in the adjacent finer block [4].

3 NUMERICAL RESULTS

Several steady-state and time-varying flow problems are chosen to demonstrate the effectiveness of the proposed 3D anisotropic AMR algorithm and show how the computational complexity is reduced. As preliminary results for inviscid flow problems governed by Euler equations, we evaluate the AMR algorithm within the unsteady shock cube flow problem and the steady-state supersonic channel flow over a bump. Comparisons between isotropic and anisotropic density profiles show a very good agreement while the anisotropic refinement manages to achieve a high level of efficiency. We next evaluate the solution of the Navier-Stokes equations for a laminar viscous fluid flow problem. The solution of the 3D subsonic flow over a flat plate is compared with the exact solution of the incompressible boundary layer equations obtained in [6]. Finally, a 3D lid-driven cavity flow problem is considered with Reynolds number $Re = 100$.

REFERENCES

- [1] X. Gao and C.P.T. Groth A parallel adaptive mesh refinement algorithm for predicting turbulent non-premixed combusting flows. *Int. J. Comp. Fluid Dynamics*, 20, 2006.
- [2] S. Northrup and C.P.T. Groth Solution of laminar diffusion flames using a parallel adaptive mesh refinement algorithm. 20th AIAA CFD Conference, 2005
- [3] L. Ivan, H. De Sterck, S. Northrup and C.P.T. Groth Multi-dimensional finite-volume scheme for hyperbolic conservation laws on three-dimensional solution-adaptive cubed-sphere grids. *JCP*, 255, 2013.
- [4] M.J. Williamschen and C.P.T. Groth. Parallel anisotropic block-based adaptive mesh refinement algorithm for three-dimensional flows. 21th AIAA CFD Conference, 2013
- [5] Z.J. Zhang and C.P.T. Groth. Parallel high-order anisotropic block-based adaptive mesh refinement finite-volume scheme. 20th AIAA CFD Conference, 2011
- [6] H. Schlichting. *Boundary-Layer Theory*. McGraw-Hill, 1979

Application of a Maximum-Entropy-Based 14-Moment Closure for Multi-Dimensional Non-Equilibrium Flows

Boone R. Tensuda¹, James G. McDonald², and Clinton P. T. Groth¹

¹ University of Toronto Institute for Aerospace Studies, 4925 Dufferin Street, Toronto, Ontario, Canada.

² Department of Mechanical Engineering, University of Ottawa, 161 Louis Pasteur, Ottawa, Ontario, Canada.

Email: boone.tensuda@mail.utoronto.ca

ABSTRACT

The predictive capabilities of a 14-moment, maximum-entropy-based, interpolative closure are explored for multi-dimensional non-equilibrium flows with heat transfer. Unlike the maximum-entropy closure on which it is based, the interpolative closure provides closed-form expressions for the closing fluxes. While still presenting singular behaviour in regions of realizable moment space, the interpolative closure proves to have a large region of hyperbolicity while remaining tractable. Furthermore, its singular nature is deemed advantageous for practical simulations. An implicit finite-volume procedure is proposed and described for the numerical solution of the 14-moment closure on two-dimensional computational domains. An implicit Newton-Krylov-Schwarz (NKS) time marching scheme is also implemented. Multi-dimensional applications of the closure are then examined for several canonical flow problems in order to provide an assessment of the capabilities of this novel closure for a range of non-equilibrium flows. The advantages of an implicit time marching scheme over a semi-implicit scheme are also considered.

1 INTRODUCTION & MOTIVATION

The prediction of transition-regime non-equilibrium flows has proven to be a challenging branch of study in computational fluid dynamics (CFD). Such flows cannot be modeled using typical continuum approaches, such as the Naiver-Stokes equations, and accurate modeling techniques, such as direct simulation Monte Carlo (DSMC) methods [1] and techniques involving direct discretization of the Boltzmann equation [7], are limited by their high dimensionality and computational cost. The method of moment closures offers an alternative technique for accurately treating transition-

regime flows with the potential of greater robustness and a significantly reduced computational cost. The purely hyperbolic and first-order quasilinear nature of some moment closures also presents several numerical advantages which extend into both the transition and continuum regimes [2].

A hierarchy of moment closures having a number of desirable properties has been proposed based on the maximization of thermodynamic entropy [4, 8]. In particular, the approximate form for the distribution function corresponds to the most likely distribution given the finite set of moments of interest and members of the hierarchy have been shown to be globally hyperbolic whenever the underlying entropy maximization problem can be solved. Unfortunately, issues with the maximum-entropy closure arise when higher-order moments that describe heat transfer are included [3]. These complications have limited the use of the maximum-entropy closure technique for general non-equilibrium flows. Recently, new, interpolative-type, maximum-entropy-based, 5-moment (one-dimensional gas) and 14-moment (three-dimensional gas) closures, initially investigated by McDonald and Groth [5], and expanded upon by McDonald and Torrilhon [6], have been proposed that successfully navigate the aforementioned issues.

2 SCOPE OF THE PRESENT STUDY

While McDonald and Torrilhon [6] have described some initial solutions of the 14-moment maximum-entropy-based interpolative closure for stationary, one-dimensional, shock structure, further investigation of the closure is certainly warranted in order to fully explore its predictive capabilities. To this end, the present study will focus on the numerical solution of the 14-moment closure for multi-dimensional non-

equilibrium flows with heat transfer. A finite-volume procedure is proposed and described for the numerical solution of the 14-moment closure on two-dimensional computational domains. Due to the high wave speeds associated with this closure, especial in the regimes of near-equilibrium and equilibrium flows, it is desirable to use a fully implicit time-marching scheme. In this study a Newton-Krylov-Shwarz (NKS) [9] implicit solver has been utilized. The implementation of this time marching scheme is summarized and a comparison to a semi-implicit scheme is presented. The application of the closure to several canonical flow problems including, but not limited to, subsonic laminar flow past a two-dimensional circular cylinder, subsonic laminar Couette flow, heat transfer between infinite flat plates, and lid-driven cavity flow are considered. The predictions will be compared to available experimental and theoretical results, as well as numerical results from other solution methods, such as DSMC, in order to provide an assessment of the capabilities of this novel closure technique for a range of non-equilibrium flows.

3 PRELIMINARY RESULTS

Some initial results are presented for subsonic flow of argon gas over a circular cylinder at a Knudsen number of one (Figure 1), and heat transfer between infinite flat plates (Figure 2). These results show many of the expected non-equilibrium phenomena such as temperature jump, counter-gradient heat flux, large boundary layers, and velocity slip. Figure 3 presents a computational cost comparison between the semi-implicit and NKS solvers applied to a Couette flow case. It is clear that even for this simple case a significant amount of computational savings result from the use of the NKS solver.

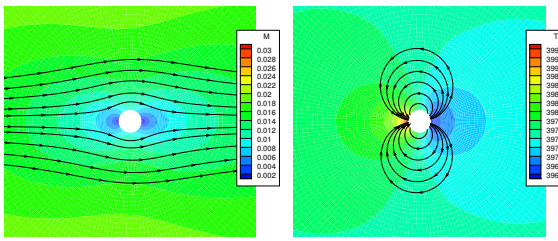


Figure 1: Non-equilibrium flow past a circular cylinder. (a) Mach number contours and velocity streamlines. (b) Temperature contours and heat flux streamlines.

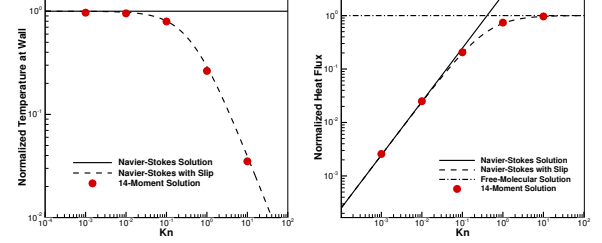


Figure 2: Heat transfer between infinite plates. (a) Normalized temperature at the wall with respect to Knudsen number. (b) Heat flux between the plates, normalized with respect to the free-molecular value, as a function of Knudsen number.

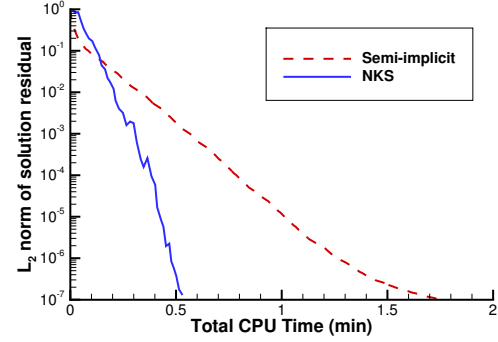


Figure 3: Comparison of convergence of the solution residuals for the Newton-Krylov-Schwarz and semi-implicit schemes for planar Couette flow.

REFERENCES

- [1] G. A. Bird. *Molecular Gas Dynamics and the Direct Simulation of Gas Flows*. Clarendon Press, Oxford, 1994.
- [2] C. P. T. Groth and J. G. McDonald. Towards physically-realizable and hyperbolic moment closures for kinetic theory. *Continuum Mech. Thermodyn.*, 21(6):467–493, 2009.
- [3] M. Junk. Domain of definition of Levermore's five-moment system. *J. Stat. Phys.*, 93(5/6):1143–1167, 1998.
- [4] C. D. Levermore. Moment closure hierarchies for kinetic theories. *J. Stat. Phys.*, 83:1021–1065, 1996.
- [5] J. G. McDonald, J. S. Sachdev, and C. P. T. Groth. Application of Gaussian moment closure to micro-scale flows with moving and embedded boundaries. Accepted to the AIAA Journal, 2014.
- [6] J. G. McDonald and M. Torrilhon. Affordable robust moment closures for CFD based on the maximum-entropy hierarchy. *J. Comput. Phys.*, 251:500–523, 2013.
- [7] L. Mieussens. Discrete velocity model and implicit scheme for the BGK equation of rarefied gas dynamics. *Mathematical Models and Methods in Applied Sciences*, 10(8):1121–1149, 2000.
- [8] I. Müller and T. Ruggeri. *Rational Extended Thermodynamics*. Springer-Verlag, New York, 1998.
- [9] S. Northrup. *A Parallel Implicit Adaptive Mesh Refinement Algorithm for Predicting Unsteady Fully-Compressible Reactive Flows*. PhD thesis, University of Toronto, 2014.

Application of CFD Modelling to the Restoration of Eutrophic Lakes

A. Najafi-Nejad-Nasser¹, S. S. Li², C. N. Mulligan³

¹*Department of Building, Civil and Environmental Engineering, Concordia University, Montreal, Canada*

²*Department of Building, Civil and Environmental Engineering, Concordia University, Montreal, Canada*

³*Department of Building, Civil and Environmental Engineering, Concordia University, Montreal, Canada*

Email¹: a_najaf@encs.concordia.ca

Email²: sam.li@concordia.ca

Email³: mulligan@civil.concordia.ca

ABSTRACT

Eutrophication in freshwater lakes refers to a dense growth of plants (algae) in the inland water bodies. The common cause of eutrophication is the addition of an excessive amount of nutrients to the lake water. Typically, among nutrients, phosphorus is the limiting factor for algae growth. Consequences of eutrophication in lakes include the depletion of oxygen supply, increased turbidity, and negative impacts in terms of other water quality parameters, as have been observed in numerous lakes around the world, including many lakes in Quebec, Canada. Thus, it is important to be able to control eutrophication in lakes. Over the past few decades, efforts to control eutrophication have aimed at reducing or eliminating fluxes of nutrients to lakes from external sources such as animal waste, agricultural fertilizers, domestic sewage, and industrial discharges of effluents from land sources. However, in many cases, the release of phosphorous from the lake bottom sediments as an internal source is more problematic than the external sources of nutrients causing eutrophication. The need to effectively control the release of phosphorus from the bottom sediments to the lake water has motivated the present study.

This paper discusses artificial circulation as a technique for the remediation of a eutrophic lake, which does not involve adding any chemical substance. Artificial circulation is generated by the injection of air bubbles into the lake water at the bottom. This paper takes the numerical prediction approach. Computational fluid dynamics (CFD)

simulations are carried out to predict bubbly flow in the lake water. The predictions are compared with laboratory experimental data. Lake circulation and turbulent mixing are treated as multi-phase bubbly flow, with water as the liquid phase and air bubbles as the gas phase. The CFD simulations are based on the Reynolds-averaged continuity and momentum equations, which allow for not only non-linearity but also dynamic interaction between the two phases. Turbulent mixing is characterised using turbulence kinetic energy, whose variations in time and space are predicted using a number of well-referenced turbulence closure models (the $k-\varepsilon$ model, the $k-\omega$ model, and the shear stress transport $k-\omega$ model). This paper compares their performance. Also, this paper discusses the Eulerian approach and the volume-of-fluid approach with respect to computational efficiency and accuracy.

In this paper, we address a number of important issues: 1) the characteristics of water circulation and turbulent mixing in a eutrophic lake by injecting air to the lake water, and implications to the quality of the lake water; 2) optimal aeration schemes for improvements to anoxic conditions and hence for the elimination/reduction of internal loading of phosphorous; and 3) maintenance of oxygenated bottom water. We show that the CFD predictions of distributed air velocity, water velocity, and air volume fraction are in good comparison with experimental data.

Application of High-Order Summation-by-Parts Operators to the Reynolds-Averaged Navier-Stokes Equations

X. Shen and D. W. Zingg

Institute for Aerospace Studies, University of Toronto, Toronto, Ontario

Email: *xy.shen@webmail.utoronto.ca dwz@oddjob.utias.utoronto.ca*

Abstract

High-order methods have been implemented to solve the steady Reynolds-averaged Navier-Stokes (RANS) equations with Spalart-Allmaras (SA) model. Summation-by-parts (SBP) operators are used for spatial discretization along with simultaneous approximation terms (SATs) to enforce boundary and interface conditions in a weak sense. Three validation cases provided by the Turbulence Modelling Resource website are tested to verify the implementation of the high-order RANS-SA model and to examine the efficiency and robustness of the high-order methods. They are a 2D zero pressure gradient flat plate, a 2D bump in a channel, and the 2D NACA0012 airfoil at various angles of attack. Work is still in progress; results to date from several grid convergence studies have shown that raising the spatial discretization to 3rd-order global accuracy leads to a substantial reduction in numerical error.

1 Introduction

While the majority of commercially available CFD programs are written with 2nd-order methods, high-order CFD methods have the potential to increase solution accuracy at reduced computational cost. With a given mesh size, a high-order method normally takes longer to obtain a converged solution; however, it can reach the same level of accuracy as a 2nd-order method on a much coarser mesh. Implementing high-order methods may have significant benefits in the numerical solution of the RANS equations [1]. This paper investigates the use of high-order SBP-SAT methods

in the numerical solution of RANS-SA equations. Results obtained using 3rd-order and 4th-order methods are compared to those from a 2nd-order method. Grid convergence studies are conducted to examine the reduction in numerical error by the high-order approach.

2 Theory

The SBP-SAT method is applied for spatial discretization in solving the turbulent flows. An SBP operator is constructed to satisfy discrete summation by parts property and is proven to be stable with the use of SAT[2, 3]. SATs correct the values of boundary or interface nodes to be the desired values by adding a penalty term. The use of SATs imposes weak boundary terms without destroying the SBP property of the difference operator. Boundary values at two neighbouring interfaces are not exactly the same and thus flow can be solved within each grid block which minimizes the information transfer among blocks.

3 Test Cases and Grids

Three geometries are studied in this paper:

1. 2D flat plate, $M = 0.2$, $Re_L = 5 \times 10^6$ ($L = 1$),
 $T_{ref} = 540R$
2. 2D bump in a channel, $M = 0.2$, $Re_L = 3 \times 10^6$ ($L = 1$), $T_{ref} = 540R$
3. 2D NACA0012, $M = 0.15$, $Re_c = 3 \times 10^6$ ($c = 1$), $T_{ref} = 540R$, at $\alpha = 0^\circ, 10^\circ, 15^\circ$,

For each test case, a series of grids provided by the Turbulence Modelling Resource website are used

for grid convergence studies. In each grid family, a coarser mesh is generated by removing every other node from the finer mesh.

4 Results and Conclusion

Results obtained so far have demonstrated that the 3rd-order method coupled with first-order upwinding dissipation scheme for the turbulent quantity generates less numerical error than the 2nd-order algorithm. Figures 1 and 2 show the drag coefficient produced by the 3rd-order method compared to the 2nd-order method for Cases 1 and 2, respectively. Numerical errors on the coarsest mesh are calculated relative to the corresponding grid converged drag coefficient value, C_d^* estimated through grid convergence studies. For example, the error in C_d obtained with the 2nd-order method on the coarsest mesh is calculated relative to C_d^* obtained by the 2nd-order method.

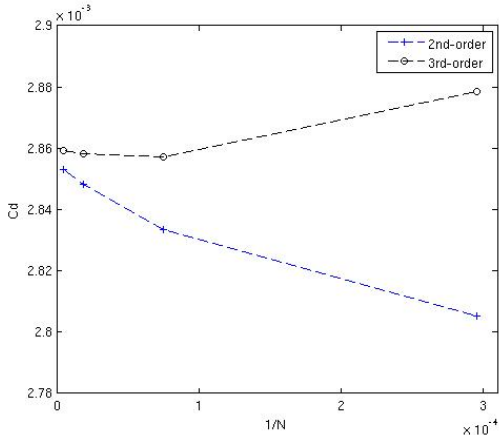


Figure 1: Grid convergence for Case 1, zero pressure gradient flat plate

Algorithm	C_d^*	$\%C_d^{(1)}$	$\%C_d^{(2)}$
2nd-order	2.8556×10^{-3}	1.75	0.77
3rd-order	2.8583×10^{-3}	0.71	0.03

Table 1: Errors for Case 1. C_d represents the drag coefficient obtained on the coarsest mesh and $\%C_d$ represents the percentage error relative to the predicted grid converged value.

Tables 1 and 2 summarize the comparison between the 2nd-order and 3rd-order methods for Cases 1 and 2, respectively. In these tables, $\%C_d^{(1)}$ represents the error on the coarsest mesh while $\%C_d^{(2)}$

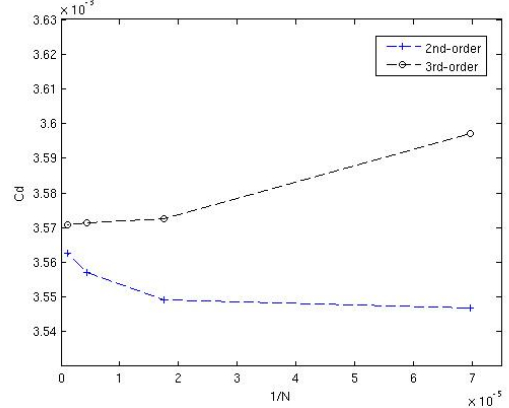


Figure 2: Grid convergence for Case 2, bump-in-channel

Algorithm	C_d^*	$\%C_d^{(1)}$	$\%C_d^{(2)}$
2nd-order	3.5755×10^{-3}	0.81	0.73
3rd-order	3.5699×10^{-3}	0.76	0.08

Table 2: Errors for Case 2. C_d represents the drag coefficient obtained on the coarsest mesh and $\%C_d$ represents the percentage error relative to the predicted grid converged value.

represents the error on the second coarsest mesh. It is shown that on the coarsest mesh, the 3rd-order method is generally more accurate than the 2nd-order method.

References

- [1] S. De Rango and D. W. Zingg, "Higher-order spatial discretization for turbulent aerodynamic computations," *AIAA Journal*, vol. 39, no. 7, pp. 1296–1304, 2001.
- [2] B. Strand, "Summation by parts for finite difference approximations for d/dx ," *Journal of Computational Physics*, vol. 110, no. 1, pp. 47–67, 1994.
- [3] D. C. Del Rey Fernández, J. E. Hicken, and D. W. Zingg, "Review of summation-by-parts operators with simultaneous approximation terms for the numerical solution of partial differential equations," *Computers and Fluids*, vol. 95, pp. 171 – 196, 2014.

Buoyant displacement flows of viscoplastic fluids in horizontal channels

Ali Eslami¹, Avinash Shevally², Nikhilesh Podduturi², Kamran Alba², Ian Frigaard^{3,4}, and Seyed Mohammad Taghavi¹

¹ Department of Chemical Engineering, Laval University, Québec, QC, Canada

² Department of Engineering Technology, University of Houston, Houston, TX, USA

³ Department of Mathematics, University of British Columbia, Vancouver, BC, Canada

⁴ Department of Mechanical Engineering, University of British Columbia, Vancouver, BC, Canada

Email: *Seyed-Mohammad.Taghavi@gch.ulaval.ca*

ABSTRACT

The displacement flow of a viscoplastic fluid by a Newtonian one is investigated numerically in a horizontal 2D channel. The fluids considered are miscible. We study a situation where the displacing Newtonian fluid is heavier than the displaced viscoplastic one. We study the effects of the presence of strong yield stress in the displaced layer and demonstrate that static residual layers of the displaced fluid are strongly present at all values of Reynolds number studied. We have also found that at lower values of Reynolds number and larger values of Bingham number the static residual layer is significantly thick, which leads to a large value of dimensionless front velocity.

1 INTRODUCTION

An important feature of a yield stress fluid is that the fluid does not deform until a critical shear stress is reached locally. Therefore, when these fluids fill ducts and are displaced by other fluids, there is a tendency for the yield stress fluid to remain stuck to the duct walls and in particular in parts of the duct where there are constrictions or corners. We have previously studied the effects of the inclination angle on the displacement of a yield-stress fluid by a Newtonian fluid of higher density in a circular pipe experimentally [1]. For brevity, we refer to these papers for a more detailed introduction and review of previous work. The main observation made in our previous works was that a strong yield-stress fluid in displacement flows can lead to the presence of two main regimes that we called center-type and slump-type displacements [1]. In the current work, we study the effects of the presence of a

yield stress for displacement flows that take place in a 2D channel geometry computationally. The novelty of our work is the consideration of a combined effect of buoyancy and yield stress effects in a horizontal channel.

2 GOVERNING EQUATIONS

We study the displacement of a Bingham fluid (fluid 2) by a Newtonian one (fluid 1) along a channel of width \hat{D} . The fluids are miscible and have different densities. We choose Cartesian coordinates (\hat{x}, \hat{y}) with \hat{x} representing the streamwise direction.¹ The dimensionless equations of motion are:

$$[1 + \phi A t] Re \left[\frac{\partial}{\partial t} \mathbf{u} + (\mathbf{u} \cdot \nabla) \mathbf{u} \right] = -\nabla p + \nabla \cdot \tau + \frac{\phi Re}{Fr^2} \mathbf{e}_g, \quad (1)$$

$$\nabla \cdot \mathbf{u} = 0, \quad (2)$$

$$C_t + \mathbf{u} \cdot \nabla C = \frac{1}{Pe} \nabla^2 C. \quad (3)$$

where \mathbf{u} denotes the velocity, p is the pressure, τ shows the deviatoric stress. Here $\mathbf{e}_g = (0, -1)$ and the function $\phi(C) = 2C - 1$ interpolates linearly between -1 and 1 for $C \in [0, 1]$. No slip conditions are satisfied at the walls, the heavy fluid enters fully developed (plane Poiseuille profile) at $x = -L/4$ and outflow conditions are applied at $x = 3L/4$. In order to make these equations dimensionless, we have used the following scaling:

$$\mathbf{x} = \frac{\hat{\mathbf{x}}}{\hat{D}}, \quad t = \frac{\hat{V}_0}{\hat{D}} \hat{t}, \quad \mathbf{u} = \frac{\hat{\mathbf{u}}}{\hat{V}_0},$$

¹In this paper, we adopt the convention of denoting dimensional quantities with the $\hat{\cdot}$ symbol and dimensionless quantities without.

$$p = \frac{\hat{D}}{\hat{\mu}_1 \hat{V}_0} \hat{p}, \quad \tau = \frac{\hat{D}}{\hat{\mu}_1 \hat{V}_0} \hat{\tau} \quad (4)$$

where $\hat{\mu}_1$ denotes the viscosity of the displacing fluid, which is Newtonian. The dimensionless groups that appear in (1-3) are the Reynolds number Re , densimetric Froude number Fr , Atwood number At and Péclet number Pe . The Newtonian displacing fluid has the constitutive law of $\tau(\mathbf{u}) = \dot{\gamma}(\mathbf{u})$ with $\dot{\gamma} = \nabla \mathbf{u} + (\nabla \mathbf{u})^T$. The displaced fluid is assumed to be a Bingham fluid, which presents a yield stress effect. For this model, we have:

$$\tau_2(\mathbf{u}) = m \left[1 + \frac{B}{\dot{\gamma}(\mathbf{u})} \right] \dot{\gamma}(\mathbf{u}) \Leftrightarrow \tau_2(\mathbf{u}) > mB, \quad (5)$$

$$\dot{\gamma}(\mathbf{u}) = 0 \Leftrightarrow \tau_2(\mathbf{u}) \leq mB \quad (6)$$

where the second invariants, $\dot{\gamma}(\mathbf{u})$ and $\tau_2(\mathbf{u})$, are defined by:

$$\begin{aligned} \dot{\gamma}(\mathbf{u}) &= \left[\frac{1}{2} \sum_{i,j=1}^2 [\dot{\gamma}_{ij}(\mathbf{u})]^2 \right]^{1/2}, \\ \tau_2(\mathbf{u}) &= \left[\frac{1}{2} \sum_{i,j=1}^2 [\tau_{2,ij}(\mathbf{u})]^2 \right]^{1/2}. \end{aligned} \quad (7)$$

The viscosity ratio m is:

$$m \equiv \frac{\hat{\mu}_2}{\hat{\mu}_1} \quad (8)$$

where $\hat{\mu}_2$ is a viscosity scale for fluid 2 (displaced) and Bingham number B can be introduced as:

$$B \equiv \frac{\hat{\tau}_Y}{\hat{\mu}_2 [\hat{V}_0 / \hat{D}_0]}. \quad (9)$$

Equations of motion are discretised using a mixed finite element, finite volume method. The Navier-Stokes equations are solved using Galerkin finite element method. The divergence-free condition is enforced by an augmented Lagrangian technique. A fixed time step is used for the Navier-Stokes equations, advancing from time step N to $N+1$. The convective velocity is approximated at time step N while the linear spatial derivatives of the velocity are approximated implicitly at time step $N+1$. The pressure is approximated at time step $N+1$ (semi-implicit method regarding the nonlinear terms). To check the accuracy of the code, various simple test problems have been implemented.

3 RESULTS

In this section we present our computational results. Fig. 1 shows examples of our results, run for $At = 0.01$,

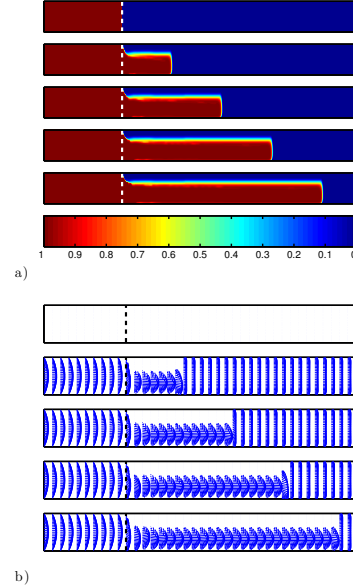


Figure 1: Examples of the results for $At = 0.01$, $m = 1$, $B = 92.7$, $Re = 500$ and $Fr = 0.61$: a) Concentration maps of the numerical simulation for times $t = [0, 11.03, 22.06, 33.09, 44.13]$; b) Velocity vector fields for the same snapshots as shown in a

$m = 1$, $B = 92.7$, $Re = 500$ and $Fr = 0.61$. At $t = 0$, the two fluids are separated by an imaginary gate valve located at $x = 0$. As time progresses, due to the imposed mean velocity, the heavy layer penetrates through the light layer and displaces it. Fig. 1a shows the concentration maps of the numerical simulation as times progresses. In this figure, it can be seen that the displaced layer remains completely static once the displacing fluid front passes a streamwise location by. As a consequence, the displacing front moves in a narrower channel (created by the static layer and the lower wall) and moves significantly faster than the imposed flow. Fig. 1b show the velocity vector fields for the same simulation. This figure confirms that the existence of a completely static residual layer, within which the velocity is zero.

REFERENCES

- [1] S. Taghavi, K. Alba, M. Moyers-Gonzalez, and I. Frigaard. Incomplete fluid-fluid displacement of yield stress fluids in near-horizontal pipes: experiments and theory. *J. non-Newt. Fluid Mech.*, 167-168:59–74, 2012.

High-order Solutions of the Negative Spalart-Allmaras Turbulence Model by a Correction Procedure via Flux Reconstruction Scheme

Farshad Navah and Siva Nadarajah

*Computational Aerodynamics Group,
Department of Mechanical Engineering, McGill University,
Montreal, QC H3A 2S6 Canada*

Email: *farshad.navah@mail.mcgill.ca*

ABSTRACT

High-order-accurate discretization methods applied to computational fluid dynamics (CFD) have recently benefited from the increasing interest of the research community. The potential of high-order methods as an efficient approach for the control and reduction of discretization errors has been established for inviscid and laminar flows. For turbulent flows modelled by the Reynolds-averaged Navier-Stokes (RANS) equations however, there is still a need for the development of robust and efficient high-order CFD solvers. The solution of the Spalart-Allmaras (SA) model of turbulence, that is conceived and extensively utilized for aerodynamic applications, has suffered from instabilities in presence of coarse spatial discretizations of the boundary layer that are typical of high-order solutions. Especially, the under-resolved representation of the SA working variable at the edge of the boundary layer introduces Gibbs oscillations that could compromise the convergence of the RANS system of equations. These instabilities have been recently addressed in a *negative* SA version of the original model that is modified to ensure convergence despite the occurrence of negative values of the working variable. This paper is concerned with the high-order solution of RANS and negative SA equations by the novel correction procedure via flux reconstruction (CPR) scheme.

1 METHODOLOGY

Most current state-of-the-art industrial computational fluid dynamics (CFD) solvers are 2^{nd} order accurate at best. This class of solvers, called *low-order*, are prone to large discretization errors that compromise the reliability of CFD as a tool for the estimation of engineer-

ing quantities such as lift and drag coefficients. High-order-accurate methods have the potential to produce lower discretization errors for the same number of degrees of freedom as their low-order counterparts and thus allow a larger flexibility in mesh generation. Furthermore, high-order methods enable the adaptation of both h , the element size, and p , the polynomial degree, that in combination, offer the full potential for optimal error control. While the efficacy of high-order methods in reducing the discretization errors is demonstrated for laminar and inviscid flows, the development of robust and efficient high-order solvers for Reynolds-averaged Navier-Stokes equations, the most popular approach for turbulence modelling, yet needs further investigation.

Recently, Huynh proposed [1] the flux reconstruction (FR) scheme, that unifies some of the most popular compact high-order methods under a common formulation. The extension of this scheme to simplexes by lifting collocation penalty is called correction procedure via flux reconstruction (CPR) [2] and is adopted as the discretization method in this paper.

1.1 Governing equations

The governing equations are the steady-state, compressible RANS equations assuming a Newtonian and calorically and thermally perfect gas. The negative SA model is detailed in [3].

The RANS-SA system is explicitly solved by a 3^{rd} order Runge-Kutta scheme.

2 RESULTS

The application case is a 2D zero-pressure-gradient flat plate with $Re = 5 \times 10^6$, $Ma = 0.2$ and $\chi_\infty = 0.3$ from NASA's Turbulence Modelling Resource (TMR).

The domain, illustrated in Figure 1, is discretized by a grid of 33×20 quadrangle elements. Three levels of polynomial discretization have been applied: P1, P2 and P3.

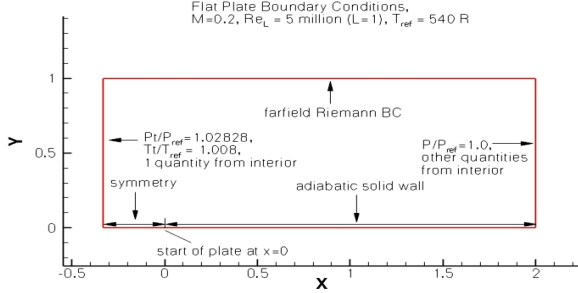


Figure 1: Domain and boundary conditions description

The results are compared to the reference solution from TMR obtained by NASA's CFL3D solver on a grid of 545×385 elements.

The relative eddy viscosity profiles at $x = 0.097$, plotted in Figure 2, exhibit improved agreements with the CFL3D profiles, as the polynomial degree is increased, to attain an excellent agreement for the P3 solution.

Increasing the order of accuracy of the discretization also improves the accuracy of the normalized velocity profiles at $x = 0.97$ that are compared, in Figure 3, to the CFL3D solution, to the theoretical inner and outer region profiles and to the law of the wall from the negative SA model [3].

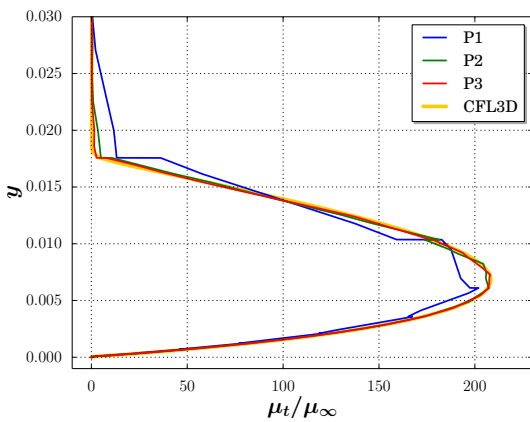


Figure 2: Relative eddy viscosity profile at $x = 0.97$.

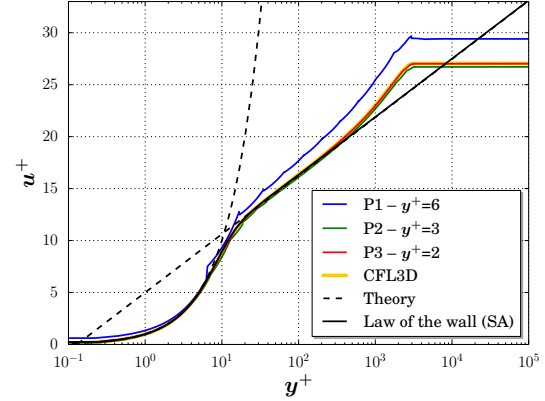


Figure 3: Normalized velocity profiles at $x = 0.97$; y^+ values in the legend refer to the normalized height of the first solution node off the wall.

REFERENCES

- [1] H. T. Huynh. A Reconstruction Approach to High-Order Schemes Including Discontinuous Galerkin for Diffusion. In *47th AIAA Aerospace Sciences Meeting*, Orlando, FL, Jan. 2009. American Institute of Aeronautics and Astronautics, AIAA Paper 2009-403.
- [2] Z. J. Wang and H. Gao. A unifying lifting collocation penalty formulation including the discontinuous Galerkin, spectral volume/difference methods for conservation laws on mixed grids. *Journal of Computational Physics*, 228(21):pp. 8161–8186, 2009.
- [3] S. R. Allmaras, F. T. Johnson, and P. R. Spalart. Modifications and Clarifications for the Implementation of the Spalart-Allmaras Turbulence Model. *7th International Conference on Computational Fluid Dynamics*, (July), 2012.

CAE-specific Criteria for Technology Readiness Levels (TRL) in the Industrial R&D Environment

Kurt Sermeus¹, Pat Piperni², Hong Yang¹

¹*Advanced Aerodynamics Department, Bombardier Aerospace, Montreal*

²*Advanced Design Department, Bombardier Aerospace, Montreal*

Email: kurt.sermeus@aero.bombardier.com

ABSTRACT

The present paper discusses the use of Technology Readiness Levels (TRL) in the planning, execution and maturity assessment of CFD software methods, or more broadly any scientific computing methods (e.g. Computational Structural Dynamics), which in this paper are termed as Computational Aided Engineering (CAE) methods and which includes methods used for Multi-Disciplinary Analysis and Optimisation (MDAO).

1. INTRODUCTION

The notion of Technology Readiness Level (TRL) has found widespread use in the industrial and governmental R&D environment. Broadly speaking a TRL is a mark between 1 and 9 to qualify in the most succinct way the state of development of a given technology. Its purpose is to facilitate the R&D management by adopting a common and generally applicable set of criteria by which the maturity of technologies can be characterized. Every technological development starts from a basic idea (TRL 1) where little is known about its eventual use, then goes through a number of development stages (TRL 2-8) to eventually be proven for an actual industrial mission (TRL 9).

The definitions of the TRL as initiated by NASA and later adopted by the US DoD [2] are based on rather general descriptions of what TRL x means in terms of hardware systems, e.g. a certain technology of rocket engine. How to apply these generally formulated TRL descriptions to simulation technologies such as CFD is often not as obvious. In the field of CFD the use of TRL is relatively new, at least at Bombardier. Traditionally the development of CFD software has been seen as a relatively linear process of specification, code implementation, verification and validation and the ‘amount’ of validation done was seen as a maturity level. However, as CFD simulation methods grow in complexity in terms of modeling

and interactions with other disciplines, the aspect of integration within a simulation environment becomes increasingly important. A given CFD method could be well validated for an isolated problem, but not mature for actual use because it lacks integration with other important elements, e.g. the CAD geometry system. The present paper proposes TRL criteria, which are in line with the commonly used US DoD’s definitions, but formulated in more specific terms that make sense to CFD – and by extension CAE – technologies. The aspect of integration of CFD methods within the larger framework of a complex CFD code or a system of several MDAO codes has been given particular attention in these criteria.

2. CAE DEVELOPMENT PATH

The CAE technology maturity has many aspects:

- Verification: correct implementation of model/method ,
- Validation: confirms accuracy of simulation models in comparison to trusted physical experiments, e.g. wind tunnel tests.
- Modeling capability: level of geometrical complexity that can be treated; in the context of aircraft this can mean for instance whether simple wing-body configurations or full aircraft configurations can be modeled.
- Efficiency, scalability: important factors that determine the cost of usage of the method for the intended application and its potential for future growth.
- Usability: how well integrated in overall process, how robust is it, documented.
- Maintainability: clean and documented implementation, level of support.

3. CAE/MDAO SPECIFIC TRL CRITERIA

The following tables list the CAE specific criteria proposed for TRL 1 to TRL 9.

The final paper will further substantiate these definitions, their background and illustrate them for particular CFD technology examples.

TRL	US DoD description	CAE specific criteria
1	Basic principles observed and reported	<p>Basic ideas of method reported in literature (a first paper) or internal memo, concept and main properties understood by BA specialists, application identified</p> <p><i>Questions to be answered:</i></p> <ul style="list-style-type: none"> - How is it different from existing tech? - How is it similar? - In what sense should it be better? - In what sense more challenging?
2	Technology concept and/or application formulated	<p>Integration of method with other elements researched at a basic abstract level, as a system/process.</p> <p>Rough estimate of technology performance, using analytical models, many assumptions. Still very speculative on interaction effects, integration.</p> <p>Paper studies, stage of invention.</p> <ul style="list-style-type: none"> - What are the integration aspects? - How will technology be verified/validated?
3	Analytical and experimental critical function and/or characteristic proof of concept	<p>Critical elements of technology implemented and tested in proof-of-concept code, each verified and validated. No integrated proof of concept of all elements yet.</p> <p>Estimate of overall system performance still subject to significant uncertainties.</p> <ul style="list-style-type: none"> - Was the main claim (advantage) of the technology demonstrated, at least at a fundamental level?

TRL	US DoD description	CAE specific criteria
4	Component and/or breadboard validation in laboratory environment	<p>All basic elements of technology integrated in a prototype code, validated together on benchmark application.</p> <p>The prototype CAE code is partially representative of the actual application (e.g. 2D) and may still have many modeling restrictions.</p> <p>Some non-critical elements may be missing (e.g. replaced by simplified ones).</p>
5	Component and/or breadboard validation in relevant environment	<p>Significant increase in integration, elements implemented in production-level code.</p> <p>Almost all functionality comparable to that expected for finalized technology.</p> <p>Proof of concept validation includes supporting elements.</p> <p>May require integration of some other enabling technologies.</p> <p>Validated on simplified test cases.</p>
6	System/ subsystem model or prototype demonstration in relevant environment	<p>Further integration into a fully functional demonstrator capability in production code.</p> <p>Test environment is close to actual production environment, some auxiliary functions (e.g. post-processing) may still be missing.</p> <p>All functions of technology fully defined.</p> <p>Extensive validation on real application cases, performance well understood.</p>

TRL	US DoD description	CAE specific criteria
7	System prototype demonstration in an operational environment	<p>Complete integration in production-ready code.</p> <p>All functions at or near final operational level of capability.</p> <p>Validation performed by application engineers on a pilot project, using real life BA problems.</p>
8	Actual system completed and operationally qualified through test and demonstration	<p>Technology fully validated and qualified for production in specified applications.</p> <p>User-level training done. Quality control (bug tracking, versioning, regression checks).</p> <p>Technology fully understood at the operational level.</p>
9	Actual system, proven through successful mission operations	<p>Technology proven in actual use. Lessons learned from application taken into account for final improvements. No further development required, only maintenance.</p>

REFERENCES

- [1] Oberkampf and Roy, Verification and Validation in Scientific Computing, Cambridge Press, 2010.
- [2] Mankins, J.C., "Technology Readiness Levels: a white paper," Advanced Concepts Office, NASA, Washington, DC, 1995.
- [3] Jimenez, H., and Mavris, D.N., "Characterization of technology insertion based on technology readiness levels," J. of Aircraft, Vol. 51, No. 1, pp. 291-302, 2014.

CFD Analysis of the Hydrodynamics of an Air-Water Multiphase System in a Rotating Toroid Wheel

N. R. Sarker¹, M. A. Islam², R. S. Sanders² and B. A. Fleck¹

¹*Department of Mechanical Engineering, University of Alberta, Edmonton, AB, Canada T6G 2G8*

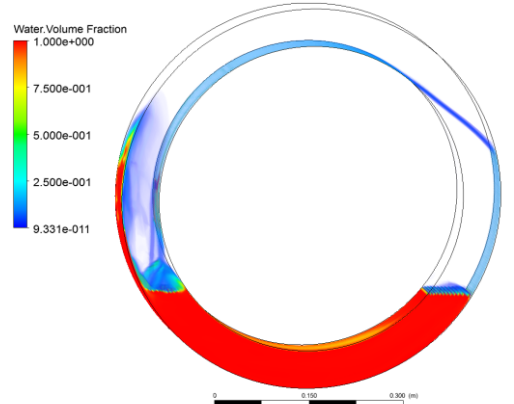
²*Department of Chemical and Materials Engineering, University of Alberta, Edmonton, AB, Canada T6G 2V4*

Email: nitishra@ualberta.ca

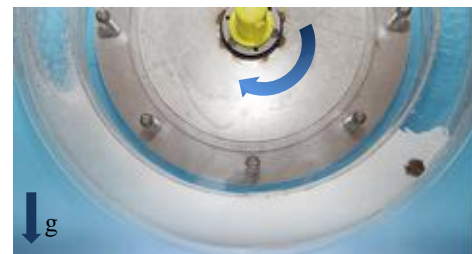
ABSTRACT

For the design and economic evaluation of slurry pipeline systems, the precise prediction of wear rate is very important [1, 2]. In Canada's oil sands industry, for example, more than \$1 Billion is spent on wear-related reliability issues each year [2]. The mechanisms governing wear are not well understood and the amount of useful wear data available is limited. Because actual pipeline wear tests are expensive and time consuming, other laboratory-scale test methods are often used (e.g. coriolis testers, impinging jet wear testers, slurry pots) [3]. One such method is the toroid wear tester as favorable comparisons between pipe wear and toroid wear tester results have been reported [1]. Under some operating conditions, however, generally accepted wear trends (say, effect of particle size or solids concentration) do not appear to hold during toroid tests. A better fundamental understanding of the hydrodynamics within a toroid wear tester is therefore required.

The present study focuses on the CFD analysis of an air-water flow induced by a rotating toroid wheel. The CFD model consists of a closed toroidal domain of 608 mm outer diameter and 60mm×65mm cross sectional area. The initial volume fractions of air and water considered inside the domain were 0.67 and 0.33, respectively. To determine the fluid velocity field, ANSYS CFX 15.0 was used in steady state mode with an unstructured 3D mesh containing about 250000 hexahedral mesh elements generated using ANSYS ICEM CFD. Grid independence tests and mesh quality parameter evaluation (such as angle, quality, and skewness) were performed to ensure high degree of confidence on the result. Both phases within the fluid domain were considered as continuous and a standard free surface multiphase model was applied. A homogenous Baseline (BSL) Reynolds Stress turbulence model with an automatic wall function was employed since the density



(a) CFD Simulation



(b) Flow in Acrylic Toroid Wheel

Fig. 1: Qualitative comparison between (a) CFD simulation and (b) photograph taken during ATW operation; N = 90 RPM

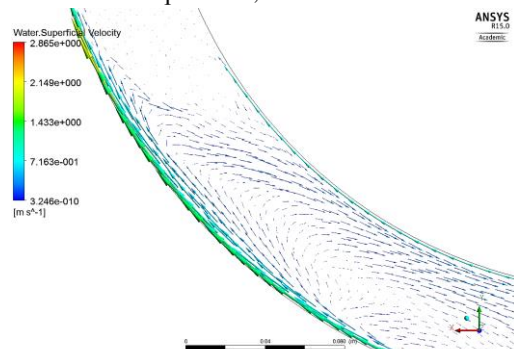


Fig. 2: Water velocity field at downstream location inside water domain; N = 90 RPM

difference based buoyancy model was considered for the study and the model included wall bounded flows in rotating fluids [4]. The fluid domain was considered stationary and a no slip rotating wall boundary condition was applied. Calculations were performed at operating speeds typically studied during wear tests, i.e. 30, 60 and 90 RPM. A qualitative comparison of the CFD simulation is made with the flow observed in a dimensionally identical acrylic toroid wheel (ATW).

Figure 1(a) shows a typical volume-rendered air-water flow situation from the CFD simulation for toroid wheel operation at 90 RPM. Figure 1(b) shows the flow in the ATW under similar operating conditions. The general similarity of the simulation result and the actual operation are apparent, particularly at the air-water interfaces. Note that the air-water interface at the downstream location is somewhat higher than the upstream location and indications of strong back-mixing at this location can be observed in both figures. Figure 2 shows the distribution of water velocity vectors in the downstream part of the water domain. It is evident from Figure 2 that water flows forward along the rotating wall due to viscous drag until it reaches the air-water interface and then flows backward through the inner core with decreasing magnitude. Figure 3 shows a typical water velocity profile along the X direction at the 6 o'clock position (bottom) of the toroid wheel at 90 RPM. This figure highlights the counter-current flow situation inside the toroid; the positive value of water velocity near wall indicates induced velocity in the direction of rotation and the negative value indicates the back-flow of water. The interface of the counter-current flow where the velocity is zero was found to occur at a normalized height of 0.06 - 0.10 depending on different locations inside water domain. Figure 3 also points to the asymmetric nature of the velocity profile in the radial direction. Comparing velocity profiles at different locations inside the toroid, it was found that for a particular wheel speed the flow at the upstream side of water domain is relatively more developed while the downstream side remains unsteady due to back-mixing phenomena. As the wheel speed increases, the disturbance in the flow field becomes more prominent as expected.

Further CFD analyses (with and without dispersed solids) focusing on velocity profiles, concentration gradients and parametric effects are being performed

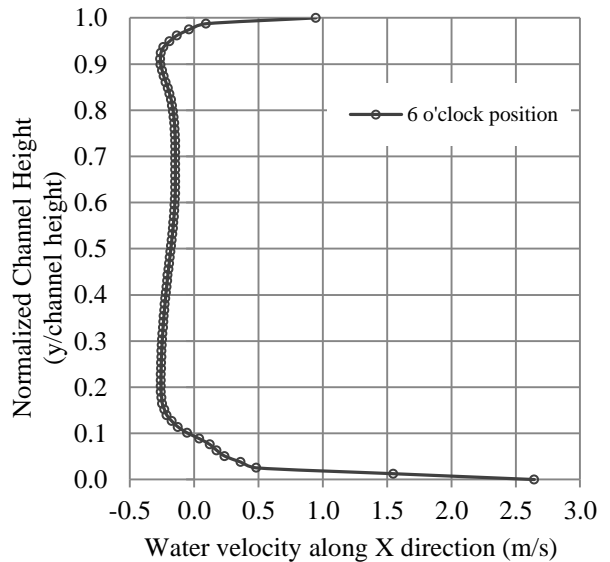


Fig. 3: Water velocity profile at 6 o'clock position inside water domain; N = 90 RPM

for better understanding of the flow characteristics in the toroid wheel. Results of these analyses will be included in the manuscript. This study will improve the understanding of the behavior of high-concentration slurry inside the toroid wear tester, which will ultimately allow for a quantitative comparison between wear rates measured in a toroid wear tester and those found in operating slurry pipelines.

[1] Cooke, R., Johnson, G. and Goosen, P. Laboratory Apparatus for Evaluating Slurry Pipeline Wear. *Economics of Wear Materials*, Calgary AB: Southern Alberta Institute of Technology, (2000).

[2] Fotty, B., Krantz, M., Been, J. and Wolodko, J. Development of a pilot-scale facility for evaluating wear in slurry pipeline systems. *18th International Conference on Hydrotransport*, BHR Group (2010), 431-443.

[3] Sadighian, A. and Sanders, R. S. Investigating key parameters affecting slurry pipeline erosion. *2013 Rio Pipeline Conference*, Rio de Janeiro, September 24-26, (2013).

[4] ANSYS CFX-Solver Modeling Guide Release 12.0. ANSYS, Inc., (2009).

CFD Investigation and Experimental Validation on the Effects of Viscosity for High Speed Liquid Jets Emitted from Needle Free Jet Injectors

Rocco Portaro, Haruka Nakayama and Hoi Dick Ng[†]

*Department of Mechanical and Industrial Engineering, Concordia University
Montréal, Québec H3G 1M8 Canada
†E-mail: hoing@encs.concordia.ca*

Extended Abstract

Hypodermic needles have long been the conventional means of delivering medication within the medical profession. However, studies suggest that needle-free liquid jet injectors can effectively deliver medication to the different layers of skin without the drawbacks of conventional hypodermic needles. In fact, this technology can further aid in implementing new types of drug therapy [1, 2]. Typical jet injectors deliver medication by compressing a column of fluid containing the medication through a nozzle. The fluid exits as a high-speed small diameter liquid jet of sufficient pressure to penetrate the skin and deliver the appropriate amount of medication. Typical needle-free injectors generally produce jets with exit velocities greater than 100 m/s and diameters ranging from 100 to 360 μm with an initial pressure change of 275 bar within 0.5 ms. The injection volume ranges from 0.1 to 1 ml with a skin penetration depth of up to 10 mm. Figure 1 illustrates the process of liquid jet injection into a ballistic gel and to air from an air-powered needle-free injector prototype [3, 4].

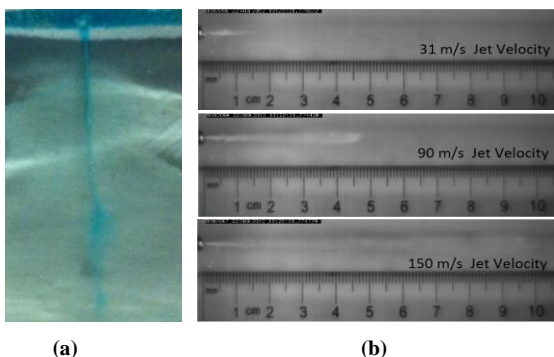


Figure 1. Photographs showing a) the jet penetration into a ballistic gel; and b) the liquid jet exiting the injector nozzle

In order to alleviate the problems with the early use of liquid jet injectors such as pain, bruising, hematomas, incomplete delivery of medication, excessive penetration and cross contamination [5, 6], much research has been conducted on improving their performance by analyzing the fluid mechanics of jet injection. Using Computational Fluid

Dynamics (CFD), this paper addresses the effect of varying drug viscosity on injector performance. These results are then validated by utilizing a custom built servo tube liquid jet injector, which is programmed to produce the same piston velocity profile as in the numerical simulations.

In this study, simulations of the high-speed liquid jet generation process from the needle-free injector are carried out using the OpenFOAM® CFD software package [7]. These simulations utilize a CFD model developed by Nakayama *et al.* [8] specifically for analyzing liquid jet injectors. The physical dimensions and the axisymmetric simulation domain are equivalent to those of the experimental prototype [3, 4] as shown in Fig. 2. The dynamic behavior of the liquid jet is approximated using a multi-phase compressible, isothermal immiscible fluids LES solver and the VOF method for the interface capturing, available in OpenFOAM®. The liquid jet is generated by dynamic mesh techniques, i.e., the liquid retained in the injector chamber is impacted by the moving boundary simulated the injector piston displacement driven by the actuator. In order to begin the computation a velocity profile which prescribes the dynamic mesh motion is necessary. This is accomplished by using model created by Portaro and Ng [3] for air powered injectors. The same mesh motion is then used in the experimental servo tube actuator in order to verify the numerical result. A typical velocity profile representative of the experimental result is given in Fig. 3

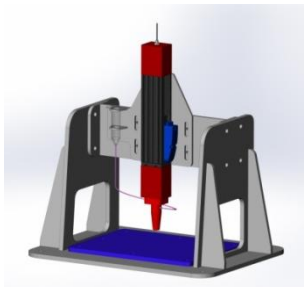


Figure 2. A detailed rendering of servo tube liquid jet injector

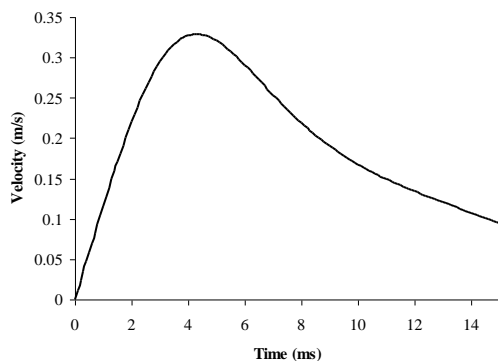


Figure 3. Velocity profile of the moving piston boundary.

Figure 4 illustrates a sample result comparing a jet with a viscosity of 0.87 cP to that of 87 cP computed with a fine mesh (i.e., with the smallest level $\Delta x = 0.01\text{mm}$ and $\Delta r = 2.5 \times 10^{-3}\text{ mm}$). From these phase fraction plots, it is possible to quantify the dispersion and the size of the jet emerging which aid in illustrating the effect of differing viscosity. Moreover the numerical studies also provide results which illustrate the behavior of the jet stagnation pressure. These traces illustrated in Fig. 5 are compared to traces obtained with the aforementioned experimental injector. Glycerol is used in order to mimic different drug viscosities throughout the course of the experiment. In practice, the increase in viscosity should aid in decreasing the size of the jet tip, decreasing jet divergence at the exit of the nozzle as well as improving delivery efficiency. The goal of this work is to determine the optimal injection viscosity that maximizes injection pressure while displaying the least amount of divergence. The experimentally validated CFD results will then make it possible to conduct further analysis between fluid properties and physical injector parameters.

References

- [1] Mitragotri S (2006) Current status and future prospects of needle free liquid jet injectors. *Nature Reviews. Drug Discovery* 5:543-548.
- [2] Mitragotri S (2005) Immunization without needles. *Nature Reviews. Immunology* 5:905-917.
- [3] Portaro R, Ng HD (2013) Experimental analysis of the performance of an air-powered needle-free liquid jet injector. Submitted to the 35th Annual Int. Conf. IEEE Eng. Medicine and Biology Society, Osaka, Japan, July 3-7, 2013.
- [4] Portaro R, Gunter AL, Ng HD (2012) Analysis of high speed liquid jets emitted from needle free jet injectors. 65th Annual Meeting of the APS Division of Fluid Dynamics, in San Diego, CA, USA, Nov. 18-20, 2012
- [5] Wijsmuller G, Snider Jr. DE (1975) Skin testing: A comparison of the jet injector with the mantoux method. *Am Rev Respir Dis.* 112:789-798.

[6] Schneider U, Birnbacher R, Schober E (1994) Painfulness of needle and jet injection in children with diabetes mellitus. *Eur. J. Pediatr.* 153:409-410.

[7] OpenCFD, OpenFOAM, The Open Source CFD Toolbox. User Guide, OpenCFD Ltd. 2009.

[8] Nakayama, H., Portaro, R. and Ng, H.D. (2013) CFD investigation of high speed liquid jets emitted from needle free jet injectors. Proceeding of the 21st Annual Conference of the CFD Society of Canada, Sherbrooke, Quebec May 6-9, 2013

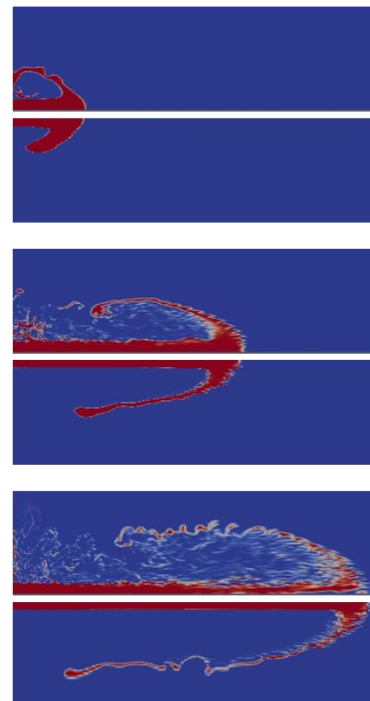


Figure 4. CFD results showing the time evolution of 0.87 cP jet (top) and 87 cP jet (bottom)

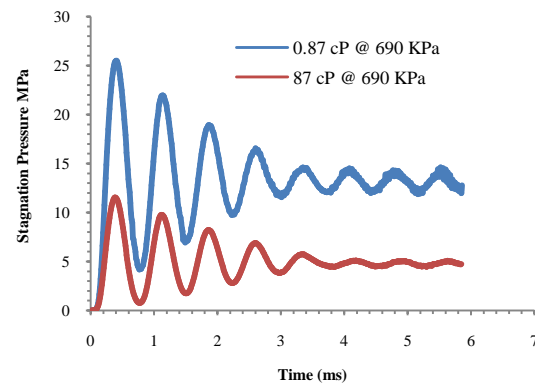


Figure 5. Numerical results illustrating injection pressure profiles for two different viscosities

CFD Investigation of a Horizontal Axis Open-Center Tidal Turbine

Amy-Lee Gunter[†], Rocco Portaro, Lyes Kadem and Hoi Dick Ng

Department of Mechanical and Industrial Engineering, Concordia University

Montréal, Québec H3G 1M8 Canada

[†]E-mail: a.k.gunter@gmail.com

Extended Abstract

Tidal energy is one of the most promising emerging renewable energy sources, which still remains largely untapped. The use of tidal turbines to convert the kinetic energy of tidal streams into electricity has been rapidly increasing as the search for new sources of renewable energy intensifies [1]. There are currently several different tidal turbine designs in large scale operation, however unlike the wind turbine industry, tidal energy is not yet a mature technology, and the optimal design is still very much a topic of intense research and development. The conditions under which a tidal turbine must operate are very unique, and must be negotiated while minimizing disruption to the surrounding marine ecosystem. The combination of efficient energy harvest technology with a low environmental impact in the design of a new type of tidal turbine is the primary focus of this research.

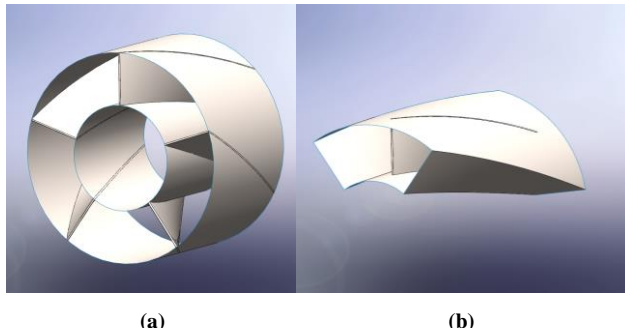


Figure 1. CAD models of a) the full turbine geometry; and b) the blade section used for CFD simulations.

Operating much like a wind turbine underwater, the tidal turbine must be able to withstand the force of a very dense and energetic flow, which reverses flow direction and height roughly twice a day, and may carry with it a large amount of debris and sediment. [2]. The current turbine designs meet this set of requirements by reinforcing the blade structure, and allowing the attack angle of the blades to be varied according to the flow direction [3]. This type of design is not optimal for minimizing destructive turbulence in the wake, and poses a threat to marine life in the form of rotating blades [4]. Using Computational Fluid Dynamics

(CFD), this paper investigates the performance of a new type of tidal turbine, which aims to address the issue of wake turbulence and blade structure integrity through the use of an open-center design. Assessment of the new design is based on the torque generation potential, as well as the amount of turbulence generated in the wake.

In this study, simulations of the horizontal axis open-center tidal turbine (HAOCTT), operating under steady flow conditions, are carried out using the ANSYS FLUENT software package. The full physical model of the new concept, shown in Fig. 1, is developed using the Solidworks CAD software, where the geometry can be parametrically designed and easily optimized. Given the axisymmetric nature of the design, the full model can be divided into five sections, each containing one blade, as shown in Fig. 1. This blade section, as well as the inlet and wake regions, is meshed using the ANSYS ICEM software package. Using periodic boundary conditions on both section faces of all three mesh domains allows for the entire flow field to be simulated at one fifth of the calculation cost. Dividing an axisymmetric flow domain in this manner is common practice in turbomachinery CFD simulations [5], where the size and complexity of the flow domain would otherwise be prohibitively calculation heavy.

In order to perform an initial analysis of the untested blade geometry and configurations, the first simulations are conducted on a stationary turbine placed in a steady flow at several stream velocities between 1.0 to 3.0 m/s. During these simulations, the flow enters the inlet region with a constant velocity normal to the boundary and turbulence intensity of 5%. The flow then enters and exits the turbine region across interfaces between the mesh zones where the nodes are perfectly matched. A $k - \omega$ SST turbulence model is used to solve for the developing flow around the blade and within the wake region, producing a pressure and velocity profile for each case, as shown in Fig. 2 and Fig. 3. The low pressure zone appearing on the back side, and high pressure zone on the front side of the blade in Fig. 3 indicate that the blade experiences a torque moment of force. Using this pressure differential across the blade surface, the magnitude of the force can be calculated, and translated into

power generation potential. These results are used to develop several different turbine models featuring various blade geometries and configurations. The most promising designs are then subjected to a rotational simulation.

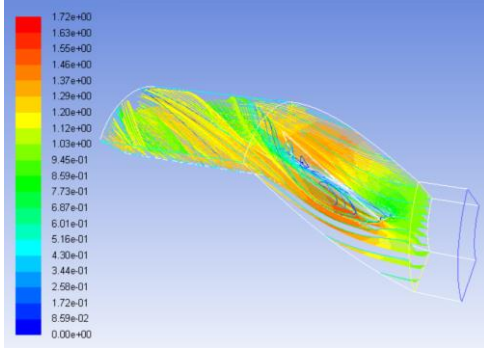


Figure 2. Velocity profile of the static turbine blade section in a 1m/s flow.

In order to model the behavior of the flow as it experiences a rotating turbine, the mesh containing the blade section is set to rotate about the turbine axis, as the inlet and wake regions are held stationary. The system is allowed to reach steady state after several full revolutions of the blade mesh, at which point the flow behavior can be analyzed. For all rotational simulations, a $k - \omega$ SST turbulence model is again used to solve for the developing flow. The time step size and number per iteration are calculated separately for each case, such that one time step corresponds to 1.8° of rotation, requiring 200 time steps per full rotation.

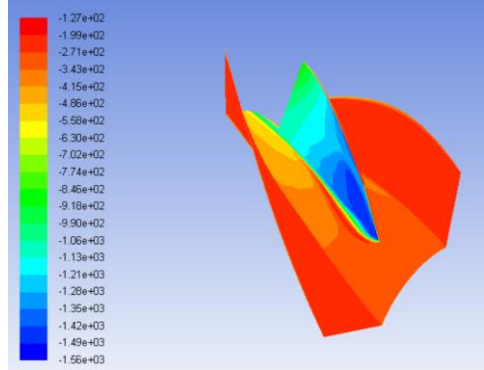


Figure 2. Pressure profile of the static turbine blade section in a 1m/s flow.

A sample result illustrating the pressure profile at steady state for a rotation speed of 15 rpm is shown in Fig 3. The model of the turbine blade section has been scaled down at a ratio of 1:25, such that the outer diameter of the shroud is 0.6m, and the inner diameter of the hub is 0.3m. This results in a blade span of 0.15m, with a length of 0.4m. The mesh generated for the case shown in Fig 3 consisted of 561,000 hexahedral cells, with a minimum cell volume of $2.091 \times 10^{-9} \text{ m}^3$. From the pressure contour plots generated during

the rotational simulations, it is possible to identify the various blade characteristics which give rise to the maximum pressure differential across the blade. In addition, the turbulence in the wake area associated with each model can be studied, providing a means to assess the impact on the marine environment. The on-going work of this research involves assessment of the variations of the HAOCTT model, in an effort to produce the most efficient and environmentally friendly design.

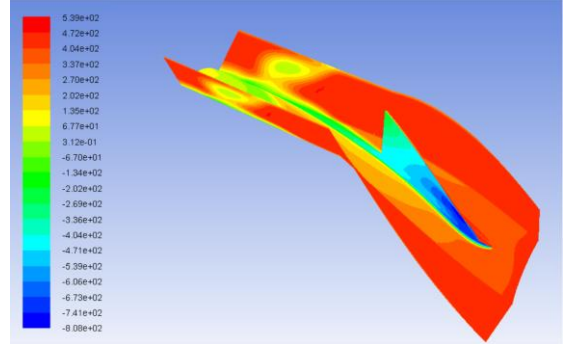


Figure 4. Pressure profile turbine blade section rotating at 15 rpm in a 1m/s flow.

References

- [1] Rourke, F. O., Boyle, F., Reynolds, A. (2010) Tidal Energy Update 2009. *Applied Energy*, Vol. 87:398-409.
- [2] Liu, P., Vietch, B. (2012) Design and optimization for strength and integrity of tidal turbine rotor blades. *Energy*, Vol. 46: 393-404.
- [3] Dimitri, V. V., Chernin, L., Yurchenko, D. V. (2013) Reliability analysis of rotor blades of tidal stream turbines. *Reliability Engineering and System Safety*, Vol. 121:26-33.
- [4] Tedds, S. C., Owen, I., Poole, R. J. (2013) Near-wake characteristics of a model horizontal axis tidal stream turbine. *Renewable Energy*, Vol. 63:222-235.
- [5] Premkumar, M., Chatterjee, D. (2015) Computational analysis of flow over a cascade of S-shaped hydrofoil of fully reversible pump-turbine used in extracting tidal energy. *Renewable Energy*, Vol. 77:240-249.

CFD Modeling and Validation of a Multipass Compact Heat Exchanger

Mohammed Ismail¹, Shahram Fotowat², and Amir Fartaj³

¹*Department of Mechanical Automotive & Materials Engineering, University of Windsor, Windsor, N9B3P4, Ontario, Canada*

²*Department of Mechanical, Automotive & Materials Engineering, University of Windsor, Windsor, N9B3P4, Ontario, Canada*

³*Department of Mechanical, Automotive & Materials Engineering, University of Windsor, Windsor, N9B3P4, Ontario, Canada*

Email: *ismailf@uwindsor.ca*

ABSTRACT

Heat transfer and flow characteristics of water are numerically studied through a compact heat exchanger. In order to satisfy the cooling demand for applications where space is limited, a multipass minichannel heat exchanger (MICHX) is used in this work. A synthesis of modeling and simulation of the MICHX is presented systematically. The heat exchanger used in this study consists of three loops. Each loop contains five slabs and four serpentines with 68 circular channels of 1mm diameter inside the serpentine slabs. Cold water is heated using hot air flow in a cross flow orientation. Air-side Reynolds number of 1380 is kept constant while water Reynolds number are varied from 110 to 160. The constant inlet temperatures of air and water are maintained 38°C and 9°C respectively. The results from numerical simulations are compared with experimental measured data for the same geometrical and operating conditions. The numerical results showed a good agreement with the experimental results.

1. INTRODUCTION

One of the critical issues of the current century is the energy conservation, transformation, and seek for development of alternative energy sources [1]. Researchers and scientists are continuously trying to resolve this vital issue effectively and efficiently. In the past decade, the renaissance in mini/micro scale thermal transport investigation has been taken place in its earnest. The revolutionary study of using a

microchannel heat sink for electronic cooling was first endeavored by Tuckerman and Pease [2]. Increased area density of the channels in MICHX creates a new level of transport method that results to a significant size reduction in applied devices. Heat exchanger with a high heat transfer surface area is needed where size is limited [3].

2. GEOMETRY MODELLING

The model and specifications of MICHX used in the numerical simulation is shown in Fig. 1 and Table 1 respectively.

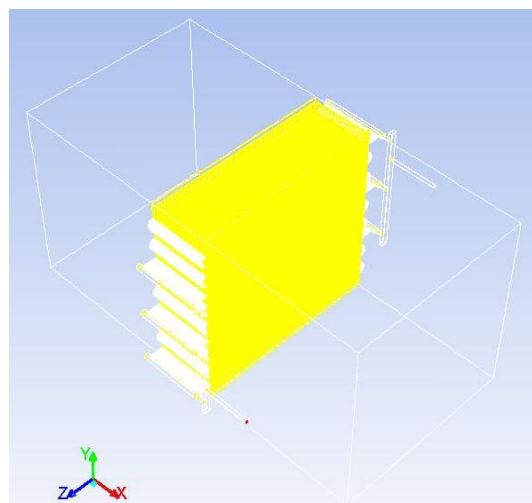


Figure 1. Computational domain of the MICHX used in simulations

Parameters	Specifications
Number of channels in a slab	68
Port or channel diameter	1mm
Port-to-port distance	1.463mm
Slab length in x-direction	100mm
Slab thickness in y-direction	2mm
Slab width in z-direction	304mm
Number of flow circuits	3
Number of flow passes	15
Fin density	12
Fin height	16mm
Fin thickness	0.1mm
Inlet & outlet header tube diameter	4.76mm

Table 1. Specifications of the MICHX test specimen

GAMBIT 2.4.6 software is used to create geometry for the MICHX and then generate mesh. The computational consists of a MICHX and a test chamber. The physical model of the MICHX is very complex. It consists of 2 headers, 6 manifolds, 15 slabs, 12 serpentine bends, 204 minichannels, and 2256 fins. Due to the complexity of the model, it is impossible to generate a single structured mesh for the whole domain. Therefore, the model is divided into several sub-sections. Structured hexahedral mesh is generated for the test chamber and fins, while unstructured tetrahedral and wedge mesh is generated for the rest of the model.

3. NUMERICAL METHOD

A three-dimensional double precision (3DDP) pressure-based low Reynolds number turbulence model is used to perform the numerical simulation. ANSYS FLUENT 13.0 is used to solve the governing equations for the steady incompressible heat transfer and fluid flow process. SIMPLE, least squares cell based, standard pressure, and second order upwind discretization solution methods are applied for all simulations.

4. RESULTS AND DISCUSSIONS

Verification of the numerical results is performed by checking %error in mass balance (MB) and heat balance (HB); these are shown in Fig. 2. The maximum absolute error in MB and HB is found 1.13% and 1.21% respectively, which are acceptable, and one can rely on the accuracy and consistency of the results.

In order to validate the model, the numerical results of water and air outlet temperatures and heat transfer rate are compared with experimental results. These

are shown in Fig. 3. The numerical results showed a good agreement with experimental measured data.

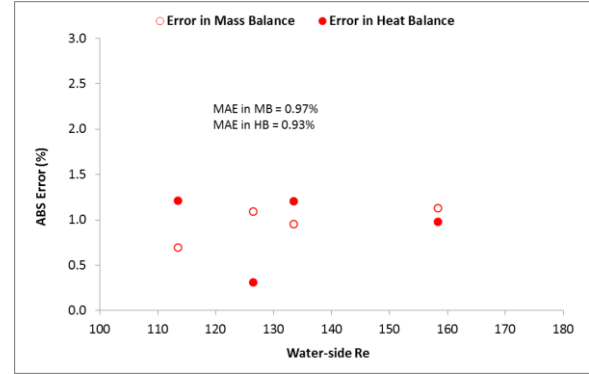


Figure 2. Absolute error in mass and heat balance

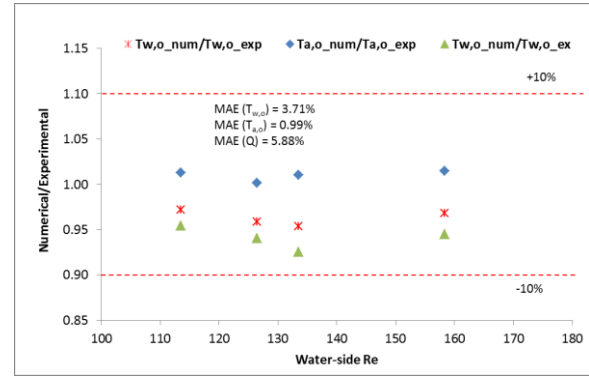


Figure 3. Comparison of numerical predictions and experimental measured data

ACKNOWLEDGEMENTS

Authors would like to thank the Natural Sciences and Engineering Research Council of Canada (NSERC) and the University of Windsor, Canada for financial support for the research.

REFERENCES

- [1] T. Dixit and I. Ghoseh. Review of micro- and mini-channel heat sinks and heat exchangers. *Renewable and Sustainable Energy Reviews*, 41: 1298–1311, 2015.
- [2] D. B. Tuckerman and R. F. W. Pease. High-performance heat sinking for VLSI. *IEEE Electron Device Letters*, 2(5): 126–129, 1981.
- [3] S.G. Kandlikar, S. Colin, S. Peles et al. Heat transfer in microchannels – 2012 status and research needs. *Journal of Heat Transfer*, 135, 091001-1–091001-18, 2013.

CFD Modelling of Mixing and Segregation of Particles in Fluidized Bed: Eulerian - Lagrangian Approach

M. Bayati¹ and C. F. Lange¹

¹*Department of Mechanical Engineering, University of Alberta, Edmonton, AB, Canada, T6G 2G8*

Email: *carlos.lange@ualberta.ca*

ABSTRACT

This article presents simulations of the segregation process in a fluidized bed using the Eulerian-Lagrangian approach. The CFDEM® Coupling code developed by DCS Computing GmbH is used as the simulation software. Particles of different size and density are fluidized in a 2-D bed to investigate the effect of the inlet velocity. Values of mean and variance of the particles' height versus time will be used for validation. Also the mixing index will be calculated to describe the segregation quality.

1 INTRODUCTION

One of the applications of fluidized beds is the segregation or mixing of particles of different density or size. The segregation process is used in different areas from pharmaceutical to oil sand industries. While the separation of solid particles is desired in a pharmaceutical process, a good mixture is required in a combustion bed boiler. Although there has been intensive research on the fluidized bed, the segregation process is still an open topic for investigation. The process is affected by several factors, such as size ratio, density ratio, properties of particles and operating conditions of the bed. Hydrodynamics of fluidized beds has been widely studied by the Eulerian-Eulerian, also known as two fluid, model. However, the lack of knowledge of particles' motions and rotations, complexity of defining size distribution and implementation of empirical models to simulate the dispersed phase reduces their level of accuracy.

This project studies the hydrodynamics of segregation process in fluidized beds and the effect of the inlet velocity on the mixing index by using Eulerian-Lagrangian approach.

2 SIMULATION METHOD

The Eulerian-Lagrangian approach is used to simulate the segregation process. The method is also known as Discrete Element Method (DEM) in which the dispersed phase is treated as particles, which are tracked. Particle-particle and particle-wall interactions are modelled by using the soft sphere model, which is based on the spring-dash model proposed by Cundall and Strack[1] and Tsuji et. al[3].

The continuous phase is simulated by solving the continuity equations and Navier-Stokes equations. The momentum exchange between the dispersed phase and the continuous phase is considered by the drag force applied to particles. Drag coefficients have been developed to model the momentum exchange of particles and gas in a dense flow.

CFDEM® coupling code developed by DCS Computing GmbH is used to simulate the segregation process. The continuous phase is simulated by the open source CFD solver, OpenFOAM® while collisions of particles are simulated and their trajectories are tracked by the DEM engine, LIGGGHTS®. The presence of particles in the flow is coupled by CFDEM® coupling. Particles are injected into the bed from the top while there is no gas imposed to the inlet. Particles will be settled after 0.5s and a compact bed will be formed. The gas is then imposed to the inlet and the fluidization process begins. Design Of Experiments (DOE) techniques will be used to define simulation parameters and to study the effect of main operating parameters and their mutual interactions on the mixing index. The model will be developed based on relevant parameters and their interactions.

3 RESULTS AND DISCUSSION

The segregation process in a fluidized bed has been studied in this report. Particles of different density and size have been considered and the effect of the inlet

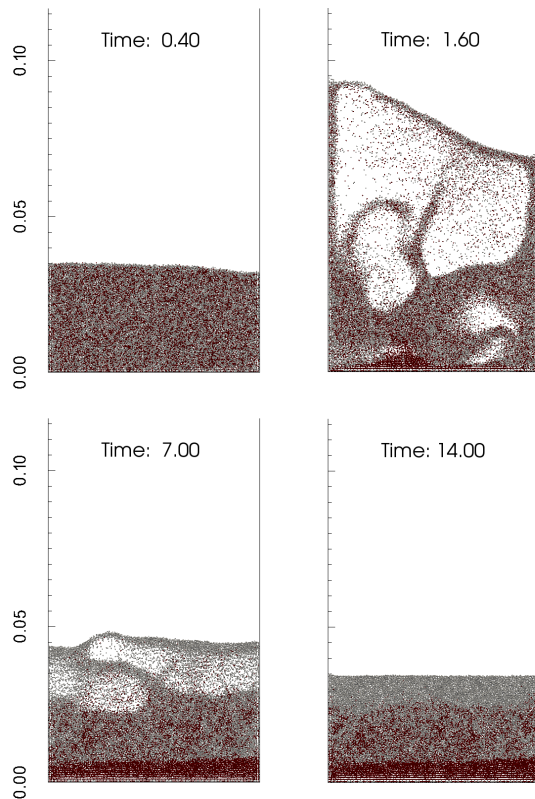


Figure 1: The initial stage of a well mixed bed and segregation process of particles of same size and different density. $\rho = 1000\text{kg}/\text{m}^3$ (light grey), $\rho = 1600\text{kg}/\text{m}^3$ (red)

velocity on the Lacey mixing index has been studied. Plots of mean height of particles and the standard deviation have been produced. Using DOE techniques, a model to describe the behaviour of the mixing and segregation will be produced. Results will be compared to numerical study of Feng et. al[2].

Figure 1 shows the initial well mixed packed bed at time 0.4 s and formation of bubbles at time 1.6 s and the segregation process at time 7 s and settlement of particles at time 14 s.

ACKNOWLEDGEMENTS

The authors are grateful to CryoEx Oil for their support.

REFERENCES

- [1] P. A. Cundall and O. D. Strack. A discrete numerical model for granular assemblies. *Geotechnique*, 29(1):47–65, 1979.

[2] Y. Feng and A. Yu. Microdynamic modelling and analysis of the mixing and segregation of binary mixtures of particles in gas fluidization. *Chemical Engineering Science*, 62(1):256–268, 2007.

[3] Y. Tsuji, T. Kawaguchi, and T. Tanaka. Discrete particle simulation of two-dimensional fluidized bed. *Powder technology*, 77(1):79–87, 1993.

CFD Modelling of the Dehydrogenation of Alkanes to Alkenes in a Fixed Bed Reactor

Tarek J. Jamaleddine^{1*}, Mohanrao Rampure² and Ramsey Bunama¹

¹ SABIC Technology and Innovation Center, Riyadh, Saudi Arabia, jamaleddine@sabic.com

² SABIC Technology and Innovation Center, Bangalore, India, rampuremr@sabic.com

¹ SABIC Technology and Innovation Center, Riyadh, Saudi Arabia, bunamar@sabic.com

Email: jamaleddine@sabic.com

ABSTRACT

The catalytic dehydrogenation reaction of alkanes to alkenes is simulated in a heterogenous fixed bed reactor (FBR). The porous medium method in ANSYS Fluent combined with the reaction model capability was utilized to predict the flow behavior and species transport in a bed of spherical particles. Physical and material properties of a dehydrogenating catalyst of Chromium Oxide (Cr_2O_3) on Aluminum Oxide Support (Al_2O_3) were employed in the model. Several reaction models were implemented using a customized User-defined Function (UDF) subroutine. Simulation results were validated against literature data for a similar process. Good agreement was observed for the conversion of alkanes to alkenes within acceptable accuracy. It is concluded that the power-law model showed the least fit for the feed conversion and product selectivity compared to the other studied reaction models. Ongoing work to implement this model in a commercial-scale reactor will be reported in a future publication.

1. INTRODUCTION

The catalytic dehydrogenation process is heavily used in the chemical industry to convert Alkanes to Alkenes. The process is performed in a fixed bed reactor at sub-atmospheric pressure conditions and temperature ranging from 540 – 670 °C. In these reactors, reaction takes place on the surface of catalyst pellets placed randomly inside the reactor volume. Chromium Oxide (Cr_2O_3) based catalyst is generally used and is supported on Aluminum Oxide (Al_2O_3) metal. Side reactions and by-product formation are some of the many challenges characterizing this process. It is thus beneficial to have a profound

understanding of the flow characteristics and reaction mechanisms in order to gain more insight into improving the system profitability.

Many researchers in the field have studied the dehydrogenation process. The most relevant to this work is a paper by Airaksinen et al. [1] who derived several kinetic models from different reaction mechanisms and tested the suitability of the models in describing the rate of dehydrogenation reaction. Al-Ghamdi et al. [2] presented a paper showing actual data for one of the largest dehydrogenation unit for MTBE production. Sanfilippo [3] discussed the current technology for the production of MTBE from isobutylene and methanol, and shed light into the type of catalyst that is widely used in this process. Chen et al. [4] proposed a kinetic model for the dehydrogenation reaction of syngas to form carbon monoxide (CO). The authors further developed a CFD model that described the flow behavior and dehydrogenation reaction in a FBR. In their model, they followed a one-way forward reaction and showed that the space velocity had less effect on the reaction outcome, whereas inlet temperature had a significant impact on the generation of hot spots in the bed.

This paper presents a 3D CFD model for the dehydrogenation reaction of isobutane to isobutylene. Model predictions for conversion and selectivity were validated against values presented in Al-Ghamdi et al. [2]. Forward and reverse reaction rates were considered in the model to accurately capture the reaction mechanisms. User-defined subroutines were used to enhance ANSYS Fluent capability and to reflect the actual reaction kinetics.

*To whom correspondence should be addressed. E-mail address: jamaleddine@sabic.com.

2. CFD MODEL DEVELOPMENT

Figure 1 shows a schematic of the geometry for CFD model. Due to symmetry, only one-fourth portion of the actual model was used in the simulation. The catalyst was assumed to be a continuous porous medium with additional source terms in the governing equations to reflect flow resistances and reaction mechanisms. The model was discretized with hexahedral elements. Finer mesh was adopted in the proximity of the reactor wall to adequately resolve the boundary layer profile in that region.

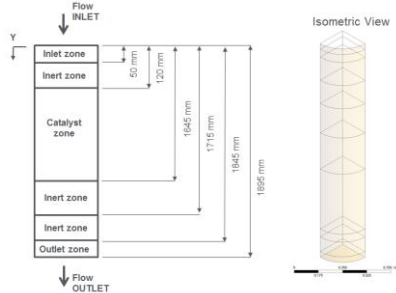


Figure 1. Schematic of the CFD model geometry

The governing equations were solved for a compressible gaseous flow using the pressure-based solver in ANSYS Fluent v16. Mixture properties were derived based on the ideal gas mixing law (Table 1). The porous regions of the reactor were treated as laminar, whereas $k-\epsilon$ turbulent model was assumed elsewhere. It took nearly 20 minutes of clock time for a compressible steady state solution to converge with residual RMS values below 10^{-4} for all equations except for the energy equation with values below 10^{-6} .

Description	Value
Thermodynamic and physical properties	
Gas mixture	Ideal gas mixing law
C_p,g (kJ/kmol.K)	Ideal gas mixing law
ρ_g (kg/m ³)	Ideal gas mixing law
μ_g (Pa.s)	Ideal gas mixing law
K_g (W/m.K)	Ideal gas mixing law
D_{lm} (m ² /s)	2.88×10^{-5}
Solid phase	
ρ_s (kg/m ³)	1520
d_p (m)	1.98×10^{-2}
Porosity, ϕ	0.36
Other model parameters	
Space velocity (hr ⁻¹)	495.068
Feed temperature (K)	853.15

Table 1. Model parameters

3. RESULTS

As can be seen in Figure 2, the mass fraction of isobutane fell sharply in the early stages of reaction with an increase in isobutylene concentration. This indicates that isobutane is consumed to generate isobutylene. It can also be concluded that slower

reaction rates occurred near the end of the catalyst region, an indication of the presence of a redundant catalyst region. These results also confirm the success of the CFD model in capturing the reaction rates.

FRANCESCA MODEL

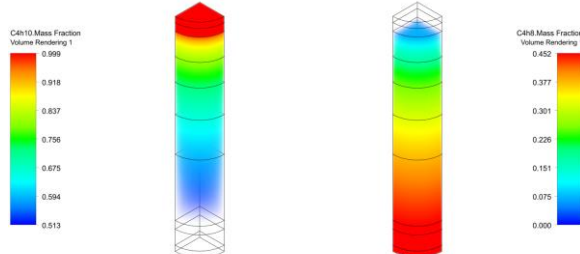


Figure 2. Mass fraction of reaction components

Figure 3 shows a comparison between the theoretical predictions and actual data. It can be drawn that Happel et al. model (presented in [1]) showed the closest fit for the isobutane conversion to isobutylene within an error of 5%. Francesca's model (also presented in [1]) however showed the closest fit for the product selectivity and yield within an error of 2% and 6%, respectively. Finally, the power-law model underestimated the conversion rate by nearly 55%.

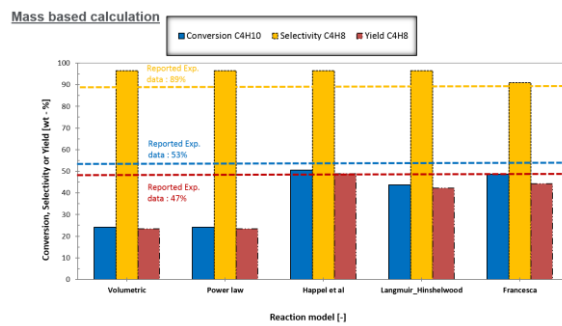


Figure 3. Theoretical predictions vs actual data

REFERENCES

- [1] S.M.K. Airaksinen, M.E. Harlin and A. Krause. Kinetic modelling of dehydrogenation of isobutane on chromia/alumina catalyst. *Ind. Eng. Chem. Res.*, 41:5619-5626, 2002.
- [2] A.A. Al-Ghamdi, A.M. Al-Bassam and J.L. Draus. Annual Meeting of the National Petroleum Refiners Association, March 20-22, 1994, San Antonio, TX, USA, paper AM-94-28.
- [3] D. Sanfilippo. Dehydrogenations in fluidized bed: Catalysis and reactor engineering. *Catalysis Today*, 178:142-150, 2011.
- [4] X. Chen, J. Dai and Z. Luo. CFD modelling using heterogeneous reaction kinetics for catalytic dehydrogenation syngas reactions in a fixed-bed reactor. *Particuology*, 11:703-714, 2013.

CFD Study of a Savonius Wind Turbine on a Rooftop

Felix Schily¹ and Marius Paraschivoiu²

Department of Mechanical and Industrial Engineering, Concordia University, 1455 De Maisonneuve Blvd.

W., Montreal, Quebec, Canada, H3G 1M8

¹Email: felixschily@gmx.de

²Email: marius.paraschivoiu@concordia.ca

ABSTRACT

Savonius turbines have the best performance at low wind speeds. Placing a turbine on the roof of a building is sounds ideal for raising the turbine at a higher elevation in the atmospheric boundary layer, but also by benefitting from the accelerated flow at the corner of the building. Nevertheless the ideal turbine and the ideal position are difficult to identify. To this end CFD simulations are employed to perform a parametric study. The turbine is mounted near the windward edge of the roof of a building. Varied parameters are the position of the turbine, blade shape, blade number and tip speed ratio. The objective is to optimize the parameters mentioned, yielding for a maximum power coefficient. As reference case, slow wind, directly facing one side of the building, is chosen. A spatial and temporal convergence study will also be performed for our three dimensional configuration.

1. INTRODUCTION

Currently, multiple studies on vertical axis wind turbines are performed in our research group and one of the main conclusion is that 2-dimensional (2D) simulations are overestimating the coefficient of power. Therefore 3-dimensional (3D) simulations are deemed essential to accurately predict this coefficient. In this paper, the 3D simulation of a Savonius turbine will be analyzed in terms of convergence requirements and results will discussed.

As a Savonius turbine is drag-based, the efficiency (i.e. power output per wind-facing area at a given wind speed) is expected to be lower than the one of lift-based wind turbines. However, a drag-based turbine also operates at a considerably lower speed than a lift-based turbine and is less sensitive regarding the shape of its blades (cheaper production, also insensitive regarding dirt on blades), which are important advantages in the projected operational scenario. The design challenge is to compensate the lack of power by positioning the turbine on the

windward roof edge, so the wind speed-up induced by the building can be used as well, as the returning blade is shielded by the edge. In [1] a standard two bladed Savonius turbine was positioned on the top of the roof but with no significant gains compared to a placement in an unperturbed flow. Here we investigate a seven cup turbine that looks more promising.

In advance of this study, the problem was investigated by a 2D CFD-study. This neglects multiple 3D effects, such as the flow next to the turbine and the building. Accordingly, the quantitative results of this study were strongly over-predicting. Qualitatively, the 2D-analysis indicated, that the most favorable design regarding the power coefficient, would be an unshrouded turbine positioned on the windward building edge.

2. MODEL PROBLEM

Consequently, the objective of the present study is, to further investigate the case of a multi-blade Savonius turbine near the windward roof edge. The focus of this investigation is on the turbine position, as well as blade shape and number. For every geometry permutation, the optimum rotational speed is determined. Ultimately a prediction of the power coefficient of the optimum design is intended, so a comparison with studies on other designs investigated currently is possible.

To be able to perform a parameter variation, several simplifications and assumptions were made. Regarding the geometry of the calculation domain, these comprise the following: The building is of cubic shape, with a height of 30.48 m. Except from the turbine, there are no other devices on the roof. The building is standing isolated, i.e. the effects of neighbor buildings are not considered. Although this assumption cannot be justified, considering the intended operational scenario, there is no way of generalizing the building's neighborhood. In a later study, this assumption might be dropped. The

building is exposed to a height-dependent (h) wind velocity profile v :

$$v = v_{ref} \left(\frac{h}{h_{ref}} \right)^{0.31}$$

Where $h_{ref} = 30.48\text{ m}$ is the height of the building and $v_{ref} = 3.89\text{ m/s}$ is the velocity at h_{ref} . The velocity is normal to one side of building; other wind velocities and angles may be investigated in later studies. The reference velocity $v_{ref} = 3.89\text{ m/s}$ was deliberately chosen close to the lower limit of wind turbine operation, as low wind speeds are considered an important operational condition in urban areas.

3. GENERAL CONSIDERATIONS REGARDING THE CALCULATION SET-UP

As the outline of the project comprises a parametric study, the general strategy of the investigation will be, to find a mesh density and time step that is within the convergence range of Richardson extrapolation [2]. Before performing the parametric study, a mesh refinement study will be conducted, to (1) determine a grid convergence index (GCI, see [2]) for the initial turbine configuration, which is assumed to remain approximately constant throughout the whole parametric study, and (2) derive an approximation of the true performance of the initial design.

The generation of the mesh requires special caution due to the fact, that unlike most exterior aerodynamic problems, this problem is dependent from three length scales of different order of magnitude (domain size, building size, turbine size), instead of two (domain and object in the flow). However, in order to keep the calculation time to a minimum for the parameter study, maximum element number is limited. For the same reason, the problem is calculated with unsteady Reynolds-averaged-Navier-Stokes equations (URANS) and a k- ϵ turbulence model [3]. Although favorable due to the flow conditions in the turbine, e.g. transient interaction of the blades' wakes with the other blades, with respect to limited computation resources, large-eddy simulation (LES) cannot be used in a parametric study. The calculation is conducted under the assumption of incompressible flow, as there are no Mach numbers over 0.1 or other causes for significant differences in the density of the air to be expected.

As mentioned before, the relevant criterion for parameter optimization is the power coefficient of the wind turbine. Generally the power coefficient C_P is defined as:

$$C_P = \frac{P}{\frac{1}{2} \rho A v_{ref}^3}$$

Here, ρ is the density of the air and A is the area of the wind turbine when projected in flow direction. $P = M \cdot \omega$ is the power generated by the turbine, with ω being the angular velocity of the turbine and M the moment of the turbine, derived from the pressure and shear stress distribution on the blades.

4. SPATIAL AND TEMPORAL CONVERGENCE STUDY

This section will describe the temporal and spatial convergence study done regarding our quantity of interest which is the coefficient of power.

5. INITIAL CONDITIONS OF THE PARAMETRIC STUDY

The initial design of the turbine features a seven-blade configuration with semi-cylindrical cups as blades. The sides of the turbine are capped. This design was arbitrarily chosen, as the 2-dimensional analysis could not take side shrouding into account, and thus does not provide any results on that aspect. However, capped sides are favorable considering the mechanical stability of the design. The turbine has a diameter and width of 2.44 m each. The cups have an inner diameter of 0.254 m and a thickness 13.5 mm.

Initially, the turbine is centered regarding the width of the building. The turbine axis is parallel to the roof's windward edge and positioned 1.4 m over the edge.

REFERENCES

- [1] P. Larin, C. Aygun, M. Paraschivoiu. CFD based Analysis of Savonius Turbine in Synergy with Flow on top of a Building. *EIC Climate Change Technology Conference (CCTC) 2015*, Paper Number 1570050033, 2015
- [2] P.J. Roache. Perspective: A method for uniform reporting of grid refinement studies. *Journal of Fluids Engineering*, Vol. 116, No. 3: 405–413, 1994
- [3] ANSYS Inc. ANSYS FLUENT Theory Guide, Release 14.0: 49-51, 2011

Comparison of Two High-Order Solution-Adaptive Schemes: Finite Volume and Discontinuous Galerkin

Pradeep Jha, Marcin Chrst, and Catherine Mavriplis

*Department of Mechanical Engineering
University of Ottawa, 161 Louis Pasteur, Ottawa, ON, K1N6N5, Canada*

Email: *pjha@uottawa.ca*

ABSTRACT

Many numerical schemes exist for the simulation of flows on computers. The Finite Volume (FV) method is one of the most commonly used numerical schemes mostly in commercial and industrial codes. Present day state-of-the-art solvers based on FV are capable of using parallel computers to adapt the grids automatically based on the local flow behavior. While most FV based solvers have a second order accuracy, recent FV schemes have been developed with fourth to sixth order accuracies. In comparison, the solvers based on the Spectral Discontinuous Galerkin (SDG) scheme have higher accuracy: of the order of six to twelve or higher. In the present article, we compare the performance a parallel solution-adaptive FV scheme, called Computational Framework for Flows and Combustion (CFFC), with a parallel solution-adaptive SDG solver. We will present results for the flow inside a cavity and a swirling flow. Performance factors such as computational speed, mesh refinement efficiency and solution accuracy will be compared.

1 INTRODUCTION

Numerical schemes based on the Finite volume (FV) method are widespread in industry and academia. FV methods discretize the entire computational domain into a number of finite volumes. All physical properties are assumed to be constant inside a given volume. These volumes interact with each other by exchanging fluxes at the volume interface. The FV method works smoothly for first-order schemes. For high-order (HO) schemes (for FV, HO schemes are of the order of 4 – 6), flux evaluation at the volume interface requires information from many neighboring cells, which increases the inter-processor communication and hence decreases the parallel-efficiency.

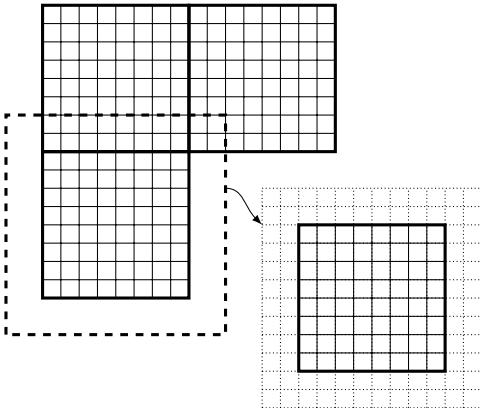


Figure 1: Ghost cells are used in a FV scheme for flux calculations

In the HO Spectral Discontinuous Galerkin (SDG) scheme (for SDG, HO schemes are of the order of 6 – 12 or higher) the computational domain is subdivided into elements. The solution inside an element is calculated using the local element-wise HO polynomial approximation of the solution. Because of the local nature of HO approximations, these schemes are friendly to parallelization. Also, like the FV method, the SDG method account for the physics of the problem (upwinding for advection problems) at the price of duplication of the variables on boundaries of elements [1]. A comparison between SDG and FV schemes performance will be interesting in many respects.

2 COMPARISON BETWEEN FV AND DG SCHEMES

We will use the HOSDG code developed at the University of Ottawa and compare its performance with

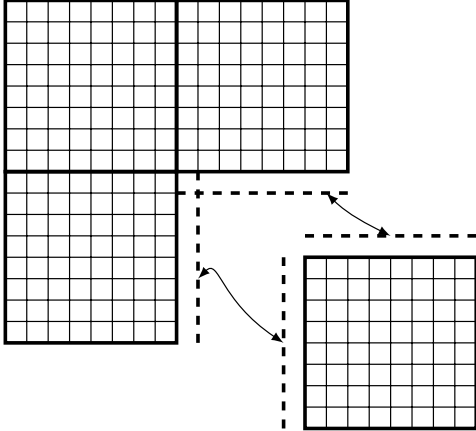


Figure 2: The information on the element face is exchanged for residual calculations in the SDG scheme

that of the *Computational Framework for Fluids and Combustion* (CFFC) developed at the University of Toronto [2]. Both these codes are state-of-the-art implementations of SDG and FV schemes in a parallel solution-adaptive framework. The CFFC tool uses a block-based approach where the entire computational domain is divided into a number of self-similar blocks, each with the same number of finite volumes. In the FV scheme, for calculating the viscous and inviscid fluxes, every cell uses the information on the neighboring cells, using the idea of ghost cells, as represented in Figure 1. In contrast, the SDG scheme exchanges the information on the faces of the elements, as shown in Figure 2. For HO schemes, the number of grid points in the FV schemes increases, and consequently the number of inter-block communications. In contrast, for the SDG schemes, the number of inter-elemental communications remain proportional to the order.

An interesting comparison will be to see how the performance of both these schemes scale with the increase in number of processors. It is expected that the SDG scheme will show better parallel efficiency compared to the FV scheme, given its minimal inter-elemental communication. Some other factors on which the parallel efficiency will depend are the implementation of the solution-adaptive algorithm for both the schemes and the load-balancing algorithm used in each case.

3 VALIDATION CASES

In order to compare the performance of the FV and the SDG schemes we will use the case shown in Figures 3 and 4. These figures show the distribution of a passive tracer with an underlying swirling velocity

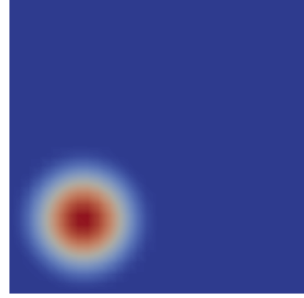


Figure 3: The initial state of the flow

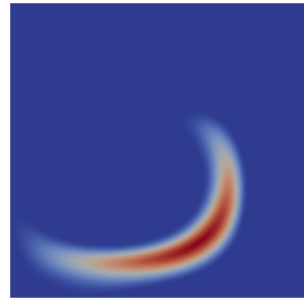


Figure 4: The final state of the flow

field [3]. The present results are obtained using the SDG scheme. The final state, in Figure 4, has a grid with four stages of refinement. The same case will be a set up on CFFC to assess the performance of the presented solver with the FV scheme. The final paper will also contain results for the driven cavity flow.

4 ACKNOWLEDGEMENTS

The authors acknowledge Prof. Clinton P. T. Groth of University of Toronto for allowing the use of the CFFC code developed in his lab.

REFERENCES

- [1] M. Chrust, A. Fabregat, and C. Mavriplis. In *Proceedings of the 21st Annual Conference of the CFD Society of Canada, Sherbrooke, QC, Canada, May 6 – 9, 2013*. CFD Society of Canada, 2013.
- [2] L. Ivan and C. P. T. Groth. *Journal of Computational Physics*, 257:830–862, 2013.
- [3] R. J. LeVeque. *SIAM Journal of Numerical Analysis*, 33(2):627–665, 1996.

Considerations in the Parallelization of a High-Order Discontinuous Galerkin Scheme

Pradeep Jha, Marcin Chrst, and Catherine Mavriplis

*Department of Mechanical Engineering
University of Ottawa, 161 Louis Pasteur, Ottawa, ON, K1N 6N5, Canada*

Email: *pjha@uottawa.ca*

ABSTRACT

With the increase in capacity of computational fluid dynamics (CFD), there has been a growing interest in the high-order (HO) schemes. HO schemes can give more accurate and stable results for fixed computational resources. In order to tap existing computational resources, it is important to parallelize a given numerical solver. In the present manuscript, we present the parallelization scheme for a HO spectral Discontinuous Galerkin (DG) direct numerical simulation solver. The presented scheme considers three approaches: (1) The spectral DG discretization scheme; (2) Parallel computing; and (3) Solution-adaptive grids. The final solver will be capable of efficiently running on massively parallel computing systems to give solutions of the order of accuracy of 8 to 12. Results will be presented for some simple geometries.

1 INTRODUCTION

There has been a massive increase in computational capacity around the globe in the last decade. The world's fastest computer, as of November, 2014, has a computational speed of 33.86 PFLOPS. Compared to the fastest computer in June, 2005, which had a computational speed of 0.136 PFLOPS, this is almost 250 times faster [6]. This massive increase in computational capacity has been largely possible due to the evolution of parallel computing hardware and knowhow [5]. For example, while the fastest computer in November, 2014, has 3,120,000 cores, the fastest computer in June, 2005, only had 65,536 cores. One should keep in mind that the increase in computational speed is not only dependent on the number of processors, but also on the speed and quality of every core in the system.

Using numerous-core systems to run a computer pro-

gram involves developing algorithms which can efficiently distribute the computational load on all the cores. These algorithms manage the communication between different cores and ensure that the load distribution is even. Message Passing Interface (MPI) [2] is a standardized and portable message-passing system designed to function on a wide variety of parallel computers.

In the present communication, we discuss the implementation of the MPI protocol for a high-order (HO) solution-adaptive flow solver based on the Discontinuous Galerkin (DG) numerical scheme [3]. The HO-DG scheme is locally computationally expensive, which reduces the number of inter-elemental communications significantly. This makes the DG scheme an excellent fit for parallel computation. In comparison to the DG scheme, both Finite Volume (FV) and Finite Difference (FD) schemes use information from more stencil points, depending on the order of accuracy of the scheme, for calculation of fluxes and solution derivatives, respectively, at every time step. This increases the amount of inter-processor communication significantly and hence affects the parallel efficiency of FV and FD schemes.

2 SOLUTION-BASED GRID ADAPTIVITY

Adaptation is handled for the DG method as for the Spectral Element method [1]. Based on desired accuracy and resource availability, a tolerance level is decided. Elements with error estimates above or below the tolerance values are marked for refinement or derefinement, respectively. Elements are refined by splitting the marked elements into four self-similar parts, and coarsened by the reverse process. Error estimates are calculated a posteriori based on the elemental spectrum of the numerical solution.

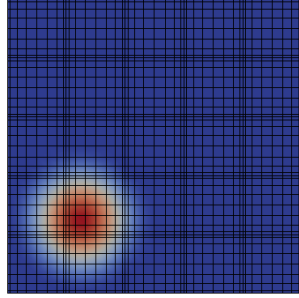


Figure 1: The initial grid and solution contour of a flow where an exponential tracer is deformed by an underlying swirling velocity field

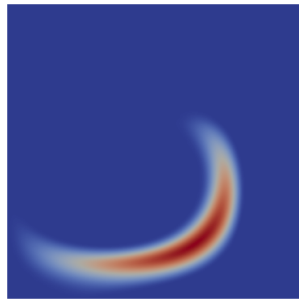


Figure 2: The final solution contour

Figures 1 and 2 show the initial and a later time, respectively, distributions of a passive tracer deformed by an underlying swirling velocity field [4]. The computational domain is discretized into 25 equally-sized elements at time $t = 0$, with 8 collocation points in each direction, as shown in Figure 1. Figure 3 shows the tracer and mesh distribution at a later time. The high density of grid points can be seen along the regions of large gradients of the tracer. Figure 3 shows four levels of h -refinement with a total of 385 elements. Both h - and p -refinement strategies are available in the solver.

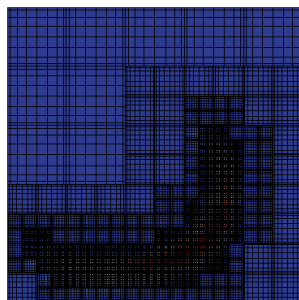


Figure 3: The final grid

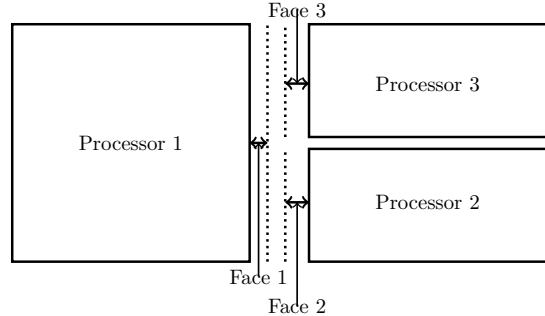


Figure 4: Parallelization of the DG scheme

3 PARALLELIZATION OF THE DG SCHEME

An important advantage of the DG scheme over other numerical schemes is that the elements only need the information on the coinciding faces to carry out the computations. This makes DG a well suited scheme for parallelization. Figure 4 shows the most complicated grid configuration in the parallel solution-adaptive scheme presented here. The parallelization involves a gather-scatter operation, where the information on the interacting faces of these three elements (faces 1, 2 and 3) are gathered respectively in an array on each face, and then communicated (using MPI) to the respective elements for calculating the respective residuals.

In order to reduce the inter-processor communication, it is important to ensure that as many neighboring elements are on the same processor as possible. The implementation of the parallel scheme is currently under active development. The details of this scheme will be presented in the final paper.

REFERENCES

- [1] H. Feng and C. Mavriplis. *Journal of Scientific Computing*, 17(1-4):385–395, 2002.
- [2] W. Gropp, E. Lusk, and A. Skjellum. *Using MPI*. MIT Press, Cambridge, Massachussets, 1999.
- [3] J. S. Hesthaven and T. Warburton. *Nodal Discontinuous Galerkin Methods*. Springer, 2008.
- [4] R. J. LeVeque. *SIAM Journal of Numerical Analysis*, 33(2):627–665, 1996.
- [5] D. A. Patterson and J. L. Hennessy. *Computer Organization and Design*. Elsevier, 2005.
- [6] E. Strohmaier, J. Dongarra, and M. Meuer. Top500 Web page. <http://www.top500.org>.

Development and Implementation of a Preconditioner for a Five-Moment One-Dimensional Moment Closure

Amir R. Baradaran and James M^cDonald

*Department of Mechanical Engineering, University of Ottawa,
161 Louis Pasteur, Ottawa, Ontario, Canada, K1N 6N5*

Email: *abara061@uottawa.ca*

ABSTRACT

Recently, a new system of first-order hyperbolic partial differential equations (PDEs) was proposed for the treatment of gases that is valid both in and for significant departures from local thermal equilibrium. In this study, the resulting system for a one-dimensional gas is studied. It consists of five first-order hyperbolic PDEs. Numerical solution of the system has proven to be difficult since, for some realistic states, the closing flux becomes infinitely large. In the present study, a preconditioner for the system is developed that scales the closing flux in order to remove the singularity from the system without altering the solution. A numerical implementation of the preconditioned system is described. Numerical solutions of several continuum and non-equilibrium flows problems are shown. Comparisons are made with classical models.

1 INTRODUCTION AND MOTIVATION

Traditionally, the Euler and Navier-Stokes equations are used to describe the time evolution of a gas flow when the gas is at or slightly deviated from the local thermal equilibrium. Despite giving accurate descriptions of gas behaviour in this regime, it is known that these two classical models lose accuracy as deviations from equilibrium become stronger. The degree to which a gas deviates from local equilibrium can be defined through the definition of the Knudsen number,

$$\text{Kn} = \frac{\lambda}{l}.$$

Here, the mean free path, λ , and characteristic length, l , are an average distance that a gas particle travels between two collisions and a length scale that characterizes flow domain respectively. Small Knudsen numbers correspond to flows with weak non-equilibrium effects. It is in this continuum-regime, $\text{Kn} < 0.01$, that

the Navier-Stokes equations have proven to be physically accurate. Although they are physically accurate, the presence of second derivatives in the system can lead to numerical difficulties on practical low-quality meshes [3].

When the Knudsen number is very large, deviations from this local equilibrium become significant. The leading method in this free-molecular regime, $\text{Kn} > 10$, is the direct simulation Monte Carlo (DSMC) method of Bird [1]. In this method, a stochastic treatment for gas particle evolution is used. Though this model is believed to be valid for all range of Knudsen numbers, its practical applicability is limited by its slow convergence rate, especially for lower-Knudsen-number situations, where the number of needed particles increases. Models based on the direct numerical discretization of high-dimensional Boltzmann equations are also assumed to be valid for any value of Knudsen number [5]. These methods require solving partial differential equations (PDEs) in a seven-dimensional phase space which results in prohibitive computational cost for practical solutions.

Many practical flows exist between these two regimes, in the so-called transition regime. Rarefied gases associated with high atmosphere flight, micro-scale flows, and flows associated with extreme gradients, such as within shock waves all exist in this regime. A robust model that remains both physically valid and computationally efficient across the continuum and transition regimes, is therefore desirable. Moment closures, derived from the Boltzmann equation, have been shown to be capable of providing such models. The promise of more accurate and affordable treatments involving less complex hyperbolic PDEs with only first-order derivative for gas flows both in the continuum and transition regimes, make these moment closures an attractive alternative to the traditional methods.

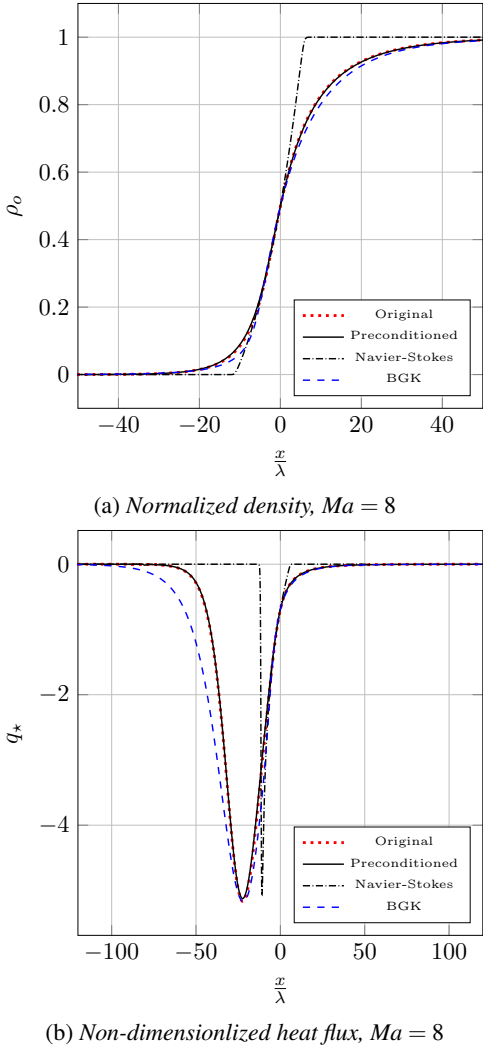


Figure 1: Normalized density and non-dimensionalized heat-transfer through a stationary shock wave.

Recently, a new moment closure of the Boltzmann equation based on an approximation of the maximum-entropy hierarchy [2] was proposed by McDonald and Torrilhon [4]. The new model has been shown to remain valid and well-posed even for strong deviations from local equilibrium and results in a set of PDEs that are strictly hyperbolic over the range of the physically realizable region [4]. Despite these advantages, the new model maintains one feature of the maximum-entropy model that is difficult to deal with in practice, it preserves a singularity in the closing flux for some physically possible states. The singularity was intentionally added to the model as it leads to very accurate predictions. However, it is difficult to deal with numerically, especially since it results in arbitrarily large wavespeeds.

2 SCOPE OF PRESENT STUDY

The objective of the current study is to develop a preconditioner matrix to overcome the problem of infinitely large wavespeeds in the moment system, since the existence of these wavespeeds leads to difficulties in numerical computation and can make numerical solution impossible in some cases. In order to construct the preconditioner, the behaviour of the wavespeeds in the model are studied over the whole physically realizable domain. An expression is suggested for each wavespeed which is shown to give a very accurate approximation for the real wavespeeds across the range of possible states. Knowledge of these wavespeeds, particularly how they behave near the singularity, is used to construct an appropriate preconditioner. The proposed preconditioner is implemented in the model and the preconditioned system is solved for several cases. Solutions derived from the preconditioned system are then compared with ones from the original system in order to validate the proposed preconditioner. Comparisons are made to other classical models in order to demonstrate the advantages of the moment-based model as compared to classical techniques. Figure 1 presents the normalized density and non-dimensionalized heat-transfer through a shock wave obtained with the original and preconditioned 5-moment systems, the Navier-Stokes equations, and the direct numerical solution of the BGK kinetic equation. It can be clearly seen that the moment closure results are in a far better agreement with the kinetic BGK solution, which is taken as the exact solution here.

REFERENCES

- [1] G. A. Bird. *Molecular Gas Dynamics and the Direct Simulation of Gas Flows*. Clarendon Press, Oxford, 1994.
- [2] C. D. Levermore. Moment closure hierarchies for kinetic theories. *J. Stat. Phys.*, 83:1021–1065, 1996.
- [3] J. G. McDonald, J. S. Sachdev, and C. P. T. Groth. Application of Gaussian moment closure to micro-scale flows with moving and embedded boundaries. *AIAA J.*, 52:1839–1857, 2014.
- [4] J. G. McDonald and M. Torrilhon. Affordable robust moment closures for CFD based on the maximum-entropy hierarchy. *J. Comput. Phys.*, 251:500–523, 2013.
- [5] L. Mieussens. Discrete velocity model and implicit scheme for the BGK equation of rarefied gas dynamics. *Mathematical Models and Methods in Applied Sciences*, 10(8):1121–1149, 2000.

Direct Numerical Simulation of the Flow Around a Wing Section at Moderate Reynolds Numbers

Seyed M. Hosseini¹, Ricardo Vinuesa¹, Philipp Schlatter¹,
Ardeshir Hanifi^{1,2}, and Dan S. Henningson¹

¹ Linné FLOW Centre, KTH Mechanics, Royal Institute of Technology, SeRC, SE-100 44 Stockholm, Sweden

² Swedish Defence Research Agency, FOI, SE-164 90 Stockholm, Sweden

Email: hosse@mech.kth.se

ABSTRACT

A three dimensional direct numerical simulation has been performed to study the flow around the asymmetric NACA-4412 wing at a moderate chord Reynolds number ($Re_c = 400,000$), with an angle of attack of 5° . The flow case under investigation poses numerous challenges for a numerical method due to the wide range of scales and complicated flow physics induced by the geometry. The mesh is optimized and well resolved to account for such varying scales in the flow. An unsteady volume force is used to trip the flow to turbulence on both sides of the wing at 10% chord. Full turbulence statistics are computed on the fly to further investigate the complex flow features around the wing. The present simulation shows the potential of high-order methods in simulating complex external flows at moderately high Reynolds numbers.

1 BACKGROUND

A clear evolutionary path could be observed looking back at the aircrafts from early days and comparing them to the state of the art modern civil aircrafts. This by large is owed to deeper knowledge of different flow phenomena around such bodies, i.e., laminar-turbulent transition, wall-bounded turbulence under pressure gradients, flow separation, turbulent wake flow, etc. Despite the conspicuous advances there still remain major challenges in terms of understanding the complex flow phenomena and a design procedure that can efficiently exploit the interacting features on an airplane. Traditionally such procedures relied heavily on experimental findings. Recent advances in supercomputers and massive parallelization have resulted determination of more and more parameters in aircraft design via computational resources in

the early stages of the design, effectively minimizing costs. Recently NASA issued a report [8] laying out a number of findings and recommendations regarding the role of CFD (Computational Fluid Dynamics) in aircraft design. The main revelations points out the necessity of accurate prediction of turbulent flows with significantly separated flow regions, more robust, fast and reliable mesh generation tools and development of more multidisciplinary simulations for both analysis and design optimization procedures. Johnson et al. [4] also discuss the changing role of CFD from a mere curiosity to a significant role in efficient designs. For instance, low order methods have been used to investigate the flow at low Reynolds numbers around an airfoil in the studies by Rodríguez et al. [6] and Calafell et al. [1]. In this study however we aim at studying such complex flow phenomena at a moderate Reynolds number along with using higher order methods.

2 SIMULATION

In the current work we study the turbulent flow around a NACA-4412 wing at a chord Reynolds number ($Re_c = 400,000$), and an angle of attack of AoA = 5° . The mesh is optimized such that it can account for all the varying scales in the flow field. The grid is designed to meet the plus units criteria, $\Delta x^+ = 10$, $\Delta y^+ = 0.2$ (at the wall), and $\Delta z^+ = 5$, where x, y, and z are the streamwise, wall-normal and spanwise coordinates, respectively. The Kolmogorov length scale is also used to determine the required spacing away from the wall and along the wake. A spanwise width of 10% chord length has been chosen. The total number of grid points in this case amounts to around 3.2 billion grid points. The flow is tripped using the a random volume forcing following the parameters in Ref. [7] at 10% chord on both the lower and the upper side. Initially

REFERENCES

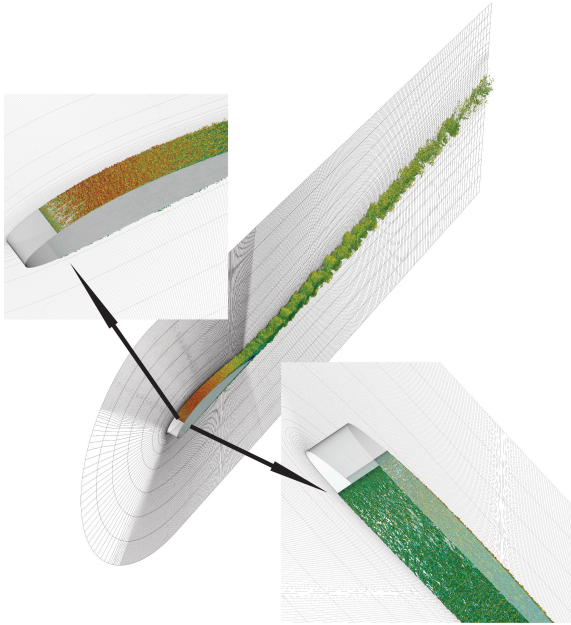


Figure 1: Instantaneous vortical structures visualized by λ_2 criterion, colored with streamwise velocity. The flow is tripped at 10% chord on both sides. The angle of attack is $\text{AoA} = 5^\circ$ and chord Reynolds number is ($Re_c = 400,000$). Black lines are the spectral element mesh.

a RANS computation is used to estimate the velocity distribution around the airfoil in order to be later fed in as the boundary condition for direct numerical simulation. The state-of-the-art Nek5000 code [2] is used for incompressible direct numerical simulation. It combines the ability of finite elements methods to handle complex geometries with the spectral accuracy provided by spectral elements. It has previously been used to study turbulent flow in a pipe [5] and flow around a wall mounted square cylinder [9] at moderately high Reynolds numbers. The code is highly scalable up to more than a million cores. The present large-scale simulation is run on 16384 processors, and is estimated to consume up to 40 million core hours. Figure ?? shows the instantaneous vortical structures identified by λ_2 criterion [3], and colored with streamwise velocity. The emergence of hairpin vortices could be seen where the flow transitions to turbulence. A small separated region along with the von Kármán-type of vortex street in the wake is visible from the figure. The final contribution will include full turbulence statistics to better characterize and understand the underlying interacting flow features.

- [1] J. Calafell, O. Lehmkuhl, I. Rodríguez, and A. Oliva. On the Large-Eddy Simulation modelling of wind turbine dedicated airfoils at high Reynolds numbers. *Proc. of the 7th International Symposium On Turbulence, Heat and Mass Transfer. Palermo, Italy*, 2012.
- [2] P. F. Fischer, J. W. Lottes, and S. G. Kerkemeier. nek5000 Web page, 2008. <http://nek5000.mcs.anl.gov>.
- [3] J. Jeong and F. Hussain. On the identification of a vortex. *Journal of Fluid Mechanics*, 285:69–94, 2 1995.
- [4] F. T. Johnson, E. N. Tinoco, and N. J. Yu. Thirty years of development and application of CFD at boeing commercial airplanes, Seattle. *Computers and Fluids*, 34(10):1115 – 1151, 2005.
- [5] G. El Khoury, P. Schlatter, A. Noorani, P. F. Fischer, G. Brethouwer, and A. Johansson. Direct numerical simulation of turbulent pipe flow at moderately high reynolds numbers. *Flow, Turbulence and Combustion*, 91(3), 2013.
- [6] I. Rodríguez, O. Lehmkuhl, R. Borrell, and A. Oliva. Direct numerical simulation of a NACA0012 in full stall. *International Journal of Heat and Fluid Flow*, 3(0):194 – 203, 2013.
- [7] P. Schlatter and R. Örlü. Turbulent boundary layers at moderate Reynolds numbers. Inflow length and tripping effects. *Journal of Fluid Mechanics*, 710:5–34, 2012.
- [8] J. Slotnick, A. Khodadoust, J. Alonso, D. Darmafal, W. Gropp, E. Lurie, and D. Mavriplis. CFD vision 2030 study: A path to revolutionary computational aerosciences. *Technical report, NASA/CR-2014-218178*, 2014.
- [9] R. Vinuesa, P. Schlatter, J. Malm, C. Mavriplis, and D. S. Henningson. Direct numerical simulation of the flow around a wall-mounted square cylinder under various inflow conditions. *Journal of Turbulence, To appear*, 2015.

Direct Numerical Simulation of Transition on a Laminar Morphing Wing: 2D vs 3D

Jérémie Laplante and Catherine Mavriplis

*Department of Mechanical Engineering
University of Ottawa, 161 Louis Pasteur, Ottawa, ON, K1N 6N5, Canada*

Email: *Catherine.Mavriplis@uottawa.ca*

ABSTRACT

Laminar flow control on aircraft wings is important for drag reduction and performance characteristics. To this end a morphing wing has been constructed and wind tunnel tested previously [1], showing laminar flow up to approximately 60% chord. The proposed paper investigates the direct numerical simulation prediction of transition on this morphing wing. Comparisons between the 2D and 3D numerical simulations will be given for Reynolds numbers of 400,000 and 500,000. The simulation is based on a high order spectral element discretization of the incompressible Navier-Stokes equations.

1 INTRODUCTION

In order to improve the performance of commercial aircraft and provide for a more environmentally-friendly product, laminar flow control is considered as a means to save on fuel consumption and hence operating costs and reduce carbon dioxide emissions. Laminar flow control attempts to extend the region of laminar flow over the surface of the wing of an aircraft, since laminar flow has a much lower skin friction drag than turbulent flow. A first attempt at changing the shape of a wing through an actuated skin was completed by a joint group of researchers of industry, academia and government [1]. The resulting morphing wing showed beneficial results, delaying transition to turbulence by up to 30% chord, thereby reducing drag by up to 22%. Confirmation of these results by direct numerical simulation is appealing in that it could then also serve to predict other conditions that were not part of the testing scenario. In an effort to do so, we present here direct numerical simulations of flow over this morphing wing profile in 2D and 3D. The focus is on characterizing the flow, determining the transi-

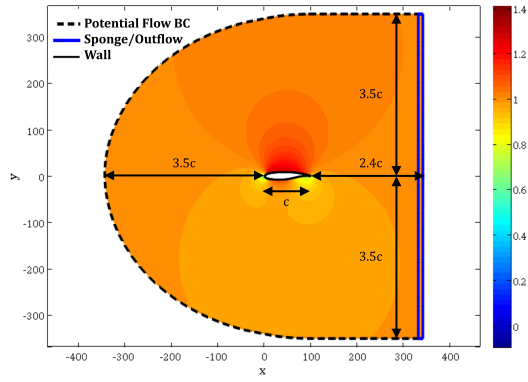


Figure 1: Computational domain for flow past a morphing wing in 2D. Boundary and initial conditions.

tion point and comparing 2D and 3D simulations to see if 2D simulations might suffice as we increase the Reynolds number. Nek5000 is the spectral element solver for the incompressible Navier-Stokes equations that is used in this investigation.

2 SIMULATION SETUP

The 2D calculations were performed on a domain indicated in Fig. 1. A potential flow vortex panel method solution [2] is used to determine the size of the domain and set inlet and farfield boundary conditions as well as initial conditions. An outflow boundary condition with a "sponge" dampening function [3] is used over the last 10% of the wake domain.

The spectral element computational grid was developed using an elliptic grid generator, controlling for spacing, orthogonality and aspect ratio of the elements. At these high Reynolds numbers, the grid appears to be quite sensitive to non-gradual changes in element

sizes and shapes. The final grid for Reynolds number $Re = 400,000$ had $K = 76,393$ elements and used elemental polynomial orders of $N = 10$. The calculation was performed in parallel on 48 cores.

The 3D calculation is quite large and the domain had to be reduced to fit on computers currently available to us. The grid extends one chord length ahead, above, and below the airfoil, while the wake region is extended to 1.5 chords. The comparable number of elements is $K = 21,248$ for the x-y plane, and $K = 7$ elements are used to cover 5% of the span with a periodic boundary condition, for a total of $K = 148,736$ elements, using $N = 10$ order polynomials. This corresponds to close to 149 million points. The calculation is launched on 512 cores.

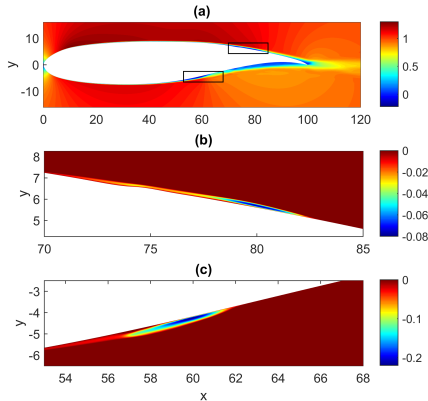


Figure 2: Time averaged flow over the morphing wing profile - 2D results at $Re = 400,000$. Separation bubbles on the upper (b) and lower (c) surfaces.

3 RESULTS

The 2D calculations for $Re = 400,000$ and zero angle of attack show a laminar attached flow on the upper surface of the airfoil up until approximately 68% chord, where a separation bubble of approximate length 14% chord forms, as shown in Fig. 2. The flow around and after separation is characterized by a series of vortices as shown in Fig. 3. Skin friction increases significantly at approximately 80-85% chord, indicating possible transition to turbulence, as shown in Fig. 4. This is confirmed by the kinetic energy of the fluctuations (not shown here for lack of space). The 3D calculations are underway and will be reported in the final paper. While the wind tunnel tests [1] report transition at around 60% chord, that result is for a larger Re of over 2 million. This paper represents a first attempt at calculating direct numerical simulation of a complex

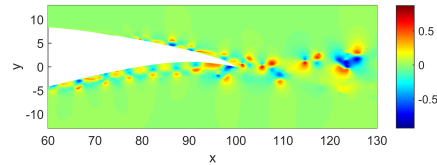


Figure 3: Velocity perturbations relative to the time averaged flow - close-up view.

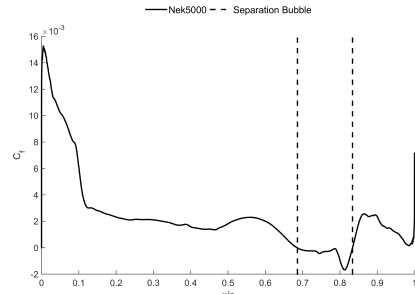


Figure 4: Skin friction coefficient for flow over the morphing wing profile - 2D results at $Re = 400,000$. The separation region is indicated by the dashed lines.

flow at such large Reynolds numbers and will lead to eventual comparison with the experiments.

The results obtained for the 2D simulation of flow past the morphing wing show that transition occurs around 80% chord at a freestream Reynolds number of 400,000. While turbulence is inherently a 3D phenomenon, we expect to see good correlation between the 2D and 3D predictions based on skin friction coefficient and other transition prediction techniques. The final paper will examine this comparison.

Acknowledgments: This problem was suggested by Éric Laurendeau of École Polytechnique de Montréal. Support from NSERC and HPCVL and SCINET computer time are gratefully acknowledged.

REFERENCES

- [1] D. Coutu, V. Brailovski, P. Terriault, M. Mamou, Y. Mébarki, and É. Laurendeau, *Smart Mater. Struct.*, 20:035019, 2011.
- [2] A. M. Kuethe, A.M. and C.-Y. Chow, *Foundations of Aerodynamics*, Fifth Edition, John Wiley and Sons, 1998.
- [3] D. Tempelmann, L.-U. Schrader, A. Hanifi, L. Brandt, et al, AIAA Paper 2011-3294.

Discontinuous Galerkin methods for incompressible continuously-stratified flow

D.T. Steinmoeller^{1†} and M. Stastna¹

¹ Department of Applied Mathematics, University of Waterloo,
200 University Ave. W, Waterloo, ON. N2L 3G1

Email: *dsteinmo@uwaterloo.ca*

ABSTRACT

The application of locally high-order element methods to incompressible flow situations has attracted recent attention in the numerical methods literature. Although accurate numerical solutions have been obtained with these methods for a suite of well-studied test problems, more work needs to be done to develop schemes that are robust in the (nearly) inviscid limit. In this limit of the parameter space, long-term stable solutions become difficult to obtain due to weak instabilities driven by spurious pressure modes as a result of the well-known LBB constraint. It can be shown that standard stabilization techniques, such as local polynomial filtering, can also fall short of stabilizing these LBB-type instabilities. In this work, we explore the Discontinuous Galerkin (DG) solution to the stratified incompressible Euler equations in the vanishing-compressibility limit. We show that locally non-smooth pressure modes may be smoothed if sufficient compressibility is retained in the model equations. We attempt to answer the question of whether solution methods for nearly incompressible flow can lead to more robust numerical solutions in the purely incompressible limit within the DG framework.

1 INTRODUCTION

Recent work [1] on DG methods for incompressible flow has suggested that numerical methods can be improved by using a numerical flux treatment derived from the artificial compressibility (AC) equations. In this paper, we follow up on this idea by considering general DG solution methods to the AC equations in the weakly compressible limit.

2 METHODS

The governing equation for a density stratified, inviscid fluid in dimensionless form read

$$\mathbf{u}_t + \nabla \cdot (\mathbf{u} \otimes \mathbf{u}) = -\nabla p - Fr^{-2} \rho \mathbf{k}, \quad (1)$$

$$\nabla \cdot \mathbf{u} = 0, \quad (2)$$

$$\rho_t + \nabla \cdot (\rho \mathbf{u}) = 0. \quad (3)$$

Here Fr is the Froude number which quantifies the relative importance of advective and buoyancy terms, and plays a role analogous to the Mach number in gas dynamics. The artificial compressibility equations are similar, except (2) is replaced with the prognostic pressure equation

$$\epsilon p_t + \nabla \cdot \mathbf{u} = 0, \quad (4)$$

where $\epsilon = (U/c)^2$.

Our spatial discretization follows the standard nodal DG approach focusing on polynomial orders ranging from $N = 4$ to $N = 8$ where advective numerical fluxes are (for simplicity) chosen to be the well-known Lax–Friedrichs flux. For the artificial compressibility equations, we choose an implicit-explicit (IMEX) based time-discretization scheme using an implicit formulation only for the terms governing the propagation of the fast sound waves allowing for an explicit treatment for the slow internal gravity waves of interest. Figure 1 shows a snapshot from a selected IMEX simulation where a numerical instability is encountered that is similar to those found for the purely incompressible equations.

ACKNOWLEDGEMENTS

This work was supported by the Natural Sciences and Engineering Research Council of Canada.

[†]Last affiliation.

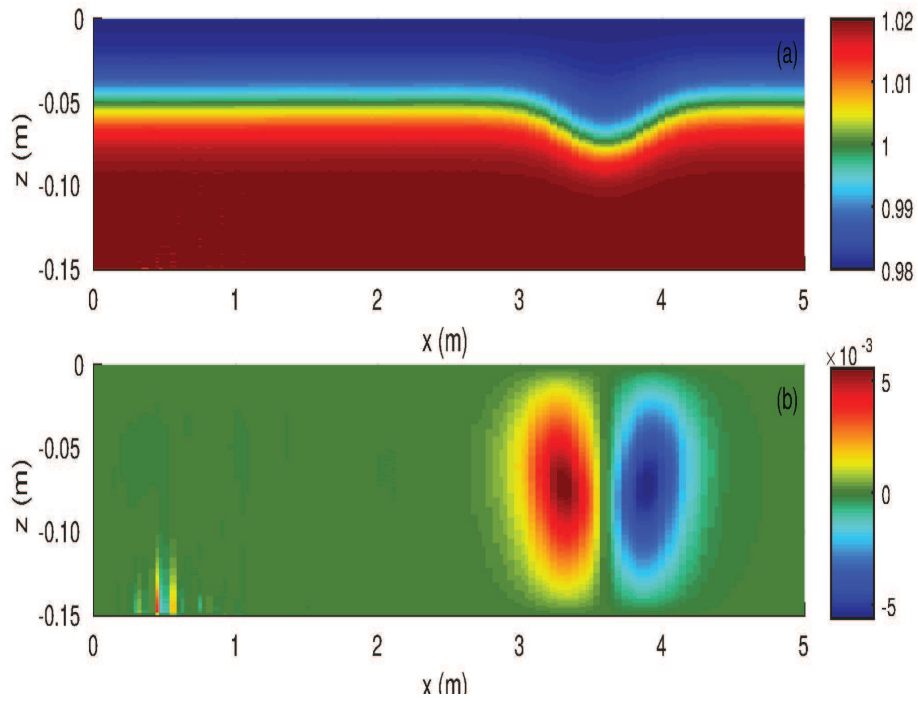


Figure 1: Snapshot of a simulation of a right-ward propagating internal solitary wave (density in the upper panel, vertical component of velocity in the lower panel) at the onset of a numerical instability. The physical time is $t = 400$ s. The numerical instability can be seen in the bottom panel near $x = 0.5$.

REFERENCES

- [1] F. Bassi, A. Crivellini, D.A. Di Pietro and S. Rebay An implicit high-order discontinuous Galerkin method for steady and unsteady incompressible flows *Comput. Fluids*, 36(10):1529–1546, 2007

Displacement flows in a plane channel with an oscillatory wall

Seyed Mohammad Taghavi¹, Kamran Alba², and Faïçal Larachi¹

¹ Department of Chemical Engineering, Laval University, Québec, QC, Canada

² Department of Engineering Technology, University of Houston, Houston, TX, USA

Email: Seyed-Mohammad.Taghavi@gch.ulaval.ca

ABSTRACT

We consider miscible displacement flows in an inclined 2D plane channel when buoyancy is significant and when a channel wall oscillates. We focus on a situation where the inertial forces are weak in comparison with viscous and buoyant forces. We rely on a thin-film approximation to simplify the governing equations and introduce the scaled conservation equations for two-layer thin-film flows. We employ a weighted residual approach to land on suitable weight functions before depth-averaging. We subsequently solve the equations numerically to furnish the interface evolution in time. For a heavy-light displacement, the heavy fluid slumps under the effect of gravity. The channel wall oscillation causes the imposed flow rate to oscillate around a fixed value with the same frequency but with a different amplitude. The model results depend on five non-dimensional parameters: χ (the ratio of buoyancy forces to viscous forces), δRe (the relative importance of inertial forces to buoyancy forces), m (the viscosity ratio), Λ (the wall oscillation amplitude), and ω (the wall frequency oscillation). We show that the wall oscillation does not modify the global displacement flow pattern a lot. However the front speed can be affected by the wall oscillation.

1 INTRODUCTION

We consider buoyant displacement flows in 2D plane channels by using a semi-analytical modeling approach. We have a case within which a heavier fluid displaces a lighter fluid downward. We have extensively studied these in our previous experimental works [3, 1]. We have shown that at large enough imposed mean flows (\hat{U}_0), the leading displacement front advances at speed \hat{V}_f that increases linearly with \hat{U}_0 (with slope larger than 1). In this paper we move one

step forward in considering an unconventional case where the 2D channel lower wall oscillates during the displacement flow. This model can be considered as a direct extension of [2, 1].

2 TWO-FLUID MODEL

We consider a two-dimensional region between two parallel plates, separated by a distance \hat{D} , that are oriented at an angle β with respect to the vertical. The slot is initially filled with fluid 2; fluid 1 is injected at $\hat{x} = -\infty$ with a mean velocity \hat{U}_0 (averaged over channel width and also over time). Cartesian coordinates (\hat{x}, \hat{y}) are as shown in Fig. 1. Both fluids are assumed to be Newtonian. Although the fluids are miscible, we consider the large Péclet number limit in which no significant mixing occurs over the timescales of interest. The dimensionless equations of motion, valid within each fluid region Ω_k , $k = 1, 2$, are:

$$\phi_k \text{Re} \left[\frac{\partial u}{\partial t} + u \frac{\partial u}{\partial x} + v \frac{\partial u}{\partial y} \right] = - \frac{\partial p}{\partial x} + \frac{\partial}{\partial x} \tau_{k,xx} + \frac{\partial}{\partial y} \tau_{k,xy} + \phi_k \frac{\cos \beta}{St}, \quad (1)$$

$$\phi_k \text{Re} \left[\frac{\partial v}{\partial t} + u \frac{\partial v}{\partial x} + v \frac{\partial v}{\partial y} \right] = - \frac{\partial p}{\partial y} + \frac{\partial}{\partial x} \tau_{k,yx} + \frac{\partial}{\partial y} \tau_{k,yy} - \phi_k \frac{\sin \beta}{St}, \quad (2)$$

$$\frac{\partial u}{\partial x} + \frac{\partial v}{\partial y} = 0. \quad (3)$$

Here $\mathbf{u} = (u, v)$ denotes the velocity, p is the pressure, and $\tau_{k,ij}$ represents the ij -th component of the deviatoric stress in fluid k . The parameter $\phi_1 = 1$, and the three dimensionless parameters appearing above are

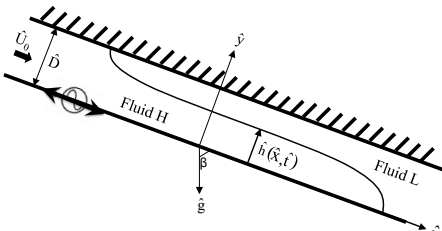


Figure 1: Schematic of displacement flow in an inclined 2D plane channel geometry. The upper wall is fixed while the lower wall oscillates with a constant amplitude and frequency.

the density ratio ϕ_2 , the Reynolds number, Re , and the Stokes number, St , defined as follows:

$$\phi_2 = \phi = \frac{\hat{\rho}_2}{\hat{\rho}_1}, \quad Re = \frac{\hat{\rho}_1 \hat{U}_0 \hat{D}}{\hat{\mu}_1}, \quad St = \frac{\hat{\mu}_1 \hat{U}_0}{\hat{\rho}_1 \hat{g} \hat{D}^2}. \quad (4)$$

Here $\hat{\rho}_k$ is the density of fluid k , $\hat{\mu}_1$ is the viscosity of fluid 1 and \hat{g} is the gravitational acceleration. In order to derive (1)-(3) we have scaled distances using \hat{D} , velocities with \hat{U}_0 , time with \hat{D}/\hat{U}_0 , and pressure and stresses with $\hat{\mu}_1 \hat{U}_0 / \hat{D}$.

On the upper wall of the slot the no-slip condition is satisfied. The lower wall however moves with the speed of $\Lambda \sin(\omega T)$, in the direction x , where $\Lambda = \hat{u}_w / \hat{U}_0$ with \hat{u}_w being the dimensional wall oscillation amplitude. If both walls were motionless, due to the scaling adopted, we would have $\int_0^1 u \, dy = 1$ in each cross-section. However, due to the wall oscillation, the upstream flow rate, which is constant otherwise, would have an oscillation the form of which can be calculated through a Poiseuille-Couette type flow analysis. After calculation, we find that $\int_0^1 u \, dy = 1 + \Lambda \sin(\omega T)/2$. The slot is assumed to be infinite in x , with the interface between fluids initially localised close to $x = 0$. We shall consider flows with buoyancy, in which the heavier fluid lies at the bottom of the slot. The fluid layers are separated by an interface ($y = h(x, t)$) which is assumed to be single-valued at each x . Across the interface, velocity and stress are continuous. The interface is simply advected with the flow, satisfying the kinematic condition.

3 SAMPLES OF RESULTS

In general our model results depend on five dimensionless parameters: χ , δRe , m , Λ , and ω . Fig. 2 shows examples of contours of q versus h and T with $m = 1$,

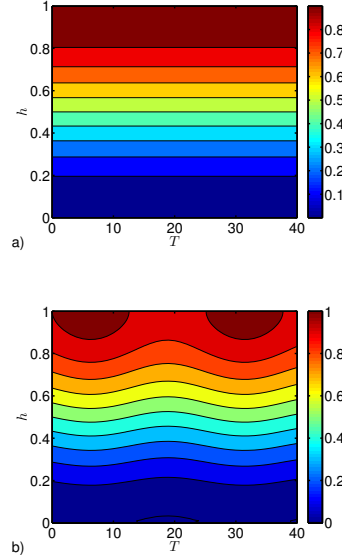


Figure 2: Examples of contours of q versus h and T with $m = 1$, $\omega = 0.25$, $\chi = 0$ and $h_\xi = 0$ for a) $\Lambda = 0$; b) $\Lambda = 0.1$.

$\omega = 0.25$ and $\chi - h_\xi = 0$ for various values of Λ . As it can be seen, the wall oscillation can alter the flow rate.

REFERENCES

- [1] S. Taghavi, K. Alba, T. Seon, K. Wielage-Burchard, D. Martinez, and I. Frigaard. Miscible displacement flows in near-horizontal ducts at low Atwood number. *J. Fluid Mech.*, 696:175–214, 2012.
- [2] S. Taghavi, T. Seon, D. Martinez, and I. Frigaard. Buoyancy-dominated displacement flows in near-horizontal channels: the viscous limit. *J. Fluid Mech.*, 639:1–35, 2009.
- [3] S. Taghavi, T. Seon, D. Martinez, and I. Frigaard. Influence of an imposed flow on the stability of a gravity current in a near horizontal duct. *Phys. Fluids*, 22:031702, 2010.

Effect of Micro-Jet Impingement on Nano-Aerosol Soot Formation in a Turbulent Paraffin-Oil Flame

Masoud Darbandi^{1,2}, Majid Ghafourizadeh¹, and Gerry E. Schneider³

¹*Center of Excellence in Aerospace Systems, Department of Aerospace Engineering, Sharif University of Technology, Tehran, P.O. Box 11365-8639, Iran*

²*Institute for Nanoscience and Nanotechnology, Sharif University of Technology, Tehran, P.O. Box 11365-8639, Iran*

³*Department of Mechanical and Mechatronics Engineering, University of Waterloo, Waterloo, Ontario, N2L 3G1, Canada*

Email: *darbandi@sharif.edu*

ABSTRACT

In this paper, the effects of micro-jet impingement on the formation of soot nano-particles and pollutants emissions in a turbulent paraffin-oil flame are investigated numerically. We study the effects on soot volume fraction, soot particles diameter, mass fractions of carbon monoxide (CO), carbon dioxide (CO₂), and benzene (C₆H₆) considering aerosol dynamics and chemistry of soot nano-particles, i.e. nucleation, coagulation, surface growth, and oxidation. In this regard, we use a two-equation standard κ - ϵ turbulence model, a PAH-inception two-equation soot model with oxidation due to OH agents, a detailed chemical kinetic consisting of 121 species and 2613 elementary reactions, and steady flamelet approach as combustion model. We take into account turbulence-chemistry interaction by using presumed-shape probability density functions PDFs. We also take into account the radiation heat transfer of soot and gases assuming optically-thin flame. In the first place, to evaluate our numerical results, we solve a documented experimental test case, i.e. a turbulent paraffin-oil flame, and compare the flame structure, i.e. the distributions of mean mixture fraction, temperature and soot volume fraction, within the flame with those of measured and reported in the experiment. Our numerical results show a good agreement with those of experiment. Then, we embed a micro-scale injector at the burner wall, split the incoming air-flow between primary and secondary streams, inject the secondary air into the burner via the micro-scale injector embedded in burner wall, and compare the results for different values of micro-impinging-jet mass flow rate. In this regard, we implement suitable boundary conditions regarding

the micro-scale embedded-injector as well as the mass flow rate of micro-impinging-jet. Our results show micro-jet impingement results in a compact-flame near the fuel-injector nozzle. Our calculations show the emission of carbon dioxide is slightly affected by micro-jet impingement while the emissions of carbon monoxide, benzene, and soot nano-aerosol are seriously changed. They show that increasing the mass flow rate of micro-impinging-jet effectively reduces the formation of pollutants within the turbulent paraffin-oil flame as well as reducing their emissions at the burner outlet. It is also found that micro-jet impingement leads to uniform profiles of temperature, soot volume fraction, and mass fractions of CO, CO₂, and C₆H₆ at the burner outlet. It is observed that the reactive flow behavior within the burner would be changed under the influence of the micro-impinging-jet. So, this paper would be a good reference for investigators studying reactive-fluid-flow control within the burner as well as pollutants reduction.

1. INTRODUCTION

To be added in full paper submission.

2. THE GOVERNING EQUATIONS

To be added in full paper submission.

3. COMPUTATIONAL METHOD

To be added in full paper submission.

4. THE BENCHMARK TEST CASE AND VALIDATION

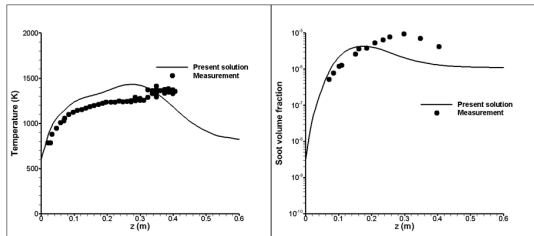


Figure 2. The current axial distributions of temperature, and soot volume fraction in a turbulent paraffin-oil nonpremixed flame and comparison with Ref. [1].

5. THE RESULTS AND DISCUSSION

We embed a micro-scale injector at the burner wall, split the incoming air-flow between primary- and secondary-air streams and inject the primary air into the burner via the micro-scale embedded injector. The dimension of micro-scale injector is 100 μm embedded at a height of $z=0.1$ m above the fuel nozzle exit. We inject a mass flow rate of 2.7 g/s of the total incoming-air via the micro-scale injector while the rest of incoming air enters the burner as primary-air. The other parameters, i.e. geometry and BCs, are similar to the benchmark test case.

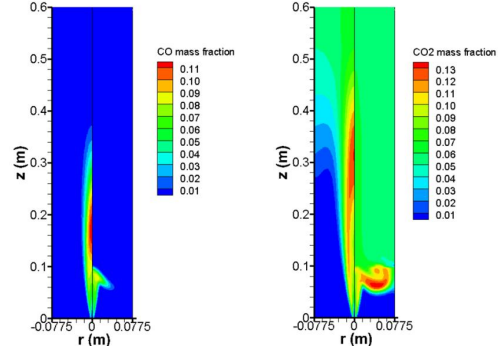
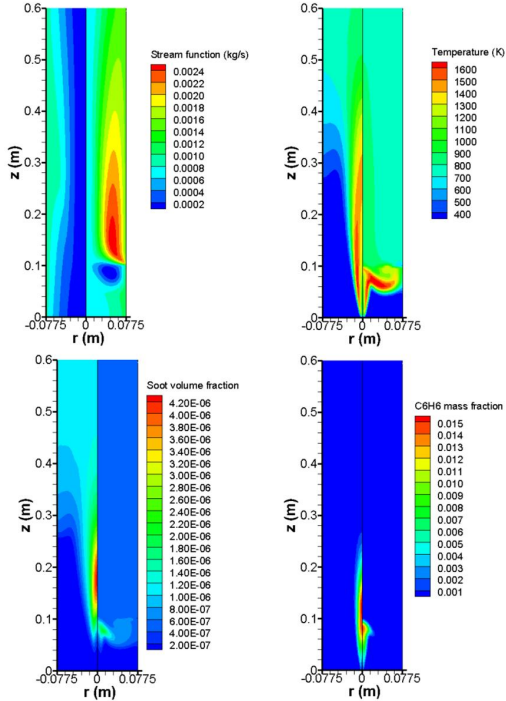


Figure 3. The effect of micro-jet impingement on the distributions of stream function, temperature, soot volume fraction, and mass fractions of C_6H_6 , CO , and CO_2 in a turbulent paraffin-oil flame.

Figure 3 shows the effect of micro-jet impingement on turbulent paraffin-oil flame. In each subfigure, the left half depicts distribution for benchmark test case, without micro-jet impingement, while the right half depicts distribution for the burner with micro-jet impingement.

CONCLUSION

We investigated the effect of micro-jet impingement on the formation of soot nano-aerosol and the emissions of carbon monoxide, carbon dioxide, benzene from a turbulent paraffin-oil flame. We first evaluated our numerical simulation by simulating a benchmark test case and then we embedded a micro-scale injector in the burner wall, split the incoming air-flow between primary and secondary streams, injected the secondary-air into the burner via the micro-scale injector, and compared the results obtained for different values of micro-impinging-jet mass flow rate. Our numerical study showed that micro-jet impingement changes the reactive flow pattern within the burner and reduces the flame length. They also showed that as the mass flow rate of micro-impinging-jet increases the emissions of soot nano-aerosol, carbon monoxide, and benzene reduce while that of carbon dioxide is slightly changed. The profiles of exhaust-gas temperature, soot volume fraction, mass fractions of CO , CO_2 , and C_6H_6 in exhaust gases also become more uniform in the case of micro-jet impingement.

REFERENCES

- [1] K. J. Young, C. D. Stewart, and J. B. Moss. Soot Formation in Turbulent Nonpremixed Kerosine-Air Flames Burning at Elevated Pressure: Experimental Measurement. *Proceeding of the Combustion Institute*:609-617, 1994.

Efficient High Order Differentiation of Implicitly-Defined Curves with Applications to Homotopy Continuation Algorithms for CFD Flow Solvers (Abstract)

David A. Brown¹ and David W. Zingg²

¹ PhD candidate

² Professor and Director, Tier 1 Canada Research Chair in Computational Aerodynamics, J. Armand Bombardier Foundation Chair in Aerospace Flight

Institute for Aerospace Studies, The University of Toronto, Toronto, Ontario, Canada

Email: *utiasdavid.brown@mail.utoronto.ca*

Homotopy continuation methods have existed for decades as algorithms for solving nonlinear systems of equations. However, only recently have these methods been developed as efficient and competitive methods for solving the discrete flow equations in CFD. The premise of homotopy continuation methods is that we begin by constructing some alternative system of equations which can be easily solved or has a known solution, which will be referred to as the homotopy system. The solution of the homotopy system is deformed to the solution of the discrete flow equations by varying some parameter $\lambda \in \mathbb{R}$. By convention, λ is decreased monotonically from 1 to 0. Since the homotopy system can be any system of equations of our choosing, there is much potential to explore these methods and we have already shown that homotopy methods can be more efficient than pseudo-transient continuation methods in many cases [3, 4].

The homotopy deformation can be represented as a curve in \mathbb{R}^N and numerical continuation is performed by attempting to trace this curve numerically from one end to the other. The curve can be traced more accurately if higher derivatives of the curve are calculated. However, previous researchers have applied homotopy methods for purposes such as the study of systems with multiple solutions for relatively small systems of equations and have not needed to calculate higher derivatives of the curve efficiently. The calculations that exist in the literature require the inversion of large dense matrices, even for CFD problems where the Jacobian of the flow residual is highly sparse and dense matrix operations would be

highly inefficient. Finite-difference approximations are possible but have limited accuracy and require previous data points, which reduce their usefulness for practical applications.

Previously we have presented a direct method for accurately calculating the tangent vector [1, 2] at the cost of one sparse linear solve and a few vector operations. Using linear algebra and differential geometry we have developed the ability to directly and accurately calculate derivatives of any order at a given point on the curve. Each additional order of derivative that is calculated requires one additional linear solve as well as several residual evaluations. This can be very useful in the construction of higher order predictors or in the analysis of homotopy deformations.

The calculation of the second derivative of the curve (known as the *curvature*) has been implemented and validated. The direct curvature calculation was compared to the finite-difference calculation at different step size $|\Delta\lambda|$ for a Laplacian-type homotopy function. The first case is inviscid flow over the NACA 0012 airfoil at Mach 0.3 and angle of attack of 1° . The mesh consists of 15390 nodes parallelized on 18 processors. This is a simple deformation exhibiting very modest curvature. The second case is performed on the same mesh but it is a transonic case at Mach 0.8 and angle of attack of 3° . The curve in this case is more complex. The calculations are plotted in Figures 1 and 2. The fact that the transonic case appears to actually exhibit lower curvature than the subsonic case is due to the

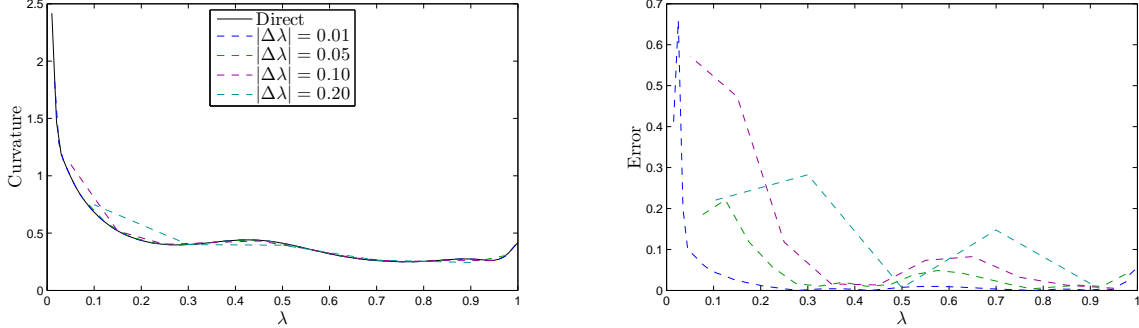


Figure 1: Comparison of direct and finite-difference curvature calculations at different step size $|\Delta\lambda|$ on the inviscid NACA 0012 airfoil at Mach 0.3 and angle of attack of 1°

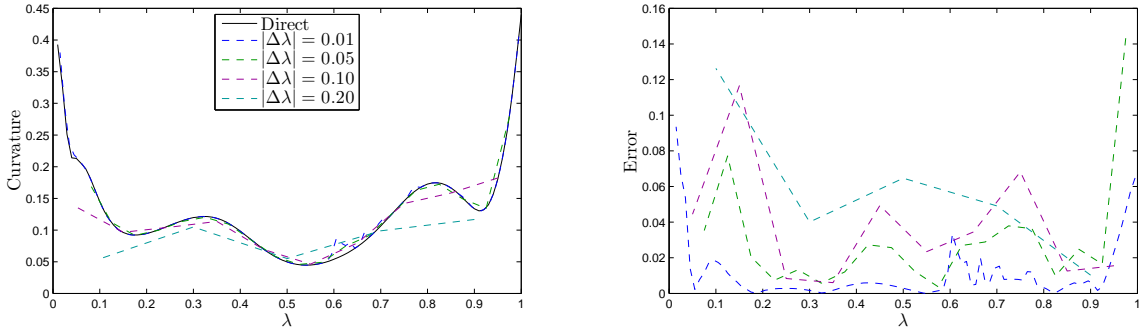


Figure 2: Comparison of direct and finite-difference curvature calculations at different step size $|\Delta\lambda|$ on the inviscid NACA 0012 airfoil at Mach 0.8 and angle of attack of 3°

parametrization, as will be explained in the final paper.

The final paper will contain the explicit details of the calculations, comparison of curvature using different homotopy systems, curvature investigation of homotopy deformations on different geometries under different flow conditions, and analysis of predictor capabilities using variable order Taylor expansions.

of the CFD Society of Canada, Toronto, Ontario, Canada, June 2014.

- [4] D. Brown and D. W. Zingg. A new monolithic homotopy continuation algorithm with CFD applications. In *Eighth International Conference on Computational Fluid Dynamics*, Chengdu, China, July 2014.

REFERENCES

- [1] D. Brown and D. W. Zingg. Advances in homotopy-based globalization strategies in computational fluid dynamics. June 2013. AIAA-2013-2944.
- [2] D. Brown and D. W. Zingg. Development of homotopy continuation methods in CFD. In *21st Annual Conference of the CFD Society of Canada*, Sherbrooke, Quebec, Canada, May 2013.
- [3] D. Brown and D. W. Zingg. Development of a monolithic homotopy continuation algorithm for CFD applications. In *22nd Annual Conference*

Equivalence between the Energy Stable Flux Reconstruction and Filtered Discontinuous Galerkin Schemes

Philip Zwanenburg¹ and Siva Nadarajah¹

Department of Mechanical Engineering, McGill University, 845 Rue Sherbrooke O, Montreal, QC H3A 0G4

Email: philip.zwanenburg@mail.mcgill.ca

ABSTRACT

The aim of this paper is to demonstrate the equivalence between filtered Discontinuous Galerkin (DG) schemes in strong and weak form and the Energy Stable Flux Reconstruction (ESFR) schemes. To this end, an alternate of the original proof is presented for the recovery of ESFR schemes from the filtering of the strong form of the DG scheme; further, the recent results demonstrating the mathematical equivalence between the DG scheme with inexact mass matrix and the ESFR g2 scheme are generalized and it is shown that the ESFR schemes can also be recovered from the filtering of the DG scheme with inexact mass matrix, using modified filter matrices. An extension to the filtering of the DG schemes in weak form is then given by demonstrating the computational equivalence of the weak and strong forms. Finally, all of the results are generally extended to higher dimensional curvilinear elements. 1D Numerical results validate theoretical derivations. A discussion concerning the extension of results presented here to other FR schemes is given in the conclusion.

Keywords: High-order, Flux reconstruction, Discontinuous Galerkin, Equivalence, Filter, Curvilinear

1 INTRODUCTION

The recently introduced Flux Reconstruction (FR) schemes [5], specifically the Energy Stable Flux Reconstruction schemes [7], have been gaining in popularity as new high-order finite element formulations. In his seminal paper, Huynh demonstrated that several existing high-order finite element methods, namely the Discontinuous Galerkin and Spectral Difference schemes, could be recovered as special cases of the more general FR formulation. It was subsequently shown by Vincent et al. that the recovered methods fit within a specific class of FR

schemes termed the Vincent-Castonguay-Jameson-Huynh (VCJH) or Energy Stable Flux Reconstruction schemes. Because of the apparent similarities between the existing high-order schemes when cast within the ESFR framework, investigators were motivated to describe these relations elegantly and have now proven that all ESFR formulations are in fact equivalent to certain filtered DG schemes in strong form; this was originally shown in 1D [1] and subsequently generalized to straight-sided tetrahedral elements [8]. Further, it has recently been demonstrated that the DG scheme in strong form with inexact mass matrix exactly recovers the ESFR g2 scheme [3, 4].

The novel contributions of this work include a general demonstration that ESFR schemes can be interpreted as filtered DG schemes in both strong and weak form. It is further shown that ESFR schemes are capable of treating nonlinear flux terms through higher-order quadrature rules in the same way as DG schemes and that the two formulations are consequently equivalent for nonlinear fluxes, a contradiction of the previous conclusion [3]. Finally, all results are generally extended to higher dimensional formulations using curvilinear elements.

We first derive the reference DG and ESFR schemes in 1D and provide much of the notation which is used throughout the paper. We then first recover the original proof [1], then generalize the result to show that all ESFR schemes can be recovered from the filtering of a DG scheme in strong form using arbitrary basis functions for both the exact and inexact mass matrix formulations; that this generalization is still equivalent for nonlinear fluxes when a higher-order quadrature is employed is also demonstrated. Next, we demonstrate the computational equivalence of the strong and weak forms, recovering the previously

demonstrated equivalence for the DG scheme [6] as a special case, and consequently extend all results to the weak formulation; we note that this is also done in the generalized 3D curvilinear element setting. Results are then extended generally to all higher dimensional formulations. 1D numerical validation has thusfar been performed to confirm theoretical results and we anticipate performing 3D testcases on curvilinear elements before the conference. Finally, conclusions, specifically discussing the possible extension of results presented here to the optimal FR (OFR) scheme [2] as well as the potential for bridging the gap between the DG and FR communities, are then given.

Due to space limitations, the derivation is omitted. A complete proof will be provided for the final submission.

ACKNOWLEDGMENTS

We would like to gratefully acknowledge the financial support of the Natural Sciences and Engineering Research Council of Canada and McGill University. Philip Zwanenburg would like to thank Nicolas Ringue for feedback and several helpful discussions.

REFERENCES

- [1] Y. Allaneau and A. Jameson. Connections between the filtered discontinuous galerkin method and the flux reconstruction approach to high order discretizations. *Computer Methods in Applied Mechanics and Engineering*, 200(49–52):3628–3636, 2011.
- [2] K. Asthana and A. Jameson. High-order flux reconstruction schemes with minimal dispersion and dissipation. *Journal of Scientific Computing*, pages 1–32, 2014. .
- [3] D. De Grazia, G. Mengaldo, D. Moxey, P. E. Vincent, and S. J. Sherwin. Connections between the discontinuous galerkin method and high-order flux reconstruction schemes. *International Journal for Numerical Methods in Fluids*, 75(12):860–877, 2014.
- [4] G. J. Gassner. A kinetic energy preserving nodal discontinuous galerkin spectral element method. *International Journal for Numerical Methods in Fluids*, 76(1):28–50, 2014.
- [5] H. T. Huynh. *A Flux Reconstruction Approach to High-Order Schemes Including Discontinuous Galerkin Methods*. American Institute of Aeronautics and Astronautics, 2014/11/06 2007.
- [6] D. Kopriva and G. Gassner. On the quadrature and weak form choices in collocation type discontinuous galerkin spectral element methods. *Journal of Scientific Computing*, 44(2):136–155, 2010.
- [7] P. Vincent, P. Castonguay, and A. Jameson. A new class of high-order energy stable flux reconstruction schemes. *Journal of Scientific Computing*, 47(1):50–72, 2011.
- [8] D. Williams and A. Jameson. Energy stable flux reconstruction schemes for advection-diffusion problems on tetrahedra. *Journal of Scientific Computing*, 59(3):721–759, 2014.

Evaluation of Hybrid RANS/LES Turbulence Models For Gas-Turbine Combustor-Relevant Flows

Jonathan P. West¹, Clinton P. T. Groth¹, and John T. C. Hu²

¹ Institute for Aerospace Studies, The University of Toronto, 4925 Dufferin St., Toronto, Ontario, M3H 5T6, Canada

² Pratt & Whitney Canada, 1801 Courtneypark Dr., Mississauga, Ontario, L5T 1J3, Canada

Email: j.west@mail.utoronto.ca

ABSTRACT

In order to investigate the use of hybrid turbulence models utilizing both Reynolds-averaged Navier-Stokes (RANS) and large eddy simulation (LES) strategies, also known as hybrid RANS/LES, for turbulent gas-turbine combustor-relevant flows, numerical simulations for several representative/benchmark cold-flow cases were performed using a standalone RANS model, a detached eddy simulation (DES) model, a standalone LES model, and a dynamic LES (DLES) model. Predictions of each model were compared to available experimental data. Through this process, the predictive performance of DES, a common hybrid RANS/LES method, was shown to be subject to several established deficiencies, such as modelled stress depletion (MSD) for some of the benchmark cases studied. However, it was shown that a very fine pre-LES zone mesh could be used to manipulate MSD regions and improve DES performance. Additionally, the predictive performance of DES was significantly improved in comparison to the other treatment techniques for turbulence for cases with complex geometry and flow features, such as swirl. The latter are more representative of the flows of practical interest here.

1 INTRODUCTION AND MOTIVATION

As discussed by Wilcox [1], Reynolds-averaged Navier-Stokes (RANS) methods for turbulence models provide a low computational cost and good near wall modelling but must model the full range of turbulent scales without resolving even large scale turbulent features. As a result, they often fail to properly capture information about unsteady flow features and turbulent mixing. Large eddy simulation (LES) methods only model turbulent structures on the smallest

scales and resolve the remaining scales without modelling. However, LES methods are generally deemed computationally too expensive near walls for practical three-dimensional geometries unless paired with an empirical wall model, which in many cases is less sophisticated than a RANS model near walls. Hybrid RANS/LES methods can potentially circumvent the weaknesses of standalone RANS and LES models by using LES outside of boundary layers and reserving RANS only for near wall and/or under resolved regions.

2 SCOPE OF PRESENT STUDY

In order to investigate the use of hybrid RANS/LES methods for turbulent combustor-relevant flows, several cold (non-reacting) flow configurations were selected as being representative of the flow types often encountered in practical gas-turbine combustion devices. The specific cases considered were as follows:

- Backward facing step case of Driver *et al.* [2];
- Propane-jet in co-flow case of Schefer [3];
- Swirl stabilized combustor case of Steinberg *et al.* [4];
- Hydrogen-jet in cross-flow case of Steinberg *et al.* [5];
- Bluff body flame stabilizer in duct flow case of Sjunnesson *et al.* [6]; and
- Bluff body burner in co-flow case of Dally *et al.* [7].

For comparative purposes, these cases were also simulated not only with a hybrid RANS/LES method but, using the same mesh, with a RANS method, an LES method, and a dynamic LES (DLES) method. The commercial code Ansys FLUENT was used as it includes implementations of all these approaches allow-

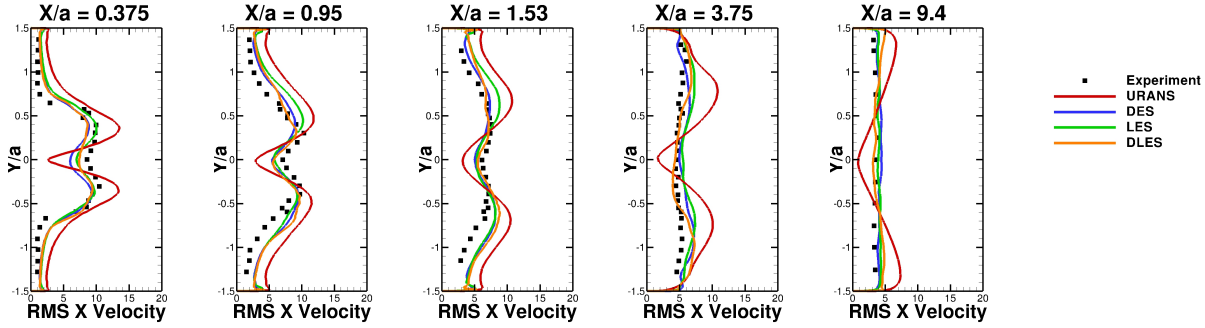


Figure 1: Unstructured mesh mean streamwise RMS velocity comparisons ($\tau_{ii}^{Modelled}$ included) (m/s).

ing for comparison with minimal change in the underlying numerical method. The specific turbulence models considered were as follows:

- RANS Model: Shear Stress Transport (SST) $k-\omega$ model of Menter *et al.* [8];
- Hybrid RANS/LES Model: Detached eddy simulation (DES) model derived from the SST $k-\omega$ RANS model of Menter *et al.* [8];
- LES Model: Smagorinsky-Lilly model proposed by Smagorinsky [9] with wall modelling; and
- DLES Model: DLES variant of the Smagorinsky-Lilly model as described in Germano *et al.* [10] with wall modelling.

Within the Ansys FLUENT solver, the SIMPLE algorithm of Patankar *et al.* [11] was utilized for pressure-velocity coupling and the second-order upwind scheme of Barth *et al.* [12] for pressure interpolation. Time advancement was accomplished with second-order dual time stepping in which subiterations at each time step were used to converge temporally discretized equations.

3 PRELIMINARY RESULTS AND ANALYSES

As an example, results for the Bluff body flame stabilizer in duct flow case of Sjunnesson *et al.* [6] are presented. This case utilizes a triangular obstruction in a duct as an analogy of a flame holder. Under cold-flow conditions this case produces vortex shedding phenomenon. Unsteady RANS (URANS), DES, LES, & DLES simulations of this case were conducted on an unstructured mesh containing 3 628 355 cells. The total simulation time used was $T = 0.15s \sim 5(L/U_{inlet})$, where L is the domain length, prior to collecting flow statistics and again for collecting flow statistics. The mean RMS velocity results are shown in Figure 1, as can be seen DES, LES, & DLES all produce good re-

sults in comparison to URANS. This is likely due to the unsteady swirling nature of the flow.

REFERENCES

- [1] D. Wilcox. *Turbulence Modeling for CFD Third Edition*. DWZ Industries, Inc., La Canada, California, 3 edition, 2006.
- [2] D. Driver and L. Seegmiller. Features of a reattaching turbulent shear layer in divergent channel flow. *AIAA Journal*, 23(2):163–171, 1985.
- [3] R. Schefer. Data base for a turbulent, nonpremixed, nonreacting propane-jet flow. Technical report, Sandia National Laboratories Combustion Research Facility, Livermore, California, 12 2011.
- [4] A. Steinberg, C. Arndt, and W. Meier. Parametric study of vortex structures and their dynamics in swirl-stabilized combustion. *Proceedings of the Combustion Institute*, 34(2):3117–3125, 2013.
- [5] A. Steinberg, R. Sadanandan, C. Dem, P. Kutne, and W. Meier. Structure and stabilization of hydrogen jet flames in cross-flows. *Proceedings of the Combustion Institute*, 34(1):1499–1507, 2013.
- [6] A. Sjunnesson, C. Nelsson, and E. Max. Lda measurements of velocities and turbulence in a bluff body stabilized flame. *Laser Anemometry*, 3:83–90, 1991.
- [7] B. Dally, D. Fletcher, and A. Masri. Flow and mixing fields of turbulent bluff-body jets and flames. *Combustion Theory and Modelling*, 2(2):193–219, 1998.
- [8] F. Menter, M. Kuntz, and R. Langtry. Ten years industrial experience with the sst turbulence model. In K. Hanjalić, Y. Nagano, and M. Tummers, editors, *In Turbulence, Heat and Mass Transfer*, pages 625–632. Begell House, Inc., 4 edition, 2003.
- [9] J. Smagorinsky. General circulation experiments with the primitive equations i: The basic experiment. *Monthly Weather Review*, 91(3):99–164, 1963.
- [10] P. Germano, U. Piomelli, P. Moin, and W. Cabot. A dynamic subgrid-scale eddy viscosity model. *Physics of Fluids*, 3(7):1760–1765, 1991.
- [11] S. Patankar and S. Spalding. A calculation procedure for heat, mass and momentum transfer in three-dimensional parabolic flows. *International Journal of Heat and Mass Transfer*, 15:1787–1806, 1972.
- [12] T. Barth and D. Jespersen. The design and application of upwind schemes on unstructured meshes. In *Aerospace Sciences Meeting*, number AIAA-89-0366 in 27. AIAA, 1989.

Flow alteration around a wall-mounted bluff body using a front splitter plate

T.K. Sheel^a, G. Nasif^b, R. Balachandar^b, and R.M. Barron^b

^a*Department of Mathematics, Trent University, Canada*

^b*Department of Mechanical, Automotive & Materials Engineering
University of Windsor, Canada*

Email: tarunsheel@trentu.ca

ABSTRACT

Three-dimensional numerical simulations using the Detached Eddy Simulation (DES) based on the unsteady $k - \omega$ SST turbulence model has been carried out to evaluate the characteristics of shallow wake flow past a wall-mounted bluff body with a front mounted rectangular splitter plate. An approaching flow with fully developed boundary layer is employed to model the effect of shallow flow. The splitter plate facilitates the separation of flow pattern in front and consequently influences the flow in the wake. Streamwise positive directed velocity is observed in the wake centerline at horizontal planes close to the bed. The flow features in the shallow wake are identified using the λ_2 -criterion. The presence of the coherent structures in the near-bed region and their influence on the wake region is discussed. The simulation results have been compared with and without the splitter plate, and the potential impact on bridge pier scour is explored.

1. OBJECTIVES

Shallow open channel flows have received much attention from researchers because of their natural occurrence in the environment. Coherent structures that are observed in shallow wakes are believed to appear as a result of interaction of the approaching boundary layer like flow with the body, interaction of the flow with the bed and flow instability. The objective of the study is to numerically investigate the flow field in the presence of the splitter plate and to obtain detailed information on the three-dimensional flow-structures occurring downstream of the bluff body immersed in an open channel flow. The effect of wall-mounted front splitter are observed and investigated carefully.

2. COMPUTATIONAL METHODOLOGY

A schematic illustration of the flow, along with the co-ordinate system adopted in this study, is shown in Figure 1. A 1.25 m length, 1.0 m width and 0.1 m deep open channel is considered as the computational domain. A sharp-edged bluff body with and without a front mounted rectangular plate is placed 0.25 m downstream of the inlet plane. The bluff body width is $D = 0.03$ m and the front mounted rectangular splitter plate is 0.04 m in length and 0.05 m in height (half of the water depth). The turbulent boundary layer velocity profile, which is extracted from a separate simulation for an 8.0 m open channel flow with water depth $H = 0.1$ m, is employed as the inlet boundary condition. The velocity near the free surface is $U_\infty = 0.45$ m/s. The flow Reynolds number is $Re \approx 7500$ based on D and U_∞ . The flow domain is discretized using approximately 8.1×10^6 polyhedral cells with a prism boundary layer clustering near the bed, around the bluff body and in the wake region. The DES based on unsteady $k - \omega$ SST turbulence model is implemented in ANSYS Fluent 14.0. This model is applicable to wall-bounded flows and incorporate modifications for low Reynolds number effects and shear flow spreading. An implicit unsteady formulation, second-order discretization and the SIMPLE algorithm have been used for pressure, momentum, turbulent kinetic energy and specific dissipation rate equations. The standard wall function is used to model the near-wall region. The values of non-dimensional wall distance Y^+ at the near-wall locations fall within acceptable limits ($Y^+ > 30$). Walls are treated as no-slip boundaries, a symmetry boundary condition is

imposed for the free surface, and an outflow condition is applied at the exit of the domain.

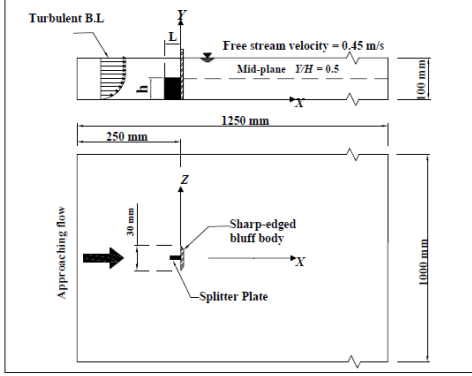


Figure 1: Schematic illustration of the flow

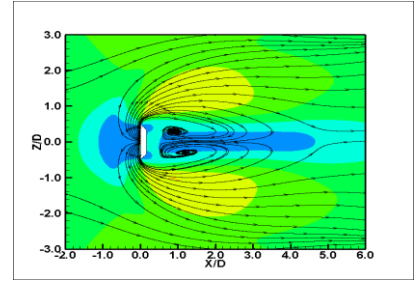
3. RESULTS AND DISCUSSIONS

The instantaneous and time-averaged quantities near the bed for the wake flow field are presented.

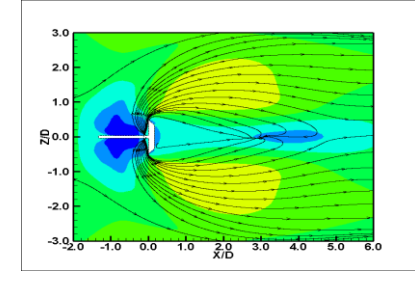
Streamtraces of the time-averaged velocity provide information on the relative mixing between different regions in the flow field. Figure 2 presents the time averaged stream traces superimposed with velocity contour at near the bed. Several horizontal slices are extracted at different locations from the bed in between range $0.01 \leq Y/H \leq 0.08$. The significant effect of splitter plate can be observed in the wake region behind the bluff body when compared with without splitter plate [1]. The dynamics of the coherent structures have a significant influence on characteristics of the shallow wake. The large scale structures are generally identified by a closed-streamline based vortex identification scheme such as λ_2 -isosurface. Figure 3 shows the λ_2 -isosurface for the present calculation shaded by x -vorticity component. It is observed that the wake flow contains a reasonable number of structures in terms of rotation. The entire depths of vortices are seen to be shed from both sides of the bluff body. The remarkable difference of shedding and rotation of vortices near the bluff body can be seen when compared with and without splitter plate.

REFERENCES

- [1] T. Sheel, G. Nasif, R. Balachandar & R. Barron, Breakdown of the horseshoe vortex around a wall-mounted bluff body using a front splitter plate, Proceeding, CFDSC-CSME 2014, Toronto, Canada.



(a)



(b)

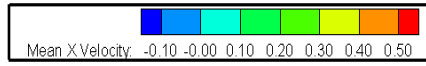
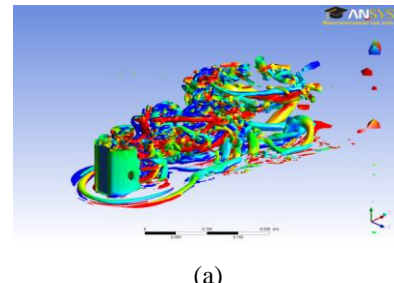
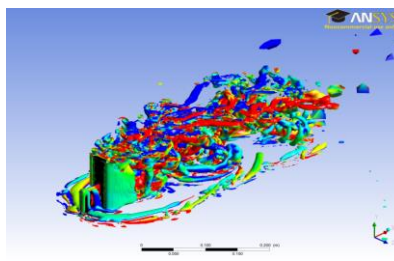


Figure 2: Streamtraces of the mean velocity field superposed with mean streamwise velocity contours for horizontal plane at $Y/H = 0.01$ (a) without splitter plate, (b) with splitter plate



(a)



(b)

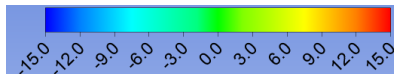


Figure 3. λ_2 -isosurface colored by x -vorticity component (a) without splitter plate, (b) with splitter plate.

Flow regimes of mesoscale circulations forced by inhomogeneous surface heating

M Alamgir Hossain and Jahrul M Alam

Department of Mathematics and Statistics, Memorial University of Newfoundland, Canada

Email: mah782@mun.ca

ABSTRACT

The urbanization is one of the extreme processes, which increases uncertainty in future climate projections. Flow regimes of mesoscale circulations associated with surface heating due to urbanization have been investigated using a wavelet based computational fluid dynamics (CFD) model. The results of our numerical model have been validated against that of a laboratory model, as well as reference numerical simulations. Characteristics of urban induced circulations have been studied for surface heat flux perturbation (H_0) between 25 W m^{-2} and 930 W m^{-2} , and the results have been analyzed against available boundary layer measurements under similar physical conditions. Our primary study shows that urban/rural heat flux anomaly introduces strong oscillations in the convective boundary layer (CBL), and transfers a fraction of the turbulent kinetic energy vertically through internal waves. Such results complement previous investigators' hypothesis that temporal oscillations in urban-induced mesoscale circulations are primarily due to downscale energy cascade. Although a further detailed study is necessary, the present numerical observations provide useful feedback for impacts of urbanization on regional climate.

1 INTRODUCTION

Human modification of the earth's surface makes city areas significantly warmer than their surrounding rural areas during the daytime when the sun heats the surface. Usually cities have a mean temperature that is 8 to 10 degrees more than the surrounding rural areas. Air circulation due to this heat source is known as the urban heat island (UHI) circulation. Surface heterogeneity due to urbanization usually triggers mesoscale circulations which influence boundary layer meteorology and atmospheric turbulence. For example, observational data analysis indicate that there is a strong

urban induced influence on local storm, precipitation, convective rolls, lake-breeze, heatwave etc [5]. The increase of clear-air turbulence by 40-90% over the period 1958-2001 in the North Atlantic, USA, and European sectors clearly demands a detailed investigation of how urbanization enhances vertical transport and mixing through internal waves. The characteristics of UHI was studied previously with theoretical models, laboratory experiments (e.g. [3]), and numerical simulations (e.g. [2, 5]).

This paper summarizes results of the numerical investigation of mesoscale circulations triggered by a wide range of surface heat fluxes, and illustrates the coherent flow regime associated with penetrative turbulence. Our simulations explains the onset of temporal oscillations due to urbanization, and indicate that a strong interaction exists between urban heating and vertical transport of turbulent energy through the mechanism of internal wave excitation. We now provide a brief outline of the methodology.

2 GOVERNING EQUATIONS

Considering the ground surface is flat, the influence of the terrain is ignored, the flow is uniform along the span-wise direction, and the Coriolis force is negligible, the following large eddy simulation model of the compressible dry atmosphere has been solved:

$$\frac{\partial \pi}{\partial t} + u_j \frac{\partial \pi}{\partial x_j} = -\pi \frac{\partial u_i}{\partial x_i}, \quad (1)$$

$$\frac{\partial u_i}{\partial t} + u_j \frac{\partial u_i}{\partial x_j} = -\theta_0 \frac{\partial \pi}{\partial x_i} + \frac{\partial \tau_{ij}}{\partial x_j} + \frac{\theta}{\theta_0} g \delta_{i3}, \quad (2)$$

$$\frac{\partial \theta}{\partial t} + u_j \frac{\partial \theta}{\partial x_j} + w\beta = \frac{\partial \tau_{\theta j}}{\partial x_j}, \quad (3)$$

where $\beta = \partial \bar{\theta} / \partial z$, δ_{ij} is the Kronecker delta and τ_{ij} is the turbulent momentum flux and $\tau_{\theta j}$ is the turbulent heat flux. The nondimensional pressure is $\pi =$

$\left(\frac{p}{p_0}\right)^{R/C_p}$, where $p_0 = 1000$ mb and $c_p = 1004 \text{ J kg}^{-1} \text{ K}^{-1}$ is the specific heat of dry air at constant pressure.

3 MODEL DESCRIPTION

The design of this UHI simulation is analogous to the large eddy simulation presented by [5]. A stably stratified atmosphere is initialized in which the average potential temperature $\bar{\theta}$ increases linearly with height i.e $\bar{\theta} = \theta_0 + \beta z$, where θ_0 is the potential temperature at the surface and β is a constant vertical gradient of potential temperature. The heating of the surface owing to the sun in the morning generates a heat flux toward the air. The nocturnal stable boundary layer tends to diminish due to this surface heat flux. Finally, a mixed layer (h) is produced due to turbulence by means of high intensity heat flux and mixed air flow. The simulation domain is taken 100 km long in the horizontal direction, 2 km wide in the vertical direction and the heated region is either 10 km or 20 km.

4 NUMERICAL METHOD

In contrast to classical atmospheric models, which typically employ an explicit scheme for predicting the resolved scale flow along with a subgrid scale parameterization scheme for the vertical mixing that is based on an ensemble mean, we have adopted a wavelet method for filtering large eddies; such a model is not usually practised in the field of atmospheric modelling. More specifically, the dynamics of the resolved flow is projected on a Krylov subspace at each time step to eliminate numerical damping of coherent eddies, where the large energy containing eddies are filtered with interpolating wavelets along with a Smagorinsky model for the subgrid scale processes (e.g. [1]).

5 RESULTS

The flow regime shows a strong dependence on the surface heat flux. For a smaller value of the surface heat flux, temporal oscillations are weak, and the mesoscale circulation is approximately steady and symmetric along the center of the UHI. This flow regime agrees with the numerical simulation of [2] and the experimental results of [3]. However, for a larger surface heat flux (e.g. $H_0 = 925.92 \text{ W m}^{-2}$), airflow shows vertical turbulent mixing, accompanying with coherent vortical structures. The mixed layer height in the turbulent region at ~ 800 m is capped with the inversion layer as shown in Fig. 1 and it can rise in adding shear turbulence due to background wind. Fi-

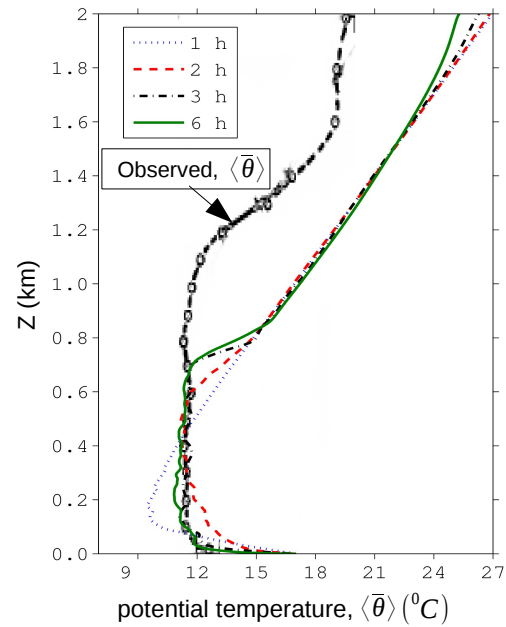


Figure 1: A comparison of $\langle\bar{\theta}\rangle$ with the field measurement of the CBL profile (e.g. [4]).

nally, the generation of gravity waves are investigated of the stable atmosphere which appears due to the penetrative convection.

REFERENCES

- [1] J. M. Alam, R. P. Walsh, M. A. Hossain, and A. M. Rose. A computational methodology for two-dimensional fluid flows. *Int. J. Numer. Meth. Fluids*, 75(12):835–859, 2014.
- [2] T. Dubois and R. Touzani. A numerical study of heat island flows: Stationary solutions. *Int. J. Numer. Meth. Fluids*, 59:631–655, 2009.
- [3] R. Kimura. Dynamics of steady convections over heat and cool islands. *J. Meteor. Soc. Japan*, 53:440–457, 1975.
- [4] C.-H. Moeng. A large-eddy-simulation model for the study of planetary boundary-layer turbulence. *Journal of the Atmospheric Sciences*, 41(13):2052–2062, 1984.
- [5] N. Zhang, X. Wang, and Z. Peng. Large-eddy simulation of mesoscale circulations forced by inhomogeneous urban heat island. *Boundary-Layer Meteorol.*, 151:179–194, 2014.

High density difference buoyant displacement flows in an inclined 2D channel

Avinash Shevally¹, Nikhilesh Podduturi¹, Ali Eslami², Seyed Mohammad Taghavi², and Kamran Alba¹

¹ Department of Engineering Technology, University of Houston, Houston, TX, USA

² Department of Chemical Engineering, Laval University, Québec, QC, Canada

Email: kalba@uh.edu

ABSTRACT

Displacement flow of a light fluid by a heavier one in an inclined 2D channel is investigated numerically. Significantly higher fluids density differences (still in the Boussinesq approximation limit) compared to our previous studies have been used in the simulations to study their effect on the back flow of the displaced fluid. It has been observed that although driving buoyancy force increases for higher density differences, the amount of displaced fluid back flow reduces due to the increased mixing of the fluids originated from the interfacial instabilities. The transition from non-instantaneous to instantaneous displacement flows is characterized on dimensionless flow map.

1 INTRODUCTION

We present a computational study of high-Péclet-number miscible displacement flows in an inclined 2D plane channel with a heavier fluid displacing a lighter one downwards (density-unstable configuration). Newtonian fluids with the same viscosity are considered in the Boussinesq limit. This study is the continuation of our previous work on 2D channel displacement flows [1, 2] which have been focused on mostly low density differences. Here, our study covers a wider range of density differences. Thus, many of the flows are strongly inertial, driven by the imposed flow rate as well as by buoyancy represented by the densimetric Froude number Fr . Our motivation comes from industrial applications present in construction and completion of oil & gas wells such as primary cementing. In such operation buoyancy and inertia are nearly always significant. The novelty of the current work is in studying channel displacement flows at higher density differences which have not been studied so far.

2 DISPLACEMENT IN CHANNELS

Our fully inertial computations solve the full 2D Navier-Stokes equations with the liquid species modeled via a scalar concentration, C :

$$[1 + \phi At][\mathbf{u}_t + \mathbf{u} \cdot \nabla \mathbf{u}] = -\nabla p + \frac{1}{Re} \nabla^2 \mathbf{u} + \frac{\phi}{Fr^2} \mathbf{e}_g, \quad (1)$$

$$\nabla \cdot \mathbf{u} = 0, \quad (2)$$

$$C_t + \mathbf{u} \cdot \nabla C = \frac{1}{Pe} \nabla^2 C. \quad (3)$$

Here $\mathbf{e}_g = (\cos \beta, -\sin \beta)$ and the function $\phi(C) = 2C - 1$ interpolates linearly between -1 and 1 for $C \in [0, 1]$. No slip conditions are satisfied at the walls. The displacing fluid enters fully developed with plane Poiseuille profile at $x = -L/4$ and outflow conditions are applied at $x = 3L/4$.

2.1 Computational method

Equations (1)-(3) are discretised using a mixed finite element, finite volume method. The Navier-Stokes equations are solved using Galerkin finite element method. The divergence-free condition is set by an augmented Lagrangian technique. A fixed time step is used for the Navier-Stokes equations, advancing from time step N to $N + 1$. The pressure is approximated at time step $N + 1$ (semi-implicit method regarding the nonlinear terms). The convective velocity is approximated at time step N while the linear spatial derivatives of the velocity are approximated implicitly at time step $N + 1$. More details of the computational methodology and the governing system of equations are given in [1].

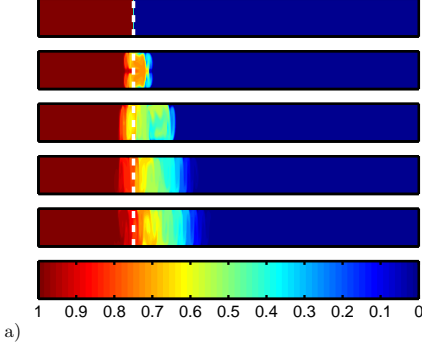


Figure 1: Snapshots of the numerical simulations at times $t = [0, 8, \dots, 32]$ run for $\beta = 0^\circ$, $Re = 100$ and $Fr = 0.054$. The last image at the bottom of the figure is the colourbar of the concentration values. The size of the domain shown is 1×105 . The dashed lines in figure a shows the position of the imaginary gate valve.

3 RESULTS

We now present the computational results. We first give a general description of the mixing pattern we have observed in our displacement flow simulations run for higher density differences. Channel displacement flows at higher density differences (or At numbers) have not been studied from the perspective of mixing and the trailing front behaviour so far. Here we aim to see how the degree of mixing and instability is different compared to our previous simulations carried for lower At [1, 2]. Figure 1 shows snapshots of a simulation with parameters $\beta = 0^\circ$, $Re = 100$ and $Fr = 0.054$. A *Rayleigh-Taylor* type mushroom initially forms due to the unstable density configuration. The figure also suggests that the mixing is very efficient across the channel (compare to Fig. 4 in [2] for instance).

We now classify our displacement flows in terms of being instantaneous or non-instantaneous, over the range of parameters computed. Figure 2 shows such a classification in the dimensionless plane of Fr and $Re \cos \beta / Fr$. The blue squares data in this figure indicate instantaneous displacement and all others are non-instantaneous flows. The figure is an extension of our previous regime classification given in Fig. 6b in [2]. Although there are approximately 20 more simulations added to our previous picture for instantaneous/non-instantaneous regime classification, we have covered a much wider range of $Re \cos \beta / Fr$ (almost twice as large) due to a higher choice of At in the current study. The pattern shown in Fig. 2 at higher $Re \cos \beta / Fr$ values suggests that the required Froude number for transitioning from a non-instantaneous to an instantaneous displacement decreases with $Re \cos \beta / Fr$. This first

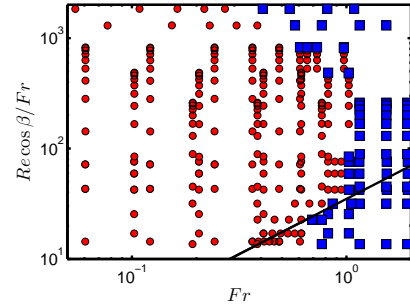


Figure 2: Classification of our results for the full range of simulations plotted in the plane of Fr and $Re \cos \beta / Fr$. The instantaneous displacement flows are marked by squares and non-instantaneous ones by circles. The arrows indicate that the non-instantaneous flows zone shrinks at higher $Re \cos \beta / Fr$ values due to a more efficient mixing.

seems counter-intuitive because at higher density differences (large $Re \cos \beta / Fr$), one expects an enhanced counter-current flow due to the buoyancy. The required mean imposed flow velocity (or correspondingly Fr) then required to overcome the back flow also is expected to be higher. However, we observe that the minimum Froude number required to transition to instantaneous flows in fact decreases with $Re \cos \beta / Fr$. One explanation is that although the density difference is higher, increased instability and transverse mixing in the system does not allow the displaced layer to travel upwards the gate valve. In fact the instability induces an efficient and strong transverse mixing suppressing the back flow and counter current motion. This is somehow similar to the famous *Boycott* effect.

REFERENCES

- [1] S. Taghavi, K. Alba, T. Seon, K. Wielage-Burchard, D. Martinez, and I. Frigaard. Miscible displacement flows in near-horizontal ducts at low Atwood number. *J. Fluid Mech.*, 696:175–214, 2012.
- [2] K. Alba, S. Taghavi, and I. Frigaard. Miscible heavy-light displacement flows in an inclined two-dimensional channel: A numerical approach. *Phys. Fluids*, 26(12):122104, 2014.

Ice Accretion Effects on Fully-articulated Rotors in Forward Flight

Daniel Kelly¹, Sahar Choukir¹, Wagdi G. Habashi¹, Marco Fossati¹, Giuseppe Quaranta² and Pierangelo Masarati²

¹ CFD Laboratory, McGill University, Montreal, QC, H3A 2S6, Canada

² Department of Aerospace Science and Technology, Politecnico di Milano, Italy

Email: daniel.kelly@cfdlab.mcgill.ca

1. INTRODUCTION

Flight into icing conditions poses particular problems for rotorcraft. Of primary concern is the accumulation and presence of ice on the blades which alters their aerodynamic shape and increases surface roughness. This circumstance has significant effects on helicopter stability, power/torque characteristics and thrust capabilities. Additionally, ice buildup alters the weight distribution on the rotorcraft, and can act to modify the inertia and aeroelastic properties of the blades themselves.

A cost-effective numerical methodology is proposed for assessing the effects of icing on rotor performance during the early design phases. This methodology aims to accelerate the development of helicopter icing protection systems, while reducing the cost and complexity of the certification process. The procedure has already been assessed in the case of the hover flight regime [1]; the present work addresses the case of forward flight.

Several approaches in the literature address icing on helicopter rotors via a tightly-coupled CFD/CSD methodology [2][3]. These approaches perform ice accretion using a 2D solver, neglecting centrifugal effects on the water film and the resulting impact on ice formations. In order to cope with the competing requirements of moderate computational efforts desired for early design phases and the interest in solution accuracy, a CFD/CSD loosely-coupled approach is proposed: a 3D ice accretion process with reference to 2D blade section airflow and droplet computations. This approach accounts for the spanwise motion of a water film, and permits more realistic heat exchange in 3D. Improved accuracy in ice geometry may thus be obtained at a minimal computational cost, comparable to 2D simulations.

2. METHODOLOGY

The methodology adopts a loose-coupling approach between solvers for airflow, ice accretion and rotor dynamics. An isolated model of the helicopter rotor is defined within a multibody context [4]. With reference to an aerodynamic library, the multibody solver identifies a trimmed condition in forward flight, iterating until a converged solution is reached. Blade motion and rotor kinematics are extracted for one complete rotation, describing flow conditions at each blade section. A series of coupled airflow and droplet impingement simulations are then conducted at each blade section in 2D. Angle of attack and induced velocity oscillations are applied through an unsteady simulation, with azimuthally-varying conditions varying according to a sinusoidal law.

The primary contribution of this work is in adopting a hybrid 2D/3D methodology for ice accretion. Here, resulting CFD solutions for aerodynamic shear stress, heat transfer and droplet impingement are gathered from each 2D section. These results are interpolated onto a 3D surface mesh of the blade to be used in the ice accretion process. A quasi-unsteady formulation accounts for water film motion and ice growth in a time-accurate fashion, applying icing in small timesteps with reference to airflow and droplet conditions at the blade's azimuthal position. The process assumes that, for the majority of the blade regions of interest for icing, airflow is dominant in the chordwise direction. Glaze ice conditions are thus better addressed by accounting for 3D motion of a water film, driven chordwise by aerodynamic forces and spanwise by centrifugal body forces.

Aerodynamic performance of the resulting 2D blade geometries are computed through a CFD flow solver, accounting for both geometric displacement and the addition of surface roughness due to icing. The

dynamics solver then computes an updated solution for rotor trim, and determines changes to the performance, dynamic behavior and vibrations of the rotor. Better capturing of the ice may be achieved through small accretion timesteps with re-meshing.

3. PRELIMINARY RESULTS

As a preliminary test for the CFD-icing approach in forward flight, a validation of the methodology is performed against icing tunnel tests from the NASA Icing Research Tunnel (IRT) [5]. These experiments used a scaled Sikorsky helicopter rotor and fuselage. 2D meshes were generated at four blade sections, representing available ice shape and performance data. Airflow, droplet impingement and icing computations were conducted with FENSAP-ICE [6].

Parameters for test condition “17” are highlighted in Table 1. The 93-second encounter was evaluated through both a single-shot and multi-shot regime with three equal accretion periods. A visualization of ice shapes at 70% span is illustrated in Figure 1. A fair agreement with experimental data is shown.

Table 1: Experimental Parameters for Test Condition “17”

Parameter	Units	Value
Tip Speed	m/s	205.7
Advance Ratio	-	0.198
Static Temp.	°C	-15.0
Liquid Water Content (LWC)	g/m ³	0.5
Vol. Diameter	μm	15 (Monodisp.)
Icing Time	sec	93

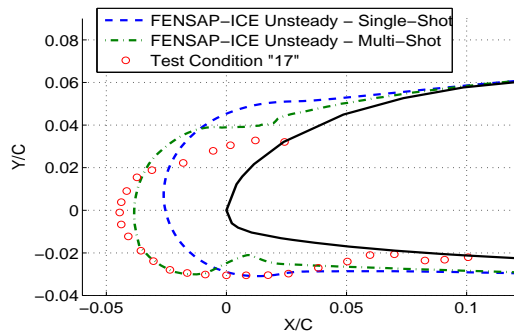


Figure 1: Resulting computational and experimental icing shapes from Test Condition “17”

4. FUTURE WORK AND FINAL REMARKS

An experimental forward flight icing case has been selected for the validation and assessment of the method as indicated in the work of Hanks et al. [7]. Results will address performance degradation in terms of time-dependent loss in thrust and increase in

torque. Secondary effects of icing will also be considered, including changes to blade vibrational characteristics, rotor inertia and pitch-link loading.

The proposed computational framework will provide a design-phase instrument that will be capable of estimating degradations as a consequence of ice accretion. This will provide a valuable tool to improve the design of ice protection systems. Moreover, the proposed method will serve as a starting point for developing more sophisticated fully-coupled approaches for the simulation of helicopter icing and dynamic characteristics.

ACKNOWLEDGEMENTS

The authors would like to thank Bell Helicopter Textron Inc. for the technical and financial support as part of a NSERC Industrial Research Chair for Multi-disciplinary Analysis and Design of Aerospace Systems. The authors would also like to thank Dr. Isik Ozcer of Ansys, Inc. for his technical advice.

REFERENCES

- [1] Kelly, D., Fouladi, H., Fossati, M., Habashi, W. G., Alicino, R., Quaranta G., and Masarati, P., "Assessment of Ice Accretion Effects on Rotor Dynamics via Multi-Body and CFD Approaches," AHS 70th Annual Forum, Montreal, Canada, 2014.
- [2] Narducci, R., Orr, S., and Kreeger, R. E., "Application of a High-Fidelity Icing Analysis Method to a Model-Scale Rotor in Forward Flight," NASA TM-2012-217122, Jan 2012.
- [3] Rajmohan, N., Bain, J., Michael, N., Lakshmi, S., Flemming, R., Egolf, T. A., and Kreeger, R., "Icing Studies for the UH-60A Rotor in Forward Flight," AHS Aeromechanical Specialists' Conference Proceedings, January 2010.
- [4] Ghiringhelli, G. L., Masarati, P., Mantegazza P., and Nixon, M. W., "Multibody Analysis of the 1/5 Scale Wind Tunnel Model of the V-22 Tiltrotor," American Helicopter Society 55th Annual Forum, Montreal, Canada, May 25-27, 1999.
- [5] Flemming, R.J., Britton, R.K., "Experimental Investigation of the Effects of Ice Accretion on a Main Rotor in the NASA Glenn Research Icing Tunnel," RITA TR 02-D-07-03.1-P3 Vol. 2, Sep. 15, 2003
- [6] Beaugendre, H., Morency F., and Habashi, W. G., "FENSAP-ICE's Three-Dimensional In-Flight," *Journal of Aircraft*, Vol. 40, (2), March 2003, pp. 239-247.
- [7] Hanks, M., Higgins, L., and Diekmann, V., "Artificial and Natural Icing Tests Production UH-60A Helicopter," United States Army Aviation Engineering Flight Activity, 1980.

Laminar and Turbulent Natural Convective Heat Transfer from a Horizontal Isothermal Circular Element with an Unheated Inner Circular Section

Patrick H. Oosthuizen

Department of Mechanical and Materials Engg., Queen's University, Kingston, Canada ON K7L 3N6

Email: *oosthuiz@queensu.ca*

ABSTRACT

Extensive studies of natural convective heat transfer from heated upward facing plane horizontal elements of various shapes have shown that a correlation equation applying to elements of various shapes can be derived as long as the Nusselt and Rayleigh numbers are expressed in terms of a suitable mean length scale. These previous studies have essentially considered only cases where the elements are composed of a single continuous area. Examples of these include circular, square and rectangular shaped elements. It is not clear that correlation equations derived for an element with a continuous area will apply in cases where the element has an outer heated section and an inner unheated section. In this study, attention has been given to steady natural convective heat transfer from an isothermal circular heated element with an inner adiabatic circular unheated section embedded in a large flat adiabatic surface. The situation considered is shown in Fig. 1.

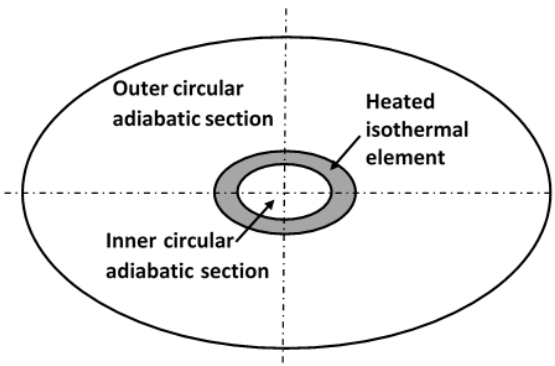


Figure 1 – Flow situation considered.

The element is at a higher temperature than the surrounding fluid. Consideration has been given to the case where the element is facing upward. This numerical study considers a range of conditions that involve laminar, transitional, and turbulent flows, and is one of a series of investigations of natural convective heat transfer rates from various horizontal heated element arrangements.

The flow has been assumed to be steady and fluid properties have been assumed constant except for the density change with temperature giving rise to the buoyancy forces. This was dealt with using the Boussinesq approach. The solution was obtained by numerically solving the governing equations subject to the boundary conditions using the commercial CFD solver ANSYS FLUENT®. The k -epsilon turbulence model was used with full account being taken of buoyancy force effects.

The heat transfer rate from the heated element expressed in terms of the Nusselt number based on the outer diameter of the element is dependent on:

- the Rayleigh number,
- the dimensionless size of the inner adiabatic element section expressed relative to the overall size of the element,
- the Prandtl number.

Results were obtained for a Prandtl number of 0.74 (i.e. for air). Rayleigh numbers between about 10^5 and 10^{14} were considered. The variation of the Nusselt number with Rayleigh number was explored in detail for various dimensionless inner adiabatic section diameters. The results were used to determine whether correlation equations can be derived that apply for all inner- to-overall element size ratios.

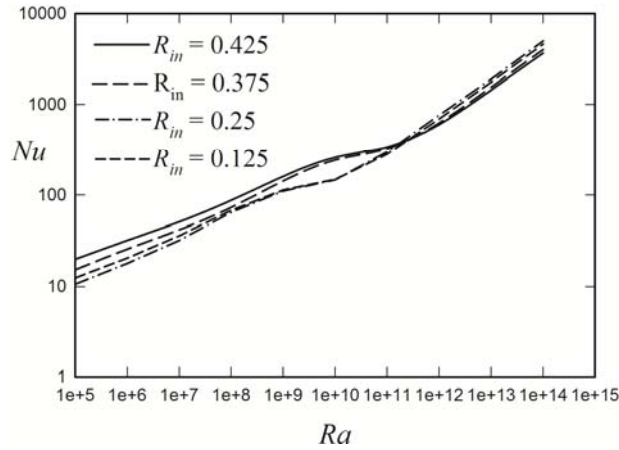


Figure 2. Variation of the mean heated element Nusselt number based on the element diameter with the Rayleigh number based on the element diameter for various values of the dimensionless inner heated element radius.

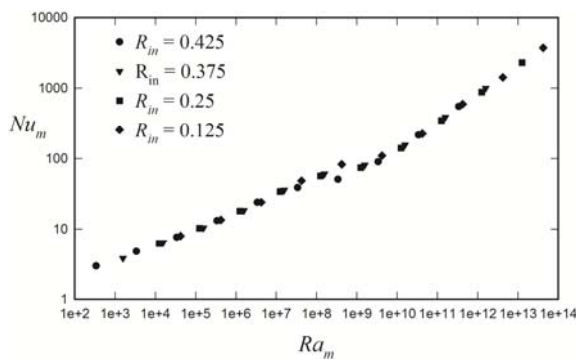


Figure 3 – Variation of the mean heated element Nusselt number based on the mean element size with the Rayleigh number based on the mean element size for various values of the dimensionless inner heated element radius.

Figure 2 shows typical variations of Nusselt number with Rayleigh number for various dimensionless inner adiabatic section sizes.

Variations of the Nusselt number based on the mean heated element size with Rayleigh number based on the mean heated element size for the dimensionless inner adiabatic section sizes for which results were given in Fig. 2 are shown in Fig. 3. The mean element size is defined by $m = 4 A / P$ where A is the surface area of the heated element and P is the total perimeter of the heated element. It will be seen from Fig. 3 that all the results in the laminar flow region fall on a single curve and that all the results in the turbulent flow region also fall on a single curve. The results in the transitional flow region, however, do not fall on a single curve.

ACKNOWLEDGEMENT

This work was supported by the Natural Sciences and Engineering Research Council of Canada (NSERC) through its Discovery Grant Program.

Laminar Free Convection from a Pair of Horizontal Cylinders: A Three-Temperature Problem

Seyed Sepehr Mohaddes Foroushani ¹, David Naylor ² and John L. Wright ¹

¹Department of Mechanical & Mechatronics Engineering, University of Waterloo, Waterloo, Canada

²Department of Mechanical & Industrial Engineering, Ryerson University, Toronto, Canada

Email: ssmohadd@uwaterloo.ca

ABSTRACT

Free-convective heat transfer from vertical arrays of horizontal cylinders has been the subject of numerous experimental and numerical studies. The vast attention this configuration has received is mainly due to its widespread application in the industry in such areas as heating and refrigeration, nuclear reactors, and electronics cooling. Although studies of free convection from arrays of horizontal cylinders usually assume uniform temperature for all the cylinders, the case where cylinders are at different temperatures has also been examined by some researchers, possibly starting with the work of Sparrow and Niethammer in 1981 [1].

Convection problems that involve more than two isothermal heat sources are identified as the multi-temperature convection problems class. The formulation of this class in terms of a single driving temperature difference and a single heat transfer coefficient, as is usually done in heat transfer research, does not properly reflect the physics of the problem. Paired heat transfer coefficients, which designate both the source and the sink of heat transfer, are suggested as a suitable alternative. The term paired is used here to refer to heat transfer between one source and another designated heat source. Overall heat transfer coefficients, on the other hand, correspond to heat transfer between one source and all the other sources. A paired heat transfer coefficient, h_{ij} , corresponding to isothermal sources at temperatures T_i and T_j , is defined according to Equation 1.

$$h_{ij} = -\frac{1}{A_j} \frac{\partial Q_j}{\partial T_i} \Big|_{h_{ij}=\text{const}} \quad (1)$$

Methods conventionally used in heat transfer research are not capable of resolving these paired

heat transfer coefficients. To address this difficulty, a new numerical technique, dubbed dQdT, is proposed. The dQdT technique entails a numerical solution of the governing equations and consequent solutions of the energy equation with perturbed boundary conditions. The condition of $h_{ij}=\text{const}$ in Equation 1 can be satisfied by solving the energy equation while the flow field and the fluid properties are fixed, *i.e.* prevented from changing after a perturbation is introduced in the temperature boundary conditions. Therefore, to calculate h_{ij} , a solution of the full set of governing equations (the baseline solution) is first obtained. Q_j is then computed by integrating the temperature field at source j . Next, T_i is perturbed by some finite amount, δT_i , and the energy equation only is solved again, using the velocity field and temperature-dependent properties from the baseline solution. The new rate of heat transfer at source j will differ from the baseline case by some amount, δQ_j . The paired heat transfer coefficient h_{ij} can then be calculated as shown in Equation 2.

$$h_{ij} = -\frac{1}{A_j} \frac{\delta Q_j}{\delta T_i} \quad (2)$$

In the present study, the dQdT technique is used to revisit the three-temperature problem of steady-state laminar free convection from two horizontal cylinders, with equal diameters but different surface temperatures, aligned vertically. A center-to-center spacing of two diameters, different Rayleigh numbers in the laminar regime ($Ra < 10^9$) and three temperature ratios, $r \in \{0.5, 1, 2\}$, are examined at $Pr=0.7$.

The commercial CFD code ANSYS FLUENT 14.0 is used to solve the steady-state equations of the conservation of mass, momentum and energy, using constant fluid properties and the Boussinesq approximation. The SIMPLE scheme was used for pressure-velocity coupling, along with second-order

discretization schemes for all of the equations. A grid convergence study was conducted using three non-uniform unstructured triangular grids. Based on the sum of total heat transfer rates at the two cylinders, a grid convergence index of 2% was obtained. In Figure 1, a schematic of the computational domain and the structure of the mesh are shown. Baseline solutions are validated against the experimental results of Sparrow and Neithammer [1].

Through paired Nusselt numbers obtained from dQdT, it is shown that while the upper cylinder has

no effect on heat transfer at the lower cylinder, the lower cylinder can influence heat transfer at the upper cylinder depending on the flow rate and the temperature ratio. It was further shown that total heat transfer from the pair is more sensitive to the temperature of the upper cylinder than to that of the lower cylinder. Likewise, compared to its effect on heat transfer at the lower cylinder, the ambient temperature has a larger effect on heat transfer at upper cylinder. The observed trends are compared to the reported results in the literature.

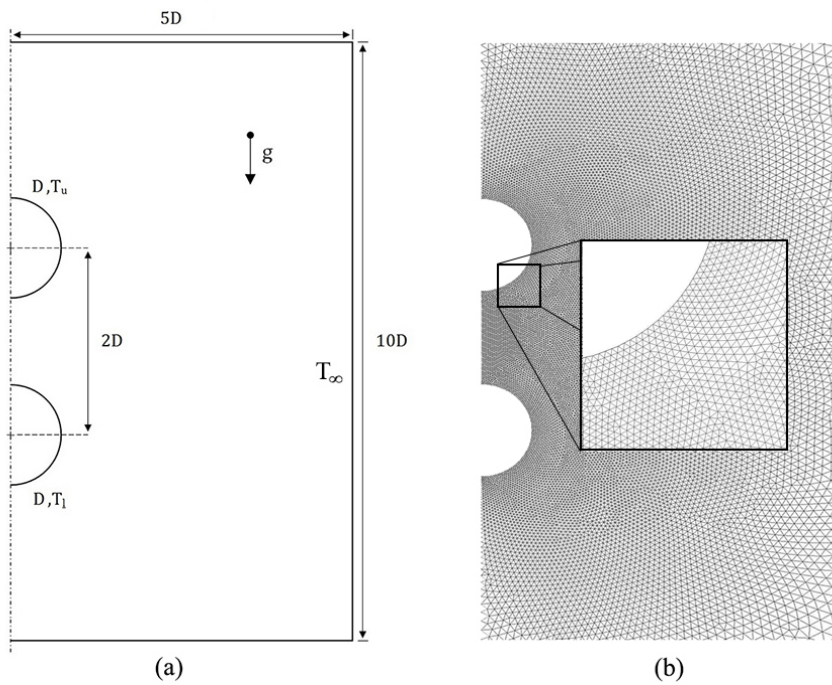


Figure 1 – Schematic of the computational domain (a) and mesh structure (b)

REFERENCES

- [1] E.M. Sparrow and J.E. Niethammer. Effect of vertical separation distance and cylinder-to-cylinder temperature imbalance on natural convection for a pair of horizontal cylinders. *Transactions of ASME*, 103:638-644, 1981

Large-eddy simulation of the flow around a single and two staggered infinite-length circular cylinders

Jody Soviak¹, BingChen Wang¹, and Eric Bibeau¹

Department of Mechanical Engineering, The University of Manitoba, Winnipeg, R3T 5V6, MB, Canada

Email: bc_wang@umanitoba.ca

Numerical simulations of turbulent flow around circular cylinders represents an important topic in fluid dynamics. The present study examines the flow field around both a single infinite length cylinder and two infinite length staggered cylinders. The staggered configuration of cylinders represents the most broad category of cylinder flows and can be defined according to the incidence angle α and horizontal and vertical center-to-center separation distances L/D and T/D respectively (see Figure for the definitions of T and L). Owing to the complex dynamics of eddy motions and interactions in the wake region, thus far, most of the studies on staggered cylinder flows are based on experimental approaches at relatively high Reynolds numbers [3]. In the literature, very few high resolution numerical and experimental studies have been reported on study of turbulence statistics of two cylinder flows. Due to the lack of published experimental data, there has been little numerical research into two cylinder flow of different physical configurations.

There are many applications of cylinder flows in engineering practice. For instance, the flow inside a shell-tube heat exchanger and wind field around a symmetrical building structure. The challenge of this type of study comes from the need for deeper understanding of the physics of the flow and dynamic interaction of different types of turbulent structures triggered by cylinders, which in turn imposes further challenges to numerical simulations in terms of modelling and predictive accuracy. Owing to the substantial advancements of computational technology over the last two decades, large-eddy simulation (LES) has become an important research tool for the simulation of turbulent flows as the results typically contain a greater level of accuracy compared to traditional turbulence modelling techniques. Thus far, LES has been applied to numerous simulations of flow around a single infinite length circular cylinder with many different sub-grid

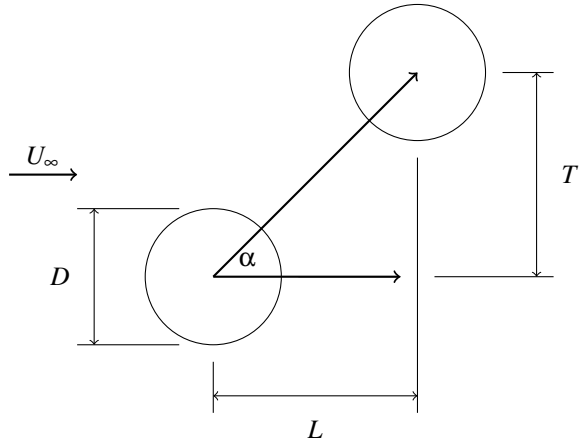


Figure 1: Two staggered cylinders

scale (SGS) models. A general literature survey confirms that the most commonly used SGS model in LES of a single cylinder is the Smagorinsky model (with either a constant or dynamic coefficient).

The current work utilises the open-source computational fluid dynamics (CFD) code OpenFOAM for examining the turbulent wake behind a single (for $Re = 3900$) and two staggered (for $Re = 3000$) infinite-length circular cylinders. Both constant and dynamic coefficient Smagorinsky models are utilized for performing LES. Based on the existing open-source code, the current research highlights the applications and improvements in open-source computational technologies. The results obtained from the simulations have been examined in terms of the first and second order turbulent statistics and the force and pressure coefficients on the cylinders. The energy spectrum at specified points in the single cylinder domain has also been examined.

Figure 2 displays the mean streamwise velocity (non-dimensionalized using the free-stream velocity (U_∞))

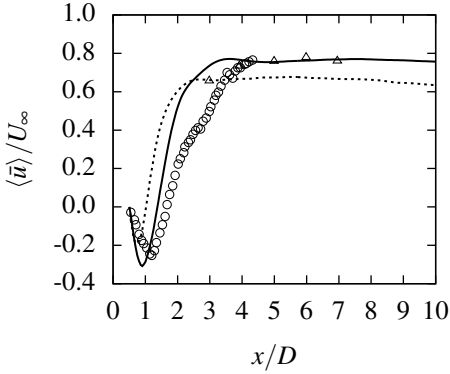


Figure 2: Non-dimensional streamwise velocity profile behind the single cylinder. Solid line: SM, dashed line: DSM, \circ : experimental data of Lourenco and Shih [1], \triangle : experimental data of Ong and Wallace [2].

within the central spanwise plane (located at $y/D = 0$) behind a single cylinder. The negative velocity observed in the immediate vicinity behind the cylinder reflects the presence of the recirculation region. Compared to the experimental data of Lourenco and Shih [1], both SGS models under-predict the length of the recirculation region; however, the result from the Smagorinsky model is closer to the experimental results. Immediately following the recirculation region, the streamwise velocity increases rapidly. In comparison with the experimental data of Ong and Wallace [2], the dynamic model slightly under-predicts the magnitude of this increase.

Figure 3 displays the mean spanwise velocity (non-dimensionalized using the free-stream velocity U_∞) for the staggered configuration at six different streamwise locations: $x/D = 1.00, 1.5, 2.00, 4.00, 7.00$ and 10.00 . The location $x/D = 0$ corresponds to the center of the downstream cylinder and the location $y/D = 0$ corresponds to the center of the separation gap between the two staggered cylinders. The first three profiles show two distinct peaks, located behind each of the two cylinders, where the pattern is in agreement with that described by Sumner [3]. Due to the asymmetrical geometry, the difference in the magnitudes of these two peaks is expected. Furthermore, in comparison with the single cylinder case, it is clear that the spanwise location ($y/D = 1.25$) of the peak for the upstream cylinder does not correspond to the centreline ($y/D = 0.5$) across the cylinder. Instead, a high pressure region caused by the downstream cylinder forces the wake to deviate away, resulting in the peak to be offset from the centreline of the upstream cylinder. As shown in Figure 3, in regions further downstream of the recirculation zone (for $x/D = 4.00 - 10.00$), the

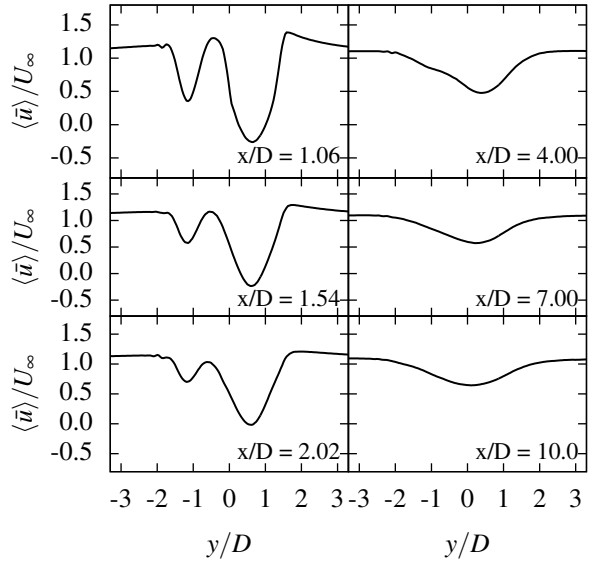


Figure 3: Non-dimensional spanwise velocity profiles at six different streamwise locations behind two staggered cylinders with the Smagorinsky Model

wake behind two cylinders merge and the profiles of $\langle \bar{u} \rangle$ exhibits a single-peaked pattern.

In the final paper, the streamwise evolutions of the velocity profiles characteristic of the single and two staggered cylinders are thoroughly examined. The dynamics of the turbulent wake flows and their interactions behind the cylinders are investigated by examining the first- and second-order velocity statistics, the pressure coefficient around the surface of the cylinders, vortex shedding frequencies and the energy spectrum.

REFERENCES

- [1] L. Lourenco and C. Shih. Characteristics of the plane turbulent near wake of a circular cylinder, a particle image velocimetry study. Technical report, CTR Annual Research Briefs, NASA Ames/Stanford University, 1994.
- [2] L. Ong and J. Wallace. The velocity field of the turbulent very near wake of a circular cylinder. *Experiments in Fluids*, 20(6):441–453, 1996.
- [3] D. Sumner. Two circular cylinders in cross-flow: a review. *Journal of Fluids and Structures*, 26(6):849–899, 2010.

Modelling of Outflow Control in Steam Assisted Gravity Drainage Process

Lei Li¹, Carlos F. Lange¹ and Yongsheng Ma¹

¹*Department of Mechanical Engineering, University of Alberta, Edmonton, Alberta, T6G 2G8*

Email: *carlos.lange@ualberta.ca*

ABSTRACT

Steam Assisted Gravity Drainage (SAGD) has been applied as a reliable oil recovery technology in oil sand industry. In SAGD, two horizontal wells i.e. injection well and production well are drilled parallel into the formation. The injection well continuously injects high pressure steam to heat the bitumen and reduce its viscosity. With the viscosity down, bitumen moves to the lower production well. Due to the dissipation along the injection well and the formation inhomogeneity, uneven steam distribution may form, which reduces production dramatically. Outflow Control Device (OCD) regulates the steam flow rate under specific pressure drop through it. OCDs coupled with slotted liner or screens are applied in the injection well to control the steam injected into the system and maintain optimized steam distribution. It is significant to research the OCD performance in order to achieve optimum design and thus guarantee high production rate. However, few detailed studies have been done on this topic and the majority of them only focus on the effect imposed on the reservoir. In our research, preliminary simulation of OCD has already been done. A more detailed and accurate model to investigate the OCD will be proposed.

1. INTRODUCTION

Steam injection control has proven to be an important method for SAGD performance improvement. However, the research on the OCD performance and its effect on the reservoir is not sufficient [1]. In order to establish an accurate model for OCD, this abstract is organized as follows. In the following section, the application conditions of OCD are introduced. As this research will be conducted by phases, the method involved and the improvement in the modelling will also be proposed in this section. At last, a brief

conclusion of the work done and a prospective outlook are put forward.

2. OCD MODELLING

The OCD analyzed here is a commercial product, which has been installed in practice. The OCD functions based on the orifices annularly located on it. The working conditions of OCD are listed as follows:

- Orifice size: 1/4in-1in (Mainly depends on the pressure drop);
- Steam quality: 92.5-95%;
- Flow rate: 200-300m³/d CWE;
- Pressure inside tool: Determined by the program at each location;
- Annular pressure (Max operating pressure): 1500-2500kPa;
- Pressure drop per orifice: 20-100kPa;
- Flow velocity per orifice: <30m/s.

The modelling of OCD will follow a sequence from simple to complex. The research will be conducted through the following three phases.

2.1 Single Phase Flow

With the given steam flow rate and inner diameter of OCD, the average steam velocity in the device can be calculated:

$$\bar{v} = \frac{Q}{\frac{1}{4}\pi d^2} = \frac{300m^3/d}{\frac{1}{4} \times 3.14 \times 0.15875^2 m^2} = 0.1755 m/s$$

Though the actual steam quality is 95%, the dry steam is assigned as the fluid to simplify the simulation. According to the steam table [2], under the pressure of 2500kPa, the steam saturation temperature is 226.1°C, the steam density is

13kg/m^3 and the steam dynamic viscosity is $1.66252 \times 10^{-5}\text{kg/m}\cdot\text{s}$. So the Reynolds number can be calculated:

$$\text{Re} = \frac{\rho v d}{\mu} = \frac{13\text{kg/m}^3 \times 0.1755\text{m/s} \times 0.15875\text{m}}{1.66252 \times 10^{-5}\text{kg/m}\cdot\text{s}} = 21785$$

For flow in the pipe, the transition Reynolds number is 4000. So the steam flow in the OCD is turbulent. With the calculation done, the boundary conditions are specified as follows:

- Inlet average velocity: 0.1755m/s ;
- Pressure of inner outlet: 2500kPa ;
- Pressure of outer outlet: 2450kPa [3];
- Two symmetry boundary;
- The other surfaces are defined as wall.

Boundary conditions are assigned to the corresponding regions. CFX has the International Association for the Properties of Water and Steam (IAPWS) embedded in the system [4], which can be invoked directly to increase the accuracy of the steam flow simulation. As a result, CFX is applied as the solver for this problem. In the initial setup, the advection scheme applied is upwind, and turbulence model is k-Epsilon. Monitoring points are set in the flow space to check the corresponding physical quantity. A sample simulation result is shown in Fig. 1.

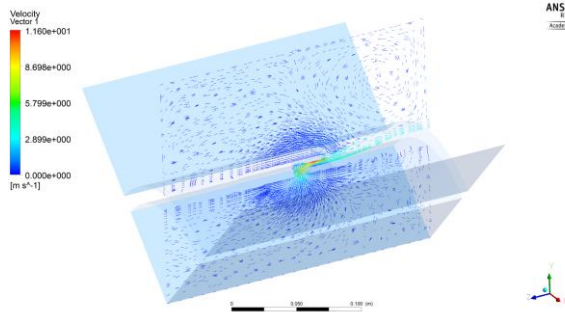


Fig. 1: Velocity vector in mid-plane.

2.2 Application Conditions

The real conditions of an existing OCD application will be approximated as much as possible. To achieve this, the OCD geometrical features, such as orifice shape and distribution, will be considered. In addition, OCD is usually tubing-deployed and covered by slotted liner or screens. So, the effect of the other parts related to OCD should also be studied. The model established in this phase will focus on the flow fields adjacent to the slotted liner and within the injection well.

2.3 Effect Analysis

In this phase, the effect of the simplification of the parameters will be investigated. Different turbulence models will be tested to figure out the best one for OCD simulation. Ideal gas model and real gas model will be compared to discover the impact on the results. OCD flow field will also be analyzed by Fluent to evaluate the different commercial software's effectiveness on OCD modelling.

3. CONCLUSION

The background of OCD application i.e. SAGD process was briefly introduced. OCD plays a vital role in achieving a balanced steam distribution along the injection well thus maintains a high production rate. Different from the research on the overall simulation of the whole reservoir, our work focuses on the flow adjacent to the OCD in order to study the flow pattern and details under various conditions. A simplified model with dry steam has already been done. Further research will be conducted according to the scheduled steps.

ACKNOWLEDGEMENTS

The authors would like to acknowledge the financial support from China Scholarship Council, University of Alberta doctoral recruitment scholarship, NSERC Discovery grant, and RGL Reservoir Management Inc collaboration fund. The authors would also like to highlight the technical input, i.e. the OCD geometrical model files, from RGL. Special thanks go to Michael Leitch for his timely support by providing the technical parameter input.

REFERENCES

- [1] Medina, M. Design and field evaluation of tubing-deployed passive outflow-control devices in steam-assisted-gravity-drainage injection wells. *SPE Production & Operations*, (Preprint, 2015)
- [2] Steam table. <http://www2.spiraxsarco.com/us/resources/steam-tables/wet-steam.asp>
- [3] S. K. Das. Well bore hydraulics in a SAGD well pair. *SPE/PS-CIM/CHOA International Thermal Operations and Heavy Oil Symposium*, 2005
- [4] CFX tutorial. <http://www.ansys.com/Industries/Academic/Tutorials/Curriculum+Resources/Tutorials,+Examples+&+Curriculum>

Modelling Particle Dispersion in a Turbulent Channel Flow by Using CFD

M. Ahmadi Golestan¹, G. Khosravi¹, S. Hallé¹, F. Morency¹

¹*Mechanical Engineering Department, École de Technologie Supérieure, Montreal, Canada*

Email: *maryam.ahmadigolestan.1@ens.etsmtl.ca*

1. INTRODUCTION

By increasing the usage of aerosol particles in industrial applications and the growing concern on inhalation exposure to these particles, many studies have been conducted focusing on their motion and deposition on surfaces in recent years [1]. The level of exposure to these aerosol particles can be estimated if numerical models can determine the main phenomena affecting their aerodynamic behaviour. This could help in the design of appropriate protection equipment for the workers. Numerical simulation of airborne particles behaviour is attractive because it gives information about their distribution everywhere in a workplace. Deposition of particles in turbulent channel flows is important process in industrial and environmental applications [2]. Therefore, in this paper we simulated particle deposition in a channel flow by Computational Fluid Dynamics (CFD) model. Compared to experimental studies, Computational Fluid Dynamics (CFD) has the advantage that it does not impose any health risk. CFD models can provide detailed spatial distribution of air velocity, pressure, temperature and contaminant concentration solving simultaneously the conservation equations of mass, momentum, energy and species concentration [3].

2. OBJECTIVES

This study aims to use CFD to predict particle concentration and velocity for 2D and 3D channel flow.

2.1. SPECIFIC OBJECTIVES

The specific objectives are to:

- Select an appropriate model and numerical method;

- Validate results with 2D and 3D channel flow by comparison with empirical correlations for velocity profile, entry length and wall particle removal rate;
- Study the effects of air flow velocity and particle size on particles dispersion in channel flow.

3. METHODOLOGY

The dispersion of airborne particles was simulated numerically using CFD (Code_Saturne, version 3.0.0). Single-phase fluid was simulated based on Eulerian unstructured co-located finite volume approach that solves incompressible Reynolds-averaged Navier-Stokes equations for meshes with cells of any shape [4]. For two phases flow (fluid containing particles), an Eulerian-Lagrangian approach was used wherein individual particles are simulated based on a Probability Distribution Function (PDF) approach [5]. In Lagrangian simulation of particle deposition, first, the flow is mathematically solved and then particles are injected into the simulated flow and particle trajectories are tracked. This one way coupling simulation is valid if the mass concentration of particles is assumed to be very much smaller than the air density. With this assumption, particles do not affect the momentum of the fluid however the fluid influences the particle momentum [6].

To validate the results of air-flow field, laminar and turbulent flow in a 2D channel was simulated. Turbulent flow was simulated by "K-epsilon linear production" model. Simulations results of laminar channel flow were validated with theoretical equations. For the turbulent flow, results were validated with empirical correlation [7]. Simulation results showed good agreement with the theoretical equations and empirical correlation. To validate the results of particle dispersion in 3D channel, it was considered that the flow containing particles is injected from the inlet. Particles were released with the same velocity as the one of the airflow. The

effects of airflow velocity and particle size on particles dispersion were studied. Velocity profile, entry length and wall particle removal rate will be compared with empirical correlations.

REFERENCES

- [1] A. Li and G. Ahmadi. Dispersion and deposition of spherical particles from point sources in a turbulent channel flow. *Aerosol Science and Technology*. 16(4): 209-226, 2007.
- [2] J. Zhang and A. Li. CFD simulation of particle deposition in a horizontal turbulent duct flow. *Chemical Engineering Research and Design*. 86 (1): 95-106, 2008.
- [3] Z. Bin, C. Chen C and Z. Tan. Modelling of ultrafine particle dispersion in indoor environments with an improved drift flux model. *Aerosol Science*. 40 (1): 29-43, 2009.
- [4] C. Beauchêne, N. Laudinet, F. Choukr, et al. Accumulation and transport of microbial-size particles in a pressure protected model burn unit: CFD simulations and experimental evidence. *BMC Infectious Diseases*. 11(1): 58-66, 2011.
- [5] K. Dorogan. Numerical schemes for the hybrid modelling of gas-particle turbulent flows. *PhD Dissertation*, Aix Marseille University, 2012.
- [6] M.R. Sippola and W.W. Nazaroff. Particle deposition from turbulent flow: Review of published research and its applicability to ventilation ducts in commercial buildings. *PhD Dissertation*, University of California, 2002.
- [7] P.J. Pritchard, *Fox and McDonald's Introduction to Fluid Mechanics*, 8th edition, Wiley, 2011.

Non-Newtonian Simulations for the Design of a Micro-Couette Blood Flow Device

Matt Laporte, Rym Mehri and Catherine Mavriplis

*Department of Mechanical Engineering
University of Ottawa, 161 Louis Pasteur, Ottawa, ON, K1N 6N5, Canada*

Email: *Catherine.Mavriplis@uottawa.ca*

ABSTRACT

A micro-Couette blood flow device has been designed previously by numerical simulation and tested experimentally. The device allows for a two fluid flow, where a first fluid (phosphate buffered saline in the case of the experiments) entrains blood, to provide a Couette-like blood layer in which to study the aggregation of red blood cells under controlled, i.e. constant shear, conditions. While the Newtonian simulations provided enough guidance to design and test the device, this paper investigates more precise definition of the flow, using non-Newtonian models. A spectral element Navier-Stokes solver is used with variable viscosity and a stress formulation to account for the non-Newtonian effects. Validation of the numerical model is presented for non-Newtonian jets, for which an analytical solution exists for power law fluids. Then non-Newtonian simulations of a polymer solution entrained by water in the device are provided and compared to experimental results of the same fluids in order to validate the model.

1 INTRODUCTION

In an effort to provide a better understanding of red blood cell aggregation, a Y microchannel device was designed, constructed and tested to provide a controlled shear micro-Couette flow. The device allows for controlled conditions under which red blood cell aggregation may be observed and quantified in order to characterize the non-Newtonian behaviour of blood. The microchannel device was designed by computational fluid dynamics using Newtonian models to predict layer thickness and velocity profiles for near constant shear rate. The device was fabricated using standard photolithography techniques out of PDMS (Poly-Di-Methyl-Siloxane). Experiments were conducted

with porcine and human blood to confirm the simulation predictions and to observe red blood cell aggregation [1]. The present paper aims to refine the simulations using non-Newtonian models to more accurately represent the blood layer in the microchannel flow.

2 SIMULATION SETUP

A Y-microchannel flow setup of water entraining a polymer solution of Polyox WSR-301 was modeled in two dimensions using a spectral element solver, Nek5000 [2] in order to validate the non-Newtonian simulation capabilities. The code allows for variable viscosity as a passive scalar as well as the full stress formulation to account for non-Newtonian effects. Spectral element methodology uses finite elements with high order polynomial approximations within each element to obtain high accuracy results to the Navier-Stokes equations. A power law fluid was used for the non-Newtonian modeling. For a power law fluid, the viscosity assigned at each point is calculated by multiplying the viscosity basis by the shear rate at that point to the exponent ($n-1$), where n is the specified power-law index. The average velocity in the water channel is 4 times that in the Polyox channel (1.0 vs. 0.25 in simulation units). The power law index for the Polyox was specified as $n=0.7868$ based on viscometer measurements of a solution of Polyox WSR-301 at 0.3% by mass. This same solution was used in the experiments. The spectral element computational grid had $K = 1280$ elements and used elemental polynomial orders of $N = 10$. The grid was refined toward the branching point and the inner walls of the branches and throughout the joined channel in the vicinity of the interface of the two liquids.

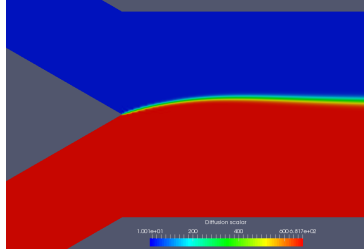


Figure 1: Calculated Polyox (red) and water (blue) layers in the microchannel downstream of the junction of the Polyox and water branches.

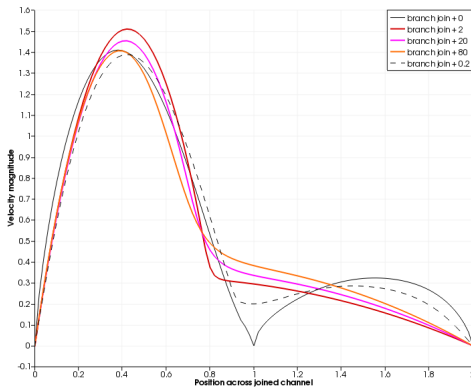


Figure 2: Calculated velocity profiles across the microchannel downstream of the junction of the Polyox and water branches.

3 RESULTS

The non-Newtonian shear-thinning behaviour of the Polyox is shown in Fig. 1 where the Polyox layer bows out into the water layer beyond the junction of the two fluids. The higher velocity water entrains the Polyox creating a layer of near constant shear as shown in the velocity profiles of Fig. 2 as the layer develops beyond the branching point. The calculated 2D velocity profiles qualitatively resemble those of the 3D experiments as shown in Fig. 3. The velocity profile of Fig. 3 is an average over 300 microns of the joined microchannel for the same geometry and conditions, albeit at a velocity ratio is 2.55 rather than 4. This corresponds roughly to an average of profiles near the +20 position profile shown in Fig. 2. The velocity distributions are also confirmed by PIV experimental results (see Figs. 4 and 5).

The comparison of the non-Newtonian simulation results with the experimental results of a flow of a polymer solution of known non-Newtonian behaviour provide confirmation that the simulation model can predict to some degree of accuracy the behaviour in the

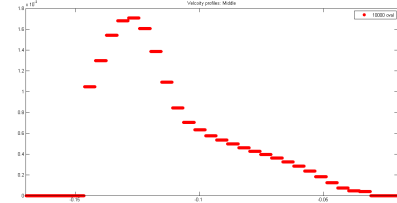


Figure 3: PIV (Particle Image Velocimetry) velocity profile over an average of 300 microns just downstream of the junction of the Polyox and water branches.

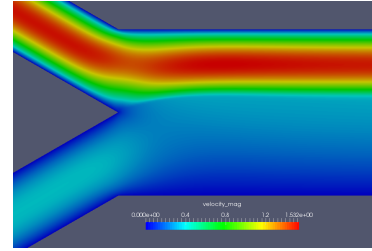


Figure 4: Calculated velocity magnitude distribution in the microchannel downstream of the junction of the Polyox and water branches.

microchannel device. Non-Newtonian simulations of blood entrained by PBS (phosphate buffered saline) in the same device will be presented and compared to experimental results in the final paper.

REFERENCES

- [1] R. Mehri, Master's Thesis, University of Ottawa, 2012.
- [2] P. F. Fischer and J. W. Lottes and S. G. Kerke-meier, <http://nek5000.mcs.anl.gov>, 2008.

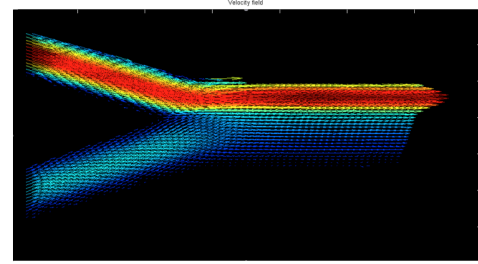


Figure 5: PIV (Particle Image Velocimetry) velocity magnitude distribution in the microchannel downstream of the junction of the Polyox and water branches.

NUMERICAL ANALYSIS OF TURBULENT CONVECTIVE HEAT TRANSFER IN HYDRO-GENERATORS

Dang D.-D.^{*,§}, X.-T. Pham^{*}

^{*} Dept. of Mechanical Engineering, École de technologie supérieure, Montréal, Québec, Canada

[§]Correspondence author. Fax: +1 514 609 3838 Email: ak58860@ens.etsmtl.ca

ABSTRACT

Upgrading procedure of hydro-generators requires a special attention on the thermal performance, besides the electro-magnetic considerations, to prevent exceeding the thermal properties of the insulating materials that can reduce the lifespan of the machine. In general, the heat generated inside the solid parts by the electromagnetic and electrical losses is channelled by the circulation of cooling air that is provided by the water-cooled radiator. In order to detect the location of hot-spot in the solid components, the conduction heat transfer was solved using the empirical correlation to evaluate the convective heat transfer coefficients for most of the convective boundaries of the rotor and stator. However, because of the complex flow structure observed, the heat transfer coefficients on the pole face and in the ventilation ducts need to be calibrated by the CFD analysis.

In the present work, the convective heat transfer coefficient was computed using the conjugate heat transfer that integrated in the commercial CFD code. And through this methodology to study the sensitivity of numerical parameters and the effect of operating conditions on the prediction of convective heat transfer coefficient on the rotor pole face. Figure 1 illustrated the two-dimensional configuration of the rotating prototype.

Two turbulence models based on RANS equations and Boussinesq eddy-viscosity approximation, the standard k-epsilon and the SST k-omega models, were employed to investigate the turbulence effect.

The Multiple Frame of Reference (MFR) was used for handling the unsteadiness of fluid flow in the rotor-stator system due to a strong interaction between the stationary and rotating components. The results computed using Frozen Rotor and Stage models were compared with the time-average transient simulation.

The energy equations for both fluid and solid domains were solved simultaneously with the constraints of heat flux balance and temperature continuity on the fluid-solid interface (conjugate conduction-convective heat transfer) for better representation of the thermo-fluid interaction.

The obtained results have shown that the fluid flow predicted by the Frozen Rotor model significantly varies depending on the rotor position relatively to the stator, meanwhile the Stage model demonstrated a good agreement with the time-averaged unsteady MFR model.

An asymmetric fluid flow and turbulent structure were obtained due to the rotation effect (at 300rpm and 50rpm), and these features have strong impact on the calculation of the heat transfer coefficient on the leading and trailing edges of the pole. It is interesting to observe the location of the minimum value of heat transfer coefficients was on the middle region of the pole.

Keywords: Multiple Frames Of Reference, conjugate heat transfer, hydro-generator, CFD, rotor-stator system, air-cooled.

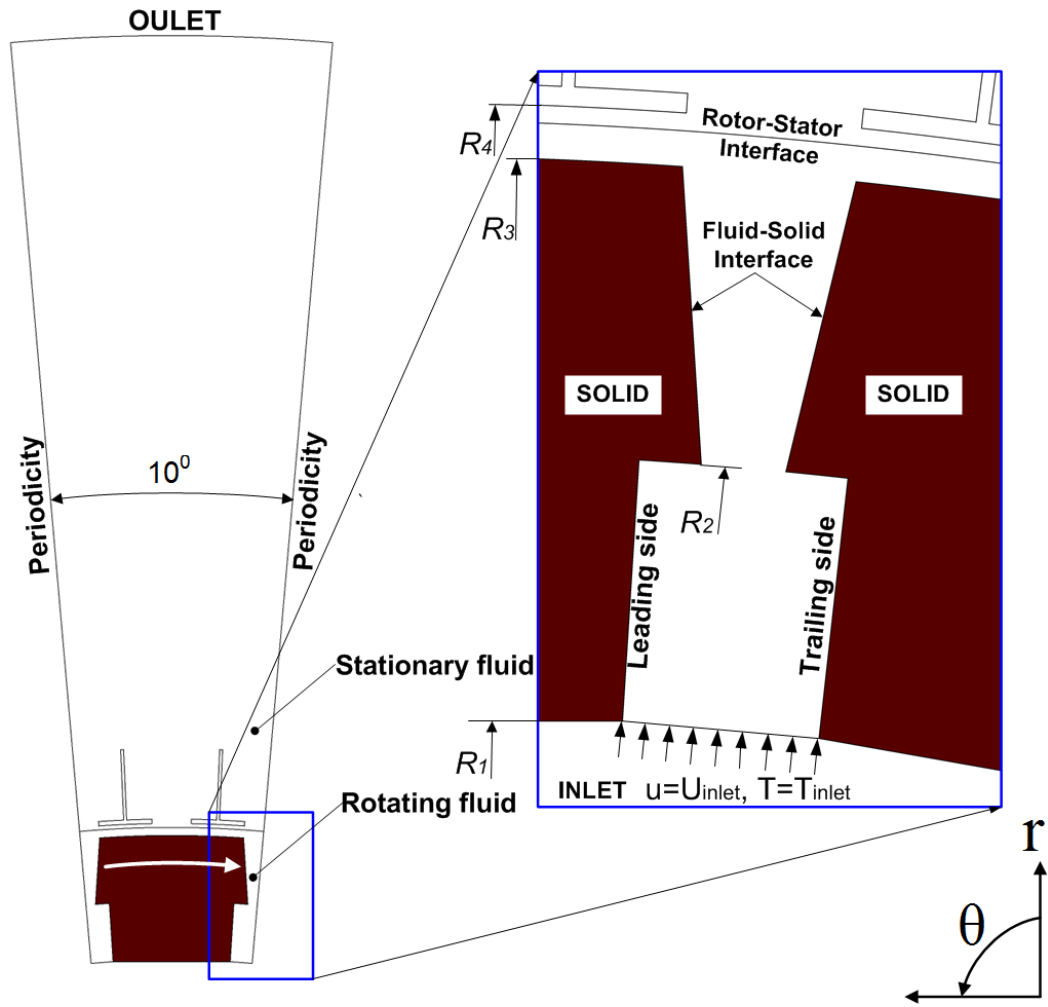


Figure 1 Geometry and computational domain

Numerical Implementation of a Plasma Actuator in a RANS Flow Solver with Experimental Comparison

M. Parenteau¹, F. Demers¹, E. Laurendeau¹, H.D. Vo¹

Department of Mechanical Engineering, Ecole Polytechnique de Montreal, Quebec, H3C 3A7, Canada

Email: *matthieu.parenteau@polymtl.ca*

ABSTRACT

Active flow control is an important research field in aerodynamics. Controlling boundary layer transition and separation is of great interest for transport aviation and there is currently considerable interest in the use of plasma actuators for active flow controls. Single-dielectric-barrier-discharge (SDBD) actuators have shown to be very promising devices.

This paper presents the results of a numerical implementation of a SDBD plasma actuator model[1] in a RANS flow solver to study the effect of plasma actuation on low-speed aerodynamics performances. This study focuses primarily on two cases, flow transition and flow separation. For both cases, the simulation is performed on the ONERA A-Airfoil which has a laminar bubble separation that triggers the boundary layer transition. In order to capture this effect, the RANS solver is coupled with the transition $\gamma - Re_\theta$ model and for validation, the simulations have been performed on a commercial (ANSY Fluent) and academic research (NSCODE[2]) RANS flow solver with experimental comparison as well.

To account for the effect of the walls of the wind tunnel where the experiments were conducted, the walls were modeled in the grid with attention to the boundary layer displacement thickness δ^* to allow an inviscid wind-tunnel wall boundary condition. Consequently, accurate results can be achieved with lower CPU time with a good convergence rate as shown in Figure 1.

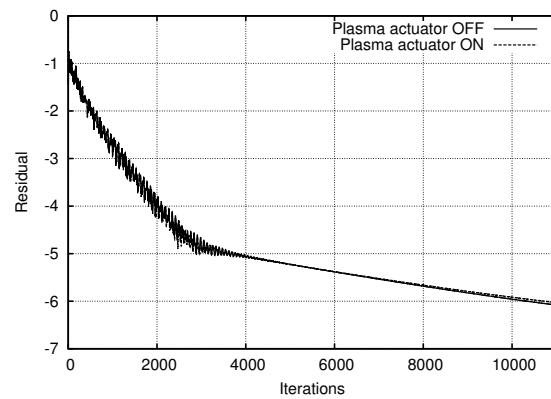


Figure 1: Convergence - 13.3 AOA & $U_\infty = 20 \frac{m}{s}$

To study the effect on boundary layer transition, the plasma actuator is placed at 26% of the chord of the airfoil with 3° angle of attack. The effect is analysed for three different freestream velocity ($15 \frac{m}{s}, 20 \frac{m}{s}, 30 \frac{m}{s}$). From Figure 2 and 3, we observed that the ionic wind pushes further downstream the laminar-turbulent transition from 31% to 52% of the chord and as a result, the friction drag is reduced. The numerical results from Figure 2 are consistent with the experimental results which confirms the quality of the grid with the wind-tunnel wall boundary implementation.

Finally, the effect on flow separation is evaluated by placing the actuator at 65% of the chord with the airfoil at 13.3° angle of attack. Without plasma actuation, flow separation occurs at around 65% of the chord, but the flow is reattached by the ionic wind generated by the SDBD as shown in Figure 4 and 5. This case is again analysed for three different freestream velocity ($15 \frac{m}{s}, 20 \frac{m}{s}, 30 \frac{m}{s}$).

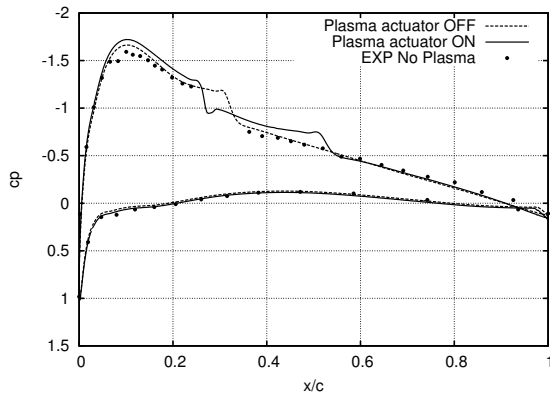


Figure 2: Pressure Coefficient - 3 AOA & $U_{\infty} = 20 \frac{m}{s}$

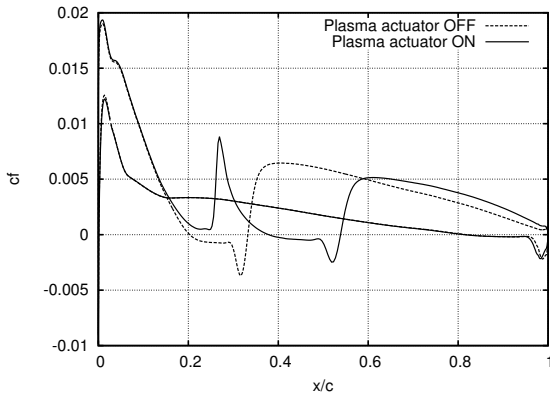


Figure 3: Friction Coefficient - 3 AOA & $U_{\infty} = 20 \frac{m}{s}$

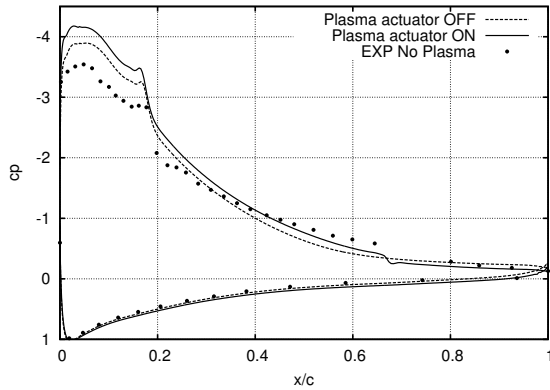


Figure 4: Pressure Coefficient - 13.3 AOA & $U_{\infty} = 20 \frac{m}{s}$

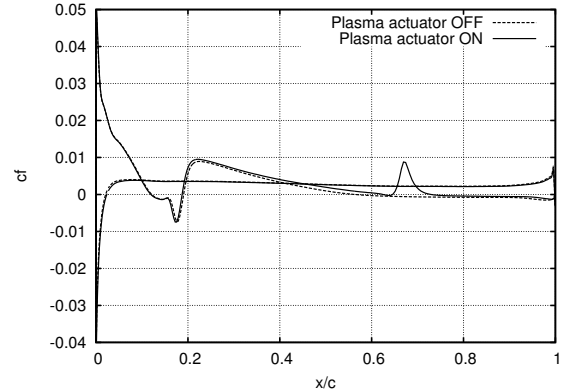


Figure 5: Friction Coefficient - 13.3 AOA & $U_{\infty} = 20 \frac{m}{s}$

The paper will discuss in detail the numerical implementation, the grid generation process and the comparisons to experimental data with/without SDBD actuators performed at Ecole Polytechnique.

REFERENCES

- [1] S. Lemire and H.D. Vo, Reduction of Fan and Compressor Wake Defect Using Plasma Actuation for Tonal Noise Reduction. *Journal of Turbomachinery*, 133(1), 011017 (2010)
- [2] Pigeon, A., Levesque, A. T., and Laurendeau, E., Two-Dimensional Navier-Stokes flow solver developments at Ecole Polytechnique de Montreal, *CFD Society of Canada 22 nd Annual Conference, CFDsc*, Toronto, CA, 2014.

Numerical Investigation of an Ethane-air Diffusion Flame Using Various Reaction Mechanisms

M L. CHIKH¹, F. MORENCY¹, M. LATEB² and F. GARNIER¹

¹ Department of Mechanical Engineering, École de Technologie Supérieure, 1100 Notre-Dame Street West, Montreal, QC H3C 1K3, Canada

² Center for Natural Resources Development and Protection, New Jersey Institute of Technology, 323 Martin Luther King Jr. Blvd., Newark, NJ 07102, United States

E-mail: mohamed-lamine.chikh.1@ens.etsmtl.ca

ABSTRACT

The combustion problems involve a strong coupling between chemistry and fluid dynamics [1]. Indeed, the non-premixed turbulent combustion is mainly based on complex and tightly coupled physical phenomena: the molecular diffusion of heat and species, turbulent flows, thermodynamic and chemical processes that require a large number of species and elementary reactions [2]. Thus, an accurate prediction of turbulent reacting flows must always firstly reproduce the phenomena that characterize the turbulent flow (e.g. heat transfer, molecular diffusion, convection, turbulent transport, etc.), and then simulate the chemistry of combustion taking into account the different species of the relevant chemical reactions (e.g. estimation of the fuel consumption rate, the formation of the combustion products, and pollutant species). Therefore, the modeling of the turbulent combustion is a task fairly complex.

In this work, a numerical study is carried out by considering a steady-state $k-\epsilon$ realizable model in order to provide a two-dimensional numerical model of an experimental setup – designed for a non-premixed ethane-air flame combustion – using Fluent software as a computational fluid dynamics tool. The study focuses on the comparison of combustion modeling results using the probability density function (PDF), which is a method that has been developed for non-premixed turbulent combustion [3], and by considering two reaction mechanisms. The first is a mechanism with a single overall reaction, available from Fluent database, while the second is a refined mechanism with two reactions of Westbrook and Dryer [4], taken from the literature.

Based on the work of Nemtallah and Habib [5] (numerical and experimental), a numerical study is

conducted and the comparison between the different results leading to the validation of the numerical model is performed over a wide ranges of different operating parameters including equivalence ratio, percentage of O₂ in the oxidizer mixture and fuel volume flow rate.

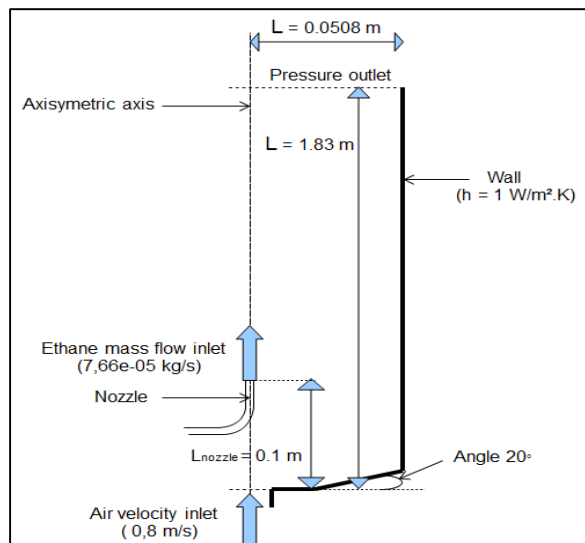


Figure 1: Diagram of the experimental setup with specific dimensions of the cylindrical combustion chamber.

The experimental setup configuration is described in the Figure 1. A central fuel jet consisting of 100% ethane (C₂H₆) – with an inner diameter of 6 mm – is emitted from a nozzle located along the central axis of a cylindrical combustion chamber. The latter is of 101.6 mm diameter (D_w) and of 1830 mm longer. The mean mass flow inlet of the fuel jet, \dot{m}_{Fuel} , is $7.66 \times 10^{-5} \text{ kg/s}$. An up-flowing air stream is supplied through an annular space of 25.4 mm diameter from the bottom of the cylinder with a constant velocity, U₀,

of 0.8 m/s. The exit section of the air flow is located at 100 mm below the fuel jet nozzle as can be seen in the Figure 1. It is worth noting that all dimensions are detailed and specified within this same figure.

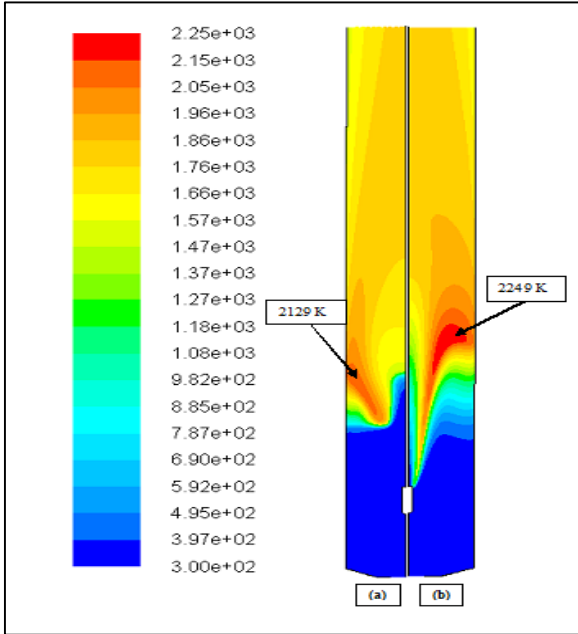


Figure 2: Overview of temperature contours (K) in the flame zone for two simulations using (a) a reduced scheme ($WD_{refined}$) and (b) a quasi-global scheme.

Through the Figure 2, one can note for both cases a quick temperature increase in the area near the Bunsen burner, which is considered one of the most important manifestations of combustion. It also shows that the distribution of the temperature along the combustion chamber is different. This difference is particularly seen at the reaction zone (flame zone) where the use of a reduced scheme seems to lead to a so-called (lifted flame). This drop seems to be induced by the additional reactions of production and destruction of the CO_2 present in the mechanism. Indeed, this fact has slowed down enough the chemical reactions to make them slower compared to the physical phenomena, such as convection and diffusion, hence the local flame extinction at the outlet of the tube carrying the fuel.

Figure 3 shows the evolution of the axial velocity along the central axis of the combustion chamber. It is to note that the use of a reduced scheme leads to the appearance of a recirculation zone upstream of the Bunsen burner. Indeed, slowing down the spread of the upstream fuel diffusion added to the Bunsen burner location, which acts as an intrusive body within the flow, induce clearly a recirculation zone at this level. However, far away from the flame zone ($x/D_{tu} >$

10) the axial velocity distribution appears to be stabilizing and decreases linearly until the exit section, with velocity values varying from 0.7 to 0.61 m/s for both schemes.

The analysis of the dynamic and temperature fields shows that the use of $WD_{refined}$ mechanism leads to a lower flame and a decrease of the temperature of the order of 5.3%. On the other hand, the use of lower chemical reactions and the slowdown of the spread of the upstream fuel induce to: (i) a lifted flame (ii) the appearance of recirculation zones which, in turn, push the flame towards the walls of the combustion chamber.

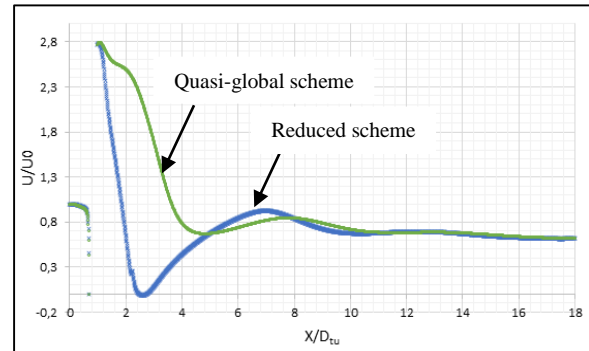


Figure 3: Comparison of the axial velocity profiles along the central axis (ox) of the combustion chamber.

REFERENCES

- [1] D. Veynante and L. Vervisch. Turbulent combustion modeling. *Progress in energy and combustion science*, 28(3): 193-266, 2002
- [2] A. Mameri, I. Fedioun and M. Boumaza. Simulation numérique d'une flamme d'hydrogène dans l'air : Confrontation avec l'expérience. *Revue des Energies Renouvelables*, 9 N°3: 229 – 236, 2006
- [3] M. Stöllinger and S. Heinz. PDF modeling and simulation of premixed turbulent combustion. *Monte Carlo Methods and Applications*, 14: 343, 2008
- [4] J. Andersen, C. L. Rasmussen, T. Giselsson and P. Glarborg. Global Combustion Mechanisms for Use in CFD Modeling under Oxy-Fuel Conditions. *Energy & Fuels*, 23: 1379–1389, 2009
- [5] M. A. Nemitallah and M. A. Habib. Experimental and numerical investigations of an atmospheric diffusion oxy-combustion flame in a gas turbine model combustor. *Applied Energy*, 111: 401-415, 2013

Numerical Investigation on Periodic Simulation of Ducted Axial Fan

Masoud Darbandi¹, Seyedali Sabzpoushan¹, and Gerry E. Schneider²

¹*Department of Aerospace Engineering, Sharif University of Technology, Tehran, P.O. Box 11365-8639, Iran*

²*Department of Mechanical and Mechatronics Engineering, University of Waterloo, Waterloo, Ontario, N2L 3G1, Canada*

Email: darbandi@sharif.edu

ABSTRACT

In this paper, we perform an acceptable simulation of an axial flow fan with relatively low amount of mesh using the periodic boundary condition. The fan we are working on may have some applications like in heat exchangers, air conditioning systems and wind tunnels which make this periodic simulation has a major difference with those common simulations have been done previously. Because of these applications, sometimes we should use a single or parallel set of our fan with upstream duct (and/or downstream duct if applicable) that may not be axisymmetric (fully cylindrical) and hence we can't apply periodic condition to the ducts and employ some slices of them. This makes the interface(s) between rotational and stationary zones very critical and we should be careful about two key points on such interfaces. Firstly, we know that face mesh at this interface must be very similar and concordant in order to avoid data missing from one zone to another (see figure 5). Secondly, there is an important constrain says the pitch ratio can't be further up than a certain limit. As a rule of thumb, for an almost reliable solution, the pitch ratio must not exceed the upper limit of about 10 (or lower limit equals to 0.1). Now, let's clarify "pitch ratio" with a relevant simple example. Prior to any explanation, it's better to mention that this simple example is necessary to examine validity and reliability of this type of periodic simulation for more complicated cases by comparing its solution with the fan experimental test and full blade rotor simulation results. However; we have a target fan with 12 blades occupy 360 degree and two ducts at its both sides (see figure 3). For this geometry, the pitch ratio equals $360/360=1$ at rotational-stationary zones interfaces. Now, suppose a periodic condition in which we employ only two

blades of the fan and have $(2/12)*360=60$ degree annulus slice cross section connected with 360 degree annulus of forward and aft ducts at two interfaces. For this geometry, the pitch ratio is $360/60=6$ (or $60/360=1/6$). The most important parameters in this simulation are the mass flow rate, the flow uniformity, and the turbulence intensities. In case of using parallel set of fans, interaction between inflow to and outflow flow from the fans also become important and we would like to study these aspects.

1. INTRODUCTION

To be added in full paper submission.

2. GEOMETRY, DOMAIN AND GRID

As you see in figure 1, length of blade is 0.5 m from root to tip (when installed on rotor's hub) and diameter of rotor disk is 2 m.



Figure 1. blade upper surface (top) and assembeled rotor disk with casing (bottom)

Maximum allowable RPM is 900 rpm and according to operating test results, mass flow rate must be near 53 kg/s (ambient pressure of about 87000 Pa). In order to eliminate swirl of flow passed through rotor disk, a stator should be embedded downstream the rotor for main applications modeling as you see in figure 2.

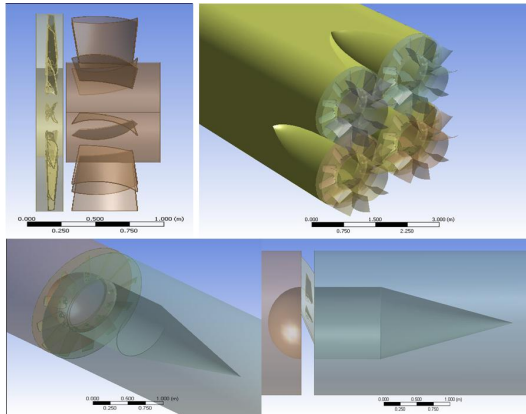


Figure 2. Side view of a rotor-stator couple - parallel set of them at the end of a duct - Full blade (12 blades) rotor disk - sliced (2 blades) rotor disk between forward and aft ducts

In figure 4, you see parts of mesh generated for blades surrounding, consisting of boundary layer and mesh concentration everywhere required.

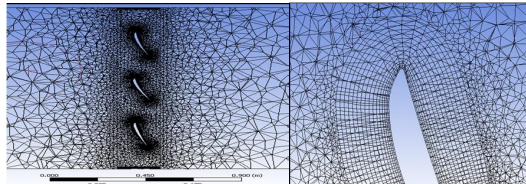


Figure 3. Cross sectional view of mesh generated for rotational zone and its surrounding

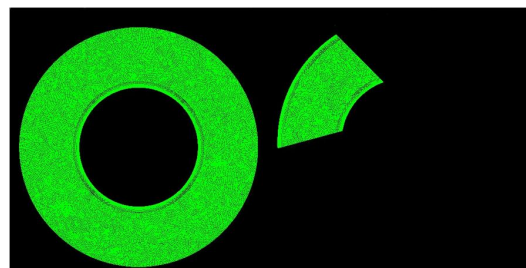


Figure 4. Matched meshing of stationary and rotational domain surfaces at their interface

The number of elements, required hardware and even convergence time of numerical solution decrease considerably if we use a section of rotor disk (and stator disk if exists) with periodic condition instead of complete 360 degree disk and this is why we try to simulate our fan by this method.

3. THE GOVERNING EQUATIONS AND COMPUTATIONAL METHOD

To be added in full paper submission.

4. THE RESULTS AND DISCUSSION

In figure 6, you can find a stream line passes through the fan (flow swirl in absence of stator) and a gage pressure contour just before the rotational domain.

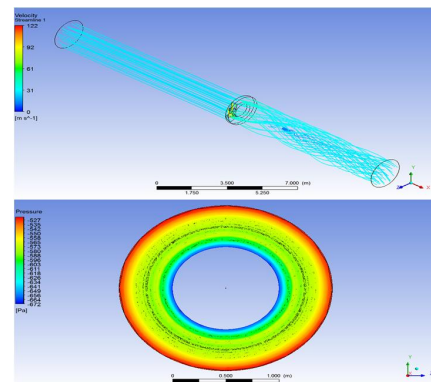


Figure 5. A sample stream line and gage pressure contour

CONCLUSION

To be added in full paper submission.

REFERENCES

- [1] J. Fidalgo. A study of fan-distortion interaction with the NASA rotor-67 transonic stage. *ASME Turbo Expo 2010: Paper GT2010-22914; Session FB-26-8, 2010*
- [2] J.D. Denton. Some limitations of turbomachinery CFD. ASME Turbo Expo 2010: Paper GT2010-22540; Session WA-29-3, 2010
- [3] F. Nicolaas le Roux. "The CFD Simulation of an Axial Flow Fan" Master Thesis. Department of Mechanical and Mechatronic Engineering, University of Stellenbosch, South Africa, 2010
- [4] M.J. Shea. "Development of a MEMS-Scale Turbomachinery Based Vacuum Pump" *Master's Thesis*. Naval Postgraduate School, Monterey, California, US, 2012

Numerical Modeling of Indirect Evaporative Cooling using a Conjugate Domain Approach

Furqan A. Khan¹ and Anthony G. Straatman

Department of Mechanical and Materials Engineering, Western University, London, Ontario

¹Email: fkhan72@uwo.ca

ABSTRACT

For a long time, evaporative cooling has been used due to its cooling potential. In this respect, direct evaporative cooling is widely used to reduce temperature of air. However, in such cases, temperature reduction is accompanied by increment in the moisture content of the air, which is undesirable at times. To overcome this limitation, indirect evaporative cooling is utilized. In indirect evaporative cooling, the temperature of product air is lowered without altering its specific humidity. This is achieved by utilizing a secondary flow of working air, which is separated from the product stream by a solid wall and cooled by evaporative cooling.

The literature survey shows that the numerical modeling of different types of indirect evaporative cooling methods requires a numerical formulation capable of simulating heat and moisture transfer in conjugate domains. To improve upon the calculations of previous researchers, the present work introduces a formulation that accounts for non-equilibrium heat and mass transfer in conjugate fluid/porous/solid domains. It is shown that the present approach gives a more complete picture of the transfer mechanisms in indirect evaporative cooling.

The problem is simulated by considering conjugate fluid/porous/solid domains. Heat and moisture transfer in each domain is modeled by considering the energy and moisture transport equations. Moreover, mathematical conditions at the interfaces are imposed to enforce continuity of heat and moisture transfer. The developed model is validated against the experimental results.

The experimental setup of Gómez et al. [1] is selected as a test case due to availability of all the necessary information. The domain considered comprises of a working channel and a product channel, separated by a polycarbonate wall are modelled. The air streams enter the heat exchanger in a cross-flow arrangement, and all the heat transfer between the streams takes

place through the polycarbonate wall. In the experimental arrangement, evaporative cooling in the working air channel is produced by spraying water from the top into the hollow working air channels. We replace the hollow working channel with a porous region that has interstitial surfaces that are assumed to be always wet in the present computational model. The simulations predict maximum deviation of 2% compared to the experimental results.

The study also investigates the temperature and moisture distributions inside the domain to show how heat and moisture transfer occur throughout the domain, and at the interfaces between the porous-solid and solid-fluid domains. The results show that the distributions of temperature throughout the different regions of the domain, and through the interfaces between the regions are smooth and without discontinuities. In the working channel, the vapour mass fraction of the air flow increases along the channel due to evaporation. However, as expected no change in vapor mass fraction occurs in the product air channel as no vapor mass transfer occurs across the separating wall. The effective diffusivities presented in the formulation are set to zero in order to enforce that no vapour transfer occurs across the separating wall.

REFERENCES

- [1] E.V. Gómez, A.T. González, and F.J.R Martínez. Experimental characterisation of an indirect evaporative cooling prototype in two operating modes. *Applied Energy*, 97:340–346, 2012.

Numerical Simulations of Developing Laminar Flows of Non-Newtonian Liquids in Straight Pipes

Iurii Lohkmanets, James I. Medvescek, Bantwal R. Baliga, and Laurent B. Mydlarski

*Department of Mechanical Engineering, McGill University
817 Sherbrooke St. W., Montreal, Quebec H3A 0C3, Canada*

Email: iurii.lokhmanets@mail.mcgill.ca, james.medvescek@mail.mcgill.ca,
bantwal.baliga@mcgill.ca, laurent.mydlarski@mcgill.ca

EXTENDED ABSTRACT

1. INTRODUCTION

Flows of non-Newtonian liquids are commonly encountered in engineering, biological systems, and the environment. Detailed discussions of such flows are available in numerous books and articles [1]. The present work was motivated by the need to ascertain pressure losses for laminar flows in the developing region of straight capillary tubes, required for designing rheometers for determining the relationship between fluid stresses and strain rate for non-Newtonian liquids. For Newtonian fluids, such data are readily available [2]. However, for non-Newtonian fluids, such data are readily available only for development lengths [3], but not pressure losses. A generalized mathematical model, applicable to both Newtonian and non-Newtonian flows, was adopted [1]. A finite volume method (FVM) was used to solve this generalized mathematical model [4,5]. Verification of this FVM was done using some analytical and numerical results available in the literature [2,3]. A continuation scheme (promotes computational efficiency), a pattern-preserving grid-refinement scheme, and an extended Richardson extrapolation procedure [5] were used in this work.

2. MATHEMATICAL MODEL

The axisymmetric calculation domain and the boundary conditions are illustrated in Fig. 1. The continuity, x -momentum, and r -momentum equations, respectively, that govern the steady, axisymmetric, two-dimensional, isothermal flows of interest were cast in generalized forms, applicable to both Newtonian and non-Newtonian fluids [1]:

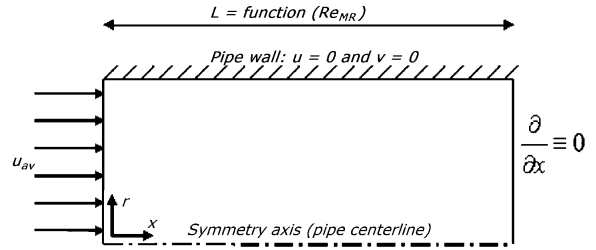


Fig. 1: Calculation domain and boundary conditions

$$\frac{\partial}{\partial x}(\rho u) + \frac{1}{r} \frac{\partial}{\partial r}(r \rho v) = 0 \quad (1)$$

$$\begin{aligned} \frac{\partial}{\partial x}(\rho uu) + \frac{1}{r} \frac{\partial}{\partial r}(r \rho vu) &= -\frac{\partial P}{\partial x} + \frac{\partial}{\partial x}\left(\mu \frac{\partial u}{\partial x}\right) \\ &+ \frac{1}{r} \frac{\partial}{\partial r}\left(r \mu \frac{\partial u}{\partial r}\right) + \frac{\partial \mu}{\partial x} \frac{\partial u}{\partial x} + \frac{\partial \mu}{\partial r} \frac{\partial v}{\partial x} \end{aligned} \quad (2)$$

$$\begin{aligned} \frac{\partial}{\partial x}(\rho uv) + \frac{1}{r} \frac{\partial}{\partial r}(r \rho vv) &= -\frac{\partial P}{\partial r} + \frac{\partial}{\partial x}\left(\mu \frac{\partial v}{\partial x}\right) \\ &+ \frac{1}{r} \frac{\partial}{\partial r}\left(r \mu \frac{\partial v}{\partial r}\right) - \frac{\mu v}{r^2} + \frac{\partial \mu}{\partial x} \frac{\partial u}{\partial r} + \frac{\partial \mu}{\partial r} \frac{\partial v}{\partial x} \end{aligned} \quad (3)$$

Here, P is a reduced pressure. The effective viscosity of the fluid, μ , is given by the following equations:

$$\mu = K[(1/2)D_{ij} : D_{ij}]^{(n-1)/2} = K \dot{\gamma}^{(n-1)} \text{ and}$$

$$\dot{\gamma} = \sqrt{\frac{1}{2} \left[2 \left(\frac{\partial v}{\partial x} + \frac{\partial u}{\partial r} \right)^2 + 4 \left(\frac{v}{r} \right)^2 + 4 \left(\frac{\partial v}{\partial r} \right)^2 + 4 \left(\frac{\partial u}{\partial x} \right)^2 \right]} \quad (4)$$

Here, K is a consistency index; D_{ij} is the rate of strain tensor; $\dot{\gamma}$ represents the magnitude of the rate

of strain tensor; and n is the flow behavior index ($n = 1$ corresponds to a Newtonian fluid; $n < 1$ to a shear-thinning fluid; and $n > 1$ to a shear-thickening fluid).

3. NUMERICAL PROCEDURES

A co-located equal-order finite volume method (FVM) was used to solve the generalized mathematical model. This FVM was adapted from the works of Patankar [4] and Baliga and Atabaki [5]. Quadratic interpolation of the dependent variables was used next to the domain boundaries [5]. In the vicinity of the inlet plane and wall of the pipe, geometrically expanding grids were used, with a geometric factor ≤ 1.05 . With these grids, almost second-order accuracy of the FVM was achieved. The discretized equations were solved using a sequential variable adjustment procedure [5]. A continuation scheme was used to enhance efficiency of the computations. An extended Richardson extrapolation scheme and a pattern-preserving grid refinement procedure were employed to estimate grid-independent solutions for selected cases, and aid the selection of the grids for the final computations.

4. RESULTS AND DISCUSSIONS

Some sample results are presented in Figs. 2 and 3. In these figures, x_D is a development length, which corresponds to the axial coordinate, x , where the centerline velocity reaches 99% of its value in the fully developed regime. A generalized Reynolds number recommended by Bird et al. [1] is used:

$$Re_{MR} = \frac{\rho u_{av}^{(2-n)} D}{K} \left\{ 8 \left(\frac{n}{6n+2} \right)^n \right\} \quad (5)$$

A local Darcy friction factor and an apparent friction factor are used to present the pressure-drop data:

$$f_{Darcy} = (-dp/dx)_{c-s,av} D / (0.5 \rho u_{av}^2) \quad (6)$$

$$f_{app} = \{(p_{x=0} - p_x)_{c-s,av} / x\} D / (0.5 \rho u_{av}^2) \quad (7)$$

5. CONCLUDING REMARKS

The methods and results presented here will be elaborated in the full paper.

ACKNOWLEDGEMENTS

The authors are grateful to Intel Corporation (U.S.A.), Natural Sciences and Engineering Research Council (NSERC) of Canada, and Fonds québécois de la recherche sur la nature et les technologies (FQRNT) for financial support of this work.

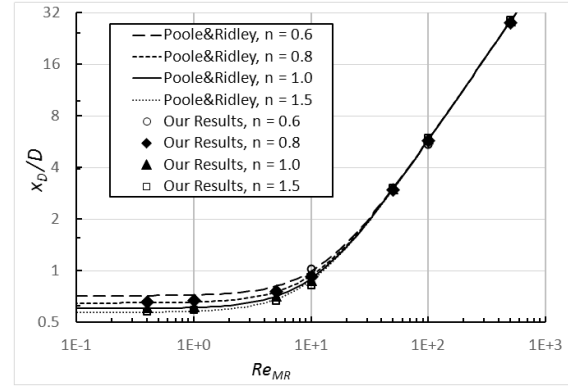


Fig. 2: Comparison of development lengths with those obtained by Poole and Ridley [3].

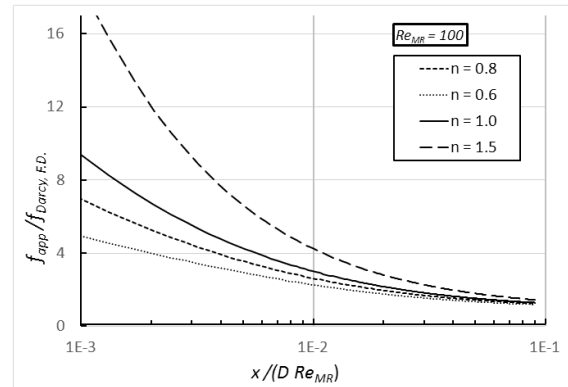


Fig. 3: Apparent friction factor normalized by the Darcy friction factor in the fully developed region.

REFERENCES

- [1] R.B. Bird, W.E. Stewart, and E.N. Lightfoot. *Transport Phenomena, 2nd Edition*, John Wiley, New York, 2002.
- [2] R.K. Shah and A.L. London. Laminar Flow Forced Convection in Ducts. *Advances in Heat Transfer, Supplement 1*, Academic Press, New York, 1978.
- [3] R.J. Poole and B.S. Ridley. Development-Length Requirements for Fully Developed Laminar Pipe Flow of Inelastic Non-Newtonian Liquids. *ASME Journal of Fluids Engineering*, 129:1281-1287, 2007.
- [4] S.V. Patankar. *Numerical Heat Transfer and Fluid Flow*, Hemisphere, Washington, U.S.A., 1980.
- [5] B.R. Baliga and N. Atabaki. Control-Volume-Based Finite Difference and Finite Element Methods. In W.J. Minkowycz, E.M. Sparrow, and J.Y. Murthy (Eds.), *Handbook of Numerical Heat Transfer, 2nd Edition*, John Wiley, New York, U.S.A. Chapter 6, 191-224, 2006.

Numerical Study of the Installed Controlled Diffusion Airfoil at Transitional Reynolds Number

Hao Wu, Paul Laffay, Alexandre Idier, Prateek Jaiswal, Marlène Sanjosé, and Stéphane Moreau

Department of Mechanical Engineering, Université de Sherbrooke, Sherbrooke, QC, J1K2R1, Canada

Email: hao.wu@usherbrooke.ca

ABSTRACT

Reynolds Averaged Navier-Stokes simulations have been carried out for the self-noise study of a controlled diffusion airfoil at chord Reynolds number of 1.5×10^5 . Two numerical setups of the anechoic open-jet facilities where experimental data on aerodynamic have been collected using hotwire measurements and particle image velocimetry are investigated to capture installation effects and to compare different turbulent models. Installation effects for the two setups with different jet nozzle size have been observed for flow with same inlet condition. In the larger nozzle case, laminar recirculation bubble is observed near the leading-edge of the airfoil while in the other case not. Different turbulent models in Reynolds Averaged Navier-Stokes simulations have been compared for such flow case and the transitional model $k\omega - sst$ shows better agreement with the experimental data, which, could be used as initialization data for future direct numerical simulation study.

1 INTRODUCTION

In the design process of a rotating machine, one major evaluation index is the noise level for a given loading. Where other noise sources can be reduced or avoided by a careful design, the trailing-edge (TE) noise is the only remaining noise source when an airfoil encounters a homogeneous stationary flow. Hence TE noise is the minimum achievable noise. It is the canonical noise problem for wall bounded problems. The study of TE noise received much attention mainly in the 1970s and early 1980s. Most of such studies during that time involve experimental measurements on 2D setups of various airfoils in freejet anechoic wind tunnels. Computational Fluid Dynamics (CFD) methods have become an important tool to study TE noise recently. In practice however, simplified

flow configurations are often employed in simulations whereas most trailing-edge aeroacoustics experiments have been conducted in open-jet wind-tunnel facilities, where the airfoil is immersed in a jet downstream of the nozzle exit. It has been seen that the proximity of the airfoil to the jet nozzle exit and the limited jet width relative to the airfoil thickness and chord length can cause the airfoil pressure loading and flow characteristics to deviate significantly from those measured in free air [1]. Installation effects thus take place for different jet configurations and require simulations to model it. The present work is aimed to present and quantify the installation effect as well as to study the influence of different turbulent models on such flow simulation. A systematic CFD study, based on Reynolds Averaged Navier-Stokes (RANS) is carried out and compared with flows over the installed controlled diffusion (CD) airfoil (a cambered airfoil originally developed at Valeo Motors and Actuators) at Ecole Centrale Lyon (ECL) and Université de Sherbrooke (UdS) anechoic chamber experiments. The results give a synthesis of the RANS study and provide guidance for the appropriate boundary conditions needed in future direct numerical simulation (DNS) studies.

2 EXPERIMENTAL AND NUMERICAL SETUP

All the measurements were done in an open jet anechoic wind tunnel shown in fig. 1(a). The test section is $30cm \times 30cm$ and the mock-up (fig. 1(b)) is an extended airfoil between the two side plates, this is done to keep the flow 2D around the airfoil. The wall pressure was measured using a Baratron capacitance manometer which is connected to a pin hole on the surface of airfoil using a capillary tube. The streamwise velocity in the wake was obtained using

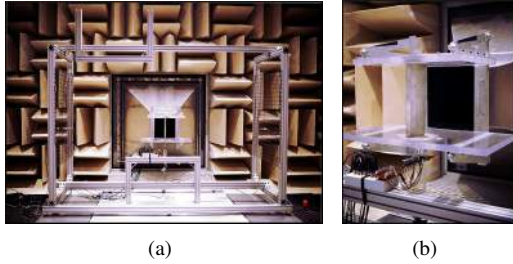


Figure 1: Presentation of the CD airfoil installation at UdS: (a) CD airfoil in the anechoic wind tunnel; (b) Close-view of the CD airfoil.

HWM (hotwire measurement) and PIV (particle image velocimetry). The flow conditions for CD airfoil are a freestream velocity V_0 of 16m/s (which gives a Mach number 0.05) and a chord Reynolds number of 1.5×10^5 . The flow is therefore turbulent or transitional. To model the turbulence, we have tested 5 turbulent models: $k\omega - sst$, rsm, $tr - k - kl - \omega$, tr-sst and $k - \epsilon$ (standard and with low Reynolds number correction). As the RANS results will serve as the initialization field for future DNS study, 3 transitional models are chosen to test their capacity to capture transition process in the simulation. Air is supposed to be an incompressible perfect gas. The geometric attack angle with respect to the wind tunnel axis is 8° . In order to introduce the installation effect, the simulation domain has included the complete nozzle geometry to assess the effect of the nozzle-airfoil interaction.

3 PRELIMINARY RESULTS

$K\omega - sst$ model shows better global behaviour among the 5 tested models thus chosen as the reference model for future RANS simulations (fig. 2). The effects of nozzle jet width is specially studied by comparing results in setups respectively at ECL and UdS. The loading of the airfoil is changed as can be seen from the pressure coefficient in fig. 3. The most significant difference is the change of laminar transition process as shown in fig. 4 . Besides, there is an obvious difference at the TE in fig. 3 between the experimental data and the simulation results at UdS. This has not been seen from the same comparison at ECL. Because of the limit of the nozzle jet width at UdS, the boundary layer at the leading-edge develops in a different way as that at ECL. At ECL, separation bubble (fig. 4) turns laminar boundary layer to a turbulent one at the leading-edge yet at UdS, the transition process is not so severe. At the end, RANS is not capable to predict the development of the transition accurately.

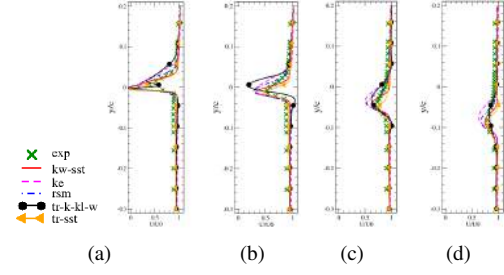


Figure 2: Wake velocity profile prediction with different turbulent models (from TE point to downstream) (a) 1mm; (b) 10mm; (c) 30mm; (d) 60mm.

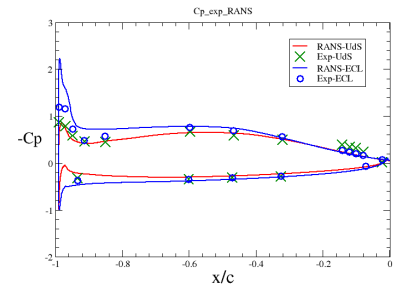


Figure 3: Comparison of pressure coefficient around airfoil.

4 CONCLUSION

On the final paper, meshing strategy and detailed RANS results will be presented for the installed airfoil with a comparison with the experimental data.

REFERENCES

- [1] S.Moreau, M.Henner, G.Iaccarino, M.Wang and M.Roger. Analysis of Flow Conditions in Freejet Experiments for Studying Airfoil Self-noise. *AIAA Journal*, Vol.41, No. 10, 2003, pp. 1895–1905.

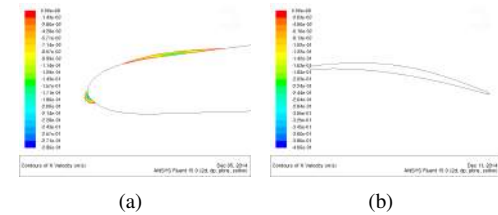


Figure 4: Velocity iso-contours: (a) Zoom view at airfoil leading-edge in ECL installation; (b) Global view of the airfoil in UdS installation.

On the similarities and differences between plane and radial wall-jets

Rayhaneh Banyassady and Ugo Piomelli

*Department of Mechanical and Materials Engineering
Queen's University
Kingston, ON, K7L 3N6, Canada*

Email: r.banyassady@queensu.ca

A wall jet is a shear flow along a wall in which an excessive momentum is injected into a region close to the wall so that the mean streamwise velocity over some region between the wall and the outer edge of the wall jet exceeds that of the external stream [1]. The typical mean streamwise velocity profile of the wall jet is shown in Figure 1; u_m is the maximum velocity and y_m is its position. The point, above y_m , where the velocity is decreased to half of the maximum velocity is $y_{1/2}$. Classically, the wall jet is divided into two shear layers: an inner layer (similar to a turbulent boundary layer) and an outer layer (similar to a half of a free jet). These two layers, with different turbulent characteristics, interact with each other. Thus, in more recent studies, a triple layer structure was proposed with an overlap layer in between the two layers.

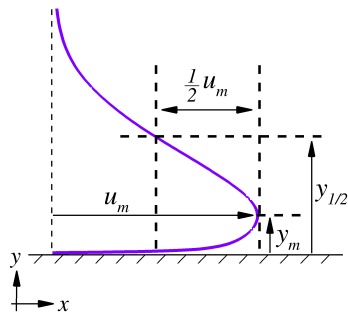


Figure 1: Typical mean streamwise velocity profile of a wall-jet.

Wall jets can be classified into plane, radial, and three-dimensional [1] wall-jets. This research focuses on the first two types. A plane wall-jet can be generated by injecting high-momentum fluid from a rectangular nozzle along the wall [1, 2]. Radial wall-jets can be generated using a radial nozzle or by impingement of a circular jet on a surface [1, 3].

The wall-jet has diverse engineering applications. Besides, it is a simple configuration to study the interaction mechanisms of two shear layers with different structural characteristics [4]. Apart from the engineering applications and the interesting structure of wall-jets, which have been motivated researchers to study this flow, the wall-jet studies up to this day focused, mostly, on one type of wall jet separate from the others. The only few studies that compared different types of wall jets considered basic characteristics and did not provide any insight into the similarities and differences between various types of wall jets [1, 5, 6]. The present study aims at investigating the details of the similarities and differences between plane and radial wall-jets by investigating the mechanism of interaction of inner and outer layers.

In this study, large-eddy simulations of turbulent plane and radial wall-jets were performed at different Reynolds numbers using the Lagrangian dynamic eddy-viscosity subgrid-scale model. The results were validated with the available experimental data in literature [2, 7]. First, a simulation of a radial and a plane wall-jet with the same inflow boundary conditions and Reynolds number were performed to study the evolution of the wall jet in streamwise direction. Then, another plane wall-jet simulation at a lower Reynolds number was performed to compare plane and radial wall-jets at the same local Reynolds number, $Re_m = u_m y_m / v$.

Compared to the plane ones, the radial wall-jets have an extra direction for expansion (azimuthal direction), which causes faster decay of velocity scales (not shown here). Thus, the resulting pressure-gradient ($\Delta P = \frac{v}{\rho u_t^3} \frac{dp}{dx}$) distributions is different (shown in Figure 2). Both plane and radial wall jets have regions of favourable pressure gradient (FPG), zero

pressure gradient (ZPG), and adverse pressure gradient (APG). However, these pressure gradients are not strong enough to cause any fundamental structural difference between plane and radial wall-jets.

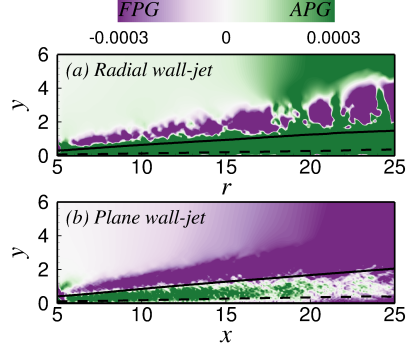


Figure 2: Contours of ΔP for the (a) radial and (b) plane wall-jet simulations; ---, y_m ; —, $y_{1/2}$.

To compare plane and radial wall-jets locally, velocity and Reynolds stresses were compared at different local Reynolds numbers. The results show that the normalized velocity profiles of plane and radial wall-jets at the same Re_m are the same (Figure 3). Various statistical analysis techniques were also employed. Contours of JPDF of streamwise and wall-normal velocity fluctuations, u' and v' , which shows the contribution of each pair of (u', v') to the total Reynolds stress, were studied in detail. Figure 4) shows these contours for a plane and a radial wall-jet at the same $Re_m = u_m y_m / \nu$ at different heights from the wall. As shown in this figure, plane and radial wall-jets have the same structural characteristics at the same Re_m .

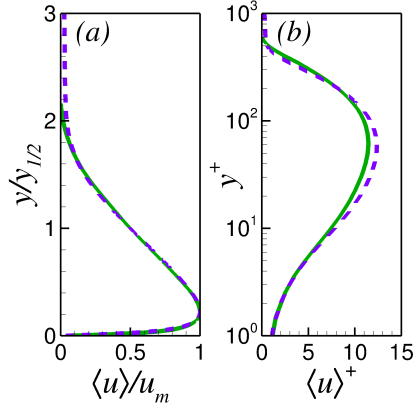


Figure 3: Mean streamwise velocity profiles, at $Re_m \approx 700$, normalized by (a) outer and (b) inner velocity-and length-scales ; —, plane wall-jet; - - -, radial wall-jet.

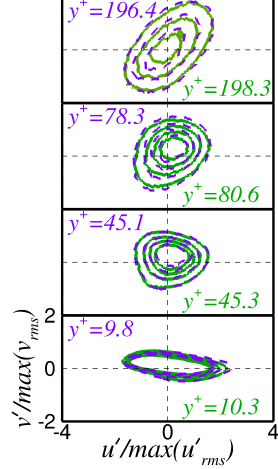


Figure 4: Contours of JPDF of streamwise and wall-normal velocity fluctuations at different heights from the wall. —, plane wall-jet at $Re_m \approx 700$; - - -, radial wall-jet at $Re_m \approx 700$. Contours increments are 0.5×10^{-5} . The outer contour line is one increment above zero.

REFERENCES

- [1] B. E. Launder and W. Rodi. The turbulent wall jet – Measurements and modeling. *Annu. Rev. Fluid Mech.*, 15:429–459, 1983.
- [2] J. Eriksson. *Experimental Studies of the plane turbulent wall jet*. Ph{D} thesis, Royal Inst. Tech., Sweden, 2003.
- [3] P. Bradshaw and E. M. Love. The normal impingement of a circular air jet on a flat surface. R & M 3205, Aeronaut. Res. Counc., London, England, 1959.
- [4] R. Banyassady and U. Piomelli. Turbulent plane wall jets over smooth and rough surfaces. *J. Turbul.*, 15(3):186–207, March 2014.
- [5] G. Padmanabham and B. H. Lakshmana Gowda. Mean and Turbulence Characteristics of a Class of Three-Dimensional Wall Jets – Part 2: Turbulence Characteristics. *J. Fluids Eng.*, 113:629–634, 1991.
- [6] T. Tanaka and E. Tanaka. Experimental studies of a radial turbulent jet (2nd Report, Wall jet on a flat smooth plate). *Bull. JSME*, 20(140):209–215, 1977.
- [7] M. Fairweather and G. Hargrave. Experimental investigation of an axisymmetric, impinging turbulent jet. 1. Velocity field. *Experiments in Fluids*, 33(3):464–471, September 2002.

On the Simulation of Porous Media Flow Using a New Meshless Lattice Boltzmann Method

S. Hossein Musavi and Mahmud Ashrafizaadeh

Department of Mechanical Engineering, Isfahan University of Technology, Isfahan, 8415683111, Iran

Email: mahmud@cc.iut.ac.ir

ABSTRACT

We propose a new meshless lattice Boltzmann method (MLLBM) for the simulation of nearly incompressible flows in porous media. As for the standard lattice Boltzmann method, the collision and the streaming operators are split. While the collision equation remains unaltered, the streaming equation is discretized using the Lax-Wendroff scheme in time, and the meshless local Petrov-Galerkin scheme in space. The Poiseuille flow is solved to validate the numerical scheme. The method is then used to simulate a flow in a porous medium. Although in general, meshless methods suffer from high computational costs, the present method shows promising accuracy and performance at a lower memory and computational costs for complex geometries, when compared with standard lattice Boltzmann methods.

1 INTRODUCTION

Since the beginning of the development of the lattice Boltzmann method (LBM), a great number of studies have been conducted to extend the capabilities of the standard lattice Boltzmann method to handle nonuniform or unstructured grids. A major trend in these studies is to apply some standard numerical techniques, such as the finite difference (FD), the finite volume (FV), and the finite element (FE) methods, for the discretization of the discrete Boltzmann equation. However, for geometrically complex problems, such as flows in porous media, where the time and computational requirements of creating good-quality meshes are significant, the idea of developing a meshless lattice Boltzmann solver naturally arises.

In this study, we employ our newly proposed meshless lattice Boltzmann method [1] for the simulation of nearly incompressible flows in porous media. The meshless feature of the proposed method makes it a

more flexible lattice Boltzmann solver, especially for cases where the mesh generation introduces significant numerical errors into the solution, or where improving the mesh quality is a complex and time-consuming process. The advantages of the present method are well illustrated in a number of test cases described in this paper.

2 FORMULATION

A full description of the MLLBM formulation is included in the full paper. However, in this abstract, we provide highlights of the main differences between the MLLBM and the LBM formulations. The MLLBM formulation starts with a standard discrete form of the Boltzmann equation using the BGK collision approximation. The solution is split into two steps. The collision step remains unaltered, while for the streaming step a pure advection equation is solved which is discretized in time using the Lax-Wendroff scheme.

In order to apply the meshless local Petrov-Galerkin scheme for space discretization, first, a local weak form is derived. The field variables are expressed in terms of nodal values by the local radial point interpolation method (LRPIM). Using a Gauss quadrature scheme a mass matrix and a stiffness matrix could be obtained to reach the fully discretized equation for a nodal point. Writing this equation for all the nodal points in the computational domain, we obtain a global system of N equations with N unknowns to be solved for each direction i after imposing the boundary conditions.

3 RESULTS

Two test cases are simulated in this study. First, to validate the numerical procedure, the plane Poiseuille flow with pressure boundary conditions is solved (see

the full paper for details). Then the method is used to simulate the flow in a granular porous medium.

3.1 Flow in a porous medium

In order to illustrate the ability of the present method to deal with complex geometries, we simulate the pressure-driven flow in a typical two-dimensional porous medium and report the permeability. Experimental studies have illustrated that flow regimes with low Reynolds numbers (typically less than 10) are Darcian, meaning that the superficial velocity is linearly proportional to the pressure gradient (Darcy's law).

In our simulation, the no-slip boundary condition is imposed on the top and the bottom walls and on the grain surfaces using the bounce-back scheme and the constant pressure boundary condition is imposed on the left and right boundaries. The pressure differences between inlet and outlet boundaries in our simulations are set so that the Reynolds number of the flow is low and the flow remains in Darcian regime.

The domain is discretized using arbitrary sets of nodal points. A total of 25284 points is shown to produce node independent results. Figure 1 shows the variation of the computed superficial velocity versus the imposed pressure gradient. The linear variation shown in this figure is in excellent agreement with that of the Darcy's law and gives a permeability of $k = 1.53 \times 10^{-5} \text{ m}^2 = 1.55 \times 10^7 \text{ Darcy}$.

Flow pressure contours inside the porous medium are depicted in Figure 2 for a dimensionless pressure gradient of 0.1. More results are provided in the full paper.

4 CONCLUSIONS

A new meshless lattice Boltzmann method (MLBM) has been developed for the simulation of the nearly incompressible fluid flows in porous media. The main advantage of our method in comparison with the previous extensions of the lattice Boltzmann method is to eliminate the need for any meshes. A feature that shows its superiority over the standard lattice Boltzmann method in complex geometries, such as porous media.

REFERENCES

- [1] S. Hossein Musavi, and Mahmud Ashrafizaadeh. Meshless lattice Boltzmann method for the simulation of fluid flows. *Physical Review E*, 91(2):023310, 2015

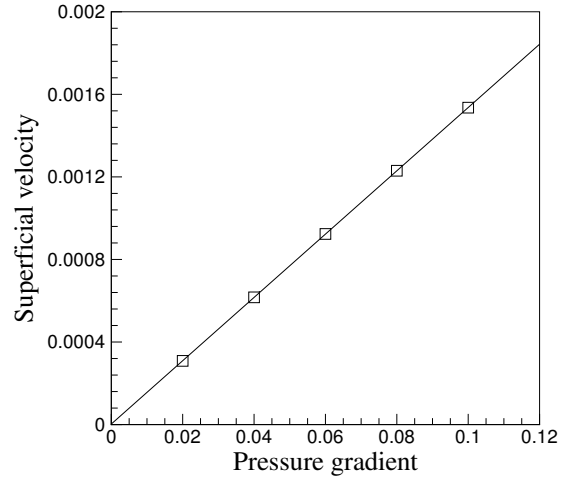


Figure 1: Variation of superficial velocity versus pressure gradient

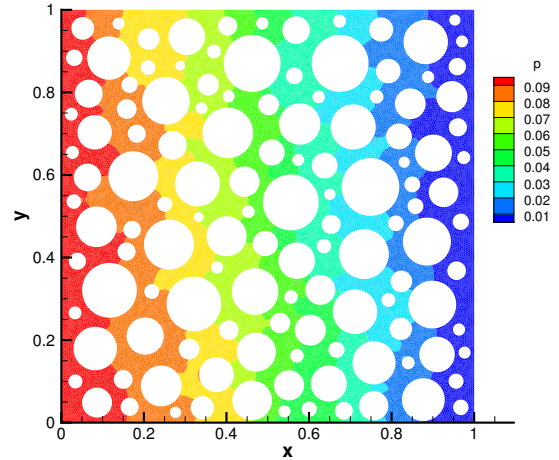


Figure 2: Pressure distribution for the flow inside the porous medium.

Optimising Flux Reconstruction Schemes for Large Eddy Simulation

Rob Watson¹ and Paul G. Tucker¹

*Department of Engineering, University of Cambridge
Trumpington Street, Cambridge, CB2 1PZ, United Kingdom*

Email: *rob.watson@eng.cam.ac.uk, pgt23@cam.ac.uk*

ABSTRACT

A flux reconstruction framework is built to solve the classical convecting isentropic vortex test case. This framework was designed to allow maximum flexibility in the solution approach, allowing the parameters to be varied in such a way that made the exploration of an extremely large number of schemes possible. To allow further investigation, this scheme variability was treated as a design space, and a genetic heuristic was used to traverse it. It was discovered that higher orders (greater than about 6th order) are not computationally favoured, probably due to the onset of Runge's phenomenon in the polynomial interpolation, and that peak efficiency occurred at 4th or 5th order. Solution point locations were also allowed to vary, as were both the interface flux calculation, and the flux correction polynomial coefficients. Optimised groups of all of these variables were generated.

1 INTRODUCTION

The increasing growth of computational resources has led to a rise in the acceptance of Large Eddy Simulation as a technique with industrial relevance. However, many existing algorithms and codes have been optimised over the last four decades to perform efficiently when computing steady Reynolds-Averaged Navier-Stokes calculations. LES places a rather higher demand on the underlying numerics of computation than does RANS — with its reduction in modelled solution content, numerical accuracy can become extremely important.

Alongside this, the need in LES to resolve quite fine scales in both space and time make it a relatively computationally intensive process — rather more so than steady RANS simulations. This, coupled with the pressure on design engineers to reduce development

windows, means that LES algorithms must be developed which are able to take advantage of the scale of modern supercomputers.

One of the potentially most useful methods for achieving this is the implementation of higher order schemes, in which the truncation error terms reduce with discretisation size at polynomial orders greater than two. This means that it should be possible to improve the numerical quality of the solution whilst reducing the total grid size. This coarser grid can reduce the communication required between parallel processes, as is required for efficient calculation on the architecture of modern computers, including for General-Purpose Graphics Processing Unit systems.

Another significant saving in computational methods for industrial applications has been the use of unstructured meshes, which allow grids to be rapidly produced for what can be extremely complex domains. Historically, these have been most straightforwardly implemented using second order, edge-based numerical schemes. High order approaches are considerably less trivial to extend to unstructured grids.

In 2007, Huynh[1] proposed a flux reconstruction approach. This resulted in a means of expressing and implementing a family of schemes, which appear to present properties that are highly favourable for use as part of an industrial LES solver. These benefits include the ability to achieve high order solutions, a reduced communications halo, and sufficient geometric flexibility to apply to unstructured meshes straightforwardly.

In this paper, we attempt to optimise the flux reconstruction framework for industrial LES applications by using a canonical test case — the isentropic convecting vortex — and trying to maximise the fidelity of the convected vortex whilst minimising the computational

time required. In order to carry out this optimisation, the characteristic values which represent each variable of the family member (*e.g.* order, mesh size, location of solution points) was broken down into a string of integers. On this stream of integers, a genetic algorithm-based optimisation was carried out, with the aim of producing a useful scheme which could form the basis for an industrial LES code.

2 OPTIMISATION WITH GENETIC ALGORITHMS

Genetic algorithms have proven to be a powerful tool for the optimisation of extremely complicated problems. They are global optimisers, which prevents them from being susceptible to being trapped by local minima. They work by mimicking the natural process of Darwinian natural selection, selecting for superior genomes — which represent points in the design space — by allowing these to reproduce and recombine to form the next generation[2].

As the available design space for these flux reconstruction schemes is likely to be extremely large and complex, it is likely that more traditional gradient descent methods would be likely to become caught in local minima.

Each of these vortex convection problems was relatively cheap to compute individually — depending on the scheme used, each computation could take between one and ten minutes. However, to properly undertake an optimisation of any fidelity on such a large design space meant that many thousands of these computations had to be undertaken. One of the great strengths of the genetic algorithm is its amenability to parallelisation, resulting in an almost perfectly parallel optimisation scheme when compared to the time taken to evaluate each point in the design space[3]. By using the genetic approach, more than 4000 processors could be used simultaneously, with one evaluation being carried out per core. This meant that, in real terms, each optimisation set could be completed in fewer than 24 hours.

3 RESULTS

Full results will be published in the full manuscript. The optimisations were successfully carried out both allowing the interpolating polynomial order to vary, and at a range of fixed orders of accuracy, and resulted in effective schemes at all orders. The schemes at fifth order enabled the optimiser to minimise the utility function most successfully, although the margin

of improvement over those at fourth order was small. At higher orders of accuracy, the optimisation process tended to push pairs of solution points together, it is thought to try and mitigate the influence on the scheme performance of Runge's phenomenon. This resulted in the optimised higher order schemes performing increasingly poorly, as measured by the utility function.

At the lower — more successful — orders it was found that the optimised solution point layout very roughly approximated some of the analytical polynomial roots which have been traditionally used for quadrature, for example, the Legendre-Gauss or Chebyshev quadratures.

ACKNOWLEDGEMENTS

We acknowledge use of Hartree Centre resources in this work. The STFC Hartree Centre is a research collaboratory in association with IBM providing High Performance Computing platforms funded by the UK's investment in e-Infrastructure. The Centre aims to develop and demonstrate next generation software, optimised to take advantage of the move towards exa-scale computing.

The funding of this work by the EPSRC under an IAA Knowledge Transfer Fellowship with Rolls-Royce plc. is gratefully acknowledged.

REFERENCES

- [1] H. T. Huynh. A flux reconstruction approach to high-order schemes including discontinuous Galerkin methods. *18th AIAA Computational Fluid Dynamics Conference*, 25th-28th June, 2007, Miami, Florida, United States. AIAA-2007-4079
- [2] P. Hajela and C.-Y. Lin. Genetic search strategies in multicriterion optimal design. *Structural Optimisation*, 4(2):99–107, 1992
- [3] R. Watson and P. G. Tucker. Distributed computing and cutback trailing edges. *AIAA SciTech 2014*, 13th-17th January, 2014, National Harbor, Maryland, United States. AIAA-2014-0227

***p*-Multigrid for High-Order Methods via Flux Reconstruction**

Liu Yang and Siva Nadarajah

Department of Mechanical Engineering, McGill University, Montreal, Quebec H3A 0C3, Canada

Email: *Liu.Yang4@mail.mcgill.ca, Siva.Nadarajah@mcgill.ca*

ABSTRACT

Fast convergence of high-order methods remains a challenging issue. As the order increases, the CFL number decreases drastically for explicit Runge-Kutta methods, thus leading to low rates of convergence. Implicit time-stepping schemes allow for higher CFL values, but requires considerable computational cost per iteration and prohibitive memory storage for the Jacobian matrix in 3D high-order cases. Multigrid methods, including *h*-, *p*- and *hp*- multigrid algorithms, offer an alternative feasible approach to accelerate the convergence rate.

The *p*-multigrid has been implemented with the spectral difference method, within the class of flux reconstruction methods [1, 2], on flow simulations by solving the Euler or Navier-Stokes equations [3, 4]. In this paper, the high-order spectral difference scheme was applied to solve the Poisson equation

$$\nabla^2 u = f.$$

A two-level *p*-multigrid method was employed to accelerate the convergence of the solution. By rewriting the equation as

$$Au = f,$$

with subscripts 'f' and 'c' denoting variables on fine and coarse level, *R* and *P* representing the restriction and prolongation operators, the two-level *p*-multigrid algorithm can be described as follows

1. Pre-smooth v_1 times.
2. Restrict the residual on the fine level

$$r_f = f - A_f u_f,$$

to the coarse level through the restriction operator,

$$r_c = R r_f = R(f - A_f u_f).$$

3. Solve the equation on the coarse level

$$A_c u_c = r_c,$$

with an initial guess $u_c^0 = 0$.

4. Correct variables on the fine level by

$$u_f = u_f^0 + P(u_c - u_c^0).$$

5. Post-smooth v_2 times.

v_1 and v_2 are pre-defined numbers of Block-Jacobi relaxation on the fine level. $v_1 = 1$ and $v_2 = 0$ were used for the results presented here.

Three major features that may distinguish various multigrid methods are: grid coarsening (how the coarse grid is chosen); restriction and prolongation operators; formation of operation matrix on the coarse level.

The *p*-multigrid method coarsens the grid by interpolating the solution variables to a lower order polynomial while keeping the geometric grid unchanged.

The error prolongation operator is defined by a simple L_2 projection over the domain Ω [5, 6], which is commonly used for the discontinuous Galerkin method.

$$P = M^{-1}N,$$

where

$$M_{i,j} = \int_{\Omega} \phi_i^p \phi_j^p d\Omega,$$

$$N_{i,j} = \int_{\Omega} \phi_i^p \phi_j^{p_c} d\Omega,$$

while ϕ^p and ϕ^{p_c} are the basis functions on fine and coarse level. The residual restriction operator is chosen to be the transpose of the prolongation operator.

$$R = P^T.$$

If A_c is evaluated through a rediscretization of the computational domain instead from A_f , the Jacobian on the fine level, then the scheme is unstable, as reported in [7, 8]. Thus, in this work, the operation matrix on the coarse level was evaluated in an algebraic approach by the Galerkin operator $A_c = RA_f P$.

Numerical simulations were carried out with a Poisson equation with periodical boundary conditions [7, 8]. The Block-Jacobi relaxation scheme was adopted on both the fine and coarse levels. The results on four different grid sizes are shown in Fig. 1. and Fig. 2. The residuals were reduced by 10 orders of magnitude for approximately 50 and 40 multigrid cycles for 4th-2nd order and 3rd-2nd order respectively and h -independent performance was achieved.

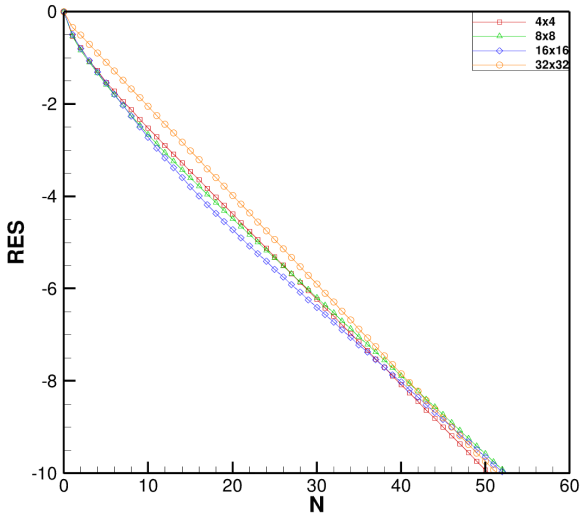


Figure 1: Convergence of Poisson equation using two-level (4th-2nd) p -multigrid.

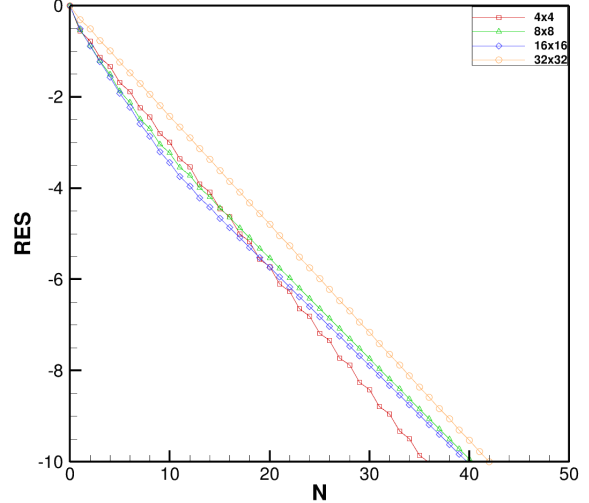


Figure 2: Convergence of Poisson equation using two-level (3rd-2nd) p -multigrid.

and implicit smoothers on unstructured triangular grids. *Computers & fluids*, 38(2):254-265, 2009

- [5] F. Bassi, A. Ghidoni, and S. Rebay. Optimal Runge-Kutta smoothers for the p -multigrid discontinuous Galerkin solution of the 1D Euler equations. *Journal of computational physics*, 230(11): 4153-4175, 2011
- [6] K. J. Fidkowski, T. A. Oliver, J. Lu, and D. L. Darmofal. p -Multigrid solution of high-order discontinuous Galerkin discretizations of the compressible Navier-Stokes equations. *Journal of computational physics*, 207(1): 92-113, 2005
- [7] H. L. Atkins, and B. T. Helenbrook. Numerical evaluation of p -multigrid method for the solution of discontinuous Galerkin discretizations of diffusive equations. *AIAA paper*, 5110, 2005
- [8] B. T. Helenbrook, and H. L. Atkins. Application of p -multigrid to discontinuous Galerkin formulations of the Poisson equation. *AIAA journal*, 44(3): 566-575, 2006
- [1] H. T. Huynh. A flux reconstruction approach to high-order schemes including discontinuous Galerkin methods. *AIAA paper*, 4079, 2007
- [2] H. T. Huynh. A reconstruction approach to high-order schemes including discontinuous Galerkin for diffusion. *AIAA paper*, 403, 2009
- [3] S. Premasuthan, C. Liang, A. Jameson, and Z. J. Wang. p -Multigrid spectral difference method for viscous compressible flow using 2D quadrilateral meshes. *AIAA paper*, 950, 2009
- [4] C. Liang, R. Kannan, and Z. J. Wang. A p -multigrid spectral difference method with explicit

Parallel JFNK Solver for Hypersonic Viscous Flows

Song Gao¹, Wagdi G. Habashi¹, Marco Fossati¹,
Dario Isola², Guido S. Baruzzi², and Isik A. Ozcer²

¹ CFD Laboratory, McGill University, Montreal, QC, H3A 2S6, Canada

² ANSYS Canada, Montreal, QC, H3A 2M7, Canada

Email: song.gao@cfdlab.mcgill.ca

1. INTRODUCTION

The study of high-speed non-equilibrium flows is of great importance for the next-generation civil transport aircraft. The flow physics of these at this regime is dominated by complex phenomena such as strong shocks, chemical non-equilibrium, thermal non-equilibrium, and the magneto-hydrodynamic effects [1]. Since the number of governing equations is not known a priori and the number of chemical species may become very big, seeking algorithms that address these flows in an accurate but at the same time computationally efficient manner is of great relevance to the aerospace industry.

The adoption of Finite Element (FE)-based method for hypersonic flows [2] has been lately reconsidered against the commonly used Finite Volume methods due to its superior accuracy, mathematical consistency and robustness over the stretched grids which may result from anisotropic mesh adaptation in boundary layer and shock waves regions. In order to overcome some of the limitations of the FE method when addressing advection-dominated problems, the node-pair (edge-based) formulation has been proposed [3] that provides a framework for a straightforward application of upwind stabilization techniques.

Critical to the numerical approach adopted is the possibility to avoid the explicit calculation and storage of the Jacobian matrix of the nonlinear residual which may become very problematic when the number of species is very high or thermodynamic nonequilibrium is considered. The Jacobian-free Newton–Krylov (JFNK) approach [4] is an elegant solution that does not require the explicit formulation of the Jacobian matrix. Along the same considerations, matrix-free numerical schemes are favored such as the Advection Upstream Splitting scheme (AUSM) proposed by Liu [5]. Other advantages offered by the AUSM scheme is the implicit upwind-

ing, which allows for stabilization in an efficient manner when implemented in a node-pair fashion.

The present work introduces a node-pair JFNK FE solver for the modeling and simulation of high-Mach flows. This serves as a prerequisite to incorporate efficiently an arbitrary mechanism of reaction with many chemical species and the complex non-equilibrium thermodynamic effects due to high-temperature conditions.

2. METHODOLOGY

The standard FE scheme is recast in the edge-based form to increase the efficiency and to enable the use of stabilization schemes AUSM+-up. The scheme is extended to second order accuracy by Monotonic Upstream-Centered (MUSCL) [6] and the slope limiter by Barth-Jespersen is used to suppress spurious oscillations [7] near shock waves. The viscous fluxes are discretized with the standard continuous Galerkin approximation but assembled in an edge-based fashion.

The discrete system of equations is solved by JFNK. The explicit calculation of Jacobian of the nonlinear residual is avoided because only the matrix-vector product is required and this is approximated by a Fréchet derivative. The pseudo-transient continuation method is also adopted to further reduce the stiffness of the system [8].

Preconditioning is a crucial step for JFNK methodology. At the present preliminary stage, ILU factorization with level zero fill-in and Symmetric Gauss Seidel (SGS) preconditioner [9] are used. Both preconditioners are performed on the first-order Jacobian, since the MUSCL reconstruction is neglected. Our goal is to achieve the true Jacobian-free preconditioner lower-upper Symmetric-Gauss-Seidel (LU-SGS) [10]. SGS is only served as an intermediate step to LU-SGS.

3. MACH 14.1 VISCOUS FLOW OVER A RAMP

This test case is a Mach 14.1 laminar viscous flow over a 24 degrees ramp. The Reynolds number based on the length of the flat plate is 103,600. The Reynolds number is low enough to ensure that the flow remains laminar. A structured mesh of 189,578 nodes and 104,583 elements is used. The numerical method is AUSM+-up with MUSCL and Barth-Jespersen slope limiter. The preconditioner used is ILU(0). The temperature and Mach contour are shown in Figure 1. The leading edge shock, the thin boundary layer, the shock-shock interaction and the shock-boundary layer interaction are clearly captured by this method.

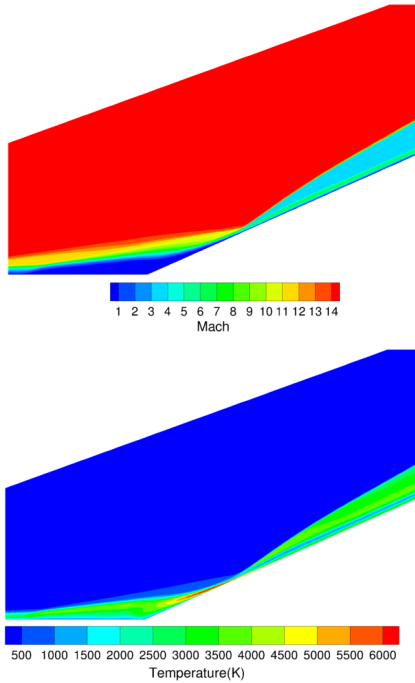


Figure 1: Mach number contour (up) and Temperature contour (down) for hypersonic flow over a 24-degree ramp.

4. FINAL REMARKS AND FUTURE WORK

A robust and accurate edge-based Jacobian-free FE solver for high-Mach flows is proposed. This formulation provides a general framework for an arbitrary number of chemical species and non-equilibrium effects. The edge-based strategy enables the implementation of the AUSM+-up stabilization scheme. The preliminary results presented confirm the accuracy of the proposed approach.

At this stage, LU-SGS is under development as a Jacobian-free preconditioning technique. The turbulence modeling in the hypersonic flow conditions is

also being investigated. Finally, validation for chemically reacting flows with non-equilibrium effects is underway.

ACKNOWLEDGEMENTS

The authors acknowledge the financial support of the Lockheed Martin Corporation though the grant G238199 and are grateful to Drs. Luke Uribarri and Ned Allen from Lockheed Martin for the continuous discussions and comments.

REFERENCES

- [1] J-H. Lee. Basic governing equations for the flight regimes of aero-assisted orbital transfer vehicles. *AIAA 19th Thermophysics Conference*, AIAA, Snowmass, Colorado, 1984.
- [2] B.S. Kirk, R.H. Stogner, P.T. Bauman and T.A. Oliver. Modeling hypersonic entry with the fully-implicit Navier-Stokes (FIN-S) stabilized finite element flow solver. *Comput. Fluids*, 92(20):281–292, 2014
- [3] V. Selmin. The node-centred finite volume approach: bridge between finite differences and finite elements. *Comput. Method Appl. M.*, 102(1):107–138, 1993
- [4] D.A. Knoll and D.E. Keyes. Jacobian-free Newton–Krylov methods: a survey of approaches and applications. *J. Comput. Phys.*, 193(2):357–397, 2004
- [5] M.-S. Liou. A sequel to AUSM, Part II: AUSM+-up for all speeds. *J. Comput. Phys.*, 214(1):137–170, 2006
- [6] B. Van Leer. Towards the ultimate conservative difference scheme, V. a second order sequel to Godunov's method. *J. Comput. Phys.*, 32:101–136, 1974
- [7] V. Venkatakrishnan. Convergence to steady state solutions of the Euler equations on unstructured grids with limiters. *J. Comput. Phys.*, 118(1):120–130, 1995
- [8] A. Jameson. Time Dependent Calculations Using Multigrid, with Applications to Unsteady Flows Past Airfoils and Wings. AIAA Paper 91-1596, AIAA 10th Computational Fluid Dynamics Conference, Honolulu, June, 1991
- [9] G. Carpentieri. An adjoint-based shape-optimization method for aerodynamic design, Delft University of Technology, 2009.
- [10] H. Luo, J.D. Baum and R. Löhner. A fast, matrix-free implicit method for compressible flows on unstructured grids. *J. Comput. Phys.*, 146(2):664–690, 1998

Piston Cooling Technology Using Jet Impingement

G. Nasif, R.M. Barron, R. Balachandar

*Department of Mechanical, Automotive & Materials Engineering
University of Windsor, Canada*

Email: *nasifg@uwindsor.ca*

ABSTRACT

Convective heat transfer of an impinging liquid jet is numerically investigated for piston cooling process. A circular jet of subcooled engine oil impinges onto the inner surface of the piston for engine operating at normal condition is considered in the study. The volume of fluid approach employing a high resolution interface capturing scheme was used to perform the two-phase flow simulations. The 3-dimensional governing Navier-Stokes equations and energy equation are numerically solved using a finite volume technique. The conjugate heat transfer method is used to obtain a coupled heat transfer solution between the solid and fluid, to predict the heat transfer coefficient and then the temperature profile in the piston. It is shown that the cooling jet can considerably decrease the volume and surface average temperature of the piston. Both piston volume and piston interior surface average temperatures are only function of oil jet Reynolds number when the engine is operating at normal condition

1. OBJECTIVE

The objective of the present study is to numerically evaluate the performance of the cooling process when an oil jet (SAE 5W30) impinges perpendicularly onto a reciprocating moving piston. Pipe nozzle sizes in the range $d = 1.0 - 3.0$ mm, for a wide range of issuing velocities, are employed in the simulations. A piston motion equation is used to capture the reciprocating motion of the piston within a piston stroke of 82.0 mm. Engine operating at normal condition, i.e. $N = 2000$ rpm is considered in this study.

2. COMPUTATIONAL METHOD

Finite volume based computations using CD-Adapco's STAR-CCM+ with polyhedral cells are

performed in the current study. The $k-\omega$ SST turbulence model is used as the turbulence model in the present study. Since the flow field involves two different immiscible fluids (oil jet in air), a numerical model to handle two-phase flow is required. Volume of fluid (VOF) is a simplified and efficient method, which provides an approach to capture the movement of the interface between the mixture phases. The VOF model can model two or more immiscible fluids by solving a single set of momentum and energy equations and tracking the volume fraction of each of the fluids throughout the domain. Therefore there is no need for additional modelling of inter-phase interaction. An additional equation will be used to transport the volume fraction of primary fluid (α). The fluid properties are evaluated based on the volume fraction in each cell element. In the current study, High Resolution Interface Capturing (HRIC) [1] is used for interface tracking with the VOF model. The interaction between the heat conduction inside the solid and the flow of fluid adjacent to the fluid-solid interface is commonly referred to as a conjugate heat transfer. The conjugate heat transfer method allows for a coupled heat transfer solution between the solid and fluid, and predicts the heat transfer coefficient more accurately than a decoupled solution. This technique is used in the current simulation to estimate the heat transfer coefficient on the solid surface due to the impingement of the oil jet.

3. MODEL SETUP

Figure 1 shows the computational domain with relevant boundary conditions. Three pipe nozzles sizes $d = 1.0, 2.0$ and 3.0 mm with various issuing bulk velocities range between $10 \text{ m/s} \leq v_f \leq 60 \text{ m/s}$, were used in the simulations. The oil exits the nozzle with a temperature of 90°C , flows as a jet towards the piston and spreads out along the piston inner surfaces. The cylinder wall is kept at 130°C . The upper surface of the piston is subjected to

convective heat transfer due to the combustion gases. A portion of combustion gases is also infiltrates through the clearance between the piston and cylinder to the crankcase with mass flow rate of 4.6 g/s at temperature of 655 °C. The transient boundary

conditions as a function of the crank angle at the bottom of the cylinder, *i.e.*, pressure, temperature, velocity components and turbulent intensities are extracted from full-scale engine simulation without cooling jet [2-4].

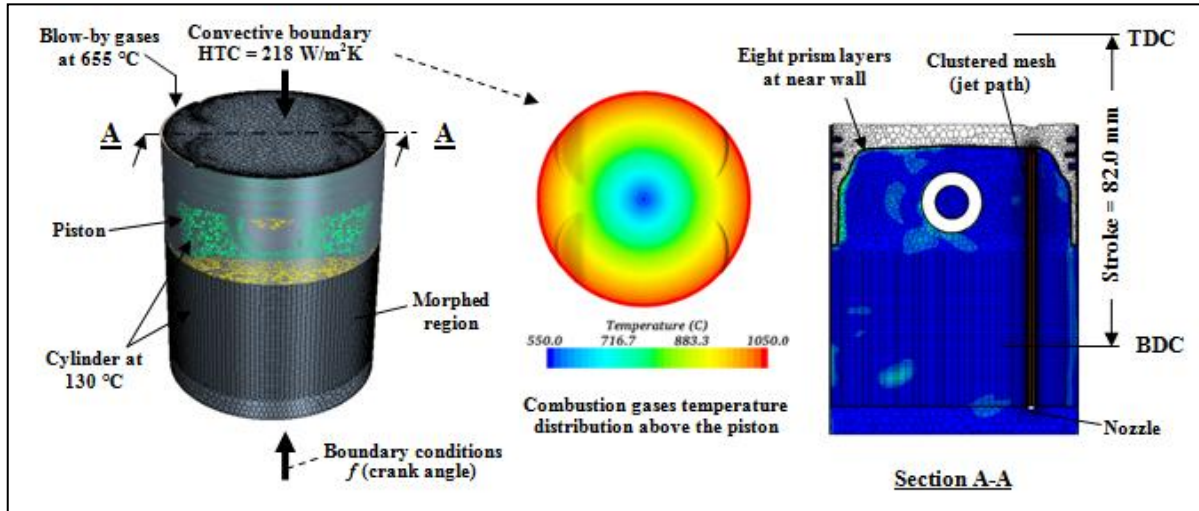


Figure 1. Computational domain with relevant boundary conditions

4. RESULTS AND DISCUSSION

The piston average temperature decreases as the jet Reynolds number increases (see Figure 2). For a given Reynolds number, the average temperature in the disc for larger nozzles (*i.e.*, 2.0 & 3.0 mm) is slightly dependent on nozzle size. One should recall that the oil flow rate is more than double with nozzle size $d = 3.0$ mm in comparison with the nozzle size $d = 2.0$ mm, therefore from practical point of view, it is preferable to use the smaller nozzle, *i.e.*, $d = 2.0$ mm.

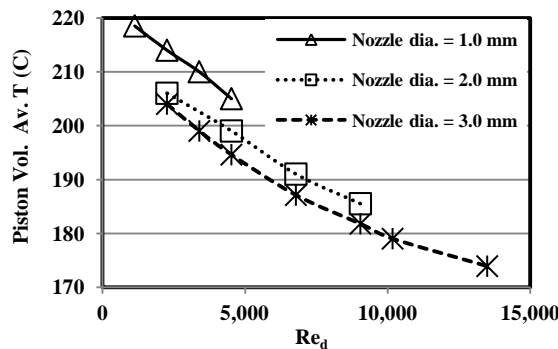


Figure 2. The effect of jet Reynolds number on the piston volume average temperature

REFERENCES

- [1] S. Muzaferija, M. Peric, P. Sames and T. Schelin. A Two-Fluid Navier-Stokes Solver to Simulate Water Entry. *Proceedings of 22nd Symposium on Naval Hydrodynamics*, Washington, DC, USA, 1989.
- [2] G. Nasif, R.M. Barron, R. Balachandar and O. Iqbal. Simulation of Jet Impingement Heat Transfer. *Proceedings of ASME 2013 Internal Combustion Engine Division (ICED), Fall Technical Conference*, Paper No. ICEF2013-19050, Dearborn, MI, USA, 2013.
- [3] G. Nasif, R.M. Barron and R. Balachandar. Heat Transfer Due to an Impinging Jet in a Confined Space. *J. Heat Trans.*, Vol. 136, No. 11; doi: 10.1115/1.4028242, 2014.
- [4] G. Nasif, R.M. Barron and R. Balachandar. Simulation of Jet Impingement Heat Transfer onto a Moving Disc. *Int. J. Heat Mass Transfer*, Vol. 80, pp 539-550, 2015.

Prediction of bioaerosols dispersion and spatial distribution in a hospital isolation room

G. Khosravi¹, M. Ahmadi Golestan¹, S. Hallé¹, F. Morency¹

¹*École de Technologie Supérieure, département de génie mécanique, Montréal, Canada*

Email: golnaz.khosravi.1@ens.etsmtl.ca

ABSTRACT

Risk of infection via the inhalation of pathogenic microorganisms is strongly related to particles diameter and airflow pattern. Ventilation systems properly designed ensure effective dilution and extraction. The objective of this paper is to determine the contaminant removal efficiency in a hospital isolation room. Computational fluid dynamic (CFD) is used to predict airflow, particle dispersion and removal efficiency.

1. INTRODUCTION

In 2003, the outbreak of severe acute respiratory syndrome [1] and the swine flu in 2010, renew the interest for airborne transmission of infectious agents and their aerodynamic behaviors in indoor spaces. Risk of infection via the inhalation of pathogenic microorganisms such as mycobacteria, bacteria and viruses, is strongly related to particles diameter and airflow. Health risk mitigation of the airborne microorganisms can be accomplished by ventilation systems that dilute and extract the potentially pathogenic aerosols. According to previous studies, the diameter of bioaerosols is generally under 100 μm , which decreases to 0.5-10 μm when the fluid of pathogenic droplets evaporates [2]. The droplets nuclei remain airborne for a long period of time and they are more likely to be inhaled by occupants. Since the evaluation of bioaerosols exposures is challenging and requires the differentiation between the biological and non-biological material [3], CFD is the most appropriate approach. It predicts air flow, particle concentration and deposition by solving conservation equations [4].

The main objective of this study is to determine the contaminant removal efficiency in a hospital isolation room.

1.1. Specific objectives

The specific objectives are as follows: i) Choose an appropriate mathematical model and numerical method for simulating airflow and bio-particle dynamic behavior into a 3D room; ii) Validate the 3D numerical simulation by comparing the air flow velocity and particle concentration to available results in literature; iii) Inject bioaerosols into a 3D isolation room and investigate the particle concentration and deposition on the solid surfaces with time.

2. METHODOLOGY

The airflow and particle dispersion models are achieved in an open source finite-volume based program, i.e., CFD package Code-Saturne (version 4.0). The code uses k- ϵ Reynolds-Average Navier-Stokes (RANS) turbulence model, which is based on the Reynolds momentum equation. For air flow simulations, k- ϵ linear production turbulence model [6] is chosen. The particle behaviors are modeled with the Lagrangian method.

For code validation, airflow and particles are injected in a chamber. The airflow velocity and particle concentration are compared to Chen [7] numerical results.

The isolation room size is length \times width \times height = 5m \times 4m \times 4m. The inlet and outlet are both 0.4m \times 0.4m on the top. Simulations are performed for three air changes per hour (ACH) namely 9, 12 and 15. The standard Ashrae-170 [5] recommends 12 ACH for an isolation room. For each simulation, particles are injected in the room from a patient lying in a bed. The contaminant removal efficiency is determined for each ACH.

3. NUMERICAL METHOD

For simulating the two phases flow an Eulerian-Lagrangian approach is used in which the fluid phase

is modeled by the Reynolds Averaged Navier-Stokes (RANS) equations, and the particle phase is modeled by Lagrangian method which uses the PDF (probability density function) and solve a set of stochastic differential equations. A first order upwind discretization scheme is used for the turbulent equations, whereas, a centered scheme approach is used for the momentum equations. The SIMPLEC algorithm (SIMPLE-Consistent) is employed to evaluate pressure-velocity coupling.

4. VALIDATION

An airflow is injected in a 3D chamber ($x=0.8\text{m}$, $y=0.4\text{m}$, $z=0.4\text{m}$, $0.04\text{m} \times 0.04\text{m}$ inlet on the top left and the same size outlet on the bottom right) according to the Chen [7] numerical work. Fig. 1 shows the computed air velocity results, compared with Chen [7] results. There is a good agreement between results, taking into account that the turbulence model is not the same. Particles are injected into the chamber to compare the concentration results with Chen results. Fig.2 shows preliminary particle volume concentration streamlines after a 8s particle injection.

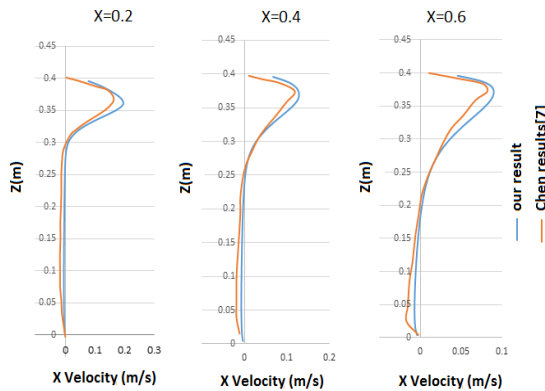


Fig.1. Comparison of airflow x velocity component at different locations for inlet velocity=0.225 m/s

5. CONCLUSION

An Eulerian-Lagrangian model is used to predict the bioparticles behavior in a hospital isolation room. The validity of the approach is verified by comparing the air flow velocity and particle concentration in a 3D chamber against the results in Chen [7] literature. The preliminary results obtained

are shown in this abstract. The comparison of particle concentration in 3D chamber and the bioparticle concentration results in the hospital room will be shown in the final paper.

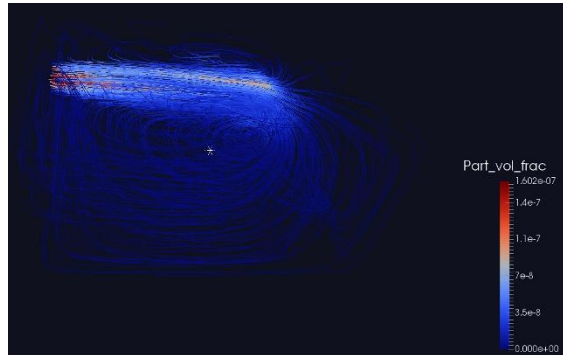


Fig.2. Particle volume concentration stream lines after 8s particle injection

REFERENCES

- [1] Y. Li, X. Haung, I. T. S. Yu, T. W. Wong and H. Qian, Role of air distribution in SARS transmission during the largest nosocomial outbreak in Hong Kong, *Indoor Air*, 15(2): 83-95, 2004
- [2] C. Chen and B. Zhao, Some questions on dispersion of human exhaled droplets in ventilation rooms: answers from numerical investigation, *Indoor Air*, 20(2): 95-111, 2010
- [3] J. Lavoie, G. Marchand, Y. Cloutier, S. Hallé, S. Nadeau, C. Duchaine and G. Pichette, Evaluation of bioaerosol exposure during hospital bronchoscopy examinations, *Environmental Science Processes and Impact*, 17:288-299, 2015
- [4] J. Jiang and X. Wang, On the numerical study of indoor particle dispersion and spatial distribution, *Air, Soil and Water research*, 5: 23-40, 2012
- [5] ASHRAE/ASHE Standard 170-2013, Ventilation of health care facilities, 20 p., 2013
- [6] V. Guimet, D. Laurence, A linearized turbulent production in the k-e model for engineering applications, 5th international symposium on engineering turbulence modelling and measurements Mallorca, Spain, 2002
- [7] F. Chen, S. C. M. Yu, A. C. K. Lai, Modeling particle distribution and deposition in indoor environments with a new drift-flux model, *Atmospheric Environment*, 40(2):357-367, 2005

Prediction of Mixing Layer Critical Reynolds Number in Different Free-Stream Temperatures

S. Rahbarimanesh and C. Mavriplis

Department of Mechanical Engineering, University of Ottawa, Ottawa, Ontario, Canada K1N 6N5

Email: *srahb100@uottawa.ca*

ABSTRACT

Effects of the high-speed side Reynolds number and temperature are investigated to predict stability behavior of a two-stream incompressible laminar mixing layer, generated at the trailing edge of a NACA0006 airfoil. A modified critical Reynolds number is defined and then maximized by using Genetic Algorithm optimization operating for a range of free-stream Reynolds numbers with different temperatures. Velocity profiles found at the end of domain in the steady simulations are fitted to a Gaussian function and used in the optimization process. The study is implemented numerically in OpenFoam® in a two-dimensional rectangular domain employing a hybrid mesh developed in Gambit®. Despite the existence of some differences, findings compare reasonably well with analytical solutions of mixing layer behind flat plates. It is shown that for relatively small shape factors, raising the high-speed side flow temperature reduces the critical Reynolds number and forces velocity profiles to become more unstable. The rate of reduction is accelerated by employing higher Reynolds numbers.

1. INTRODUCTION

Free and bounded mixing layers in practical aerodynamics engineering are declared as a means to evaluate distinctive aspects of laminar-turbulent mechanisms of fluid mixing. Early investigations of incompressible laminar mixing layers behind flat plate splitters show that steady behavior of the two-stream flow can be generalized by using a Blasius-type similarity variable for each stream [1]. Furthermore, stability of these similar profiles over flat plates can be estimated from a universal graph correlating critical Reynolds number and shape factor [2]: with increasing shape factor, critical Reynolds number decreases and instability occurs earlier.

For flows with temperature dependent properties, stability of the boundary layer has been shown to be enhanced by imposing more negative pressure gradients [3]. Uncertainty in prediction of instability in these flows with small shape factors points to a need to investigate the effects of temperature changes on the onset of instability.

2. SOLUTION METHODS

2.1 Numerical Simulation

Following the experiment of Hollingsworth [4], a mixing layer with a fixed velocity ratio of 2 between the upper and lower sides resulting from airflow over the two-dimensional NACA0006 airfoil is studied numerically using OpenFoam and a hybrid grid generated in a rectangular computational domain. High-speed side free-stream Reynolds number is investigated from 10,000 to 150,000 in a range of temperatures between 250 K and 400 K. IcoFoam and SimpleFoam solvers were chosen for unsteady and steady simulations, respectively. The BuoyantBoussinesqPimpleFoam (BBPF) solver was also used for solving the unsteady energy equation.

2.2 Analytical Procedure

Simplified forms of the famous Falkner-Skan wedge flows were analytically derived by Lock [5]. In the current study, corresponding steady-state Falkner-Skan equations with appropriate boundary conditions were solved as a boundary value problem in Matlab® to validate the numerical results at the last station of domain.

Assuming that pressure gradient can be estimated as a function of time [3], an unsteady partial differential streamwise momentum equation was solved in Matlab. Boundary and initial conditions for this equation were specified in terms of Gaussian functions fitted to steady-state results explored in the numerical simulations.

2.2.1 Stability Analysis

The universal plot of Wazzan [2] on instability analysis does not predict the critical Reynolds number for all ranges of shape factor found in wall bounded shear layers. Thus, a different approach was chosen as the objective function to estimate the onset of instability in the mixing layer: critical Reynolds number defined by Hughes and Reid [6] was used and then maximized by using a genetic algorithm in Matlab.

3. RESULTS AND DISCUSSION

Fig.1 compares velocity profiles found by numerical simulation with those of the analytical solution. The difference between the profiles is mainly due to the presence of mild pressure gradients in the mixing layer due to the airfoil as shown by the numerical solutions.

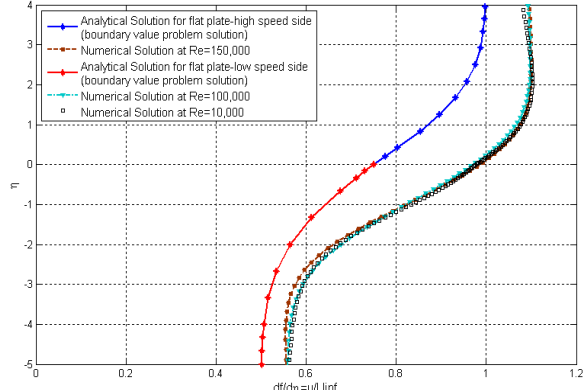


Fig. 1: Comparison of numerical mixing layer velocity profiles with analytical solution at different Re numbers

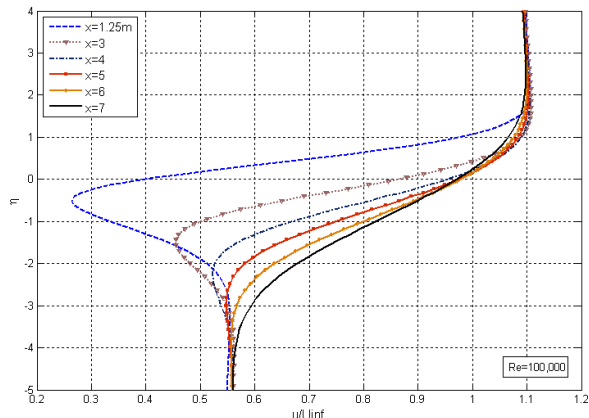


Fig. 2: Numerical solution: Evolution of the dimensionless velocity profiles in streamwise direction at $Re=100,000$

Streamwise evolution of the mixing layer at $Re=100,000$, $T=300K$ is observed in Fig. 2. As shown, double-peak behavior of the flow is eliminated gradually in further downstream regions

showing smoothed-out, developed profiles in the last station.

Effects of the upper side free-stream temperature on the behavior of the mixing layer are shown in Fig. 3.

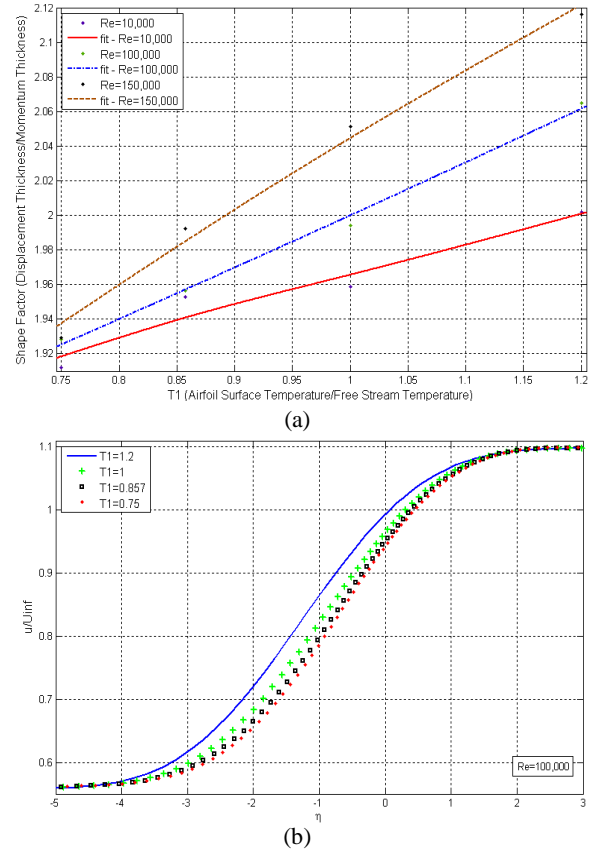


Fig. 3: Effects of free-stream temperature; (a) shape factors, (b) last-station velocity profiles at $Re=100,000$

As indicated, increase in the free-stream temperature over the airfoil pushes the onset of instability further upstream of the mixing layer.

Velocity profiles in the last station of the domain at various free-stream Re and temperatures as well as estimated values of critical Re number found by the optimization process will be discussed in the paper.

4. REFERENCES

- [1] H. Schlichting, "Boundary Layer Theory," 8th ed., Springer, 2000, pp. 127-200.
- [2] A. R. Wazzan, et al., "Tollmien-Schlichting waves and transition," *Prog. Aerosp. Sci.*, vol. 18, no. 2, pp. 351–392, 1979.
- [3] F. M. White, "Viscous Fluid Flow", 3rd ed., McGraw-Hill, 2006, pp. 128-135, 337-362.
- [4] D. K. Hollingsworth, *Experimental Thermal and Fluid Science* 11, 1995, pp.210-222.
- [5] R. C. Lock, *Q. J. Mech. Appl. Math.*, vol. 4, pp. 42–63, 1951.
- [6] T. H. Hughes, and W. H. Reid, *J. Fluid Mech.*, vol. 23, pp. 715–735, 1965.

Reynolds-averaged and wall-modelled large-eddy simulations of impinging jets with embedded azimuthal vortices

Wen Wu and Ugo Piomelli

Department of Mechanical and Materials Engineering, Queen's University, Kingston, ON, Canada, K7L 3N6

Email: w.wu@queensu.ca, ugo@me.queensu.ca

Helicopter brownout is a problem that has recently received considerable attention. When a helicopter hovers near the ground, the rotor-tip vortices are convected towards the ground and interact with the wall-jet like, high-Reynolds number, turbulent flow near the solid ground. An undesirable effect of this interaction is the lifting up of sediment particles that may be entrained in the wake and affect the pilot's visibility.

Due to the simplicity of the configuration and the similarity between the flow and the rotor wake, the round impinging jet has been used as a model of the wake of a rotorcraft hovering near the ground. It has also been used frequently to test and validate turbulence models for the Reynolds-Averaged Navier-Stokes (RANS) equations. Forcing the jet is useful to amplify the instability, leading to more coherent azimuthal eddies, locked at the forcing frequency.

The studies of impinging jets shows the critical role of the primary vortex in the flow, and the complexity in predicting its dynamics due to the highly unsteady, three-dimensional flow, which is difficult to model within the framework of the RANS equations. Although eddy-resolving methods such as LES have shown their potential, their computational cost remains an issue. An alternative, which becomes more feasible as the available computational power increases, is to use Wall-Modelled LES (WMLES) [2].

The goal of this article is to explore the accuracy of both Unsteady RANS (URANS) models and WMLES to the same problem studied by Wu and Piomelli [3] using resolved LES. The evaluation of these techniques, in a case in which resolved LES data is available to guide the modelling effort, may contribute to the development of better lower-level models.

A round impinging jet whose Reynolds number being 6.6×10^4 was studied [4, 3]. The jet outlet-to-target wall distance was $H/D = 1$. The exciting

frequency was 75Hz. The computation domain size was $3.5D(0.25D - 3.75D) \times 1D \times \pi/3$ in r , z and θ directions. Phase-averaged or filtered Navier-Stokes equation were solved using a well-validated finite-difference code based on staggered grid. At the inflow and top boundaries, profiles of time-varying mean flow velocity and maps of arbitrary turbulent fluctuations were assigned. Periodic and convective boundary conditions were imposed in the azimuthal direction and outflow. No-slip conditions are applied on the wall, except in the logarithmic-law WMLES.

Three RANS models, the Spalart-Allmaras (SA) model, the $k - \omega$ model and the $k - \epsilon$ two-layer model, are used. Two WMLES techniques are used. In the first, the log-law WMLES, the entire wall layer is bypassed, and the velocity at the first grid point, which is located ideally in the logarithmic region, can be related to the wall stress by assuming a logarithmic velocity profile. The second is the Delayed Detached-Eddy Simulation (DDES), a hybrid approach in which the RANS equations are solved in attached, thin shear layers, while the LES is used in separated flow.

The mean radial velocity profiles obtained by URANS and WMLES are shown in Figure 1. Near the impingement region all models agree well with each other. Downstream, the SA model yields a wall-jet velocity profile similar to that of the resolved LES, although the maximum velocity is about 8% larger, the wall jet is wider for $r/D < 2.0$. The wall jet velocity predicted by the $k - \omega$ SST model shows a much wider wall jet, and, in the outer shear layer, a back flow can be seen. The maximum velocity also decays faster, and is 15% smaller than the resolved LES value for $r/D > 1.5$. The $k - \epsilon$ two-layer model predicts the velocity similar to the $k - \omega$ SST model. WMLES and DDES show good agreement with the resolved LES results.

None of the URANS model is able to predict the correct vortex dynamics (Figure 2). Even the generation

of the primary vortex in the jet shear layer is, in some cases, slower, presumably because of the damping of the shear-layer instability due to the large eddy viscosity predicted there by the URANS models; the result is a much weaker primary vortex, which decays more rapidly. The SA model, designed for wall-bounded flow, is the least accurate in this region. The $k - \omega$ SST model and the $k - \epsilon$ two-layer model have the same behaviour in the jet shear layer. In the near-wall region, however, the ω equation is triggered, resulting in improved prediction of the separation. DDES and WMLES shows better agreement with the resolved LES.

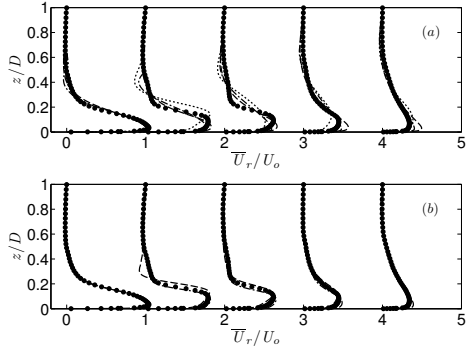


Figure 1: Profiles of \bar{U}_r at $r/D = 1.0$ to 3.0 by (a) URANS: • resolved LES; – SA ; ··· $k - \omega$ SST; - - - $k - \epsilon$ two-layer. (b) WMLES: • resolved LES; – DDES; - - - log-law WMLES.

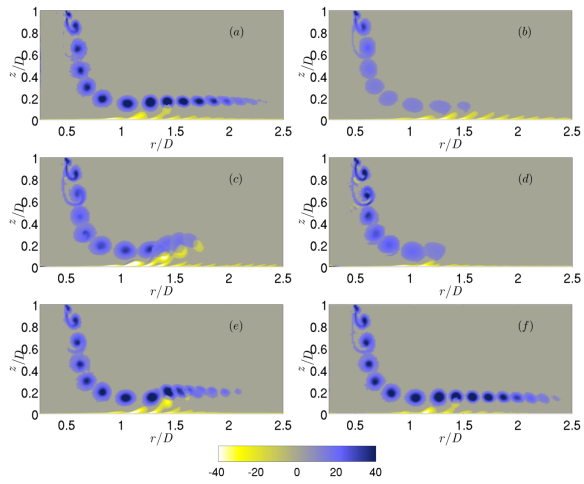


Figure 2: Contours of phase-averaged vorticity at levels -40 to 40 . Time interval between each set of contours is $0.25T$. (a) resolved LES; (b) SA; (c) $k - \omega$ SST; (d) $k - \epsilon$ two-layer; (e) DDES; (f) log-law WMLES.

The magnitude of the TKE in the region between the primary and secondary vortices varies significantly (Figure 3). The SA model does not predict the TKE correctly. The $k - \omega$ SST case, surprisingly, shows very low levels of TKE during the vortex interaction, but as shown before, stronger separated vorticity is

predicted. The weak turbulence in this region is the reason for the slow decay of the vortex pair predicted by this model. The $k - \epsilon$ two-layer model predicts very large TKE during the interaction, even though the separated vorticity can barely be observed. In the WMLES cases the stochastic TKE in the shear layer between the primary and secondary vortices is lower than it in the resolved LES case, although the separated vortex by DDES is stronger . The primary vortex survives the interaction only in the WMLES cases , in which the secondary region of high stochastic TKE in the vortex core appears, matching the resolved LES results.

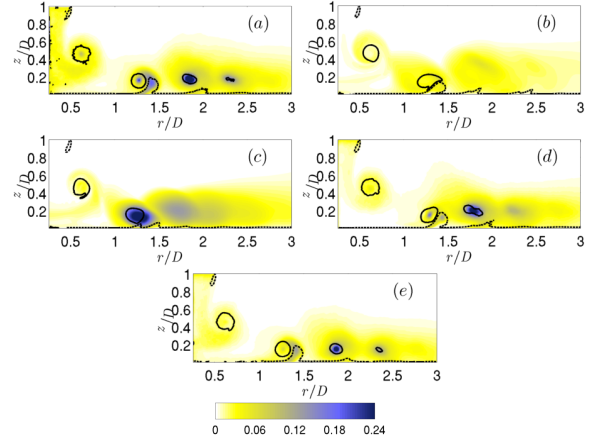


Figure 3: Contours of the stochastic TKE at $\phi = 6/8$, normalized by U_o^2 . (a) Resolved LES; (b) $k - \omega$ SST; (c) $k - \epsilon$ two-layer; (d) SA WMLE ; (e) log-law WMLES.

We thus conclude that the URANS approach was not very successful: $k - \omega$ SST model showed a superiority over the others; SA did not predict the vortex generation correctly, and $k - \epsilon$ two-layer underpredicts the separation. The hybrid WMLES, both gave the most accurate results.

REFERENCES

- [1] U. Piomelli and E. Balaras. Wall-layer models for large-eddy simulations. *Annu. Rev. Fluid Mech.*, 34 (2002), pp. 349–374.
- [2] W. Wu, and U. Piomelli. Large-eddy simulation of impinging jets with embedded azimuthal vortices. *J. Turbul.* 16 (2014), pp. 44–66.
- [3] J. Geiser and K.T. Kiger. Vortex ring breakdown induced by topographic forcing. *Journal of Physics: Conference Series*, 318 (2011), p. 062013

Shock Capturing for High-Order Correction Procedure via Reconstruction Methods

Nicolas Ringue and Siva Nadarajah

Department of Mechanical Engineering, McGill University, Montreal, QC, Canada

Email: nicolas.ringue@mail.mcgill.ca

ABSTRACT

In this paper, shock capturing schemes for the solution of the compressible Euler equations of gas dynamics using the high-order Correction Procedure via Reconstruction (CPR) method are considered. In the presence of flow discontinuities (shocks and contact discontinuities), high-order approximations exhibit Gibbs-type oscillations that pollute the solution and potentially prevent convergence. Shock capturing schemes are therefore needed to eliminate spurious high-frequencies and obtain stable solutions. Approaches commonly used to stabilize high-order discontinuous Galerkin (DG) discretizations are based on the use of limiters or on addition of artificial dissipation.

In this work, artificial viscosity schemes proposed by Persson and Peraire [2], as well as some limiting procedures are studied within the CPR framework. Our goal is to compare those approaches and assess their limitations in order to develop an efficient and robust shock capturing methodology for high-order solutions of transonic and supersonic flows using the CPR scheme.

These shock capturing schemes have been successfully used to obtain high-order solutions of unsteady problems. Steady problems involving shocks appear to be more challenging, especially when implicit methods are employed. Scalar conservation laws have been considered to first test several shock capturing methods. A simple steady advection equation with a steep manufactured solution is solved using the CPR scheme. Figure 1 presents the solution obtained in this case using 10 P_5 elements. Since no shock capturing is used, spurious oscillations alter the solution in the shock region and produces an error that is convected downstream. In contrast, figure 2 shows the solution obtained with the addition of artificial dissipation. The use of this shock capturing method results

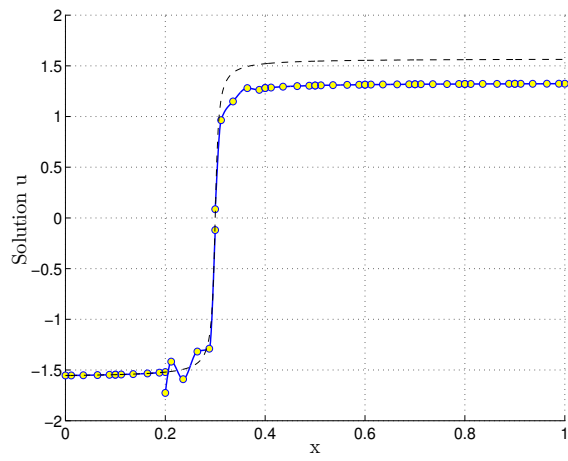


Figure 1: Steady advection equation numerical (blue) and exact (black) solutions on 10 sixth order (P_5) elements (no shock capturing).

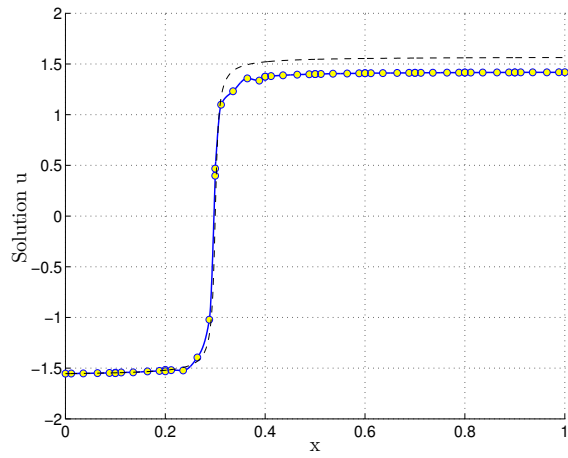


Figure 2: Steady advection equation solution using artificial viscosity-based shock capturing.

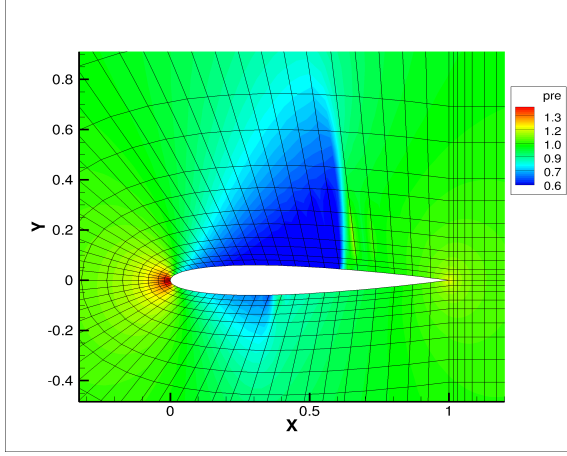


Figure 3: Pressure field for the transonic flow over a NACA 0012 airfoil on P_2 elements.

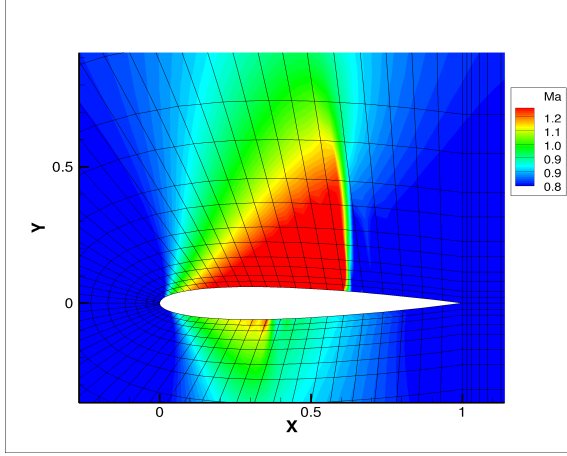


Figure 4: Mach number field for the transonic flow over a NACA 0012 airfoil on P_2 elements.

in less spurious oscillations in the shock region and hence in a globally more accurate solution. The use of limiters, particularly the WENO limiter recently proposed by Du et al. [1], appears less computationally costly although not as efficient as artificial viscosity to eliminate spurious oscillations. Further comparisons between limiters and artificial viscosity approaches remain to be carried out in order to verify this fact.

The two-dimensional case of a transonic inviscid flow over a NACA 0012 airfoil is also considered to assess the reliability and robustness of the proposed shock capturing schemes. The steady solution of this case (Mach 0.8, $\alpha = 1.25^\circ$) is computed using an implicit Newton-Krylov algorithm. The physical artificial viscosity method [2] is used to stabilize the so-

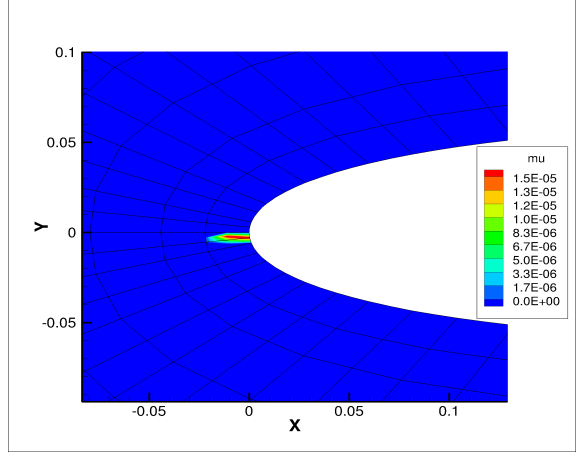


Figure 5: Artificial viscosity field (converged solution).

lution. Computations reveal a certain difficulty for this method to obtain a converged solution. In order to improve its robustness, a smoothing of the piecewise constant artificial viscosity field is proposed in order to ensure continuity at the element interfaces. This enhances the convergence properties of the implicit solver. Figures 3 and 4 show the converged solution obtained for this case. An interesting feature of the present shock capturing scheme is that a reduced amount of artificial dissipation is actually added to ensure convergence (see figure 5). Once the solution is converged, no dissipation seems needed in the shock region. Note also that the shock is represented within a single cell.

However, this method still exhibits a certain sensitivity to the artificial viscosity model parameters. Several options are currently studied in order to improve its robustness. Other artificial viscosity models (Laplacian artificial viscosity and artificial bulk viscosity), as well as a line-search algorithm for the implicit backward Euler solver and a possible automation for the choice of the shock capturing scheme's parameters are currently investigated and expected to improve the robustness of the method.

REFERENCES

- [1] J. Du, C.-W. Shu, and M. Zhang. A simple WENO limiter for the CPR framework on unstructured meshes. *Applied Numerical Mathematics*, 2015.
- [2] P.-O. Persson and J. Peraire. Sub-cell shock capturing for discontinuous Galerkin methods. In *44th Aerospace Sciences Meeting*. AIAA, 2006.

Simulation of Integrated Nozzle/Jet Compressible Subsonic Turbulent Flow

A. Ghasemi and Xianguo Li

Department of Mechanical and Mechatronics Engineering, University of Waterloo

200 University Avenue West, Waterloo, Ontario, Canada N2L 3G1

Email: *a6ghasem@uwaterloo.ca.*

ABSTRACT

Compressible subsonic flow of turbulent round jet is simulated. Smooth contraction nozzle is attached to the free jet region to provide appropriate real-time inlet conditions. Unsteady compressible Navier-Stokes equations are solved using the rapid distortion RNG $k - \varepsilon$ turbulence model. Computational domain is spatially discretized using a finite volume approach. Gas flow accelerated in the smooth contraction nozzle, is issued at a Mach number $Ma = 0.35$ and a temperature of $T = 310$ K. The corresponding Reynolds number $Re = U_j D / v$ equals 1.9×10^5 . Transition of the jet into the domain is temporally tracked until a quasi-steady jet is formed.

1. INTRODUCTION

Shear flows generated in the form of jets, are used for variety of applications in industry such as mixing, heating, cooling and cleaning. In addition, they have been subject of many fundamental experimental [1] and numerical [2,3] studies. Free jets issued from different shapes of nozzle openings [4,5] result in different flow features in the jet. In addition, single and multiphase jets [6] can be similar in some aspects and different in other characteristics. One of the important characteristics of jets is the level of entrainment [7] and mixing. Entrainment and mixing are highly affected by the formation and dynamics of the vortical structures in the shear layer [8]. It should be noted that, above mentioned studies have been mainly conducted for fully developed steady jet. However, many industrial applications of transitional and starting jets have made them an interesting topic of research with fundamental and practical importance [9].

In the present study, unsteady compressible Navier-Stokes equations are solved with rapid distortion RNG $k - \varepsilon$ turbulence model using a finite volume

approach. Smooth contraction nozzle is included in the jet computational domain to allow an integrated solution. Unsteady simulations are carried out for the transition of starting jet, and conducted until reaching steady state jet conditions.

2. PROBLEM DEFINITION AND SIMULATION APPROACH

Figure 1 shows the computational domain, including the smooth contraction nozzle and free jet region. Gas flow enters the jet region at a Mach number $Ma = 0.35$ and a temperature of $T = 310$ K. The equivalent Reynolds number $Re = U_j D / v$ is 1.9×10^5 . Compressible subsonic flow of turbulent round jet is simulated by solving unsteady compressible Navier-Stokes equations:

$$\frac{\partial \bar{\rho}}{\partial t} + \frac{\partial(\bar{\rho}\tilde{u}_i)}{\partial x_i} = 0 \quad (1)$$

$$\begin{aligned} \frac{\partial \bar{\rho}\tilde{u}_i}{\partial t} + \frac{\partial \bar{\rho}\tilde{u}_i\tilde{u}_j}{\partial x_j} &= -\frac{\partial \bar{p}}{\partial x_i} + \frac{\partial}{\partial x_j} \left[2\mu S_{ij} - \frac{2}{3}\mu \frac{\partial \tilde{u}_j}{\partial x_i} \delta_{ij} \right] \\ &\quad - \frac{\partial}{\partial x_j} (\tau_{ij}) \end{aligned} \quad (2)$$

Where, is the $S_{ij} = \frac{1}{2} \left(\frac{\partial \tilde{u}_i}{\partial x_j} + \frac{\partial \tilde{u}_j}{\partial x_i} \right)$ and τ_{ij} are the strain rate and Reynolds stress tensors. In order to couple the continuity and momentum equations, density is related to pressure using the equation of state $P = \rho R T$. Therefore, additional energy equation needs to be solved to obtain temperature. In addition to the above equations, the transport equations for turbulent kinetic energy and turbulence dissipation rate should be solved to obtain the closure of Reynolds stress term. The above equations are discretized using a finite volume approach with first-order upwinding of the convective terms. In addition, a second-order accurate Crank-Nicolson scheme is

implemented for time marching. Mass flow rate is imposed as nozzle inlet boundary condition. Nozzle wall is treated with a no-slip condition. Outflow boundaries are subjected to zero normal Gradient Neumann condition. A Cartesian grid is generated for the finite volume discretization of the domain. The grid is locally refined using adaptive mesh refinement.

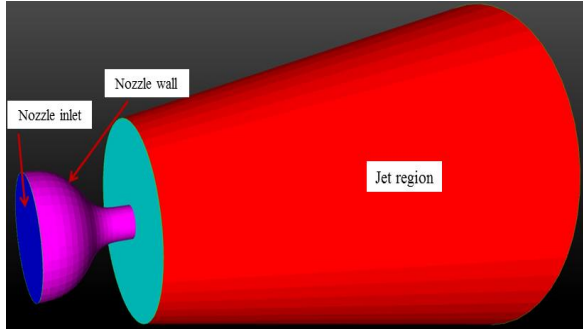


Fig. 1: The computational domain

3. RESULTS AND DISCUSSION

In Figure 2, the velocity magnitude is shown in the central plane of a quasi-steady jet. Flow is accelerated through the smooth contraction nozzle. This smooth contraction can prevent secondary flows by developing a thin boundary layer at the nozzle exit. Near the jet centerline potential core is maintained up to 6.5 diameters downstream. Due to the ambient flow entrainment, the jet is expanding with the downstream distance.

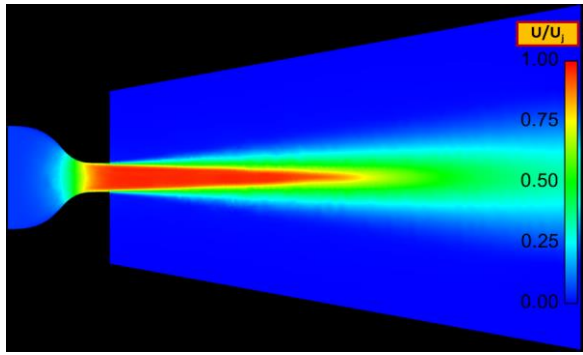


Fig. 2: The velocity distribution in the central plane

4. CONCLUSION

Compressible subsonic flow through the smooth contraction nozzle is simulated during the formation and evolution of turbulent round jet. Unsteady compressible Navier-Stokes equations are solved using the rapid distortion RNG $k - \varepsilon$ turbulence

model for a transient jet until a steady state condition is obtained. It is shown for a steady state jet, that gas flow is accelerated through the smooth contraction nozzle. A potential core region is formed up to 6.5 nozzle diameters downstream in the near-field of the jet. The jet region expands with downstream distance due to ambient air entrainment.

ACKNOWLEDGEMENTS

The financial support of the Natural Science and Engineering Research Council of Canada (NSERC) via a discovery grant is greatly appreciated.

REFERENCES

- [1] A.M. Shinneeb, J.D. Buggand R. Balachandar. Quantitative investigation of vortical structures in the near-exit region of an axisymmetric turbulent jet. *Journal of Turbulence*, 9(19):1-20, 2008.
- [2] C. Bogey and C. Bailly. Large eddy simulations of transitional round jets: Influence of the Reynolds number on flow development and energy dissipation. *Physics of Fluids*, 18(6), 1-14, 2006.
- [3] J. Kim and H. Choi. Large eddy simulation of a circular jet: effect of inflow conditions on the near field. *Journal of Fluid Mechanics*, 620:383-411, 2009.
- [4] A. Ghasemi, V. Roussinova and R. Balachandar. A study in the developing region of square jet. *Journal of Turbulence*, 14(3):1-24, 2013.
- [5] A. Ghasemi, V. Roussinova, R.M. Barron, and R. Balachandar. Reynolds number effects in the near-field of a turbulent square jet. *Experimental Thermal and Fluid Sciences*, 61:249-258, 2015.
- [6] A. Ghasemi, R.M. Barron and R. Balachandar, Spray-induced air motion in single and twin ultra-high injection diesel Sprays, *Fuel*, 121: 284–297, 2014.
- [7] A. Ghasemi, V. Roussinova, R.M. Barron and R. Balachandar. Analysis of entrainment at the turbulent/non-turbulent interface of a square jet. *ASME Congress & Exposition*, 1-7, 2013.
- [8] J. Philip and I. Marusic. Large-scale eddies and their role in entrainment in turbulent jets and wakes, *Physics of Fluids*, 24(5):1-10, (2012).
- [9] P.S. Kruegera and M. Gharib. The significance of vortex ring formation to the impulse and thrust of a starting jet. *Physics of Fluids*, 15(5):1271-1281, 2003.

Stochastic Methods For Reproducing The Continuity Effect In Turbulent Particle-Laden Flows

S. Murray, M. F. Lightstone, S. Tullis

McMaster University, Hamilton, ON, Canada

Email: *murrasa@mcmaster.ca, lighstm@mcmaster.ca, stullis@mcmaster.ca*

Particle-laden flows are a class of two-phase flows in which one of the phases is a continuously connected fluid, and the other phase is comprised of small, immiscible, typically dilute particles dispersed throughout the fluid. The modelling of turbulent particle-laden flows can be applied to a tremendous range of phenomena of environmental and industrial interest, such as the dispersion of pollutants in the atmosphere, fluidization and turbulent mixing in combustion processes, deposition of medicinal aerosols in the extrathoracic airway, processing and transport of liquid/solid nuclear waste and water droplet formation within clouds. Many physical/chemical processes depend upon the local concentration of the dispersed species, hence the development of accurate computational models of these processes depends on the ability to reproduce particle clustering and dispersion. Even single phase turbulent flows pose enormous challenges for researchers; often many simplifying assumptions are required to make meaningful predictions. This difficulty is exacerbated with the addition of a particle phase, since a balance must be sought in simulating the turbulence in a manner which is computationally tractable, but does not sacrifice the detailed correlated information “seen” by the dispersed particles.

In much particle-laden flows literature, the aim is to reproduce dispersion, defined as $\langle y_p^2(\tau) \rangle$, where

$$y_p(\tau) = x_p(t + \tau) - x_p(t) \quad (1)$$

and x_p represents the position of a dispersed particle (treated in the Lagrangian frame of reference). The brackets $\langle \cdot \rangle$ indicate an average over the particle ensemble. Related to dispersion is the particle Lagrangian velocity autocorrelation:

$$R^L(\tau) = \frac{\langle u_p(x_p(t), t) u_{p,j}(x_p(t + \tau), t + \tau) \rangle}{\sqrt{\langle (u_p(x_p(t))^2) \rangle} \sqrt{\langle (u_p(x_p(t + \tau), t + \tau))^2 \rangle}} \quad (2)$$

If the only fluid information available is the time-averaged statistics (as in the Reynolds-averaged Navier-Stokes (RANS) context), one can stochastically generate a history of correlated fluid velocities seen by individual particles, according to a discretized Langevin equation, in a manner which reproduces these statistics (often in addition to reproducing the expected autocorrelations). This information is then used to integrate the (Lagrangian) momentum equation for an individual particle. Such methods are known as stochastic separated flow (SSF) models. A generalized governing stochastic differential equation of the particle velocity random variables is [10]:

$$du_p = f(u_p, x_p, t) dt + g(u_p, x_p, t) dW \quad (3)$$

where W is a Wiener process. Such a construction yields histories of u_p which are Markovian by construction. It is expected that autocorrelations exhibit a spatial as well as temporal dependence, and the spatial autocorrelations exhibit qualitatively different behaviour between the ballistic and inertial ranges. To ensure the random variables u_p are centred, however, the process W must likewise exhibit a spatial dependence, and self-similarity is therefore not guaranteed, which can lead to an inconsistency between imposed and effective autocorrelations. In fact it has been shown that such treatments are dependent on timestep [6]. While homogenous Langevin treatments are consistent, they yield exponentially decaying autocorrelations - and there exists an important scenario in which such behaviour is unrealistic: the lateral dispersion of heavy particles with high drift velocity (due to the presence of a body force). In such cases, it has been demonstrated analytically [1], numerically [3], and experimentally [8] that the lateral autocorrelations exhibit significant negative loops (referred to as the *continuity effect*) which the aforementioned Langevin treatment is unable to capture - this naturally has important implications for the suitability of SSF for captur-

ing dispersion in such scenarios.

A method which reproduces negative autocorrelation loops necessitates that the particles have an enhanced “memory”; a potential means for accomplishing this is to kinematically simulate the underlying turbulence, rather than the velocity histories of individual particles. Kinematic simulation (KS) (with its basis in the work of Kraichnan [5]) allows a turbulent-like field to be constructed from randomly oriented trigonometric function elements, in a manner consistent with the expected second-order Eulerian statistics. KS has attracted attention due to its purported ability to reproduce realistic dispersion of *pairs* of particles, and in turn, concentration variances of passive scalars [2]. The applicability of KS to *single-particle* Lagrangian statistics, however, has received considerably less attention, which we address here.

The applicability of both SSF and KS to reproducing the continuity effect for heavy dispersed particles, and in turn, dispersion, is tested. A variety of numerical simulations are carried out, in which an ensemble of virtual heavy particles were advected according to three methods:

- Direct numerical simulation
- KS “turbulence” (according to the method of [7])
- SSF (according to the method of Hennick [4])

In all cases the particles are subjected to a body force sufficiently large such that the continuity effect would, in theory, be present. A key result is that KS is able to qualitatively reproduce the lateral autocorrelations of the particle ensemble, whereas SSF is not (Fig. 1). As a result, KS successfully reproduces the reduction in lateral dispersion, without appeal to further empiricisms, unlike SSF. The appropriate scale relations of dispersion (according to Taylor [9]) are indeed recovered, though the extent of dispersion is somewhat underpredicted by KS.

REFERENCES

- [1] G. T. Csanady. Turbulent diffusion of heavy particles in the atmosphere. *J. of the Atm. Sci.*, 20:201–208, 1963.
- [2] P. Durbin. A stochastic model of two-particle dispersion and concentration fluctuations in homogeneous turbulence. *Journal of Fluid Mechanics*, 100(02):279–302, 1980.
- [3] S. Elghobashi and G. C. Trusdell. Direct simulation of particle dispersion in a decaying isotropic turbulence. *J. Fluid Mech.*, 242:655–700, 1992.
- [4] E. A. Hennick and M. F. Lightstone. A comparison of stochastic separated flow models for particle dispersion in turbulent flows. *Energy & Fuels*, 14:95 – 103, 2000.
- [5] R. H. Kraichnan. Diffusion by a random velocity field. *Physics of Fluids*, 13(1):22–31, 1970.
- [6] M. Lightstone. Self-consistency and the use of correlated stochastic separated flow models for prediction of particle-laden flows. *Int. J. CFD*, 21(9-10):329–334, 2007.
- [7] F. Nicolleau and A. Abou El-Azm Aly. Can kinematic simulation predict richardson’s regime? *New Approaches in Modeling Multiphase Flows and Dispersion in Turbulence, Fractal Methods and Synthetic Turbulence*, pages 43–57, 2012.
- [8] W. Snyder and J. L. Lumley. Some measurements of particle velocity autocorrelation functions in a turbulent flow. *J Fluid Mech*, 48:41–71, 1971.
- [9] G. I. Taylor. Diffusion by continuous movements. *Proc. London. Math. Soc.*, 20:196 – 212, 1921.
- [10] D. Thomson. Random walk modelling of diffusion in inhomogeneous turbulence. *Quarterly Journal of the Royal Meteorological Society*, 110(466):1107–1120, 1984.

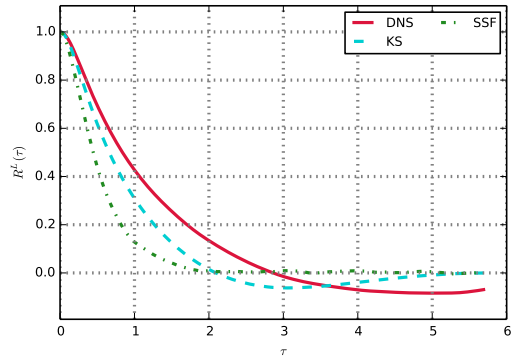


Figure 1: $R^L(\tau)$, perpendicular to the direction of the mean drift of the inertial particles

Stratified Instabilities on the sub-centimeter scale

M. Stastna¹, A. Koberinski², J. Ladan¹

¹ Department of Applied Mathematics, University of Waterloo,
200 University Ave. W, Waterloo, ON. N2L 3G1.

² Department of Philosophy, Western University,
add address

Email: mmstastn@uwaterloo.ca

ABSTRACT

Gravity currents are perhaps the most well studied phenomenon in buoyancy driven fluid mechanics. Most studies concentrate on the large head region which often dominates turbulence production and mixing. In the parameter regime of small length scales and low diffusivity (moderate Reynolds number, high Schmidt number) the dynamics of the gravity current head laminarizes. In this regime transition to turbulence is dominated by the so-called lobe cleft instability of the advancing front and Rayleigh Taylor instability of the large region beneath the gravity current behind the advancing head, and is thus vitally dependent on the no slip boundary conditions at the bottom of the domain and the accurate representation of sharp density interfaces. We discuss numerical simulation, as well as laboratory experiments in what we term the ‘coating regime’.

1 SUMMARY

Gravity currents are quasi-horizontal flows formed when a fluid of higher density collapses into a second fluid of lower density. Naturally occurring examples include pyroclastic outflows from volcanic explosions, dust storms (or haboobs), and freshwater river outflows into the salty coastal ocean [1]. In the laboratory, gravity currents can be easily generated by trapping dense fluid behind a barrier then suddenly removing the barrier. This is termed ‘lock-exchange’ in analogy with the sudden opening of a canal lock. Due to its effect on the refractive index, salt is often used to increase the fluid density and hence the resulting flow is a low Schmidt number flow due to the large contrast between the diffusivity of salinity and the viscosity of water under room temperature conditions.

In this contribution we employ high resolution, pseudo

spectral DNS to examine the fine scale dynamics of a small, salt-like gravity current in what we term the ‘coating regime’. This regime occurs when the Reynolds number is modest and the Schmidt number is low enough to decrease molecular mixing between the thin layer of high density fluid left behind by the gravity current and the less dense fluid trapped beneath the advancing front near the bottom boundary of the tank. The coating occurs due to no-slip boundary conditions at the bottom of the tank, forcing the gravity current up and over the less dense fluid. We find that this coating regime gives rise to RT instabilities, which three dimensionalize and penetrate through the dense overlying fluid. At times these instabilities connect to less dense fluid flowing into the gravity current through lobe-cleft instabilities at the wave front. Besides this connection via lobe-cleft instabilities, we find that the dynamics of the coating regime develop largely independently of the conditions at the wave front. Qualitatively similar structures were observed experimentally.

We consider a $20 \times 2 \times 2$ cm tank, resolved with a grid of $2560 \times 64 \times 256$ points. Figure 1 shows the development of the density field in a horizontal plane, parallel to the bottom boundary at $z = 0.6$ mm. The Reynolds and Schmidt numbers for the simulation were approximated as 150 and 210, respectively.

ACKNOWLEDGEMENTS

This work was supported by the Natural Sciences and Engineering Research Council of Canada.

REFERENCES

- [1] Simpson, J., *Gravity Currents in the Environment and the Laboratory*, Cambridge University Press, Cambridge, 1997.

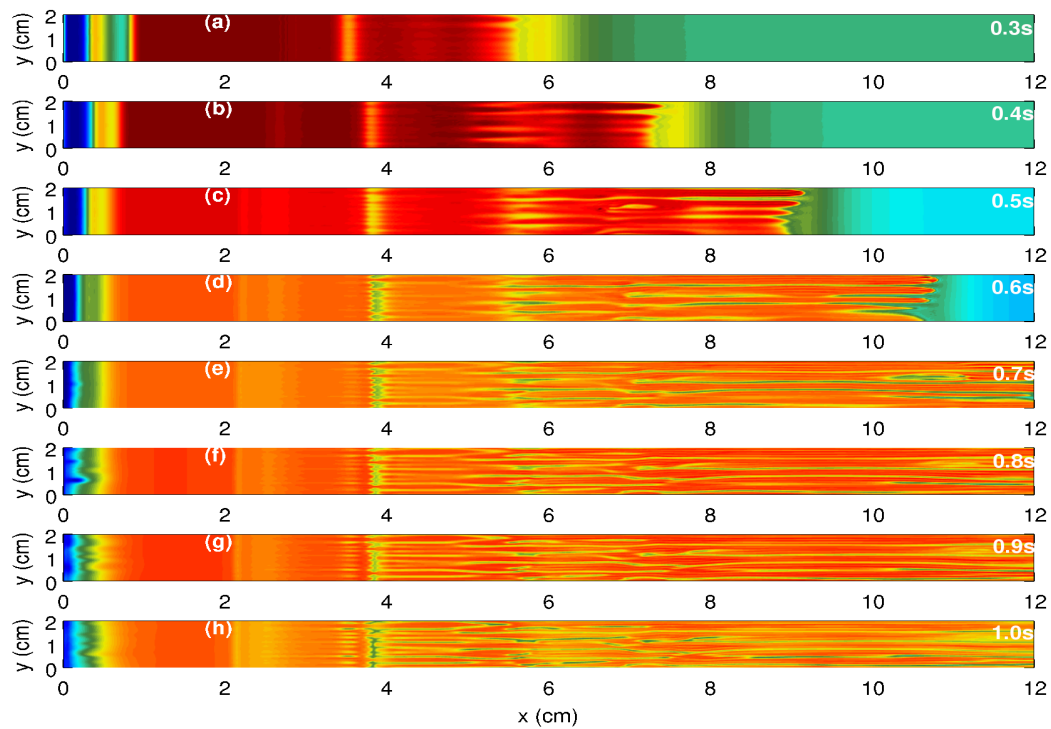


Figure 1: Density x - y slices of the gravity current at a height of $z = 0.6$ mm, focusing on the rising less-dense sections protruding through the coating layer of the gravity current. Slices are shown at regular time intervals from $t = 0.3$ s through $t = 1.0$ s (a–g). Dense fluid is indicated by warm colours, light fluid by cool colours, with dark green indicating the ambient density.

The Effects of Wall Roughness on Adverse Pressure Gradient Boundary Layer

Pouya Mottaghian, Junlin Yuan and Ugo Piomelli

*Department of Mechanical and Materials Engineering,
Queen's University, Kingston, ON, K7L 3N6, Canada*

Email: pouya.mottaghian@me.queensu.ca

ABSTRACT

Separation of the turbulent boundary layer, is among the most critical phenomena that determine the efficiency of flow devices, ranging from airplane wings to turbine and compressor blades, to curved ducts. In many of these cases roughness is present, and increases the wall friction, due to the contribution of pressure drag. In this study Large-eddy Simulations are carried out on flat-plate boundary layer over smooth and rough surfaces in the presence of an adverse pressure gradient, strong enough to induce separation. Roughness causes early flow separation due to increased momentum deficit and decrease of turbulent kinetic energy production.

1 INTRODUCTION

We consider the turbulent flow over a flat plate with a suction and blowing velocity profile imposed at the freestream. This velocity profile induces a strong adverse pressure gradient (APG) that causes the flow to separate and then to reattach downstream. This type of pressure-driven separation is relevant to many flows (airfoils, ducts, etc.) and, unlike the case of geometry induced separation (such as that in the backward-facing step), the prediction of both separation and reattachment is challenging. Previous numerical simulations of this flow in the turbulent regime [1] have shown that large coherent structures are generated in the separation zone and lifted upward into the shear layer and over the separated-flow region. Near the reattachment point these structures impinge on the wall and break apart, generating a highly unsteady three-dimensional flow.

The effect of roughness is known to alter to some extent these dynamics, but the knowledge of the interaction between APG leading to separation and rough-

ness is limited. Boundary layers subjected to strong APG on a rough wall have been studied experimentally in flows over a hill or a ramp [2, 3], where the roughness was shown to cause earlier separation, and a larger separation bubble compared to the smooth-wall flow. This has been attributed to a larger mean momentum deficit on the rough wall. However, roughness is also expected to lead to higher turbulence intensities, which should contribute to a delay of the separation. Therefore, the cause of the earlier separation is not yet fully understood. In this study, we carry out large-eddy simulations (LES) of flat plate boundary layers to investigate the physics underlying rough wall flow separations.

2 PROBLEM FORMULATION

The simulations are performed using a well-validated code that solves continuity and momentum equations on a staggered grid using second-order, central differences for all terms, and a second-order semi-implicit time advancement [4]. The deceleration is imposed by a spatially varying freestream velocity in the wall-normal direction, $V_\infty(x)$ (Fig. 1); An immersed-boundary method (IBM) based on the volume-of-fluid approach [5] is used to model the roughness as a dense distribution of randomly rotated ellipsoids (sand grains). A smooth-wall and a rough-wall case are simulated in the same conditions. Grid sizes for the smooth and rough case have, respectively, $2560 \times 384 \times 384$ and $2048 \times 384 \times 384$ grid points. The roughness Reynolds number, $k^+ = ku_\tau/\nu$ (where u_τ is the friction velocity, ν the kinematic viscosity), is 60 in the upstream equilibrium region.

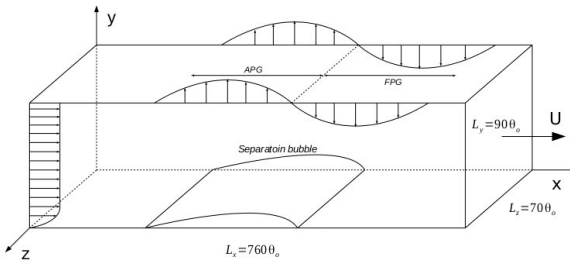


Figure 1: Computational setup.

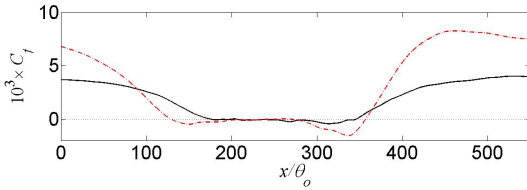


Figure 2: Streamwise development of the friction coefficient.

3 RESULTS

Figure 2 shows the friction coefficient $C_f = 2\tau_w/\rho U_{\infty,o}$ (where $U_{\infty,o}$ is the freestream velocity at the inlet) above the roughness sublayer. In the rough-wall case the flow separates earlier than on the smooth wall, and the separation bubble is longer and taller than the smooth case. In the roughness sublayer, APG leads to faster decrease of $\langle \bar{u} \rangle$ (compared to the outer layer) due to larger small-scale separations downstream of roughness elements which do not emerge from roughness sublayer until $x/\theta_o = 170$; an increasingly larger percentage of the xz -plane is associated with zero or negative $\langle \bar{u} \rangle$, leading to the earlier separation. Note that, inside the roughness layer, the mean velocity becomes negative even earlier.

The mean streamwise-velocity profiles at two locations are shown in (Fig. 3). Roughness leads to lower mean momentum in the boundary layer due to the higher Reynolds shear stress and the increased momentum deficit is the main reason of early separation at rough wall flow.

The roughness effect on the turbulence intensity is shown by the TKE contours in Fig. 4. The APG is found to noticeably decrease the TKE magnitude on the rough wall for $100 < x/\theta_o < 130$; it can be shown that this is due to a significant decrease of TKE production. Furthermore, after separation, the turbulent intensity increases in the shear layer because turbulent eddies detach from the wall and grow significantly inside the separating shear layer; in this process, the

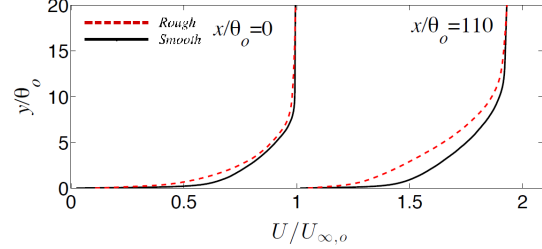


Figure 3: Evolution of the streamwise mean velocity in the upstream equilibrium region ($x/\theta_o = 0$) and immediately before separation ($x/\theta_o = 110$).

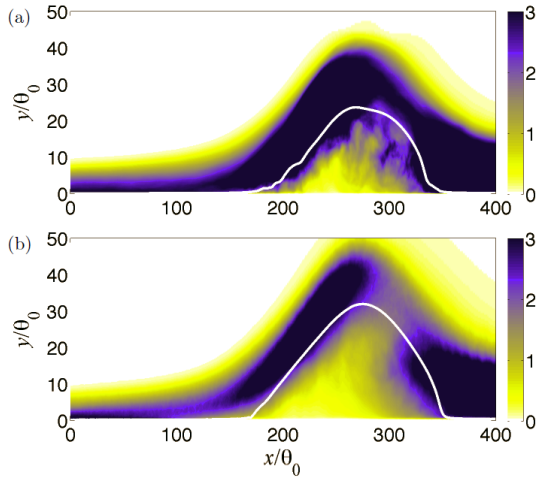


Figure 4: Contours of TKE normalized by $u_{t,o}^2$ in (a) smooth and (b) rough cases. White line: dividing streamline.

structures depend on the outer layer input, i.e., the freestream deceleration and acceleration, instead of that from the wall, i.e., the roughness.

REFERENCES

- [1] Y. Na and P. Moin, *J. Fluid Mech.*, vol. 370, pp. 175–201, 1998.
- [2] S. Song, D. B. DeGraaff, and K. Eaton, *Int. J. Heat Fluid Flow*, vol. 21, pp. 512–519, 2000.
- [3] S. Cao and T. Tamura, *Journal of wind engineering*, vol. 94, pp. 1–19, 2006.
- [4] A. Keating, U. Piomelli, K. Bremhorst, and S. Nešić, *J. Turbul.*, vol. 5, p. N20, 2004.
- [5] A. Scotti, *Phys. Fluids*, 18:31701, 2006.

The lattice Boltzmann method for compressible flows at high Mach number

Yao Deng¹, Fue-Sang Lien², and Eugene Yee³

¹ Department of MME, The University of Waterloo, Waterloo, Canada

² Department of MME, The University of Waterloo, Waterloo, Canada

³ Defence Research and Development Canada, Suffield Research Centre, Medicine Hat, Alberta, Canada

Email: y27deng@uwaterloo.ca

ABSTRACT

The lattice Boltzmann method (LBM) is a mesoscopic-level “particle-based” method representing a density distribution that can be used to solve certain types of partial differential equations (PDEs). More specifically, LBM provides a very simple numerical procedure for simulating the Boltzmann equation at the microscopic level, whose appropriate coarse graining leads to the standard hydrodynamic equations (in the long wavelength limit) that express the conservation of mass (continuity equation) and momentum (Navier Stokes equation) at the continuum level. Owing to the fact that LBM offers numerous advantages such as simplicity, efficiency and accuracy over more traditional methodologies, it has been increasingly used by researchers in recent years for the simulation of turbulence and multi-phase and multi-component flows in porous media.

In the initial development of LBM, researchers focused on the simulation of very low-Mach-number incompressible and isothermal flows [1]. These methodologies are not suitable (e.g., unstable and unreliable) for the simulation of fluid flows at larger Mach numbers. Currently, there is no consensus on the “correct” method for application of LBM to the simulation of compressible high-Mach-number flows (which necessarily requires the development of a model for LBM that leads to the correct Newtonian thermo-hydrodynamics in the long wavelength limit). Nevertheless, there has been some important recent developments on models for LBM that can simulate high-Mach-number compressible flows, most notably the Kataoka-Tsutahara (KT) model [2] and Qu’s model [3].

In this paper, we present and compare results for a number of benchmark test cases of compressible flows

obtained with the KT model and Qu’s model. To this purpose, these thermal LBM models have been implemented using a number of different finite volume advection schemes such as the simple upstream differencing scheme (UDS) and various total variation diminishing (TVD) schemes such as the Monotonic Upstream-Centered Scheme for Conservation Laws (MUSCL) and the weighted essentially non-oscillatory (WENO) schemes [3, 4]. Typical benchmark tests such as the shock tube problem and the double Mach reflection problem have been implemented in order to validate the two compressible LBM models and the proposed advection schemes used with these models. These simulations demonstrate the capability of LBM in the simulation of compressible flows at high Mach numbers and will provide the guidance for future researchers who are interested in finding the most appropriate LBM models and advection schemes for specific compressible flow applications.

REFERENCES

- [1] Chen, S.-Y., Chen, H.-D., Martnez, D. and Matthaeus, W. Lattice Boltzmann model for simulation of magnetohydrodynamic. *Physical Review Letters*, 67(27):3776–3779, 1991
- [2] Kataoka, T. and Tsutahara, M. Lattice Boltzmann model for the compressible Navier-Stokes equations with flexible specific-heat ratio. *Physical Review E*, 69(3), 035701, 2004
- [3] Qu, K. Development of lattice Boltzmann method for compressible flows, PhD thesis, Northwestern Polytechnical University, China, 2009
- [4] Wang, Y., He, Y.-L., Zhao, T.-S., Tang, G.-H. and Tao, W.-Q. Implicit-explicit finite-

difference lattice Boltzmann method for compressible flows. *International Journal of Modern Physics C* 18(12):1961–1983, 2007

The Numerical Performance Comparison between Nominal and As-Manufactured Heat Transfer Enhancement Surfaces

A.J.M. Buckrell¹, F.-S. Lien²

¹ University of Waterloo, Waterloo, Canada, ajmbuckr@uwaterloo.ca

² University of Waterloo, Waterloo, Canada, fue-sang.lien@uwaterloo.ca

The performance of heat transfer enhancement (HTE) surfaces in compact heat exchangers (CHE) is the focus of study in many analytical/empirical [1], experimental [2, 3], and more recently, numerical studies [4, 5]. Understanding the heat transfer and pressure drop performance within these surfaces is critical to developing new and more efficient heat transfer enhancement surfaces.

Many previous studies place focus on developing models to predict the performance of HTE surfaces [1], however, although experimental testing and validation is used for comparison of results [2, 5], a critical step is left out of the process: fully understanding what the post-manufactured part looks like in comparison to the nominal geometry used for modelling. The variation in manufactured geometry, combined with uncertainty introduced in testing can lead to a significant departure between the expected and actual CHE performance.

The focus of the present study is to take an in-depth look at the geometry created during the manufacturing process and compare it with nominal CAD data. Furthermore, an investigation into the effects of turbulence models on heat transfer and pressure drop predictions is conducted and recommendations for modifications to normal CAD models are suggested as a means to improve performance predictions. This study represents the first in-depth look at the small scale flows within bluff body type HTE's in either a numerical or experimental context.

A 3D reconstruction method is performed, in which a CHE sample is assembled into a digital model of the physical geometry. Significant departures from nominal geometry are observed, including rounding of HTE surface edges and thinning of material. Numerical simulations are performed on the acquired geometry, and improved agreement with experimental results is observed.

A study of the impact of turbulence models is performed. The results indicate that there is a significant variability based on the model selected for simulation. Furthermore, LES predicts a fully turbulent flow at the highest Re tested. Further investigation is ongoing to determine the Re at which the flow becomes turbulent and the Re at which the onset of unsteady flow occurs. LES models are observed to provide the best overall agreement with experimental results.

Modifications to nominal CAD data are performed, and results are compared with those obtained using the real geometry derived through the 3D reconstruction process. Tested Re range from 8 to 600. LES results show a significant improvement with modified geometry in comparison to those using nominal CAD data.

References

- [1] R.M. Manglik and A.E. Bergles, *Heat Transfer and Pressure Drop Correlations for the Rectangular Offset Strip Fin Compact Heat Exchanger*, Exp. Therm. Fluid Science **10**, pp. 171-180 (1995).
- [2] J. Stasiak and M.W. Collins and M. Ciofalo and P.E. Chew, *Investigation of Flow and Heat Transfer in Corrugated Passages - I. Experimental Results*, Int. J. Heat Mass Transfer **39**, 1, pp. 149-164 (1996).
- [3] X. Gao and B. Sundén, *PIV Measurement of the Flow Field in Rectangular Ducts with 60 degree Parallel, Crossed and V-Shaped Ribs*, Exp. Therm Fluid Science **28**, pp. 639-653 (2004).
- [4] K. Suzuki and E. Hirai and T. Miyake and T. Sato, *INumerical and Experimental Studies on a Two-Dimensional Model of an Offset-Strip-Fin Type Compact Heat Exchanger used at Low Reynolds Number*, Int. J. Heat Mass Transfer **28**, 4, pp. 823-836 (1985).
- [5] M. Ciofalo and J. Stasiak and M.W. Collins, *Investigation of Flow and Heat Transfer in Corrugated Passages - II. Numerical Simulations*, Int. J. Heat Mass Transfer **39**, 1, pp. 165-192 (1996).

Thermocapillary Migration of a Deformable Droplet

Babak Samareh¹, Arash Kashani², and Javad Mostaghimi¹

¹*Mechanical and Industrial Engineering Department, University of Toronto, Canada*

²*Simulent Inc., Toronto, Canada*

Email: *mostag@mie.utoronto.ca*

ABSTRACT

In the present study a parallel three dimensional Volume of Fluid (VOF) method is developed to simulate Marangoni convection in immiscible fluids with variable surface tension. Conservation equations are solved based on cell-averaged one-field volume tracking scheme. Evaluating the convective term in the energy equation along the boundary between the fluids highly depends on the position and orientation of the interface; hence, using average cell values simply ignores the interface shape and leads to computational uncertainty. As a remedy to this issue, the original idea behind the volume tracking method is used not only to advect mass and momentum but also energy across cells. To verify the proposed algorithm, results are compared against theoretically predicted thermocapillary migration velocity of a droplet at the limit of zero Marangoni number. However, at relatively high Marangoni numbers, thermal boundary layers are very thin and challenging to resolve. To demonstrate the capabilities of the heat transfer module, simulation of a Fluorinert droplet moving in silicon oil under applied temperature gradient in microgravity is compared against the available experimental results and the migration velocity of the droplet is reported.

1. INTRODUCTION

Thermal fluctuations in a two phase interfacial flow can alter the dynamics of the interface due to the dependence of the surface tension on temperature. Variations of the surface forces along the interface, known as Marangoni forces, can impact the flow field via induced interfacial flows which in turn change the interfacial temperature distribution. An example of temperature dependent flow dynamics is the thermocapillary motion of droplets and bubbles caused by the variations of interfacial tension when placed in another fluid and subjected to a temperature

gradient. In the present study, a fully 3D parallel Volume of Fluid (VOF) multi-phase flow solver is employed to capture Marangoni effects during thermocapillary migration of a drop.

2. GOVERNING EQUATIONS

In an Eulerian frame, the continuity, momentum, and energy equations are solved, coupled with Young's front tracking algorithm to reconstruct the interface between the two-phases. The surface tension force, which is non-zero only at the interface, is expressed as:

$$\mathbf{F}_{ST} = \sigma(T)K\nabla f + \nabla_{\parallel}\sigma(T)|\nabla f| \quad (1)$$

where K is the local interface curvature and ∇_{\parallel} the tangential surface derivative. The first term on the right hand side corresponds to the temperature-dependent normal surface tension component, while the second term corresponds to the Marangoni force. The problem of the thermocapillary migration of a drop is characterized by the following non-dimensional parameters: the capillary number, which gives the ratio of the tangential to normal stresses at the drop interface, the Reynolds number, and the Marangoni number, which represents the relative importance of convective transport of energy with respect to molecular transport, defined by:

$$Ma = \frac{U\rho_b C_{pb} r_0}{k_b} = \frac{\sigma_T |\nabla T| r_0^2}{\mu_b \alpha_b} \quad (2)$$

3. NUMERICAL IMPLEMENTATION

Energy equation is discretized using the finite volume approach with volume averaged quantities used to approximate cell centered variables. It is shown that evaluating the convective terms in the energy equation at the boundary between the fluids highly depends on the position and orientation of the interface [1]; hence, using average cell values simply

ignores the interface shape and leads to computational uncertainty. A remedy to this issue is to use Young's volume tracking algorithm to find the exact mass of each fluid crossing cell boundaries and calculate the associated energy transfer, as shown in Figure 1.

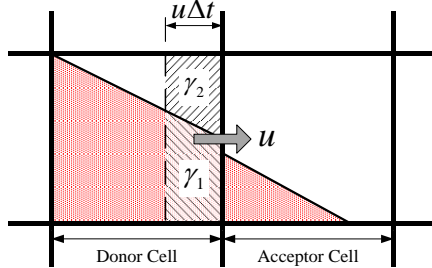


Figure 1 Mass and momentum transfer based on Young's algorithm

Energy transfer can be expressed as:

$$\text{Energy Transfer} = u(\rho_1 h_1 \gamma_1 + \rho_2 h_2 \gamma_2) \quad (3)$$

with γ_1 and γ_2 being the volume of each fluid transferred from the donor to acceptor cell.

The normal component of the surface tension force is calculated using the Balanced Force formulation and following the Continuum Surface Force (CSF) model. The tangential derivative of the surface tension is obtained by subtracting the normal component from the surface tension gradient, and is then converted into a volumetric force to generate the surface tension driven flow:

$$\nabla_{\parallel}\sigma = \nabla\sigma - (\nabla\sigma \cdot \hat{\mathbf{n}})\hat{\mathbf{n}} \quad (4)$$

4. RESULTS

In the case of large Marangoni number, the migration velocity of a Fluorinert FC-75 droplet of diameter $D = 10.7$ mm in Dow–Corning DC-200 series silicon oil of nominal viscosity of 10 centistokes is computed and results are compared to the experiments conducted during the Life and Microgravity Science (LMS) mission aboard the NASA Space Shuttle Columbia, reported by Hadland et al. [2]. The test cell used in the present study is a rectangular cavity of length 60 mm with a square cross section of 45×45 mm, filled with silicon oil. The cold wall is held at a constant temperature of $T_c = 283$ K, hot wall has a temperature of $T_h = 343$ K and the side walls are held at a steady linear temperature profile between the cold and hot walls, resulting in a temperature gradient of $|\nabla T| = 1000$ K/m. After the desired steady temperature gradient in the bulk liquid is established, a needle is inserted by software commands from the

ground to inject a Fluorinert droplet of specified size. The droplet is then released from the tip of the needle by rapidly withdrawing the needle. Surface tension parameters between silicon oil and Fluorinert are $\sigma_0 = 0.007$ N/m and $\sigma_T = -3.6 \times 10^{-5}$ N/mK with a reference temperature of $T_0 = 313$ K, resulting in $Re = 17.79$ and $Ma = 1723$ evaluated at the center of the test cell.

Figure 2 (sample result) shows the rise velocity of the droplet against the vertical position in the test cell. It also shows the numerical results calculated by Hermann et al. [3] using the Refined Level Set Grid (RLSG) method. Similar to this study, they have used an idealized initial condition where the droplet has the same initial linear temperature distribution as the bulk phase. In contrast to current study, the droplet motion in [3] is unrealistic and does not agree with the experiments.

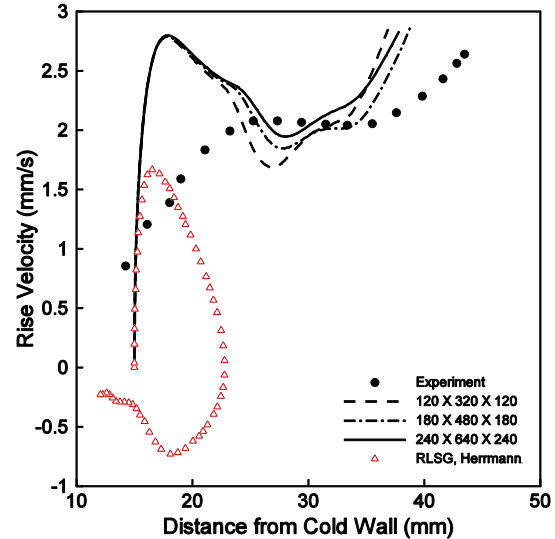


Figure 2 Numerical and experimental rise velocity against vertical position in test cell

REFERENCES

- [1] V. Mehdi-Nejad, J. Mostaghimi, S. Chandra, Modeling heat transfer in two-fluid interfacial flows, International Journal for Numerical Methods in Engineering 61 (2004) 1028-1048
- [2] P.H. Hadland, G. Balasubramaniam, R. Wozniak, R.S. Subramanian, Thermocapillary migration of bubbles and drops at moderate to large Marangoni number and moderate Reynolds number in reduced gravity, Experiments in Fluids 26 (1999) 240-248
- [3] M. Hermann, J.M. Lopez, P. Brady, M. Raessi, Thermocapillary motion of deformable drops and bubbles, Proceedings of Centre for Turbulence Research (2008) 155-170

Three-dimensional numerical analysis for stratified iso-viscous miscible displacement pipe flows

S. Yoon¹, K. Alba² and I.A. Frigaard^{1,3}

¹ Department of Mathematics, University of British Columbia, Canada

² Department of Engineering Technology, University of Houston, US

³ Department of Mechanical Engineering, University of British Columbia, Canada

Email: sungho.yoon5@gmail.com

ABSTRACT

We numerically investigate the three-dimensional displacement flows that a displacing fluid is denser than a displaced fluid (i.e., a density unstable configuration) by using the framework of finite element approximation. This study consists of the benchmarks with the experimental results in Taghavi et. al. [1] to observe the three-dimensional flowing patterns on the internal layers in the displacement flows. At low imposed velocity in the viscous regime the heavier fluid downwards underneath the lighter one, the front on the displacing fluid is dragged with a bump-shaped form by the inertial effect in the existence of the secondary flow regions, showing that the residual wall layers are squeezed on the sides of the pipe.

1 MODEL OVERVIEW

The computational domain is illustrated in Fig. 1-(top), and the mesh structure for a pipe is presented in Fig. 1-(bottom). In model equations, the Navier Stokes (NS) equations for mass and momentum balances and the convection (CE) equation for mass transfer are introduced, and these are approximated by using a standard, mixed $Q_2 - Q_1 - Q_2$ Galerkin method for (\mathbf{u}, p, c) on a quadrilateral mesh in \mathbb{R}^3 . For the solutions of \mathbf{u} and p the projection-type method with BDF-2 version proposed by Guermond et.al. [2] is employed and the solution for concentration c for a variable density between two fluids is also employed with BDF-2 version with the entropy viscosity method [3] for numerical stabilization of the convection term. The NS and CE equations are decoupled in an explicit manner under CFL constraint. Overall the finite element method for discretizing the set of equations is employed by the assist of deal.II object-oriented, C++, finite element li-

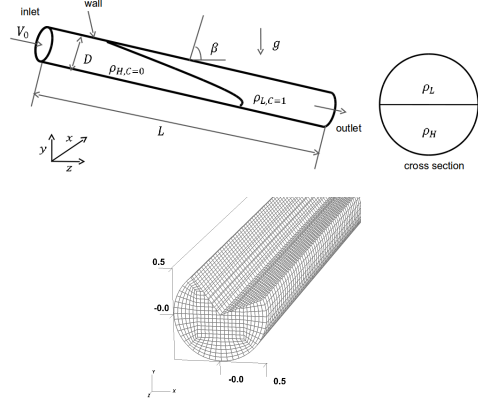


Figure 1: The schematic diagram showing three-dimensional pipe displacement flows with two fluids (heavy and light)-(top) and the mesh structure for a pipe (bottom).

brary [4]. On each discretized step the resultant linear equation is solved by the iterative solver (GMRES or CG) with the suitable preconditioner (ILU or algebraic multigrid) on the MPI library supported by Trilinos library package for the parallel computations. All of simulations are carried out with the CPUs of $12 \sim 24$ upon the Intel-Xeon processors supported by WestGrid (www.westgrid.ca).

2 RESULTS

We show the simulation results on the flow condition $\beta = 85^\circ$ and $At = 0.0035$ in the viscous regime defined in [1], where β is the inclination angle from the vertical and At is the Atwood number. In Fig. 2, The two types of plot are demonstrated: 1. the velocity

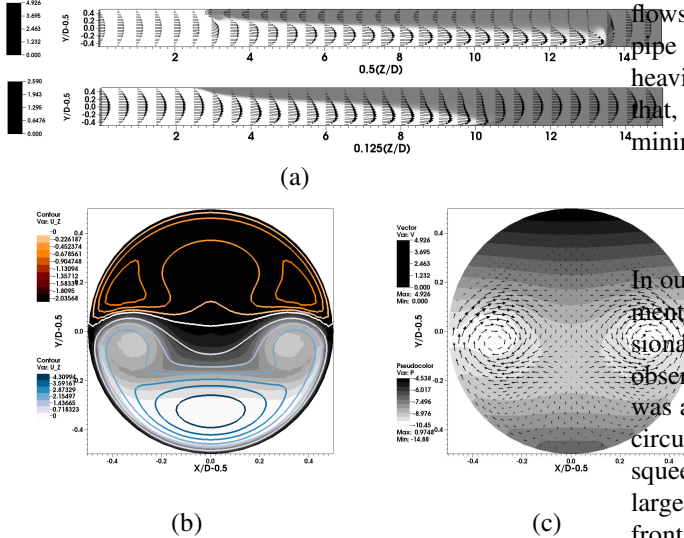


Figure 2: (a) The velocity plots projected on the $z - y$ plane over the concentration distribution with grey colour are plotted in each case of V_0 of 8.1mm/s and 32.3mm/s at $\beta = 85^\circ$ and $At = 0.0035$. (b) The concentration (grey colours) and the axial velocity (contours) and (c) the pressure (grey colours) and the vector plots for (v_x, v_y) are plotted on the cross section near front at $V_0 = 8.1\text{mm/s}$.

(v_x, v_y) plots projected on $z - y$ plane; 2. the field variables for secondary flowing pattern on the cross section at $V_0 = 8.1\text{mm/s}$. At $V_0 = 8.1\text{mm/s}$, the advancing front is being dragged forming an inertial bump in the transverse direction with which the back flows are generated, whereas for the front at $V_0 = 32.3\text{mm/s}$ it spreads out in the flow direction further than the front bump disappears in the stabilizing effect, implying that imposed velocity changes the front shape. This seems to be explained by which a larger inertial force acts on displacement further to conserve the kinetic energy being supplied by a Poiselle flow in the viscous dominant flow condition. This agrees with the results in Taghavi et. al. [1].

Through three dimensional simulations, it allows for observing the internal behaviours of the displacement flows. The displacement pattern on the cross section near front at $V_0 = 8.1\text{mm/s}$ with an inertial bump is presented. In Fig. 2-(b), when the flow is sufficiently developed in time, the lighter fluid (black colour) is displaced underneath the heavier (white colour) by which the front is dragged by inertial effect. Such an unstable configuration leads that the lighter fluid moves upwards with the pressure difference between centres and sides of the pipe followed by the secondary

flows are generated azimuthally along the sides of the pipe as shown in Fig. 2-(c). This also induces that the heavier fluid located at the sides dispersed upwards so that, consequently, the re-circulating flows toward a minimum of the pressure near both sides are observed.

3 CONCLUSION

In our study, we have presented the miscible displacement flows with imposed velocities in the three dimensional structure under the viscous regime. We have observed that the inertial bump near the dragged front was appeared in low imposed velocity V_0 , and the re-circulation zone with secondary flows was found in squeezing the residual layer near sides of the pipe. At larger V_0 , it was also seen that the inertial bump on the front disappeared by the stabilizing effect with a larger inertial force.

ACKNOWLEDGEMENTS

This research has been carried being, supported financially by NSERC and Schlumberger through CRD project 444985-12. This research was also enabled by support provided by WestGrid (www.westgrid.ca)

REFERENCES

- [1] S.M. Taghavi, K. Alba, T. Seon, K. Wielage-Burchard, D.M. Martinez and I.A. Frigaard. Miscible displacement flows in near-horizontal ducts at low Atwood number. *J. Fluid Mech.*, 696:175–214, 2012.
- [2] J. Guermond, and A. Salgado. A splitting method for incompressible flows with variable density based on a pressure Poisson equation. *Journal of Computational Physics.*, 228:2834–2846, 2009.
- [3] J.-L. Guermond, R. Pasquetti and B. Popov. Entropy viscosity method for nonlinear conservation laws. *Journal of Computational Physics.*, 230:4248–4267, 2011.
- [4] W. Bangerth, R. Hartmann and G. Kanschat. deal.II - a general purpose object oriented finite element library. *ACM Transactions on Mathematical Software.*, 33:1–27, 2007.

Trailing front behavior in heavy-light displacement flows in an inclined 2D channel

K. Alba¹, S.M. Taghavi² and I.A. Frigaard^{3,4}

¹ Department of Engineering Technology, University of Houston, Houston, TX, USA

² Department of Chemical Engineering, Laval University, Quebec, QC, Canada

³ Department of Mathematics, University of British Columbia, Vancouver, BC, Canada

⁴ Department of Mechanical Engineering, University of British Columbia, Vancouver, BC, Canada

Email: *kalba@uh.edu*

ABSTRACT

We numerically study the displacement flow of two iso-viscous Newtonian fluids in an inclined channel formed by two parallel plates. The heavier displacing fluid moves the lighter displaced fluid in the downward direction. Three dimensionless groups largely describe these flows: the duct inclination (β), the densimetric Froude number (Fr) and the Reynolds number (Re). The behavior of the trailing front i.e. the displaced fluid front which advances in the opposite direction of the mean flow, is explored over a wider range of parameters. The displacement flows with and without back flow are called non-instantaneous and instantaneous respectively. These flows are classified in a two-dimensional ($Fr; Re \cos \beta / Fr$)-plane. For inclination angles closer to vertical, further exotic behaviours in the trailing front are observed due to stronger buoyant forces in the streamwise direction.

1 INTRODUCTION

We present a computational study of high-Péclet-number miscible displacement flows in an inclined 2D plane channel with a heavier fluid displacing a lighter fluid downwards, i.e. density-unstable configuration. Iso-viscous Newtonian fluids in the Boussinesq limit are considered. This study continues our previous work on 2D channel displacement flows [1, 2] which have been focused at near-horizontal channels. Here, our study covers the full range of channel inclinations (β) and extends from the exchange flow limit (zero imposed flow) into ranges with significant Reynolds number (Re). The novelty of the current work is in investigating channel displacement flows at higher inclinations which have not been studied from the perspective of the trailing front so far.

2 DISPLACEMENT IN CHANNELS

The fluids have the same viscosity but different densities. The displacing fluid is denser than the displaced fluid. The computations that we have carried out are fully inertial, solving the full 2D Navier-Stokes equations with the liquid species modeled via a scalar concentration, C :

$$[1 + \phi At] [\mathbf{u}_t + \mathbf{u} \cdot \nabla \mathbf{u}] = -\nabla p + \frac{1}{Re} \nabla^2 \mathbf{u} + \frac{\phi}{Fr^2} \mathbf{e}_g, \quad (1)$$

$$\nabla \cdot \mathbf{u} = 0, \quad (2)$$

$$C_t + \mathbf{u} \cdot \nabla C = \frac{1}{Pe} \nabla^2 C. \quad (3)$$

Here $\mathbf{e}_g = (\cos \beta, -\sin \beta)$ and the function $\phi(C) = 2C - 1$ interpolates linearly between -1 and 1 for $C \in [0, 1]$. No slip conditions are satisfied at the walls, the heavy fluid enters fully developed (plane Poiseuille profile) at $x = -L/4$ and outflow conditions are applied at $x = 3L/4$.

2.1 Computational code

Equations (1)-(3) are discretised using a mixed finite element, finite volume method. The Navier-Stokes equations are solved using Galerkin finite element method. A fixed time step is used for the Navier-Stokes equations, advancing from time step N to $N+1$. The convective velocity is approximated at time step N while the linear spatial derivatives of the velocity are approximated implicitly at time step $N+1$. The pressure is approximated at time step $N+1$ (semi-implicit method regarding the nonlinear terms). More details of the computational methodology and the governing

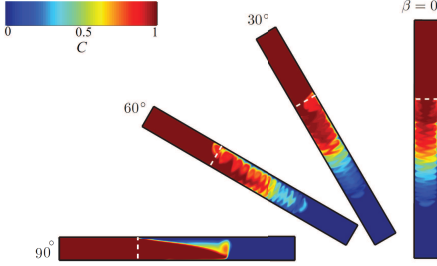


Figure 1: Change in iso-viscous displacement flows with β for $Re = 300$ and $Fr = 0.61$. The field of view is 1×75 with the white dashed lines indicating the position of the imaginary gate valve. The color bar at the top left of the figure shows the corresponding concentration value, C , with 0 referring to the pure displaced fluid and 1 to the pure displacing fluid. The snapshots are taken at $t = 20.6$.

system of equations are given in [2]. More details of the computational methodology is given in [2].

3 RESULTS

We now present the computational results. We first give a general phenomenological description of the main regimes we have observed in our displacement flow simulations.

3.1 Displacement flows: main qualitative features

Figure 1 shows typical results from our simulations, primarily illustrating the effect of inclination angle β on the flow pattern. The concentration values in the numerical simulations shown in Fig. 1 are calibrated so that they vary between 0 (displaced fluid) and 1 (displacing fluid). The data shown are obtained for $Re = 300$ and $Fr = 0.61$. Similar to the pipe exchange flows, the degree of mixing and disorder in the system increases as we move towards the vertical ($\beta \rightarrow 0^\circ$). The flow pattern for more horizontal inclinations remains qualitatively similar to viscous flows of two separated layers; see $\beta = 90^\circ$ in Fig. 1.

3.2 Instantaneous and non-instantaneous displacements

An important large scale feature of the displacement flows is whether they are instantaneous or not. By instantaneous displacement we mean that the displaced

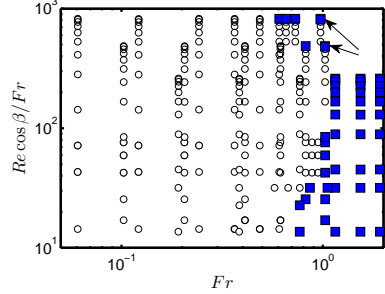


Figure 2: Classification of our results for the full range of simulations plotted in the plane of Fr and $Re \cos \beta / Fr$. The instantaneous displacement flows are marked by squares and non-instantaneous ones by circles. The arrows indicate that the non-instantaneous flows zone shrinks at higher $Re \cos \beta / Fr$ values due to a more efficient mixing.

fluid does not travel upstream of the gate valve once the simulation/experiment starts. If the displacement is non-instantaneous we have inevitably had a back-flow of the displaced fluid layer. From the industrial point of view this characteristic is very important if it is sustained, as it implies a residual of displaced fluid. Ideally we want to always displace instantaneously and avoid back flow. We now classify our displacement flows in terms of being instantaneous or non-instantaneous, over the range of parameters computed. Figure 2 shows such a classification in the dimensionless plane of Fr and $Re \cos \beta / Fr$. The blue squares in this figure indicate instantaneous displacement and all others are non-instantaneous flows.

REFERENCES

- [1] S. Taghavi, T. Seon, D. Martinez, and I. Frigaard. Buoyancy-dominated displacement flows in near-horizontal channels: the viscous limit. *J. Fluid Mech.*, 639:1–35, 2009.
- [2] S. Taghavi, K. Alba, T. Seon, K. Wielage-Burchard, D. Martinez, and I. Frigaard. Miscible displacement flows in near-horizontal ducts at low Atwood number. *J. Fluid Mech.*, 696:175–214, 2012.

Transient Substrate Pressure Variation in the Shock Induced Spray Process

Sichang Xu¹, Kevin Mrozinski¹, Jean-Paul Martins¹, Gary W. Rankin¹ and Bertrand Jodoin²

¹*Department of Mechanical, Automotive and Materials Engineering, University of Windsor, Windsor, Ontario, Canada, N9B3P4.*

²*Department of Mechanical Engineering, University of Ottawa, Ottawa, Ontario, K1S5T3.*

Email: rankin@uwindsor.ca

ABSTRACT

A simplified computational fluid dynamic model of the flow field associated with the shock induced spray process is used to explain the unexpected results from a recent experimental study. The pressure variation with time measured on the target substrate, at a location which coincides with the intersection of the transient jet axis, was found to have different characteristic shapes depending on the jet stand-off distance, supply pressure and frequency. In order to explain these seemingly anomalous results a commercial computational fluid dynamic package was used to simulate the process. The numerical pressure trace shapes observed are in good qualitative agreement with the experimental trace shapes. The different substrate pressure variations with time are analyzed and correlated with the transient flow field of the supersonic jet which forms in the space between the jet exit and the substrate.

1. INTRODUCTION

The Shock Induced Spray Process (SISP) is a relatively new technique for coating surfaces with various types of protective materials [1]. It falls into the category of a cold spray process in which heated but solid particles are accelerated to supersonic speed by a steady gas jet and caused to impact on the substrate to be coated. The fact that the deposited particles remain in the solid or semi-solid state as they impact the substrate results in less residual stress in the coated material. The fundamental difference in the case of the SISP is that the process does not occur at a steady state. Shock waves are periodically formed in a long tube as the result of a high pressure gas valve which is rapidly opened and closed at a set

frequency. The shock wave and subsequent supersonic flow accelerates and further heats the particles as they travel down the long tube. They exit the tube and cross a small gap before impacting and being deposited on the substrate.

A comprehensive numerical solution of a complete SISP arrangement has been conducted and reported in the literature [2, 3]. One of the questions which arose during this work concerns the transient formation of a standing bow shock wave near the surface of the substrate. It is known that this shock wave is detrimental to the deposition process in the case of the traditional, steady, cold spray process [4]. In order to determine the importance of this phenomenon in the case of SISP, an experimental study was conducted [5].

The experiments involved testing a geometrical model of the SISP which would allow a high speed camera to record Schlieren flow visualization images of flow in the gap region between the exit of the SISP tube and the substrate. A dynamic surface mounted pressure transducer was placed at the centre of the substrate which coincided with the jet axis. The pressure traces obtained from the substrate transducer exhibited different shapes depending on the gap distance, supply pressure and pulsation frequency. In some cases the pressure continued to rise and then eventually fall. In some cases however, the pressure rose then dropped to an approximately constant value before rising again and finally falling. In order to qualitatively explain the distinctly different behavior it was decided to conduct a simple numerical study which, unlike the previous numerical work, focuses specifically on the region in question.

2. SIMPLIFIED COMPUTATIONAL FLUID DYNAMIC MODEL

The numerical model geometry is schematically represented in Figure 1. It should be noted that this diagram is not to scale since the tube length L_1 (813 mm), is considerably larger than the other dimensions ($R_1 = 2.72$ mm, $R_2 = 3.46$ mm, $R_3 = 46$ mm, $L_2 = 25$ mm, $L_3 = 20$ mm and $L_4 = 801$ mm). In the case of the experiment the tube is rectangular in shape, however an axially symmetric approximation is employed in the current model in order to reduce computational time. The radii were determined using the equivalent diameter concept. This approximation is considered to be acceptable due to the qualitative nature of the objective of this work. The substrate and tube wall are modeled as impermeable adiabatic boundaries with no slip while the surroundings are approximated as pressure outlets as indicated. Although not shown in the diagram, the tube wall was given a thickness of 0.1 mm. The tube exhaust is shown for convenience of labeling and is not a flow boundary. Unlike the complete numerical model, this case does not include a sub-model of the valve and its functioning. An estimation regarding the pressure variation with time at a location after the valve is used instead. It is based on experimental measurements made in a similar SISP arrangement [2] and has been scaled to approximate the current supply pressure and frequency values.

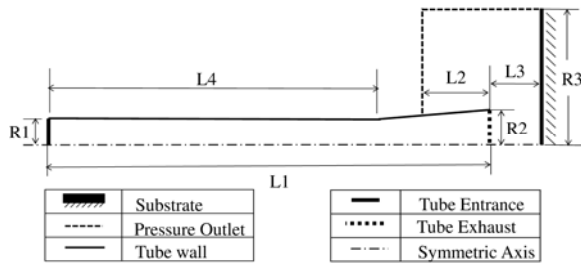


Figure 1. Schematic Diagram of Model Geometry.

A grid which consists of a total of 28,035 cells with a finer mesh in regions of high velocity gradient is used to mesh the flow field.

A commercial computational fluid dynamics program, ANSYS Fluent 14, is used to solve the pertinent flow equations using the density based implicit solver. Second order upwind solvers are selected for the pressure, momentum and energy equations. The Spalart-Allmaras model is used to approximate the turbulence effect.

An initial steady state solution is obtained for the starting value of the transient inlet pressure waveform. Once the steady state is reached the

solution is switched to transient and a second order implicit technique used. A time step size of 2e-06 seconds is found to be sufficiently small to resolve the transient events of interest.

3. NUMERICAL STUDY

The above mentioned numerical model is used to investigate the transient substrate pressure traces corresponding to the set of supply pressures (3), stand-off distances (3) and pulsation frequencies (4) considered in the experimental study. These are then compared with the experimental results.

4. RESULTS

An example of the numerical solution for the substrate pressure variation with time, for a supply pressure of 3.35 MPa, stand-off distance of 20 mm and frequency of 12 Hz is shown in Figure 2. This qualitatively agrees with the shape observed experimentally for similar operating conditions although the magnitude of the pressure values do not.

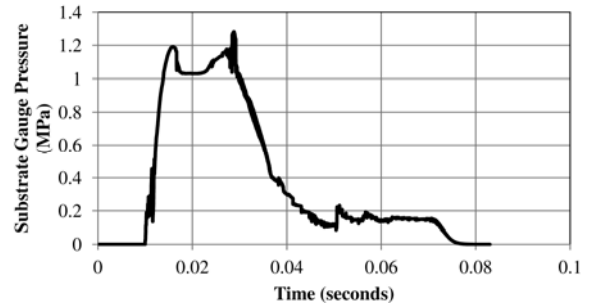


Figure 2. Substrate Pressure Trace for a Supply Pressure of 3.45 MPa, Stand-off Distance of 20 mm and Frequency of 12 Hz.

The final paper will include a complete comparison of the experimental and numerical results along with a discussion of the trends in the shape changes with each of the operating parameters.

The reasons for the changes in the trace shapes will also be investigated and discussed in view of the changing supersonic jet flow pattern.

REFERENCES

Due to a lack of space the references will be included in the full paper.

Treatment of Non-Conforming Faces in the Framework of Spectral Discontinuous Galerkin Discretization

Marcin Chrust and Catherine Mavriplis

*Department of Mechanical Engineering
University of Ottawa, 161 Louis Pasteur, Ottawa, ON, K1N 6N5, Canada*

Email: *marcin.chrust@uottawa.ca*

ABSTRACT

Recent revolution in high performance computing (HPC) leading to the emergence of many-core heterogeneous parallel computing systems offering unprecedented performance has drawn the interest of the scientific community back to high order methods. Characterized by low dissipation and dispersion properties, favourable computational intensity and suitability for efficient parallelization, high order methods are becoming an increasingly more common choice for many industrial applications. The success of computational codes in industrial realms depends on two key aspects: their robustness and the associated computational cost. Typical industrial applications involve multi-scale physics and complex geometries which, combined with "a priori" generated fixed computational grids, often results in under-resolved simulations. Insufficient grid resolution leads to large aliasing errors and undermines the robustness of a code. Both mentioned aspects can be, to a large extent, addressed by grid adaptation. We discuss the development of our *hp*-adaptive high order Discontinuous Galerkin (DG) framework for the incompressible Navier-Stokes equations. The focus of this paper is on the treatment of fluxes on the non-conforming faces. Both the polynomial interpolation and the mortar element method are discussed and compared highlighting their key numerical properties.

1 INTRODUCTION

High order methods can be used to solve time dependent partial differential equations with higher accuracy and at a lower cost compared to traditional low order schemes. However, although this family of numerical methods is becoming increasingly popular, low order codes still prevail in industry. The primary reason for this situation is the lack of robustness of high or-

der methods, which are prone to large aliasing errors and even instabilities, if the solution is under-resolved. Since the local features of the solution are generally not known at the stage of generation of the grid, the grid is usually insufficiently refined in regions of large solution gradients. Under-resolution combined with inherent low dissipation and usually insufficient built-in artificial dissipation mechanisms characteristic for high order methods lead to less reliable codes. This deficiency can be efficiently addressed by *hp*-adaptation. Adaptive grid methods allow to adjust the grid resolution depending on the evolution of the solution. The computational grid can be refined in regions where the solution is not smooth (e.g. shocks, geometric singularities) or exhibits high gradients, and coarsened in smooth regions. The indirect advantage of grid adaptation is reflected in the minimization of the number of degrees of freedom required to fully resolve the solution. In this paper we focus on the treatment of non-conforming faces in the framework of the spectral Discontinuous Galerkin method.

2 GRID ADAPTATION AND TREATMENT OF NON-COMFORMING FACES

We consider here the non-linear scalar advection equation discretized using the spectral Discontinuous Galerkin framework recapitulated in [1]. The numerical flux on *hp*-non-conforming faces will be calculated using *i*) polynomial interpolation and *ii*) mortar projection developed originally for the spectral element method in [4]. The polynomial interpolation method consists in, as the name suggests, using high order polynomial interpolation to match different discretizations on non-conforming faces, while the mortar element method involves introducing an additional element, called mortar, onto which the solution is projected using the least square projection; the flux is then

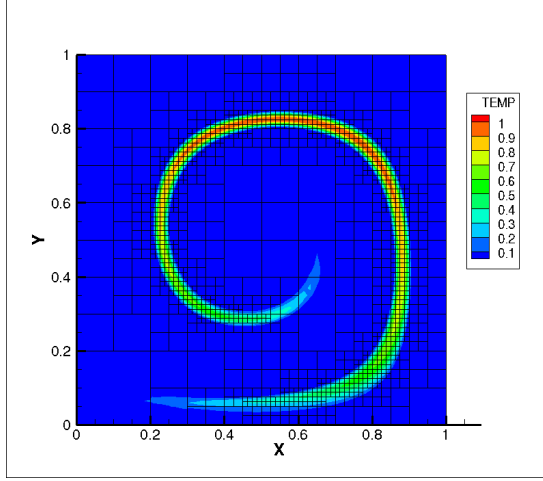


Figure 1: Tracer distribution at $t = T/2$ shown with h -adapted grid of $K = 1300$ elements and $N=8$ polynomial order, maximum number of adaptation levels $L_{max}=4$. Non-conforming faces handled using the mortar element method.

calculated on the mortar, and finally projected back to elements. The latter method can be shown to have two important properties: global conservation and satisfies the outflow condition ([2]), while the polynomial interpolation method is easier to implement and is computationally less expensive.

3 RESULTS

The two dimensional test case simulating the evolution of a passive tracer with an underlying periodic swirling velocity field [3] will serve as a test case for the purpose of this communication. Figure 2 shows the norm of the difference in the tracer distribution between the solution after one period and the initial solution: $\epsilon = ||T_T - T_0||$ as a function of the number of allowed h -adaptation levels, L_{max} , and the element polynomial order, N .

4 CONCLUSION

The results obtained for the scalar advection equation indicate that the choice of treatment of non-conforming faces in the spectral Discontinuous Galerkin framework has an important effect on the discretization error. The mortar projection method results in more accurate handling of non-conforming faces at the price of increased computational requirements. Similar studies have been conducted for the full incompressible Navier-Stokes equations and will be presented in the final paper.

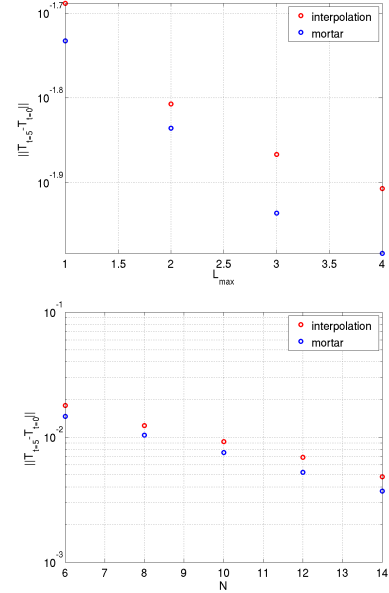


Figure 2: Comparison of the error between the implementations using the mortar element method and polynomial interpolation for handling non-conforming faces as a function of: *top*: the maximum allowed h -adaptation levels, L_{max} and *bottom*: the element polynomial order, N .

REFERENCES

- [1] M. Chrust, A. Fabregat, and C. Mavriplis. An adaptive Discontinuous Galerkin solver for the incompressible Navier-Stokes equations. In *Proceedings of the 21st Annual Conference of the CFD Society of Canada, Sherbrooke, QC, Canada, May 6 – 9, 2013*. CFD Society of Canada, 2013.
- [2] D. A. Kopriva, S. L. Woodruff, and M. Y. Hussaini. Computation of electromagnetic scattering with a non-conforming discontinuous spectral element method. *International Journal for Numerical Methods in Engineering*, 53(1):105–122, 2002.
- [3] R. J. LeVeque. High-resolution conservative algorithms for advection in incompressible flow. *SIAM Journal of Numerical Analysis*, 33(2):627–665, 1996.
- [4] C. Mavriplis. *Nonconforming Discretizations and A Posteriori Error Estimators for Adaptive Spectral Element Techniques*. PhD thesis, Massachusetts Institute of Technology, 1989.

Turbulent Schmidt Number Sensitivity of Adjoint-based Pollutant Quantification

Carol Brereton¹, Lucy Campbell² and Matthew Johnson¹

¹*Department of Mechanical and Aerospace Engineering, Carleton University, Ottawa, Ontario*

²*School of Mathematics and Statistics, Carleton University, Ottawa, Ontario*

Email: matthew.johnson@carleton.ca

ABSTRACT

Fugitive pollutant emissions, such as methane gas leaks, are important industrial greenhouse gas sources that are difficult to locate and quantify. Combining wind information and downstream concentration sensor data as an optimization problem can potentially characterize leaks, but results depend on dispersion estimates. To isolate turbulent Schmidt number effects, synthetic cases based on Project Prairie Grass were simulated for specified Schmidt numbers. The gradient-based LBFGS optimization algorithm combined with the gas transport adjoint characterized emissions for various turbulent Schmidt numbers (25%-200% of the actual value) using the previously modelled sensor data. Results were shown to be strongly influenced by the prescribed turbulent Schmidt number inducing variations in the predicted emission rates of -19% to +475% relative to the original synthetic release rate.

1. INTRODUCTION

Fugitive emissions, often caused by leaking valves, leaking seals, loose fittings, process faults, and evaporation losses [1], are important greenhouse gas sources. Their repair and maintenance rely on both location and quantification within industrial facilities that may contain thousands of potential pollutant emitters. An alternative to current manual search methods is combining CFD predicted wind fields with concentration sensors to characterize upwind emissions.

L-BFGS optimization, requiring knowledge of the gradient obtained with the gas transport adjoint to reduce computational time, can characterize emissions sources as demonstrated in two-dimensional proof-of-concept simulations [2]. Due to flow field complexity around bluff bodies such as

buildings, simulations have now been extended into three dimensions. For dispersion modelling, the turbulent Schmidt number, or ratio of eddy viscosity to diffusivity, must be assumed.

Many CFD codes default to a constant turbulent Schmidt number of 0.7 to 0.9 [3], but a review of values shows potentially broader variation [3]. For open fields, ranges between 0.17 and 1.34 have been observed in tracer experiments with no clear correlation to atmospheric stability, wind speed, or time of day [4].

Unlike direct tracer methods, the current algorithm does not assume information about the location or number of leaks. This additional complexity makes it difficult to directly anticipate the effects of the turbulent Schmidt number. Several synthetic cases with known turbulent Schmidt values were modelled to determine virtual sensor readings. These readings were then fed into the emission characterization algorithm for a range turbulent Schmidt numbers to determine the change in predicted emission rate.

2. DISPERSION MODELLING

The pollutant gases are negligible relative to the bulk flow so the wind field computation and gas dispersion are separated. Assuming a non-buoyant inert gas, gas concentration (C) with a known wind velocity (\mathbf{u}), given sources S and diffusion (D) can be predicted by [2]

$$\frac{\partial C}{\partial t} + \nabla \cdot (C\mathbf{u} - D\nabla C) - S = 0. \quad (1)$$

3. TURBULENT SCHMIDT NUMBER

The diffusional properties of the gaseous pollutant are an important factor in simulations of downwind

concentrations. The turbulent Schmidt number (Sc_t) is defined as the ratio of turbulent eddy viscosity (ν_t) to turbulent diffusivity (D_t) [3]:

$$Sc_t = \frac{\nu_t}{D_t}. \quad (2)$$

For RANS flows, the turbulent eddy viscosity can be found from turbulent kinetic energy and dissipation, estimated from empirical profiles [5]. Turbulent diffusivity was assumed to dominate (i.e. $D \approx D_t$).

4. SOURCE OPTIMIZATION

Potential source locations are defined in every cell of the discretized domain with a zero source initialization and optimized using the L-BFGS algorithm [6]. Model misfit g is half the squared difference between current guess and desired concentration at the sensors. Integrating over the domain space Ω and between times t_0 to t_f with the scalar adjoint variable λ multiplied by Eq. 1 (or zero) to simplify computation gives

$$J = \int_{t_0}^{t_f} \int_{\Omega} g - \lambda \left(\frac{\partial C}{\partial t} + \nabla \cdot (C\mathbf{u} - D\nabla C) - S \right) d\mathbf{x} dt, \quad (3)$$

the total cost function to be minimized. This can be manipulated so that the only unknown is the adjoint variable computed by integrating Eq. 4 backwards in time (similar to inverting the gas transport with sensor locations acting as sources).

$$\begin{aligned} -\frac{\partial \lambda}{\partial t} + \nabla \cdot (-\lambda \mathbf{u} - D \nabla \lambda) &= \frac{\partial g}{\partial C} \\ \lambda(\mathbf{x}, t = t_f) &= 0 \end{aligned} \quad (4)$$

Outlet: $\lambda = 0$
Inlet: $\lambda \mathbf{u} + D \nabla \lambda = 0$

The OpenFOAM toolkit was used to implement the transport solvers.

5. PRELIMINARY TEST CASE

An open field with sensor positions based on Project Prairie Grass (PPG) [7] was discretized in a 45600 cell mesh and a domain size of 300 m \times 200 m \times 150 m with near ground refinement. Wind conditions and average emission rates were taken from four PPG release experiments. A forward transport release with $Sc_t = 0.7$ (typical assumed value) was simulated to act as a comparison case. Source location and quantification were performed for several cases changing only Sc_t from the lower physical range of 0.175 to the upper range of 1.4.

6. RESULTS AND DISCUSSION

Underestimating Sc_t in the current cases could produce an overestimation of almost 5 times the desired value. Over-estimation of Sc_t reduced the source strength prediction by approximately 20% (See Fig. 1). For the current case, assuming a higher turbulent Schmidt number results in an improved prediction. Different assumptions for actual turbulent Schmidt number on the current and more complex flow fields are currently underway.

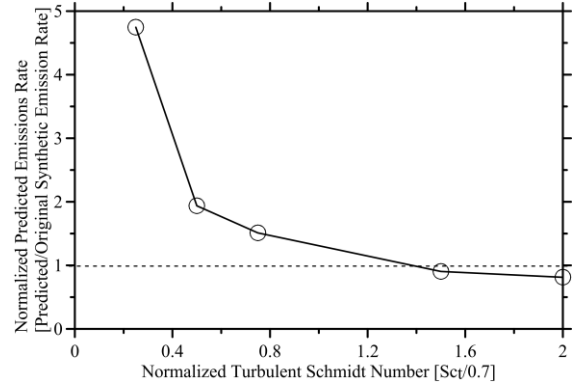


Figure 1: Normalized emission rate prediction versus normalized turbulent Schmidt number

REFERENCES

- [1] J. N. Carras et al. Fugitive emissions. In *2006 IPCC guidelines for national greenhouse gas inventories*, Intergovernmental Panel for Climate Change, Hayama, Japan, 2006
- [2] I. Joynes. Proof-of-Concept Inverse Micro-Scale Dispersion Modelling for Fugitive Emissions Quantification in Industrial Facilities. *Master's Thesis, Carleton University*, 2013
- [3] Y. Tominaga and T. Stathopoulos. Turbulent Schmidt numbers for CFD analysis with various types of flowfield. *Atmos. Environ.*, 41:8091–8099, 2007
- [4] T.K. Flesch. Turbulent Schmidt number from a tracer experiment. *Agric. For. Meteorol.*, 111:299–307, 2002
- [5] P.J. Richards and R.P. Hoxey. Appropriate boundary conditions for computational wind engineering models using the k-epsilon turbulence model. *J. Wind Eng. Ind. Aerod.*, 46&47:145–153, 1993
- [6] D.C. Liu and J. Nocedal. On the limited memory BFGS method for large scale optimization. *Math. Program.*, 45:503–528, 1989
- [7] M.L. Barad. Project Prairie Grass, a field program in diffusion, vols. 1 and 2. *Geophys. Res. Papers U.S.*, 59, 1958

Contributed Sessions

CS-AMPRE Applied Problems and Methods in Research & Education

Computational and Statistical Challenges with High Dimensionality: Efficient Algorithms for Feature Selection based on Manifold Learning

Abdelkader Baggag, Ehsan Ullah and Halima Bensmail

Qatar Computing Research Institute, Qatar Foundation, {abaggag, eullah, hbensmail}@qf.org.qa

Dimensionality reduction algorithms transform data for the sake of easier computation and to reduce the effect of noise and in order to extract the main features from the data. Geometrically intuitive and mathematically rigorous insight can be gained by leveraging the information content of the data, i.e., while the data is extrinsically high-dimensional, there is evidence that it lies near a low-dimensional manifold. This information is essential in the design of efficient and scalable algorithms.

In this project, we will combine geometric approaches with modern linear algebra and multivariate analysis to design efficient and scalable algorithms for feature selection. The algorithms are essentially optimization techniques on the Grassmann/Stiefel manifold. These algorithms are validated on synthetic data and on H¹-NMR data where the number peaks exceeds far more the number of samples.

References

- [1] "From Manifold to Manifold: Geometry-Aware Dimensionality Reduction for SPD Matrices" by Mehrtrash T. Harandi, Mathieu Salzmann, and Richard Hartley.

Computational Thinking in Teaching Accounting

H. Shodiev¹, A. Czegledi²

¹ Department of Physics and Computer Science, Wilfrid Laurier University, Waterloo, Canada, hshodiev@wlu.ca

² School of Business, Conestoga College, Kitchener, Canada, Aczegledi@conestogac.on.ca

Computational thinking (CT) concepts can be used across disciplines to facilitate efficient problem solving by recognizing computable problems and approaching thinking process differently and more effectively. Although there is an active discussion around implementation of CT in teaching at different scale and domain, research on teaching CT concepts mostly takes place within computer science and the science, technology, engineering and math fields. [1]

Our study focused on using CT concepts in teaching accounting. Critical thinking and problem solving skills are important requirements for accounting professionals. A series of studies shows that students need more help in developing these skills [2]. The gap between the skills taught at different level and those expected by employers is especially problematic for those students seeking employment as managerial accountants [3]. Managerial accounting classes provide sufficient coverage of traditional topics such as overhead allocation and master budgets, but less focus on the more contemporary topics such as ethics and continuous improvement [3]. Those contemporary topics require more critical thinking skills and problem solving skills.

Successful accounting students require the ability to analyze data, use professional judgement and see “the big picture” in order to provide information for making financial decisions. Using CT will assist accounting degree students in developing these skills. We will present benefits of using CT in accounting education with application in managerial accounting. CT allows students to see various possible solutions for managerial accounting problems and in the process improving their critical thinking and problem solving thinking skills as well as mastering managerial accounting concepts.

Keywords: Computational thinking, critical thinking skills, problem solving skills, accounting, managerial accounting.

References

- [1]Betul C. Czerkawski and Eugene W. Lyman III, *Exploring Issues About Computational Thinking in Higher Education*, TechTrends, Volume 59, Number #2, pp. 57-65 (2015).
- [2]Pamela Weaver, Marie Kulesza, *Critical Skills for New Accounting Hires: What's Missing from Traditional College Education?*, Academy of Business Research Journal, pp. 34-49, (2014)
- [3] Cable, R. J., Healy, P. & Mathew, E., *Teaching future management accountants*. Management Accounting Quarterly, pp. 44-50 (2009)

New Hyper Binomial Probability Distribution

M. L. Mbodj¹, Y. Gningue²

¹UCAD (Université Cheikh Anta Diop), Sénégal (Ph D program in maths) mbodj.lamine@hotmail.fr

²Laurentian University, Canada, (Maths and Computer Science) ygningue@cs.laurentian.ca

Abstract. Our aim in this presentation is to introduce a new probability distribution we named hyper binomial distribution which generalizes the usual binomial probability Refs. [1, 2, 3]. In this general situation, the Bernouilli Distribution [1] concerns more than one trial with the success associated to a finite set A being connected to another finite set B . The finding of a new formula which evaluates the number of functions from a finite set A to a finite set B allows us to define that generalized law. Then we establish the hyper binomial distribution by checking all the probability definition properties. Some examples of problems are presented in order to have a clear and better understanding of that new probability law. We extend the result to the situation where the set B is infinite but bounded. That extension is performed by the discretization of the initial set B . Finally we introduce an application to a situation in finance before providing some concluding remarks.

Keywords. Binomial probability, Bernouilli distribution, hyper binomial distribution, Beta distribution, Newton's binomial formula.

References

- [1] A. Papoulis, *Bernoulli Trials. Probability, Random Variables, and Stochastic Processes*, 2nd Edition, New York: McGraw-Hill, p. 57–63, (1984).
- [2] N. L. Johnson, S. Kotzand and A. Kemp, *Univariate Discrete Distributions* , 2nd Edition, J., Wiley, (1993).
- [3] T. Cover and J. Thomas, *Elements of Information Theory*, 2nd Edition, J., Wiley, (2006).

Optimal and Robust Designs of Step-stress Accelerated Life Testing Experiments for Proportional Hazards Models

Xiaojian Xu¹, Wan-Yi Huang²

¹ Brock University, St catharines, xxu@brocku.ca

² Brock University, St catharines, wh13oq@brocku.ca

Accelerated life testing (ALT) is broadly used to obtain reliability information of a product in a timely manner. The proportional hazards (PH) model is often utilized for reliability analysis. In this paper, we focus on designing ALT experiments for reliability prediction when a PH model is adopted. We consider a PH model in the form of

$$\lambda(t; \mathbf{s}) = \lambda_0(t) \exp(\beta^T \mathbf{s}) \quad (1)$$

where $\lambda_0(t)$ is the baseline hazard rate function at the time of t , \mathbf{s} is the column vector of stress levels used in an ALT test, and β is a vector of unknown parameters.

When an ALT experiment under constant stress levels is still too lengthy, a step-stress ALT scheme is often used to reduce the times to failure even further. In comparison to constant-stress ALTs, [1] has shown that step-stress ALTs outperform constant-stress ALT when there is heavy censoring for the constant-stress tests at lower stress levels. Therefore, we explore the method of optimal design construction for multiple step-stress ALT plans with censoring.

In order to illustrate our method, we consider $\lambda_0(t)$ to be either a simple linear or a quadratic function. For each case, we have constructed the optimal step-stress ALT designs under three different design criteria: D-, A-, and Q-optimality. The maximum likelihood method has been used for estimating the model parameters. The information matrix has been derived and both optimal stress-changing times and optimal stress levels have been obtained for each scenario considered.

Note that the classical designs are optimal only if the model assumed is correct. Due to the nature of prediction made from ALT experimental data, attained under the stress levels higher than the normal condition, extrapolation is encountered. In such case, the assumed model can not be tested. For possible imprecision in an assumed PH model, the method of construction for robust designs is also explored. As an example, we investigate the optimal and robust designs for the situation where $\lambda_0(t)$ in the fitted PH model is simple linear but the true $\lambda_0(t)$ is actually quadratic. The optimal stress-changing times and optimal stress levels are determined by minimizing the asymptotic variance, asymptotic squared bias, and asymptotic mean squared error, respectively. In addition, simulations and comparison of the resulting designs and the classical optimal designs such as those derived in [2] are presented.

References

- [1] I. H. Khamis. *Comparison between constant and step-stress tests for Weibull models*. International Journal of Quality and Reliability Management, vol 14, pp. 74-81 (1997).
- [2] C. Hu, R. D. Plante and J. Tang, *Stepstress Accelerated Life Tests: a Proportional Hazards-based Nonparametric Model*. IIE Transactions, vol 44, pp. 754-764 (2012).

Spatial dependence modeling and allocation of wind/solar resources using C-Vine copulas and value-at-risk

A. Narayan¹ and K. Ponnambalam¹

¹*Department of Systems Design Engineering
University of Waterloo, Waterloo, ON, Canada N2L 3G1 {apurva.narayan,ponnu}@uwaterloo.ca*

The investment in wind and solar power is mainly driven by the aim to maximize the penetration of the renewable energy. The investment decisions on the actual placement are driven by the aim to maximize the expected annual energy of the turbines and solar panels. The result of such an approach is an increased concentration of the wind farms at a location with higher average wind speeds and solar panels with high solar insolation. This strategy may be optimal in a few cases but for a majority of cases the setup is unfavourable for the energy suppliers and the economy because of large fluctuations in the overall renewable energy output. We analyze the stochastic dependencies of wind speed, wind power (from a standard wind turbine) for three different sites with four sub-sites. We gather that these dependencies turn out to be non-linear but are constant over time. We utilize the copula theory to determine the non-linear dependencies and the value at risk of energy production for a given allocation set of wind turbines and solar panels. We derive optimal allocation plans, and conclude that optimized allocation of wind generation may substantially stabilize the overall energy supply on daily as well as hourly basis.

References

- [1] J. S. Benth and F. E. Benth, *Analysis and modelling of wind speed in New York*, Journal of Applied Statistics, vol. 37, pp. 893-909, (2010)
- [2] H. Joe, *Multivariate Models and Multivariate Dependence Concepts*, Taylor & Francis, (1997).
- [3] Sklar, A., *Fonctions de répartition à n dimensions et leurs marges*, Publ. Inst. Statist. Univ. Paris 8: 229-231, (1959).
- [4] E. C. Brechmann and U. Schepsmeier, *Modeling Dependence with C- and D-Vine Copulas: The R Package CDVine*. Journal of Statistical Software, vol. 52, pp. 1-27, 2, (2013).
- [5] R. J. Bessa, J. Mendes, V. Miranda, A. Botterud, J. Wang and Z. Zhou, *Quantile-copula density forecast for wind power uncertainty modeling*, PowerTech, 2011 IEEE Trondheim, pp. 1-8, (2011).
- [6] S. Gill, B. Stephen and S. Galloway, *Wind Turbine Condition Assessment Through Power Curve Copula Modeling*, Sustainable Energy, IEEE Transactions on, vol. 3, pp. 94-101, (2012).
- [7] S. Hagspiel, A. Papaemmanouil, M. Schmid and G. Andersson, *Copula-based modeling of stochastic wind power in Europe and implications for the Swiss power grid*, Appl. Energy, vol. 96, pp. 33, (2012).
- [8] H. Valizadeh Haghi, M. Tavakoli Bina, M. A. Golkar and S. M. Moghaddas-Tafreshi, *Using Copulas for analysis of large datasets in renewable distributed generation: PV and wind power integration in Iran*, Renewable Energy, vol. 35, pp. 1991-2000, 9, (2010).
- [9] G. Papaefthymiou and D. Kurowicka, *Using Copulas for Modeling Stochastic Dependence in Power System Uncertainty Analysis*, Power Systems, IEEE Transactions on, vol. 24, pp. 40-49, (2009).
- [10] R. T. Clemen and T. Reilly, *Correlations and Copulas for Decision and Risk Analysis*, Management Science, vol. 45, pp. 208-224, (1999).
- [11] R. B. Nelsen, *An Introduction to Copulas* (2nd ed. ed.) (2006).
- [12] O. Grothe and J. Schnieders, *Spatial dependence in wind and optimal wind power allocation: A copula-based analysis*, Energy Policy, vol. 39, pp. 4742-4754, (2011).
- [13] P. Kumaraswamy, *A generalized probability density function for double-bounded random processes*, Journal of Hydrology, vol. 46, pp. 79, (1980).

CS-BSM Mathematics and Computation in Biological Sciences and Medicine

A Computational Model of Dynamic Cell Fates Via Signal Regulation in Retina Angiogenesis

A. Aylward ¹, C. Calmelet ², A. Madamanchi ³

¹ University of California, San Diego, USA anthony.aylward@gmail.com,

² California State University, Chico, USA cocalmelet@csuchico.edu,

³ Vanderbilt University, Nashville, USA akmadamanchi@gmail.com

We present a hybrid mathematical model to simulate the morphological and signaling features observed in the postnatal development of a retina vascular network. We study the underlying mechanisms guiding the endothelial cells in forming new sprouts and new branching. We discuss the effects of specific molecules and signaling pathways in determining tip/stalk cell fates responsible for the development of the nascent blood vessels. We obtain some numerical solutions of the model, analyze their dependence on physical parameters of the system, and discuss their biological interpretation. The numerical outcomes show similarities with the development of the retinal vascular network *in vivo*.

A numerical study of the effects of inhomogeneous media in Diffusion Weighted Imaging

J. Cervi^{1†}, G. Lewis¹, D. Aruliah¹

¹ Faculty of Science, University of Ontario Institute of Technology, Canada

† jessica.cervi@uoit.ca

Diffusion Weighted Imaging (DWI)—a common Magnetic Resonance Imaging (MRI) technique—is used to infer material properties of tissues from the average diffusion of water molecules over brief time intervals [3]. In particular, an Apparent Diffusion Coefficient (ADC) can be reconstructed from the MR signal under the assumption of homogeneous tissues [2]. Unfortunately, the complex structure of a typical volume element of physiological tissue contains many types of cells of different shapes and sizes separated from extracellular space by semi-permeable barriers and is thus far from homogeneous.

To better understand the effect of inhomogeneous media in DWI, we model a cellular medium with a one-dimensional system of idealized cells separated by non-uniformly spaced semi-permeable membranes and extracellular space [1]. Finite difference solutions of the associated PDE model can be used to compute a Displacement Probability Distribution Function (DPDF) as seen in figure 1. The DPDF in turn is used to reconstruct an MRI signal by averaging the solutions obtained using different initial conditions. We also compute an ADC from the second moments of the DPDF for comparison to the DWI approach. Finally, we investigate the effect of an inhomogeneous model on the higher-order moments (e.g., the kurtosis) of the DPDF and the ADC in general.

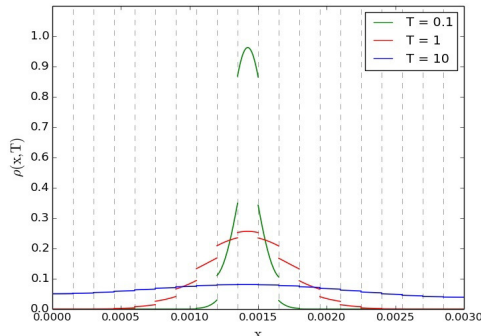


Figure 1: Distribution $\rho(x, T)$ of water particles from an instantaneous source at the centre of the middle region of a 20-region system for reduced permeability $P = 0.5$ at reduced times $T = 0.1, 1, 10$. In figure, the dashed vertical lines represent the semi-permeable membranes.

References

- [1] J.E. Tanner, *Transient diffusion in a system partitioned by permeable barriers. Application to NMR measurements with a pulsed gradient*, J. Chem. Phys. **69**, 1748, (1978).
- [2] A. Szafer, J. Zhong, J.C. Ghore, *Theoretical Model for Water Diffusion in Tissues*, Magn Reson Med, **33**, pp. 697-712 (1995)
- [3] Hagmann, Patric, et al. *Understanding Diffusion MR Imaging Techniques: From Scalar Diffusion-weighted Imaging to Diffusion Tensor Imaging and Beyond*, Radiographics **26**, pp.205-223 (2006)

A Quantitative Model of Cutaneous Melanoma Diagnosis Using Thermography

E. Agyingi¹, T. Wiandt², S. Maggelakis³

¹ Rochester Institute of Technology, USA, eoasma@rit.edu

² Rochester Institute of Technology, USA, tiwsma@rit.edu

³ Rochester Institute of Technology, USA, sxmsma@rit.edu

Cutaneous melanoma is the most commonly diagnosed cancer and its incidence is on the rise worldwide. Early detection and differentiation of a malignant melanoma from benign cutaneous lesions provides an excellent chance for treating the disease. Thermography is a non-invasive tool that can be used to detect and monitor skin lesions. We model heat transfer in a skin region containing a lesion. The model which is governed by the Pennes equation uses the steady state temperature at the skin surface to determine whether there is an underlying lesion. Numerical simulations from the model ascertain whether the lesion is malignant or benign.

Assessing the Robustness of Limited Sampling Strategies

L. Kheibarshekan¹, J. li^{1,2}, F. Nekka^{1,2}

¹ Faculté de Pharmacie, Université de Montréal

² Centre de recherches mathématiques, Université de Montréal

Therapeutic drug monitoring (TDM) is a routine clinical practice for many drugs, immunosuppressive agents in particular, which exhibit significant inter- and intra-individual pharmacokinetic (PK) variability and a narrow therapeutic range. With the aim to optimize treatment efficacy and minimize toxicity, TDM uses appropriate blood sampling to estimate surrogates that correlate well with the drug effect. The area under the plasma drug concentration-time curve (AUC) is one of these surrogates which uses estimation attracts increasing interest. Although many methods have been proposed to estimate AUC, they generally require a large number of blood sampling for a reliable estimation. To reduce this inconvenience, limited sampling strategies (LSS) have been developed, with the involvement of three or less blood samples while keeping a reasonable accuracy [1].

The multiple linear regression (MLR) and the Bayesian are the two usual LSS approaches for the estimation of AUC, noted R-LSS and B-LSS, respectively [2]. The development process of LSS in a clinical setting, generally involves a full sampling to be used as a reference dataset, with 6 to 10 blood samples for each patient. Then a reference AUC (AUC_{ref}) is estimated from this dataset using the trapezoidal method, and set as the AUC target. R-LSS are then established using different subsets of blood sampling to estimate AUC, that are reliable enough compared to AUC_{ref} . The B-LSS approach requires the use of several well-established drug concentrations in addition to population pharmacokinetic (Pop-PK) model for the estimation of AUC.

Regardless of the method used, evaluation of the LSS is critical to achieve a reliable prediction. The criteria most frequently used for the evaluation of LSS involve the calculation of bias and precision. Although these criteria inform the validity of the LSS, the predictive power of these LSS and transferability in fact has not to be taken for granted when different patient subpopulations and contexts are involved. This explains the variety of LSS reported for the same drug by different research groups. Therefore when using a specific LSS, the degree of transferability or reproducibility in a clinical setting or a population different from the one for which it has been established should be assessed. We will refer to this transferability property as the robustness of the LSS [3]. This is the main objective of the current work. In this study we present a comprehensive approach to quantify the robustness of LSS with respect to between subject variability (BSV) and residual variability (RV). We can achieve an accurate and robust LSS by taking advantages of both multiple linear regression (MLR) and Bayesian approach. Our result shows the importance of the BSV and also variability ratio (BSV/RV %) for the robustness probability. For this model, for low BSV, no matter what the RV is, the robustness probability is always relatively high.

References

- [1] M. J. Moore and P. Bunting and S. Yuan and J. J. Thiessen, *Development and validation of a limited sampling strategy for 5-fluorouracil given by bolus intravenous administration*, Ther Drug Monit. **15**, 5, pp. 394-9 (1993).
- [2] S. Sarem and J. Li and O. Barriere and C. Litalien and Y. Theoret and A. L. Lapeyraque and F. Nekka, *Bayesian approach for the estimation of cyclosporine area under the curve using limited sampling strategies in pediatric hematopoietic stem cell transplantation*, Theor. Biol. Med. Model. **11**, 1, pp. 39 (2014).
- [3] A. F. van der Meer and M. A. E. Marcus and D. J. Touw and J. H. Proost and C. Neef, *Optimal Sampling Strategy Development Methodology Using Maximum A Posteriori Bayesian Estimation*, Therapeutic Drug Monitoring **33**, 2, pp. 133-146 (2011).

Coupled and Multi-scale Lattice Boltzmann Modeling of Bidomain type models in Cardiac Electrophysiology

S. Corre¹ and A. Belmiloudi²,

¹ INSA-IRMAR, Rennes, France, Samuel.Corre@insa-rennes.fr

² INSA-IRMAR, Rennes, France, Aziz.Belmiloudi@math.cnrs.fr

In this work, coupling Lattice Boltzmann Models (LBM) in simulation of cardiac electrophysiology are developed in order to capture the detailed activities of macro- to micro-scale transport processes. The propagation of electrical activity in the human heart is mathematically modelled by bidomain type systems (see e.g., [1] and [2] and the references therein). As transmembrane potential evolves, we take in account domain anisotropical properties using intracellular and extracellular conductivity, such as in a pacemaker or an electrocardiogram, in both parallel and perpendicular directions to the fibers. The bidomain system represents multi-scale, stiff and strongly nonlinear coupled reaction-diffusion models (governing the dynamics at cellular and tissue levels) that consists of a set of ordinary differential equations coupled with a set of partial differential equations. Due to dynamic and geometry complexity, numerical simulation and implementation of bidomain type systems are extremely challenging conceptual and computational problems but are very important in many real-life and biomedical applications. This communication suggests a new modified LBM scheme, reliable, efficient, stable and easy to implement in the context of such bidomain systems with nonlinear Robin type boundary conditions in complex geometry boundaries. The concept of LBM, which is efficient in terms of parallelization, is based on Boltzmann equations which describe the evolution of particles in kinetic theory. LBM has two main phases: one, local, which models the collision between particles and the second, along each direction of interpolation, which models the transport phase (see e.g, [3] and [4] and the references therein). The numerical results demonstrate the effectiveness and accuracy of our approach using general methods for bidomain type systems and show good agreement with analytical solutions and numerical results reported in the literature.

Keywords: Coupled Lattice Boltzmann, Reaction-Diffusion system, Bidomain models, Ionic models, Cardiac electrophysiology, multi-scale system.

References

- [1] A. Belmiloudi, *Robust control problem of uncertain bidomain models in cardiac electrophysiology*, Journal of Coupled Systems and Multiscale Dynamics, 1 (2013) 332-350.
- [2] P. Colli Franzone, G. Savaré, Degenerate evolution systems modeling the cardiac electric field at micro- and macroscopic level, in: A. Lorenzi, B. Ruf (Eds.), Evolution Equations, Semigroups and Functional Analysis, Birkhauser, Basel, (2002) 49-78.
- [3] A. J.C. Ladd, *Numerical simulations of particulate suspensions via a discretized Boltzmann equation. Part 1. Theoretical foundation*, Journal of Fluid Mechanics, 271 (1994) 285-309.
- [4] X. Yang, B. Shi, Z. Chai, *Coupled lattice Boltzmann method for generalized Keller-Segel chemotaxis model*, Computers and mathematics with applications 68 (2014) 1653-1670.

Effects of a Mixed Immuno-chemotherapy of Tumor by Impulsive Control

Qing Wang¹, Zhijun Wang², David J. Klinke³

¹ Shepherd University, USA, qwang@shepherd.edu

² Shepherd University, USA, zwang@shepherd.edu

³ West Virginia University, USA, david.klinke@mail.wvu.edu

Chemotherapy, radiation therapy and surgery have been the traditional methods of cancer treatment. Recent clinical data have shown potential benefit in harnessing the power of the immune system in combination with chemotherapy. In order to investigate the impact of dosage and timing in mixed immuno-chemotherapies on tumor growth, we developed a multi-scale mechanistic model using a system of impulsive ordinary differential equations to capture the activation and differentiation of naïve CD8+ T cells into effector cytotoxic T cells in the lymph node following adenovirus-mediated vaccination against a tumor antigen, the trafficking of the resulting cytotoxic T cells into blood and tumor microenvironment, the production of cytokines within the tumor microenvironment, and the interactions between tumor cells, T cells and cytokines that control tumor growth. The parameters of the multi-scale model were calibrated to published experimental data. Based on the calibrated model, impulsive control was applied to in silico screening of the optimal therapeutic dosage and timing in mixed adenovirus vaccination therapy and chemotherapy to control tumor growth. The simulation results may provide cost-effective and efficient immune-chemotherapy regimens for optimal clinical response. The study is supported by the NIGMS of the NIH grant as part of the West Virginia INBRE (P20GM103434).

***Escherichia coli* Contamination Spread in Ground Beef Production**

Petko Kitanov¹, Allan R. Willms²

¹ University of Ottawa, Ottawa, Canada, pkitanov@uottawa.ca
² University of Guelph, Guelph, Canada, AWillms@uoguelph.ca

Human illness due to contamination of food by pathogenic strains of *Escherichia coli* is a serious public health concern and can cause significant economic losses in the food industry. Recent outbreaks of such illness sourced from ground beef production motivates the current work.

Most ground beef consumed in North America is produced in large facilities where many carcasses are butchered and various pieces of them are ground together in large batches. These batches are produced sequentially. If, after leaving the facility, ground beef from a particular batch is discovered to be contaminated with *E. coli*, and if the production facility is determined to be the likely source of this contamination, government regulations require the recall and destruction of all meat and sources associated with the contaminated batch. This regulation is broad for public safety reasons, but much of the meat destroyed under it is likely not contaminated, and its destruction is a large economic loss to the producer. Nonetheless, very little real information is available on the probability of contamination of previous and subsequent batches of ground beef given that one is contaminated.

Assuming that the source of *E. coli* contamination in the hot batch is a single carcass, we model the probability that previous and subsequent batches are also contaminated. The contamination is assumed to initially reside on the fat layer of a single carcass, which moves through the production facility. Trimmings from cuts of this carcass are placed in a time-dependent manner into bins that are later used as input to ground beef production. The model takes into account the fact that each batch of ground beef is generated from several different raw sources, both trimming bins from within the facility and often frozen material from other facilities, each with various fat content and differing likelihoods of being contaminated themselves. The primary determinant is the spread of each carcass across the trimming bins, and this is highly dependent on the operational procedures of the meat production facility. Given an estimate of this spread as well as information on the identity and mass of all input to the ground beef batches, we compute the probability that batches produced before and after the hot batch are also contaminated. Very little data is available for testing the model, however, we do compare our results with data from a genetic study of ground beef production, which provides some verification.

This model may help the beef industry to identify the likelihood of contamination in other batches and potentially save money by not needing to cook or recall unaffected batches of ground beef.

In-host HIV model describes differences in disease progression among patients infected with HIV-1 subtypes A, C and D.

D. W. Dick¹, L. M. Wahl²

¹ Western University, London, Canada, ddick8@uwo.ca

² Western University, London, Canada, lwahl@uwo.ca

Most HIV research focuses on HIV-1 subtype B, which is prevalent in North America and Western Europe. However HIV-1 subtype C is predominant in Africa and in fact global prevalence of subtype C has grown to make up 51% of all HIV-1 infections worldwide [1]. To date, differences in disease progression and epidemiology among subtypes are poorly understood. An in-host mathematical model of disease progression has been designed to test hypotheses about HIV subtypes. This model of disease progression allows us to assess which virologic and immunological parameters differ significantly among subtypes. Differences in disease progression among subtypes may have important implications for disease transmission, timing initiation of antiretroviral therapy, the rapid spread of HIV-1 subtype C and the global HIV epidemic more generally.

References

- [1] Denis M Tebit and Eric Arts, *Tracking a century of global expansion and evolution of HIV to drive understanding and combat disease*, Lancet Infect Dis. **11**, pp. 45-56 (2011).

Mathematical Model of HIV and HCV Co-infection

B. D. Aggarwala¹

¹ University of Calgary, Canada, aggarwal@ucalgary.ca

In many developing countries, with very high population densities, co-infection with both HIV and HCV is fairly common. This is perhaps because, in such situations, people live in close proximity and generally, are not well cared for. Medical facilities are minimal, so that infections spread easily and persist. Also, people who are already infected with HIV or HCV, are likely to have "risky" behavior (risk factors for both HIV and HCV are almost the same) so that contacts are fairly common (sexual, sharing needles and other). Considering all this, one may assume that a certain fraction of people suffering from HIV are also suffering from HCV and vice versa.

We present a mathematical model which describes the development of co-infection with HCV and HIV, in such situations. We assume that, while susceptible people become infected with HIV and/or HCV through physical contact (sexual, sharing needles, and so on), co-infection occurs simply because they live in close proximity to each other. We also assume that a certain percentage of people who are infected with HCV in a densely populated environment are also infected with HIV, and vice versa.

We find that our model has only one relevant solution, apart from the disease-free one. In the solution, 34% of people infected with HIV are also infected with HCV. This is consistent with other findings in the literature.

We calculate the basic reproduction number and give numerical examples.

Mathematical Study of the Pest Control for Jatropha Curcas Plant

Priti Kumar Roy*, Jahangir Chowdhury, Fahad Al Basir

*Centre for Mathematical Biology and Ecology
Department of Mathematics, Jadavpur University
Kolkata - 700032, India*

*Corresponding Author Email:pritiju@gmail.com
Research is supported by UGC, Government of India.

Jatropha Curcas is one of the drought resistant plants that are well-growing even in poor soil and producing seeds containing 37 % of Jatropha oil or triglycerides for 50 years. Jatropha plants are frequently utilized as the best option for generating the Jatropha oil that is used to make Biodiesel in the most cost-effective and eco-friendly way. The plants are affected by mainly six types of pests. Disease of the plants especially through pests inhibits the maximum production of seeds. In this paper, we formulate a set of non-linear differential equations, which consists Jatropha plants, susceptible pests, infected pests and virus population. We mathematically study the control of pests which is extinguished by Nuclear Polyhedrosis Virus, without any damage to the host plants. Our analytical study shows that bio-control is one of the most cost effective ways for maximum production of Jatropha seeds. Results from our numerical study of the model are consistent with the analytical results.

Keywords: Jatropha Curcas, Biodiesel, Nuclear Polyhedrosis Virus (NPV), Susceptible Pests, Infected Pests, Bio-control.

References

- [1] Venturino E., Roy P. K., Basir F. A., Datta A., *Mathematical Overview to Control the Vector Borne Disease of Jatropha Curcas Plant: A Theoretical Approach - The plantation model*, In preparation 2015.
- [2] Bhattacharya D. K., Karan S. P., *On bionomic model of integrated pest management of a single pest population*, J. Differ. Equat. Dyn. Syst., Vol. 12(4), pp. 301-330, 2004.

Mobile Genetic Elements in Prokaryotes: Analysis of the Birth-Death-Diversification Model

N.E. Drakos¹, L.M. Wahl²

¹ University of Western Ontario, London, Canada, ndrakos@uwo.ca

² University of Western Ontario, London, Canada, lwahl@uwo.ca

Mobile genetic elements (MGEs) are regions of DNA that are involved in the intracellular and intercellular movement of genetic material. They are prevalent in all genomes, and are of immense importance in evolution. There exist many models for describing the dynamics of mobile genetic elements in prokaryotes. Most of these models include duplication, deletion, horizontal gene transfer (HGT) and selection. Recently, the birth-death-diversification model was developed to describe the dynamics of a particular class of MGEs, mobile promoters [1]. A novel feature in this model was that the authors included diversification of MGEs.

The birth-death-diversification model consists of two levels: first, the copy-level model is a multi-type branching process used to describe the number of copies per genome, and secondly, the genome-level model is a markov-chain process which describes the number of families in each genome. In this research, we analyze the equilibrium solutions, extinction probabilities and extinction times of this new model using a combination of analytic, numeric and simulation techniques.

A finding of our analysis is that although diversification does not change the number of copies of MGEs in a family, it nonetheless increases both survival and growth rates of MGE families. This is through the influence of diversification on HGT rates; unlike duplication, deletion and diversification, HGT rates appear not to be dependent on family sizes. Therefore, increased diversification indirectly increases HGT rates, which in turn increase the number of MGE families. This analysis demonstrates the subtle interaction between diversification and HGT, and suggests that this interplay is important to consider when modelling prokaryotic MGEs.

References

- [1] M.W. van Passel and H. Nijveen and L.M. Wahl, *Birth, death, and diversification of mobile promoters in prokaryotes*, Genetics **297**, 1, pp. 291-299 (2014).

Population dynamics of lysogenic and lytic strategies during phage-bacteria interactions

Q. Ali¹, L. Wahl²

¹ University of Western Ontario, London, qali6@uwo.ca

² University of Western Ontario, London, lwahl@uwo.ca

Bacteriophage, viruses that infect bacteria, sometimes incorporate their genetic material into the host cell DNA but do not harm the host (lysogeny), rather than using cellular resources to produce new phage, ultimately killing the host (lysis). A mechanistic understanding of the conversion of lambda-phage from lysogeny to lysis has been well developed empirically as well as theoretically at a molecular level. From an evolutionary perspective, however, the decision-making strategy of bacteriophage to pursue either lysogeny or lysis is not well understood. In this contribution, a deterministic population model is developed to study the interaction of wild type bacteria with both lytic and lysogenic viruses. The interesting phenomenon of conversion, from a lysogenic life cycle to a lytic cycle, is also considered in the model. Quantitative parameter estimates have been obtained from the primary experimental literature. Although the basic reproductive ratio is always higher for lytic phage, we explore scenarios in which lysogeny has an evolutionary advantage. A sensitivity analysis by parametric variations is performed to study the impact of parameter values on phage fitness.

Populations Dynamics and Infections in Honey Bees

M. Betti¹, L.M. Wahl², M. Zamir³

¹ University of Western Ontario, London, Canada mbetti@uwo.ca

² University of Western Ontario, London, Canada lwahl@uwo.ca

³ University of Western Ontario, London, Canada zamir@uwo.ca

The global decline of honey bee populations has been a persistent problem in recent history, with potentially detrimental effects on agriculture. The current consensus is that this problem is multi-faceted and pesticide use as well as disease may contribute to colony collapse [1]. We have recently proposed a model which combines the dynamics of the spread of disease within a bee colony with the underlying demographic dynamics of the colony, including both hive bees and foraging bees [2]. This model allowed comparisons of the fate of the colony under exposure to environmental hazards such as pesticides or insecticides, or under exposure to an infectious disease. The average age of recruitment to foraging (AARF) was found to be predictive of the health of a bee colony exposed to a disease threat. Here we extend this work to include age-structure for both the hive and foraging bee populations. This approach allows us to accurately predict changes in the AARF in response to either disease or environmental hazards, and to monitor the resulting changes in hive and forager demographics. Our aim is to develop demographic patterns of decline that are hallmarks for either disease or pesticide exposure, with the goal of better distinguishing the two in field studies.

References

- [1] D. vanEngelsdorp, J. D. Evans, C. Saegerman, et al. Colony collapse disorder: A descriptive study. *PLoS ONE*, (4)8: e6481, (2009).
- [2] M. I. Betti, L. M. Wahl, M. Zamir. Effects of Infection on Honey Bee Population Dynamics: A Model. *PLoS ONE*, 9(10): e110237, (2014).

Provirus as a Reservoir of Viral DNA

A. Nadeem¹ and L.M. Wahl²

¹ Western University, London, Canada, anadeem4@uwo.ca

² Western University, London, Canada, lwahl@uwo.ca

Recent work has shown that the bacterium *E. coli*, when under attack by bacteriophage lambda, can reduce the expression of the receptor that the virus uses as a point of entry, in order to defend itself. In response, the virus can evolve rapidly, gaining the ability to attack through a novel receptor [2]. Very recently, virus lambda has been observed to acquire this ability by using genetic information buried within the host's DNA (J. Meyer, personal communication). This adaptation is only possible because the virus has access to valuable genetic sequences which were left as provirus (remnant viral DNA) within the host's genome by earlier generations of temperate viruses. This phenomenon raises some significant questions, namely what are the factors that may select for the viruses to become temperate and whether the "remains" of previous generations of virus in the host genome provide a benefit to extant viruses for long-term survival. For this purpose, we model the evolutionary dynamics of virus and bacteria using a system of differential equations, including the probabilities that virus in previous generations may leave genetic material in the host genome, and that recombination may allow these genes to transfer back to the virus genome at a later time. The main aim of this study is to understand the importance of provirus and the ability of the virus to use its host as a time capsule to carry information that is detrimental to the host. These questions are of substantial importance since over 8% of the human genome consists of proviral DNA [1].

References

- [1] Casjens, Sherwood. "Prophages and Bacterial Genomics: What Have We Learned so Far?" *Molecular Microbiology* 49.2 (2003): 277-300.
- [2] Meyer, J. R., D. T. Dobias, J. S. Weitz, J. E. Barrick, R. T. Quick, and R. E. Lenski. "Repeatability and Contingency in the Evolution of a Key Innovation in Phage Lambda." *Science* 335.6067 (2012): 428-32.

Regulation and Interaction of Cytokines During a Cytokine Storm

M. Wilcox¹, A. Willms²

¹ University of Guelph, Ontario, Canada, wilcoxm@uoguelph.ca

² University of Guelph, Ontario, Canada, awillms@uoguelph.ca

Cytokine storms are a potentially fatal exaggerated immune response consisting of an uncontrolled positive feedback loop between immune cells and cytokines. The dynamics of cytokines are highly complex and little is known about specific interactions. Although cytokine storms have many biological consequences, the greatest interest to us are the dynamics involved in cancer. Researchers at the Ontario Veterinary College have encountered cytokine storms during virotherapy. Instead of the virus having positive effects, the body becomes overloaded and severe negative effects occur. Multiple mouse trials were conducted where a virus was injected. In each case a fatal cytokine storm occurred. A nonlinear differential equation model of the recorded cytokine amounts was produced to obtain some information on their mutual interactions. Optimization techniques revealed cytokine interaction parameters where cytokines with the largest regulatory effects were further studied. Results provide insight into the complex mechanism that drives the storm and possible ways to prevent such immune responses.

CS-CACO Computational Algebra, Combinatorics and Optimization

Continuous Approaches To Quadratic Boolean Problems Solving

O. Pichugina¹, S. Yakovlev²

¹ Brock University, St.Catarines, Canada, op13ci@brocku.ca

² National University of Internal Affairs, Kharkov, Ukraine, svsyak@mail.ru

To solve the quadratic boolean problem $f(x) = x^T Ax + b^T x \rightarrow \min_{x \in B_n}$, $B_n = \{0,1\}^n$ there are proposed continuous approaches based on inscribing B_n into a sphere $S_r(a)$, $a = (1/2)^n$, $r = \sqrt{n}/2$. In our paper we introduce two different methods to solve the problem.

Method 1. The polyhedral-spherical method [1] for solving discrete problems modified for B_n using the following representation $B_n = S_r(a) \cap P_n$, $P_n = \text{conv}B_n$. It allows us to combine two types of relaxations namely the quadratic problems: a) over P_n ; b) over $S_r(a)$. The method is branch and bound where branching is based on B_n -decomposition into two identical $n-1$ -dimensional sets ($B_n = B_n^{0i} \cup B_n^{li}$, $B_n^{ai} = \{x \in B_n : x_i = a\}$, $i = \overline{1, n}$). The method implies a solution of similar to the original subproblems on P_n -faces of different dimensions. It includes the improvement of lower bounds by the quadratic problem solving over spheres and polyhedra, upper bounds – by projections on B_n of the corresponding points of minimum.

Method 2. The penalty method used for the following function:

$$F(x, \mu, \lambda) = f(x) + \mu \cdot \left(\sum_{i=1}^n \left(x_i - \frac{1}{2} \right)^2 - \frac{n}{4} \right) + \lambda \cdot \sum_{k=1}^2 \sum_{i=1}^n \left(\left(x_i - \frac{1}{2} \right)^{2k} - \frac{n}{2^{2k}} \right)^2. \quad (1)$$

The formula (1) includes functional representation [2] of B_n as a set of tangent points of two smooth surfaces (term 3), and the sphere belonging condition (term 2).

In the present work we have been using the method of convex extension of functions from vertex located sets into R^n [3]; a convex quadratic problem explicit solutions over R^n and $S_r(a)$.

Both our methods can be extended to other classes of functions and sphere located sets. In particular, method 1 can be applied to functions with known global minima over a sphere and for the sets with known analytic description of their convex hulls. Method 2 is applicable for any vertex located sets with known functional representation.

References

- [1] O. Pichugina and S.Yakovlev, *Polyhedral-Spherical Approach to Solving Some Classes of Combinatorial Optimization Problems*, in *Proceedings of the 6th International School-Seminar on Decision Theory*, Uzhgorod, Ukraine, pp. 152-153 (2012).
- [2] O. Pichugina and S.Yakovlev, *Penalty function method for solving optimization problems over combinatorial sets inscribed into a sphere*. Submitted (Jan 2015).
- [3] S.Yakovlev, *The Theory of Convex Continuations of Functions at the Vertices of Convex Polygons*. Computational Mathematics and Mathematical Physics. 34, 7, pp. 959–965 (1994).

Exact Solution of a Boundary Value Problem using Computer Algebra System

Pratibha¹

¹ Department of Mathematics, Indian Institute of Technology Roorkee, Roorkee, India, pratifma@iitr.ac.in

The problem of incompressible potential flow past a sphere in contact with a plane is studied. The velocity at large distance is taken to be uniform and parallel to the plane. This problem is an excellent example where symbolic computation systems can be exploited in order to solve a second order differential equation subject to the boundary conditions.

We used the analytic continuity to re-expand the solution at different points along the axis and matched it to the other end. We obtain a solution that is more accurate and efficient than a numerical one using a computer algebra system. All the routines required for this purpose were developed in MAPLE. These routines are extremely efficient in terms of computer memory and CPU time.

Improving the NNA for the Travelling Salesman Problem using a Modified Vogel Method

D. Almaatani¹, Y. Gningue², M. Takouda³, H. Zhu⁴

¹Laurentian University, Canada, (Maths and Computer Science) dalmaatani@laurentian.ca

²Laurentian University, Canada, (Maths and Computer Science) ygningue@cs.laurentian.ca

³Laurentian University, Canada, (Finance and Operation) mtakouda@laurentian.ca

⁴Nipissing University, Canada, (Computer Science and Maths) haibinz@nipissingu.ca

Abstract. The Travelling Salesman Problem (TSP) consists of finding the lowest cost or the shortest path tour T between n cities Refs. [1, 2, 3]. In term of graph, TSP includes to find the Hamiltonian cycle associated with the shortest total distance or a total minimal cost. The TSP, known as an NP-hard problem in combinatorial optimizations, plays very important role in operations research and theoretical computer science. Indeed, in the theory of computational complexity, the decision step of the TSP belongs to the class of NP-complete problems [3] and is one of the simplest but most intensively studied problems in optimizations. The TSP has several applications such as planning, logistics, and the manufacture of microchips. Even though the problem is computationally difficult, a large number of heuristics [2] and exact methods are known. In this presentation, we propose a new heuristic algorithm for the TSP. It uses the Modified Vogel Method (MVM) to improve the Nearest Neighbor Algorithm (NNA) [1] which is at first introduced. Then, the Modified Vogel Method (MVM) is applied into the TSP in the following section. Finally, an example of illustration and numerical tests are presented in the fourth section followed by the concluding remarks.

References

- [1] G. Gutin, A. Yeo and A. Zverovich. *Traveling salesman should not be greedy: domination analysis of greedy-type heuristics for the TSP*, Discrete Applied Mathematics 117 (2002), 81-86
- [2] S. S. Ray, S. Bandyopadhyay and S. K. Pal. *Genetic Operators for Combinatorial Optimization in TSP and Microarray Gene Ordering*, Applied Intelligence, 2007, 26(3). pp. 183-195.
- [3] Z. Weixiong. *A note on the complexity of the Asymmetric Traveling Salesman Problem*, Oper. Res. Letters 20 (1997) 31-38

Numerical verification of mixed precision algorithms using Monte Carlo arithmetic

M. Baboulin¹, C. Denis², A. Khabou¹

¹ Université Paris-Sud, Orsay, France, {baboulin,khabou}@iri.fr

² Ecole Normale Supérieure de Cachan, CMLA, Cachan, France, christophe.denis@cmla.ens-cachan.fr

Large scale simulations produced in scientific applications require an increasing amount of memory and energy consumption. It becomes then crucial to reduce these quantities in order to prepare for the exascale computing [1]. The design of mixed precision algorithms has been successfully applied in [2] to accelerate the solution of linear systems. Mixed precision algorithms can be also used to reduce memory and energy consumption since they perform the most expensive part of the computation in the lowest precision. However, it is essential to estimate the numerical accuracy of mixed precision algorithms and to compare it to the original algorithms in fixed precision.

In this work, we focus on the numerical verification of mixed precision algorithms by studying the round-off error propagation [3] in the solution of dense linear systems. This is achieved by using the Monte Carlo arithmetic instead of the IEEE-754 arithmetic. The Monte Carlo Arithmetic (MCA) tracks rounding errors by applying randomization to the input and output operands, forcing the results of floating point operations to behave like random variables [4]. This turns a given execution into trials of a Monte Carlo simulation, which allows us to obtain statistics on the effects of rounding errors over a number of executions. The Monte Carlo Arithmetic Library (MCALIB) [5] implements variable precision MCA for single and double precision floating point arithmetic in the C language. We use source-to-source compilation methods implemented using the C Intermediate Language (CIL) so that modifications of the existing source code are not required and floating point operations are automatically translated to function calls.

In this paper, we first describe the mixed precision algorithms designed to solve linear systems. Then we discuss the numerical verification obtained with MCALIB on a set of linear systems that have different condition numbers and that we solved using mixed and fixed precision algorithms.

References

- [1] I. S. Duff, *European Exascale Software Initiative: Numerical Libraries, Solvers and Algorithms*, Euro-Par 2011: Parallel Processing Workshop, Lecture Notes in Computer Science, **7155** (2011).
- [2] M. Baboulin, A. Buttari, J. Dongarra, J. Kurzak, J. Langou, P. Luszczek, S. Tomov, *Accelerating scientific computations with mixed precision algorithms*, Computer Physics Communications, **180**, 12, pp. 2526-2533 (2009).
- [3] C. Denis, *Numerical verification of an industrial code to simulate accurately large scale hydrodynamics events*, International Water Journal, **2**, pp. 46-51 (2013).
- [4] D. S. Parker, *Monte Carlo Arithmetic: exploiting randomness in floating-point arithmetic*, Technical Report CSD-970002, UCLA Computer Science Department (1997).
- [5] M. Frechting, P. H. W Leong, *MCALIB - a tool for automated rounding error analysis*. ACM Transactions on Programming Languages and Systems, In press, accepted 23 Aug 2014.

Quasi-Cyclic Codes over Finite Chain Rings

K. Guenda¹ and T.A. Gulliver²,

¹ Faculty of Mathematics, University of Algiers (USTHB), Algeria, ken.guenda@gmail.com

² Dept. of Electrical and Computer Engineering, University of Victoria, Victoria, BC, Canada, agullive@ece.uvic.ca

A finite *chain ring* R is a finite ring such that its ideals are ordered by inclusion. The class of codes over finite chain rings is an important class of codes with many practical applications in areas such as signal processing, DNA computing, quantum computing and cryptography. Quasi-cyclic codes are well-known error correcting codes which includes many optimal codes. Further, they are used in several code-based cryptosystems [1, 5]. A linear code is called quasi-cyclic of order l if it is invariant under the permutation $i \mapsto i + l \bmod n$, or equivalently C is quasi-cyclic if for all $c \in C$ we have $T^l(c) \in C$, where $T : i \mapsto i + 1$ is a circular shift. The order l of C is the smallest integer satisfying this property. Several authors [3, 4] have investigated quasi-cyclic codes over finite fields and more generally over finite chain rings.

This work solves one of the most challenging problems for quasi-cyclic codes, namely the equivalence of these codes over finite chain rings. The main result is a proof that two quasi-cyclic codes are equivalent if and only if their constituent codes are equivalent. In some cases, this allows us to reduce the equivalence problem for quasi-cyclic codes to the equivalence of cyclic codes, which can be solved using the approach in [2]. This result also enables us to find conditions on the existence of self-dual quasi-cyclic codes and more generally isodual quasi-cyclic codes over finite chain rings. For example, it is proven that if q is odd then there are no μ_e -isodual quasi-cyclic codes for any multiplier permutation.

References

- [1] T.P. Berger, P.-L. Cayrel, P. Gaborit and A. Otmani, *Reducing key length of the McEliece cryptosystem*, Progress in Cryptology - AFRICACRYPT 2009, LNCS 5580, 77–97, 2009.
- [2] K. Guenda and T.A. Gulliver, *The equivalency problem for cyclic combinatorial objects*, CanaDAM, 2013.
- [3] S. Ling and P. Solé, *On the Algebraic structure of quasi-cyclic codes II: Chain rings*, Des. Codes. Cryp., 30, 113–130, 2003.
- [4] S. Ling and P. Solé, *On the algebraic structure of quasi-cyclic codes III: Generator theory*, IEEE Trans. Inform. Theory, 51(7), 2692–2700, 2005.
- [5] A. Otmani, J.-P. Tillich, and L. Dallot, *Cryptanalysis of two McEliece cryptosystems based on quasi-cyclic codes*, Math. Comput. Sci., 3(2), 129–140, 2010.

Random butterfly transformations for accelerated parallel machines

M. Baboulin¹, A. Rémy¹

¹ Université Paris-Sud and Inria, Orsay, France, baboulin@lri.fr

² Université Paris-Sud and Inria, Orsay, France, aremy@lri.fr

Randomized algorithms are becoming very attractive in high-performance computing (HPC) since they are able to outperform deterministic methods while still providing very accurate results. In recent works, we designed randomized algorithms [1, 2] based on random butterfly transformations (RBT) [3]. These randomized solvers have the advantage of reducing the amount of communication in dense factorizations by removing completely the pivoting phase which degrades performance in Gaussian Elimination (GE). The process to solve the general linear system $Ax = b$ is the following:

1. Compute the randomized matrix $A_r = U^T AV$, with U and V belonging to a class of random matrices called *recursive butterfly matrices* [3],
2. Factorize A_r using GE without pivoting (LU factorization),
3. Solve $A_r y = U^T b$,
4. Solution is $x = Vy$.

We propose in this work to design efficient RBT algorithms that take advantage of current accelerators like GPUs and Intel Xeon Phi. In these algorithms, the matrix is transferred and randomized on the accelerator. During the block LU factorization, the panel is factored on the CPU host, while the updates are performed on the accelerator. Then the triangular solves are performed on the accelerator. The solution can be improved by using iterative refinement on the accelerator if required, and one iteration is generally sufficient to get satisfactory accuracy. The CUDA implementation of our RBT solver outperforms the classical partial pivoting version from MAGMA [4]. For large enough matrices (from size 6000), the obtained performance on GPU is about 20-30% faster than the partial pivoting version. The time spent in the randomization phase represents 1-2% of the total time (3-4% for small matrices). Note that the randomization performed on the Intel Xeon Phi coprocessor has been optimized using SIMD instructions and OpenMP.

References

- [1] M. Baboulin and J. Dongarra and J. Hermann and S. Tomov, *Accelerating Linear System Solutions using Randomization Techniques*, ACM Transactions on Mathematical Software, **39**, 2 (2013).
- [2] M. Baboulin and D. Becker and G. Bosilca and A. Danalis and J. Dongarra, *An efficient distributed randomized algorithm for solving large dense symmetric indefinite linear system*, Parallel Computing, **40**, 7, pp. 213-223 (2014).
- [3] D. S. Parker, *Random Butterfly Transformations with Applications in Computational Linear Algebra*, Technical Report CSD-950023, UCLA Computer Science Department (1995).
- [4] S. Tomov and J. Dongarra and M. Baboulin, *Towards dense linear algebra for hybrid GPU accelerated manycore systems*, Parallel Computing **36**, 5&6, pp. 232-240 (2010).

CS-CPC Computational Physics and Chemistry

A Force Balance Model for Rise, Impact and Bounce of Bubbles in Clean Systems

R. Manica¹, E. Klaseboer², D. Chan³

¹ Institute of High Performance Computing, Singapore, manicar@ihpc.a-star.edu.sg

² Institute of High Performance Computing, Singapore, evert@ihpc.a-star.edu.sg

³ The University of Melbourne, Australia, D.Chan@unimelb.edu.au

A force balance model that takes into account effects of buoyancy, drag, added mass and thin film drainage is proposed for the rise and impact of air bubbles against solid horizontal surfaces. The boundary condition at the air-water interface is taken to be stress-free which is consistent with bubbles in clean water systems. Numerical simulations of the governing equations for the position and velocity of the center of mass of the bubbles are compared against experimental data. Features that are compared include bubble terminal velocity, bubble accelerating from rest to terminal speed and bubble impacting and bouncing off different solid surfaces for bubbles that have already attained terminal speed and for bubbles that have not yet. Excellent agreement between theory and experiments indicates that the forces included in the model constitute the main physical contributions to the bouncing phenomenon while other effects such as shape oscillations of the bubble play a secondary role. In Figure 1, we show numerical results for the velocity of the bubble as well as thin film drainage during multiple impacts with the solid surface.

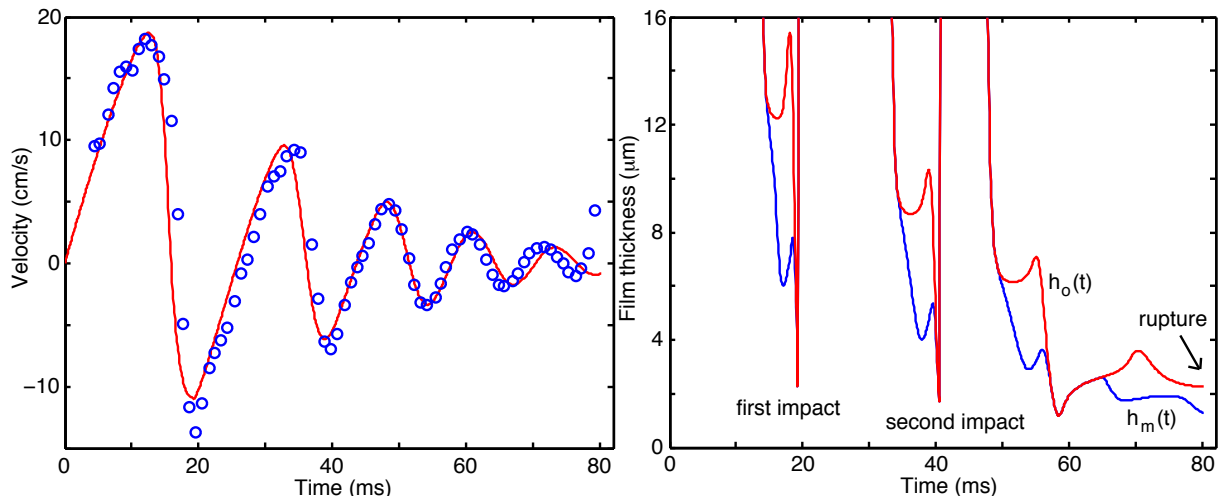


Figure 1: (a) Comparison between our model (line) and experimental rising velocity (circles) of Kosior et al. for a bubble ($R=0.74\text{mm}$) that is released from a syringe 3 mm away from a solid surface. The bubble bounces multiple times.
 (b) Central $h_o(t)$ and minimum $h_m(t)$ film thickness during impacts of the bubble onto the surface.

References

- [1] M.H.W. Hendrix, R. Manica, E. Klaseboer, D.Y.C. Chan, C.-D. Ohl, *Spatiotemporal evolution of thin liquid films during impact of water bubbles on glass on a micrometer to nanometer scale*, Phys. Rev. Lett. **108**, 247803 (2012).
- [2] E. Klaseboer, R. Manica, M. H. W. Hendrix, C-D. Ohl, and D. Y. C. Chan. *A force balance model for the motion, impact, and bounce of bubbles*. Phys. Fluids, **26**, 092101 (2014).
- [3] D. Kosior, J. Zawala, M. Krasowska, K. Malysa, *Influence of n-octanol on the bubble impact velocity, bouncing and the three phase contact formation at hydrophobic solid surfaces*. Colloids Surf. A: Physicochem. Eng. Aspects **441**, 788-795 (2014).

Accurate Determination of Concentration Dependent Material Properties in Electrochemical Systems Using *In-Situ* NMR and Inverse Modelling

Athinthra Krishnaswamy Sethurajan¹, Sergey A. Krachkovskiy², Ion. C. Halalay³, Gillian R. Goward², Bartosz Protas⁴

¹ School of Computational Science and Engineering, McMaster University, krisha9@mcmaster.ca

² Department of Chemistry, McMaster University, {sergey.k.goward}@mcmaster.ca

³ General Motors Global R&D - Warren, ion.c.halalay@gm.com

⁴ Department of Mathematics, McMaster University bprotas@mcmaster.ca

We consider an extension of the Planck-Nernst model to the transport of ionic species in concentrated binary Li-ion battery electrolyte solutions in which the effect of high salt concentrations is accounted for by a concentration-dependent diffusion coefficient and transference number. The concentration dependences are determined in an optimal manner through the solution of an inverse problem using concentration profiles obtained from *in-situ* ^{19}F NMR imaging measurements. This experiment is modeled by a 1D time-dependent partial differential equation describing the evolution of the lithium salt concentration with prescribed initial concentrations and fluxes at boundaries. The material properties are reconstructed with minimal assumptions, by using methods of variational optimization to minimize the least-square error between the experimentally determined and simulated concentration values. The optimization problem is solved using a gradient-based method with a careful treatment of uncertainties resulting from the presence of noise in the experimental data. Thus obtained dependencies of the diffusion coefficient and transference number on the salt concentration are consistent with results derived through other experimental techniques. It is also demonstrated that, with such optimally determined material properties, the Planck-Nernst model can provide a more accurate description of ion transport in concentrated binary electrolyte solutions.

Dynamics of disc-shaped colloids in nematic liquid crystal

A. Antipova¹, C. Denniston²

¹ University of Western Ontario, Canada, aantipov@uwo.ca

² University of Western Ontario, Canada, cdennist@uwo.ca

We examine the behavior of (ferromagnetic) micron-sized structures such as disc-shaped colloidal particles in a nematic liquid crystal using Lattice Boltzmann algorithm. Without any external forces the position of the disc with respect to the liquid crystal director minimizes the free energy of the system and no distortion of the director field is observed. When the rotating magnetic field is present, the torque on the disc with homeotropic surface anchoring should change with analogy to electrostatic energy, which implies the disc continues turning following the field. However, when the disc reaches some critical position and the director field around it is highly distorted, the disc suddenly flips to minimize the free energy. Position and motion of pairs of such discs under similar conditions can be controlled by the angular velocity of magnetic field, its magnitude and initial configuration of the system. As a result of analysis of discs' dynamics, a new way to control self-organization of disc particles was produced. We also will demonstrate some results on ferromagnetic torus micro-colloidal particle in nematic with more complicated boundary conditions.

Molecular-Dynamics Simulations Using Spatial Decomposition and Task-Based Parallelism

Chris M. Mangiardi¹, Ralf Meyer²

¹ Laurentian University, Sudbury, Canada, cmangiardi@laurentian.ca

² Laurentian University, Sudbury, Canada, rmeyer@cs.laurentian.ca

Molecular-Dynamics (MD) simulations are an integral method in the numerical studying of material-sciences. In order to utilize the full processing power of these systems, algorithms must be updated to account for newer hardware. This contribution discusses an algorithm for large-scale MD simulations using modern multi- and many-core systems on distributive computing networks.

The proposed hybrid method utilizes spatial decomposition [1] for use with the Message Passing Interface (MPI) to distribute the system onto multiple nodes, in combination with the cell task method [2] used for task-based parallelism on each node. This allows for the improved performance of task-based parallelism on single systems, in addition to the benefit of distributive computing allowed by MPI.

Results from benchmark simulations on Intel Xeon processors, and Intel Xeon Phi co-processors are presented. Results show that the hybrid method provides better performance than either spatial decomposition or cell task methods alone on single nodes, and scales well as additional nodes are added, using a variety of system configurations.

References

- [1] S. Plimpton, *Fast Parallel Algorithms for Short-Range Molecular Dynamics*, Journal of Computational Physics, **117**, pp. 1-19 (1995).
- [2] R. Meyer, *Efficient Parallelization of Short-Range Molecular Dynamics Simulations on Many-Core Systems*, Physical Review E **88**, 053309 (2013).

Solutions of Time-Fractional Diffusion Equations with Reflecting and Absorbing Boundary Conditions using Matlab

Iftikhar Ali, Nadeem A. Malik and Bilal Chanane

King Fahd University of Petroleum and Minerals, PO Box 5046, Dhahran, 31261, Saudi Arabia.

Email: iali@kfupm.edu.sa; namalik@kfupm.edu.sa; Chanane@kfupm.edu.sa

The main objective of this work is to develop Matlab program for solving time-fractional diffusion equation (TFDE) with reflecting and absorbing boundary conditions on finite and infinite domains, see [1, 2, 3].

Essentially, there are two major codes one for finding the exact solution of the TFDE and other for finding the numerical solution of the TFDE. The code for finding the exact solutions is based on the solutions techniques given in Metzler and Klafter [4, 5], whereas the code for finding the numerical solutions is based on the explicit and implicit finite difference schemes given by Yuste and Acedo [6] and Langlands and Henry [7] respectively.

Finally, we illustrate the effectiveness of the codes by applying them to TFDEs with sharp initial data and for various reflecting and absorbing conditions both on finite and infinite domains. The results show the difference of solutions between the standard diffusion equation and the time-fractional diffusion equation.

References

- [1] Ali, Iftikhar, and Nadeem A. Malik, *Hilfer fractional advection-diffusion equations with power-law initial condition; a numerical study using variational iteration method*, Computers & Mathematics with Applications 68, no. 10 (2014): 1161-1179.
- [2] Ali, Iftikhar, Nadeem Malik, and Bilal Chanane, *Fractional diffusion model for transport through porous media*, in 5th International Conference on Porous Media and Their Applications in Science, Engineering and Industry, June 22-27, 2014, USA.
- [3] Nadeem A. Malik, Iftikhar Ali, and Bilal Chanane, *Numerical solutions of non-linear fractional transport models in unconventional hydrocarbon reservoirs using variational iteration method*, in 5th International Conference on Porous Media and Their Applications in Science, Engineering and Industry, June 22-27, 2014, USA.
- [4] Metzler, Ralf, and Joseph Klafter, *The random walk's guide to anomalous diffusion: a fractional dynamics approach*, Physics reports 339, no. 1 (2000): 1-77.
- [5] Metzler, Ralf, and Joseph Klafter, *Boundary value problems for fractional diffusion equations*, Physica A: Statistical Mechanics and its Applications 278, no. 1 (2000): 107-125.
- [6] Yuste, Santos B., and L. Acedo, *An explicit finite difference method and a new von Neumann-type stability analysis for fractional diffusion equations*, SIAM Journal on Numerical Analysis 42, no. 5 (2005): 1862-1874.
- [7] Langlands, T. A. M., and B. I. Henry, *The accuracy and stability of an implicit solution method for the fractional diffusion equation*, Journal of Computational Physics 205, no. 2 (2005): 719-736.

The fourth-order density gradient expansion of a fluid free energy

G. Piatkovska¹, C. Denniston²

¹ University of Western Ontario, London, Canada, gpiatkov@uwo.ca

² University of Western Ontario, London, Canada, cdennist@uwo.ca

The fourth-order density gradient expansion of a fluid free energy density is constructed from microscopic measurements. The gradient expansion coefficients are determined for liquid water by means of measurements of correlation functions of TIP3P water in a molecular dynamics computer simulation. The second-order coefficient is found to be negative and its value agrees with the one recently calculated using linear response measurements, while the fourth-order coefficient is positive and ensures the stability of the gradient expansion. Implications for coarse-graining are discussed, including the choice of density (mass versus number) and interpretation of correlations.

CS-DSDE Applications of Dynamical Systems and Differential Equations

Bifurcations in the solution structure of market equilibrium problems

F. Etbaigha¹, M. Cojocaru²

¹ University of Guelph, Guelph, ON, Canada {fetbaigh}@uoguelph.ca

² University of Guelph, Guelph, ON, Canada {mcojocar}@uoguelph.ca

In this study, the well-known market disequilibrium model with excess supply and demand is investigated to determine if it exhibits changes in the structure and number of equilibrium states for specific choices of parameter values. The current market model [1] consisting of the supplies, demands, shipments, excess supplies and excess demands is extended from a simpler spatial price equilibrium model (see [2]) and is caused by price controls, i.e., the supply and demand prices are regulated by price floors and price ceilings, respectively, which are assumed to be known and fixed. The market equilibrium conditions allowing excess supply and demand are formulated as a variational inequality problem [1, 2].

We propose to examine the effects of changing pricing functions at supply or demand locations on the number of arising market equilibrium states; specifically, there are well-known conditions under which market models in [1, 2] exhibit a unique equilibrium state (shipments, excess supply, demand etc.); we investigate the conditions under which changes in the pricing functions lead to a non-unique structure in the market model. We conduct our analysis by modelling the markets via a projected dynamical system [3, 4], which is a type of constraint ODE whose critical points are the market equilibrium states of the economic model.

We show a market example with two supply markets and three demand markets; the variational inequality and projected dynamical system of market conditions are formulated. We introduce a parameter in the supply price without influencing the solution to see if the dynamic behavior of the solution exhibits any bifurcation as the parameter is varied.

KEY WORDS. Bifurcation theory, variational inequality, projected dynamical system, supply and demand

References

- [1] A. Nagurney, *Disequilibrium and variational inequalities*, Journal of computational and applied mathematics. **211**, 33(2), pp. 181-198 (1990).
- [2] A. Nagurney, *Network economics: a variational inequality approach*, Vol. 10. Springer Science & Business Media, (1998).
- [3] Cojocaru, M.-G. and Jonker, L. B., *Existence of solutions to projected differential equations on Hilbert spaces*, Proceedings of the AMS, Volume 132, Number 1, 183-193 (2004).
- [4] Cojocaru, M.-G., *Monotonicity and existence of periodic cycles for projected dynamical systems on Hilbert spaces*, Proc. Amer. Math. Soc. 134 (2006) 793-804.

Dynamic Boundary Stabilization of Schrödinger Equation through a Kelvin-Voigt Damped Wave Equation

Lu Lu, Jun-Min Wang

Beijing Institute of Technology, Beijing, China, lulu0408100@126.com

In this paper, we present a dynamic boundary feedback controller (DBFC) for a Schrödinger equation, where DBFC is a wave equation with Kelvin-Voigt damping in order to stabilize the Schrödinger equation. The coupled Schrödinger-wave system (as shown in Fig.1.) is written as follows:

$$\begin{cases} y_t(x, t) + iy_{xx}(x, t) = 0, & 0 < x < 1, t > 0, \\ z_{tt}(x, t) - z_{xx}(x, t) - \alpha z_{xxt}(x, t) = 0, & 1 < x < 2, t > 0, \\ y(0, t) = z(2, t) = 0, & t \geq 0, \\ y(1, t) = kz_t(1, t), & t \geq 0, \\ \alpha z_{xt}(1, t) + z_x(1, t) = -iky_x(1, t), & t \geq 0, \end{cases}$$

where $\alpha > 0, k \neq 0$. The two equations are coupled at $x = 1$ with interconnected conditions and fixed at each end.

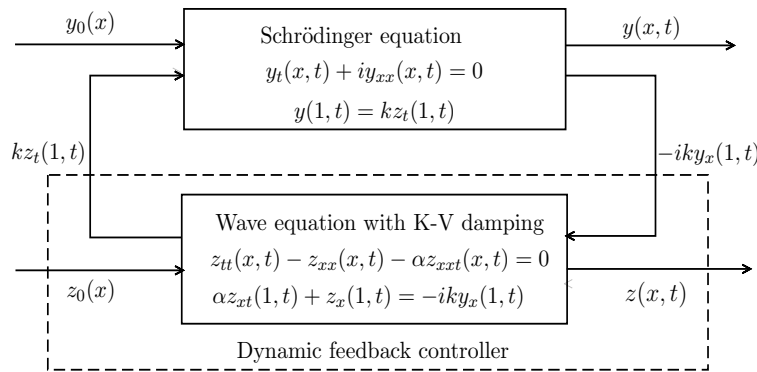


Figure 1: Dynamic boundary feedback for the coupled system

We first set up the system operator and show it generates a C_0 -semigroup of contractions, and the system is well-posed. By detailed spectral analysis, we obtain that the residual spectrum is empty and the continuous spectrum contains only one negative point. Moreover, all the eigenvalues of the system lie in the open left half plane, and their real parts approach negative infinity, by giving the asymptotic expressions of the eigenvalues. Therefore, this controller design moves the eigenvalues of the Schrödinger and wave equations into the second quadrant. It follows that the C_0 -semigroup generated by the system operator achieves strong stability.

Existence and stability of a synchronous oscillation in a neural system with delayed coupling

Israel Ncube¹

¹ College of Engineering, Technology, & Physical Sciences,
Department of Mathematics, Alabama A & M University,
Huntsville, AL 35762, U.S.A.,
Ncube.Irael@gmail.com

The article deals with a particular case of a two neuron network with two discrete time delays. We analyse the linear stability for the particular equilibrium $(0, 0)$, and address the Hopf bifurcation which may occur as one of the delays crosses some critical values. The network under consideration has no self-connections, and thus only one time delay appears in the characteristic equation.

The purpose of the article is to investigate the existence and stability of a nonconstant periodic oscillation $[x(t), x(t)]$ of the following system of delay differential equations:

$$\begin{aligned} x'_1(t) &= -ax_1(t) + b(|x_1(t-R) - x_2(t-R)|) \cdot g[x_2(t-\bar{R})], \\ x'_2(t) &= -ax_2(t) + b(|x_1(t-R) - x_2(t-R)|) \cdot g[x_1(t-\bar{R})], \end{aligned} \quad (1)$$

where $a > 0$ is the leakage term, $R, \bar{R} > 0$ are discrete delays, and the function $b : \mathbb{R} \rightarrow \mathbb{R}$ denotes the coupling, and is given by

$$b(|x_j(t-R) - x_{j+1}(t-R)|) = f(|x_j(t-R) - x_{j+1}(t-R)|) - \sigma, \quad j \bmod 2.$$

The coupling $b(z)$ is modelled so that it is negative in a small neighbourhood of the origin and then becomes positive if z exceeds a constant $\sigma > 0$, say.

Global Stability of Coupled Lorenz Systems Controlled with Two Adaptive Controllers

Yan Wu¹

¹*Georgia Southern University, USA, yan@georgiasouthern.edu*

One-dimensional flows in a coupled loop thermosyphon system are governed by the interconnected Lorenz systems

$$\begin{cases} \dot{x}_1 = \sigma(y_1 - x_1) - \gamma(x_1 - x_2) \\ \dot{y}_1 = R_1 x_1 - y_1 - x_1 z_1 + u_1 \\ \dot{z}_1 = x_1 y_1 - z_1 - \eta(z_1 - z_2) \\ \dot{x}_2 = \sigma(y_2 - x_2) - \gamma(x_2 - x_1) \\ \dot{y}_2 = R_2 x_2 - y_2 - x_2 z_2 + u_2 \\ \dot{z}_2 = x_2 y_2 - z_2 - \eta(z_2 - z_1) \end{cases} \quad (1)$$

where the x -variables represent fluid velocity, and the other states are analogous to fluid temperature. As the Rayleigh numbers R_i increase, the flow evolves through the stages from heat conduction, convection, to chaos. The control objective is to stabilize the flow when the Rayleigh numbers are in the chaotic regime, while maintaining that the system parameters are not known *a priori*. The controllers u_1 and u_2 , which are inserted in the y -equations, have two components: one is a proportional state feedback with the y -variable and the second part is a wavelet network that synthesizes the uncertainties or the dynamics not considered through modeling. We prove global stability of the adaptive control system (1) with uncertainties or disturbances present in the system. We also demonstrate the control efficiency with numerical simulations.

Homoclinic Structure for a Generalized Davey-Stewartson System

C. Babaoglu¹, I. Hacinliyan²

¹ Istanbul Technical University, Istanbul, Turkey, ceni@itu.edu.tr

² Istanbul Technical University, Istanbul, Turkey, hacinliy@itu.edu.tr

Homoclinic orbits is a fundamental tool for the study of chaos in deterministic nonlinear dynamics. In a neighborhood of such an orbit, an extended knowledge of geometric structures lead one to a better understanding of chaotic dynamics. In this study, we analyze the homoclinic structure for the generalized Davey-Stewartson (GDS) equations, given as

$$\begin{aligned} iA_t + \delta A_{xx} + A_{yy} &= \chi |A|^2 A + b (\varphi_{1,x} + \varphi_{2,y}) A, \\ \varphi_{1,xx} + m_2 \varphi_{1,yy} + n \varphi_{2,xy} &= (|A|^2)_x, \\ \lambda \varphi_{2,xx} + m_1 \varphi_{2,yy} + n \varphi_{1,xy} &= (|A|^2)_y, \end{aligned} \quad (1)$$

where $A : R_x \times R_y \times R_t^+ \rightarrow C$, $\varphi_1 : R_x \times R_y \times R_t^+ \rightarrow R$ and $\varphi_2 : R_x \times R_y \times R_t^+ \rightarrow R$. A is the scaled amplitude of the free short transverse wave mode and φ_1 and φ_2 are the scaled free long longitudinal and long transverse wave modes, respectively [1].

Homoclinic structure of nonlinear Schrodinger equation (NLS) is considered by Ablowitz and Herbst in [2]. They have shown how this structure associated with the cubic NLS equation may be obtained from the N-soliton solutions of the defocusing NLS equation. We follow a similar approach and first observe that the fixed point in the GDS system is hyperbolic. Then, we provide an analytic description of the characteristics of homoclinic orbits via soliton type solutions. These solutions that we obtain from Hirota's method are also supported by numerical computations.

References

- [1] C. Babaoglu and S. Erbay, *Two-dimensional wave packets in an elastic solid with couple stresses*, Int. J. Non-Linear Mech. **39**, pp. 941-949 (2004).
- [2] M.J. Ablowitz and B.M. Herbst, *On homoclinic structure and numerically induced chaos for the nonlinear Schrödinger equation*, SIAM J. Appl. Math. **50**, pp. 339-351 (1990).

Investigating an Exemplar Dynamic Model for Sound Classification

B. Goodman¹ and P.F. Tupper¹

¹ Simon Fraser University, Burnaby, BC, Canada, bgoodman@sfu.ca

We investigate an exemplar dynamic model for classifying sounds into categories. For example, one might want to tell the difference between someone saying the word “bet” and the word “bit.” In order to do this, you must classify the vowel sound as either “e” or “i.” One way of modelling this is by using exemplar dynamics.

An exemplar is the detailed memory of sound modelled as a vector that is N-dimensional. The dimensions represent different characteristics of the sound we are classifying such as frequencies. In the model, the hearer of the sound has a collection of exemplars that they know the categorization of. Upon hearing a new sound they then classify it using the exemplars.

In our work, we are classifying new sounds by shortest distance to the weighted average of each exemplar category. We study the long-term behaviour of this system within a population of speakers. During our presentation I will discuss the work we have done and our results.

Modeling the effect of climatic factors on malaria transmission

G.J Abiodun¹, P. Witbooi¹, K. Okosun²

¹ University of the Western Cape, Republic of South Africa, 3109433@myuwc.ac.za, pwitbooi@uwc.ac.za

² Vaal University of Technology, Republic of South Africa, kazeemo@vut.ac.za

In this study, a climate-based mathematical model to investigate the impact of temperature and rainfall on malaria transmission is developed and analysed. The basic reproduction number (\mathcal{R}_0) is derived along with stability analysis. The effect of the larval death rate on the reproduction number is also investigated. The model is validated on observed malaria transmission in Limpopo Province, South Africa, giving a reasonable fit and in particular, detecting accurately all the spikes in malaria prevalence. The model provides a numerical basis for further refinement towards prediction of the impact of climate variability on malaria transmission.

References

- [1] K.O. Okosun and O.D. Makinde, *Modeling the impact of drug resistance in malaria transmission and its optimal control analysis*, Int. J Phy. Sci. **6**, 28, pp. 6479-6487, (2011).
- [2] E.P. Paul and M. Edwin, *Modeling Climate Change and Malaria Transmission*, Adv. Exp. Med. and Bio., 673 pp. 184-199, (2010).

Numerical Solutions for Accelerated and Decelerated MHD Falkner-Skan Flows

A. Malek¹, R. Naseri²

¹ Tarbiat Modares University, Tehran, Iran, mala@modares.ac.ir

² Tarbiat Modares University, Tehran, Iran, naserir@modares.ac.ir

In studying magneto-hydro-dynamic (MHD) Falkner-Skan flows, the first three questions are the question of existence, multiplicity and uniqueness of similarity solutions for the nonlinear differential equations arising in this subject. Although, there are lots of research works in the case of accelerating flows (see Refs. [1, 2]), there is little work in the case of decelerated nonlinear differential equations arising in MHD Falkner-Skan flows. Accelerating flows for positive parameter β may be written as the third order nonlinear differential equation

$$\varphi'''(\eta) = -\varphi(\eta)\varphi''(\eta) - \beta(1 - \varphi'(\eta)^2) + M^2(\varphi'(\eta) - 1), \quad (1)$$

under the following boundary conditions

$$\varphi(0) = 0, \quad \varphi'(0) = 0, \quad \text{and} \quad \varphi'(\eta) = 1 \quad \text{as} \quad \eta \rightarrow \infty. \quad (2)$$

For $\beta = 0$, it is called constant flow, while for $\beta < -M^2$ Eqs. (1)-(2) represent decelerated flows. In the year 2010, for both $\beta \geq 0$ and for $-M^2 < \beta < 0$ unique solutions are derived [1, 2]. In their proofs they use the monotone property of the $\varphi(\eta)$ together with its first and second derivatives monotonicity. In the year 2015, Naseri, Malek and Van Gorder [4] proposed a novel algorithm based on techniques in Ref. [3] that can derive solutions in either of cases, i.e., accelerated, constant and decelerated flows. In this talk, we show that solutions to the problem (1)-(2) exist for negative values of the parameter β such that $\beta < -M^2$. This leads to discuss some links between accelerated and decelerated MHD Falkner-Skan flows. Numerical simulations are given. Existence, multiplicity and uniqueness of the solutions for different type of parameters are discussed.

References

- [1] R. A. Van Gorder, K. Vajravelu. *Existence and uniqueness results for a nonlinear differential equation arising in MHD Falkner-Skan flow*, Commun. Nonlinear Sci. Numer. Simulat. 15, pp. 2272-2277 (2010).
- [2] R. A. Van Gorder, K. Vajravelu. *Corrigendum to existence and uniqueness results for a nonlinear differential equation arising in MHD Falkner-Skan flow*. Commun. Nonlinear Sci. Numer. Simulat. 15, pp. 2272-2277 (2010). Commun. Nonlinear Sci. Numer. Simulat. 17, pp. 5294-5295 (2012).
- [3] R. Naseri, A. Malek. *Optimization technique in solving laminar boundary layer problems with temperature dependent viscosity*, Numer. Algor. 66, pp. 663-668 (2014)
- [4] R. Naseri, A. Malek and R. A. Van Gorder. *On existence and multiplicity of similarity solutions to a nonlinear differential equation arising in magnetohydrodynamic Falkner-Skan flow for decelerated flows*, Math. Meth. Appl. Sci. DOI: 10.1002/mma.3363, (2015), in press.

On Stabilization of an Unbalanced Lagrange Gyrostat

D. Chebanov, N. Mosina, J. Salas

City University of New York - LAGCC, USA, {dchebanov, nmosina}@lagcc.cuny.edu

In this paper we investigate dynamical properties of a system of two coupled gyrostats. By definition, a gyrostat is a mechanical system consisting of a rigid carrier and other bodies connected to it such that their motion relative to the carrier does not alter the distribution of masses of the mechanical system. Examples of such systems include a rigid body to which axes of several symmetric rotors are connected, or a rigid body with cavities completely filled with a homogeneous fluid [1, 2]. Mechanical models involving gyrostats have a number of applications; for instance, they are of interest in aerospace engineering, since they are used for controlling the attitude dynamics of spacecraft and for stabilizing its rotations [3, 4].

We consider a mechanical system S consisting of two gyrostats G_1 and G_2 with carriers B_1 and B_2 , respectively. The body B_1 is attached to an immovable base at one of its points O_1 , while the bodies B_1 and B_2 are coupled at a common point O_2 ($\neq O_1$) by an ideal spherical joint. We assume that each gyrostat G_k has the mass distribution analogous to the one of a Lagrange top, the attachment point(s) of B_k lie on the dynamic symmetry axis of G_k , and the gyrostatic moment of G_k is directed along this axis. The system S moves under the gravitational attraction of a point mass μ located at a fixed point P as discussed in [5].

We investigate a problem of the stability of the state of motion of system S with the following property: one of the gyrostats permanently rotates about its dynamic symmetry axis coinciding with the axis O_1P , whereas the other gyrostat is at rest. While studying this problem, we show the existence of an interesting stabilization effect: for any Lagrange gyrostat that is in its unstable equilibrium position, there is another Lagrange gyrostat such that, when the two gyrostats are coupled to form a chain S , the rotation of the latter gyrostat can be used to stabilize the former one. A similar stabilization effect was discovered for a system of two heavy Lagrange tops moving about a fixed point [6, 7, 8]. Our paper extends the results of [6, 7, 8] to a case of a system of two gyrostats moving in a non-homogeneous gravitational field.

We establish and analyze the stabilization conditions in the space of the basic mechanical parameters characterizing system S . Given the parameters of the gyrostat to be stabilized, we provide recommendations on how the parameters of the stabilizing gyrostat should be chosen to guarantee the desired stabilization effect.

References

- [1] J. Wittenburg, *Dynamics of Multibody Systems*, Springer-Verlag, Berlin (2008).
- [2] N.N. Moiseyev and V.V. Rumyantsev, *Dynamic Stability of Bodies Containing Fluid*, Springer, New York (1968).
- [3] P.C. Hughes, *Spacecraft Attitude Dynamics*, John Wiley & Sons, New York (1986).
- [4] V.V. Beletsky, *The Motion of a Satellite about its Centre of Mass in a Gravitational Field*, Moscow University Press, Moscow (1975).
- [5] D. Chebanov, *Precessional motions of a chain of coupled gyrostats in a central Newtonian field*, in *Proceedings of the ASME 2014 International Design Engineering Technical Conferences and Computers and Information in Engineering Conference (IDETC/CIE 2014)*, Buffalo, NY, paper DETC2014-35590 (2014).
- [6] M.E. Lesina, *Stabilization of an unbalanced Lagrange gyroscope at rest*, Mekh. Tverd. Tela, **11**, pp. 88-92 (1979).
- [7] I.P. Varkhalev, A.Ya. Savchenko, and N.V. Svetlichnaya, *On the stabilization of an unbalanced Lagrange gyroscope at rest*, Mekh. Tverd. Tela, **14**, pp. 105-109 (1982).
- [8] A.Ya. Savchenko, I.A. Bolgrabskaya, and G.A. Kononyhin, *Stability of Motion of Systems of Coupled Rigid Bodies*, Naukova Dumka, Kyiv (1991).

Power Geometry For Finding Periodic Solutions in System of ODE

A. Soleev¹, F.A. Halimov²

¹ Samarkand State University, Uzbekistan, {asoleev}@yandex.ru
² Samarkand State University, Uzbekistan, ahalimov@samdu.uz

In a vicinity of a stationary solution we consider a real analytic system of ODE of order four, depending on a small parameter ε (see [1])

$$dy_i/dt = a(\varepsilon)y_i + f_i(\varepsilon, y_1, y_2, \bar{y}_1, \bar{y}_2), \quad i = 1, 2 \quad (1)$$

and the corresponding complex conjugate equations. We look for families of periodic solutions which contract to the stationary solution $y_1 = y_2 = \bar{y}_1 = \bar{y}_2 = 0$, when the parameter ε tends to zero. We apply the general methods of Power Geometry (see [1]) for the study of complex bifurcations for local resolutions of singularities.

First of all, we bring the system to a normal form in a vicinity of a fixed point, then we compute the set A containing all the families of periodic solutions that contract to this fixed point. These families can be written as asymptotic power series in a small parameter. To obtain the first few terms of these series from the normal form, we single out the first approximation of the system (truncated system) and study it in detail. In the nondegenerate case it is the truncated system that determines character of the bifurcations and their asymptotic. The higher terms in the normal form allow one to make the asymptotic expansion of the family more precise. Thus, the computation of these families of periodic solutions is performed over the coefficients of the terms of the normal form. For concrete systems, the computation of the coefficients of terms in the normal form can be made only up to terms of some finite degree. In this case it is important to compute all coefficients of the terms of the lowest degree (that appear in the truncated system) (see [1,2]).

After some calculation we have proved the following

THEOREM. *There exist systems (1), in which 10 families of real periodic solutions bifurcate from the stationary point $y=0$, when ε passes through zero.*

Here we show how works methods Power Geometry for the real system of ODEs of order four near a stationary point, depending on a small parameter. We have received that there exist systems (1), in which ten families of real periodic solutions bifurcate from the stationary point, when the parameter tends to zero. In the same manner, one can study periodic solutions of the Hamiltonian system with two degrees of freedom near a resonant periodic solution. Generally, bifurcations of periodic modes in resonant cases from Poiseuille flow, Couette flow and other flows were investigated by this way (see [1,2,4]).

References

- [1] A.D. Bruno, *Power Geometry in Algebraic and Differential Equations*, "Nauka", Moscow, 1999; English transl. Elsevier, 386 p. (2000).
- [2] A. D. Bruno and A. Soleev, *Local uniformization of branches of a space curve and Newton polyhedra*, St. Petersburg Math. J. **3** pp. 53-81 (1992).
- [3] E. Bierstone and P. D. Milman, *Uniformization of analytic spaces*, J. Amer. Math. Soc. **2** pp. 801-836 (1989).
- [4] P. O. Drazin, *Nonlinear Systems*, Cambridge Univ. Press, 292 p. (1992).

Stabilization of the Kuramoto-Sivashinsky equation

Rasha al Jamal¹ and Kirsten Morris²

¹ Business Analyst, Operations Excellence, Air Canada, Brampton, ON, Canada rasha.aljamal@aircanada.ca

² Dept. of Applied Math., University of Waterloo, Waterloo ON, Canada, kmorris@uwaterloo.ca

Financial support of Natural Sciences and Engineering Research Council of Canada (NSERC) for this research is gratefully acknowledged.

The Kuramoto-Sivashinsky equation is a nonlinear partial differential equation that models reaction-diffusion systems. It is related to various pattern formation phenomena where turbulence or chaos appear; see for example, [7]. The stability of the equilibria depends on the value of a positive parameter v ; the set of all constant equilibria are unstable when the instability parameter $v < 1$. Analytical results using the linearization as well as numerical studies of the dynamics of the KS equation have indicated that the KS equation is unstable for small values of a parameter v . In [5] it is shown that the set of all constant equilibria for the KS equation is unstable when the instability parameter $v < 1$. Furthermore, the zero equilibrium of the KS equation is Lyapunov stable when $v = 1$.

The whole state of the system cannot be measured, so the case where a single scalar measurement $y(t)$ is available is considered. The natural question is how to stabilize the KS equation, using only this partial information? The conventional approach of designing an output-feedback control to the KS equation is by approximating the PDE by a system of ODE's and then linearizing the system of ODE's [3, 4, 6]. Although numerical results were encouraging, verification that this approach is valid has not been previously shown. It is shown that Fréchet differentiability of the C_0 -semigroup corresponding to the closed-loop system is the key condition for this method to be valid. [1, 5]. It is then proven that stabilizing the closed-loop linearized approximated KS equation will stabilize the nonlinear infinite-dimensional KS equation, provided that the approximation satisfies certain natural assumptions. Thus, spillover is avoided.

Furthermore, it was assumed in earlier works that the number of measurements is equal to the number of the unstable eigenfunctions corresponding to the linearized KS equation. In this talk, it is shown that a single output-feedback control can locally exponentially stabilize the KS equation around a constant equilibrium, even when there are multiple unstable eigenvalues in the linearized equation.

References

- [1] R. Al Jamal and K. Morris. Output feedback control of the Kuramoto-Sivashinsky equation. preprint, 2013.
- [2] A. Armaou and P. Christofides. Feedback control of the Kuramoto-Sivashinsky equation. *Physica D: Nonlinear Phenomena*, 137(1-2):49 – 61, 2000.
- [3] A. Armaou and P. Christofides. Robust control of parabolic PDE systems with time-dependent spatial domains. *Automatica*, 37(1):61 – 69, 2001.
- [4] P. Christofides and A. Armaou. Global stabilization of the Kuramoto-Sivashinsky equation via distributed output feedback control. *Systems and Control Letters*, 39:283 – 294, 2000.
- [5] R. Al Jamal and K. Morris. Linearized stability of partial differential equations with application to stabilization of the Kuramoto-Sivashinsky equation. *Submitted*, 2014.
- [6] Y. Lou and P. Christofides. Optimal actuator/sensor placement for nonlinear control of the Kuramoto-Sivashinsky equation. *IEEE Transactions on Control Systems Technology*, 11(5):737 – 45, 2003.
- [7] G. Sell and Y. You. *Dynamics of evolutionary equations*, volume 143. Springer-Verlag, 2000.

Symmetry-Breaking Bifurcations in Laser Systems with All-to-All Coupling

Juancho A. Collera

University of the Philippines Baguio, Gov. Pack Road, Baguio City 2600 Philippines, jacollera@up.edu.ph

A system of n semiconductor lasers with all-to-all coupling is considered where lasers are coupled through their optical fields and with delay arising from the finite propagation time of the light from one laser to another. The system is described using the Lang-Kobayashi rate equations [2], and the resulting system of delay differential equations has symmetry group $S_n \times S^1$. This equivariant property is then utilized to find symmetric solutions [1], and classify symmetry-breaking steady-state and Hopf bifurcations [3].

References

- [1] K. Engelborghs, T. Luzyanina, and G. Samaey, *DDE-BIFTOOL v. 2.00 user manual: a matlab package for bifurcation analysis of delay differential equations*, Technical report, Department of Computer Science, K. U. Leuven, Leuven (2001).
- [2] H. Erzgraber, B. Krauskopf, and D. Lenstra, *Compound laser modes of mutually delay-coupled lasers*, SIAM J. Appl. Dyn. Syst. **5**, 1, pp. 30-65 (2006).
- [3] M. Golubitsky, I. Stewart, and DG. Schaeffer, *Singularities and groups in bifurcation theory II*. Springer-Verlag, New York (1988).

The quantum finite square well problem and the Lambert W function

S. R. Valluri¹, Ken Roberts²

¹ Physics and Astronomy, and Applied Mathematics Departments, Western University, London, Canada; King's University College, London, Canada, valluri@uwo.ca, vallurisr@gmail.com

² Physics and Astronomy Department, Western University, London, Canada, krobe8@uwo.ca

We present a solution to the quantum mechanics problem on the allowable energy levels of a bound particle in a one-dimensional finite square well. The method is a geometric-analytic technique utilizing the conformal mapping

$$w \rightarrow z = w \exp(w) \quad (1)$$

between two complex domains. The solution of the finite square well problem can be seen to be described by the images of simple geometric shapes, lines and circles, under this map and its inverse image. The technique can also be described using the Lambert W function. One can work in either of the complex domains, thereby obtaining additional insight into the finite square well problem and its bound energy states. There are a variety of applications possible with the use of this remarkable function, including possible utility for the design of devices which respond to a change in the number of bound states, such as Quantum Well Infrared Photodetectors (QWIPs) [1].

The Lambert W description of the finite square well problem is best visualized as a conformal map between two complex planes, produced by the mapping (1), the Lambert W function being the multi-branch inverse of that mapping. The axial rays in the z -plane map to the Lambert W lines in the w -plane, whose intersections with the circle of radius R about the origin give the solutions to the FSW problem. Here R (a unitless number) is the strength of the quantum well. Alternatively, the circle of radius R about the origin in the w -plane maps to a multi-loop closed curve in the z -plane, whose intersections with the axial rays also give the solutions to the FSW problem. Thus one may approach the problem situation working in either the w -plane (as is traditional), or in the z -plane – the choice of plane being determined by the convenience of other aspects of the particular problem which may be simpler in one or the other of those representations.

This technique bears some similarities to the method used in [2] to determine the fringing fields of a parallel plate capacitor. Because the mapping is conformal, the angles between the corresponding intersections of curves in each plane are equal. That suggests some possibilities for design of materials to be sensitive to slight changes in their environment, and leads back to the topic of the quantum well infrared photodetector (QWIP) which is mentioned above. A discussion of this topic is outlined in [3].

References

- [1] Harald Schneider, Hui Chun Liu, *Quantum Well Infrared Photodetectors: Physics and Applications*, Springer, 2007.
- [2] S. R. Valluri, D. J. Jeffrey, R. M. Corless, "Some applications of the Lambert W function to physics", *Canadian Journal of Physics*, vol 78, no 9 (September 2000), pp 823-831.
- [3] Ken Roberts, S. R. Valluri, "Solution of the quantum finite square well problem using the Lambert W function", ArXiv:1403.6685.

**CS-ENV Mathematical Modeling in
Environmental Sciences and Models for
Complex Media**

Fractal Modelling of Hydrocarbon Bearing Rocks using Iterative Function Systems

Kamal¹, S. Chanda²

¹ Indian Institute of Technology Roorkee, Roorkee, India, kamalfes@iitr.ac.in

² Indian Institute of Technology Roorkee, Roorkee, India,

We present an efficient method to analyze well-log data in hydrocarbon exploration using **Iterative Function Systems (IFS)** of a dynamic process.

Data created from a theoretical model of hydrocarbon bearing earth formations are used to generate IFS images for several physical parameters. The entire data range is scanned, using a mathematical method called coarse graining, in four bins and selecting a specific data window.

Since Earth is a dynamic system, the physical variations in the mathematical model of hydrocarbon bearing rocks manifest interesting fractal patterns. A four cornered chaos-game was analyzed and definite patterns like sierpinski gasket and straight line are seen indicating boundaries of hydrocarbon bearing formations. The process may be automatized for digital data interpretation.

Influence of the Coriolis force on internal waves in Lake Simcoe

B. Flood¹, M.Wells¹

¹ University of Toronto, Ontario, Canada, bryan.flood@mail.utoronto.ca

We will present new observations of thermocline dynamics obtained during the 2014 field season (August 18th – September 30th) in Kempenfelt Bay, Lake Simcoe, Ontario. Large amplitude internal waves, some in excess of 15 metres amplitude, were observed within the thermocline in the narrow, channel-like bay. We will show that Coriolis forces strongly influence the propagation of internal waves in the bay. A lateral tilt across the 2-3km wide bay of as much as 6 metres was observed due to the geostrophic balance of the Coriolis force.

The Burger number, Bu (see Eq. (1)), is the ratio of rotational to stratification forces (see Ref. [1]), and is useful in determining which physical processes dominate in a lake. It is defined as

$$Bu = \left(\frac{NH}{\Omega L} \right)^2 = \left(\frac{Ro}{Fr} \right)^2, \quad (1)$$

where N is the stratification frequency, H and L are the vertical and horizontal scales, respectively, Ω is the Earth's angular rotation rate, Ro is the Rossby Number and Fr is the Froude Number.

Kempenfelt bay is large enough to have a $Bu \approx O(1)$ resulting in the thermocline movements being strongly influenced by Coriolis forces. Fig. 1 depicts the variation of the thermocline (taken as the 12°C isotherm) depth away from the mean depth for three successive observations. It can be seen from these visualizations that the wave is propagating counterclockwise along the shoreline of the bay. This is typical of Kelvin waves, which develop as a direct result of the Coriolis force acting upon the wind-induced internal waves. The internal wave has dominant periods of approximately 70 and 4 hours.

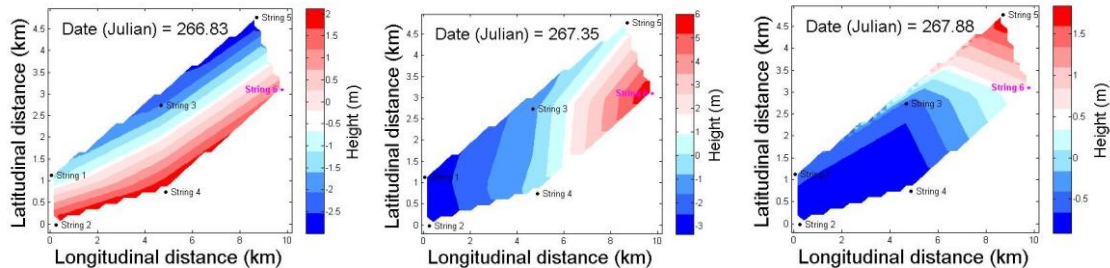


Figure 1: Temporal visualization of the variation from mean depth (m) of the internal wave in Kempenfelt Bay, Lake Simcoe.

The development of the internal Kelvin wave, and potential implications of the physical dynamics of the Coriolis-influenced internal waves in Lake Simcoe will be discussed with relation to biological activity and water quality conservation efforts.

References

- [1] B. Cushman-Roisin, *Introduction to Geophysical Fluid Dynamics*, Prentice Hall, New Jersey, USA, pp. 132 (1994).

Persistent Homology for Analyzing Environmental Lake Monitoring Data

B. Fraser, R. Wachowiak-Smolikova, M. P. Wachowiak

Nipissing University, North Bay, Canada, bfraser826@community.nipissingu.ca, {renatas, markw}@nipissingu.ca

Topological Data Analysis (TDA) consists of new methods for analyzing large, high-dimensional, heterogeneous, and noisy data that are characteristic of modern scientific and engineering applications [1]. In one TDA method, persistent homology (PH), a filtration [2] of a simplicial complex is generated from point clouds and analyzed for topological features. Betti numbers are computed across varying spatial resolutions, based on a proximity parameter r , where the n -th Betti number equals the rank of the n -th homology group [1]. The lower dimensional numbers can be understood to represent the number of connected components and voids in the complex. Features persisting in a long r -interval generally represent the shape of the data [1]. At low values of r , the topological features identified are more likely to appear by chance and not be meaningful.

In this study, PH is used to identify features and to assess changes in limnological data in environmentally-important Lake Nipissing, Ontario. Properties were collected on different days from a sonde sensor attached to a commercial cruise vessel, resulting in a large amount of high-dimensional data. Although statistical analysis provides insight into lake parameters, PH may help clarify these findings by algorithmically identifying high-dimensional, deformation invariant features. Open source PH programs are available for generating the simplicial complex filtration by incrementing r by a predetermined step size, but in this work, a custom Matlab program based on code by A. Cutbill was used to add a single edge at each iteration, incrementing r by the smallest possible amount, resulting in the finest possible filtration – in this case, of a 2-complex.

PH was applied to data from transects on two consecutive days, using five of the collected properties (temperature, conductivity, dissolved oxygen concentration, pH, and chlorophyll). On the first day, the Betti 1 number indicated a 2D hole during an interval with $r > 0.45$ (Figure 1, circled), whereas this feature was not present on the next day. This persistent hole may indicate interactions among properties on the first day (e.g. pH and dissolved oxygen affecting chlorophyll activity), but the interactions were inhibited on the following day. Hence, PH can be a preliminary step in determining how further analysis should proceed by identifying features that can be related to known environmental conditions in the lake. From these preliminary results, TDA, used in conjunction with statistical analysis and visualizations, is promising as a tool for obtaining insight into large, heterogeneous, noisy data collected from environmental monitoring sensors.

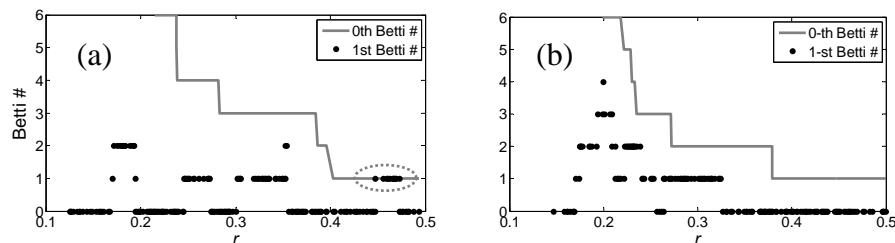


Figure 1: Persistence diagram. (a) 2-D void in 5-D subset of lake monitoring data for September 3, 2011, generally persisting for $r > 0.45$ (dotted circle). (b) The same properties for Sept. 4, 2011. No voids are apparent for this day.

References

- [1] G. Carlsson, *Topology and Data*, American Mathematical Society. **46**, 1, pp. 255-308 (2009).
- [2] A. Zomorodian, *Fast construction of the Vietoris-Rips complex*. Computers & Graphics. **34**, 3, pp. 263-271 (2010).

Stochastic Modeling and Performance Analysis for Electric Vehicle Charging Stations

J.-R., Kim¹, S.-Y., Son², J.-M., Lee³ and H.-T., Ha⁴

¹ Yongin University, R. Korea, jerimkim@yongin.ac.kr

² Gachon University, R. Korea, xtra@gachon.ac.kr

³ Gachon University, R. Korea, jals8224@naver.com

⁴ Gachon University, R. Korea, htha@gachon.ac.kr

The significantly increasing adoption of electric vehicles (EVs) is expected in near future. Widely spread convenient charging station infrastructure is an essential necessary condition for the success of wide public spread of EVs in public sector. In this paper, we propose a stochastic model for EVs' battery charging system and obtain its performance measure, from which efficient operational decisions can be made. The most challenge for the model is utilizing a very flexible non-homogeneous Poisson process with hidden Markov chain for modeling the complexity of the time varying behavior of EVs into the system. The random factors for the parking time and requested amount of charging energy, and the constraints for the number of parking lots (charging facility) are also considered in the model. We analyze the performance of the charging system under the policy that, when the total consumption of EVs in charge overshoot the upper power limit, the EVs in charge will share the power for charging. The performance of battery charging system is measured based on the probability that incoming EVs are fully charged during its parking time. We obtain Laplace-Stieljes transformation of the proposed performance measure via deriving the distribution of the number of inbounding EVs and the distribution of the consumed power amount during their parking times. Euler algorithm, which is a well known Laplace inversion method using Fourier inversion, is utilized to numerically calculate the performance measure for numerical examples. In the examples, we also showed sensitivity analysis of the minimal total power so that an arbitrary inbounding EV is fully charged during the parking time.

CS-FINANCE Financial Mathematics and Computation

First passage time of skip-free Markov chains with application to ruin theory

P. Patie¹, M.C.H. Choi²

¹ Cornell University, Ithaca, USA, pp396@cornell.edu
² Cornell University, Ithaca, USA, cc2373@cornell.edu

In this talk, we develop the potential theory of skip-free Markov chains and characterize the distribution of their first passage times, with potential overshoot, to a fixed level. We recall that a Markov chain on a denumerable state space is said to be, for instance, *upward skip-free* if it has upward jump of unit size, yet it can have downward transition of arbitrary magnitude. Karlin and McGregor [5] have shown that the first passage time upward from state x to state y , where $x < y$, is a convolution of geometric random variables for birth-and-death processes, that is for Markov chains which are both upward and downward skip-free. This fascinating result has been extended to upward skip-free Markov chains by two different interesting methods, namely a spectral approach by Abate and Whitt [1] and an intertwining approach by Fill [4] and Diaconis and Fill [2].

Unfortunately, little is known about the more delicate case when $x > y$, that is in the presence of overshoot as the skip-free property no longer apply. To overcome this difficulty, we suggest an original and comprehensive approach based on a combination of potential theory and the theory of Martin boundary as exposed by Dynkin [3] and Woess [6]. The motivation underlying our approach is to take advantage of the upward skip-free property to characterize explicitly the upper Martin boundary, and, by means of tools from potential theory, we develop methodologies to study the first passage time downward. We also discuss spectral representation of the probability generating function of this positive random variable. Finally, we shall explain how our approach allows one to get detailed information, regarding the (finite-time) ruin probability as well as the so-called Gerber-Shiu function in the framework of general discrete-time risk models.

References

- [1] J. Abate and W. Whitt, *Spectral Theory for Skip-Free Markov Chains*, Probab. Engr. Inform. Sci., 3: 77-88 (1989).
- [2] P. Diaconis and J.A. Fill, *Strong stationary times via a new form of duality*, Ann. Probab., 18: 1483?1522 (1990).
- [3] E.B. Dynkin, *Boundary theory of Markov processes (the discrete case)*, Russian Math. Surveys, 24: 1-42 (1969).
- [4] J.A. Fill, *On Hitting Times and Fastest Strong Stationary Times for Skip-Free and More General Chains*, J. Theoret. Probab., 22: 587-600 (2009).
- [5] S. Karlin and J. McGregor, *Coincidence properties of birth and death processes*, Pacific J. Math., 9, 1109-1140 (1959).
- [6] W. Woess, *Denumerable Markov chains*, EMS Textbooks in Mathematics, European Mathematical Society (EMS), Zurich (2009).

Machine learning: modeling risky behaviour in financial fraud detection

*Deitra Sawh and Kumaraswamy Ponnambalam
Systems Design Engineering, University of Waterloo*

Fraud detection models have drawn attention since the financial crisis of 2008 because of their frequency, size, and technological advances leading to financial manipulation. Statistical methods dominate industrial fraud detection systems at banks, insurance companies and financial marketplaces. However, most efforts so far are only focused on anomaly detection problems and simple rules. There are unsolved issues in modeling the behaviour of risky agents in the real-world financial markets using machine learning.

This paper studies the challenges posed by fraud detection and investigates the use of Reinforcement Learning (RL) to model risky human behaviour. We then hybridize the model with a Hidden Markov Model (HMM) to classify fraudulent samples. We first study an insider trading example to demonstrate how learning algorithms can mimic risky agents. The classification power of the model is demonstrated by applying it to a real-world based database for debit card transaction fraud.

The RL-HMM hybrid model shows high sensitivity rates while exhibiting low false positive rates. These two metrics are ideal for industrial implementation because of high levels of identification at a low cost.

Numerical Solution of Backward SDEs: Regression Later Algorithm

Kossi K. Gnameho¹, Mitja A. Stadje², Antoon Pelsser³

¹ Maastricht University, k.gnameho@maastrichtuniversity.nl

² Tilburg University, Dept. of Econometrics and Operations Research, m.a.stadje@uvt.nl

³ Maastricht University, a.pelsser@maastrichtuniversity.nl

The aim of the work is to seek efficient numerical methods to implement the pricing methods for realistic insurance products. Precisely we are concerning by the numerical approximation of a backward stochastic differential equations (BSDE). These equations are a new class of stochastic differential equations with a prescribed terminal value. In our work we will study the particular case of a forward backward stochastic differential equations (FBSDE) on a fixed time interval $[0, T]$ with the horizon $T > 0$.

Inspired by the works of E. Pardoux and S. Peng [5] and others authors [4],[1]... under some regularity assumptions of the coefficients of the FBSDE , we can represent it's solution as a solution of a regular quasi-linear parabolic partial differential equation (PDE). By exploiting the Markov property of the solution of the forward backward stochastic differential equations (FBSDE), we have developed a probabilistic numerical regression named "Regression later algorithm" based on the least squares Monte Carlo and the previous connection between a quasi-linear parabolic partial differential equation and the FBSDE.

The method is inspired from the work of Gobet et al. [3] and the work of E. Beutner and al. [2]. We have derived a convergence result of our probabilistic numerical scheme and provided numerical experiments in the context of option pricing problems to test the performance of the Regression later algorithm.

Keywords: BSDE , FBSDE , SDE's, PDE, Regression, Hilbert space, Projection, Numerical scheme, Monte Carlo, Pricing, Options

References

- [1] V. BALLY AND A. MATOUSSI, *Weak solutions for spdes and backward doubly stochastic differential equations*, Journal of Theoretical Probability, 14 (2001), pp. 125–164.
- [2] E. BEUTNER, A. PELSSER, AND J. SCHWEIZER, *Fast convergence of regress-later estimates in least squares monte carlo*, Available at SSRN 2328709, (2013).
- [3] E. GOBET, J. LEMOR, AND X. WARIN, *A regression-based Monte Carlo method to solve backward stochastic differential equations*, Annals of Applied Probability, 15 (2005), pp. 2172–2202.
- [4] J. MA, P. PROTTER, AND J. YONG, *Solving forward-backward stochastic differential equations explicitly a four step scheme*, Probability Theory and Related Fields, 98 (1994), pp. 339–359.
- [5] E. PARDOUX AND S. PENG, *Backward stochastic differential equations and quasilinear parabolic partial differential equations*, in Stochastic partial differential equations and their applications, Springer, 1992, pp. 200–217.

The 2015 AMMCS-CAIMS Congress
Waterloo, Ontario, Canada
June 7-12, 2015

On double barrier exit probabilities for the classical risk process with diffusion

D. Teneng¹

¹ University of Tartu, Estonia, dean_teneng@yahoo.com

We study double barrier exit probabilities for risk processes with spectrally positive Levy perturbations. We derive Pollaczek-Hinchin type formulas using scale functions and obtain analytical results amenable to implementation for the case of exponentially distributed claim size distributions. Approximations for heavy-tailed claim size distributions are analogously obtained.

Pricing Options with Hybrid Stochastic Volatility Models

G. Jones¹, R. Makarov²

¹ Wilfrid Laurier University, Waterloo, Canada, j.glynis@gmail.com

² Wilfrid Laurier University, Waterloo, Canada, rmakarov@wlu.ca

We introduce a hybrid stochastic volatility model where the asset price process follows the Heston model and the stochastic interest rate process is governed by a two-factor model. Two cases are considered. First, it is assumed that there is no correlation between the interest rate and the asset price. Fourier techniques are used to derive analytical pricing formulae for plain vanilla options. In the second case we introduce a correlation between the asset price and the interest rate and use Monte Carlo simulations for pricing options. To reduce the stochastic error, we use the control variate method where an estimator of the option value for the uncorrelated case is used as a control variate. The options are priced with a varying correlation coefficient. We observe that the control variate method allows us to speed up Monte Carlo computations by a factor with the magnitude of several hundreds. The efficiency of the method is higher for smaller values of the correlation coefficient. We then study the impact a correlation between the two processes has on option prices using Monte Carlo simulations. It has been noticed that the call option price is an increasing function of the correlation coefficient.

Series Approximations for Value-At-Risks and Expected Shortfalls of Financial Delta-Gamma Methods

Hyung-Tae Ha

Gachon University, R. Korea, {htha}@gachon.ac.kr

A new approach using series approximation to the computation of Value-at-Risks of Delta-Gamma method in financial risk management is presented in this paper. The density and distribution functions of the Delta-Gamma methods are approximated on the basis of orthogonal polynomial expansions with respect to a proper reference density function that is expressed as a difference of two asymptotic approximants. The corresponding Value-At-Risks and its asymptotics are easily obtained analytically via the general Cornish-Fisher expansions. The proposed series approximation is not limited to the case that the risk factor returns are with multivariate Gaussian distributions but can be extended to the heavy tailed distribution with multivariate t distribution unlike Edgeworth expansion and Saddlepoint approximation. In many practical situations, its actual accuracy of the proposed method is accurate more than sufficiently in addition to simple and fast computation of the approximation. Numerical examples are provided.

Simulation of timer options under stochastic interest rates

Yongzeng Lai¹, Bowen Hu²

¹ Wilfrid Laurier University, Waterloo, Canada, ylai@wlu.ca

² Wilfrid Laurier University, Waterloo, Canada, huxx0670@mylaurier.ca

A timer option is similar to a vanilla European option with a random maturity date specified by the first time when the accumulated variance of the underlying asset reaches a given budget level. A timer call option was first traded by Société Générale Corporate and Investment Banking (SG CIB) in 2007. Pricing timer options receives increasing attention in the recent mathematical finance community. However, discussion on pricing timer options were mainly on stochastic volatility models for the underlying asset prices driven by Brownian motions and deterministic interest rates in the literature. This talk will present simulation of timer options under stochastic volatility models driven by some Levy processes for the underlying asset prices and stochastic interest rates.

Semi-parametric time series modelling with autocopulas

A. Ware¹, I. Asadzadeh²

¹ University of Calgary, Alberta, Canada, aware.ucalgary.ca

² University of Calgary, Alberta, Canada, iasadzad@ucalgary.ca

In this paper we present a new approach for finding the distribution of financial time series showing non-linear dependency. Due to the existence of linear and non linear dependencies in the series we develop an application of so-called autocopulas for such data. The linear and non-linear dependencies in the series are unknown thus we cannot use standard copula models to capture them. Instead we apply empirical copulas and use the inverse distribution function method to generate independent time series. Our approach here is semi-parametric and is characterized by a non-parametric copula and parametric marginals. One advantage of using autocopulas is that they represent nonlinear dependencies well, and make it possible to study the interdependence of values of the series at different extremes separately. The time series that we study represents daily cash flows derived from the product of daily natural gas price and daily temperature deviations from normal levels. In addition we deal with seasonality by means of a time dependent normal inverse Gaussian (NIG) distribution fitted to the raw values.

By comparing the generated time series with the input data, our method can capture the main characteristics as depicted in Figure. 1.

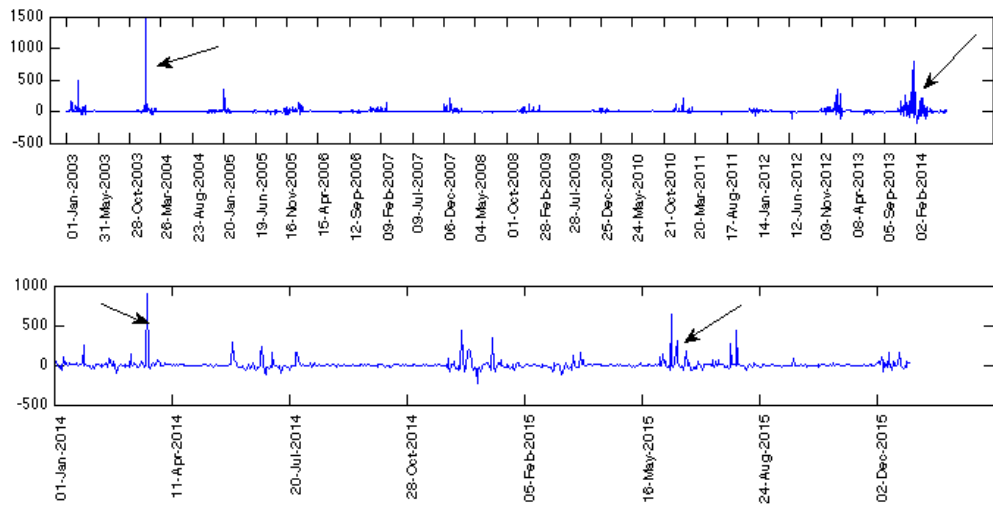


Figure 1: The above figure shows the input data for 11 years and below is the simulate path for 2 years. Note that arrows in the plot show the spikes due to high weather deviation from normal and high spot price deviation from next foreword month

References

- [1] R. B. Nelsen, *An Introduction to Copulas, Second Edition*, New York, NY 10013, USA. (2006).
- [2] X. Chen and Y. Fan, *Estimation of copula-based semiparametric time series models*, Journal of Economics, pp. 307-335 (2006)
- [3] A. J. Patton, *Copula based models for financial time series*, Handbook of financial time series, pp. 767-785 (2009).
- [4] G. Pumi and S. Lopez, *Simulation of Univariate Time Series Using Copulas*, (2010).
- [5] Barndorff-Nielsen, O. E., *Normal inverse Gaussian distributions and stochastic volatility modelling*, Scandinavian Journal of Statistics 24, no. 1 pp. 1-13 (1997).

CS-MECHE Computational Mechanics and Engineering

An effective high-order shock-capturing limiter for discontinuous Galerkin methods

S. Moe¹, J.A. Rossmanith², D.C. Seal³

¹ University of Washington, smoe@uw.edu

² Iowa State University, rossmani@iastate.edu

³ Michigan State University, seal@math.msu.edu

In this work, we present a novel shock capturing limiter for the discontinuous Galerkin (DG) method. It can be viewed as either an extension of the recent maximum principle preserving (MPP) limiter devised by Zhang and Shu [1] to be able to handle shocks, or as an extension of the older finite volume limiter developed by Barth and Jespersen [2] to the DG framework. Our limiter constructs *local* upper and lower bounds for the solution by sampling nearest neighbors, and then limits the solution to stay within these bounds. It is simple to implement, has minimal communication, is effective at capturing shocks, and retains genuine high-order accuracy of the solution in smooth regimes. Numerical results including problems that require positivity preservation in one and two dimensions on structured and unstructured grids are presented that indicate the robustness of the method.

References

- [1] X. Zhang and C.-W. Shu. *Maximum-principle-satisfying and positivity-preserving high-order schemes for conservation laws: survey and new developments*, Proc. R. Soc. Lond. Ser. A Math. Phys. Eng. Sci., **467**, (2011).
- [2] T. Barth and D. Jespersen. *The design and application of upwind schemes on unstructured meshes*, American Institute of Aeronautics and Astronautics, (1989).

Free Vibration Analysis of Axially Functionally Graded Beams using the Differential Quadrature Method

H. Sakurai¹

¹ National Institute of Technology, Sendai College, Japan, {co-operative education center}@snct

In recent years, functionally graded syntactic foam sheets have been developed, and their applications in absorbing impact energy materials have been attracting much interest^[1]. When we use beams constructed of functionally graded materials (FGMs) for absorbing impact energy, it's necessary to analyze the FGM beams having an Young's modulus varying in the longitudinal direction. The objective of the present research is to carry out free longitudinal and flexural vibration analysis of axially varying FGM beams using the differential quadrature method^[2]. Consider a FGM beam, clamped at one end, and free to move at the other, as shown in Figure 1. The length of the beam is l , the cross section area A , moment of inertia I , the mass density ρ and the Young's modulus is $E(X)$, varying in the longitudinal direction.

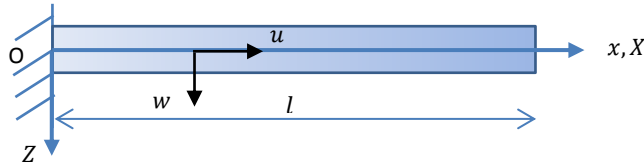


Figure 1: A clamped-free FGM beam with Young's modulus varying in the longitudinal direction.

The governing equations of the longitudinal and flexural vibration of the FGM beam are given respectively by:

$$e(x) \frac{d^2u}{dx^2} + \frac{de(x)}{dx} \frac{du}{dx} + \omega_l^2 u = 0 \quad (1), \quad e(x) \frac{d^4w}{dx^4} + 2 \frac{de(x)}{dx} \frac{d^3w}{dx^3} + \frac{d^2e(x)}{dx^2} \frac{d^2w}{dx^2} - \omega_f^2 w = 0, \quad (2)$$

where $x = X/l$ is the dimensionless longitudinal coordinate, u is the axial displacement, w is the transverse displacement, $e(x) = E(x)/E_0$ denotes the function representing the variation of the Young's modulus. $\omega_l^2 = \rho \bar{\omega}_l^2 l^2 / E_0$, $\omega_f^2 = \rho A^2 \bar{\omega}_f^2 l^4 / E_0 I$ are the dimensionless circular frequencies, with E_0 is the Young's modulus at a reference position, and $\bar{\omega}_l, \bar{\omega}_f$ the dimensional natural circular frequencies. First, analysis of homogeneous beams with non-uniform cross section are performed, and through comparison of the present results and known exact solutions^[3-4], the validity of the present method is shown. Furthermore, the effect of the variation of Young's modulus on the natural frequencies and mode shapes of the vibration of FGM beams is made clear

References

- [1] Kishore, R. Shankar and S. Sankaran, *Gradient syntactic foams: Tensile strength, modulus and fractographic features*, Materials Science and Engineering, A412, pp.153–158(2005).
- [2] C. Shu and H. Du, *Implementation of clamped and simply supported boundary conditions in the GDQ in the free vibration analysis of beams and plates*, International Journal of Solids and Structures, Vol.34, No.7, pp.819-835(1997).
- [3] B.M. Kumar and R.I. Sujith, *Exact solutions for the longitudinal vibration of non-uniform rods*, Journal of Sound and Vibration, 207(5), pp.721-729(1997).
- [4] S. Abrate, *Vibration of non-uniform rods and beams*, Journal of Sound and Vibration, 185(4), pp.703-716(1995).

High-Order Semi-Implicit Time-Stepping Methods for Navier-Stokes Equations

K.C. Loy¹, Y. Bourgault²

Department of Mathematics and Statistics, University of Ottawa, Canada, ¹*kloy024@uottawa.ca,* ²*ybourg@uottawa.ca*

Much attention has been given to higher-order time-discretization method to solve time-dependent PDE problems. The application of such methods for solving Navier-Stokes equations, for order two and higher, still remains very challenging. Typically, more stable implicit methods like backward differentiation formulae (BDF) are favoured for solving Navier-Stokes equations. Unfortunately, these methods suffer from the need to iterate with fixed point methods at each time step because of the nonlinear advection. Semi-implicit approaches, which treat the nonlinear term using extrapolation strategy, are one of the remedy to avoid the machinery of Newton's or Picard iteration. These numerical methods are not new [1, 2, 3], but interestingly the application of such higher order semi-implicit schemes have not seriously been attempted for Navier-Stokes equations. The goal or our work is to investigate and develop semi-implicit methods for computing unsteady incompressible flows modelled by Navier-Stokes equations using Taylor-Hood mixed finite elements, to have equally accurate solutions in space.

We first study Semi-Implicit Backward Differentiations (SBDF) of order 2 and 3 and show how they can successfully compute non-stationary flows, such as the Von Karman alley and unsteady lid-driven cavity flow. Our numerical experiments have shown that even though SBDF methods might be more restrictive on the maximal time step for stability than its implicit counterpart, they provide accurate results up to the order of 2 and 3 in time for both velocity and pressure. SBDF methods are competitive for unsteady flows, as accuracy is the limiting factor for picking the time step, no nonlinear system is to be solved and the matrix is frozen across time-steps (with a constant time step). However, one still needs to solve a saddle-point problem for handling the incompressibility condition. Recently, Guermond and Minev [4] proposed a way to avoid such saddle-point problems. Their semi-implicit time-discretization method is based on higher-order pseudo-compressibility and deferred correction methods. It solves separately advection-diffusion problems for velocity and regular pressure updates at each time step, while recovering higher-order accuracy with a multi-stage approach. Splitting and projection methods are limited to at most second order accuracy in time [5], but the analysis and numerical simulation with this new scheme has proven successful in reaching arbitrary order in time. In our talk, we will present some analysis and numerical benchmarks using SBDFn methods and the one proposed by Guermond and Minev, in all cases for Taylor-Hood P2-P1 mixed finite elements. The discussion on several open problems, challenges and possible further numerical improvements for both schemes will end this talk.

References

- [1] M. Ethier and Y. Bourgault, *Semi-Implicit Time-Discretization Schemes for the Bidomain Model*. SIAM Journal of Numerical Analysis. **46**, 5, pp. 2443-2468 (2008).
- [2] U. M. Ascher, S. J. Ruuth and B. T. R. Wetton, *Implicit-Explicit Methods for Time-Dependent Partial Differential Equations*. SIAM Journal of Numerical Analysis. **32**, 3, pp. 797-823 (1995).
- [3] W. Kress and P. Lötstedt, *Time Step Restrictions Using Semi-Implicit Methods for the Incompressible Navier-Stokes Equations*. Computer Methods in Applied Mechanics and Engineering. **195**, pp. 4433-4447 (2006).
- [4] J.-L. Guermond and P. D. Minev, *High-Order Artificial Compressibility for the Navier-Stokes Equations, Part I: Theory*, (2014) Submitted.
- [5] J.-L. Guermond, P. D. Minev and J. Shen, *An Overview of Projection Methods for Incompressible Flows*, Computer Methods in Applied Mechanics and Engineering. **195**, pp. 6011-6045 (2006).

Investigation of the Reynolds Number Effect on Fluid-elastic Instability of Moving Cylinder Arrays

A. Ghasemi¹, N. Kevlahan²

¹ School of Computational Science and Engineering, McMaster University, Hamilton, ON, Canada, ghasea@mcmaster.ca

² Department of Mathematics and Statistics, McMaster University, Hamilton, ON, Canada, kevlahan@mcmaster.ca

Because of its practical importance in industrial applications, many attempts have been made to understand the instability of flow-induced vibrations of a periodic array of elastically mounted cylinders. It has been suggested that the onset of instability depends on parameters such as geometry, Scruton number and natural frequency of cylinders as well as the mean velocity of the cross flow. Presently, there is considerable evidence from experimental measurements and CFD simulations that the Reynolds number is also an important parameter. Unfortunately, this effect has not been addressed clearly by theoretical models. Moreover, the available experimental results give conflicting evidence as to whether increasing Reynolds number and turbulence intensity are stabilizing or destabilizing. We investigate this problem using a high resolution pseudo-spectral scheme to solve the Navier-Stokes equations (with no turbulence modelling) and employ Brinkman volume penalization to impose no-slip boundary conditions on the surfaces of the moving cylinders. We have developed a parallel code to simulate the flow efficiently on a large number of processors. We vary mean velocity, Reynolds number and Scruton number, to better understand the role of turbulence in resonant and non-resonant fluid-elastic instabilities. In addition to summarizing simulation results, we also describe the features of our efficient and accurate numerical tool for fluid-elastic instability.

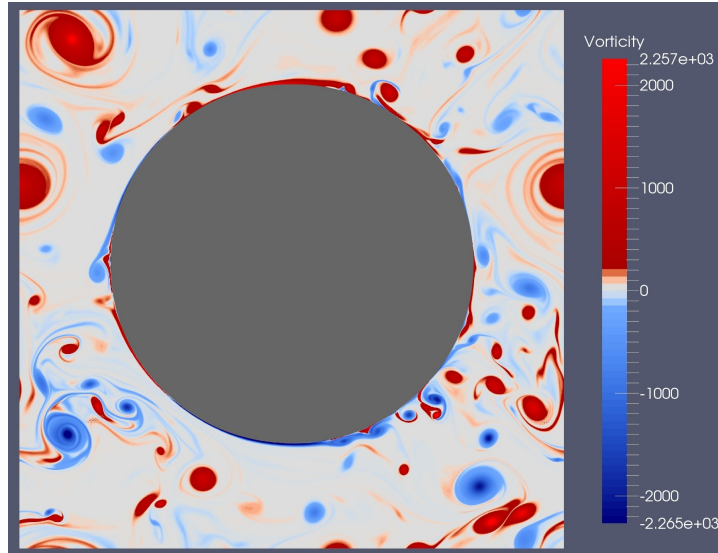


Figure 1: Vorticity field at $\text{Re} = 20,000$.

Mode coalescence of instability in two-fluid flows

A. Kaffel¹, A. Riaz¹

¹ Department of Mechanical Engineering, University of Maryland, College Park, MD 20742, USA, dr.kaffel@gmail.com

We examine the flow stability of two fluids with different density and viscosity. A multi-domain Chebyshev collocation spectral method along with QZ eigenvalue solver are used to solve the coupled Orr-Sommerfeld stability equations for the whole spectrum of eigenvalues and associated eigenfunctions. The derivation of the asymptotics of these modes shows that the numerical eigenvalues are in agreement with the analytic formula in the long and short wave limits. The behaviour of unstable modes, corresponding to the shear and interfacial modes, and their dependence on the flow parameters are studied in detail. A parametric study was carried out to investigate the effects of various parameters on the stability characteristics of these modes to understand the nature of the competitive instabilities arising in two-phase flows. We discuss the structure of the spectra and the shapes of eigenfunctions. Due to viscosity contrast, we found that the eigenfunctions undergo a rapid change in their derivatives at the interface and exhibit characteristic extrema in the neighborhood of the interface and near the critical points. The interactions and branch exchange between the interfacial and shear modes are also investigated. There are instances when the flow becomes unstable to more than one unstable mode and coalescences between different modes occur in the stable and/or in the unstable region of the spectrum.

Key words: Linear stability, two-phase flow, interfacial instability, coalescence, eigenfunctions, Chebyshev collocation spectral method.

References

- [1] P.G. Drazin., *Introduction to Hydrodynamic Stability*, Cambridge University Press, Cambridge, (2002).
- [2] P.J. Schmid and D.S. Henningson, *Stability and Transition in Shear Flows*, in *Appl. Math. Sci.*, Springer; Vol. 142, New York, (2001).
- [3] D.D. Joseph and Y.Y. Renardy., *Fundamentals of two-fluid dynamics, Part I: Mathematical theory and applications*, in Springer Verlag, New York (1993).

Server Side Algorithms for WHLK Framework

N. Gupta¹, S. Jamwal²

¹ University of Jammu, India, nis.decent@gmail.com

² University of Jammu, India, jamwalsnj@gmail.com

Software piracy is the most significant and burning issue in the age of Internet. Software piracy has been a direct threat for software vendors in terms of revenue and, therefore, a number of effective and efficient techniques were employed for detection and prevention of software piracy. One of very important technique is software watermarking and using registration keys. This paper proposes the Server-side algorithms for registration and embedding the watermark into the software using WHLK approach. We have tested the algorithms and the analysis of the proposed algorithms proves that these registration algorithms are more reliable and efficient in comparison to other techniques.

References

- [1] Business Software Alliance, *Ninth Annual BSA Global Survey of PC User Attitudes*. [Online]. Available: (http://globalstudy.bsa.org/2011/downloads/study_pdf/2011_BSA_Piracy_Study-Standard.pdf).
- [2] Business Software Alliance, *Ninth Annual BSA Global Survey of PC User Attitudes*. [Online]. Available: (http://globalstudy.bsa.org/2011/downloads/study_pdf/pr_india_en.pdf).
- [3] W. Zhu, C. Thomborson, F. Wang, *A Survey of Software Watermarking*, in *Proceedings of IEEE International Conference on Intelligence and Security Informatics*, LNCS 3495, Springer-Verlag Berlin Heidelberg, Germany, pp. 454-458 (2005).
- [4] Q. Liu, *Techniques Using Exterior Component against Software Piracy*, in Technical Report, Department of Computer Science, University of Auckland, New Zealand.
- [5] Y. Zhang, L. Jin, X. Ye, D. Chen, *Software Piracy Prevention: Splitting on Client*, in *Proceedings of International Conference on Security Technology*, IEEE Computer Society, Washington, DC, USA, pp. 62-65 (2008).
- [6] P. Djekic and C. Loebbecke, *Preventing application software piracy: An empirical investigation of technical copy protections*, in *Journal of Strategic Information Systems*, Elsevier, 16, pp. 173-186 (2007).
- [7] V.K. Sharma, S.A.M. Rizvi, S.Z. Hussain, A.S. Chauhan, *Dynamic Software License Key Management Using Smart Cards*, in *Proceedings of International Conference on Advances in Computer Engineering*, IEEE Computer Society, pp. 244-246 (2010).
- [8] I. Kamel and Q. Albluwi, *A robust software watermarking for copyright protection*, in *Journal of Computers and Security*, Elsevier, 28, 6, pp. 395-409 (2009).
- [9] A. Kulkarni and S. Lodha, *Software Protection through Code Obfuscation*, in Project Report, Tata Research Development and Design Centre, Pune (2012).
- [10] I.J. Jozwiak and K. Marczaik, *A Hardware-Based Software Protection Systems – Analysis of Security Dongles with Time Meters*, in *Proceedings of Second International Conference on Dependability of Computer Systems*, IEEE Computer Society Washington, DC USA, pp. 254-261 (2007).
- [11] A. Nehra, R. Meena, D. Sohu, O.P. Rishi, *A Robust Approach to Prevent Software Piracy*, in *Proceedings of Students Conference on Engineering and Systems*, IEEE, pp.1-3 (March 2012).
- [12] N. Gupta, S. Jamwal, D. Padha, *Watermark, Hardware Parameters and License Key: An Integrated Approach of Software Protection*, in *International Journal of Advanced Research in Computer Science and Software Engineering*, 3, 5, pp. 1285-1289 (May 2013).
- [13] N. Gupta, S. Jamwal, D. Padha, *WHLK: Framework for Software Authentication and Protection*, in *IEEE African Journal of Computing & ICT*, IEEE, Nigeria, 7, 1, pp. 69-80 (2014).

The Distributive Interoperable Executive Library for Multi-disciplinary System-wide Simulations

K. Wong¹, J. Coan², N. Moran³, J. Pollack⁴

¹ University of Tennessee, Knoxville, TN, USA, kwong@utk.edu

² Maryville College, Knoxville, TN, USA, jason.coan@my.maryvillecollege.edu

³ University of Tennessee, Knoxville, TN, USA, nmoran1@vols.utk.edu

⁴ University of Tennessee, Knoxville, TN, USA, jpollac1@vols.utk.edu

As HPC capability and software adaptability continues to expand, the interest to perform complex system-wide simulations involving multiple interacting components grows. In this paper, we present a novel integrative software platform – the Distributive Interoperable Executive Library (DIEL) – to facilitate the collaboration, exploration, and execution of multiphysics modeling projects suited for a diversified research community on emergent large-scale parallel computing platforms. It does so by providing a managing executive, a layer of numerical libraries, a number of commonly used physics modules, and two set of native communication protocols. DIEL allows users to plug in their individual modules, prescribe the interactions between those modules, and schedule communications between them. The DIEL framework is designed to be applicable for preliminary concept design, sensitivity prototyping, and productive simulation of a complex system. The DIEL framework is designed to be an integrated, community-driven, non-proprietary capability that follows an agile development process allowing users to efficiently validate, verify, maintain, and expand new computational models, algorithms, analytics, and tools. Figure 1 shows the functional block diagram of DIEL. The managing core (EXECUTIVE) and the communication units (COMMLIB) are the critical building blocks of DIEL. These are interconnected with an integrator of numerical libraries and an interface for tools. An analyzer module performs data analytics, sensitivity analysis, and parametric optimization during the life cycle of a simulation. The science modules are distinct computer codes implemented by users to perform their simulations. By leveraging this framework, a biomedical heart simulation is built to showcase the functionalities and the interacting workflow managed in DIEL. The framework will be released as an open source product called openDIEL [1] under LGPL license. The openDIEL framework will provide a data archiving tool that will allow the archiving of distributed scientific datasets.

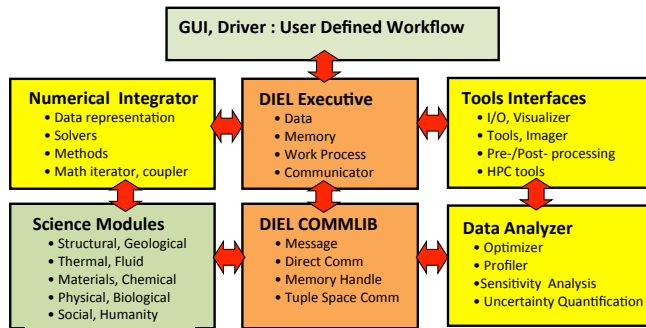


Figure 1: Functional Blocks of DIEL

References

[1] openDIEL: <http://cfdlab.utk.edu/openDIEL>

The High-order Path-conservative Scheme for a Model of Compressible Non-conservative Two-phase Flow

Yueling. Jia¹, S. Jiang², Baolin.Tian³, E.F. Toro⁴

¹ Institute of Applied Physics and Computational Mathematics, Beijing, China, jia_yueling@iapcm.ac.cn

² Institute of Applied Physics and Computational Mathematics, Beijing, China, jiang@iapcm.ac.cn

³ Institute of Applied Physics and Computational Mathematics, Beijing, China,tian_baolin@iapcm.ac.cn

⁴ University of Trento, Trento, Italy, toro@ing.unitn.it

The 4-shock Riemann Solver and the high-order path-conservative scheme, via the MUSCL reconstruction and the Runge-Kutta technique, are considered for A 2-dimensional model of non-conservative two-phase flow [1,2,3]. Numerical results demonstrate its accuracy and robustness, which can be used in a wide range of applications in science and engineering.

$$\begin{aligned}
 & \frac{\partial}{\partial t} \alpha_g + u_I \frac{\partial}{\partial x} \alpha_g + v_I \frac{\partial}{\partial y} \alpha_g = 0 \\
 & \frac{\partial}{\partial t} (\alpha_g \rho_g) + \frac{\partial}{\partial x} (\alpha_g \rho_g u_g) + \frac{\partial}{\partial y} (\alpha_g \rho_g v_g) = S_1 \\
 & \frac{\partial}{\partial t} (\alpha_g \rho_g u_g) + \frac{\partial}{\partial x} (\alpha_g \rho_g u_g^2 + \alpha_g p_g) + \frac{\partial}{\partial y} (\alpha_g \rho_g u_g v_g) - p_I \frac{\partial}{\partial x} \alpha_g = S_2 \\
 & \frac{\partial}{\partial t} (\alpha_g \rho_g v_g) + \frac{\partial}{\partial x} (\alpha_g \rho_g u_g v_g) + \frac{\partial}{\partial y} (\alpha_g \rho_g v_g^2 + \alpha_g p_g) - p_I \frac{\partial}{\partial y} \alpha_g = S_3 \\
 & \frac{\partial}{\partial t} (\alpha_l \rho_l) + \frac{\partial}{\partial x} (\alpha_l \rho_l u_l) + \frac{\partial}{\partial y} (\alpha_l \rho_l v_l) = S_4 \\
 & \frac{\partial}{\partial t} (\alpha_l \rho_l u_l) + \frac{\partial}{\partial x} (\alpha_l \rho_l u_l^2 + \alpha_l p_l) + \frac{\partial}{\partial y} (\alpha_l \rho_l u_l v_l) + p_I \frac{\partial}{\partial x} \alpha_g = S_5 \\
 & \frac{\partial}{\partial t} (\alpha_l \rho_l v_l) + \frac{\partial}{\partial x} (\alpha_l \rho_l u_l v_l) + \frac{\partial}{\partial y} (\alpha_l \rho_l v_l^2 + \alpha_l p_l) + p_I \frac{\partial}{\partial y} \alpha_g = S_6
 \end{aligned} \tag{1}$$

where $p_I = \sum \alpha_k p_k$, $u_I = \sum \alpha_k \rho_k u_k / \sum \alpha_k \rho_k$. K_g , γ_g , K_l , γ_l and ρ_0 are constants,

$$p_g = K_g \rho_g^{\gamma_g}, \quad p_l = \frac{K_l}{\rho_0^{\gamma_l}} \rho_l^{\gamma_l} - K_l \tag{2}$$

References

- [1] R. Saurel and R. Abgrall, *A multiphase Godunov method for compressible multi-fluid and multiphase flows*, J.comput.Phys. **150**, pp. 425-467 (1997).
- [2] D. Schwendeman, C. Wahle and A. Kapila, *The Riemann problem and a highresolution Godunov method for a model of compressible two-phase flow*, J.comput.Phys., **212**, pp. 490-526 (2006).
- [3] B. Tian, E.F.Toro and C.E.Castro, *A path-conservative method for a five-equation model of two-phase flow with an HLLC-type Riemann solver*, Computers and fluids, **46**, pp. 122-132 (2011).

CS-MODELING Partial Differential and Integral Equations in Mathematical Modeling

A Simple Method for Solving PDEs on Point Clouds

A. Elmoataz^{1,2}, Z. Lakhdari^{1,2}

¹ Université de Caen Basse-Normandie, CNRS, UMR 6072 GREYC, F-14032 Caen, France, abderrahim.elmoataz-billah@unicaen.fr

² ENSICAEN, CNRS, UMR 6072 GREYC, F-14050 Caen, France, zakaria.lakhdari@unicaen.fr

Many applications in the natural and applied sciences require the solutions of Partial Differential Equations (PDEs) on surfaces or Point Clouds. Examples of such applications areas arise in biological systems, image processing, computer graphics and Machine learning.

Many methods have been developed for solving PDEs on surfaces. While most of these methods do not immediately extend to point clouds, they could generally be used if point clouds were first reconstructed into a suitable surface [1,2], a process that can be highly complex.

PDEs on surfaces are traditionally handled by techniques that roughly classified in three categories whether they make use of either explicit, implicit or intrinsic representations of the surfaces [3,4].

In this paper, we will present a general and a simple framework for solving PDEs on point clouds without parametrization or connection information. With this approach, 3D point clouds are represented by a weighted graph. Then we use the framework of Partial difference Equations (PdEs) on graphs [5,6] to transcribe PDEs in the discrete setting. Conceptually PdEs mimic PDEs on a general discrete domain by replacing the differential operators by non-local difference operators such as: difference, gradient, divergence, p-laplacian,etc. Our approach allows to transpose and extend many processes in classical image processing to solve many PDEs on surfaces and point clouds.

Applications to image processing on point clouds such as restauration, inpainting or colorization will be presented.

References

- [1] J. Liang, R. Lai, T. Wai Wong and H. Zhao, *Geometric understanding of point clouds using laplace-beltrami operator in CVPR*, pp. 214–221, (2012).
- [2] R. Lai, J. Liang, and H.K. Zhao, *A local mesh method for solving pdes on point clouds*. Inverse Probl. Imag., vol. 7, no. 3, pp. 737–755, (2013).
- [3] C.B Macdonald, B. Merriman and S.J Ruuth, *simple computation of reaction-diffusion processus on point clouds*, Proc. Natl.Sci, 110(23), (2013)
- [4] F. Lozes, A. Elmoataz, O. Lezoray, *Partial difference operators on weighted graphs for image processing on surfaces and points clouds*, IEEE Transaction on Image Processing, 23(9),3896-3909, (2014)
- [5] A. Elmoataz, O. Lezoray, and S. Bougleux, *Nonlocal discrete regularization on weighted graphs: a framework for image and manifold process ing*, IEEE T. Image Process., vol. 17, no. 7, pp. 1047–1060, (2008).
- [6] A. El Chakik, A. Elmoataz, X. Desquesnes, *Mean Curvature Flow on Graphs for Image and Manifold Restoration and Enhancement*. Signal Processing, vol. 105, pp 449-463, (2014).

Approximate Solution of Some Boundary Value Problems

M. Chumburidze

Akaki Tsereteli State University, Kutaisi, Georgia, atsu@atsu.edu.ge

We consider a non-classical model of partial differential equations arising in couple-stress thermo-elasticity (**CPTE**), which was formulated by Green-Lindsay. In particular, we investigate the boundary value problems of two-dimensional pseudo oscillations systems of **CPTE** for isotropic homogeneous elastic media of the form:

$$\begin{aligned} \forall x \in \Omega: & (\mu + \alpha) \Delta u(x, \tau) + (\lambda + \mu - \alpha) \text{grad} \text{div} u + 2\alpha \text{rot} u_3 - \gamma_\tau \text{grad} u_4 - \varsigma \tau^2 u = h^{(1)}(x) \\ & (\nu + \beta) \Delta u_3(x, \tau) + 2\alpha \text{rot} u - 4\alpha u_3 - I \tau^2 u_3 = h_3(x) \end{aligned} \quad (1)$$

$$\begin{aligned} \Delta u_4(x, \tau) - \frac{\tau}{\varphi_\tau} u_4 - \eta \tau \text{div} u = h_4(x) \\ \forall z \in \partial\Omega: & u = f_k^{(1)}(z), \quad (\delta_{1k} + \delta_{2k})(\nu + \beta) \frac{\partial u_3}{\partial n} + (\delta_{0k} + \delta_{3k}) u_3 = f_{3k}, \\ & (\delta_{1k} + \delta_{3k}) \frac{\partial u_4}{\partial n} + (\delta_{0k} + \delta_{3k}) u_4 = f_{4k}, \quad k = \overline{0,3} \end{aligned} \quad (2)$$

where, $x = (x_1, x_2), z = (z_1, z_2)$ are points of two-dimensional Euclidean space- R^2 , Ω is a finite domain in R^2 bounded by closed surface $\partial\Omega$ Holder's class, $u = (u_1, u_2)$ is the displacement vector, u_3 is characteristic of the rotation, u_4 is the temperature variation, $\alpha, \beta, \gamma, \mu, \eta, \nu, I, \varsigma$ are constants of **CPTE** [1], δ_{jk} ($j,k=0,3$) is a Kronecker's symbol, $\tau_0 > \tau_1 > 0$ are constants of relaxation, Δ is a two-dimensional Laplacian operator,

$$\text{rot} u_3 = \left(\frac{\partial u_3}{\partial x_2}, -\frac{\partial u_3}{\partial x_1} \right)^T, \text{rot} u = \left(\frac{\partial u_2}{\partial x_1} - \frac{\partial u_1}{\partial x_2} \right), \gamma_\tau = \gamma(1 + \tau_1 \tau), \frac{1}{\varphi_\tau} = \frac{1}{\varphi}(1 + \tau_0 \tau), \tau = \sigma + iq, \sigma > 0.$$

$$H = (h^{(1)}, h_3, h_4) = (h_1, h_2, h_3, h_4) \in C^{1,\alpha}(\Omega), F = (f_k^{(1)}, f_{3k}, f_{4k}) = (f_{1k}, f_{2k}, f_{3k}, f_{4k}) \in C^{1,\alpha}(\partial\Omega), \alpha > 0, k = \overline{0,3}$$

are given functions. Approximate solutions for (1)-(2) boundary value problems are constructed by using the generalized Fourier series method, potential method and method of singular integral equations [1, 2]. we will see that:

$$U^N(x) = \sum_{k=1}^N \sum_{j=1}^k X_k b_k^j \Phi^{j-4} \left[\frac{j-1}{4} \right] \left(x - x \left[\frac{j+3}{4} \right], i\tau \right) - \frac{1}{2} \int_{\Omega} \Phi(y - x, i\tau) H(y) dy \quad (3)$$

where, $U = (u, u_3, u_4) = (u_1, u_2, u_3, u_4)$ is solution of the problem (1)-(2), Φ is the matrix of fundamental solutions of (1), which is constructed by the elementary functions [1], X_k are Fourier series coefficients, which are represented by the boundary data (2), b_k^j are coefficients of the orthonormalization.

References

- [1] M. Chumburidze and D. Lekveishvili, *Approximate Solution of Some Mixed Boundary Value Problems of the Generalized Theory of Couple-Stress Thermo-Elasticity*, World Academy of Science, Engineering And Technology, vol:8, no:6, paper number28, pp.161-163, New York, USA,(2014)
- [2] M. Chumburidze and D. Lekveishvili, *Effective solution of boundary value problems of the theory of thermo piezoelectricity for a half-plane*, AIP Conference Proceedings 1570, pp. 290-297, AIP Publishing LLC, USA(2013)

Boundary Integral Equation Method in the Mathematical Theory of Double Porosity Materials

M. Svanadze

Ilia State University, Tbilisi, Georgia, svanadze@gmail.com

The mathematical theories of double porosity media, as originally developed for the mechanics of naturally fractured reservoirs, have found applications in many branches of engineering, technology and, in recent years, biomechanics. The mathematical models for elastic materials with double porosity are introduced by several authors (see [1-3] and references therein), where the basic PDEs involve the displacement vector field and the pressures associated with the pores and fissures.

In the last decade there has been interest in investigation of problems of the mathematical theories of elasticity and thermoelasticity for solids with double porosity. In this connection, the existence, uniqueness and stability of solutions of the boundary value problems (BVPs) and initial-BVPs are proved, the properties of plane and acceleration waves are established (for details see [4-6]).

Recently, the theory of elasticity for materials with a double porosity structure is presented [7], where the basic PDEs involve the displacement vector field and the volume fraction fields associated with the pores and the fissures.

In this paper, the mathematical theory of materials with a double porosity structure [7] is considered and a wide class of the internal and external BVPs of steady vibrations are investigated. Indeed, the fundamental solution of the system of PDEs of steady vibrations in the considered theory is constructed by elementary functions, the Green's formulas and Somigliana-type integral representation of regular vector and classical solution of the system of equations of steady vibrations are obtained. The uniqueness theorems for solutions of the BVPs are proved. The basic properties of surface (single-layer and double-layer) and volume potentials are established. The singular integral operators of the mathematical theory of materials with a double porosity structure are studied. Finally, the existence of regular (classical) solutions of the internal and external BVPs by means of the boundary integral equation method (potential method) and the theory of singular integral equations are proved.

References

- [1] R. Gelet, B. Loret and N. Khalili, *Borehole stability analysis in a thermoporoelastic dual-porosity medium*, Int. J. Rock Mech. Min. Sci. **50**, pp. 65-76 (2012).
- [2] E. Rohan, S. Naili, R. Cimrman and T. Lemaire, *Multiscale modeling of a fluid saturated medium with double porosity: Relevance to the compact bone*, J. Mech. Phys. Solids **60**, pp. 857-881 (2012).
- [3] Y. Zhao and M. Chen, *Fully coupled dual-porosity model for anisotropic formations*, Int. J. Rock Mech. Min. Sci. **43**, pp. 1128-1133 (2006).
- [4] M. Ciarletta, F. Passarella and M. Svanadze, *Plane waves and uniqueness theorems in the coupled linear theory of elasticity for solids with double porosity*, J. Elast. **114**, 1, pp. 55-68 (2014).
- [5] E. Scarpetta, M. Svanadze and V. Zampoli, *Fundamental solutions in the theory of thermoelasticity for solids with double porosity*, J. Therm. Stresses **37**, pp. 727-748 (2014).
- [6] M. Svanadze, *Uniqueness theorems in the theory of thermoelasticity for solids with double porosity*, Mecanica **49**, pp. 2099-2108 (2014).
- [7] D. Iesan and R. Quintanilla, *On a theory of thermoelastic materials with a double porosity structure*, J. Therm. Stresses **37**, pp. 1017-1036 (2014).

Compressibility Coefficients in Nonlinear Transport Models in Unconventional Gas Reservoirs

Iftikhar Ali, Nadeem A. Malik and Bilal Chanane

King Fahd University of Petroleum and Minerals, PO Box 5046, Dhahran, 31261, Saudi Arabia.

Email: iali@kfupm.edu.sa; namalik@kfupm.edu.sa; Chanane@kfupm.edu.sa

Transport processes in unconventional hydrocarbon reservoirs such as shale gas reserves are not well understood at the present time [1]. They are characterized by extremely low permeability which is a major hurdle in the extraction of gas from the reservoirs. Furthermore, in tight porous media the pore radius (R) may become comparable to the mean free path of the atoms (l), and the transport processes is governed by the Knudsen number, $K_n = l/R$. The process is highly non-linear because the system parameters are strongly dependent upon the pressure field, and cannot be described by simple diffusion equation like Darcy's law, see Refs. [2, 3].

In some transport models such as in Cui [4], Civan [5], several key model parameters, say γ , appear which are strongly dependent upon the pressure $p(x, t)$ in the reservoir, where x is the space coordinate, and t is the time. Each parameter γ has an associated compressibility factor $\beta_\gamma = \beta_\gamma(p)$, which is the relative rate of change of the parameter with respect to changes in the pressure, [6]

$$\beta_\gamma = \frac{\partial \ln \gamma}{\partial p}. \quad (1)$$

γ could be the density (ρ), the permeability (K), the Knudsen number (K_n), etc. In this research, we investigate the gas compressibility factors associated with, the gas deviation factor (β_Z), gas density (β_ρ), gas viscosity (β_μ), permeability (β_K), and the porosity (β_ϕ) of the source rock, as a function of pressure, and their effect on the apparent diffusivity and the apparent convective velocity that appear in the model.

References

- [1] Bustin, R. M., Bustin, A., Ross, D., Chalmers, G., Murthy, V., Laxmi, C., and Cui, X., *Shale gas opportunities and challenges*, Search and Discovery Articles, 40382, 20-23, (2009).
- [2] Ziarani, Ali S., and Roberto Aguilera, *Knudsen's permeability correction for tight porous media*, Transport in porous media 91.1 (2012): 239-260.
- [3] Nadeem A. Malik, Iftikhar Ali, and Bilal Chanane, *Numerical solutions of non-linear fractional transport models in unconventional hydrocarbon reservoirs using variational iteration method*, in 5th International Conference on Porous Media and Their Applications in Science, Engineering and Industry, June 22-27, 2014, USA.
- [4] Cui, X., A. M. M. Bustin, and R. M. Bustin, *Measurements of gas permeability and diffusivity of tight reservoir rocks: different approaches and their applications*, Geofluids, pp. 208 - 223 (2009).
- [5] Civan, F., C. S. Rai, and C. H. Sondergeld, *Shale-gas permeability and diffusivity inferred by improved formulation of relevant retention and transport mechanisms*, Transport in Porous Media 86.3 (2011), pp. 925-944.
- [6] Ali, Iftikhar, Nadeem A. Malik, and Bilal Chanane, *Time-fractional nonlinear gas transport equation in tight porous media: An application in unconventional gas reservoirs*, in International Conference on Fractional Differentiation and Its Applications (ICFDA), pp. 1-6. IEEE, 2014.

Fourth-Order Finite Difference Schemes for Numerical Solution of PDEs Using the Cartesian Cut-Stencil Method*

R.M. Barron, M. Esmaeilzadeh, R. Balachandar

University of Windsor, Windsor, Canada, az3@uwindsor.ca, esmaeilm@uwindsor.ca, rambala@uwindsor.ca

A generalized finite difference method (GFDM), referred to as a cut-stencil method, for the numerical solution of partial differential equations (PDEs) is discussed in this paper. Unlike the traditional finite difference method, GFDM can be applied on an arbitrarily shaped physical domain by using localized Cartesian coordinate systems and mappings from the physical stencil to a generic computational stencil, as illustrated in Fig. 1. Previous research (see eg., Refs. [1,2]) has demonstrated that this GFDM can be used to solve model PDEs arising in many areas of engineering and applied sciences.

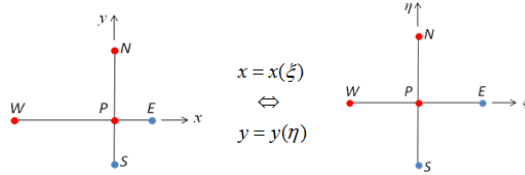


Figure 1: Mapping from physical to generic computational stencil in 2D

The Cartesian cut-stencil method is a simplified version of the GFDM. On a uniform Cartesian mesh without boundary cuts, it reverts to the traditional FDM. However, since it can be applied on complex domains, the Cartesian cut-stencil method is a viable alternative to other discretization schemes such as the finite volume and finite elements methods. These methods are not without difficulties, and in particular for this discussion, the development of high-order schemes is problematic.

The development and implementation of two 4th-order schemes within the cut-stencil FDM framework, one based on Hermitian form and one based on a stencil confinement strategy, is presented in this paper. A typical comparison of the local truncation error (LTE) for 2nd and 4th-order solutions of the convection-diffusion equation is illustrated in Fig. 2. Table 1 demonstrates that the 4th-order scheme can achieve the same level of solution accuracy as the 2nd-order scheme with approximately 1/10th the number of nodes.

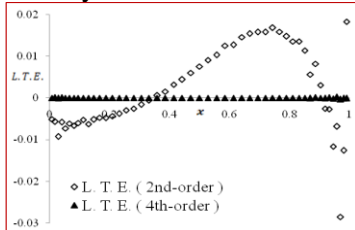


Figure 2: LTE for 2nd and 4th-order schemes

2 nd -order		4 th -order	
# of cells	max. abs. LTE	# of cells	max. abs. LTE
200	5.0E-5	20	4.2E-5
400	1.3E-5	40	1.0E-5

Table 1: Mesh size required for prescribed accuracy

References

- [1] J.J.Situ, R.M. Barron and M. Higgins, *Cell-centred finite difference methodology for solving partial differential equations on an unstructured mesh*, in *Advances in Mathematical and Computational Methods: Addressing Modern Challenges of Science, Technology and Society*, AIP, AMMCS2011, Waterloo, Canada, eds. I. Kotsireas, R. Melnik, B. West, pp, 65-68 (2011).
- [2] R.M. Barron, M. Esmaeilzadeh and S. He, *A Cartesian cut-stencil method for the finite difference solution of the convection-diffusion equation in a complex domain*, 22nd Annual Conf. of the CFD Society of Canada, CFD2014, Toronto, Canada (2014).

Non-singular formulation of boundary integral equations in physics and engineering

D. Y. C. Chan¹, E. Klaseboer², Q. Sun³

¹ School of Mathematics and Statistics, University of Melbourne, Australia, D.Chan@unimelb.edu.au

² Institute of High Performance Computing, Singapore, evert@ihpc.a-star.edu.sg

³ Department of Mechanical Engineering, National University of Singapore, Singapore, q.sun@nus.edu.sg

The classic differential equations in physics and engineering such as the Laplace equation for electrostatic problems, the Helmholtz equation for wave propagation, the Stokes and Oseen equation that describe low Reynolds number hydrodynamics and the equations for linear elasticity all belong to mathematical structure of the Moisil–Theodorescu–Mises–Bitsadze system [1]

$$\nabla \times \mathbf{V} + 2(\mathbf{a} \times \mathbf{V}) = -\nabla \chi \quad \text{and} \quad \nabla \cdot \mathbf{V} = 0, \quad (1)$$

and their solutions can be found by solving boundary integral equations that involve Green's functions of the system as kernels. The boundary integral equation (BIE) formulation is attractive because only unknowns on boundaries need to be found thereby reducing the dimension of the problem by one. Although the resulting system of equations involve a full matrix, $O(N \log N)$ algorithms are available that can handle problems with millions of degrees of freedom. However, the inherent singularities of the Green's function kernels require highly complex of the implementation and place limits on the precision that can be attained [2].

We have developed non-singular formulations of the above classic differential equations in physics and engineering in which all singularities associated with the Green's function kernels are removed analytically [3-7]. This facilitates the use quadratic surface elements and standard Gauss quadrature to evaluate the surface integrals. This approach yields an order of magnitude improvement in precision compared to standard BIE methods for the same number of degrees of freedom or achieves comparable precision with a 90% reduction in the number of degrees of freedom required. In addition, numerical instabilities that arise in problems in which boundaries are very close together are completely eliminated. This is particularly important in nanotechnology applications where it is common for characteristic dimensions to have very different length scales.

References

- [1] M. Zabarankin, Cauchy integral formula for generalized analytic functions in hydrodynamics Proc. Roy. Soc. **A468** pp. 3745-3764 (2012).
- [2] Y. Cao, L. Wen, J. Xiao and Y. Liu, A fast directional BEM for large-scale acoustic problems based on the Burton–Miller formulation, Engin. Anal. Bound. Elements **50** pp. 47-58 (2015).
- [3] E. Klaseboer, Q. Sun and D. Y. C. Chan, Non-singular boundary integral methods for fluid mechanics applications, J. Fluid Mech. **696** pp. 468-478 (2012).
- [4] Q. Sun, E. Klaseboer, B. C. Khoo and D. Y. C. Chan, Stokesian dynamics of pill-shaped Janus particles with stick and slip boundary conditions, Phys. Rev. E. **87** pp. 043009: 1-5 (2013).
- [5] Q. Sun, E. Klaseboer, B. C. Khoo and D. Y. C. Chan, A robust and non-singular formulation of the boundary integral method for the potential problem, Engin. Anal. Bound. Elements **43** pp. 117-123 (2014).
- [6] Q. Sun, E. Klaseboer, B. C. Khoo and D. Y. C. Chan, A robust and non-singular formulation of the boundary integral method for the potential problem, Phys. Fluids **27** pp. 23102:1-19 (2015).
- [7] Q. Sun, E. Klaseboer, B. C. Khoo and D. Y. C. Chan, Boundary regularised integral equation formulation of the Helmholtz equation in acoustics, Roy. Soc. Open Sci. **2** pp. 140520 -140529 (2015).

Optimal dissipation in partial differential equations

K. Morris¹, A. Vest²

¹ Dept. of Applied Mathematics, University of Waterloo, Canada, kmorris@uwaterloo.ca

² Dept. of Applied Mathematics, University of Waterloo, Canada, avest@uwaterloo.ca

Consider the abstract control problem

$$\dot{z}(t) = Az(t) + Bu(t); \quad z(0) = z_0,$$

where A generates a C_0 -semigroup on a Hilbert space \mathcal{L} and B is a bounded operator into \mathcal{L} , with a suitable quadratic cost functional that penalizes the control and/or the state of the system. Provided the system satisfies some technical assumptions and using optimal control theory, it is possible to prove the existence of an optimal control that can be expressed as a feedback.

Assuming that the control operator B depends on the location of the actuator through a parameter r that lies in a set Ω , i.e.

$$B = B(r); \quad r \in \Omega,$$

it is possible to introduce a second layer of optimization by trying to find the best (in a sense to be defined) actuator location. The existence of an optimal actuator location along with the convergence of numerical approximations were studied recently by Morris in [4].

In many situations, the actuator location also affects (at least locally) the dynamics of the system, for example a piezo-electric patch on a plate modifies locally the physical properties of the plate. Hence, the goal of this work is to study and understand the case where the generator of the semigroup also depends on r , i.e.

$$A = A(r), \quad r \in \Omega.$$

The previous results of Morris [4] will be extended to this more general framework.

One special case of this problem is to optimize damping in a structure. For example, given a vibrating string or beam and a given amount of damping material, what is the best location and shape for the damping? A vibrating string with a viscous damping that acts on a part of the string has been considered by Cox and Zuazua [1], Fahroo and Ito [2], Hébrard and Henrot [3]. Here B is the zero operator and \mathcal{L} will be a product space. These earlier results will be extended, and the problem of optimal damping for a vibrating beam discussed.

References

- [1] S. Cox, E. Zuazua, *The rate at which energy decays in a damped string*, Comm. Partial Differential Equations **19**, pp. 213–243 (1994).
- [2] F. Fahroo, K. Ito, *Variational formulation of optimal damping designs*, Contemporary Mathematics, **209**, pp. 95–114 (1997).
- [3] P. Hébrard, A. Henrot, *A spillover phenomenon in the optimal location of actuators*, Siam Journal of Control and Optimization, **44**, 1, pp. 349–366 (2005).
- [4] K. Morris, *Linear-Quadratic optimal actuator location*, IEEE Transactions on Automatic Control, **56**, 1, pp. 113–124 (2011).

Regularization for ill-posed problems in Banach space

M. A. Fury¹, B. M. Campbell Hetrick²

¹Penn State Abington, Abington, Pennsylvania, USA *{maf44}@psu.edu*

²Gettysburg College, Gettysburg, Pennsylvania, USA *bcampbel@gettysburg.edu*

We investigate regularization for the abstract Cauchy problem

$$\begin{aligned} \frac{du}{dt} &= Au, & 0 \leq t < T \\ u(0) &= x \end{aligned} \tag{1}$$

where $-A$ generates a uniformly bounded holomorphic semigroup $\{e^{-zA} : \operatorname{Re} z \geq 0\}$ on a Banach space X . The problem is generally ill-posed as solutions do not depend continuously on initial data. For example, defining $A = -\Delta$ and $X = L^p(R)$, $1 < p < \infty$, yields the backward heat equation. We prove continuous dependence on modeling by estimating a known solution $u(t)$ of (1) by the solution of an approximate well-posed problem

$$\begin{aligned} \frac{dv}{dt} &= f_\beta(A)v, & 0 \leq t < T \\ v(0) &= x \end{aligned} \tag{2}$$

where $\beta > 0$ produces a small change in the model. Many examples of the approximate operator $f_\beta(A)$ have been applied in both Hilbert space and Banach space such as Lattes and Lions's $f_\beta(A) = A - \beta A^2$ [3] and Showalter's $f_\beta(A) = A(I + \beta A)^{-1}$ [4], each of error order $e^{C/\beta}$. Recently, as regularization has been sought for non-linear problems, a less severe amplification factor of the error is required. For example, Boussetila and Rebbani [1] introduce a modified quasi-reversibility method

$$f_\beta(A) = -\frac{1}{pT} \ln(\beta + e^{-pTA}), \quad \beta > 0, \quad p \geq 1 \tag{3}$$

which has error order $\frac{C}{\beta}$. In [2], Huang applies (3) in Banach space and uses a perturbed initial condition to establish regularization. In our paper, we use a different approach by substituting $f_\beta(A)$ as defined by (3) into equation (2). For initial data $x \in \operatorname{Ran}(e^{-2TA})$ and assuming stabilizing conditions on $u(t)$, e.g. $\|u(T)\| \leq M'$, we prove an estimate of the form

$$\|u(t) - v_\beta(t)\| \leq C\beta^{1-\frac{t}{T}} M^{\frac{t}{T}}, \quad 0 \leq t < T$$

where C and M are constants independent of β . Thus, regularization may be accomplished by considering a small change in the initial data and letting $\beta \rightarrow 0$. The theory applies to partial differential equations, particularly the backward heat equation in L^p spaces. In future work, we intend to extend our study to non-linear problems in Banach space and obtain similar results.

References

- [1] N. Boussetila and F. Rebbani, *A modified quasi-reversibility method for a class of ill-posed Cauchy problems*, Georgian Math J. **14**, pp. 627-642 (2007).
- [2] Y. Huang, *Modified quasi-reversibility method for final value problems in Banach spaces*, J. Math. Anal. Appl. **340**, pp. 757-769 (2008).
- [3] R. Lattes and J. L. Lions, *The Method of Quasireversibility, Applications to Partial Differential Equations*, Amer. Elsevier, New York, 1969.
- [4] R. E. Showalter, *The final value problem for evolution equations*, J. Math. Anal. Appl. **47**, pp. 563-572 (1974).

Spectral Convergence and Turing Patterns for Nonlocal Diffusion Systems

Peter W. Bates¹, Guangyu Zhao²

¹ Michigan State University, East Lansing, USA, bates@math.msu.edu

² University of the West Indies, Barbados, gyzhao23@gmail.com

Many physical and biological processes occur with long-range interaction, which oftentimes is not negligible, giving rise to spatially nonlocal operator equations. These operators are diffusive-like but are bounded rather than unbounded as is the case of the diffusion operator. This talk presents our recent study on the spectra of a class of nonlocal diffusion operators on smoothly bounded domains. The class of nonlocal operators under consideration takes the form:

$$(L_\varepsilon w)(x) := \int_{\Omega} \varepsilon^{-2} J_\varepsilon(x-y) [w(y) - w(x)] dy, \quad w \in L^2(\Omega), \quad \Omega \subset \mathbb{R}^n \ (n \geq 1), \quad (1)$$

where $\Omega \subset \mathbb{R}^n$ is a bounded open region with smooth boundary, $\varepsilon > 0$, $J_\varepsilon(x-y) = \varepsilon^{-n} J(\frac{x-y}{\varepsilon})$, $J \in C_c(\mathbb{R}^n)$ is a radially symmetric function, and $J \geq 0$. It is shown that as the scaling parameter ε tends to zero, the spectra of such nonlocal operators converge to the spectrum of a Laplace operator with Neumann boundary condition.

As an application, the established spectral convergence is utilized to investigate Turing patterns for nonlocal diffusion systems:

$$\begin{cases} \frac{\partial u(t,x)}{\partial t} = \int_{\Omega} \varepsilon^{-2} J_\varepsilon(x-y) [u(t,y) - u(t,x)] dy + f(u(t,x), v(t,x)), \\ \frac{\partial v(t,x)}{\partial t} = d \int_{\Omega} \varepsilon^{-2} J_\varepsilon(x-y) [v(t,y) - v(t,x)] dy + g(u(t,x), v(t,x)), \end{cases} \quad d > 0. \quad (2)$$

With the usual Turing conditions on the kinetic systems under consideration, we obtain nonlocal diffusion driven instability for these systems as the scaling parameter ε approaches zero.

References

- [1] F. Andreu, J. M. Mazón, J. D. Rossi and J. Toledo, *A nonlocal p-Laplacian evolution equation with Neumann boundary conditions*, J. Math. Pures Appl., **90**, pp. 201-227 (2008).
- [2] F. Andreu, J. M. Mazón, J. D. Rossi and J. Toledo, *Nonlocal diffusion problems*, Math. Surveys Monogr., Amer. Math. Soc., Providence, RI, 2010.
- [3] P. W. Bates and G. Zhao, *Existence, uniqueness and stability of the stationary solution to a nonlocal evolution equation arising in population dispersal*, J. Math. Anal. Appl., **332**, pp. 428-440 (2007).
- [4] P. Fife, *Some nonclassical trends in parabolic and parabolic-like evolutions*, Trends in Nonlinear Analysis, Springer, Berlin, pp. 153-191 (2003).

CS-POST AMMCS-CAIMS2015 Poster Session

A Study of N-Acetyl aspartic acid/Creatine Ratio in the White Matter of HIV Positive Patients and Its Application

V.Midya¹, U.S.Chakraborty²

¹ Indian Statistical Institute, Delhi, India, midya006@gmail.com

² Seth G.S. Medical College & KEM Hospital, India, ulhaas@gmail.com

A total of 50 patients were enrolled in the study, and MRI brain with MR spectroscopy was done. Out of these, 35 were HIV positive patients (cases). 15 patients with HIV negative status who also underwent MRI for unrelated pathologies were enrolled as controls. They also underwent MRI brain with MR spectroscopy. Tuberculosis was the most common neurologic disease found in the HIV positive group, consisting of 9 patients. Two patients had healed granulomas. Seven of these patients had tuberculous meningitis amongst which a further 2 had vasculitic infarcts. Another two in this group had tuberculomas. Prominent lipid lactate peaks on the spectra obtained from the lesions confirmed the diagnosis of tuberculoma. PML was seen in 6 patients. NAA/Cr was found to be reduced in all the patients, and in fact the value was further reduced compared to the HIV positive group as a whole. Raised choline and myoInositol peaks were also found in all the patients. Toxoplasmosis was seen in 4 patients. MR Spectroscopy showed lipid – lactate peaks confirming the diagnosis. A single patient with brain abscess was seen where also the spectroscopic data from the lesion confirmed the diagnosis with a lactate peak as well as amino acid resonances at characteristic locations. 2 patients had HIV encephalopathy on the imaging study. Their spectra also revealed lowered NAA peaks along with raised choline peaks. 2 patients with cryptococcosis showed characteristic imaging finding of enlarged Virchow Robin (perivascular) spaces. They revealed elevated choline peaks in addition to reduced NAA. No trehalose peaks were identified. MR Spectroscopy was also done in 4 patients of vascular thrombosis, two arterial and two venous, where the MR Spectroscopic findings were not specific. In 7 patients no focal lesions could be identified on conventional MRI sequences however on MR spectroscopic analysis NAA was found to be reduced in comparison to the controls. The values of NAA/Cr were determined after duly processing the spectroscopic data from both cases and controls. Each group (Cases and controls) were divided on the basis of age into two age groups: Lesser than or equal to 40 years, and greater than 40 years. In all three groups the values of the mean NAA/Cr ratio was significantly (p-value less than 0.05) reduced in comparison to controls. An ancillary finding was the reduction of NAA/Cr further in cases of PML. Combined use of both the conventional and advanced MRI sequences is advisable as spectroscopy helps in confirming the diagnosis of opportunistic infection of the CNS in HIV positive patients. NAA/Cr ratio is reduced in HIV positive patients and is a marker for HIV infection of the brain even in the absence of imaging findings of HIV encephalopathy or when the patient is symptomatic due to neurologic disease of other etiologies.

References

- [1] De Cock, K. M., Jaffe, H. W. & Curran, J. W. Reflections on 30 years of AIDS. *Emerg. Infect. Dis.* **17**, 1044–8 (2011).
- [2] Clifford, D. B. HIV-associated neurocognitive disease continues in the antiretroviral era. *Top. HIV Med.* **16**, 94–8.
- [3] Valcour, V., Sithinamsuwan, P., Letendre, S. & Ances, B. Pathogenesis of HIV in the central nervous system. *Curr. HIV/AIDS Rep.* **8**, 54–61 (2011).
- [4] Kranick, S. M. & Nath, A. Neurologic complications of HIV-1 infection and its treatment in the era of antiretroviral therapy. *Continuum (Minneap. Minn.)*. **18**, 1319–37 (2012).

A DFT study on the sorption of organoarsenicals onto Iron Oxide Hydroxides

Adrian Adamescu¹, Hind Al-Abadleh², Ian Hamilton²

¹ University of Waterloo, Waterloo, Canada

² Wilfrid Laurier University, Waterloo, Canada

Organic arsenicals can occur naturally and can be introduced anthropogenically into the environment from a variety of sources. Their bioavailability and transport depends highly on their interactions with reactive soil components such as iron oxide hydroxides. Understanding the mechanisms of binding at the liquid solid interface is helpful for the development of more accurate modeling tools and for the design of remediation technologies.

We present density functional theory (DFT) calculations of energies, activation barriers, vibrational frequencies and Gibbs free energies of adsorption for various ligand exchange reactions of organoarsenicals with iron oxide hydroxide clusters. It is shown that these reactions are thermodynamically favourable and that there are activation barriers greater than 20 kJ/mol along the reaction pathway in order to go from outer-sphere to inner-sphere complexes.

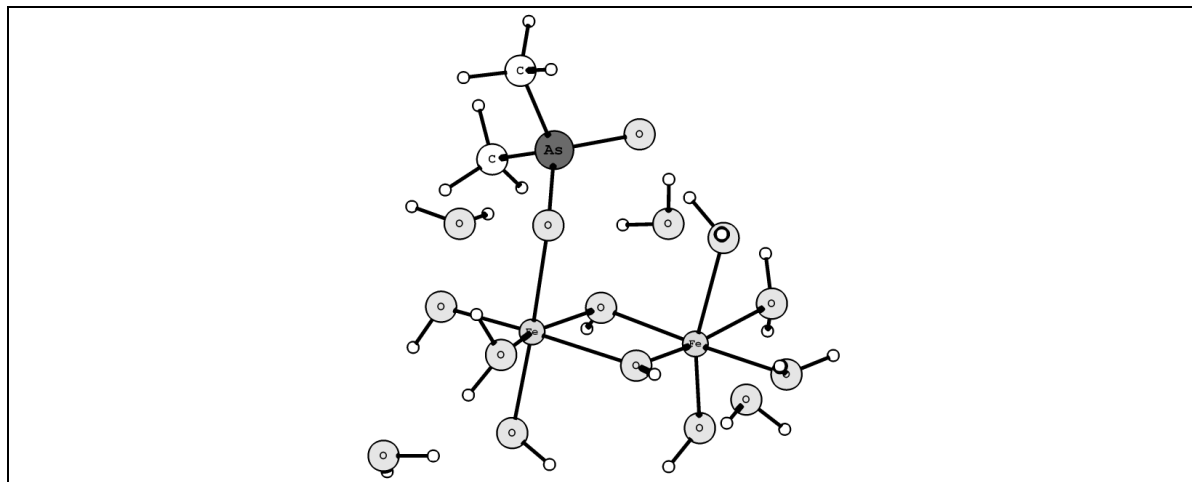


Figure 1: Dimethylarsinic acid forming an inner-sphere monodentate mononuclear complex with an iron oxide hydroxide.

References

- [1] A. Adamescu, I. Hamilton and H. Al-Abadleh. Density Functional Theory Calculations on the Complexation of p-Arsanilic Acid with Hydrated Iron Oxide Clusters: Structures, Reaction Energies and Transition States. *Journal of Physical Chemistry A*, **2014**, 118, 5667-5679.

A mathematical model of the influence of prevention among the homeless people on decrease of the incidence of tuberculosis in the northeastern Poland.

M. Bodzionch¹, J. Romaszko², A. Siemaszko¹

¹ Faculty of Mathematics and Computer Science, University of Warmia and Mazury in Olsztyn, Poland,

mariusz.bodzionch@matman.uwm.edu.pl, artur@uwm.edu.pl

² Family Medicine Unit, University of Warmia and Mazury in Olsztyn, Poland, jerzy.romaszko@uwm.edu.pl

According to the European Centre for Disease Prevention and Control, incidence of tuberculosis in Europe has been decreasing by an average of around 4% a year. In Poland, in the last decade, the average decrease amounted around 26% (by an average of around 2.8% a year). This phenomenon has different dynamics in different parts of the country and the geographical distribution of the dynamics of the decrease is fairly chaotic. The largest decrease (53%, by an average of around 6.4% a year) in the incidence of tuberculosis was observed in the Warmia and Mazury province (the north-eastern region of Poland). The region has a population of about 1.5 million people including about 1000-1500 homeless people. In this region, in the years 2004, 2005, 2006 and 2011, sequentially, four programs of active detection of pulmonary tuberculosis infections in the environment of homeless people were implemented. Reducing the reservoir of infectious bacteria, reducing the amount of outbreaks of infection with respect to the infectious disease, which can be transmitted by droplet transmission only, should lead to decrease in the incidence of infections in general population, especially that the infection spreads in not only the environment of homeless people but is also transmitted to general population.

The relationship between poverty and the incidence of tuberculosis is well known for over 100 years. Homelessness, as a special form of poverty, increases many times the risk of developing tuberculosis disease. We also know that homeless people in many countries are a noticeable proportion of patients which are hospitalized with diagnosed tuberculosis, e.g. it is estimated that 6.3% of all newly diagnosed cases of tuberculosis in the United States relate to homeless people.

It gives the fairly attractive hypothesis about the relationship between the observed decrease in the incidence and preventative actions which were carried out by us. The aim of the study was to demonstrate that the observed decrease in the incidence of tuberculosis was due to the preventive actions which were carried out in the environment of homeless people.

We consider two populations: homeless and not homeless people. Suppose that the disease is such that both of these populations can be divided into two distinct classes: the susceptibles and the infectives. We have built a SIS-type mathematical model to describe numbers of individuals in each of the four classes, which take into account four programs of active detection of pulmonary tuberculosis infections in the environment of homeless people. We used numerical techniques to generate model parameters fitted to experimental data. Further simulations showed that the decrease of incidence of tuberculosis in the next decade will be by an average of around 4% a year in the Warmia and Mazury province. Whereas, assuming that the programs of active detection of pulmonary tuberculosis infections in population of homeless people will be repeated, the expected average decrease in the incidence of infections in the considered region could even amount to 7% a year. The simulations demonstrate the importance of prevention in eliminating outbreaks of infectious diseases to reduce the spread of the infectious disease in general population, in particular, among the people who are characterized by an increased risk of developing tuberculosis disease.

A Statistical Study on Using Perfusion Computed Tomography (PCT) on Brain Tumours

I.Thiraviaraj¹, V.Midya²

¹ Seth G.S. Medical College & KEM Hospital, Mumbai, India, inthulanthiraviaraj@gmail.com

² Indian Statistical Institute, Delhi, India, midya006@gmail.com

A total of 33 patients with histopathologically proven diagnosis of gliomas were analyzed. Of these 6 were grade II gliomas, 7 were grade III and 20 were grade IV gliomas. Multiple factors have to be studied while diagnosing and grading gliomas. Inclusion of perfusion adds to the confidence in stratifying patients diagnosed with a glial tumour. Of the 4 perfusion parameters rCBV (relative cerebral blood volume) was the one that was most sensitive and specific in assessing the grade of gliomas. The cut off value calculated is 2.19625. rCBF (relative cerebral blood flow) also had good correlation with the grade of the tumour. However on comparison with rCBV it proved inferior. The cut off value calculated is 2.165. nMTT (normalized Mean transit time) and nTTP (normalized Time to peak enhancement) had no correlation with the tumour grade. rCBV cannot be used in differentiating grade III from grade IV tumours. High grade gliomas occur in older population in comparison with their low grade counterparts. However they can be seen in any age group. Perfusion CT can be used for grading gliomas in any location. Both thalamic gliomas and lobar gliomas show high values of rCBV and rCBF relative to normal uninvolving white matter. Both anterior cerebral artery and middle cerebral artery can be used for obtaining arterial curves. Basilar artery can also be used in cases of posterior fossa tumours; however MCA (Middle cerebral artery) should be preferred for standardization of values. Haemorrhage, necrosis and corpus Callosum involvement occur in GBMs more commonly than in grade III tumours and are not frequent in low grade tumours. Multiple ROIs (Region of interest) have to be drawn to find out the area with highest rCBV. These areas have to be mentioned while reporting cases of gliomas because targeted biopsies can be planned accordingly to prevent misdiagnosis.

References

- [1] Anne G. Osborn. *Diagnostic Neuroradiology*. 1st ed. India: Elsevier,2009. Print.
- [2] Scott W. Atlas. *Magnetic Resonance Imaging of the Brain and Spine*. 4th ed. Philadelphia : Lippincott Williams & Wilkins, 2009. Print.
- [3] Axel, L. Cerebral blood flow determination by rapid-sequence computed tomography: theoretical analysis. *Radiology* **137**, 679–86 (1980).
- [4] K.A. Miles, M. Hayball, A.K. Dixon. Colour perfusion imaging: a new application of computed tomography. *Lancet*. 337(8742):643-5. Mar 1991
- [5] M. Koenig, E. Klotz, B. Luka, D.J. Venderink, J.F. Spittler, L. Heuser. Perfusion CT of the brain: diagnostic approach for early detection of ischemic stroke. *Radiology* 209(1):85-93, October 1998
- [6] Allmendinger, A. M., Tang, E. R., & Lui, Y. W. (2012). Imaging of Stroke: Part 1, Perfusion CT—Overview of Imaging Technique, Interpretation Pearls, and Common Pitfalls, (January), 52–62. doi:10.2214/AJR.10.7255
- [7] Hoeffner, E. G., Case, I., Ct, R. T., Jain, R., Gujar, S. K., Shah, G. V, Deveikis, J. P., et al. (n.d.). Radiology Cerebral Perfusion CT :Technique and Clinical Applications
- [8] Eastwood, J. D., Lev, M. H. & Provenzale, J. M. Perfusion CT with iodinated contrast material. *AJR. Am. J. Roentgenol.* **180**, 3–12 (2003).

A Study on Pattern of Speech Modulation Spectrum of Toddlers with Autism Spectrum Disorder (ASD) and Typically Developing Children (TD)

V.Midya¹

¹*Indian Statistical Institute, Delhi, India, midya006@gmail.com*

The main objective of this study is to find some statistical measures or some combination of statistical measures which will significantly differentiate between ASD and TD children based on theirs speech modulation spectrum. For dimensionality reduction, singular value decomposition technique has been applied on the speech modulation spectrum matrices. Based on the singular values, it is found that the measures Median, 3rd Quartile Deviation (Q_3) and Inter Quartile Range (IQR) show significant difference (p-value less than 0.05) between ASD and TD children. Further it is found that ASD Median and TD Median, ASD Q_3 and TD Q_3 , ASD IQR and TD IQR are significantly uncorrelated (p-value is more than 0.05), which in turn points to the high robustness of these measures. The intra converging validity for above mentioned ASD measures and TD measures are also very high (p-value is less than 0.05), so these three measures can be grouped together which enables these combination of measures to be statistically very significant.

References

- [1] Sullivan K, Sharda M, Greenson J, Dawson G and Singh NC (2013) A novel method for assessing the development of speech motor function in toddlers with autism spectrum disorders. *Front. Integr. Neurosci.* 7:17. doi:10.3389/fnint.2013.00017.
- [2] Singh, L., and Singh, N. C. (2008). The development of articulatory signatures in children. 671 *Developmental Science*, 11, 467-473.
- [3] Singh, L., Shantisudha, P., and Singh, N. C. (2007). Developmental patterns of speech production in children. *Applied Acoustics*, 68, 260-269.
- [4] Singh, N. C., and Theunissen, F. E. (2003). Modulation spectra of natural sounds and ethological theories of auditory processing. *The Journal of the Acoustical Society of America*, 114, 3394-3411.

A Tensor Decomposition Approach Based on User Trust for QoS Web Service Recommendation

S. Chai¹, W. Feng^{1,2}

¹ Queen's University, Kingston, Canada, chai@cs.queensu.ca

² Trent University, Peterborough, Canada, wfeng@trentu.ca

Quality of Service (QoS) plays a significant important role in web services, which is the measure of web service quality and availability [1]. QoS performance is closely related to the user when the service is confronted with change. User trust is a mark of confidence correlated for ensuring quality of web service. The trust relationship between the users usually address participant's confidence and helps to make value judgments for QoS. Therefore, the trust relationship of users should pay more attention in the recommendation system.

The most widely used way for obtaining user trust value is collaborative filtering methods. This method uses the similar QoS records to predict service for a user. The recent study of the literature has been proposed to revise collaborative filtering methods. Xu et al. [2] Build the two models which called service neighborhood-based MF model and the user neighborhood-based MF model. They identify the similar neighbors through similarity computation. Lin et al. [3] propose a social-trust-based mechanism for dynamic collaboration. The legal agreement and characteristics are bound to a social trust network of web services. It recommends trust services in collaboration. Unfortunately, all users are considered separately from the service in these methods. They use the single similar relationship which cannot capture the trust when looking for different services. To overcome this issue, Zhang et al. [4] propose the trust recommendation algorithm using the Tucker tensor model. The Tucker uses a user-service relation represented by the context information. A trust relationship to improve the QoS recommendations should be considered on this algorithm..

To avoid loss trust, while maintaining user-service relation, we propose a tensor decomposition approach based on user trust relationship. The tensor object represented by three dimensional user-user-service matrix for maintaining the original QoS data. The decomposition algorithm is improved for tensor objects by applying tensor rank-one decomposition. Approaches for the research include modeling and experiment in the WS-DREAM dataset. The dataset contains 150 files, where each file includes 10,000 Web service invocations on 100 Web services by a service user. And there are totally more than 1.5 million Web service invocations. Compared with the classic ways, the experiments result shows that proposed method can reduce the training time and get the optimal solution fast.

References

- [1] A. Mani and A. Nagarajan. Understanding quality of service for Web services. IBM dW, <http://www-106.ibm.com/developerworks/library/ws-quality.html>, (2002)
- [2] Xu, Y., Yin, J., Wu, Z., He, D., & Tan, Y. Reliability Prediction for Service Oriented System via Matrix Factorization in a Collaborative Way, In Proceedings of Service-Oriented Computing and Applications (SOCA), 2014 IEEE 7th International Conference, pp. 125-130 (2014)
- [3] Lin, S. Y., Yang, Y. C., Lo, C. C., & Chao, K. M. A Social Trust Based Recommendation Mechanism for Web Service Dynamic Collaboration, In Proceedings of Service-Oriented Computing and Applications (SOCA), 2013 IEEE 6th International Conference, pp. 318-322 (2013)
- [4] Zhang, W., Sun, H., & Liu, X. An Incremental Tensor Factorization Approach for Web Service Recommendation, In Proceedings of Data Mining Workshop (ICDMW), 2014 IEEE International Conference, pp. 346-351 (2014)

Approximate controllability of neutral stochastic integro-differential systems with impulsive effects

M. Li¹, X. Li²

¹ Donghua University, Shanghai, P. R. China, meiliuvic@gmail.com

² Donghua University, Shanghai, P. R. China, lixiangdhu@163.com

In this paper, we study the approximate controllability of the following neutral stochastic integro-differential systems with impulsive effects of the form

$$\begin{cases} d[x(t) + F(t, x_t)] = [-Ax(t) + \int_0^t \gamma(t-s)x(s)ds + Bu(t)]dt + G(x, x_t)dW(t), & t \in J, t \neq t_k, \\ \Delta x(t) = I_k(x(t^-)), & t = t_k, k = 1, 2, 3 \dots m, \\ x_0 = \phi, & t \in [-r, 0], \end{cases} \quad (1)$$

where $J = [0, T]$, ϕ is \mathcal{F} -measurable and $-A$ generates an analytic semigroup on a separable Hilbert space H with inner product $\langle \cdot, \cdot \rangle$ and norm $\|\cdot\|$. $u(\cdot) \in L_2^{\mathcal{F}}(J, U)$ is the control function where U is a Hilbert space. $\gamma(\cdot)$ is a family of closed linear operators to be specified later. B is a bounded linear operator from U into H . Define the Banach space $D(A^\alpha)$ with the norm $\|x\|_\alpha = \|A^\alpha x\|$ for $x \in D(A^\alpha)$, where $D(A^\alpha)$ denotes the domain of the fractional power operator $A^\alpha : H \rightarrow H$. Let $H_\alpha := D(A^\alpha)$ and $C_\alpha = C([-r, 0], H_\alpha)$ be the space of all continuous functions from $[-r, 0]$ into H_α . Define K be another separable Hilbert space. Suppose $W(t)$ is a given K -valued wiener process with a finite trace nuclear covariance operator $Q \geq 0$. $F : [0, T] \times C_\alpha \rightarrow H$, $G : [0, T] \times C_\alpha \rightarrow L_2^0(K, H)$ and $I_k : H \rightarrow H$ are appropriate functions to be specified below. Here $L_2^0(K, H)$ denotes the space of all Q -Hilbert-Schmidt operators from K into H . For every $t \in J$, the history function x_t is defined by $x_t(\theta) = x(t + \theta)$ for $\theta \in [-r, 0]$, $\Delta x(t)$ denotes the jump of x at t , $\Delta x(t) = x(t^+) - x(t^-) = x(t^+) - x(t)$. Sufficient conditions are established for the approximate controllability. The results are obtained by using the theory of analytic resolvent operator and the contraction mapping principle. Particularly, the compactness of the analytic resolvent operator is not needed in this paper. An example is presented to illustrate the obtained conclusions. Our results extend those of Dauer and Mahmudov [1], Shen and Sun [2], Mokkedem and Fu [3].

References

- [1] J. P. Dauer, N. I. Mahmudov, Controllability of stochastic semilinear functional differential equations in Hilbert spaces, Journal of Mathematical Analysis and Applications **290**, pp. 373-394 (2004).
- [2] L. J. Shen, J. T. Sun, Approximate controllability of stochastic impulsive functional systems with infinite delay, stochastic semilinear functional differential equations in Hilbert spaces, Automatica **48**, pp. 2705-2709 (2012).
- [3] F. Z. Mokkedem, X. Fu, Approximate controllability of semi-linear neutral integro-differential systems with finite delay, Applied Mathematics and Computation **242**, pp. 202-215 (2014).

Approximate controllability of semi-linear neutral stochastic integro-differential inclusions with infinite delay

M. Li¹, M. Liu²

¹ Donghua University, Shanghai, P. R. China, meiliuvic@gmail.com

² Donghua University, Shanghai, P. R. China, 12467566@qq.com

In this paper, we are interested in the approximate controllability of the following semi-linear neutral stochastic integro-differential inclusions with infinite delay in a Hilbert space:

$$\begin{cases} d[x(t) + F(t, x_t)] \in [-Ax(t) + Bu(t) + \int_0^t \gamma(t-s)x(s)ds]dt + G(t, x_t)d\omega(t), & t \in J := [0, T], \\ x(t) = \phi(t) \in L_2(\Omega, \mathcal{B}), \text{ for a.e } t \in J_0 := (-\infty, 0], \end{cases} \quad (1)$$

where $-A$ is the infinitesimal generator of an analytic semigroup of bound linear operator $S(t)$, $t \geq 0$, on a separable Hilbert space H with inner product $\langle \cdot, \cdot \rangle$ and norm $\|\cdot\|$. The control function $u(\cdot)$ takes values in $L_2(J, U)$ of admissible control functions for a separable Hilbert space U and B is a bounded linear operator from U into H . $\gamma(\cdot)$ is a family of closed linear operators. Let K be another separable Hilbert space with inner product $\langle \cdot, \cdot \rangle_K$ and norm $\|\cdot\|_K$. Suppose $\{\omega(t)\}_{t \geq 0}$ is a given K -valued Brownian motion or Wiener process in a finite trace nuclear covariance operator $Q \geq 0$. $F : J \times \mathcal{B} \rightarrow H$ and $G : J \times \mathcal{B} \rightarrow \mathcal{P}(L_Q(K, H))$ are respectively measurable and multivalued measurable mapping, where $\mathcal{P}(L_Q(K, H))$ is the family of all nonempty subsets of $L_Q(K, H)$ and $L_Q(K, H)$ denotes the space of all Q -Hilbert-Schmidt operators from K into H . The histories $x_t : (-\infty, 0] \rightarrow H$, $x_t(\theta) = x(t + \theta)$, $\theta \leq 0$, belongs to an abstract phase space \mathcal{B} . Sufficient condition are formulated and proved for the approximate controllability of such system. The results are obtained by using the Krasnoselkii fixed point theorem, the fraction power theory, α -norm and the theory of analytic resolvent operator. An example is provided to illustrate the applications of the obtained results. Our results extend those of Liu [1], Balasubramaniam and Ntouyas [2], Mokkedem and Fu [3].

References

- [1] Bing Liu, Controllability of impulsive neutral functional differential inclusions with infinite delay, Nonlinear Analysis **60**, pp.1533-1552 (2005).
- [2] P. Balasubramaniam, S. K. Ntouyas, Controllability for neutral stochastic functional differential inclusions with infinite delay in abstract space, Journal of Analysis and Applications **324**, pp.161-176 (2006).
- [3] Fatima Zahra Mokkedem, Xianlong Fu, Approximately controllability of semi-liner neutral integro-differential system with finite delay, Applied Mathematics and Computation **242**, pp.202-215 (2014).

Asymptotic behavior of heavy-tailed renewal-reward process and applications

C.C.Y. Dorea¹, D.B. Ferreira², M.A. Oliveira³

¹ Universidade de Brasilia, Brasilia-DF, Brazil, changdorea@unb.br

² Universidade Federal do Rio Grande do Norte, Natal-RN, Brazil, debora@ccet.ufrn.br

³ Instituto Federal de Brasilia, Brasilia-DF, Brazil, magno.oliveira@ifb.edu.br

Consider a renewal-reward process $S_{N(t)} = \sum_{k=1}^{N(t)} X_k$ and let $\{\tau_n\}$ be the interarrival times. It is well-known that, under regularity conditions, $S_{N(t)}$ is asymptotically Gaussian provided X_n and τ_n have finite second moment. However, in modelling risk processes or heavy traffic networks, the assumption of the finiteness of the second moment may not be compatible. Also, the independency of the processes $\{S_n\}$ and $\{N(t)\}$ might be not realistic. In this case, heavy-tailed distributions arise as a proper alternative and dependency structures between τ_n and the reward X_n should be explored. By making use of the Mallows-Wasserstein distance we derive CLT type results for heavy-tailed renewal-reward dependent processes. Applications include bounds for the ruin and buffer overflow probabilities in finite time.

Key Words: heavy-tailed distribution, stable laws, Mallows distance, renewal-reward process.

References

- [1] C.C.Y. Dorea and D.B. Ferreira, *Conditions for equivalence between Mallows distance and convergence to stable laws*, Acta Mathematica Hungarica **134**, pp. 1-11 (2012).
- [2] C.C.Y. Dorea and M.A. Oliveira, *The Donsker's theorem for Levy stable motions via Mallows distance*, Markov Proc. and Related Fields **20**, pp. 167-172 (2014).

Computational Thinking Across Disciplines

J.Mueller¹, H.Shodiev², J.Dhaliwal², A.Khattak², I.Murphy¹ and D. Beckett¹

¹*Faculty of Education Wilfrid Laurier University, Waterloo, Canada, jmueller@wlu.ca*

²*Department of Physics and Computer Science, Wilfrid Laurier University, Waterloo, Canada, hshodiev@wlu.ca*

Abstract

Computational thinking is an emerging component of broader 21st century thinking required by all learners to actively participate in a digital economy. Utilizing graphical computer coding software in a variety of subjects, across disciplines, will provide a foundation for critical, creative thinking and decision making [1]. In this work we study problem solving skills through Computational Thinking core concepts using K-12 system curriculum based modules. Teaching computational thinking techniques across a broad range of subjects can be challenging. We offer a method by which modules can be built around curriculum requirements in and out of STEM disciplines. This method will provide tools with which teachers can identify how different computational concepts could apply to their subject matter and how this could map into a Scratch based project. New rubrics are presented for developing problem-based modules. Student problem solving ability is expected to improve following an intervention that teaches computational thinking through Scratch coding modules across disciplines and grades (4 to 10).

Keywords: Computational thinking, critical thinking skills, problem solving skills, Scratch programming, graphical programming

References

- [1] ISTE standards for students. <http://www.iste.org/standards/standards-for-students>

Effects of Cross-diffusion in Biofilm Model of Competition for a Shared Resource

Kazi A. Rahman¹, Hermann J. Eberl¹

¹*Dept. Mathematics and Statistics, University of Guelph, Guelph, Canada, {krahman,heberl}@uoguelph.ca*

We investigate the effects of cross-diffusion (CD) when two different species are interacting with each other using a biofilm model that includes competition for a shared resource. The effects of cross-diffusion compared to non cross-diffusion model considering two different active biofilm colonies with equal constant growth and decay rates has been investigated. We have also investigated this cross-diffusional effects with random inoculation. The presence of cross-diffusion in the model has potential impact locally, in particular the relative local distribution of species, but it does not affect overall lumped quantities such as the total number of species. In addition, cross-diffusion slows down the interaction process between species.

Elimination of bacterial plasmids by engineered unilateral incompatibility

R. Gooding-Townsend¹, S. ten Holder¹, B. Ingalls¹

¹ University of Waterloo, Waterloo, Canada, bingalls@uwaterloo.ca

Plasmids are extra-chromosomal genetic elements that are commonly found in bacteria and are readily passed from cell to cell [1]. They often confer traits that improve host fitness in specific environments (such as resistance to antibiotics and heavy metals). Antibiotic resistance plasmids represent a significant health concern, as they provide a means for pathogenic bacterial strains to rapidly acquire resistance to multiple antibiotics, making treatment of infections difficult. We propose an approach to the elimination of target plasmids from bacterial populations (e.g. in clinical environments).

Elimination of plasmids from laboratory populations is standard practise, where the goal to produce a plasmid-free isolate, rather than to eradicate a plasmid from a population. Two commonly used methods for the plasmid *curing* task are chemical treatment (which interferes with plasmid replication), or displacement by incompatibility [2]. We employ an engineered form of incompatibility in our approach, as discussed below.

Maintenance of a plasmid within a host imposes a metabolic load. To ensure their successful propagation, plasmids have evolved control mechanisms to ensure they will persist within their host population. One such mechanism is copy number control, by which plasmids regulate their rate of replication. The resulting copy number is low enough to ensure the host's metabolism is not overloaded, but high enough to ensure that the cell division events do not result in plasmid-free daughter cells. Plasmids that share a common copy number control mechanism are called incompatible, as they cannot both be stably maintained in a given host. Unilateral incompatibility can be achieved by engineering a plasmid that is compatible with the target plasmid, but codes for the components that limit replication of the target. As a proof of principle, we have engineered such a plasmid to displace the ColE1 plasmid from a laboratory strain of *Escherichia coli* and confirmed eradication.

To investigate the performance of this eradication approach, we have developed mathematical models of the plasmid dynamics within the population. The dynamics of plasmid copy number control have been modelled using both deterministic differential equations and stochastic processes [3]. The dynamics of plasmid incompatibility has been addressed as well [4]. Combining these approaches, we have constructed a stochastic model of unilateral incompatibility. We used Gillespie's stochastic simulation algorithm [5] and approximations via Poisson processes to explore the model's dynamics. We used this model to explore the performance of the eradication mechanism under a range of conditions and control mechanism pairings. These results will be used for model-based design as we move forward with further experimental implementations.

References

- [1] D. Summers, *The Biology of Plasmids*, Wiley, New York, (1996).
- [2] R. P. Novick, *Plasmid Incompatibility*, *Microbiology Review* **51**, pp. 381-395 (1987).
- [3] J. Paulsson and M. Ehrenberg, *Noise in a minimal regulatory network: plasmid copy number control*, *Quarterly Reviews of Biophysics* **34**, pp. 1-59 (2001).
- [4] Ishii, K., Hashitomo-Gotoh, T. and Matsubara, K., *Random replication and random assortment for plasmid incompatibility in bacteria*, *Plasmid* **1**, pp. 435-445 (1978).
- [5] D. T. Gillespie, *Exact Stochastic Simulation of Coupled Chemical Reactions*, *The Journal of Physical Chemistry* **81** pp. 2340–2361 (1977).

Fixation Probability of Budding Viruses

J. Reid¹, L.M. Wahl²

¹ University of Western Ontario, London, Canada jreid222@uwo.ca

² University of Western Ontario, London, Canada lwahl@uwo.ca

Human viruses can be classified based on their utilization of one of three major egress mechanisms. The first is lysis of the cell, which results in cellular apoptosis, and thus, cell death. The other two mechanisms, budding and exocytosis, retain viability of the cells. Budding is a form of egress where the virions steal a portion of the cellular membrane to gain a viral envelope. Finally, exocytosis occurs when virions are packaged in vesicles and transported to the cell membrane, where they fuse and are released. While non-enveloped viruses commonly utilize exocytosis, some enveloped types may also employ it.

When the genomes of viruses are replicated, there is a chance that mutations occur. These mutations can be beneficial, deleterious, or silent, and may affect any property associated with the organism. Over time, these mutations either become fixed in the growing population of progeny, or become extinct, based on selective pressures that promote or oppose the mutant population. The fixation of novel mutations is the underlying process by which viruses adapt to environmental pressures such as new antiviral pharmaceuticals, or in order for them to infect a new host.

To model the growth phase of budding viruses I have created a system of delay-differential equations,

$$\frac{dF}{dt} = \left(-\frac{1}{a} - \frac{1}{v}\right)F + \frac{1}{b}I, \quad (1)$$

$$\frac{dI}{dt} = \frac{1}{a}F - I(t - \tau), \quad (2)$$

$$\frac{dB}{dt} = I(t - \tau) - \frac{1}{d}B, \quad (3)$$

where F represents the free viruses that are not attached to a host cell, I represents the cells that are infected by the virus but not yet in the budding stage, and B represents the infect cells that are budding free viruses. Parameters a , v , b , and d represent the attachment, clearance, budding, and cell death times respectively.

Numerical simulations were used to track the virions throughout a growth phase, followed by a transmission bottleneck as the virus infected a new host. Starting with a wild-type population, beneficial mutations were introduced, to examine fixation probabilities. Specific examples of the effects of beneficial mutations are: increasing the attachment rate, increasing the cell's lifetime, increasing the budding rate and reducing the probability of clearance. In parallel analytical work, the fixation probabilities are estimated by a probability generating function that represents the number of offspring in this mutant lineage at any given time.

In summary, the main goal of this study is to understand the evolution of budding viruses from a mathematical point of view. The findings shed light on mechanisms of adaption used by budding viruses of significant importance to human health, when faced with selective pressures such as antiviral drugs.

Interaction of double-stranded DNA inside single-walled carbon nanotubes

M. Alshehri¹, B. Cox², J. Hill³

¹ Department of Mathematics, College of Science, King Saud University, Saudi Arabia mhalshehri@ksu.edu.sa

² School of Mathematical Sciences, The University of Adelaide, Adelaide, SA, Australia, barry.cox@adelaide.edu.au

³ School of Mathematical Sciences, The University of Adelaide, Adelaide, SA, Australia, jim.hill@adelaide.edu.au

Deoxyribonucleic acid (DNA) is the genetic material for all living organisms, and as a nanostructure offers the means to create novel nanoscale devices. Here, we investigate the interaction of deoxyribonucleic acid inside single-walled carbon nanotubes. Using classical applied mathematical modeling, we derive explicit analytical expressions for the encapsulation of DNA inside single-walled carbon nanotubes. We adopt the 6-12 Lennard-Jones potential function together with the continuous approach to determine the preferred minimum energy position of the dsDNA molecule inside a single-walled carbon nanotube, so as to predict its location with reference to the cross-section of the carbon nanotube. An analytical expression is obtained in terms of hypergeometric functions which provides a computationally rapid procedure to determine critical numerical values. We observe that the double-strand DNA can be encapsulated inside a single-walled carbon nanotube with a radius larger than 12.30 Å, and we show that the optimal single-walled carbon nanotube to enclose a double-stranded DNA has radius 12.8 Å. We are assuming that the DNA molecule adopts a double helical geometry. With reference to a rectangular Cartesian coordinate system (x, y, z) , a typical point on the surface of the DNA is given by

$$\mathbf{G}(\Theta, t) = \left(\frac{R}{2} \left[\cos \Theta + \cos(\Theta - \phi) + t(\cos \Theta - \cos(\Theta - \phi)) \right], \frac{R}{2} \left[\sin \Theta + \sin(\Theta - \phi) + t(\sin \Theta - \sin(\Theta - \phi)) \right], \frac{c\Theta}{2\pi} \right),$$

where $R = 10$ Å is the radius of the dsDNA helix, $c = 34$ Å is the unit cell length, ϕ is the helical phase angle parameter and the parametric variables t and Θ are such that $-1 < t < 1$, and $-\pi < \Theta < \pi$.

Similarly, with reference to the rectangular Cartesian coordinate system (x, y, z) , a typical point on the surface of the tube has the coordinates $(a \cos \theta, a \sin \theta, z)$, where a is the radius of the carbon nanotube and $-\infty < z < \infty$ and $-\pi < \theta < \pi$.

We derive the total interaction energy for a DNA molecule into a carbon nanotube using the Lennard-Jones potential together with the continuum approximation, which is given by

$$E = \eta_1 \eta_2 \int_{S_1} \int_{S_2} \left(-\frac{A}{\rho^6} + \frac{B}{\rho^{12}} \right) dS_1 dS_2,$$

where η_1 and η_2 denote the atomic liner surface densities of the first and the second molecules, respectively, and A and B are the attractive and repulsive constants, respectively. The distance ρ between a typical surface element on the CNT and another on the DNA is given by

$$\begin{aligned} \rho^2 &= a^2 - aR[\cos(\Theta - \theta) + \cos(\Theta - \theta - \phi) + t[\cos(\Theta - \theta) - \cos(\Theta - \theta - \phi)]] \\ &\quad + R^2[\cos^2(\phi/2) + t^2 \sin^2(\phi/2)] + (z - c\Theta/2\pi)^2. \end{aligned}$$

Legendre-Galerkin Method for Solving Fredholm Integral Equations of the First Kind

B. Neggal¹, F. Rebbani², N. Boussetila³,

¹ Applied Mathematics Laboratory, University Badji Mokhtar Annaba, P.O.Box 12, Annaba 23000, Algeria
bilel-negal@hotmail.com

² Applied Mathematics Laboratory, University Badji Mokhtar Annaba, P.O.Box 12, Annaba 23000, Algeria
faouzia.rebbani@univ-annaba.org

³ Department of Mathematics, FMISM, Guelma University, P.O.Box 401, Guelma 24000, Algeria
n.boussetila@gmail.com

In this talk, a numerical approach based on the Legendre-Galerkin Method is proposed to approximate the solution of Fredholm integral equations of the first kind. We also establish some error estimates are also given under a suitable assumptions on the exact solution. Finally, some numerical examples will be stated to show the accuracy of this method. Many problems in applied mathematics and engineering can be formulated as Fredholm integral equations of the first kind:

$$Kf(x) = \int_a^b k(x,y)f(y)dy = g(x), \quad (1)$$

where the kernel $k(.,.)$ and the right-hand side g are smooth real-valued functions. The determination of the solution f is an ill-posed problem in the sense of Hadamard; in the sense that the solution (if it exists) does not depend continuously on the data. In this work, we suggest a numerical procedure based on the Legendre-Galerkin projection method, where the solution is projected onto a subspace generated by Legendre polynomials.

References

- [1] K. Maleknejad , K. Nouri , M. Yousefi, Discussion on convergence of Legendre polynomial for numerical solution of integral equations, *Applied Mathematics and Computation* 193 (2007) 335–339.
- [2] G. Andrews , R. Askey , R. Roy , *Special Functions*, Cambridge Uni Press(1999).
- [3] Ben-yu Guo , Zhong-qing Wang, Legendre–Gauss collocation methods for ordinary differential equations, *Adv Comput Math* (2009) 30:249–280.
- [4] K.Maleknejad, R.Mollapourasl and M. Alizadeh, Convergence analysis for numerical solution of Fredholm integral equation by Sinc approximation, *CommunNonlinear SciNumer Simulat* 16 (2011), 2478-2485.

Long-time Dynamics of the Critical Surface Quasigeostrophic Equation

P. Constantin¹, A. Tarfulea², V. Vicol³

¹ Princeton University, USA, *const@math.princeton.edu*

² Princeton University, USA, *tarfulea@math.princeton.edu*

³ Princeton University, USA, *vvcoll@math.princeton.edu*

Nonlinear forced dissipative partial differential equations can generate physical space patterns which evolve in a temporally complex manner. As parameters are varied, the dynamics may transition from simple to chaotic and ultimately to fully turbulent. Nevertheless, several forced nonlinear dissipative PDE of hydrodynamic origin have been shown to have finite dimensional long-time behavior. This has been proved if certain minimal conditions are satisfied; chief among them is the property that linearizations about time evolving solutions are dominated in a certain sense by the linear dissipation. This is the case for semilinear dissipative PDE such as the Navier-Stokes system in 2D, or subcritical quasilinear damped systems. For our case, we focus on the long time behavior of the critical, quasilinear, forced surface quasigeostrophic (SQG) initial-value problem

$$\partial_t \theta + u \cdot \nabla \theta + \kappa \Lambda \theta = f, \quad u = \mathcal{R}^\perp \theta = (-\mathcal{R}_2 \theta, \mathcal{R}_1 \theta), \quad \theta(\cdot, 0) = \theta_0.$$

Here the spatial domain is the 2D torus, \mathcal{R}_j is the j^{th} Riesz operator, and $\Lambda = (-\Delta)^{1/2}$. The SQG equation, similar in structure to the 3D Euler equations in vorticity form, describes the evolution of a surface temperature field θ in a rapidly rotating, stably stratified fluid with potential vorticity [4, 5]. The nonlinearity has the same differential order as the nonlocal dissipation, so that the above system (for large data) cannot be treated as a perturbation of a fractional heat equation.

Proving global regularity for solutions of the unforced equation is nontrivial and has been obtained only in the last few years (see [3] and references therein). We improve the robustness of the nonlinear lower bound for the fractional Laplacian established in [3] by using the smallness of α in the C^α control to replace the (now unneeded) “only small shocks” condition.

The dynamics of the SQG equation have also been of recent interest (see, for example, [2]). The existence of a compact finite dimensional attractor, however, requires an infinite dimensional loss of information. With our new proof of regularity that is more direct and more explicitly quantitative than all prior ones, the loss of information is reflected in the long-time bounds that eventually become independent of the initial data θ_0 . This is entirely nontrivial for a critical quasilinear system, but it is true here because the smoothing effect is controlled by the L^∞ norm. The latter result is based on a new uniform nonlinear Poincaré inequality, which is of independent interest.

References

- [1] P. Constantin, A. Tarfulea, and V. Vicol, *Long time dynamics of forced critical SQG*, Communications in Mathematical Physics **335**, 1, pp. 93-141 (2015).
- [2] P. Constantin, A. Tarfulea, V. Vicol, *Absence of anomalous dissipation of energy in forced two dimensional fluid equations*, Archive for Rational Mechanics and Analysis **212**, 3, pp. 875-903 (2014).
- [3] P. Constantin and V. Vicol, *Nonlinear maximum principles for dissipative linear nonlocal operators and applications*, Geometric and Functional Analysis **22**, 5, pp. 1289-1321 (2012).
- [4] I.M. Held, R.T. Pierrehumbert, S.T. Garner, and K.L. Swanson, *Surface quasi-geostrophic dynamics*, Journal of Fluid Mechanics **282**, pp. 1-20 (1995).
- [5] P. Constantin, A.J. Majda, and E. Tabak, *Formation of strong fronts in the 2-D quasigeostrophic thermal active scalar*, Nonlinearity **7**, 6, pp. 1495-1533 (1994).

Macrohedging in a Financial Market of Semimartingales

M. Abdelghani¹ & A. Melnikov²

¹ University of Alberta, Edmonton, Canada, mnabdelghani@gmail.com

² University of Alberta, Edmonton, Canada, melnikov@ualberta.ca

Traditional hedging requires that one hedges individual assets comprising the portfolio. On the other hand, macrohedging is about reducing several underlying risk factors, such as, volatility of interest rate, volatility of exchange rates and variability of a portfolio of assets as a *whole*. In a macrohedge one must carry on an investment policy to maximize returns, and a hedge policy that reduces the risk of the entire portfolio, a balance sheet or a financial entity with hedge instruments, such as, futures and option contracts.

Let $(\Omega, \mathcal{F}, \mathbf{F} = (\mathcal{F}_t)_{t \geq 0}, \mathbf{P})$ be the standard stochastic basis and that the financial market evolves on this basis over a time horizon $[0, T]$. The market is composed of two baskets of assets: the portfolio basket of assets and a set of hedging instruments. For example, a portfolio basket can be bonds and stocks whereas hedging instruments can European put options ‘closely related’ to stocks. Let $X = (X^1, X^2, \dots, X^n)$ be a vector of n assets determining the value V of the portfolio π . The portfolio basket or space of assets is \mathbf{X} and $X \in \mathbf{X}$. Let \mathbf{Y} be the space of hedging instruments and $Y = (Y^1, Y^2, \dots, Y^m)$ is the vector of instruments in \mathbf{Y} . We associate with X the filtration $\mathbf{F}^X = (\mathcal{F}_t^X)_{t \geq 0}$ which we assume complete and right continuous. With Y we associate the filtration $\mathbf{F}^Y = (\mathcal{F}_t^Y)_{t \geq 0}$, which we also assume to be complete and right continuous. Together $\sigma(\mathcal{F}_t^X \cup \mathcal{F}_t^Y) \subseteq \mathcal{F}_t$ for all t . The space of all possible self-financing predictable portfolios is Π and the vector $\pi = (\pi_1, \pi_2, \dots, \pi_n) \in \Pi$. All securities and hedge instruments in this market are cadlag semimartingales. Note that in general $[X^i, Y^k] \neq 0$ and $\mathcal{F}^X \cap \mathcal{F}^Y \neq \emptyset$ for all t and (i, k) . In other words, the spaces \mathbf{X} and \mathbf{Y} overlap. This overlap is needed for the hedging instruments to be useful.

The value V of portfolio π is given by $V = \sum_i \pi_i X^i = \pi' X$. We let $\mathbf{F}^V = (\mathcal{F}_t^V)_{t \geq 0}$ be the filtration associated with the value process V and assume that, it is right continuous and complete and $\mathbf{F}^V \subseteq \mathbf{F}^X$. Now, let us consider the hedging portfolio λ over the set of the hedge instruments Y having the value, $U = \lambda' Y$. Similarly, we require that λ be self-financing and predictable. Let Λ be the set of all self-financing portfolios over \mathbf{Y} for which $\lambda \in \Lambda$. We let $\mathbf{F}^U = (\mathcal{F}_t^U)_{t \geq 0}$ be the filtration associated with the value process U and assume that, it is right continuous and complete and $\mathbf{F}^U \subseteq \mathbf{F}^Y$.

The *macroportfolio* is $\phi = (\pi, \lambda)$ is composed of both the assets and hedge instruments and has a value $Z = V + U = \pi' X + \lambda' Y$. Therefore, one can define macrohedging as all those methods by which one can select a hedge portfolio λ given the investment portfolio π . One can understand macrohedging as a hierarchical optimization problem where one first finds a portfolio that maximize returns then a hedge portfolio that minimized the risk of the entire portfolio. Risk minimization can be achieved by minimizing a risk measure, such as, the variance, Value-at-Risk or quadratic variation of the macroportfolio value Z .

We will consider finding λ in a semimartingale market by minimizing the “quadratic projection” of Z on the space \mathbf{Y} where quadratic projection is computed in the sense of the *quadratic variation* of Z with Y . Hence, given the portfolio and its associated value (π, V) and hedge instruments Y such that, $\mathbf{E}[V, V]_t < \infty$, $\mathbf{E}[Y, Y']_t < \infty$ and the matrix $[Y, Y']_t$ is not singular for all $t \geq 0$ then one can simply write $\lambda = d[V, Y'] / d[Y, Y']$ for which $[Z, Y'] = 0$. With this choice of λ , $[Z, Z]$ is minimized.

Minimal Total Variation Infilling to Determine Radiological Aerosol Deposition from Dose

I. Zwiers¹, L. Lebel²

¹ Canadian Nuclear Laboratories, Chalk River, Ontario, ian.zwiers@cnl.ca

² Canadian Nuclear Laboratories, Chalk River, Ontario

In the event of radiological aerosol dispersal there is a need to determine the likely pattern of contaminant deposition based on scattered measurements of radiation dose. Lebel et al [1], found that a linear deposition to dose relationship is not reliable. Total variation infilling techniques from image processing, as pioneered by Starck, Candès and Donoho [2], and others, are tested as a constraint on potential contamination patterns under radiation-transport deconvolution. The technique is demonstrated against validated field data from aerosol dispersal device tests conducted at the Suffield proving grounds in Alberta in 2012, Korpach et al. [3].

References

- [1] L. Lebel, P. Bourgoiun, S. Chouhan, N. Ek, V. Korolevych, A. Male, D. Bensimon and L. Erhardt, *Atmospheric Dispersion Modeling of the Full Scale RDD Experiments with Operational Models in Canada Part II: Radiation Modeling and Finite Cloud Effects*, to appear in Health Physics (2015).
- [2] J.-L. Starck, D. Donoho and E. Candès, *Very High Quality Image Restoration by Combining Wavelets and Curvelets*, in *International Symposium on Optical Science and Technology* (2001).
- [3] E. Korpach, L. Erhardt, R. Berg, L. Lebel, C. Liu, I. Watson, and D. Quayle, *Cloud shine and ground shine measurements from the DRDC Suffield Full Scale RDD Experiments* to appear in Health Physics (2015).

Non-Local Delays and Depth Dependence in an NPZ Model

Matt Kloosterman¹, Sue Ann Campbell², Francis Poulin³

¹ University of Waterloo, Waterloo, Canada *{mklooste}@uwaterloo.ca}*

² University of Waterloo, Waterloo, Canada *{sacampbe}@uwaterloo.ca*

³ University of Waterloo, Waterloo, Canada *{fpoulin}@uwaterloo.ca*

The study of planktonic ecosystems is important as they make up the bottom trophic levels of aquatic food webs. These ecosystems have an inherent heterogeneity with respect to depth, as the light needed for photosynthesis is more abundant near the water's surface, yet the required nutrients tend to sink to deeper levels. In order to better understand these dynamics we use a closed Nutrient-Phytoplankton-Zooplankton (NPZ) model where the variables depend on time as well as a vertical spatial dimension. We allow movement in space through diffusion as well as transport due to sinking, floating, and swimming. Additionally, since dead matter takes time to be recycled into usable nutrient, various types of delays are incorporated into the model. Due to sinking and diffusion, it is necessary to make the delays non-local so that the state variables can depend not only on the past values, but also on values at other points in space. With this model we study equilibrium solutions and their stability while varying parameters such as the length of delay and the total biomass in the system. We verify these results through numerical simulations. In doing so, we better our understanding of how properties such as total biomass, recycling time, depth, the difference in behaviours among different species of plankton, and various physical properties affect the overall ecosystem.

Non-Smooth Bifurcations in the Mean-Field System for a Network of Type 1 Neurons with Adaptation

W. Nicola¹, S.A. Campbell¹

¹ University of Waterloo, Ontario, Canada wnicola@uwaterloo.ca

The mean-field system for a coupled network of type 1 neurons with spike frequency adaption is a piecewise-smooth continuous system of two ordinary differential equations. Due to the nature of these equations, the mean-field system displays a series of non-smooth bifurcations. In particular, there are two analytically resolvable non-smooth co-dimension two bifurcations that occur [1]. One involves the collision between a Hopf bifurcation equilibria and the switching manifold for the system. The other involves the collision between a saddle-node bifurcation equilibria and the switching manifold. Various other non-smooth co-dimension 1 bifurcations also emanate out from these two points. We discuss how these two points are related to the underlying behavior of the type 1 network of neurons, and how general these points are for an arbitrary piecewise-smooth continuous dynamical system. We also discuss how the mean-field system can be regularized via analyzing the original network of neurons in the low noise limit.

References

- [1] W. Nicola, S.A. Campbell, *Non-smooth Bifurcations of Mean Field Systems of Two-Dimensional Integrate and Fire Neurons*, arXiv:1408.4767 (2014)

Numerical simulation of the seasonal thermocline in Lake Ontario using FVCOM

M. Wilson¹, J. Shore², L. Boegman¹ R. Yerubandi³

¹ Queen's University at Kingston, Canada

² Royal Military College of Canada, Kingston, Canada

³ Environment Canada, Canada Centre for Inland Waters, Burlington, Canada

In large lakes, such as Lake Ontario, three-dimensional numerical models have difficulty in accurately reproducing the formation of the thin seasonal thermocline present in field observations (Boegman et al. 2001; Huang et al. 2010; Hodges et al. 2000). Models typically produce a thermocline which is more diffuse than real lake conditions (Hodges et al. 2000). This results from poor parameterization of sub-grid-scale turbulent mixing (via the turbulence closure scheme) and numerical diffusion which cause the model runs to overestimate vertical mixing (Laval et al. 2003). Cumulative effects of poor turbulent closure parameterization and numerical diffusion are more pronounced as the length of simulation increases and, therefore, seasonal investigations are heavily impacted (Hodges et al. 2000). Consequently, there is a need for more accurate turbulent closure parameterizations to improve simulation of the seasonal thermocline and associated fluxes from the epilimnion to the hypolimnion.

In the present study, the Finite Volume Coastal Ocean Model (FVCOM) is employed to assess the relative accuracy of various turbulence closure schemes included in the Global Ocean Turbulence Model (GOTM) in simulating the seasonal thermocline in Lake Ontario through comparison against observed temperature profiles. Within GOTM, several turbulent mixing schemes are available, including k-epsilon and Mellor-Yamada formulations, which can be applied using multiple stability and length scale methods. In this study, FVCOM employs an unstructured triangular mesh grid with a (maximum resolution at the shoreline of ~200 m and minimum resolution in the middle of the lake of ~7000 m). Thirty-one terrain following sigma levels are employed in the vertical direction. The model is forced with a wind field created using data from eleven stations around Lake Ontario in 2010 and interpolated onto the unstructured grid. Model results utilizing a non-uniform wind field have been shown to produce more accurate temperature and current structure than results obtained using uniform wind forcing (Laval et al. 2003).

In addition to validation against field observations, the FVCOM results will be compared to results from other three-dimensional numerical models (ELCOM, POM and CANDIE) applied to Lake Ontario with similar grid resolutions (Huang et al. 2010). Once the optimal closure scheme has been identified, a sensitivity analysis will be applied to weigh the computational cost versus the benefits of increased vertical resolution in reducing numerical diffusion.

References

- [1] Boegman, L., Loewen, M.R., Hamblin, P.F. and Culver, D.A. 2001. Application of a two-dimensional hydrodynamic reservoir model to Lake Erie. *Can. J. Fish. Aquat. Sci.* 58: 858-869.
- [2] B. Hodges, B.R., Imberger, J., Laval, B., Appt, J., Modelling the Hydrodynamics of Stratified Lakes- Hydroinformatics 2000 Conference, Iowa Institute of Hydraulic Research,23-27 July 2000
- [3] Huang, Anning, et al. Hydrodynamic modeling of Lake Ontario: An intercomparison of three models. *Journal of Geophysical Research: Oceans* (1978–2012) 115.C12 (2010)
- [4] Laval, B., Imberger, J., Hodges, B. R., & Stocker, R. (2003). Modeling circulation in lakes: Spatial and temporal variations. *Limnology and Oceanography*, 48(3), 983-994.
- [5] Laval, Bernard, Ben R. Hodges, and Jörg Imberger. Reducing numerical diffusion effects with pycnocline filter. *Journal of Hydraulic Engineering* 129.3 (2003): 215-224.

On the agreement between small-world-like OFC model and real earthquakes

D.S.R. Ferreira^{1,2}, A.R.R. Papa², R. Menezes³, R.P. Freitas¹, V.S. Felix¹

¹ LISComp Laboratory, Federal Institute of Rio de Janeiro, Paracambi, RJ, Brazil, douglas.ferreira@ifrj.edu.br

² Geophysics Department, National Observatory, Rio de Janeiro, RJ, Brazil, papa@on.br

³ BioComplex Laboratory, Computer Sciences, Florida Institute of Technology, Melbourne, USA, rmenezes@cs.fit.edu

Despite all the existing knowledge about the production of seismic waves through slips on faults, much remains to be discovered regarding the dynamics responsible for these slips. A key step in deepening this knowledge is the study, analysis and modeling of the seismic distributions in space and time. Aiming to contribute to the understanding of earthquake dynamics, in this paper we implemented simulations of the model developed by Olami, Feder and Christensen (OFC model), which incorporate characteristics of self-organized criticality (SOC) and has played an important role in the phenomenological study of earthquakes, because it displays a phenomenology similar to the one found in actual earthquakes. We applied the OFC model for two different topologies: regular and “small-world” [1, 2], where in the latter the links are randomly rewired with probability p . In both topologies, we have studied the distribution of time intervals between consecutive earthquakes and the border effects present in each one. In addition, we also have characterized the influence that the probability p produces in certain characteristics of the lattice and in the intensity of border effects, as shown in Figures 1 (a) and 1 (b). Furthermore, in order to contribute the understanding of long-distance relations between seismic activities we have built complex networks of successive epicenters from synthetic catalogs produced with the OFC model, using both regular and small-world topologies. In our results distributions arise belonging to a family of non-traditional distributions functions [3], as we can see in Figure 1 (c), which agrees with previous studies using data from actual earthquakes [4]. Our results reinforce the idea that the Earth is in a critical self-organized state and furthermore point towards temporal and spatial correlations between earthquakes in different places.

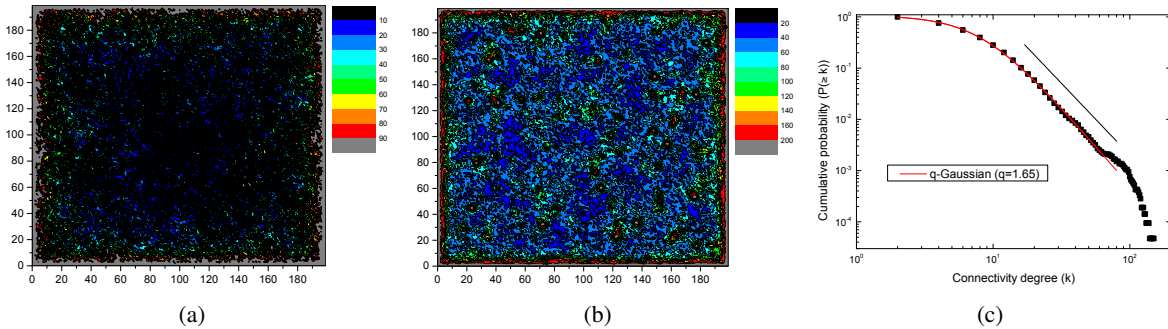


Figure 1: Map of epicenters distribution through a lattice. (a) Regular lattice. (b) Small-world lattice with $p = 0.006$. We can see that the border effects are considerably smaller in the small-world topology. (c) Cumulative distribution of connectivities in small-world topology.

References

- [1] F. Caruso, et al., *Olami-Feder-Christensen model on different networks*, EPJ B **50** (1-2), pp.243-247 (2006).
- [2] D. Watts and S. Strogatz, *Collective dynamics of ‘small-world’ networks*, Nature **393**, pp. 440-442 (1998).
- [3] S. Thurner and C. Tsallis, *Nonextensive aspects of self-organized scale-free gas-like networks*, EPL **72**, pp. 197-203 (2005).
- [4] D. Ferreira, A. Papa, R. Menezes, *Small world picture of worldwide seismic events*, Physica A **408**, pp.170-180 (2014).

Optical spectra of helical gold nanorods and emergence of the plasmon transition

Harold Hodgins¹, Ian Hamilton¹, Jay Foley², Stephen Grey²

¹ Department of Chemistry, Wilfrid Laurier University, Waterloo, Ontario, Canada

² Center for Nanoscale Materials, Argonne National Laboratory, Argonne, Illinois, USA

Background Hamilton et. al [1] examined the stability of multi-strand 7-1 helical Au24, Au32 and Au40 structures (recent work includes Au48, Au56, and Au64) with three, four and five gold atoms in the central strand and 21, 28 and 35 gold atoms in the coaxial tube using relativistic density functional theory. They demonstrated that the helical gold nanorods are stable structures at zero Kelvin (the corresponding nonhelical gold nanorods are not) and that are competitive, both energetically and chemically, with alternate cage and compact structures. Whereas the central strand is linear, the seven strands comprising the coaxial tube that surrounds the central strand are helical. This could potentially result in novel optoelectronic properties for these nanostructures.

Gray et. al [2] have examined excited-state plasmon modes in small linear atomic chains using time-dependent quantum mechanical methods and found that linear atomic chains with as few as 100 active electrons could display plasmonic features. With two active electrons per gold atom, the small helical gold nanorods are in this range. Piccini et. al [3] found that plasmonic behaviour appears in gold nanowires at lengths greater than 2nm. Since the Au64 nanorod is just above 2nm in length plasmonic behaviour in the smaller nanorods is interesting.

Objectives To examine the novel plasmonic behaviour resulting from the helical character of the noble metal strands and it's dependence on nanorod length.

Methodology We are using time-dependent density functional theory (TDDFT) as implemented in the Gaussian software package and including relativistic effects with the lanl2dz basis set and the long ranged corrected BP86 exchange/correlation functional to obtain the Absorbance and CD spectra of the nanorods.

Results The Absorbance spectrum of Au40 shows promising symptoms of plasmonic behaviour. Partial results from Au64 are encouraging.

Significance The small helical gold nanorods could potentially be used as interconnects in nanostructured optoelectronic devices. Because plasmons are generated at optical frequencies, their oscillations are extremely rapid. They are therefore capable of encoding much more information than is possible for conventional electronic devices.

As the size of the metal structures becomes smaller, quantum effects become more important and it essential to understand them. Differences between gold nanowires and gold nanorods in terms of plasmonic behaviour have consequences in the manufacturing of nanostructured optoelectronic devices.

Future Work We plan to extend this work to larger nanorods.

References

- [1] Xiao-Jing Liu, Ian Hamilton, Robert P. Krawczyk and Peter Schwerdtfeger, J. Comp. Chem. 2012, 33, 311-318.
- [2] A. Eugene DePrince III, Matthew Pelton, Jeffrey R. Guest and Stephen K. Gray, Phys. Rev. Lett. 2011, 107, 196806.
- [3] GiovanniMaria Piccini, Remco W. A. Havenith, Ria Broer, and Mauro Stener, J. Phys. Chem. C 2013, 117, 17196-17204.

Sensitivity Analysis For Stochastic Models Of Biochemical Reaction Networks

A. Monjur Morshed¹, B. Brian Ingalls², C. Silvana Ilie³

¹ University of Waterloo, Waterloo, Canada, m6morshe@uwaterloo.ca

² University of Waterloo, Waterloo, Canada, bingalls@uwaterloo.ca

³ Ryerson University, Toronto, Canada, silvana@ryerson.ca

In the study of Systems Biology it is necessary to simulate cellular processes and chemical reactions that comprise biochemical systems. This is achieved through a range of mathematical modelling approaches. Standard methods use deterministic differential equations, but because many biological processes are inherently probabilistic, stochastic models must be used to capture the random fluctuations observed in these systems. The presence of noise in a system can be a significant factor in determining its behavior. The Chemical Master Equation is a valuable stochastic model of biochemical kinetics. One particularly important tool in the study of biochemical systems is sensitivity analysis, which aims to quantify the dependence of a system's dynamics on model parameters. A number of approaches to sensitivity analysis of these models have been developed [1, 2]. We provide a comparison of these methodologies in order to identify which approach is most efficient depending of the features of the model. This result can serve as a guide to efficient sensitivity analysis, which can serve as a foundation for the formulation, characterization, and verification of models.

References

- [1] D. F. Anderson, *An Efficient Finite Difference Method For Parameter Sensitivities of Continuous Time Markov Chains*, SIAM J. Numer. Anal. **50**, 2237 (2012).
- [2] M. Rathinam, P. W. Sheppard, and M. Khammash, *Efficient Computation of Parameter Sensitivities of Discrete Stochastic Chemical Reaction Networks*, J. Chem. Phys. **132**, 034103 (2010).

Stable Variables and Application in Non Life Insurance

A. Laouar¹, K. Boukhetala², R. Sabre³

¹ Hight school of marine Sciences and coastal planning(ENSSMAL), Algiers, Algeria, amel.laouar@gmail.com

² University of science and technology Houari Boumediene (USTHB).Algiers, Algeria, kboukhetala@usthb.dz

³ AgroSup,Dijon,France. r.sabre@agrosupdijon.fr

Abstract : For an insurance company it's often essential to develop adequate strategies for efficient portfolio management to deal with probable risks. To do this, it is often sought to develop representative mathematical models, to be used as tools for analysis, forecasting and simulation for decision support. The choice of model is very important and as we know Gaussian process and variables have been studied for a long time and their usefulness in stochastic and statistical modelling is well accepted. However, they don't allow for large fluctuations and may sometimes be inadequate for modelling high variability, especially in finance and non life insurance. that's why it's important to focus on other family of laws and processes such as stable random variable's and processes which naturally appear as alternative modeling tools. There are several reasons which have led us to choose the stable distributions for our work and modelization, they are a very rich class of probability distributions can represent different asymmetries and heavy tails. This class was characterized by Lévy (1925) in this work the sum of independent and identically distributed variables. This class has a great importance in the theory of extreme values, because stable distributions can be characterized from the Generalized Central Limit Theorem given by Gnedenko and Kolmogorov (1954) and indicates that if the condition of finite variance is not respected. The only possible limit law of the sum of n random variables (iid), is a Stable law.

In the most general case a risk process representing the behaviour of a non life insurance company is described as follows :

$$R(t) = u + ct - S(t) \quad (1)$$

Where u is the initial capital of the insurance company, c is the constant premium rate over time and $S(t)$ is the claim process defined by :

$$S(t) = \sum_{i=1}^{N(t)} X_i \quad (2)$$

- o $\{X_i\}_{i \geq 1}$ Sequence of iid positive random variables, which represent claim severities.

- o N_t describes the number of claims in $(0, t]$, we assume that X_i and N_t are independent.

As we can see that the aggregate claim amount $S(t)$ is a random sum of random variables. And for good risk management of insurance company, it needed to have good modelling of this sum (claim process), which depends essentially of claims amounts and their frequencies. To do this, we must examine sequences of real data to have the best estimate of the claim amounts distribution, and we propose to check if we are in the presence of infinite variance law or not, and more specifically the stable law.

References

- [1] H. Cramér, *Collective Risk Theory*. Skandia Jubilee Volume, Stockholm (1955).
- [2] V.M. Zolotarev, *One-Dimensional Stable Distributions*. American Mathematical Society, Providence, RI (1986).
- [3] A. Janiko and A. Weron, *Simulation and chaotic behavior of α -stable process*. Marcel Dekker, INC, New York (1994).
- [4] V.M. Zolotarev and V. Uchaikin, *Chance and stability : Stable distribution and their application*. Modern probability and statistics. Netherlands, Utrecht, VSP. Tokyo, Japan (1999).
- [5] L. d'Estampes. *Traitement statistique des processus alpha-stables, Mesure de dépendance et identification des AR stable, Test séquentiels tronqués*. Thèse de doctorat soutenue à l'institut national de polytechnique de Toulouse le 24 octobre2003.

A Survey On a Class of Intersection Graph: Self-graphoidal Graph

P. K. Das¹, K. R. Singh²

¹ NERIST, Arunachal Pradesh, [pdk_ma@yahoo.com](mailto:pkd_ma@yahoo.com)
² NIT, Arunachal Pradesh, karamratan7@gmail.com

We consider only non-trivial, simple, finite and connected graphs here. A graphoidal cover of a graph G [1] is a collection ψ of (not necessarily open) paths in G such that every path in ψ has at least two vertices, every vertex of G is an internal vertex of at most one path in ψ and every edge of G is in exactly one path in ψ . A graph G is called a graphoidal graph if there exists a graph H and a graphoidal cover ψ of H such that $G \cong \Omega(H, \psi)$. Also, the graph G is said to be self-graphoidal if it is isomorphic to one of its graphoidal graphs. In this article, we present a comprehensive review of the progress made till date on self-graphoidal graphs.

References

- [1] B.D. Acharya and E. Sampathkumar, Graphoidal covers and graphoidal covering number of a graph, *Indian J. Pure Appl. Math.*, 18(10)(1987), 882-890.
- [2] S. Arumugam, B. D. Acharya, E. Sampathkumar, Graphoidal covers of a graph: a creative review, in *Proc. National Workshop on Graph Theory and its applications, Manonmaniam Sundaranar University, Tirunelveli, Tata McGraw-Hill, New Delhi* (1997) 1–28.
- [3] K. R. Singh, P. K. Das, On self-graphoidal graphs, *Thai Journal of Mathematics*, 8(3), (2010) 575–579.
- [4] K. R. Singh, P. K. Das, On Helly Graphoidal Graphs.(Communicated)
- [5] K. R. Singh, P. K. Das, Further Results on Self-graphoidal Graphs.(Communicated)

Switching dynamics in the *Aplysia* bag cell neuron

K. Keplinger¹, S. Campbell²

¹ University of Waterloo, Canada, keegankeplinger@gmail.com

² University of Waterloo, Canada, sacampbe@uwaterloo.ca

Persistent neural response is a mechanism by which a brief stimuli can induce long-term firing behavior in the nervous system. Qualitative similarities in persistent neural responses are prevalent across species, including motoneurons in turtles, the escape response of lamprey, and numerous cortical regions relating to memory and attention. Persistent activity is often associated with peptide release, as is the case with mammalian maternal function in birth and lactation through the release of oxytocin. Here, we develop an ion-conductance neuron model to reproduce persistent behavior in *Aplysia* reproduction. In *Aplysia*, bag cell neurons in the abdominal ganglia respond to a brief pulse with persistent neural oscillations, known as the afterdischarge, inducing the release of peptides associated with egg-laying. After several minutes of persistent activity, the neuron transitions to a refractory period where it can function as a normal threshold neuron, but afterdischarge cannot be invoked until the refractory period ends. Mounting evidence suggests intrinsic cellular mechanisms, namely calcium, are responsible for the transition to persistent oscillations and the refractory period. Development of the *Aplysia* bag cell model is in collaboration with the experimental lab of Neil Magoski at Queen's University, which provides data and insightful observations to inform the development of the mathematical model.

Using Sign Patterns to Detect Periodicity in Biological Systems

G.J. Culos¹, D.D. Olesky¹, P. van den Driessche¹

¹ University of Victoria, Victoria, Canada

Many models in the physical and life sciences, formulated as dynamical systems of ordinary differential equations, have a positive steady state, with the qualitative behavior of this steady state determined by the eigenvalues of its Jacobian matrix. Our interest lies in detecting if this steady state is linearly stable or if the system has periodic solutions arising from a Hopf bifurcation. We address this by considering the sign pattern, a matrix with entries from $\{+, -, 0\}$, of the Jacobian matrix and its set of allowed refined inertias. The refined inertia $ri(A)$ of an n -by- n real matrix A is a 4-tuple $(n_+, n_-, n_z, 2n_p)$ where n_+ (n_-) is the number of eigenvalues with positive (negative) real part, n_z is the number of zero eigenvalues, and $2n_p$ is the number of nonzero pure imaginary eigenvalues. A Hopf bifurcation may be possible if the sign pattern of the Jacobian matrix allows the set of refined inertias $\mathbb{H}_n = \{(0, n, 0, 0), (0, n - 2, 0, 2), (2, n - 2, 0, 0)\}$. In most cases we also need to consider magnitude restrictions on the entries of the Jacobian matrix that are a consequence of the particular model. Our aim is to complement other studies that have relied on algebraic evaluation of the Routh-Hurwitz criteria. We illustrate the usefulness of sign pattern analysis with several biological examples, including metabolic-genetic circuits, biochemical reaction networks, and predator-prey.

References

- [1] E. Bodine, L. Deaett, J.J. McDonald, D.D. Olesky, and P. van den Driessche. Sign patterns that require or allow particular refined inertias. *Linear Algebra and its Applications*, 437(9):2228–2242, 2012.
- [2] C. Garnett, D.D. Olesky, and P. van den Driessche. Refined inertias of tree sign patterns. *Electronic Journal of Linear Algebra*, 26:620–635, 2013.
- [3] R. D. Holt. Spatial heterogeneity, indirect interactions, and the coexistence of prey species. *The American Naturalist*, 124:377–406, 1984.
- [4] M. Mincheva and M. R. Roussel. Turing-Hopf instability in biochemical reaction networks arising from pairs of subnetworks. *Mathematical Biosciences*, 240(1):1–11, 2012.
- [5] Ed Reznik, Tasso J Kaper, and Daniel Segrè. The dynamics of hybrid metabolic-genetic oscillators. *Chaos*, 23(1):013132, 2013.

Index of Authors

A

Abdelghani, M., 193, 677
Abgrall, R., 30
Abiodun, G., 620
Abrar, B., 83
Abudiab, M., 235
Abukhdeir, N., 201, 309
Adamescu, A., 662
Adcock, B., 398
Adem, A., 236
Adler, J., 400
Afshar, S., 283
Aggarwala, B., 592
Agyingi, E., 105, 586
Ahmadi Golestan, M., 516, 545
Akbari, A., 69
Akewe, H., 295
Akhmetgaliyev, E., 276
Aksoylu, B., 277
Al-Abadleh, H., 662
Alaei, N., 64
Alam, J., 502
Alba, K., 417, 458, 490, 504, 566, 568
Albert, R., 10
Aleman, D., 153
Alexander, M., 363
Algarni, S., 405
Ali, I., 611, 654
Ali, Q., 595
Alipanahi, B., 211

Almaatani, D., 602
Alshehri, M., 674
Alter, O., 217
Alvarez, A., 191
Alwan, M., 170, 176, 177
Amarala, S., 401
Anand, M., 338, 346, 358, 376
Ananiev, S., 449
Anco, S., 35, 228, 229, 238, 267
Andjelkovic, M., 205
Andreguetto Maciel, G., 285
Andrews, M., 351
Antipova, A., 609
Ao, W., 291
Apaloo, J., 162, 166
Arat, S., 223
Arredondo, J., 134
Aruliah, D., 585
Asadzadeh, I., 640
Ashlock, D., 154
Ashrafizaadeh, M., 535
Assous, F., 81, 394
Atarodi, M., 300
Athar, S., 164, 214
Aylward, A., 584
Azarderakhsh, R., 60
Azimzadeh, P., 402

B

Babaoglu, C., 618

- Baboulin, M., 603, 605
 Badescu, A., 190
 Badu, S., 242
 Baer, S., 255
 Baggag, A., 578
 Bakker, L., 132
 Balachandar, R., 500, 543, 655
 Baltzer, J., 163
 Banyassady, R., 533
 Baradaran, A., 482
 Barclay, P., 161
 Bardeleben, M., 563
 Barlow, L., 358
 Barron, R., 500, 543, 655
 Barton, M., 374
 Barutello, V., 139
 Baruzzi, G., 541
 Basir, F., 353, 593
 Bates, P., 659
 Bauch, C., 165, 338, 346, 351, 358, 376
 Bayati, M., 472
 Behrouzifar, A., 441
 Belair, J., 96, 99, 284
 Belmiloudi, A., 588
 Bennett, M., 36, 61
 Bensmail, H., 578
 Benson, T., 400
 Berezansky, L., 97
 Bernard, C., 182
 Berry, T., 109, 113, 114
 Best, J., 256–258
 Betti, M., 596
 Beyer, H., 277
 Biasse, J., 67
 Bibeau, E., 512
 Bielecki, T., 12
 Bihlo, A., 414
 Bilel, N., 675
 Bilinsky, L., 255
 Biros, G., 215
 Bobak, C., 47
 Bodzionch, M., 663
 Boegman, L., 314, 681
 Bohun, C., 324
 Boreland, B., 44
 Boukhetala, K., 685
 Bourgault, Y., 308, 403, 418, 644
 Boussaid, N., 274
 Bowman, J., 397
 Boyle, G., 264
 Bramburger, J., 106
 Braverman, E., 97
 Brereton, C., 574
 Brinkerhoff, J., 443
 Broucke, M., 172
 Brown, D., 494
 Brown, J., 162, 163, 166
 Bruin, N., 64
 Bruno, O., 272, 276
 Bruzon, M., 230
 Buckrell, A., 563
 Budd, C., 14
 Bunama, R., 474
 Buono, P., 143
 Burhani, H., 90
 Burkowski, F., 208, 210
 Butler, L., 140
- C**
- Calmelet, C., 584
 Campbell Hetrick, B., 658
 Campbell, L., 307, 574
 Campbell, S., 103, 251, 287, 679, 680
 Cao, S., 282
 Cecile, A., 358
 Celiker, F., 277
 Celler, A., 407

- Cervi, J., 585
Chai, S., 666
Chakraborty, U., 661
Chalmers, N., 424, 438
Chan, D., 607, 656
Chanane, B., 654
Chanda, S., 628
Chang, X., 415
Chaskalovic, J., 81, 394
Chebanov, D., 141, 622
Cheeseman, A., 50
Chen, G., 173
Chen, H., 244
Chen, L., 339
Chifman, J., 223
Chikh, M., 524
Choi, M., 633
Choi, S., 59
Choukir, S., 506
Chowdhury, J., 353, 593
Christlieb, A., 80
Chrust, M., 478, 480, 572
Chumburidze, M., 652
Church, K., 169
Cio, Y., 408
Coan, J., 648
Cohen, A., 183
Coifman, R., 110
Cojocaru, M., 159, 164, 214, 614
Colapinto, C., 49
Collera, J., 625
Consta, S., 52, 54–56
Constantin, P., 676
Constas, S., 57
Coons, M., 71
Corbett, B., 363
Corless, R., 330
Corre, S., 588
Cossu, R., 305
Costanzino, N., 183
Coulier, P., 380
Craig, M., 99
Craig, W., 279
Cressman, R., 156, 157, 166
Cui, Z., 190
Cusumano, J., 218
Cyr, E., 400
Czegledi, A., 579
- D**
- Damaren, C., 152
DANG, D., 520
Dang, D., 187
Daniels, L., 204
Dar, A., 228
Darbandi, M., 83, 300, 441, 492, 526
Darve, E., 380
Das, P., 686
Dastjani-Farahani, K., 300
Davarpanah Jazi, S., 306
Dawes, A., 341
Dawson, T., 374
Day, T., 350
Daymond, M., 304
de la Rosa, R., 230
De Sterck, H., 382, 385, 399, 434
de Vries, G., 341
deBoer, R., 342
Demers, F., 522
Deng, Y., 561
Denis, C., 603
Denniston, C., 312, 609, 612
Dhaliwal, H., 670
Diamessis, P., 303
Dias, C., 240
Dick, D., 591
Dierich, F., 449

- Dionne, B., 106
 Dogan, G., 220
 Dorea, C., 669
 Dowdall, J., 378
 Drakos, N., 594
 Drapaca, C., 216, 218
 Drusvyatskiy, D., 209
 Dsilva, C., 110
 Dubickas, A., 74
 Dumitrache, A., 329
 Dunn, J., 158
 During, B., 262
 Dutot, M., 331
 Dzalilov, Z., 102
- E**
 Eberl, H., 326, 329, 343, 352, 355, 361, 671
 Ebrahimi, M., 221
 El-Gebeily, M., 48
 El-Hage, G., 428
 Elias, Y., 72
 Elmoataz, A., 651
 Elsenhans, A., 62
 Emerenini, B., 352
 Emili, E., 117
 Ernsthausen, J., 123
 Eslami, A., 458, 504
 Esmaeilzadeh, M., 432, 655
 Esquivel-Avila, J., 294
 Etbaigha, F., 614
 Evans, D., 218
- F**
 Fartaj, A., 470
 Feaver, A., 66
 Feick, R., 145, 148, 150
 Felix, V., 682
 Feng, T., 89
 Feng, W., 88, 90, 229, 666
- Feng, X., 80
 Fernandes, B., 202
 Ferreira, D., 669, 682
 Filatova, T., 374
 Fischer, P., 32
 Fishelov, D., 112
 Fleck, B., 464
 Flood, B., 629
 Foley, J., 683
 Fossati, M., 506, 541
 Foster, J., 315, 335
 Fotowat, S., 470
 Fraser, B., 630
 Freitas, R., 682
 Freret, L., 451
 Friedrich, B., 149
 Frigaard, I., 322, 323, 406, 417, 458, 566, 568
 Fury, M., 658
- G**
 Galagusz, R., 275
 Galstyan, A., 278
 Galvani, A., 347, 373
 Gao, H., 194
 Gao, S., 541
 Garnier, F., 524
 Garvie, M., 337
 Gaudreau, P., 413
 Gaur, D., 411
 Gear, W., 110
 Georgiou, N., 125
 Geurts, B., 430
 Ghafarian, N., 197
 Ghafourizadeh, M., 492
 Ghasemi, A., 553, 645
 Ghodsi, A., 211
 Giannakis, D., 108, 109, 115
 Gibson, P., 332
 Girardin, R., 241

- Giuliani, A., 447
 Gnameho, K., 635
 Gningue, Y., 580, 602
 Gong, X., 390
 Gong, Z., 390
 Gonzalez-Meler, M., 163
 Gonzalez-Sales, M., 99
 Gooding-Townsend, R., 672
 Goodman, B., 619
 Goward, G., 608
 Graf, I., 321
 Greenhalgh, S., 347
 Greenwood, P., 253, 369
 Grey, S., 683
 Groth, C., 382, 434, 451, 453, 498
 Guenda, K., 604
 Gulliver, A., 604
 Gully, A., 335
 Gunter, A., 468
 Gupta, N., 647
 Guthrey, P., 271
 Guy, R., 75
- H**
- Ha, B., 248
 Ha, H., 631, 638
 Habashi, W., 506, 541
 Habibi, M., 247
 Hacinliyan, I., 618
 Haddar, H., 269
 Hajaiej, H., 274
 Halalay, I., 608
 Halimov, F., 623
 Halle, S., 516, 545
 Halloway, A., 166
 Hamilton, I., 662, 683
 Hanifi, A., 484
 Hare, K., 74
 Harlim, J., 109, 113
- Harnanan, S., 310
 Haslam, M., 268
 Haynes, R., 383, 410
 Hejazi, A., 180
 Henderson, K., 358, 376
 Henningson, D., 484
 Higgs, P., 246, 359
 Hillairet, C., 188
 Hlynka, A., 167
 Hodgins, H., 683
 Hossain, M., 502
 Hossain, S., 411
 Hosseini, B., 325, 409
 Hosseini, S., 484
 Howse, A., 399
 Hu, B., 639
 Hu, J., 498
 Hu, X., 289
 Huang, H., 390
 Huang, J., 87, 89
 Huang, M., 244
 Huang, W., 581
 Huguet, G., 258
 Humphries, A., 99
 Humphries, T., 407
 Huo, X., 357
 Hurd, T., 37
 Hyndman, C., 188
- I**
- Ibrahim, S., 274
 Idels, L., 97
 Idier, A., 531
 Ilie, S., 388, 684
 Ingalls, B., 672, 684
 Ingram, P., 63
 Inoue, J., 260
 Islam, M., 464
 Ismail, M., 470

- Isola, D., 541
 Ivan, L., 382, 434
 Ivanov, A., 102
- J**
 Jabbari, A., 314
 Jaber-Douraki, M., 354
 Jackson, K., 180, 187
 Jacobson, M., 73, 78
 Jaiswal, P., 531
 Jakubowski, T., 128
 Jalbert, E., 329
 Jamaleddine, T., 474
 Jamwal, S., 647
 Jankauskas, J., 74
 Jao, D., 60
 Javadpour, F., 200
 Jemcov, A., 445
 Jha, P., 422, 478, 480
 Jia, Y., 649
 Jiang, W., 333, 334, 364
 Jiang, Z., 269
 Jiao, Y., 188
 Jin, X., 374
 Jodoin, B., 570
 John, L., 557
 Johnson, M., 574
 Jones, G., 637
- K**
 Kabacaoglu, G., 215
 Kadem, L., 468
 Kaffel, A., 646
 Kamal, T., 628
 Kang, N., 196
 Kapral, R., 244, 245
 Karimfazli, I., 322
 Kashani, A., 564
 Keita, S., 308
- Kelly, D., 506
 Keplinger, K., 687
 Kettlewell, B., 334
 Kevan, P., 343
 Kevlahan, N., 384, 645
 Kevrekidis, L., 110
 Kevrekidis, Y., 116
 Khabou, A., 603
 Khajehpour, P., 211
 Khajepour, A., 283
 Khalique, C., 226, 235
 Khan, F., 528
 Khan, M., 219
 Khani, S., 311
 Khattak, A., 670
 Kheibarshekan, L., 587
 Khodadadi-Yazdi, M., 300
 Khosravi, G., 516, 545
 Khulief, Y., 48
 Kim, C., 250
 Kim, I., 318
 Kim, J., 631
 Kirr, E.-W., 38
 Kiss, I., 125
 Kitanov, P., 590
 Kiyak, H., 176
 Klaseboer, E., 607, 656
 Klinke, D., 589
 Kloosterman, M., 287, 679
 Knipl, D., 375
 Knudstrup, S., 254
 Koberinski, A., 557
 Kobti, Z., 167
 Kovacic, M., 143
 Kowalik-Urbaniak, I., 50
 Koykka, C., 224
 Krachkovskiy, S., 335, 608
 Kreinin, A., 185

- Krishnaswamy Sethurajan, A., 608
 Krislock, N., 209
 Krivodonova, L., 424, 426, 438, 447
 Krone, S., 348
 Kroukamp, O., 361
 Kroumi, D., 155
 Kunze, H., 44–47
 Kwak, M., 186
 Kwok, F., 410
- L**
- La Torre, D., 42, 45, 46, 49
 Laffay, P., 531
 Laforest, M., 408
 Lai, X., 100
 Lakhdari, Z., 651
 Lalín, M., 68
 Lamoureux, M., 328
 Lange, C., 472, 514
 Laouar, A., 685
 Laplante, J., 486
 Laporte, M., 518
 Larachi, F., 490
 Larsen, K., 348
 Laskowski, M., 370
 Lateb, M., 524
 Laubenbacher, R., 223
 Laurendeau, E., 522
 Lauter, K., 72
 Lawley, S., 256
 Lawrence, H., 148
 Lebel, L., 678
 LeBlanc, V., 106, 288, 378
 Lee Slew, K., 428
 Lee, H., 60
 Lee, J., 631
 Lessard, S., 155
 Levere, K., 46
 Lewis, G., 585
 Lewis, M., 143
 Li, J., 99, 587
 Li, L., 514
 Li, M., 293, 344, 667, 668
 Li, S., 455
 Li, X., 208, 210, 364, 553, 667
 Li, Y., 419
 Lien, F., 561, 563
 Lightstone, M., 555
 Lindner, S., 65
 Linhananta, A., 241
 Liu, H., 335
 Liu, W., 293
 Liu, W.K., 16
 Liu, X., 98, 170, 171, 174–178
 Liuzzi, D., 49
 Lizotte, D., 201
 Lo, C., 181
 Lokhmanets, I., 529
 Lopez, C., 223
 Lorin, E., 395
 Lorinczi, J., 126
 Loy, K., 644
 Lu, L., 189, 615
 Lutscher, F., 285, 367, 378
 Lynch, D., 163
- M**
- M. Wahl, L., 372
 Ma, L., 221
 Ma, Y., 514
 MacLachlan, S., 400
 MacPhee, D., 439
 Madamanchi, A., 584
 Maggelakis, S., 586
 Maggioni, M., 111
 Majedi, H., 197, 203
 Makarov, R., 192, 637
 Malek, A., 621

- Malevanets, A., 53
 Malik, N., 654
 Mallat, S., 18
 Malmskog, B., 70
 Mamon, R., 194
 Mangiardi, C., 610
 Mao, D., 85
 Margrave, G., 328
 Marsiglio, S., 49
 Martins, J., 570
 Maruthi, N., 436
 Masic, A., 355
 Matida, E., 428
 Mavriplis, C., 422, 478, 480, 486, 518, 547, 572
 Mbodj, M., 580
 McCluskey, C., 94, 157
 McDonald, J., 453, 482
 McKenzie, R., 119, 121
 McLeish, D., 182
 McLenaghan, R., 142
 McNickle, G., 163, 166
 McVittie, J., 91
 Medlock, J., 347
 Medvescek, J., 529
 Mehri, R., 518
 Melnik, R., 198, 242
 Melnikov, A., 193, 677
 Mendivil, F., 43, 333, 334
 Menezes, R., 682
 Mestdag, T., 135
 Metelka, J., 147
 Metzler, A., 192
 Meyer, R., 610
 Michel, L., 274
 Midya, V., 661, 664, 665
 Mikhailov, A., 244
 Miller, M., 428
 Miskovic, Z., 196, 199, 202, 204
 Moe, S., 642
 Moghadas, S., 363, 370
 Mohaddes Foroushani, S., 510
 Mohammad, K., 383
 Mohammadi, M., 187
 Moorthy, A., 326
 Moran, N., 648
 Morency, F., 516, 524, 545
 Morgan, J., 337
 Morris, K., 283, 624, 657
 Morris, S., 296
 Morshed, M., 684
 Morsky, B., 165
 Mosina, N., 622
 Mostaghimi, J., 564
 Mosunov, A., 78
 Mottaghian, P., 559
 Moyles, I., 387
 Mrozinski, K., 570
 Mueller, J., 670
 Muir, P., 393
 Mulligan, C., 455
 Murphy, I., 670
 Murray, S., 555
 Musavi, H., 535
 Musgrave, J., 285
 Mydlarski, L., 529
- N**
- Nadarajah, S., 460, 496, 539, 551
 Nadeem, A., 597
 Naeem, I., 231
 Najafi Nejad Nasser, A., 455
 Nakano, S., 407
 Nakayama, H., 466
 Nakhaei, N., 319
 Narayan, A., 582
 Naseri, R., 621
 Nasif, G., 500, 543

- Nategholeslam, M., 246
 Navah, F., 460
 Nave, J., 275, 302, 381, 414
 Naylor, D., 510
 Naz, R., 227
 Ncube, I., 616
 Ndeffo-Mbah, M., 347
 Nedialkov, N., 121, 122
 Nekka, F., 587
 Nelson, L., 331
 Ng, H., 466, 468
 Ngwa, M., 105
 Nian, K., 392
 Nicola, W., 251, 680
 Nigam, N., 409
 Nijhout, H., 257
 Nikitina, L., 307
 Nikrityuk, P., 449
 Nkounkou, H., 403
 Nowack, S., 338
 Nykamp, D., 250
- O**
 Odesskii, A., 137
 Offin, D., 143
 Oh, M., 55
 Okosun, K., 365
 Oleskey, D., 688
 Oliveira, M., 669
 Oosterlee, K., 20
 Oosthuizen, P., 508
 Ornik, M., 172
 Ortega, J., 190
 Otero, D., 42
 Ozman, E., 72
- P**
 Pacard, F., 291
 Padgett, J., 388
 Paliy, M., 56
 Pannekoucke, O., 117
 Papa, A., 682
 Paraschivoiu, M., 476
 Parenteau, M., 522
 Parker, D., 374
 Pashaie, A., 152
 Pasini, D., 313
 Patie, P., 129, 633
 Pavel, L., 152
 Peakall, J., 305
 Pelinovsky, D., 270, 315
 Perelson, A., 373
 Perez-Arancibia, C., 272
 Peterson, S., 333, 334
 Petras, A., 389
 Pham, T., 520
 Piatkovska, G., 612
 Pichugina, O., 600
 Piomelli, U., 314, 430, 533, 549, 559
 Piperni, P., 462
 Pirvu, T., 186
 Pitre, R., 318
 Plotkin, S., 243, 247
 Pocas, D., 286
 Podduturi, N., 458, 504
 Pollack, J., 648
 Pongui Ngoma, D., 403
 Ponnambalam, K., 282, 582, 634
 Portaluri, A., 138
 Portaro, R., 466, 468
 Poulin, F., 287, 679
 Pouransari, H., 380
 Prabhakar, S., 198, 242
 Prada, J., 232
 Pratibha, N., 601
 Prieto-Langarica, A., 258
 Protas, B., 608

- Proulx, L., 386
 Provost, S., 194
 Pryce, J., 119, 121, 122
 Pugh, M., 296
 Pyzza, P., 258
- Q**
 Qian, Z., 189
 Qiao, T., 333, 334
 Quaife, B., 215, 391
 Quaranta, G., 506
- R**
 Rémy, A., 605
 Rabbani, M., 372
 Rabin, N., 112
 Radovanovic, P., 202
 Rael, R., 160
 Rahbarimanesh, S., 547
 Rahman, K., 361, 671
 Rajaratnam, K., 142
 Rampure, M., 474
 Rankin, G., 570
 Rao, S., 436
 Rasmussen, C., 70
 Rastelli, G., 136
 Ratti, V., 343
 Rechnitzer, A., 61
 Recio, E., 238, 267
 Reed, M., 256, 257
 Reesor, M., 184
 Reid, J., 673
 Resch, J., 426
 Riahi, M., 269
 Rimbu, A., 96, 284
 Ringue, N., 551
 Roberts, K., 626
 Roberts, M., 397
 Roberts, S., 146
- Robertson, B., 245
 Robertson, C., 145, 147, 148
 Roettger, E., 75
 Romaszko, J., 663
 Rosa, M., 237
 Rosenhaus, V., 233
 Roshanaei, V., 153
 Rossmanith, J., 271, 642
 Rottler, J., 247
 Rouhi, A., 430
 Roustaei, A., 323
 Rowat, P., 252
 Roy, P., 353, 593
 Roy, T., 418
 Rubinstein, M., 77
 Ruiz Galan, M., 46
 Ruuth, S., 389
- S**
 Sabre, R., 685
 Sabzpushan, S., 526
 Safavi-Naeini, S., 197, 203
 Safouhi, H., 413
 Saha, A., 411
 Sakurai, H., 643
 Samareh, B., 564
 Sanders, R., 464
 Sanjose, M., 531
 Santoprete, M., 136
 Sarker, A., 410
 Sarker, N., 464
 Sarnak, P., 77
 Sauer, T., 114
 Saunders, J., 76
 Sawh, D., 634
 Scalas, E., 125, 261
 Schily, F., 476
 Schlatter, P., 484
 Schneider, G., 83, 300, 441, 492, 526

- Schreiber, S., 22
 Scott, M., 204
 Seal, D., 80, 642
 Semnani, B., 203
 Seo, G., 368
 Sermeus, K., 421, 462
 Shan, C., 293, 362
 Shankar, R., 233
 Sharma, P., 199
 Sharma, V., 273, 337
 Shaw, J., 317
 Sheel, T., 500
 Shen, J., 415
 Shen, X., 456
 Sheriff, F., 52
 Shevelly, A., 458, 504
 Shi, K., 171
 Shirokoff, D., 275
 Shodiev, H., 579, 670
 Shontz, S., 216
 Shore, J., 681
 Shu, H., 289
 Shuai, Z., 371
 Sideroff, C., 445
 Siemaszko, A., 663
 Silva, J., 69
 Sylvester, A., 73
 Simmons, S., 132
 Skelton, A., 377
 Skippon, T., 304
 Slevinsky, R., 413
 Smerlak, M., 265
 Smirnov, R., 133
 Smith?, R., 349
 Soleev, A., 623
 Soltani, S., 57
 Son, S., 631
 Sonner, S., 352
 Soontiens, N., 310
 Soviak, J., 512
 Spiteri, R., 416
 Stange, K., 72
 Stastna, M., 310, 316, 317, 488, 557
 Stechlinski, P., 178
 Steinbrecher, A., 120
 Steinman, D., 219
 Steinmoeller, D., 488
 Stenflo, O., 43
 Stephens, D., 445
 Stockie, J., 325, 409
 Stoica, C., 131
 Straatman, A., 528
 Subich, C., 301
 Sudarsan, R., 327
 Suderman, R., 201
 Sugati, T., 177
 Sun, F., 282
 Sun, Q., 656
 Suvakov, M., 205
 Svanadze, M., 653
 Swishchuk, A., 95
- T**
- Tadic, B., 205
 Taghavi, S., 490, 504, 568
 Takouda, M., 602
 Talmon, R., 110
 Tan, G., 121, 122
 Tan, P., 401
 Tang, Q., 80
 Tarfulea, A., 676
 Tarfulea, N., 213
 Tawagi, P., 428
 Taylor, B., 318
 Tcheng, A., 381
 Ten Holder, S., 672
 Teneng, D., 636

- Tensuda, B., 453
 Thiraviaraj, I., 664
 Thommes, E., 214
 Thual, O., 117
 Ting, F., 291
 Toaldo, B., 127
 Torabi Ziaratgahi, S., 416
 Torti, S., 223
 Tracinà, R., 234
 Trinh, P., 297
 Trummer, M., 407
 Tucker, P., 537
 Tufail, N., 228
 Tullis, S., 555
 Tuminaro, R., 400
 Tupper, P., 396, 619
 Tyson, R., 331, 348, 367
- U**
 Ullah, E., 578
 Urbach, D., 153
- V**
 Valen-Sendstad, K., 219
 Valluri, S., 626
 van den Driessche, P., 340, 688
 van den Hoogen, J., 162
 van Veen, L., 404
 Vanden-Eijnden, E., 24
 Verriest, E., 104
 Vest, A., 657
 Vicol, V., 676
 Vinuesa, R., 484
 Vo, H., 522
 Voronin, Y., 209
 Vrscay, E., 42, 50, 333
 Vujićić, T., 158
- W**
 Wachowiak, M., 630
 Wachs, A., 322, 406
 Wahl, L., 356, 360, 591, 594–597
 Waite, M., 311
 Wan, A., 414
 Wan, J., 401
 Wang, B., 512
 Wang, J., 615
 Wang, L., 289, 344
 Wang, Q., 412, 589
 Wang, R., 188
 Wang, S., 89, 92, 339
 Wang, Z., 103, 589
 Ward, M., 297
 Watmough, J., 289
 Watson, R., 537
 Wei, J., 291
 Wells, C., 373
 Wells, M., 305, 306, 629
 West, J., 498
 White, D., 341
 Wiandt, T., 105, 586
 Wilcox, M., 598
 Wild, E., 154, 159
 Wild, G., 158, 224, 366
 Williams, H., 73, 75
 Williams, K., 331
 Willms, A., 377, 590, 598
 Wilson, M., 681
 Winlaw, M., 385
 Wolf, T., 137, 229
 Wolfaardt, G., 329, 361
 Wolkowicz, G., 292, 368
 Wolkowicz, H., 208–210
 Wong, A., 92
 Wong, K., 648
 Wright, J., 510
 Wu, H., 531

- Wu, J., 91, 92, 290
 Wu, W., 549
 Wu, Y., 335, 617
- X**
- Xi, L., 299
 Xiao, Y., 370
 Xiaoyan, H., 82
 Xie, W., 175
 Xie, X., 415
 Xin, G., 92
 Xu, F., 157
 Xu, S., 570
 Xu, W., 189
 Xu, X., 581
 Xu, Y., 92, 207
- Y**
- Yakovenko, V., 263
 Yakovlev, S., 600
 Yang, H., 462
 Yang, J., 56
 Yang, L., 539
 Yang, T., 87
 Yazdani, S., 69
 Yee, E., 561
 Yerubandi, R., 681
 Yi, Y., 26, 293
 Yodzis, M., 346
 Yoon, S., 417, 566
 Yu, P., 356
- Yuan, J., 559
 Yuan, Y., 292
- Z**
- Zabarasz, N., 28
 Zaccour, G., 39
 Zafar, M., 273
 Zamir, M., 596
 Zhang, K., 175
 Zhang, Q., 88
 Zhang, S., 150
 Zhang, W., 345, 356
 Zhao, G., 659
 Zhao, Y., 129
 Zhao, Z., 108
 Zheng, X., 181
 Zhong, S., 171, 174
 Zhou, A., 184
 Zhou, M., 366
 Zhu, A., 360
 Zhu, H., 101, 171, 222, 339, 345, 602
 Zhu, S., 87
 Zielinski, A., 282
 Zingg, D., 456, 494
 Zochowski, M., 254
 Zou, X., 100, 364
 Zubov, V., 328
 Zucker, J., 286
 Zwanenburg, P., 496
 Zwiers, I., 678

The AMMCS-CAIMS 2015 Congress
Book of Abstracts

ISBN: 978-0-9918856-1-9